Study of the resistance to biodeterioration of innovative low-carbon cementitious materials for application in sewer networks

Amr Aboulela

THESIS

For the award of a

DOCTORATE OF THE UNIVERSITÉ DE TOULOUSE

Issued by Institut National des Sciences Appliquées of Toulouse

---

Presented and defended by

Amr ABOULELA

21st of January 2022

Study of the resistance to biodeterioration of innovative low-carbon cementitious materials for application in sewer networks

---

Doctoral school: **MEGEP – Mechanics, Energetics, Civil & Process Engineering**

Department: **Civil Engineering**

Research laboratories:

LMDC - Laboratoire Matériaux et Durabilité des Constructions de Toulouse

TBI - Toulouse Biotechnology Institute, Bio & Chemical Engineering

Thesis supervised by

Alexandra BERTRON, Matthieu PEYRE LAVIGNE and Cédric PATAPY

Jury

M. Eric VAN HULLEBUSCH, Reviewer
M. Burkan ISGOR, Reviewer
Mme Josée DUCHESNE, Examiner
M. Mark ALEXANDER, Examiner
M. Cyrill GRENGG, Examiner
M. Cédric PATAPY, Co-supervisor
M. Matthieu PEYRE LAVIGNE, Co-supervisor
Mme Alexandra BERTRON, Supervisor

THESE

En vue de l'obtention du

DOCTORAT DE L'UNIVERSITÉ DE TOULOUSE

Délivré par l'Institut National des Sciences Appliquées de Toulouse

Présentée et soutenue par

Amr ABOULELA

Le 21 janvier 2022

Étude de la résistance à la biodétérioration de matériaux cimentaires innovants et bas carbone pour une application dans les réseaux d'assainissement

Ecole doctorale : **MEGEP - Mécanique, Energétique, Génie civil, Procédés**

Spécialité : **Génie civil**

Unité de recherche :
LMDC - Laboratoire Matériaux et Durabilité des Constructions de Toulouse
TBI - Toulouse Biotechnology Institute, Bio & Chemical Engineering

Thèse dirigée par
Alexandra BERTRON, Matthieu PEYRE LAVIGNE et Cédric PATAPY

Jury

M. Eric VAN HULLEBUSCH, Rapporteur
M. Burkan ISGOR, Rapporteur
Mme Josée DUCHESNE, Examinatrice
M. Mark ALEXANDER, Examinateur
M. Cyrill GRENGG, Examinateur
M. Cédric PATAPY, Co-directeur de thèse
M. Matthieu PEYRE LAVIGNE, Co-directeur de thèse
Mme Alexandra BERTRON, Directrice de thèse

Study of the resistance to biodeterioration of innovative low-carbon cementitious materials for application in sewer networks

By Amr Aboulela

Doctoral thesis in Civil Engineering, National Institute of Applied Sciences of Toulouse

Abstract

Biodeterioration of cementitious materials in sewer networks is a major concern for health and economic reasons. Mainly, it is due to the biological oxidation of H_2S into H_2SO_4 leading to a local and a progressive dissolution of the cementitious matrix and the precipitation of expansive products likely to provoke cracks. In the literature, it is widely established that calcium aluminate cement (CAC) has a better resistance in such environments compared to Portland cement (PC). The better performance of CAC was mainly linked to the high aluminum content of this material and to the physic-chemical properties of the cement matrix (mineralogical phases, porosity…). In addition, recent studies revealed the potential role of iron in the resistance of materials in such environments, however, without clarifying this role.

This thesis, carried out in collaboration between Holcim and the National Institute of Applied Sciences (INSA) in Toulouse, aimed to (i) study the behavior and the deterioration mechanisms of different low-CO_2 cementitious materials (calcium sulfoaluminate cement and alkali-activated slag) exposed to a microbial attack in sewer conditions; (ii) evaluate the impact of partially substituting PC with mineral additives, rich in aluminum and/or iron, on the durability of the materials; (iii) understand the mechanisms of interactions between the cement matrix, the aggressive environment and the biofilm; (iv) use and optimize of a numerical model, based on the coupling of materials' chemistry and the transport of species in solution, to include biological transformations of sulfur species.

The experimental work was carried out in laboratory conditions using an accelerated test (BAC test), developed at INSA Toulouse, with the aim of simulating the biological conditions encountered in sewer networks. The BAC test consists of inoculating cementitious specimens with activated sludge before exposing the cement-based materials to a trickling solution containing tetrathionate ($S_4O_6^{2-}$) as a soluble reduced sulfur source. This test made it possible to create favorable conditions for the development of a sulfur-oxidizing activity at acidic pH and to evaluate the behavior of a large panel of materials of different chemical and mineralogical compositions (based on Portland cement, calcium aluminate cement, calcium sulfoaluminate cement and alkali-activated materials). The BAC test simulates severe exposure conditions with a pH ranging between 3 and 2.5 for the active deterioration phase. The biodeterioration process was monitored during several 3-months experimental campaigns in terms of analyses of the composition of the leached solutions, bacterial populations and modification of the microstructure, the chemistry and the mineralogy of the cement matrices. Moreover, the results from this experimental protocol were used as a database for the

calibration of a reactive-transport model to assess the behavior of materials in chemical and/or biological conditions.

Part of the work, focused on the analyses of sulfur species produced during the selected sulfur-oxidizing activity, showed that in acidic conditions disproportionation of the sulfur substrate took place. In addition to the quantification of the production of polythionate reaction intermediates, this phenomenon was responsible for the presence of elemental sulfur (S^0) precipitations on the surface of materials. These analyses made it possible to estimate the amount of acid in direct contact with the material.

The analyses of the transformation of sulfur species were completed by an identification of the populations involved in the process of deterioration of cementitious materials in sewer conditions. *Acidithiobacillus* and *Thiomonas* species were the main bacteria identified, with the latter being able to disproportionate tetrathionates in absence of oxygen. *Acidithiobacillus ferrooxidans* were detected on materials containing Fe-rich mineral additives. The comparison between the populations developed on the surface of the material and the populations found in the deteriorated zones of the material did not show any major difference.

A performance indicator (PIeqOH) was developed by evaluating the leaching of chemical elements/compounds (in particular calcium, aluminum, iron, magnesium and sulfate which define the neutralizing capacity of the materials). This performance indicator was used to establish a classification of materials according to their resistance to sulfuric acid attack in these exposure conditions. The PIeqOH was validated using the CAC and PC and the results were consistent with the literature.

Besides the very good resistance of calcium aluminate cement, certain calcium sulfoaluminate cement (CSA)-based materials have shown better behavior than Portland cements (PIeqOH of 1.3 times higher) in the experimental conditions. Calcium sulfoaluminate clinker (CSAC) and calcium sulfoaluminate clinker with gypsum (CSAG) showed better performance than calcium sulfoaluminate clinker with anhydrite (CSAC). The evolution of the mineralogical phases of the three studied CSA-based materials consisted of the dissolution of AFt and AFm phases and the formation of gibbsite-like AH_3 on the surface. The better resistance of CSA-based materials was mainly attributed to the presence of aluminum hydroxide (AH_3) as well as its chemical stability in acidic environments. Moreover, the mineralogical form of aluminum-bearing phases was a key factor in the resistance of such phases; i.e. the simple increase of the aluminum content in the materials by non-reactive mineral additives was shown to be insufficient to improve the performance of cementitious materials.

The lack of consensus on the iron impact on the deterioration mechanisms of cementitious matrices led to studying its influence in the conditions of the BAC test. The results showed that iron remained relatively inactive during the very aggressive microbial attack. Neither the iron concentration nor the form in which it was present showed any impact on the development of microbial activities. In addition, the use of non-reactive iron-rich mineral additives did not seem to significantly improve the durability of the cement-based materials.

Alkali-activated slag-based materials were formulated in the laboratory to study the deterioration mechanisms of innovative and alternative materials to Portland cement. In the experimental conditions of the BAC test, the deterioration mechanisms of these materials closely resembled to those of Portland cement and consisted of a very strong decalcification of the hydrated phases of calcium aluminosilicate (C-A-S-H), leading to the formation of an aluminosilicate gel on the surface.

HYTEC software (reactive-transport model based on thermodynamic database) was used to represent the experimental data for PC and CAC materials. In a first approach simulating only sulfuric acid attack at two different pH, the results showed differences in terms of performances between PC and CAC; however, these results were not consistent with the experimental results. In order to improve the simulation approach by adding biological reactions to the model, new chemical reactions, adapted to HYTEC, were proposed based on the experimental data obtained from the transformation of the sulfur compounds in the experimental conditions. Such equations were used to reproduce the evolution of the microbial activity on the surface of the materials in the conditions of the BAC test. In this study, due to the lack of time, the coupling of the chemical reactive-transport model and the biological-like model was not carried out; however, this work could be a perspective of this study.

In the end, through this work, a better understanding of the alteration mechanisms of different innovative materials was achieved. The leached solutions allowed the classification of the materials according to their performances. Potential key factors to improve the resistance of cementitious binders in such environments were highlighted by a thorough study of the evolution of the microstructure and the modification of the chemistry and mineralogy of the materials. The development of the numerical models has opened doors for studying alternative cement-based materials and for optimizing the formulation of the binders.

Keywords: biodeterioration; cementitious materials; calcium sulfoaluminate; alkali-activated slag; durability; microorganisms; sewer; sulfuric acid.

Etude de la résistance à la biodétérioration de matériaux cimentaires innovants et bas carbone pour une application dans les réseaux d'assainissement

Par Amr Aboulela

Thèse de doctorat en Génie Civil, Institut National des Sciences Appliquées de Toulouse

Résumé

La biodégradation des matériaux cimentaires dans les réseaux d'assainissement est une préoccupation majeure pour des raisons sanitaires et économiques. Elle est principalement due à l'oxydation biologique de H_2S en H_2SO_4 conduisant à une dissolution locale et progressive de la matrice cimentaire ainsi qu'à la précipitation de produits expansifs susceptibles de provoquer des fissurations. Dans la littérature, il est largement établi que le ciment d'aluminates de calcium (CAC) a une meilleure résistance dans de tels environnements en comparaison avec le ciment Portland (PC). Les meilleures performances du CAC sont principalement attribuées à la forte teneur en aluminium de ce matériau et aux propriétés physico-chimiques de la matrice cimentaire (phases minéralogiques, porosité…). D'autre part, des études récentes révèlent le potentiel rôle du fer dans la résistance des matériaux présents dans de tels environnements, sans toutefois permettre de clarifier ce rôle.

Cette thèse, réalisée en collaboration entre Holcim et l'Institut National des Sciences Appliquées de Toulouse, avait pour objet (i) d'étudier le comportement et les mécanismes de détérioration des différents matériaux cimentaires bas-CO_2 (ciment sulfoalumineux et laitier alcali-activé) exposés à une attaque microbienne en condition d'assainissement; (ii) d'évaluer l'impact de la substitution d'une partie du ciment Portland par des additions minérales, riches en aluminium et/ou en fer, sur la durabilité des matériaux; (iii) de comprendre les mécanismes d'interactions entre la matrice cimentaire et le biofilm; (iv) d'optimiser un modèle numérique, basé sur le couplage de la chimie des matériaux et le transport des espèces en solution, par l'intégration des transformations biologiques des espèces soufrées.

Le travail expérimental a été réalisé dans les conditions du laboratoire en utilisant un test accéléré (BAC test), développé à l'INSA de Toulouse, afin de simuler les conditions biologiques rencontrées dans les réseaux d'assainissement. Le BAC test consistait à ensemencer des échantillons de ciment avec de la boue activée avant de les exposer à une solution de ruissellement contenant du tétrathionate ($S_4O_6^{2-}$) comme source soluble de soufre réduit. Ce test a permis d'avoir des conditions favorables au développement d'une activité sulfo-oxydante à pH acide et d'évaluer le comportement d'un large panel de matériaux de compositions chimiques et minéralogiques différentes (à base de ciment Portland, ciment alumineux, ciment sulfoalumineux et matériaux alcali-activés). Le BAC test simule des conditions d'exposition sévères avec un pH compris entre 3 et 2,5 pour la phase active de la détérioration. Le processus de biodétérioration a été suivi au cours de plusieurs campagnes expérimentales de 3 mois en termes d'analyses de la composition des solutions lessivées,

populations bactériennes et de modifications de la microstructure, de la chimie et de la minéralogie des matrices cimentaires. Les résultats issus de ce protocole expérimental ont servi comme base de données pour calibrer le modèle chimie-transport permettant d'évaluer le comportement des matériaux dans des conditions chimiques et/ou biologiques.

Une partie du travail, orientée sur les analyses des espèces soufrées produites lors de l'activité sulfo-oxydante sélectionnée, a montré que dans les conditions acides, la dismutation du substrat soufré avait lieu. Outre la quantification de la production d'intermédiaires réactionnels de type polythionate, ce phénomène est responsable de la présence de précipitation de soufre élémentaire (S^0) sur la surface des matériaux. Ces analyses ont également permis d'estimer la quantité d'acide réellement en contact avec le matériau.

Les analyses de la transformation des espèces soufrées ont été complétées par une identification des populations impliquées dans le processus de détérioration des matériaux cimentaires dans les conditions d'assainissement. Les espèces *Acidithiobacillus* et *Thiomonas* sont les principales bactéries identifiées, avec le dernier qui est capable de dismuter les tetrathionates en absence d'oxygène. *Acidithiobacillus ferrooxidans* ont été détectées sur les matériaux contenant des additions minérales, tels que la bauxite et le HardCem. La comparaison entre les populations développées sur la surface du matériau et les populations retrouvées dans les zones détériorées du matériau n'ont pas montré de différence majeure.

Un indicateur de performance (PIeqOH) a été développé par l'évaluation de la lixiviation des éléments/composés chimiques (notamment le calcium, l'aluminium, le fer, le magnésium et le sulfate, qui définissent le pouvoir tampon des matériaux). Cet indicateur a permis d'établir un classement des matériaux selon leurs résistances à l'attaque d'acide sulfurique dans ces conditions. Le PIeqOH a été validé en utilisant des matériaux à base de ciment Portland et de ciment alumineux et les résultats ont été en accord avec la littérature.

Mis à part la très bonne résistance du CAC, certains matériaux à base de ciment sulfoalumineux ont montré un meilleur comportement que les ciments type Portland (PIeqOH 1.3 fois supérieur) dans les conditions expérimentales. Cette résistance a été attribuée principalement à la présence de l'hydroxyde d'aluminium (AH_3) ainsi que sa stabilité chimique en conditions acides. De plus, la forme minéralogique des phases alumineuses est un facteur clé de la résistance de telles phases; i.e. la simple augmentation de la teneur en aluminium dans les matériaux par l'ajout des additions minérales non-réactives s'est avérée insuffisante pour améliorer les performances des matériaux cimentaires.

Le non-consensus de l'impact du fer sur les mécanismes de détériorations des matrices cimentaires a conduit à une étude de son influence dans les conditions du BAC test. Les résultats ont montré que le fer reste relativement inactif pendant une attaque microbienne très agressive. Ni la concentration en fer, ni la forme sous laquelle il est présent n'ont montré d'impact sur l'installation de l'activité microbienne. De plus, l'ajout des additions minérales riches en fer non réactif n'a pas amélioré la durabilité des matériaux cimentaires.

Des matériaux à base de laitier alcali-activé ont été formulés au laboratoire afin de tester la résistance de matériaux innovants alternatifs au ciment Portland. Les mécanismes de détérioration de ces matériaux ressemblaient beaucoup aux ceux du ciment Portland et ont consisté à une décalcification très forte des phases hydratées d'aluminosilicate de calcium (C-A-S-H), arrivant jusqu'à la formation d'un gel silicoalumineux en surface.

Enfin, HYTEC (model chimie-transport basé sur une base de données thermodynamique) a été utilisé pour représenter les données expérimentales pour le PC et le CAC. Dans une première approche utilisant de l'acide sulfurique uniquement à 2 pH différents, les résultats ont montré des différences en termes de performances entre les 2 matériaux ; cependant, ces résultats n'ont pas été en accord avec les résultats expérimentaux. Afin d'améliorer l'approche du modèle en ajoutant les réactions biologiques, des réactions chimiques nouvelles, adaptées pour HYTEC, ont été proposées en se basant sur des données expérimentales obtenues de la transformation des espèces soufrées dans les conditions du BAC test. Ces équations ont été utilisées pour reproduire l'évolution des activités microbiennes sur la surface des matériaux. Dans cette étude, le couplage du modèle chimie-transport et le modèle biologique n'a pas été fait par manque de temps ; cependant, ce travail pourrait être fait dans une étude perspective.

Pour finir, à travers ce travail, une meilleure compréhension des mécanismes d'altération de différents matériaux innovants a été obtenue. Les solutions lessivées ont permis de classer les matériaux selon leurs performances. Les facteurs clés pour améliorer la résistance des liants cimentaires dans de tels environnements ont été mis en évidence par une étude approfondie de l'évolution de la microstructure et de la modification de la chimie et de la minéralogie des matériaux. Le développement des modèles numériques a ouvert des portes pour étudier des matériaux cimentaires alternatifs et pour optimiser la formulation des liants.

Mots-clefs : biodétérioration; acide sulfurique; durabilité; matériaux cimentaires; microorganismes; réseaux d'assainissement; ciment sulfoalumineux; laitier alcali-activé.

Acknowledgement/Remerciement

Tout d'abord, je souhaiterais commencer par remercier très chaleureusement mes encadrants de thèse.

J'adresse mes remerciements à ma directrice de thèse, Alexandra Bertron (LMDC), pour ces 5 dernières années de collaboration. Je la remercie de m'avoir fait confiance pour réaliser ce travail de thèse, ainsi que pour toutes les opportunités qu'elle m'a permis de vivre pendant la thèse, que ce soient les voyages dans le cadre de conférences ou la rédaction d'articles scientifiques. Elle m'a appris à connaitre et aimer la recherche et je lui en serai toujours reconnaissant.

Je remercie également Cédric Patapy (LMDC), pour son suivi régulier, sa rigueur et sa bonne humeur. Je tiens à le remercier très particulièrement pour son aide sur les techniques analytiques avancées que nous avons pu mettre en place ensemble, et grâce à son réseau.

Il est impossible d'oublier Matthieu Peyre Lavigne (TBI), sans qui cette thèse n'aurait pas vu le jour. Je tiens d'abord à remercier Matthieu sur le plan humain pour sa bienveillance et son soutien sans faille, en particulier durant les moments difficiles. Je le remercie également pour son aide sur le plan scientifique et pour l'accompagnement pendant ces 5 années. Merci à lui de m'avoir initié aux domaines de la thermodynamique et du génie des procédés.

Enfin, je remercie Samuel Meulenyzer et Bruno Huet (Holcim Innovation Centre), pour leurs encadrements, leurs suivis et leurs bonnes humeurs. Merci aussi à eux de m'avoir permis de découvrir l'environnement industriel.

Je tiens à remercier Alain Sellier et Jean-Paul Balayssac, directeurs du Laboratoire Matériaux et Durabilité des Constructions, et Mathieu Sperandio et Claire Dumas, animateur(rice) de l'équipe Symbiose au Toulouse Biotechnology Institute.

Je souhaite également remercier les membres du jury : Burkan Isgor et Eric Van Hullebusch, rapporteurs de thèse, Mark Alexander et Cyrill Grengg, examinateurs, et Josee Duschesne, Présidente du Jury. Merci de m'avoir fait l'honneur de lire mon manuscrit (ce n'était pas un travail facile), merci aussi de m'avoir proposé de multitudes pistes de recherche pour les prochaines années de ma carrière universitaire.

Je tiens ensuite à exprimer toute ma gratitude envers le Service Chimie du LMDC, pour leur extrême compétence, gentillesse et disponibilité. Je tiens à remercier en particulier Vanessa Mazars pour son aide et sa patience après les nombreuses fois que j'ai grillé le filament du MEB (et pour m'avoir fait découvrir le thé à la vanille), Maud Schiettekatte pour tout le temps qu'elle a dû passer avec moi à l'ICP et à la HPIC (plus que 4000 échantillons analysés lors de cette thèse), et enfin Guillaume Lambaré pour son expertise et son aide à réaliser les essais de caractérisation (et aussi pour son stock de cartons).

Mes remerciements s'adressent également à l'équipe technique du TBI de l'EAD9, Evrard Mengelle, Simon Dubos et Mansour Bounouba, pour leur aide technique à la résolution des problèmes avec le BAC test. Je n'oublierai pas non plus les bons moments passés au foot (surtout les blessures).

Je tiens à remercier l'ensemble de personnels du LMDC et du TBI.

Je remercie sincèrement mes amis avec qui j'ai partagé des moments inoubliables et qui m'ont permis d'oublier momentanément la charge de travail avec les soirées, les repas, les pause-café, le foot, le canoé, le ski, les jeux-vidéo ou autres : Arthur, Laura, Hugo, Virginie, Marlène, Mansour, Tarek, Mathilde, Emilie, Sidonie, Léa, Irene, Erika, Matteo, Beatrice, Clémence et Omar. Je remercie tout particulièrement Marie pour tous les moments partagés, que ce soit l'encadrement des stagiaires, les vols de 12 heures pour l'Afrique du Sud, les conférences ou les voyages.

Je remercie évidemment mes parents, Abir et Khaled, ainsi que mes sœurs, Sara et Dina, d'avoir toujours était là pour moi et de m'avoir soutenue pendant tout ce parcours. Merci également à mes beaux-parents, Jocelyne et Jean-Christophe, et à mes beaux-frères, Victor et Gabriel, pour m'avoir supporté et encouragé pendant toute la durée de la thèse, et plus particulièrement pendant les derniers mois de rédaction qui n'ont pas toujours été des plus agréables.

Je remercie de tout mon cœur ma femme, Daphnée, dont l'affection, l'amour, le soutien et l'encouragement constants m'ont été d'un grand réconfort et ont contribué à l'aboutissement de ce travail. Merci de m'avoir accompagné tout le long de ce chemin.

Enfin, au risque d'être mal compris, mais en toute modestie et sincérité, j'aimerai me remercier moi-même d'avoir tenu le coup lorsque la situation ne s'y prêtai guère. Cette remarque peut paraître incongrue, mais une thèse est souvent parsemée de situations difficiles à gérer, bien qu'instructives. Cela dit je ne regrette rien, et je suis à présent heureux d'avoir pu franchir ce cap.

Notation

Materials designation

PC	Portland cement
CAC	Calcium aluminate cement
CSA	Calcium sulfoaluminate cement
AAS	Alkali-activated slag

Mineralogical phases

C_3S	Tricalcium silicate, alite
C_2S	Dicalcium silicate, belite
C_3A	Tricalcium aluminate
C_4AF	Tetracalcium aluminoferrite
$C_4A_3\check{S}$	Tetracalcium trialuminate sulfate, ye'elimite
CH	Portlandite
C-S-H	Calcium silicate hydrate
C-A-S-H	Calcium aluminosilicate hydrate
Et	Ettringite
Ms	Monosulfoaluminate hydrate
Mc	Monocarboaluminate hydrate
$C\check{S}.H_2$	Gypsum
$C\check{S}$	Anhydrite
H_2SO_4	Sulfuric acid

Sulfur-bearing species

H_2S	Hydrogen sulfide
S^0	Elemental sulfur
$S_2O_3^{2-}$	Thiosulfate
$S_4O_6^{2-}$	Tetrathionate
$S_5O_6^{2-}$	Pentathionate
$S_6O_6^{2-}$	Hexathionate
SO_3^{2-}	Sulfite
SO_4^{2-}	Sulfate

Properties

w/c	Water to cement ratio
w/b	Water to binder ratio
wt.%	Weight percentage

Techniques

SEM	Scanning electron microscopy
EDS	Energy dispersive spectroscopy
XRD	X-ray diffraction
TGA	Thermogravimetric analyses
ICP	Inductively coupled plasma
OES	Optical emission spectroscopy
HPIC	High performance ionic chromatography
HPLC	High performance liquid chromatography

Table of contents

General introduction

General introduction

In the aim of building a more sustainable world, the United Nations (UN) has fixed in 2015 an objective to guarantee the access to water and to sewer networks for everyone by 2030 and to ensure sustainable management of water resources. Moreover, in 2020, the UN published a report recalling that 46% of the world population (around 3.6 billion people) were still lacking safely managed sanitation services [1].

On the other hand, the average service-life of sewer networks in France is estimated at 60 years, which leads to expensive repair and renovation works, often difficult to implement [2]. The cost of the rehabilitation work of sewer pipelines in France was estimated at 1 billion €/ year given the age of the structures [3]. In the objective of reducing the maintenance costs of sewage networks and of designing new infrastructures that are more durable and resistant to deterioration mechanisms, it is essential to fully understand the phenomena that take place within sewer networks leading to their deterioration.

Cementitious materials are widely used in sewage network manufacturing and represents around half of the amount of sewer pipes. Concrete is used in the construction of new sewer pipes, in the rehabilitation of old structures or as a sacrificial layer on the surface of cast iron pipes [4]. During their service life, concrete pipes are subject to different types of deteriorations; e.g. default in the assemblage (defect in pipe connections, joints displacement), environmental aggression (growth of tree roots, land movement) or deterioration by effluents and microorganisms (concrete corrosion, gas attack) [4].

The deterioration of cementitious materials in sewer networks is a major concern for societal (connection of a growing part of the world's population), ecological (environmental pollution due to the deterioration of the networks) and economic (rehabilitation work of sewer networks) reasons.

The biodeterioration of cement-based materials in sewer environments is linked to the transformation of sulfur species by sulfur-oxidizing microorganisms proliferating on the pipes' surface. The production of sulfuric acid and the decrease in the surface pH of the concrete leads to severe deterioration of the structure. However, the durability of cementitious materials exposed to such conditions highly depends on the nature of the binder. Field's experiments around the world showed that materials based on calcium aluminate cement (CAC) exhibited better resistance than materials based on Portland cement (PC). The better resistance of CAC was mainly attributed to its particular chemical and mineralogical composition, especially its high aluminum content.

While the biodeterioration mechanisms of PC- and CAC-based are well studied in the literature, other relatively recent materials (calcium sulfoaluminate cement and alkali-activated slag) showed promising behavior against some external chemical attacks but were not yet studied in such conditions. Further, aluminum and iron were reported to influence the

deterioration mechanisms of cementitious binders exposed to biogenic sulfuric acid attack in sewer environments. However, this influence is not very well understood and needs to be further investigated.

In the objective of developing new resistant and durable materials, this research work aimed at:

(i) Developing an overall performance indicator allowing the comparison of a wide variety of binders, exposed to biogenic acid attack in laboratory conditions using a biological test (the BAC test).
(ii) Studying the behavior and deterioration mechanisms of various low-CO_2 cementitious materials (calcium sulfoaluminate cement and alkali-activated slag) exposed to microbial attack in sewer conditions.
(iii) Assessing the impact of partially substituting Portland cement with mineral additives, rich in aluminum and/or iron, on the durability of the materials.
(iv) Understanding the interaction mechanisms between the cement matrix and the microorganisms.
(v) Optimizing a numerical model, based on coupling the chemistry of materials and the transport of species in solution, by including the biological transformations of sulfur species.

The next chapters present a biogeochemical study of the performance of innovative cement-based materials of different chemical and mineralogical composition exposed to sewer environments in laboratory conditions. Cement pastes based on Portland cement (PC), calcium aluminate cement (CAC), calcium sulfoaluminate cement (CSA) and alkali-activated slag (AAS) were prepared. In addition, the investigation of the influence of the aluminum-bearing phases was carried out on three different calcium sulfoaluminate materials while the influence of the aluminum content was studied by adding bauxite at 10% to an AAS material. Furthermore, the influence of iron was studied using 4 binders (3 PC-based and 1 AAS-based materials) by incorporating a high-iron mineral addition (HardCem) at two different rates (20 and 10%) in PC and AAS materials respectively as well as having two PC-binders (sulfate-resistant type) with twice the initial iron content of the control material. The combination of all these materials aimed to cover the three main aspects detailed in the literature concerning the pending questions on the role of aluminum in the resistance of calcium sulfoaluminate materials, the role of iron in the deterioration process and, finally, the performance of alkali-activated slag materials in such conditions.

The cementitious materials were tested using a biological test (BAC test) in laboratory conditions. The BAC test consisted of inoculating the surface of cementitious materials with activated sludge then exposing these materials to a trickling solution containing tetrathionate ($S_4O_6^{2-}$) as a reduced sulfur source. The development of a microbial activity results in the deterioration of the cement-based materials. The representativeness, the reproducibility and

the repeatability of the testing protocol have been demonstrated. The BAC test is currently being considered for standardization on the European scale.

Chapter III presents the study of the possible transformation pathways of tetrathionate used as reduced sulfur substrate in the process of biodeterioration of cementitious materials in the BAC test. The different forms of sulfur were studied by analyzing the leached solutions during 3 months of exposure period of the materials by High Performance Liquid Chromatography (HPLC). This method, coupled with the literature review, was used as a basis to develop a numerical model capable of determining the formation of different polythionates and the amount of acid produced by microorganisms on the surfaces of materials according to the state of progress of the deterioration. This approach was then evaluated on four different families of cementitious materials, i.e. Portland cement, calcium aluminate cement, calcium sulfoaluminate cement and alkali-activated slag.

Chapter IV tackles the behavior of cementitious materials with respect to the leaching of the cement matrix. The first part of this chapter dealt with the classification of the studied cement-based binders according to their resistance to the biogenic sulfuric acid attack based on the development of a performance indicator based on the leaching of the five major elements of a cement matrix (calcium, aluminum, iron, magnesium and sulfate). This performance indicator aims to compare cementitious binders of very different chemical and mineralogical natures. The second part studied the correlation between the leaching kinetics of the cementitious matrix and the reactivity of the different hydrated phases. This study intended to investigate the possible influence of iron and aluminum (in terms of concentration and mineralogical form) on the microbial activity as well as the understanding of the reactivity of Fe- and Al-bearing phases vis-à-vis the acid attack.

Chapter V presents the study of the influence of the physico-chemical properties of the cementitious materials on their resistance against biogenic sulfuric acid attacks in the BAC test conditions. The deterioration phenomena were analyzed at a macroscopic level to study the development of microorganisms at the surface of the materials. Microscopic analyses concerned mainly the modification of the chemical and mineralogical composition. These analyses allowed to evaluate the correlation between the deteriorated depths and the performance indicators from chapter IV. Moreover, the concentration of aluminum and the mineralogical forms of AH_3 were investigated and were compared between calcium aluminate cement and calcium sulfoaluminate cement. The impact of the mineral additions (e.g. HardCem and Bauxite) in terms of iron and aluminum concentrations as well as their reactivity with the acid attack were studied. Finally, the mechanisms of deterioration of alkali-activated slag materials were evaluated.

Chapter VI presents a modeling approach for simulating biodeterioration phenomena using reactive-transport model (HYTEC®). The results from the three previous chapters were compiled to build a 1D model with two approaches; chemical and bio-chemical. The first part consisted of simulating an acid attack on cementitious materials with similar parameters to

the BAC test (flow of the solution, temperature, regulated pH…) using a chemical sulfuric acid instead of the reduced sulfur form (*tetrathionate*). A second part was based on the numerical model issued from the study of the sulfur cycle in chapter III. The different bio-chemical reactions were used to take into account the biofilm aspect (use of reduced sulfur source, impact of pH on microbial activity, quantity of acid produced…) in the simulations in order to better represent the biodeterioration of materials.

This multidisciplinary work was carried out in partnership with Holcim Innovation Center (HIC) and two research laboratories of INSA Toulouse: Laboratoire Matériaux et Durabilité des Constructions (LMDC) and Toulouse Biotechnology Institute (TBI).

Chapter I

Literature review

1. CHAPTER I - LITERATURE REVIEW

Table of contents

1.1. INTRODUCTION

The biodeterioration of cementitious materials in sewage environment is essentially due to biochemical processes. It has been estimated to represent around 10% of the deterioration of German sewer networks (Figure I-1) [4]. Concrete corrosion was linked to biogenic sulfuric acid attack for the first time by Parker [5,6]. Sulfate reducing bacteria (SRB) are developed in stagnant zones of the canalization systems, where they reduce the sulfate found in the wastewater stream to produce hydrogen sulfide (H_2S). The hydrogen sulfide diffuses in the air and gets in contact with the sewer concrete walls where gaseous diffusion phenomena will ease the penetration of the hydrogen sulfide into the interstitial solution via the surface pores. Since sound concrete has an alkaline pH, chemical redox reactions will cause the decrease of the pH leading to the development of sulfur oxidizing bacteria (SOB), at pH 9, which start to oxidize the sulfur species and produce sulfuric acid [6]. The sulfuric acid produced by microorganisms on the material's surface is at the origin of a severe biochemical attack on the cementitious material.

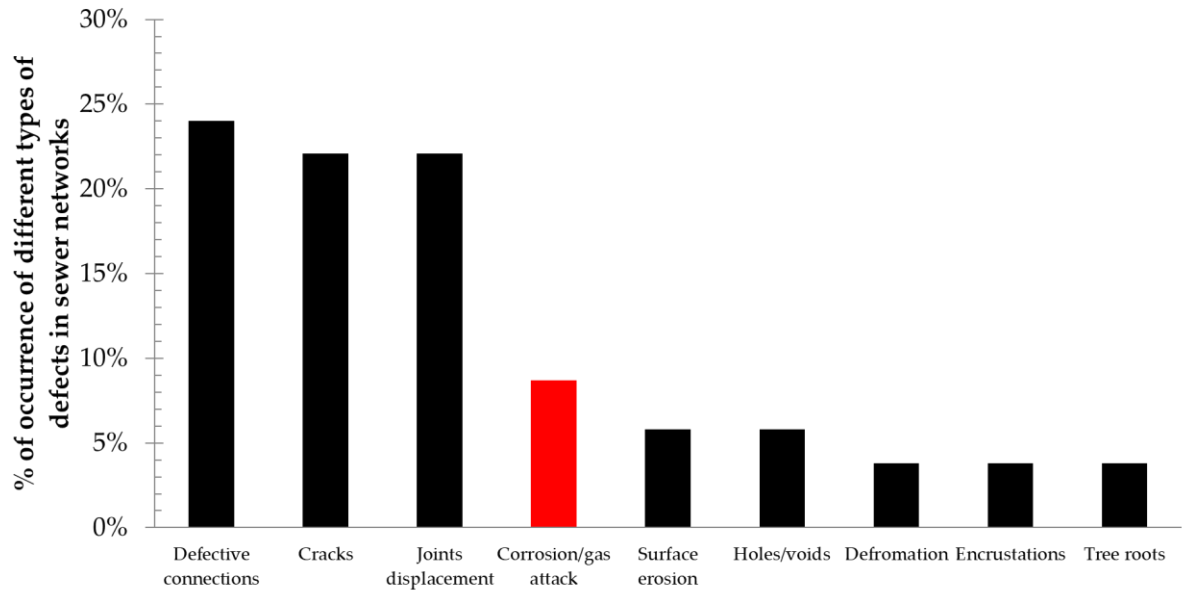

Figure I-1. Degradation mechanisms and the frequency of their occurrences in German sewer systems, after [4]

This research work aims to draw up a database of (i) the biological phenomena in sewer networks; (ii) the different in-situ campaigns and their results; (iii) the alteration mechanisms induced by biodegradation for Portland cement and calcium aluminate cements; (iv) the performance of potentially innovative binders such as Portland cement with supplementary cementitious materials (slag, metakaolin, silica fume and fly ash), geopolymers and super sulfated cements against biological attack to clarify the positioning of these binders for sewers networks (v) the different formulation parameters probably impacting the durability of tested materials.

1.2. SEWER NETWORKS

The materials used in the sewer systems have evolved in time. Cementitious materials are widely used nowadays in sanitation networks, either as pre-cast structures or as a part of rehabilitation and reparation works. In 1999, a study on sewer systems in Germany showed that the two main materials employed into their construction were concrete (46%) and stone (38%). However, bricks, ductile iron and plastics were used as well but in fewer amounts as seen in Table I-1.

Table I-1. Principal materials used in German sewer networks [4]

Material	Percentage
Concrete	46%
Stoneware	38%
Bricks	6%
Ductile iron	5%
Plastics	5%

In 1900, Olmstead and Hamlin have studied the deterioration of sewer networks in Los Angeles and found that the mortars used as joints between the bricks have been damaged by swelling phenomena [7]. Years later, Parker has proposed a direct link between microorganisms and concrete deterioration based on experiments conducted in an Australian sewage system. The study has successfully identified the species of microorganisms associated with the degradation as well as the global alteration mechanisms which was defined to consist of an acid attack leading to leaching of cementitious cations – for instance, Ca^{2+} and Al^{3+} – followed by a sulfate attack inducing precipitation of secondary sulfate-bearing phases, such as gypsum and/or ettringite. Moreover, the conclusion made by Parker was that the degradation of cementitious materials, in sewers environment, was a mix of chemical and biological attacks [5,6].

Since then, more studies took place on the phenomena and led to the acknowledgement of the main source of the deterioration - the sulfur compound - with its dominant phase in wastewater, sulfate [8].

1.2.1. Biological activity in sewer networks

The biological activity in sewerage conditions consists of two major types of autotrophic microorganisms, sulfate-reducing bacteria (SRB) and sulfur-oxidizing bacteria (SOB). Figure I-2 summarizes the phenomena encountered in the pipes.

The process of sulfuric acid attack on cementitious materials in sewer environment can be summarized into three stages. The first stage occurs when mud sediments in areas with low

abrasive forces and with long retention times of the wastewater. In these particular zones, oxygen and nitrate concentrations are very low due to fermentation processes; hence, sulfate reduction is initiated by different sulfate-reducing bacteria (SRB). As sulfate is used as an electron acceptor in the absence of oxygen and nitrate, hydrogen sulfide (H_2S) is produced as a side product of the anaerobic oxidation of organic matter by SRB [5,6,9,10]

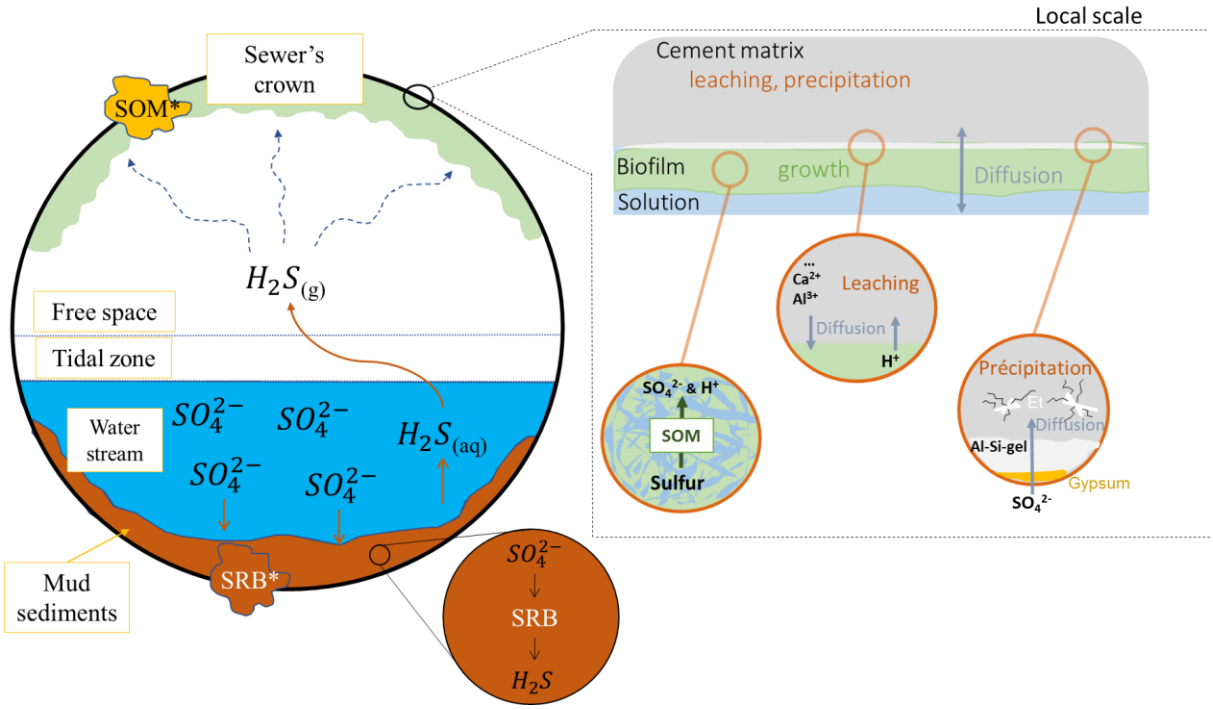

Figure I-2. Biological activity and sulfur transformation [6,9,11,12]

The second stage consists of the diffusion of hydrogen sulfide in the air above the water flow due to a dissociation process that is a function of pH, temperature and concentration of oxidized sulfur compounds in the wastewater. The wastewater encountered in such environment has a pH range between 6 and 8; hence, the proportion of dissolved sulfide as H_2S in the water is about 50% leaving the other 50% under the form of HS-. Due to pH limitation, the concentration of S^{2-} in the waste-water stream is neglected (Figure I-3). Gaseous H_2S, carbon dioxide (CO_2) and methane (CH_4) are formed and partly degassed into the atmosphere in sewerage pipes.

The third and last stage starts with the dissolving and accumulation of CO_2 and H_2S in the porosity of the concrete. Thereafter, H_2S decomposes into HS^- or S^{2-} and H^+ depending on the pH of the concrete. Since, traditional concrete is initially a strong alkaline porous material with a pH ranged between 12 and 13, an abiotic reduction of concrete pH to approximately 9 results from chemical acid-base reactions due to carbonation and polythionic acids generated by chemical oxidation of H_2S [13,14].

Depending on the physiochemical properties of the material, the abiotic oxidation of H_2S could lead to precipitation of associated sulfur species – such as elemental sulfur S^0 or thiosulfate – which could provide an energy source for biological production of sulfuric acid. However, while the high alkaline medium present in concrete limits the bacterial growth [14], it has been

reported in [10] that a very significant decrease in pH was observed on the surface of concrete compared to the decrease calculated from purely chemical neutralization reactions. Such decrease was related to biotic activity on concrete surface; however, the contribution of the abiotic and biotic decrease of pH in the early stages of concrete corrosion is still in debate.

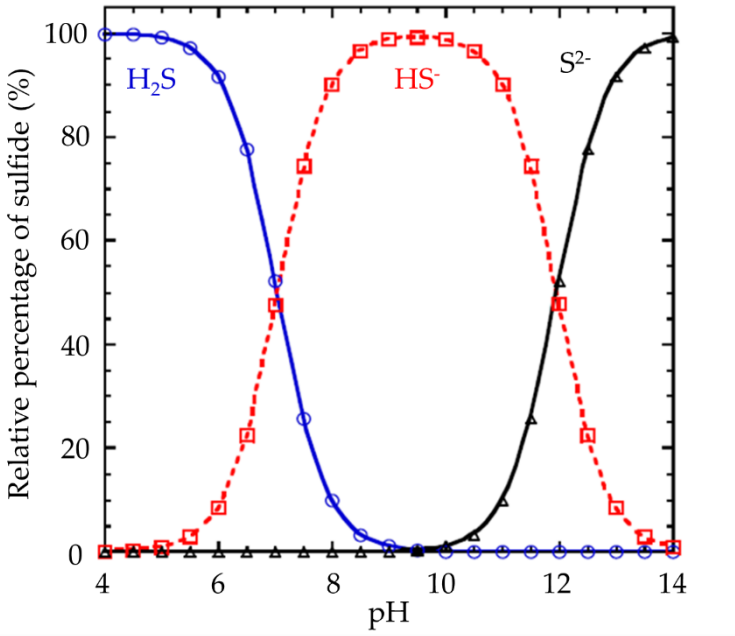

Figure I-3. Speciation of sulfide as a function of pH

Nevertheless, when pH drops to 9 and the environmental conditions – temperature and relative humidity – are suitable for bacterium growth, autotrophic SOB are developed on the concrete surface. These bacteria are mainly responsible for the bio-chemical transformation of sulfide to sulfate.

1.2.2. Microbial succession on concrete exposed to sewer environments

The development of microorganisms on concrete surface is bounded by the environmental conditions. The main parameters are the temperature, the relative humidity, the concrete's alkalinity and the nutrients availability. A description of the bacterial succession in sewage environments together with mineralogical aspects in aerobic part of microbial induced concrete corrosion (MICC) is presented in Figure I-4.

The initial high pH of the concrete creates an obstacle for bacterial growth, and hence, the aggression on the cementitious matrix is initiated by an abiotic attack where hydrogen sulfide starts to condensate on the canalization's walls/crown. Sulfate diffusion into the cementitious matrix through its interconnected open porosity initiates the leaching of calcium rich hydroxides but generally with no significant mass loss. Carbon dioxide (CO_2) also contributes to the deterioration in early stages through its reaction with leached Ca^{2+} ions resulting in the precipitation of calcite ($CaCO_3$) and a gradual pH decreasing.

The abiotic attack results in the decrease of concrete surface pH from 13 to 9, consequently, allowing the growth of neutrophilic sulfate oxidizing microorganisms (NSOM).

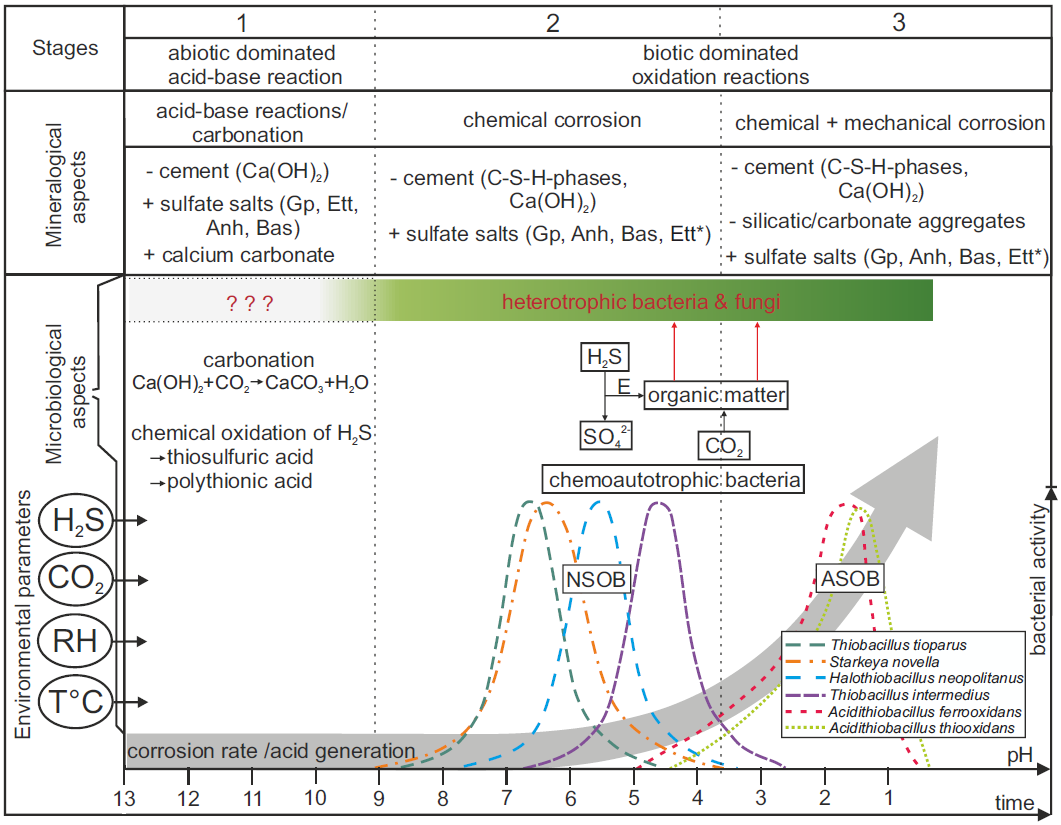

Figure I-4. Description of microbial and mineralogical aspects of the aerobic part of concrete corrosion [15], based on an adapted corrosion model of Islander et al. [9]

Neutrophilic Sulfur Oxidizing Bacteria (NSOB)

The second stage of concrete corrosion is characterized by the growth of NSOB on the concrete surface at pH around 9 to 9.5 [9,16]. It has been shown that *Thiobacillus thioparus, Thiobacillus novellus, Thiobacillus intermedius and Thiobacillus neapolitanus* are present in the initial and intermediate bacterial colonies and that their succession is function of the medium pH [9,17].

The evolution of NSOB is associated with a production of biogenic H_2SO_4 and a progressive pH decrease. Such pH decrease induces the dissolution of the cementitious mineral phases together with the precipitation of neo-formed sulfate salts resulting in mass loss of the material. However, while main identified precipitated sulfate salts are gypsum, basanite, anhydrite [18–20], ettringite has been observed in several studies principally at the interface between the highly deteriorated concrete layer and the non-corroded concrete where high alkaline conditions are still dominant with presence of high sulfate amounts in the pores solution [19,20].

Acidophilic Sulfur Oxidizing Microorganisms (ASOM)

Low pH conditions become an inhibitor for most of the neutrophilic bacteria, leading to the third stage of concrete corrosion where acidophilic bacteria dominate the biofilm.

Thiobacillus genus was identified as the principal source of acid production; hence, the most destructive to concrete. Such species cannot exist at a pH higher than 6.5 and they perform remarkably well in acidic mediums as the produced sulfuric acid does not fully prevent their activity [5,9]. Furthermore, *Thiobacillus thiooxidans* bacteria was the most reported bacteria found in the biofilm at the late stages of concrete corrosion. They favor polysulfide and elemental sulfur as substrates rather than hydrogen sulfide. The transformation process of hydrogen sulfur to polysulfide and elemental sulfur is done by neutrophilic microorganisms and/or by chemical reactions prior to the development of *Thiobacillus* genus

It has been demonstrated that the development of ASOB is accompanied by a rapid increase of sulfate production. However, while ASOB reach their maximum growth rate at pH 2, the medium might become inhibitory for *T. thiooxidans* if the pH falls down to 1; hence, slowing down the acid production to a certain limit where the acid neutralization capacity of the cementitious material balances the acid production by the bacteria [9,10].

Several studies have described other types of ASOB capable of producing sulfuric acid in different conditions compared to *T. thiooxidans*. For instance, *Thiomonas intermedia* and *Acidiphilium acidophilium* bacteria have been identified with the former being a chemoautotroph which produces sulfuric acid in pH between 5 and 7 and the latter being able to develop autotrophically or mixotrophically using various sulfur compounds as well as heterotrophically using organic compounds and is capable of reducing iron [17,21]. Moreover, *Acidithibobacillus ferrooxidans* bacteria have been reported in various studies [10,18,22,23], however, the impact of such bacteria on concrete biodeterioration is still under debate.

However, the results of many studies showed that bacteria species vary from one environment to another and depend strongly on the environmental conditions and the nutrient supplies.

1.3. PATHWAYS FOR SULFUR OXIDATION

In the literature, mainly H_2S, SO_4^{2-} and S^0 are mentioned as the sulfur-bearing compounds identified in the deterioration process of concrete in sewers. However, other soluble sulfur compounds with different degrees of oxidation can be found, depending on the conditions, including sulfides (HS^- and S^{2-}), thiosulfate ($S_2O_3^{2-}$), dithionate ($S_2O_6^{2-}$), trithionate ($S_3O_6^{2-}$), tetrathionate ($S_4O_6^{2-}$), pentathionate ($S_5O_6^{2-}$), hexathionate ($S_6O_6^{2-}$) and sulfite (SO_3^{2-}). Figure I-5 shows an illustration of the sulfur oxidation pathways by biotic and abiotic mechanisms. In aerobic conditions and in the presence of SOB, the end products of the oxidation of tetrathionate are sulfate and hydronium ions.

The study of sulfur oxidation in sewer networks (field conditions) is challenging due to various difficulties: (i) The relatively long time needed for sulfur-oxidizing bacteria to development which could take from several months to several years depending on the conditions of the networks and the cementitious materials; (ii) the difficulty in collecting liquid samples which were in direct contact with the cementitious materials, in particular if the

materials were suspended in the aerial part of the network; (iii) the complexity of accessing the in-situ site, etc. Hence, accelerated laboratory biological tests could be used as an alternative to real life exposure in order to reproduce the sulfur cycle.

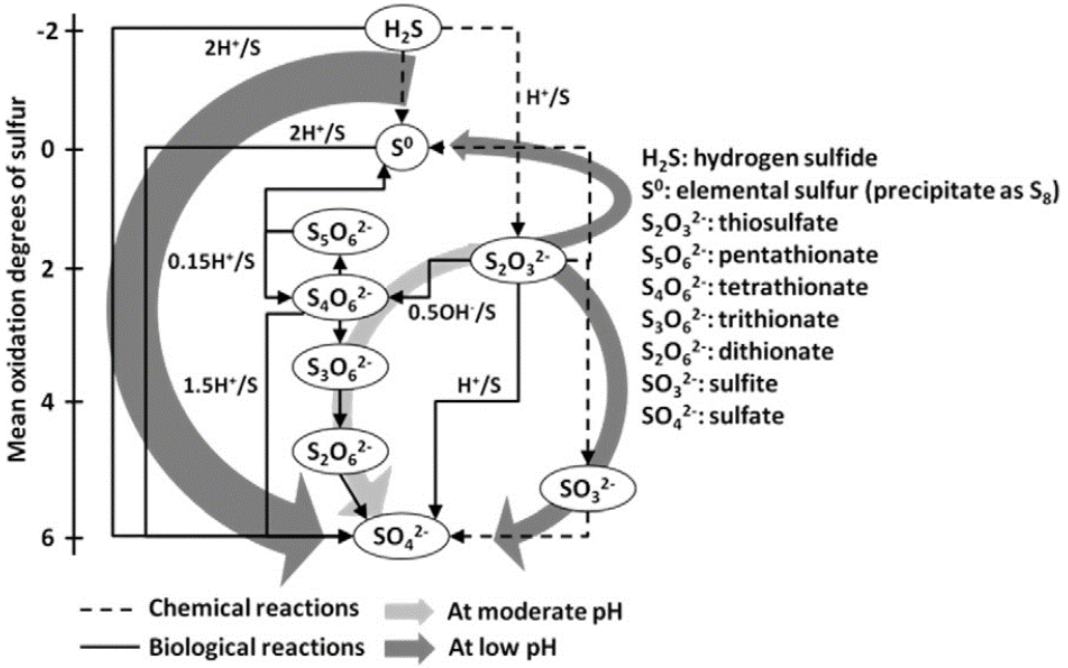

Figure I-5. Sulfur oxidation cycle by biotic and abiotic mechanisms, Peyre Lavigne et al. [24], adapted from Islander et al. [9]

Several tests operating according to various principles have been developed, including the tests of the University of Toulouse and the University of Hamburg [24,25]. These accelerated tests were validated in terms of representativeness of the biodeterioration phenomena of cementitious materials [26,27]. Thus, the study of the impact of the cement materials on the reaction pathways of sulfur oxidation in presence of sulfur-oxidizing bacteria was carried out using the University of Toulouse accelerated laboratory test: the BAC test (3 months of exposure) [20,24,26,28]. This test uses tetrathionate ($S_4O_6^{2-}$) as a soluble reduced sulfur source instead of hydrogen sulfide to allow an accurate mass balance of sulfur species in a more secure environment.

In the literature, tetrathionate oxidation is described as an intermediate reaction in the oxidation of reduced sulfur compounds, such as thiosulfate, through the S(IV)-I pathway (for tetrathionate intermediate) where tetrathionate is first formed during the thiosulfate oxidation and then oxidized into sulfate, involving sulfite SO_3^{2-} as intermediate [29]. The following reactions (**Eq.I-1, Eq.I-2 and Eq.I-3**) describe this phenomenon:

$$S_2O_3^{2-} + 0.25\ O_2 + H^+ \rightarrow 0.5\ S_4O_6^{2-} + 0.5\ H_2O \qquad \textbf{Eq.I-1}$$

$$S_4O_6^{2-} + 2\ O_2 + 3\ H_2O \rightarrow 4\ SO_3^{2-} + 6\ H^+ \qquad \textbf{Eq.I-2}$$

$$SO_3^{2-} + 0.5\ O_2 \rightarrow SO_4^{2-} \qquad \textbf{Eq.I-3}$$

In a study carried out in acid-mine drainage, higher sulfate production was obtained from elemental sulfur than from tetrathionate using SOB. The high acidic conditions were identified to cause the hydrolysis of tetrathionate into disulfane-monosulfonic acid ($H_2S_3O_3$) before forming thiosulfate and elemental sulfur [30–32] with a fraction of tetrathionate being oxidized. The disproportionation of tetrathionate in such conditions was described using the following reaction (**Eq.I-4**) [30]:

$$S_4O_6^{2-} + H_2O \rightarrow S_2O_3^{2-} + S^0 + SO_4^{2-} + 2\ H^+ \qquad \textbf{Eq.I-4}$$

Moreover, tetrathionate biological disproportionation was identified in anaerobic conditions with *Thiomonas Intermedia K12* [33]. The findings of the study on *Thiomonas Intermedia K12* suggested that some tetrathionate were oxidized via disulfane-monosulfonic acid to form trithionate and sulfate while the resulting electrons were used to reduce tetrathionate and form thiosulfate, pentathionate, hexathionate and elemental sulfur [34,35]. Reactions (**Eq.I-5**, **Eq.I-6**, **Eq.I-7** and **Eq.I-8**) present the described pathways for tetrathionate reduction by disulfane-monosulfanate ($S_3O_3^{2-}$):

$$S_3O_3^{2-} + S_4O_6^{2-} \rightarrow S_2O_3^{2-} + S_5O_6^{2-} \qquad \textbf{Eq.I-5}$$

$$2\ S_3O_3^{2-} + S_4O_6^{2-} \rightarrow 2\ S_2O_3^{2-} + S_6O_6^{2-} \qquad \textbf{Eq.I-6}$$

$$S_3O_3^{2-} + S_5O_6^{2-} \rightarrow S_2O_3^{2-} + S_6O_6^{2-} \qquad \textbf{Eq.I-7}$$

$$4\ S_3O_3^{2-} \rightarrow 8\ S^0 + 4\ SO_3^{2-} \qquad \textbf{Eq.I-8}$$

In acidic environments, thiosulfate is chemically reactive and can decompose via a disproportionation reaction into colloidal sulfur (S^0), that may later precipitate as crystals of elemental sulfur (S^0), and in S(IV)-oxides such as sulfite (SO_3^{2-}) and bisulfite (HSO_3^-) [36]. This process is generally described by the following reaction (**Eq.I-9**) [37]:

$$S_2O_3^{2-} + H^+ \rightarrow S^0 + HSO_3^- \qquad \textbf{Eq.I-9}$$

In addition, thiosulfate could also be oxidized biologically into sulfate by the following reaction (**Eq.I-10**) [38]:

$$S_2O_3^{2-} + 2\ O_2 + H_2O \rightarrow 2\ SO_4^{2-} + 2\ H^+ \qquad \textbf{Eq.I-10}$$

The reactivity of hexathionate and thiosulfate was studied in moderate acidic conditions (pH ranged between 4 and 5), and the precipitation of elemental sulfur and the production of different polythionates and sulfite were observed, using different reactions to represent the system (using $S_3O_3^{2-}$ as an intermediate) [39].

Moreover, physical properties of the concrete could have an impact on the biological activity. For instance, the roughness of the concrete surface has an influence on the formation of the biofilm. To enable the initial adhesion of bacteria on concrete, its surface must present cavities

suitable with the size of bacteria. Afterwards, more bacteria are brought to the surface, either by aerosol or by wastewater, and get to hold on to the bacteria already on the surface, creating micro-colonies. These micro-colonies evolve in time and form biofilms [40].

1.4. INVESTIGATION OF THE PERFORMANCES OF CEMENT-BASED MATERIALS IN SEWER NETWORKS

Different types of cementitious materials were exposed to in-situ conditions in different regions of the world in order to understand their alteration mechanisms and to evaluate their performances against biological aggression in sewage conditions. This section is dedicated to five main campaigns that were carried out in South Africa, Japan, Australia, France and Austria.

The first campaign was carried out by a research team at the University of Cape Town. The project consisted in exposing calcium aluminate cement (CAC) and ordinary Portland cement (OPC) based concrete to in-situ conditions in a sewer network in Virginia, South Africa. The temperature varied between 0 and 30°C and the H_2S concentration ranged from 70 ppm to 140 ppm. Figure I-6 shows the results obtained on the different specimens exposed to live conditions from 2008 to 2013.

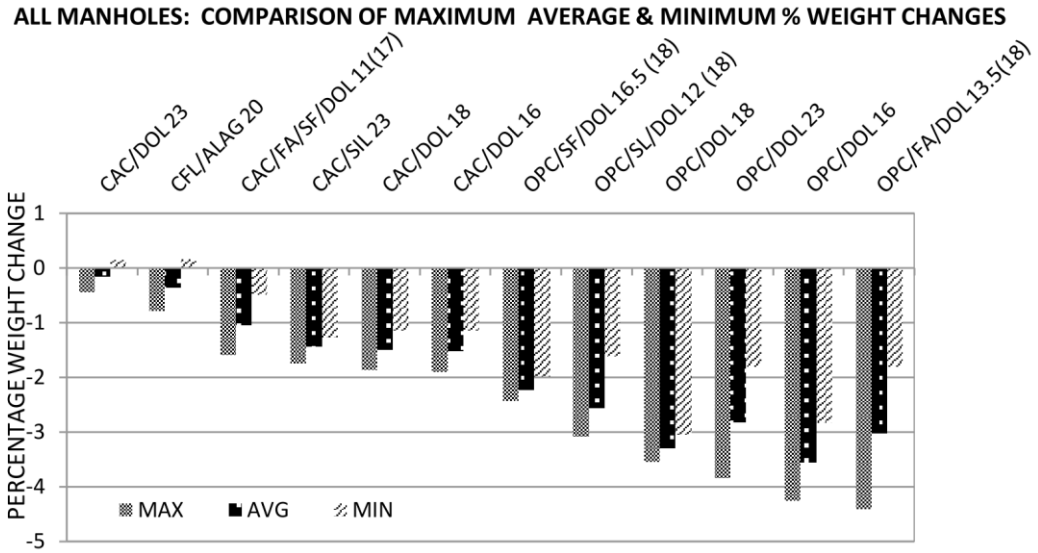

Figure I-6. Comparison of weight loss of different binders exposed to live conditions in Virginia sewers project between 2008 and 2013 [41]. OPC: ordinary Portland cement; CAC: calcium aluminate cement; FA: fly ash; SF: silica fume; DOL: dolomite-based aggregates; SIL: silica-based aggregates. The numbers in the binders' designation (11, 12, 13.5, 16, 16.5, 18, 20, 23) refer to the binder percentage in the concrete

The main results of the Virginia Sewer project showed that CAC binder resisted better than OPC binder – both with siliceous aggregates – in terms of degradation rate (0.8-1.2 mm/year for CAC and > 5 mm/year for OPC). These results were based on weight loss measurements but due to the lack of a standardized method, the comparison between different studies could be complicated. Also, a positive effect of dolomite aggregates on OPC performance was found as the dissolution rates of OPC and dolomite aggregates were very similar resulting in

smoother surface and less aggregates fallout. The dissolution rate for OPC/dolomite and OPC/siliceous were 3.1 mm/year and 7.5 mm/year respectively. However, siliceous aggregates are known to resist acid attacks, which mean that the deleterious effect of acid was mainly concentrated on the binder.

Another campaign was performed by a research team from Shimane University. Investigations were carried out in a Tokyo sewer system, which was constructed with OPC and siliceous aggregates concrete. This sewer was found to be heavily deteriorated [42]. The hydrogen sulfide concentrations in the atmospheric part of the canalization varied between 5 and 400 ppm and the temperature ranged between 10 and 30°C. Several concrete samples were extracted from different parts of the pipe wall with a sound sample from the bottom part, which was not attacked, with 88 mm of thickness and 1000 mm of diameter.

The corrosion rate was the highest at the sewage level with 4.7 and 4.3 mm/year – the thickness was less than the half of the sound sample – for the left and the right parts respectively. The rate decreased while going upwards with the lowest value recorded for the crown with 1.4 mm/year. Mineralogical and chemical analyses showed the formation of gypsum, calcite, ettringite and barite in the heavily corroded zones. Furthermore, expansion, cracking and disintegration of the binder were recorded (Figure I-7).

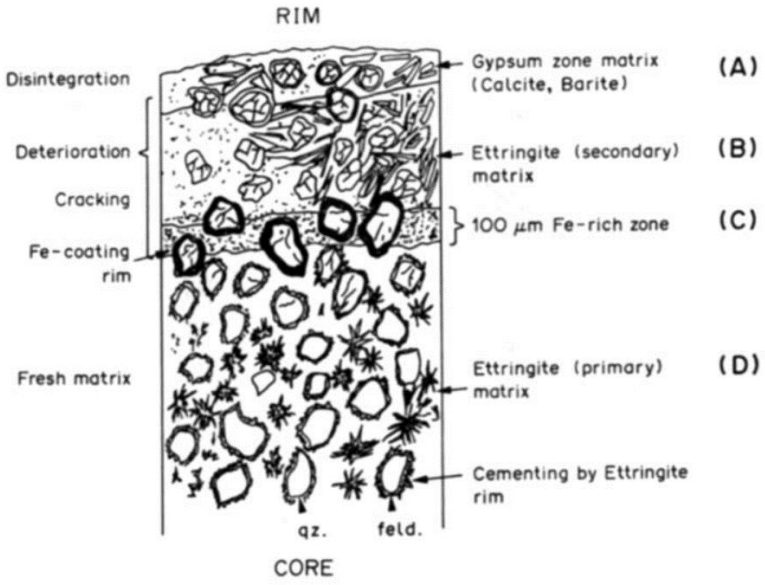

Figure I-7. Schematic representation of the distribution of secondary phases (gypsum, calcite and ettringite) in the deteriorated zone [42]

Still in Japan, a research team from Hokkaido University exposed OPC mortars in a sewer canalization system in Hachinohe, where concrete was found severely deteriorated [10]. They placed the specimens at 30 cm above the water level. The average H_2S concentration in the atmospheric area was 30 ± 20 ppm. The first sample was removed after 1 month and then the frequency of sampling was roughly every 2 weeks until 147 days. The final samples were removed after 1 year of exposure.

Figure I-8-A reports the evolution of pH measured on the surface of concrete specimens and the specimens' weight loss. Stabilization of pH around 1.6 was recorded starting from day 102. The concrete specimens have suffered from a negligible mass loss (< 3%) in the first 174 days. However, after 1 year, a significant mass loss was recorded at 37%. Figure I-8-B shows the progression in sulfate concentration on the concrete surface with an important increase at day 174 was measured at 20 mg-S/g.

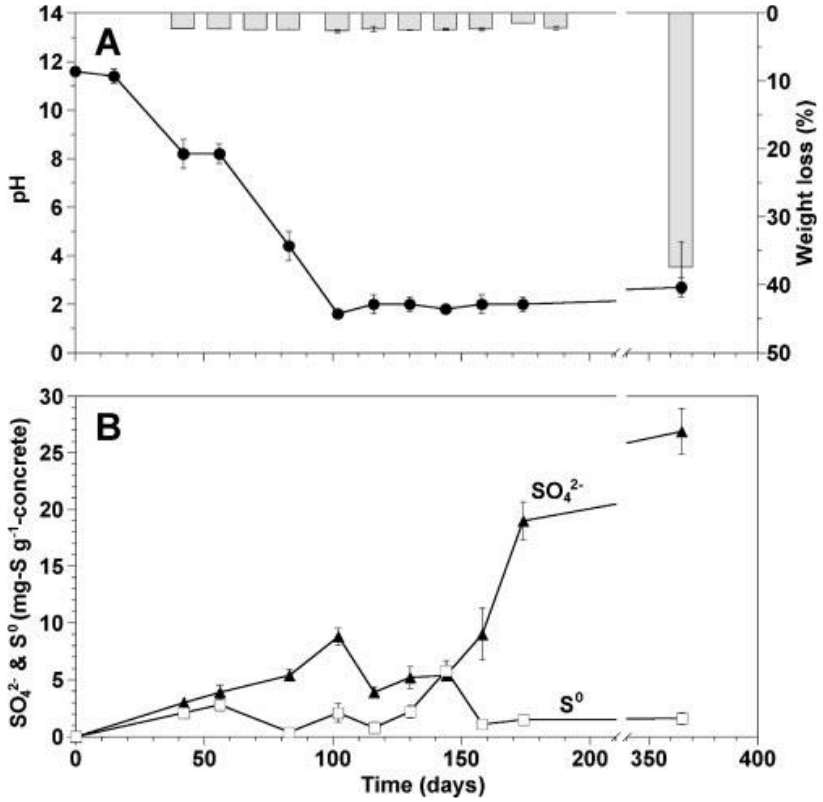

Figure I-8. (A) pH evolution and mass loss of concrete specimens exposed to sewage environments (B) SO_4^{2-} and S^0 concentrations measured on the surface of concrete specimens [42]

A third campaign was carried out by Australian researchers where they exposed new and old – extracted from sewer covers which were in use for 70 years – concrete samples to different sewer networks in Australia with different environmental conditions (Sydney, Melbourne and Perth) [43]. The concrete was made of OPC with siliceous aggregates. The test lasted 5 years, running from 2010 till 2015, with sampling frequency every 6 to 8 months for the first 3 years then once a year for the last 2 years. The conditions in the sewage are reported in Table I-2. Note that Perth pipe system was sealed while Sydney's and Melbourne's were ventilated, explaining the high concentration of H_2S in Perth's sewers.

The new concrete analyses showed an initiation period in which the concrete surface pH declines from alkaline (≈12.5) to neutral values (≈6) between 9 and 36 months due to abiotic reactions with CO_2 and H_2S. On the other hand, regarding the old concrete, the initial surface pH was at 8, which is coherent with the presence of an existing degraded layer. The abiotic initiation period did not take place as the pH was already adequate for microbial colonization. During the abiotic attack period, the concrete's mass loss was insignificant. However, the exposure conditions had an influence on the period of time required to reach neutral pH.

Table I-2. Average values of environmental conditions [43]

Sewer location	H_2S concentration (ppm)	Temperature (°C)	Relative Humidity (%)
Sydney A	2	22	94
Sydney B	3	21	94
Melbourne A	1.5	20	100
Melbourne B	6	21	100
Perth A	125	26	97
Perth B	423	27	91

Later on, the corrosion process was activated by the development of ASOM and the corrosion rate was different in respect with the location of the sewer. Figure I-9 shows the corrosion rate for new and old concrete samples at Melbourne and Perth locations. The authors came to conclusion that the initiation period slightly delays the active corrosion phase but do not have an impact on the deterioration of concrete.

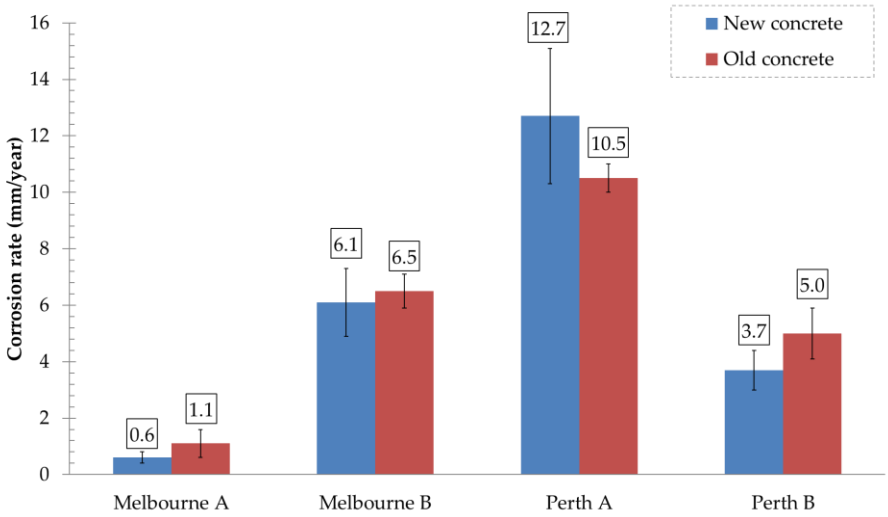

Figure I-9. Corrosion rate for new and old concrete samples exposed at Melbourne and Perth sewer systems [43]

A fourth campaign was conducted in France on mortars with different type of binders exposed to sewage environment [44]. H_2S concentrations varied between 0 and 250 ppm with a mean value of 100 ppm. Temperature ranged from 8 to 30°C in winter and in summer respectively. The exposed mortars formulations were made of OPC and CAC with siliceous sand. Every 4 months, the samples were photographed, weighed and the surface pH was measured. Moreover, biofilms studies were carried out to identify the microbial population.

After 2 years of exposure, visual analyses (Figure I-10) showed that OPC samples suffered more deterioration than CAC samples. Further analyses provided quantitative mass change with a mass loss of 14% for OPC samples and a slight mass gain of 1% for CAC samples which might be due to precipitation of certain phases such as gypsum and/or ettringite. Microbiological analyses revealed diversity in the biofilm showing that the microbial

population was different on each type of cement. Additionally, the quantity of biomass was higher on OPC mortars than on CAC mortars. This might be due to an inhibitory effect of the calcium aluminate matrix on the microbial activity. Although this theory has been proposed by several authors in the literature [45–47], the mechanisms are not yet well understood and seem to have been contradicted by laboratories studies performed in very aggressive conditions [12].

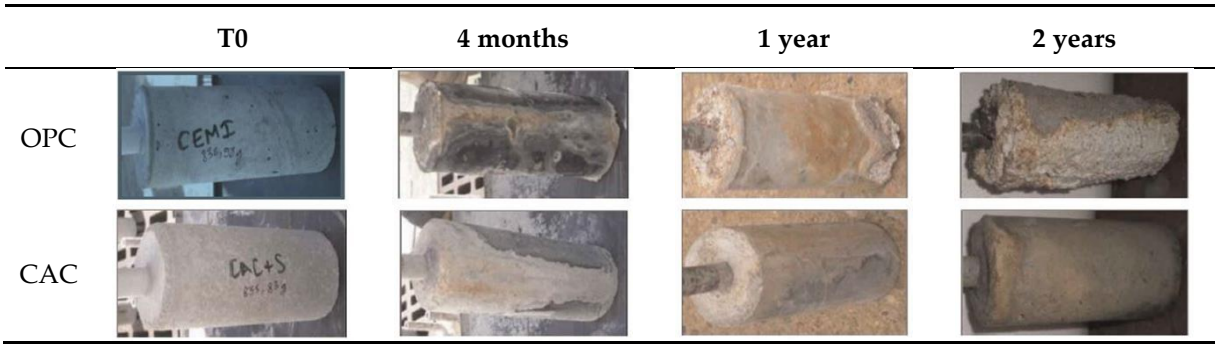

Figure I-10. Observed visual changes on OPC & CAC mortars, unbrushed, over 2 years of exposure in sewage environment [44]

The fifth campaign took place in Austria where samples from existing sewer network evaluated as heavily corroded were analyzed [18,48]. The concrete specimens were extracted from different manholes severely damaged and presenting a few centimeters of a porous zone (Figure I-11). The concrete manhole was made of a mix of fly ash and ordinary Portland cement (C_3A-free) for the binder with either siliceous or calcareous aggregates. The average H_2S concentration was recorded over a 6 weeks-period with a mean value of 6 ppm and variation between 0.1 and 367 ppm (with the use of $FeCl_2$ to stabilize the sulfur). However, during the sampling, the H_2S concentration was up to 84 ppm. Also, CO_2 and CH_4 concentrations were even higher with 2600 ppm and 1760 ppm respectively.

Figure I-11. A scheme of a manhole and the sampling cut with a clear view of the transition zone (TZ) [48]

The corrosion rate ranged between 0.1 and 1 cm/year. Portlandite and C-S-H were completely dissolved in the degraded zone. The decalcification of such phases resulted in the precipitation of sulfate salts. Gypsum was massively formed (42 wt.%). Further, bassanite and anhydrite were formed with 16 wt.% and 3 wt.% respectively. The aggregate's nature was studied in parallel. Siliceous aggregates resisted better against acidic attack while calcareous aggregates were totally dissolved.

Moreover, previous studies reported that oxygen depletion was achieved at about 400 to 600 μm deep in the degraded zone [10]. However, Grengg has observed *A. ferroxidans* bacteria in deeper zones (~ 3cm deep) where a higher concentration of iron was observed as well. While *A. thiooxidans* bacteria are likely to be inhibited by the absence of oxygen and the high Fe accumulation, *A. ferroxidans* dominated the interior part of the degraded zones. These microorganisms are able to produce sulfuric acid in anaerobic conditions by using ferric iron as an electron acceptor while sulfur compounds are used as the electron donor. In conclusion, it seems that *A. ferroxidans* have an important role in concrete biodeterioration, at least in the presence of iron, as they provide sulfuric acid in the inner deteriorated zones closer to the corrosion front.

Summary

The main highlights of the five on-site tests, conducted worldwide, are summarized in Table I-3. The results showed the need to highlight the role of microorganisms in the deterioration process as well as to enhance the understanding of the biodeterioration mechanisms of cementitious materials in sewer networks. Furthermore, the two main cementitious materials used in these studies were ordinary Portland cement and calcium aluminate cement with the latter resisting better to biological aggression than the former [44,49]. Moreover, calcareous aggregates were attacked by the acid along with the cementitious binder but, on the other hand, siliceous aggregates resisted the aggression although the dissolution of the binder around the aggregates led to the fall-out of the latter. Since there is no standardized method for measuring the degradation, weight loss measurements were adapted as an indicator for degradation. However, some phases are susceptible to precipitate, such as gypsum and/or ettringite, which could lead to an increase in specimens' weight. Hence, weight loss measurements seem not to be the adequate indicator for measuring the degradation of cementitious materials in sewer networks, especially in the short term.

Also, *A. thiooxidans* might not be the only main ASOB causing the deleterious damage to concrete as *A. ferroxidans* has been proven to exist in anaerobic zones in the biofilm – mainly at the interface between the sound and the deteriorated zones in the cementitious material – and to use iron instead of oxygen to oxidize sulfur species into sulfuric acid [48]. Finally, the emphasizing of the abiotic phase prior to the development of microorganisms was shown to have a moderate effect on the deterioration of the cementitious matrix [43].

However, there is a lack of information about other cementitious materials. For instance, blended Portland cement with supplementary cementitious materials (SCM) show not only economic and environmental interests but are proven to generally improve the durability of Portland cement against external attacks (e.g. leaching by pure water [50], deicing salts [51], seawater attack [52], sulfate attack [53], etc).

Table I-3. Summary of the experimental in-situ results and the associated environmental conditions on the biodegradation of cementitious materials in sewer networks; N.A.: data not available; OPC: ordinary Portland cement; CAC: calcium aluminate cement; FA: fly ash

Reference	location	Period	Environmental conditions		Aggregates	Corrosion rate (mm/year)	
			[H_2S] (ppm)	T (°C)		OPC	CAC
[41,49]	South Africa (Virginia)	14 years	70 - 140	0 - 30	Siliceous	> 5	0.8 – 1.2
					limestone	1.7 – 2.5	N.A.
[42]	Japan (Shiman)	12 years	5 - 400	10 - 30	Siliceous	4.3 – 4.7	N.A.
[10]	Japan (Hachinohe)	1 year	30 ± 20	30	N.A.	Mass loss = 37%	N.A.
[43]	Australia (Sydney, Melbourne, Perth)	5 years	1.5 – 6 (Sydney and Melbourne) 125 – 423 (Perth)	20 – 22 (Sydney and Melbourne) 26 – 27 (Perth)	Siliceous	Melbourne Sound concrete = 0.6 and 6.1 Corroded concrete = 1.1 and 6.5 Perth Sound concrete = 3.7 and 12.7 Corroded concrete = 5 and 10.5	N.A.
[11,44]	France	2 years	0 - 250	8 - 30	N.A.	Mass loss = 14%	Mass gain < 1%
[18,54]	Austria	1 year	0.1 - 367	N.A.	N.A.	OPC + FA = 0.1 – 10	N.A.

1.5. DETERIORATION MECHANISMS OF CONVENTIONAL MATERIALS EXPOSED TO SEWER ENVIRONMENTS

Biodeterioration, i.e. deterioration induced by microorganisms, can lead to physical, chemical and microstructural alteration of cementitious matrix resulting in the loss of its properties, the drop of mechanical strengths and, in some cases, the total destruction of material.

Over the years, the degradation of cementitious materials in sewer networks was the subject of many research works. In-situ tests and laboratory tests were carried out to understand the alteration mechanisms of the cementitious matrix in sewage environments [10,20,25,41,49,55].

However, while main identified precipitated sulfate salts are gypsum, basanite, anhydrite [18–20], ettringite has been observed in several studies [20,56] principally at the interface between the highly deteriorated concrete layer and the non-corroded concrete where high alkaline conditions are still dominant with presence of high sulfate amounts in the pores solution. Moreover, elemental sulfur was identified mainly on the materials surface and is likely formed by abiotic and/or biotic oxidation of H_2S.

In-situ investigations showed that CAC binders have a better resistance to biodeterioration than OPC. Several authors have suggested that there is an interaction between the microorganisms and the cementitious matrix which explains the different behavior of CAC binders as a function of the nature of the test, chemical or biological [11,49].

However, there is a lack of information about Portland-based alternative binders that show a better resistance than ordinary Portland cements to chemical attacks. For example, supplementary cementitious materials (SCM), such as slag, metakaolin, fly ashes and silica fume, might improve the resistance of ordinary Portland cement to acid attack due to their pozzolanic effect, additional aluminum input and/or their ability to clog the porosity. Nevertheless, the resistance of such blends against biological degradation has been little or not discussed in the literature.

1.5.1. Ordinary Portland cement

The ordinary Portland cement has a relatively high alkaline pH (around 12.5) which will decrease gradually to 9 due to the abiotic neutralization of Portlandite (CH) and C-S-H phases by H_2S and CO_2.

While the carbonation of CH and C-S-H leads to the precipitation of calcium carbonate (calcite, aragonite, vaterite) [57,58], the positive difference of volumes between hydrated cement phases and neo-formed calcium carbonate is generally known to generate important modifications of the microstructure, such as porosity, connectivity, pore size distribution, etc. However, it is generally recognized that carbonation phenomenon reduces the porosity.

Furthermore, while the carbonation of CH and C-S-H initiates simultaneously, the carbonation of the former slows down progressively due to the less accessibility to CH [59].

As the pH continues to drop, NSOB develop followed by ASOM leading to the production of sulfuric acid. The degradation of the cementitious matrix by sulfuric acid is a coupled aggression by the acid H^+ and by the sulfate ions SO_4^{2-} leading to a severe aggressive attack

The acid penetrates into concrete via its surface porosity by diffusion mechanisms. It gets into contact with the interstitial solution and starts to dissociate following **Eq.I-11**:

$$H_2SO_4 \rightarrow SO_4^{2-} + 2\ H^+ \qquad \textbf{Eq.I-11}$$

The increase of the concentration of hydronium ions in the solution induces a decrease of the concrete pH. Consequently, the dissolution of the main phases of cement, such as Portlandite and C-S-H, is initiated (reactions **Eq.I-12** and **Eq.I-13)**. An amorphous silica gel is formed due to the calcium leaching from the C-S-H. Note that **Eq.I-13** is a simplified reaction for C-S-H since aluminum can be incorporated into C-S-H and can be found within the residual silica gel formed from the dissolution of C-S-H.

$$Ca(OH)_2 + 2\ H^+ \rightarrow Ca^{2+} + 2\ H_2O \qquad \textbf{Eq.I-12}$$

$$xCaO.ySiO_2.zH_2O + 2x\ H+ \rightarrow x\ Ca^{2+} + y\ Si(OH)_4 + (x+z-2y)\ H_2O \qquad \textbf{Eq.I-13}$$

The concentration of calcium ions released from the leaching process of Portlandite and C-S-H increases resulting, in presence of a sufficient concentration of sulfate ions in the interstitial solution, in gypsum ($CaSO_4.2H_2O$) precipitation (**Eq.I-14** and **Eq.I-15**):

$$Ca(OH)_2 + SO_4^{2-} + 2\ H_2O \rightarrow CaSO_4.2H_2O \qquad \textbf{Eq.I-14}$$

$$xCaO.ySiO_2.zH_2O + x\ SO_4^{2-} + 2\ H_2O \rightarrow CaSO_4.2H_2O + y\ Si(OH)_4 \qquad \textbf{Eq.I-15}$$

The solubility of the calcium sulfate is low, as shown in Table I-4. Therefore, the calcium salt reacts with the aluminate-bearing phases of the cementitious matrix, resulting in the formation of secondary expansive ettringite following reaction **Eq.I-16**:

$$3\ CaSO_4.2H_2O + Ca_3Al_2O_6 + H_2O \rightarrow Ca_6Al_2(SO_4)_3(OH)_{12}.26H_2O \qquad \textbf{Eq.I-16}$$

The precipitation of secondary expansive products, such as gypsum and ettringite may lead to the formation of microcracks. These cracks could lead to the penetration of bacteria inside the cementitious material resulting in a more aggressive and a more severe attack due to the production of sulfuric acid in contact with sound concrete [48].

Table I-4. Solubility of calcium salts of some acids [60]

Calcium salts of acid	Solubility in water (wt.% or g/cm^3)
Calcium sulfate	0.20
Calcium chloride	46.08
Calcium nitrate	56.0
Calcium fluoride	0.02
Calcium formate	35.2
Calcium acetate	52.0
Calcium oxalate	6.7×10^{-4}

1.5.2.Calcium aluminate cement

The calcium aluminate cement (CAC) is considered as an alternative to OPC in some applications. Its high cost - four to five times more expansive than OPC - limits its usage to some domains where OPC is considered inept.

Calcium aluminate cement presents a fast-hardening property, which can reach, after 24 hours, the same mechanical strength obtained with an OPC after 28 days, and many advantages compared to OPC owing to its chemical and microstructural composition that allows it to better resist to severe conditions, such as sulfate attack, acid attack, bacterial attack, high temperature, thermal and hydric cycles, freezing-thaw cycles, etc [61].

In order to obtain such high mechanical strength and good durability, it is recommended to have water-to-cement ratio lower than 0.4 and cement content higher than 400 kg.m^{-3}. However, Table I-5 shows typical chemical compositions of calcium aluminate cements and in particular their aluminum content. The increase in the aluminum content is accompanied with a decrease in the calcium content.

Table I-5. Chemical composition of different calcium aluminate formulations [62]

Cement type	CaO	SiO_2	Al_2O_3	Fe_2O_3
Ciment Fondu	37-39	3-5	38-40	15-18
40% Alumina	42-48	5-8	40-45	< 10
50% Alumina	34-39	4-6	49-55	< 3,5
70% Alumina	27-29	< 0,8	69-72	< 0,3
80% Alumina	17-20	< 0,4	79-82	< 0,25

In the literature, the different hypotheses for explaining the better resistance of calcium aluminate cements to biological attack are: (i) the hydration of calcium aluminate cement leads to the formation of aluminous products, less soluble than Portlandite, such as amorphous AH_3

with Ks = $6.31x10^{-32}$ and crystallized AH_3, known as Gibbsite, with Ks = $1.95x10^{-34}$ [62]; (ii) the higher neutralization capacity of the acid compared to Portland cement [63]; (iii) the gain in buffer capacity when its phases start to dissolve[63,64]; (iv) the aluminum hydroxide stability down to a pH between 3 and 4 [11,65]; (v) the inhibitory effect of aluminum ions on the microorganisms [44,66].

The key factor in the resistance of CAC lies in its chemical and microstructure nature. The main hydrates are C_3AH_6 and AH_3. AH_3 has the particularity to be chemically stable down to pH 3-4; however, for pH conditions < 3, its dissolution leads to the release of 3 hydroxide ions which gives the cementitious matrix a better acid neutralization capacity. Moreover, the decalcification of CAC hydrates, mainly C_3AH_6, by acid leads to the precipitation of additional alumina gel which creates a physical barrier slowing down the penetration of more acid. The aluminum ions released from AH_3 in highly acidic conditions (pH 1 to 2) may inhibit the microorganisms' cells function or at least to reduce their sulfuric acid production. Nonetheless, it has been demonstrated that ASOB are able to resist to very high concentrations of soluble aluminum [67], which would suggest that the inhibition would be rather effective on less-resistant bacteria, such as NSOB. Anhydrous grains also might have an influence on the resistance of CAC as they have high alumina content.

Figure I-12 and Figure I-13 show a comparison between ordinary Portland and calcium aluminate cements in terms of acid neutralization capacity. On one hand, the study on cement pastes proved that CAC performs better against acid attack than Portland cement owing to its chemical and microstructural composition. On the other hand, adding synthetic calcium aluminate aggregates (ALAG™), which have a similar composition to calcium aluminate cement, improved the neutralization capacity of calcium aluminate mortars by a factor of 4.

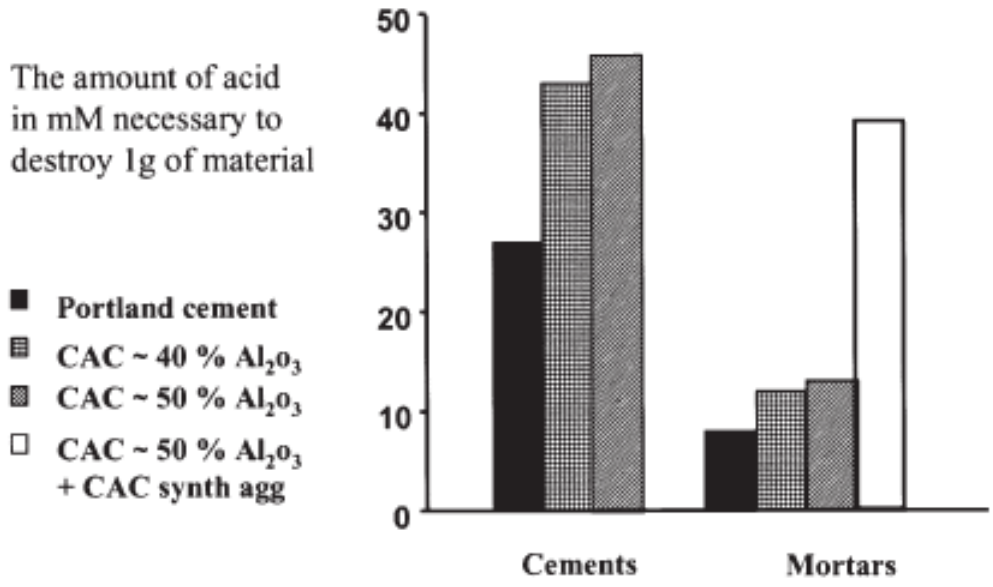

Figure I-12. Acid neutralization capacity for Portland and CAC pastes and mortars [64]

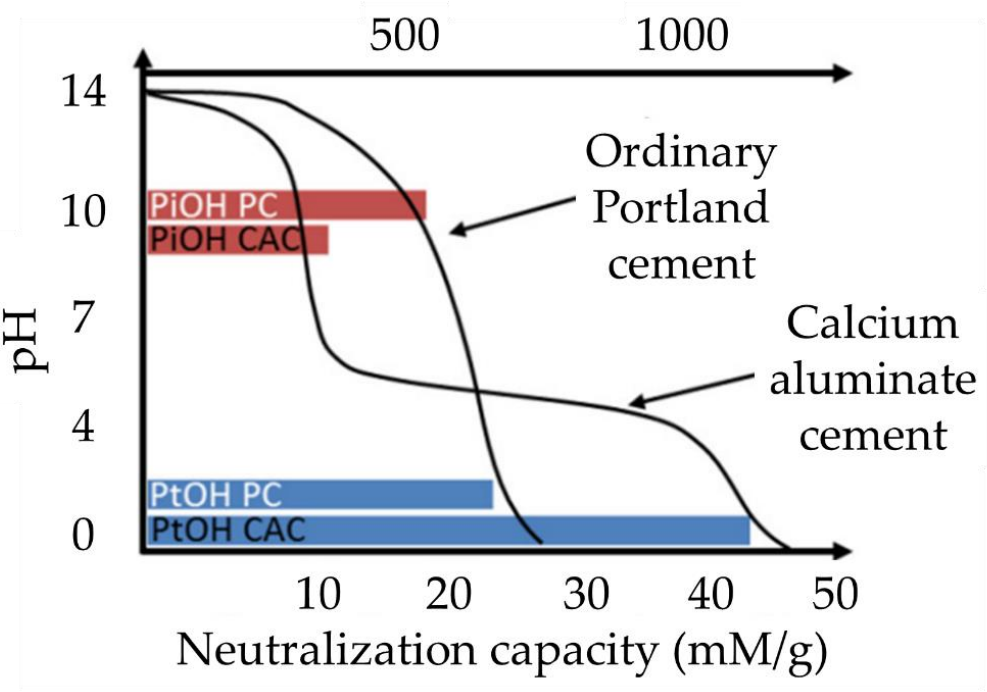

Figure I-13. Acid neutralization capacity of OPC and CAC [67], adapted from [68]

The biogenic produced sulfuric acid attacks the different hydrates of the cementitious matrix – composed mainly of calcium aluminate phases, such as : CAH_{10}; C_2AH_8 and C_3AH_6 – leading firstly to the leaching of Ca^{2+} ions and the precipitation of aluminum hydroxide (AH_3) according to the following reactions (**Eq.I-17**, **Eq.I-18** and **Eq.I-19**):

CAH_{10}: $CaAl_2(OH)_8.6H_2O + 4\ H^+ \rightarrow Ca^{2+} + 2\ Al(OH)_3\ (s) + 8\ H_2O$ **Eq.I-17**

C_2AH_8: $Ca_2Al_2(OH)_{10}.3H_2O + 4\ H^+ \rightarrow 2\ Ca^{2+} + 2\ Al(OH)_3\ (s) + 7\ H_2O$ **Eq.I-18**

C_3AH_6: $Ca_2Al_2(OH)_{12} + 6\ H^+ \rightarrow 3\ Ca^{2+} + 2\ Al(OH)_3\ (s) + 6\ H_2O$ **Eq.I-19**

When the pH drops to a level lower than 3, the AH_3 becomes unstable and Al^{3+} ions are released into the interstitial solution. Once the interstitial solution is over-saturated with Ca^{2+}, Al^{3+} and SO_4^{2-}, secondary expensive ettringite starts to precipitate creating internal stresses and resulting in microcracks which can lead to more penetration of acid and the decrease in the mechanical strength.

The behavior of calcium aluminate based cementitious matrix was proven to be different according to the nature of the test (chemical or biological). It has been found that OPC had a better resistance than CAC regarding a pure chemical attack by sulfuric acid (Figure I-14), however, the CAC has performed better against biological attack [49,69].

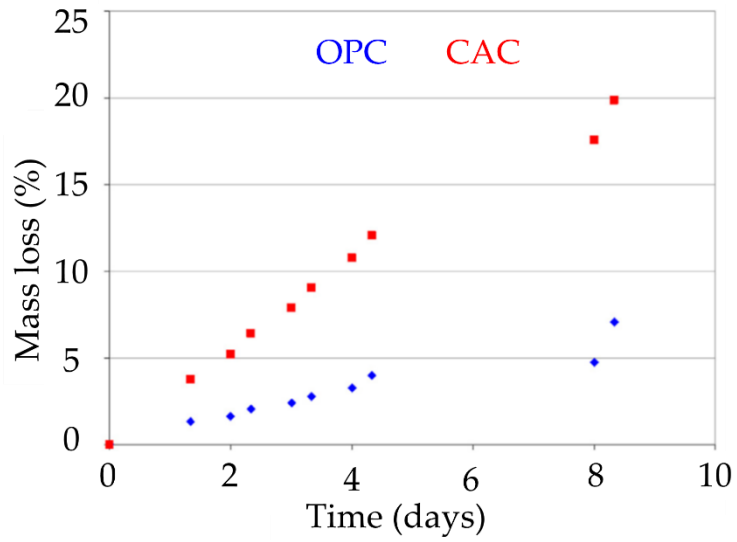

Figure I-14. Mass loss of OPC and CAC samples subjected to pure chemical attack by immersion in sulfuric acid at pH 1 [69]

Between 1984 and 1999, the Hamburg test was developed to evaluate the resistance of cementitious-based materials to biodegradation in sewers conditions. CAC specimens used in this test showed a better resistance compared to other materials, such as OPC, sulfate resistant cement and BFSC. Figure I-15 shows the evolution of pH measured on concrete surface for different formulations. The pH of CAC-based materials (SC and CC) stabilized at 3 and 2 respectively while the pH of OPC-based materials went down to 1. The first results showed also a "stifling effect" on the bacterial activity by the release of Al^{3+} ions.

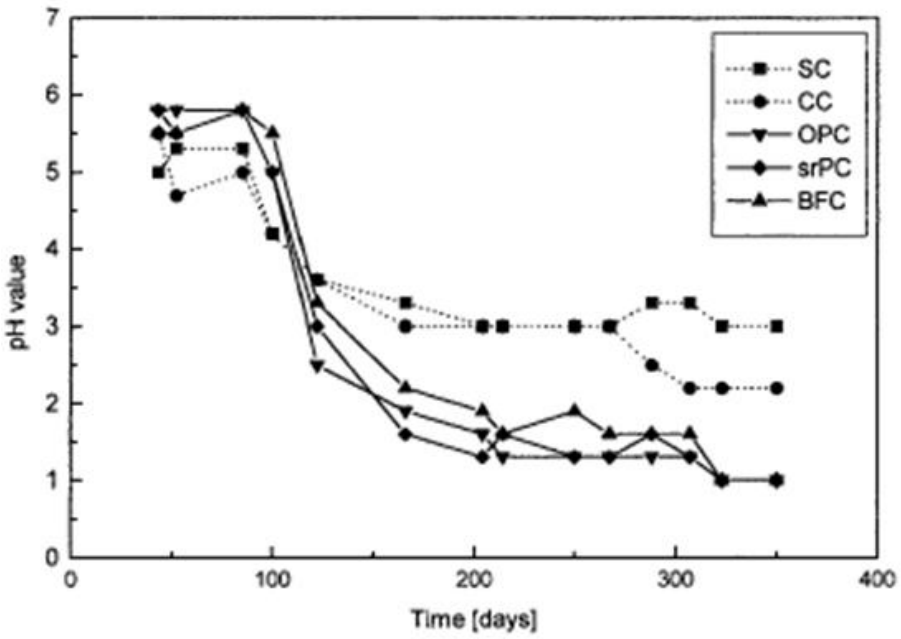

Figure I-15. The evolution of the pH measured on concrete specimens' surface using Hamburg test chamber [70]

Saucier and Lamberet proposed a more complex explanation. Not only the release of aluminum ions is the only reason behind the resistance of CAC mortars and concrete against the biodeterioration but different arguments are concerned such as that CAC could contain

other minor ions which will act on the microbial activity as well; or the absence of oligo-elements - required for the growth of the microorganisms – in the CAC matrix [47].

Another test was conducted on CAC mortar samples by where the samples were exposed to a biological degradation. The test consisted of laying activated sludge collected from wastewater treatment plant on the top of the specimens then trickling a nutrient solution containing the necessary elements for the growth of bacteria with thiosulfate as the reduced sulfur. The test campaign consisted of measuring the degraded depth along with chemical and microstructural analyses.

Generally, the results showed a better behavior of CAC against biogenic sulfuric acid. Precipitation of gypsum and delayed formation of ettringite due to the stability of AH_3 down to a pH of 3-4 were verified. In addition, an aluminum gel was formed on the material's surface, which could create a protective barrier that led to the reduction of acid penetration (needs to be deeper investigated). The bacterial activity was also influenced by the chemical and mineralogical composition of CAC specimens as the selection of SOB has been delayed compared to blast furnace slag cement (BFSC) specimens tested at the same time and in the same conditions. The influence of CAC on microorganisms was also reported in-situ where low biodiversity was identified compared to PC and geopolymer materials, which suggested an impact on the growth of microorganisms [71]. Moreover, as shown on Figure I-16, the degraded depths were recorded for the two types of cementitious materials after 107 days of exposure to accelerated biodegradation, showing a smaller degraded layer with 150 μm for CAC comparing to 700 μm for BFSC.

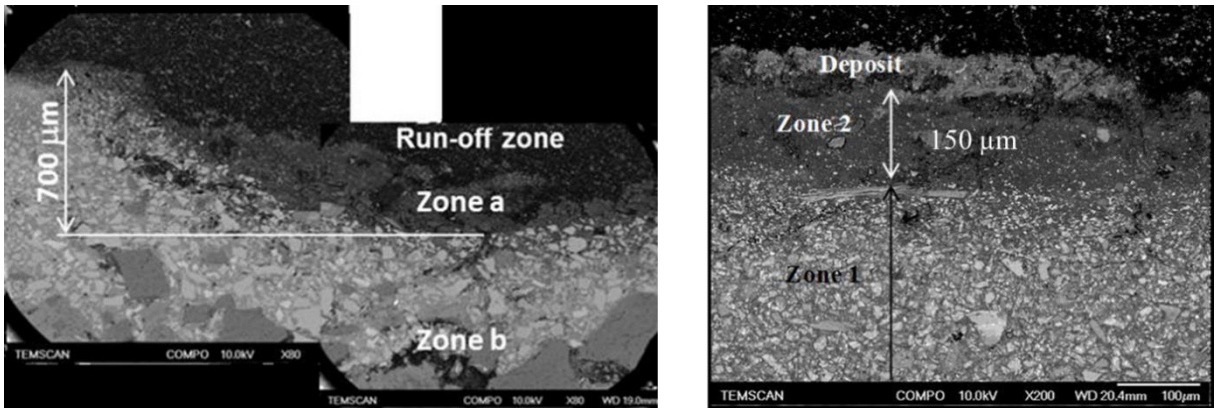

Figure I-16. Degraded depths by SEM analyses. Left: BFSC ; right: CAC [20]

1.6. POTENTIAL PATHWAYS FOR IMPROVING THE RESISTANCE OF CEMENTITIOUS BINDERS

Several new binders are potentially interesting for developing cementitious materials resistant to biological attacks. These binders would make it possible to develop an alternative to CAC-based binders which present a high cost. These new binders are presented in this section from the point of view of the main characteristics of their mineralogical and chemical compositions and the few data available on their durability.

1.6.1.Calcium sulfoaluminate cements

Ettringite-based binders are now used widely in different applications. Mainly, they are employed in contexts where relatively high early mechanical strength, an improved durability against certain external aggressions and an expansive behavior – contrary to conventional ordinary cement – are required. Furthermore, they could be employed into cold-weather constructions, fabrication of pre-cast elements, self-leveling screeds and even energy storage [72].

Expansive binders were originally used in late 1940's as a shrinkage compensator to OPC by mixing calcium aluminate (C_5A3) and anhydrite ($C\check{S}$) with the OPC clinker. Since then, more work has been carried out on ettringite-based binders. However, this study focuses mainly on calcium sulfoaluminate cement (CSA).

The first use of sulfoaluminate cement as an independent binder goes back to the 1970s and was implemented at an industrial scale in China by the China Building Materials Academy (CBMA) [73].

This chapter presents the mineral composition of CSA clinker and its hydration processes. The main hydrates of CSA cement are ettringite and AH_3 but they might also contain secondary phases such as AFm phases, calcium aluminate hydrate, C-S-H and even Portlandite. However, the secondary phases strongly depend on different parameters during the clinkerization and/or the hydration processes. The production of CSA is known to be a low energy process compared to OPC. Moreover, CSA has a very high mechanical strength in early ages, an improved durability against certain external aggressions and an expansive behavior on the contrary to OPC which is subject of shrinkage.

CSA clinker is made mainly from limestone, bauxite and sulfate source [74]. The production of CSA requires a smaller quantity of limestone comparing to OPC (40% for CSA and 80% for OPC) which reduces the CO_2 emissions (by ≈ 35%) coming essentially from decarbonation processes. Ye'elimite ($C_4A_3\check{S}$) is the major compound of CSA clinker. A comparison of CO_2 emissions of the major elements of OPC clinker (C_3S and C_2S) and CSA clinker ($C_4A_3\check{S}$) is presented in Table I-6 and shows that ye'elimite can divide the emissions of CO_2 by 3 compared to main OPC anhydrous phases C_3S and C_2S.

Table I-6. CO_2 emissions from principal components of cement [74]

Component	CO_2 emissions (kg/mol of product)
C_3S	0.58
C_2S	0.52
$C_4A_3\check{S}$	0.22

Sulfoaluminate-belite contains ye'elimite (≈ 65%) as a principal compound and belite (≈ 20%) as secondary component. CSA-belite clinker are mainly mixed with a source of sulfate

(gypsum or anhydrite). The interest of using anhydrite is to reduce the economic cost and to reduce the CO_2 footprints since it's a natural product obtained from quarries.

The chemical composition of CSA is different from OPC. It's characterized by the relatively high sulfur content, the higher amount of aluminum oxide and the reduced quantity of calcium and silica. Table I-7 shows a typical chemical composition of OPC and CSA.

Table I-7. Weight percentage of chemical composition of typical CSA & OPC [75]

Clinker	SiO_2	Al_2O_3	Fe_2O_3	CaO	SO_3
CSA	3 – 13	25 – 40	1 – 3	36 - 45	8 - 15
OPC	17 – 25	3 – 8	0.5 – 6	59 – 67	/

The mineralogical composition is different as well. The absence of C_3S, the presence of ye'elimite, the low quantity of calcium aluminate and the high dose of calcium sulfate (gypsum or anhydrite) are the main characteristics of such cement. Among the anhydrous phases for sulfoaluminate-belite, we can identify:

- Ye'elimite
- Belite
- Calcium aluminate
- Calcium ferro-aluminate
- Stratlingite
- Free Lime
- Anhydrite/gypsum

Hydration products of calcium sulfoaluminate binders

Calcium sulfoaluminate cement is composed essentially of ye'elimite and other minor phases (C_2S, C_2AS, CT, C_4AF) mixed with a calcium sulfate source (mainly gypsum or anhydrite). Its hydration is carried out via dissolution-precipitation phenomena since the solubility of anhydrous grains is higher than the solubility of hydrates phases.

The ye'elimite is, generally, the most active phase of such cements and its hydration is the main responsible of the rapid strength gain (formation of AFt/AFm and gibbsite). The ye'elimite hydration process depends on the presence of anhydrite/gypsum and/or calcium hydroxide CH [76].

In the absence of calcium sulfate source, ye'elimite reacts with water to form calcium mono-sulfoaluminate and aluminum hydroxide (**Eq.I-20**). This process is known to be a quite slow reaction in terms of kinetics, and shows a long dormant period [77].

$$C_4A_3\check{S} + 18\ H \rightarrow C_3A.C\check{S}.H_{12} + 2\ AH_3 \quad \text{(monosulfoaluminate formation)} \qquad \textbf{Eq.I-20}$$

With presence of anhydrite or gypsum, the kinetics of the reaction is quicker [78]. For a ratio of ye'elimite over calcium sulfate higher than 0.5, ettringite is formed along with mono-sulfoaluminate and aluminum hydroxide (**Eq.I-21**). The proportion of ettringite and mono-sulfoaluminate in the products depends on the proportions of ye'elimite and calcium sulfate in the mix [76].

$$2\ C_4A_3\check{S} + 2\ C\check{S}H_2 + 52\ H \rightarrow C_3A.3C\check{S}.H_{32} + C_3A.C\check{S}.H_{12} + 4\ AH_3 \qquad \textbf{Eq.I-21}$$

If the amount of sulfate gets higher, mono-sulfoaluminate is not formed and only ettringite is produced (**Eq.I-22**). However, in either way, aluminum hydroxide (AH_3) is formed.

$$2\ C_4A_3\check{S} + 2\ C\check{S}H_2 + 34\ H \rightarrow C_3A.3C\check{S}.H_{32} + 2\ AH_3 \qquad \text{(ettringite formation)} \qquad \textbf{Eq.I-22}$$

Portlandite can be formed from the hydration of belite (C_2S) or if the cement includes initially free lime. The abundancy of sulfate and portlandite in the mix can lead to the formation of only ettringite (**Eq.I-23** and **Eq.I-24**).

$$C_4A_3\check{S} + 8\ C\check{S}H_2 + 6\ CH + 74\ H \rightarrow 3\ C_3A.3C\check{S}.H_{32} \qquad \textbf{Eq.I-23}$$

$$C_4A_3\check{S} + 8\ C\check{S} + 6\ CH + 90\ H \rightarrow 3\ C_3A.3C\check{S}.H_{32} \qquad \textbf{Eq.I-24}$$

Table I-8 presents the different proportion of produced phases as a function of ye'elimite over calcium sulfate ratio. After the hydration of most of ye'elimite and the production of gibbsite, ettringite and/or mono-sulfoaluminate, the rest of the anhydrous phases starts to react.

Table I-8. Water consumption from the hydration of ye'elimite and formation of ettringite [79]

Moles number	$C_4A_3\check{S}/C\check{S}H_2$	Ye'elimite	Water	Gypsum	Ettringite
Eq.I-21 (Without CH)	1	2	52	2	1
Eq.I-22 (Without CH)	0.5	1	34	2	1
Eq.I-23 (With CH)	0.125	1	74	8	3

Figure I-17 shows the proportion of the different phases as a function of time and Figure I-18 shows the different phases as a function of the gypsum added.

Studies were carried out on the understanding of the influence of calcium sulfate nature (gypsum/anhydrite) on the hydration mechanisms [80]. The influence was highlighted in the first days of the hydration. As for gypsum, its dissolution is faster than anhydrite; hence, it favors the rapid formation of ettringite and accelerates the kinetics of the hydration. However, for the anhydrite, its dissolution is slower which mean that the ye'elimite can partially react, in presence of calcium sulfate, to form mono-sulfoaluminate. After several days, the influence on the kinetics is not significant but it may have some consequences on the mechanical strength as well as the hydration degree.

The quantity of calcium sulfate, also, varies the dimensional stability of mortars made of CSA cement. In general, calcium sulfate favors the formation of ettringite over mono-sulfoaluminate. Ettringite has more molar volume than mono-sulfoaluminate which means less porosity in the cementitious matrix and hence the higher the mechanical resistance.

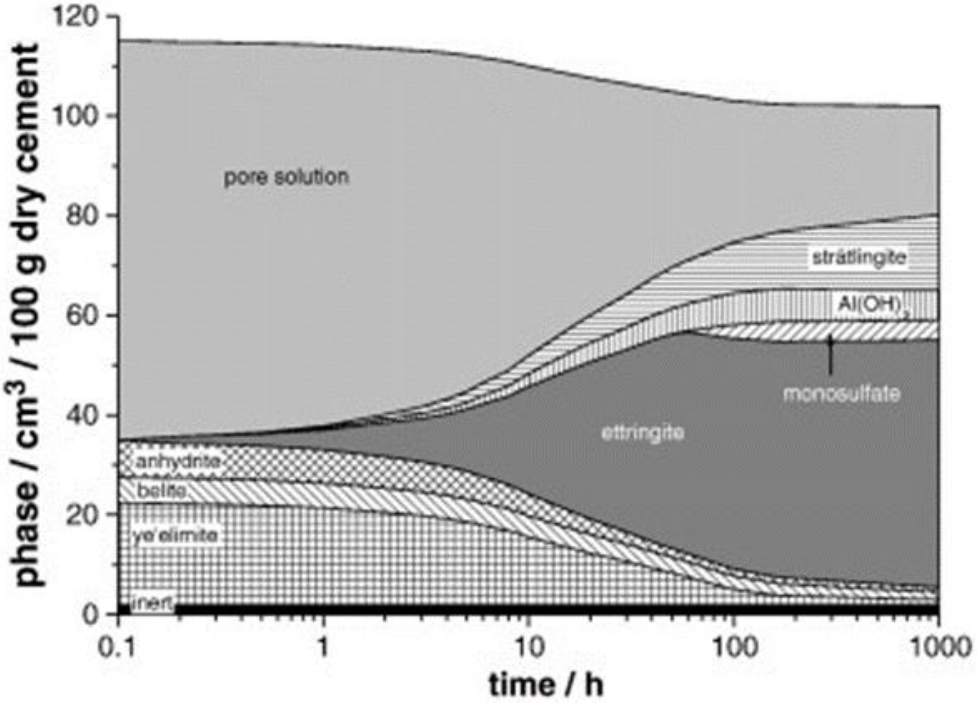

Figure I-17. Different phases' development of a CSA as a function of hydration time [77]

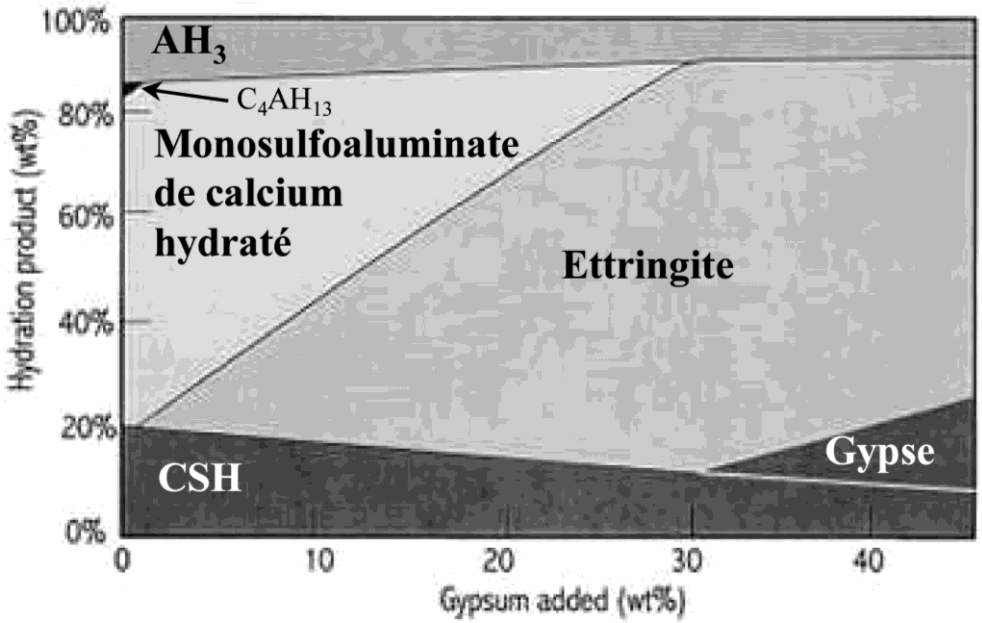

Figure I-18. Gypsum influence of a CSA on the hydration products [81], adapted from [74]

The addition of limestone filler allows the formation of hemicarboaluminate and monocarboaluminate which belong to AFm phases [82]. These two are more stable than monosulfoaluminate and hence, they indirectly stabilize the ettringite.

The CSA reacts more quickly compared to OPC, which means that in early stages, the hydration heat gets to its maximum. Mostly, between 2 and 12h or, sometimes, between 2 and 24h [76]. The hydration of CSA is known to be a low energy consuming process associated with low CO_2 emissions [74]. With no adjuvants added, high heat emissions occur during the first 10 hours after mixing the clinker with water. The increase in the amount of calcium sulfate added to the mix allows the reduction of heat emissions flux, Table I-9.

Table I-9. The decrease of heat flux with the increase of added sulfate for sulfoaluminate cements [83]

Maximum heat flux	Time	Calcium Sulfate added
≈ 42 W/kg	30 min.	10 %
≈ 23 W/kg	3 hours	20 %
≈ 12 W/kg	5 hours	30 %

The reason for this early strength development is unveiled by microstructure analyses which showed the formation of ettringite needles, along with mono-sulfoaluminate, aluminum hydroxide and calcium silicate hydrates, provoking a denser microstructure. Generally, the CSA reaches higher early and late strengths than OPC. For the best setting time, strength development and volume stability, 15-25 wt.% of gypsum is added, otherwise, ettringite continues to precipitate after the 1st day, whereas the cement matrix is hardened, leading to microcracks.

The rapid strength gain is essentially due to the rapid development of ettringite, which becomes after 24h the main responsible of the strength evolution. Later, the mechanical strength continues to increase because of the hydration of other phases, especially belite (C_2S). Zhang and Glasser worked on 1:2.5 cement:sand cubic mortars, under 20°C and RH > 98%. They used a CSA clinker containing 18% gypsum and had a specific area of 3840 cm2/g. The water to cement ratio was about 0.43. Table I-10 shows the mechanical strength obtained at 1 and 3 days of hydration.

Table I-10. Mechanical Strength on cubic mortars for 1 and 3 days [74]

	Mechanical Strength	
	Compressive (MPa)	**Flexural (MPa)**
1 day	44.2	7.6
3 days	53.9	7.5

Durability of calcium sulfoaluminate binders

Calcium sulfoaluminate cement remains a relatively recent cement compared to Portland cement. The durability of such binder is still being tested in different environments, such as leaching by pure water, sulfate-rich soil, acid attacks, carbonation and seawater attack [74,81,84–86].

Berger et al. investigated the resistance of cement pastes made of a CSA clinker and a CSA cement (mixture of CSA clinker with 20 wt.% of gypsum) to leaching phenomena by pure water [84]. The leaching experiment was carried out in controlled laboratory conditions with pH and temperature regulated at 7.0 and 20°C respectively.

The main results of this study were that the decalcification was controlled by diffusion mechanisms and that CSA-based materials showed a better resistance to decalcification than Portland cement (w/b = 0.40) (Table I-11). Moreover, the flux of sulfate in the leached solution was higher for CSA clinker compared to CSA cement.

Table I-11. Kinetics of decalcification of the cementitious matrix of different cement paste exposed to leaching by pure water in regulated conditions

	Decalcification rate (mmol/dm^2.d$^{0.5}$)	**Reference**
PC	13.00 ± 2.00	[87]
CSA clinker	8.60 ± 0.02	[84]
CSA cement (CSA clinker + 20 wt.% of gypsum)	6.80 ± 0.06	[84]

Regarding the microstructure of the materials, the authors determined two deteriorated layers (outer and inner). The outer deteriorated layer was composed mainly of AH_3 and exhibited high porosity and low mechanical strength and the inner layer was less porous and denser than the outer layer. Additionally, they concluded that the formation of ettringite instead of monosulfoaluminate hydrates, by adding gypsum, increased the resistance of the material to attack by pure water due to the lower solubility of ettringite.

Another study has compared the performance of mortars made of calcium sulfoaluminate cement and of Portland cement exposed to sodium sulfate solution (at 5%) and sulfuric acid solution (at 1%) [86].

The CSA binders showed lower dimensional modifications when exposed to sodium sulfate attack (Figure I-19) and lower volumetric change when exposed to sulfuric acid attack (Figure I-20) than Portland cement.

This behavior was probably linked to the particular chemical and mineralogical composition of CSA cement. The low content of free lime and the absence of C_3A phase are the main reasons for the high resistance of such binders to sulfate attack [85,88]. The secondary ettringite precipitation in Portland cement is responsible for the strains in the microstructure of the hardened cement paste, while secondary ettringite does not theoretically occur in CSA binders when exposed to sulfate attack [62,85,88].

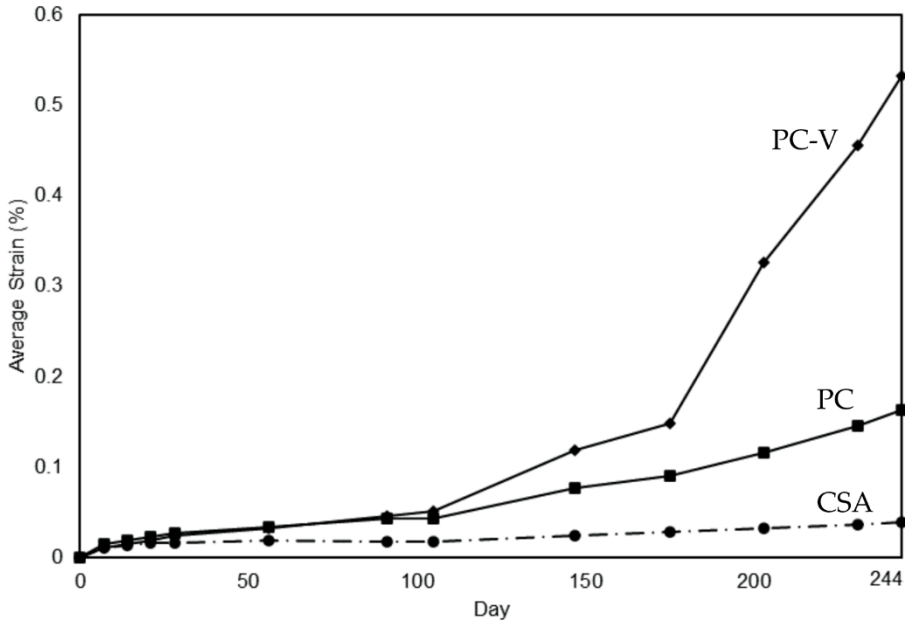

Figure I-19. Average strain (in %) for PC, PC type V (PC-V) and CSA mortars exposed to sodium sulfate solution (5%) according to ASTM C1012 [86]

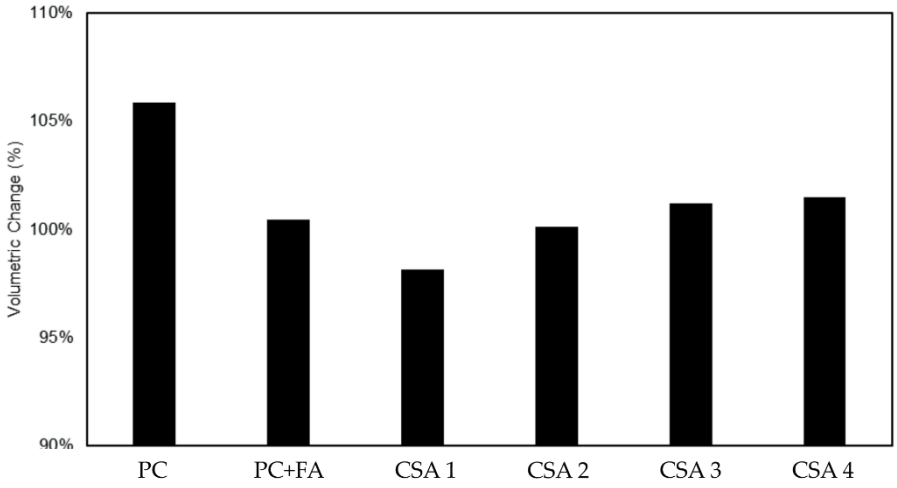

Figure I-20. Volumetric change (in %) for PC, PC+FA and different formulations of CSA mortars exposed to sulfuric acid solution (at 1%) [76]

Figure I-21 shows that the carbonation rate of CSA tended to be higher than PC-based materials. High amounts of calcite were detected in the carbonated layer with lower amounts of ettringite compared to sound core [89]. The carbonation of the hydrated cement paste leads to the decrease in pH (typically around 12-13) and impacts the stability of the ettringite phase, which becomes chemically instable in environments with pH < 10.6 [80]. The destabilization of ettringite might result into its dissolution; hence, deteriorating the microstructure of CSA materials.

The problem with seawater is the presence of chloride ions that, if they penetrate inside the concrete, can decrease its pH and initiate the corrosion of the reinforcement bars. Glasser and Zhang analyzed some samples taken from a concrete pipe made of CSA cement in contact with sea water for 14 years [74]. They noticed that the steel bars were not corroded despite a

concrete cover of only 8 mm. Moreover, they analyzed 1 mm from the surface of the cementitious lining in contact with seawater and identified 3 zones:

- Inner zone: unaltered concrete, rich in chloride and anhydrous clinker grains.
- Intermediate zone: a progressive decrease in calcium content and the absence of anhydrous phases which were chemically modified by the seawater.
- Outer zone: High substitution of Ca^{2+} by Mg^{2+} and an adhesive bio-precipitated layer of $CaCO_3$.

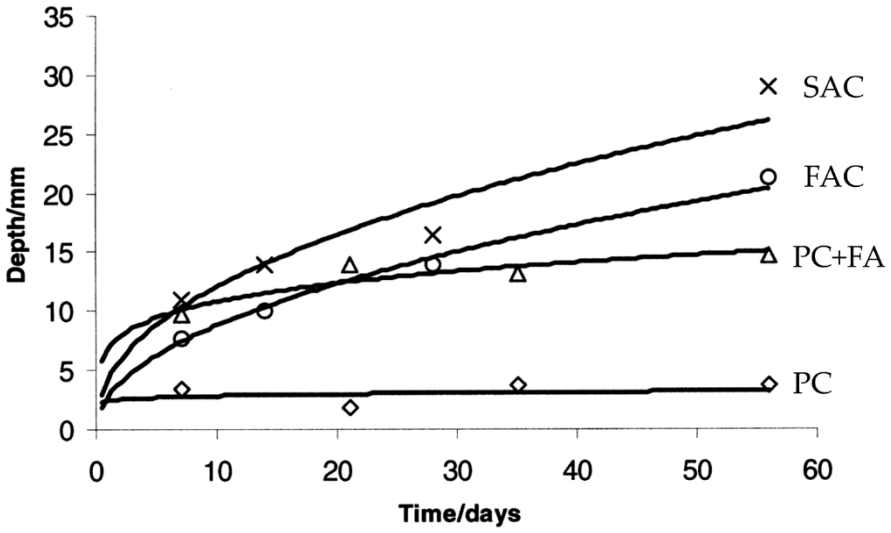

Figure I-21. Evolution of the carbonation depth (using accelerated carbonation techniques) for calcium sulfoaluminate cement (SAC), calcium ferroaluminate cement (FAC) compared to Portland cement (PC) and Portland cement with fly ash (PC+FA) [89]

The authors were not able to precisely determine the reason for the resistance to chloride progression; however, the suggested that the physical properties (e.g. permeability of oxygen, initial porosity and pore size distribution) and the chemical and mineralogical composition (e.g. low content of unreactive anhydrite) could play a key role in understanding such phenomena for CSA-based materials.

1.6.2.Portland cement + mineral additives

The previous section showed that calcium aluminate cement exhibited higher durability than Portland cement in sewer conditions. The better resistance of CAC was mainly attributed to its high initial alumina content and to the higher chemical resistance of its aluminum-bearing phases, in particular aluminum hydroxide (AH_3). Thus, increasing aluminum content in Portland cement and eventually decreasing the amount of portlandite could improve its durability against such aggressive environments. Moreover, calcium sulfoaluminate cement is known to have a high initial alumina content and aluminum hydroxide is one of its main hydrated phases. However, the durability of such binder was still to be tested in these conditions and the deterioration mechanisms are yet to be investigated.

This section presents potential binders having an increased aluminum content either by incorporating mineral or pozzolanic additives to Portland cement or by having a completely different chemical and mineralogical nature of the cement, such as the case of calcium sulfoaluminate cement.

1.6.2.1. Supplementary cementitious materials rich in aluminum

Environmental regulations and pollution controls have led to an increase in the industrialization of waste and by-products materials which can be used as supplementary cementitious materials (SCM) such as ground granulated blast furnace slag, metakaolin, silica fume and fly ash. The incorporation of such materials in concrete does not only reduce the pollution level but enhance the properties and the durability of Portland cement.

Supplementary cementitious materials are characterized by a lower calcium content compared to Portland cement. The nature and/or chemistry of such materials – which need to be activated by the Portland cement to react – affect the hydrates produced during the hydration and, therefore, the strength and the durability of the blended product. For instance, the mechanical strength development of blended cement is slower than in OPC due to the nature – latent hydraulic and/or pozzolanic properties – of the SCM.

Three main effects are observed when SCM are mixed with Portland cement. The first one is the reduction of calcium hydroxide (Portlandite) content in the blend due to pozzolanic reactions to produce mainly C-S-H and other hydrates. The second effect is the decrease in pore size due to the additional hydrates formed during the pozzolanic reaction. These hydrates increase the solid volume leading to a denser and more compacted structure. The third effect concerns the structure of C-S-H hydrates, which is the most important phase in a Portland cement. Incorporating SCM into Portland cement matrix leads to the formation of C-S-H with lower C/S ratio than C-S-H produced in plain Portland cement. The decrease in C/S ratio in C-S-H structure in Al-rich environment leads to an increase in C-S-H Al uptake (Figure I-22) [90,91].

The mechanisms of degradation of ordinary Portland cement are widely studied in the literature. The precipitation of secondary expansive phases is due to the leaching of Ca^{2+} and Al^{3+} ions coming mainly from calcium hydroxide (Portlandite) and calcium silicate hydrates (C-S-H).

Based on the in-situ and laboratory results performed on Portland cement and calcium aluminate cement, the decrease in calcium content – in particular calcium hydroxide – and the increase in the aluminum content in the cementitious matrix could be two important factors regarding the durability of cementitious materials in sewage environments. Hence, there is an interest in testing Portland cement with supplementary cementitious materials.

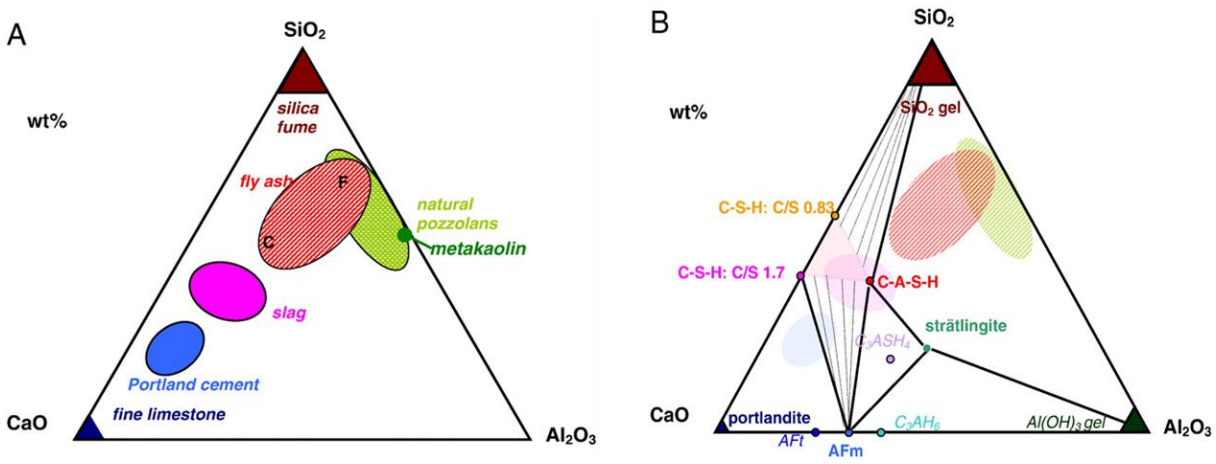

Figure I-22. (A) The repartition of cementitious materials in the CaO-SiO_2-Al_2O_3 system; (B) The hydrate phases in the CaO-SiO_2-Al_2O_3 system [91]

1.6.2.1.1. Ground granulated blast furnace slag (GGBFS)

Ground granulated blast furnace slag (GGBS) is a by-product of metallurgical furnaces producing iron and steel and is obtained by quenching the molten slag in water to produce granular glassy product which is then dried and grounded into a fine powder. GGBS presents high latent hydraulic properties, which means that they react in presence of activators like calcium-rich solutions. GGBS can be mixed with OPC in order to reduce the calcium hydroxide content and improve the durability of blended cements especially against sulfate attack [63].

Hydration products of blended PC/slag binder

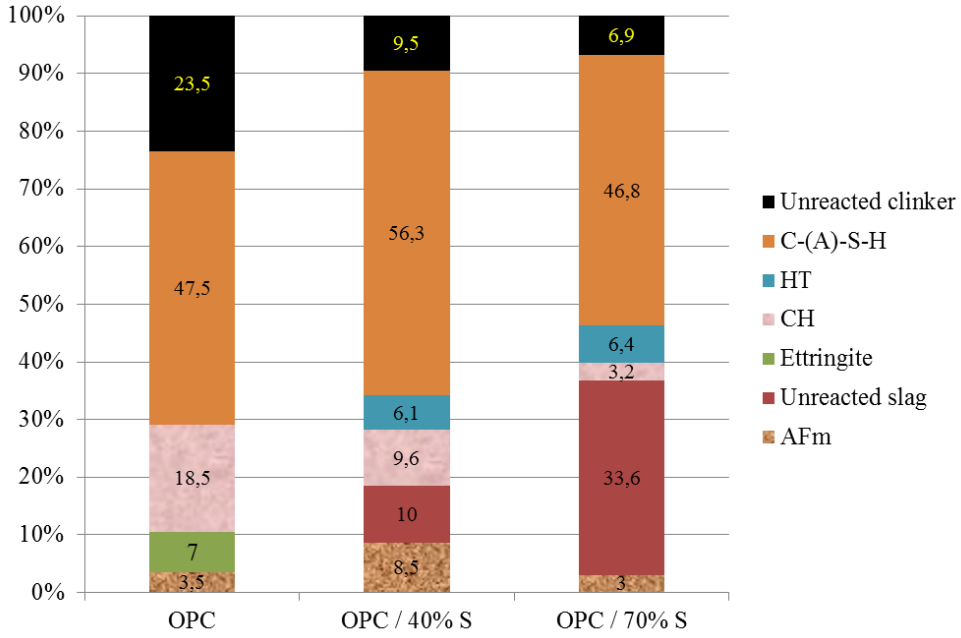

Figure I-23. Impact of slag percentage replacement (0%; 40% and 70%) on the phase assemblage after 90 days hydration [63]

However, the chemical and microstructure compositions of blended cements depend highly on the percentage replacement (PR). For instance, as described on Figure I-23, only 40% of

GGBS replacement has decreased the Portlandite content by two and for 70% of slag replacement, the Portlandite content has decreased by a factor of six, nevertheless, an increase in unreacted slag accompanied the decrease of Portlandite. Other phases develop as well resulting from the fact that the supplementary cementitious materials (SCM) affect the hydration mechanisms of Portland cement. For example, ratios of Si/Ca and Al/Ca in C-A-S-H phase increased with higher GGBS additions.

Durability of blended PC/slag binder

The durability of blast furnace slag cements has been tested in several environments. For instance, the durability against chloride ions penetration, sulfate attack and alkali-silica reactions were proven to be improved by incorporating slag in the cement mix [63,92,93]. Therefore, researchers turned to test such blends against acid attack to understand their alteration mechanisms.

The behavior of OPC, CAC and BFSC samples exposed to a laboratory test using a corrosion chamber to simulate biogenic sulfuric acid attack in sewage environments was evaluated [70]. The room temperature was at 30°C with 98% of RH. The chamber air contained H_2S concentration at 10 ± 5 ppm. The cementitious samples were inoculated with different strains of *Thiobacillus thiooxidans*, *T. intermedius*, *T. novellus* and T.*neapolitanus*.

All mortars were prepared with siliceous sand except the SC samples which were prepared with Alag™ aggregate, which had the same mineralogical composition as CAC Fondu. The results of weight loss of the different cementitious materials are reported on Figure I-24.

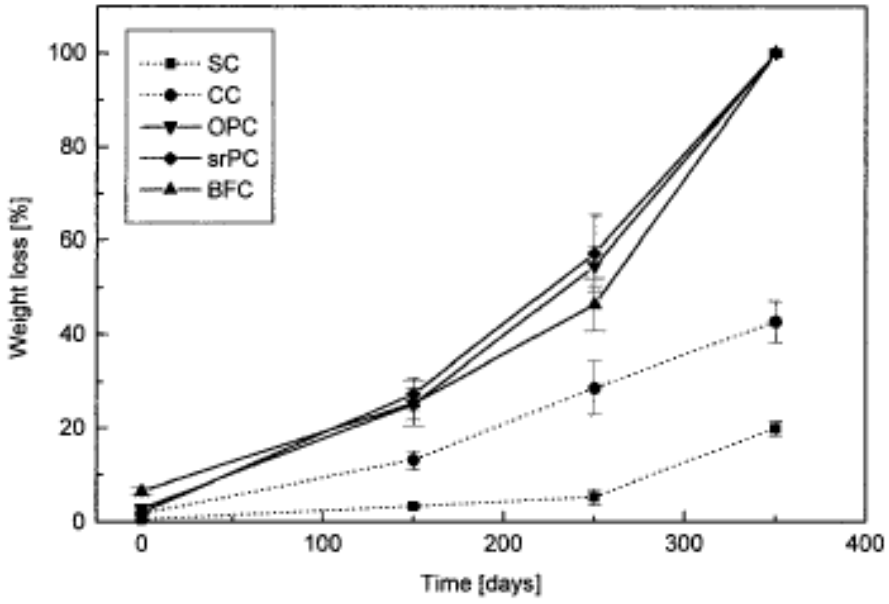

Figure I-24. Weight loss recorded for different mortars using the simulation chamber [70]

OPC and BFSC have been completely dissolved after 350 days of incubation in the simulation chamber while SC and CC – CAC samples – have suffered from 20 and 40% of weight loss for the same period. Moreover, the amount of biogenic produced sulfuric acid depended on the type of the cementitious materials. For instance, after an incubation of 80 days, the amount of

the acid produced by the microorganisms was higher on OPC and BFSC than on CAC. The authors attributed this behavior to the mineralogical composition of the different cements, the lower neutralization capacity of OPC and BFSC and the inhibitory effect of Al^{3+}.

They have also compared the performance of the three materials in chemical and biological sulfuric acid attack with the results reported on Figure I-25. The results showed the difference in the behavior of each cement according to the type of test. Nevertheless, BFSC performance can be situated between OPC and CAC.

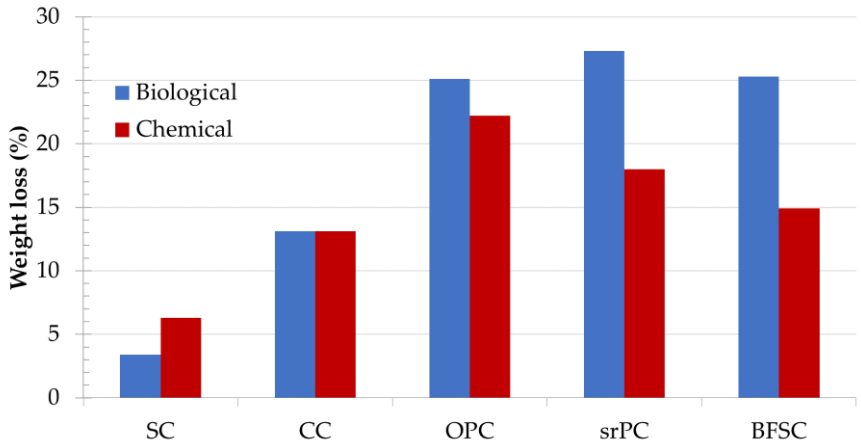

Figure I-25. Comparison of weight loss of mortar samples subjected to biological (after 150 days) and chemical tests (after 33 renewals of the solution) [70]

Another research team has exposed BFSC (with slag content ranging from 66 to 80%) to a laboratory test simulating the biological aggression in sewage network. One test cycle consisted of four steps of 17 days total: 3 days of H_2S gas incubation at 250 ppm; 10 days of immersion in 600 ml of the culture medium at pH 7; 2 days of rinsing to simulate the high flow of water stream on rainy days and finally 2 days of drying. The concrete corrosion was simulated in 4 cycles.

During cycle 2, solution analyses showed an increase in sulfate concentration from 0 to 2-4 g SO_4^{2-}/l, confirming the biological activity. This was in accordance with the solution's pH as it dropped rapidly from 8 to 3 after 3 days and continued to decrease until pH 1 after 10 days. After 4 cycles of testing, change in thickness varied between -0.3 mm and -0.8 mm with limestone aggregates concrete having a limited decrease in radius than inert aggregates concrete.

However, as shown on Figure I-26, the cement type seemed to be the key parameter in weight loss measurements by comparing OPC and BFSC specimens with the same aggregates and production method. The mass loss for concrete with slag cement was higher than concrete with Portland cement. The aggregates had a slight effect but, nevertheless, the results were contradictory with the change in thickness results. A hypothesis was that the density of removed materials was higher for limestone concrete (aggregates and cement mortar) than for inert concrete (cement mortar only).

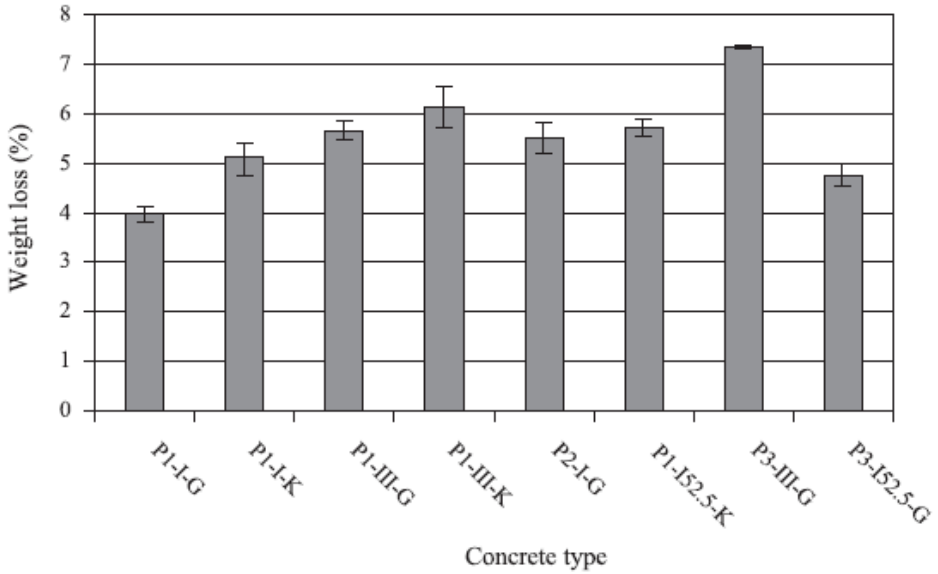

Figure I-26. Weight loss of Portland cement (I) and slag cement (III) with different production methods (P1, P2 and P3) and different aggregates (K: Limestone; G: inert) exposed to microbiological test [94]

Parts of pipes with a BFSC mortar coating were exposed to a test simulating the microbiological corrosion of cementitious materials [20]. Figure I-27 reports the results obtained by SEM observations on the BFSC specimen. Microcracks were observed at the area in contact with the biofilm (100 µm) and a major crack at 400 µm from the surface that seemed to be due to the precipitation of secondary expensive ettringite. The total degraded depth was 700 µm with the outer zone (in contact directly with the biofilm) was highly decalcified (represented by a darker gray shade).

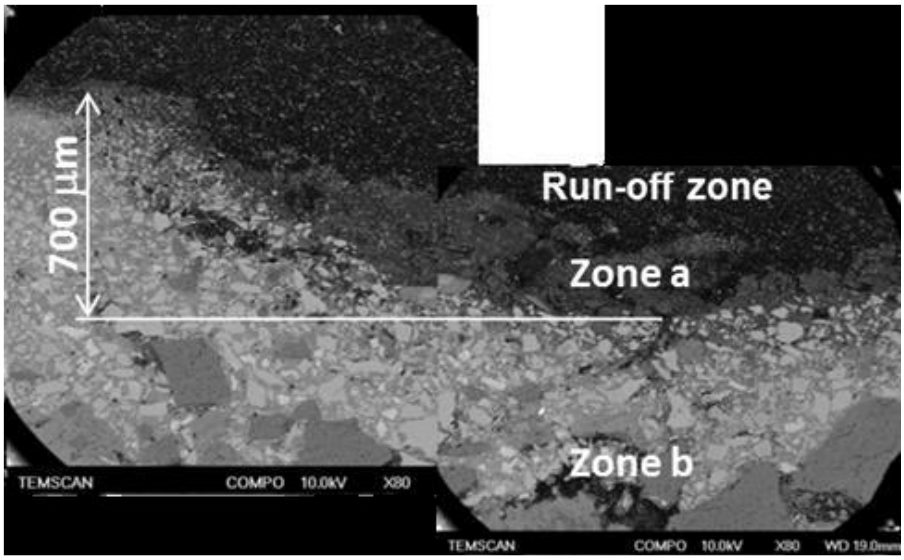

Figure I-27. SEM observations (BSE mode) showing the total degraded depth [20]

1.6.2.1.2. Fly ash

Fly ash (FA) is a coal-combustion residue composed of fine particles mainly captured by filtration systems in coal-burning electric power plants. It consists essentially of SiO_2, Al_2O_3, Fe_2O_3 and alkalis but its chemical composition can vary depending on the nature of the coal

and the production process. A typical chemical composition of ASTM type F FA is presented in Table I-12.

Table I-12. Chemical composition of ASTM type F FA [95]

	SiO_2	Al_2O_3	Fe_2O_3	CaO	MgO	Na_2O	K_2O	Ig. loss
Fly ash	54.7	22.8	7.4	8.9	1.8	0.7	0.6	1.9

Hydration products of blended PC/fly ash binder

In cement industry, FA is used as a supplementary cementitious material due to its pozzolanic properties. Blended cement containing FA has often a higher strength and durability comparing to plain Portland cement. The pozzolanic reaction of FA is similar to that of SF, the alumina-silicate component reacts with calcium hydroxide, formed from the hydration of calcium silicate in Portland cement, to produce calcium silicate hydrates and calcium aluminum hydrates. The additional C-S-H and C-A-H densify the structure of the blend by reducing the total porosity of the system.

The impact of FA on the phase assemblage of the blended cement was studied. First observation was that the consumption of portlandite was less marked comparing to SF as FA contains CaO which is an additional source of calcium and also due to the limitation of FA reactivity. Second observation was that ettringite content decreases and AFm phases are more abundant in systems where FA is blended with Portland cement as the former contains an important amount of Al_2O_3 and a very low content of SO_3. Third observation was that for aluminum rich FA, stratlingite may form. However, its formation depends on other factors such as the reactivity of the FA and the uptake of Al in C-S-H. Figure I-28 shows a thermodynamic model (assuming a complete hydration of OPC) predicting phase assemblage for blended cements as a function of FA replacement level.

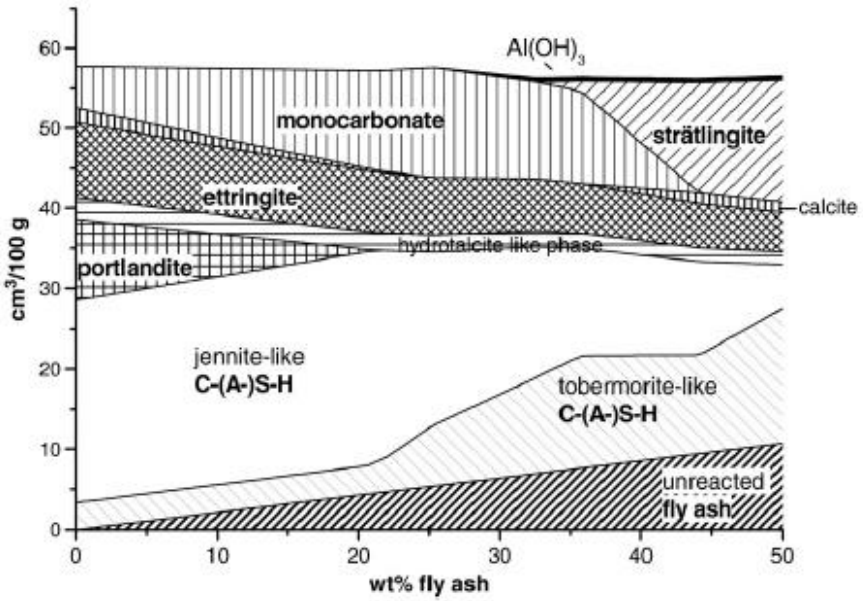

Figure I-28. Thermodynamic model of phase assemblage as a function of replacement percentage by fly ash, assuming a complete hydration [91]

Durability of blended PC/fly ash binder

Several authors have tested the resistance of OPC/FA blended mortars to chemical aggressions and in particular sulfuric acid attack. For instance, mortars of OPC/FA were tested with replacements of cement by FA of 10; 30; 50 and 70% in a 2% H_2SO_4 solution for 3 years (Figure I-29).

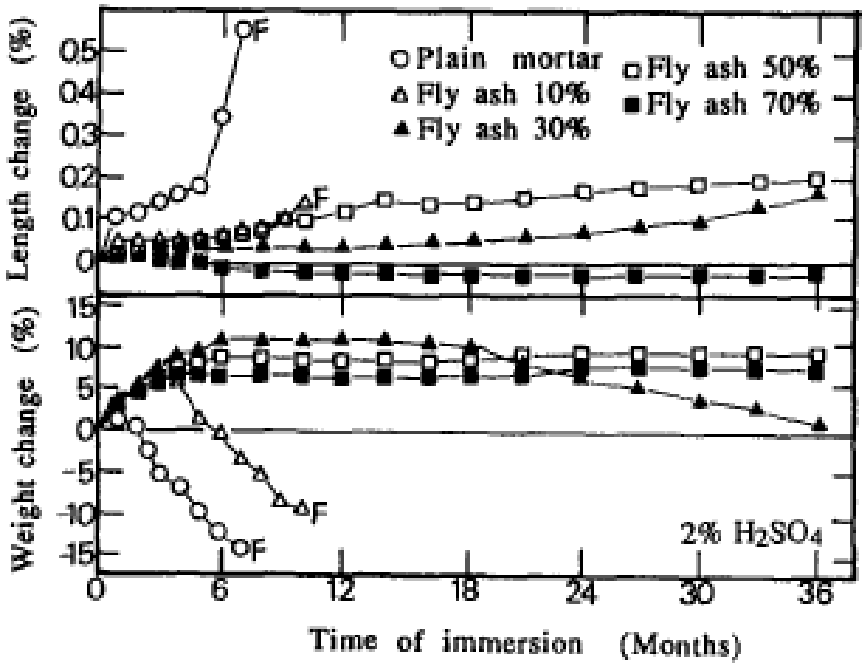

Figure I-29. Length and weight change for plain OPC and blended OPC with fly ash mortars during 3 years of exposure to 2% sulfuric acid solution [95]

The concentration of sulfuric acid in the solution was controlled periodically. After one year of exposure, the first results showed that OPC/FA blended systems with fly ash replacement higher than 30% have maintained a relatively good shape comparing to plain OPC cement which completely decomposed after 7 months. However, gypsum precipitation was found in higher quantity in blended mortars than in plain mortars. Despite the high replacement of cement by fly ash, the authors remarked that it was impossible to effectively stop the sulfuric acid attack on OPC/FA mortars for long-term exposure [95].

Roy et al. have tested a series of OPC/FA specimens with 0 – 30 wt.% replacements. The test was in accordance with ASTM C-267 (standard test method for chemical resistance of mortars) and consisted of immersing the specimens in 1% and 5% sulfuric acid solutions for 28 days. The results showed that by increasing the fly ash replacements, the mortars have gained in weight. This might be due to the saturation of the specimen with water and/or the precipitation of secondary phases inside the cementitious matrix. However, the study did not go any further than pH observation. The pH of the acidic solution changed to alkaline values at the end of the test for 1% of H_2SO_4 and, on the other hand, the pH of the 5% H_2SO_4 has remained acidic. Moreover, OPC/FA specimens were completely deteriorated after 28 days of immersion in the 5% H_2SO_4 solution.

Another study was carried out to evaluate the impact of high-volume fly ash (HVFA) on the resistance of concrete to sulfuric acid attack. The influences of standard and steam curing were studied as well. The test consisted of an immersion of mortar samples into sulfuric acid solution at concentration of 5% for 60 days. The results showed a negligible improvement of acid resistance due to FA incorporation into the cementitious matrix for standard curing samples. However, starting from 40 wt.% replacement by FA, under steam-curing conditions, the mortars showed higher resistance as the weight loss decreased from 8% for plain OPC mortar to 1% for 70 wt.% FA [96].

1.6.2.1.3. Metakaolin

Metakaolin was reported in the literature as a supplementary cementitious material for the first time in 1960's where it was used in the construction of Jupia dam in Brazil with a replacement of 30% of cement by volume [97]. Since then, the industrial use of metakaolin or cement-metakaolin mixes was build up in many countries around the world but still not used as much as other SCMs such as slags or fly ashes.

Hydration products of blended PC/metakaolin binder

Metakaolin is known to be a high water consumer material due to its relatively high specific surface and to the flat form of its particles which can influence the properties – especially at fresh state – of the final mix [98].

Clays' structure is a combination of tetrahedral silicon (Si) and octahedral aluminum (Al) sheets but different cations can replace Al^{3+} in the structure, such as Mg^{2+}, Fe^{2+}, Fe^{3+} and Mn^{2+}. The thermal activation process, which consists of heating the mineral to a certain temperature to eliminate structural water, is called dehydroxylation [99]. The removal of hydroxyl groups (**Eq.I-25**) from the kaolinite ($Al_2Si_2O_5(OH)_4$) leads to a metastable state and a more disorder in the structure (Figure I-30). This metastable state is called metakaolin.

$$AS_2.H_2 \rightarrow AS_2.H_X + (2\text{-}x)\ H \qquad \textbf{Eq.I-25}$$

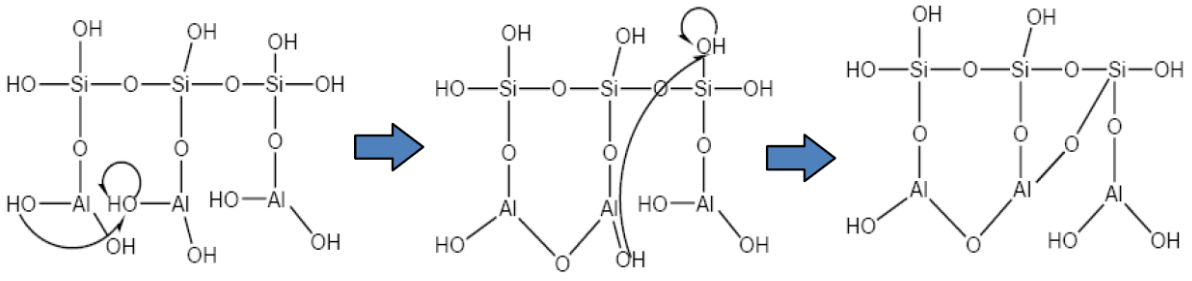

Figure I-30. Schematic process of the dehydroxylation of kaolinite [100]

The fineness of metakaolin particles can be situated between that of silica fumes and that of cement. Also, while the specific surface of metakaolin is largely higher than that of cement which gives it a higher reactional surface, the high specific surface increases the water demand in the mix. The chemical composition of metakaolin consists of mainly aluminum and silica (>

90%) but it might contain, depending on the purity of kaolinite, many non-reactive secondary phases like quartz – which could limit the water demand of metakaolin – or iron oxides. These secondary phases might have an impact on some properties of the product such as its rheology or its reactivity [98].

The metakaolin – resulted from the dehydroxylation of kaolinite - presents a pozzolanic activity. In addition, Kaolin – which is composed essentially from kaolinite – is sedimentary clay and can be found all around the world. Thus, metakaolin is considered a valuable substitute for cement in concrete industry.

As metakaolin is considered as a pozzolanic material, silica will react with calcium hydroxide (portlandite) to produce calcium silicate hydrates (C-S-H) which is the responsible of the pozzolanic setting of the paste. However, since metakaolin is rich in aluminum, other reactions take place as well as producing different hydrated phases, e.g. katoite, stratlingite and other AFm phases.

Limestone calcined clay cement (LC3) is another type of binders containing Portland cement and metakaolin recently developed to reduce the environmental impact of cementitious binders [101–104]. This binder is composed of about 50% of Portland clinker mixed with calcined clays (or kaolinite) and limestone. The main hydration reaction of such binder could be summed in the following reaction (**Eq.I-26**) [105,106]:

$$A(\text{from calcined clay}) + C\check{C} + 3\ CH \rightarrow C_3A.C\check{C}.H_{11} \qquad \textbf{Eq.I-26}$$

Calcined clays (not only calcined kaolinite) are more available than the other SCM (slag, FA and SF) which will become limited resources.

Durability of blended PC/metakaolin binder

The overall durability of ordinary Portland cement is improved by incorporating metakaolin as SCM. In fact, a significant reduction in the pores size was observed when replacing cement by 20 wt.% of metakaolin [107]. This diminution in the pores size leads to modifications in the transport properties of water and hence, the diffusion rates of aggressive ions [98,108].

Bucher has compared concrete specimens in terms of chloride migration coefficient. Concrete with metakaolin has an equivalent or lower coefficient than OPC based concrete with the optimal replacement rate was around 15% which led to a decrease of 30% of chloride migration coefficient [98].

Decalcification is the main pathology observed during an acid attack on cementitious material. Calcium hydroxide dissolves firstly then followed by silicate hydrates and alumina-silicate hydrates. The dissolution of these hydrates creates a concentration gradient with the exterior medium leading to the decalcification phenomenon.

The substitution of cement by metakaolin has slightly improved the durability of mortars against chemical aggression. However, the resistance of mortars containing metakaolin to sulfuric acid at 1% increased with the increase of metakaolin substitution level up to 15% [109].

The resistance of partially replaced cement mortars by metakaolin increases proportionally with the increase of metakaolin replacement level. In fact, incorporating 15% of metakaolin in the cementitious mix improved significantly the resistance of the material immersed in 7% H_2SO_4 (pH ≈ 0.3) and 3% H_2SO_4 (pH ≈ 0.6) solutions by volume (Figure I-31) [110]. Moreover, the authors implied that the positive effect of metakaolin on the durability of mortars could be attributed not only to their influence on the porosity decrease and the consumption of calcium hydroxide but also to the formation of more chemically stable hydrates – mainly calcium aluminate hydrates (C_2ASH_8, C_4AH_{13} and C_3AH_6) – in acidic conditions than calcium silicate hydrates (C-S-H).

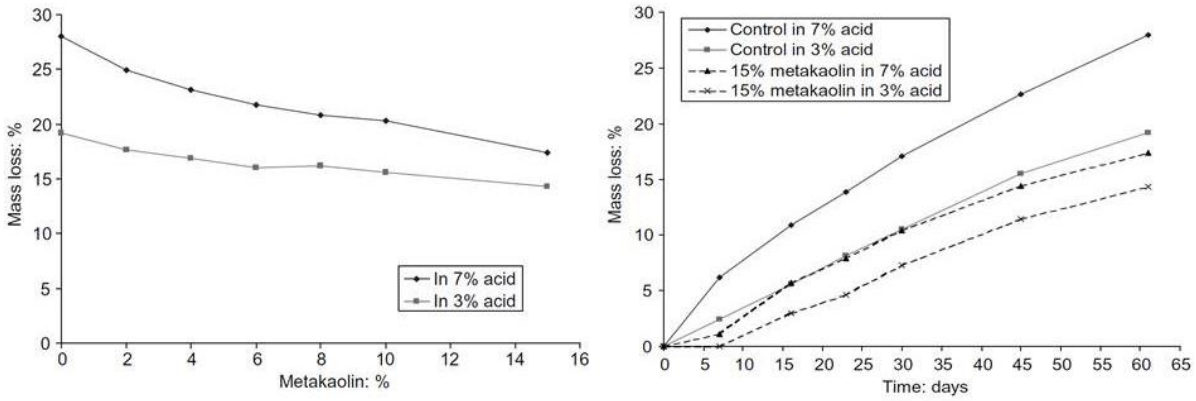

Figure I-31. Influence of metakaolin incorporation on the performance of mortars against sulfuric acid attack by immersion [110]

Another study showed that, after 32 weeks of exposure to 2.5% H_2SO_4 solution, the total weight loss for plain Portland cement was equal to 40%. However, by replacing 10, 20 and 30% of cement by metakaolin, the total weight loss was about 30% (Figure I-32) [111].

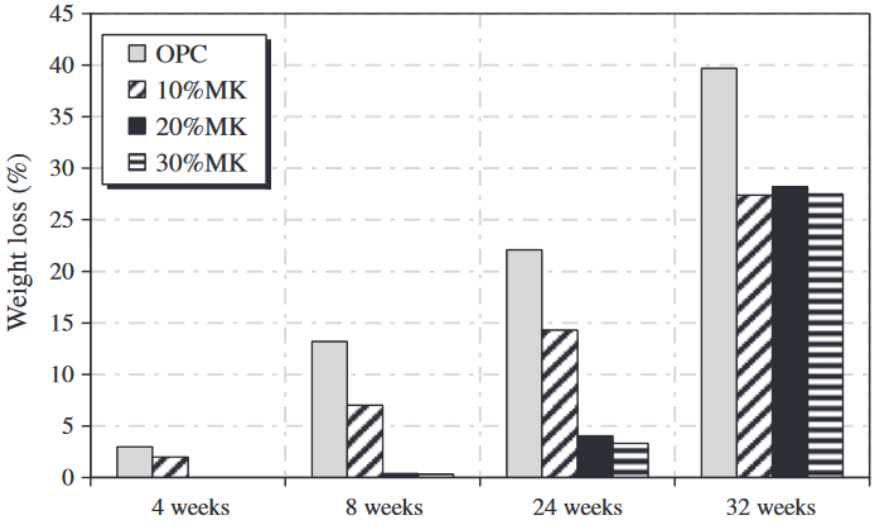

Figure I-32. Total weight loss of mortars immersed in 2.5% H_2SO_4 [111]

In another context, metakaolin seem to enhance the durability of cementitious materials against exogenous sulfate attack. The comparison of different replacement levels of metakaolin and fly ash mortars immersed in sodium sulfate (Na_2SO_4) solution (sulfate concentration at 16g/l) showed that metakaolin-modified mortars presented no dimension changes while plain Portland mortars showed a significant expansion. Nevertheless, the best resistance to Na_2SO_4 was attributed to a replacement level of 15% of cement by metakaolin [112].

Another study has showed that incorporating metakaolin in the mix could lead to a rapid formation of ettringite in the cementitious matrix, even at high temperature, which could decrease the risk of the formation of delayed expansive ettringite [113].

1.6.2.2. Cementitious matrices rich in iron

Iron is present typically in an ordinary Portland cement relatively small amounts, mainly in the form of C_4AF. As such phase exhibits a very slow hydration reaction, most of iron remains in the anhydrous form and very few irons might get incorporated into AFt/AFm phases [62,114].

During the acid attack on Portland cement, the amount of iron in conventional cements is mostly insignificant compared to calcium and silicon, and to a lower extent aluminum. However, the iron content could be increased through the addition of iron-rich minerals (e.g. hematite) to cementitious binders. The potential of iron to influence the resistance of binders, in particular exposed to sewer conditions, has been discussed in very few studies in the literature.

A study carried out on deteriorated concrete samples, made of CEM I 42.5 N C_3A-free mixed with fly ash, and extracted from an Austrian sewer system [48]. An accumulation of iron was detected at the degradation front between the deteriorated and the sound zones, as presented in Figure I-33. At such depth, anaerobic conditions were assumed and *A. ferrooxidans* bacteria were detected instead of *A. thiooxidans*, identified on the surface of the material.

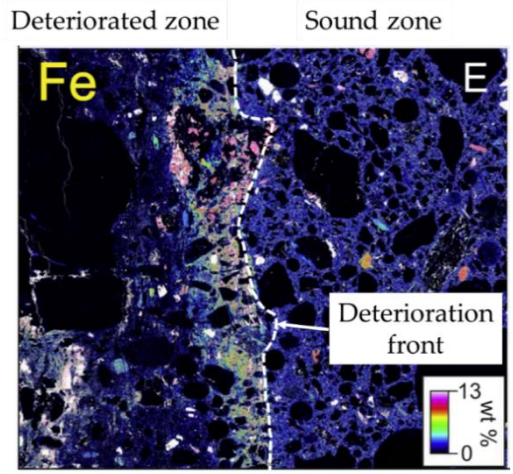

Figure I-33. Elemental mapping showing the accumulation of iron at the interface between the deteriorated and the sound zones of the concrete sample exposed to sewer environments [48]

The authors explained the particular behavior of iron to be linked to the microbial activities and the pH of the deteriorated zone. During the biogenic attack, dissolution of cementitious phases releases OH^- which increases locally the pH of certain zones. For a relatively elevated pH (3-4) and in aerobic conditions, ferric iron (Fe^{3+}) precipitates in several mineralogical forms (lepidocrocite, goethite and parabutlerite). Therefore, Grengg et al. concluded on the possible production of sulfuric acid directly at the interface with the sound zone via *A. ferrooxidans* in presence of high iron content in the medium.

Another study was focused on the impact of heavy metals (Fe, Cu and Co) on the resistance of geopolymers to sulfuric acid attack [115]. The incorporation of inert iron in the form of hematite to a geopolymer with high alkali content (Na:Al = 1.39) resulted in improving the overall durability of the geopolymer to chemical sulfuric acid attack at pH 2. After exposure to sulfuric acid attack, the high-Fe geopolymer (containing 5 wt.) presented lower compressive strength and porosity change as well as low leaching of aluminum and silicon, showing less modification of the microstructure and the chemistry of the binder compared to the same geopolymer without iron addition.

Finally, a preliminary work (Holcim internal documents) showed an improvement of the performances of Portland cement concrete mixes exposed to field sewer conditions when Fe-rich mineral additive (HardCem) had been added to the mix. Several hypotheses were proposed to explain the reason behind the enhancement of the resistance of such material, e.g. (i) the inert grains improved the erosion resistance of the binder and led to less deterioration via physical phenomena; (ii) the dissolution of iron from the attack on the HardCem grains influenced the microbial activity and led to decrease the severity of the attack; and (iii) the partial substitution of the cement by the mineral additive decrease the amount of matter susceptible to react with the acid. However, the impact of such additives on the deterioration mechanisms is still not clear and further investigations are required, in particular on the interaction of Fe-rich additives with the cementitious matrix and with the microorganisms as well as the resistance of such additives to sulfuric acid attack.

1.6.3.Alkali-activated materials

The use of alkali activated materials in building construction goes back to the 1940s [116,117]. Recently, in the aim of reducing greenhouse emissions, the industry was more interested in the reuse of by-products from other industries, e.g. slag and fly ash. Several studies were carried out to compare the carbon footprint of Portland cement and alkali-activated binders showed that the production of the latter resulted in a reducing of 40-80% of CO_2 emissions [118–120].

Alkali-activated materials (AAM) are being used as substitutes to Portland cement in the aim of reducing the environmental impact of cement production and to encourage the reuse of industrial by-products. Developing new cement-free binders with similar properties to

Portland cement was a challenge since the AAM present different chemical and mineralogical composition and physical and transfer properties.

1.6.3.1. Alkali-activated slag

Alkali-activated slag (AAS) is a sub-family of AAM which is obtained by an alkaline attack on the amorphous aluminosilicate of slag. Slag when mixed with an alkaline solution yields a material which set and harden resulting in developing binding properties.

A main difference between the alkaline activation of slag and the activation of slag by cement and gypsum in blended cements is the rapid and high development of mechanical strength and the higher resistance against external attacks [121–123].

Alkali-activators and hydration of alkali-activated slag

Slag is considered to be a high calcium by-product which is activated in moderately alkaline conditions [124]. The high pH of the alkaline activator induces the dissolution of slag and initiates a series of reactions, described in **Eq.I-27**, **Eq.I-28** and **Eq.I-29** [125,126].

$$\equiv Si\text{-}O^{-} + R^{+} \rightarrow \equiv Si\text{-}O\text{-}R \qquad \textbf{Eq.I-27}$$

$$\equiv Si\text{-}O\text{-}R + OH^{-} \rightarrow \equiv Si\text{-}O\text{-}R\text{-}OH^{-} \qquad \textbf{Eq.I-28}$$

$$\equiv Si\text{-}O\text{-}R\text{-}OH^{-} + Ca^{2+} \rightarrow \equiv Si\text{-}O\text{-}Ca\text{-}OH + R^{+} \qquad \textbf{Eq.I-29}$$

The alkaline cation (R^{+}) plays an important role in the early stages of the hydration process via cationic exchange with calcium ions. The nature of the alkaline cation could have a significant impact on the hydration reactions and in particular on the setting time of the binder [121,127]. Although, the use of potassium hydroxide (KOH) as an alkaline activator was reported to produce high mechanical strength at 1 day, the development of mechanical strength scales down after 1 day, as seen in Figure I-34 [128].

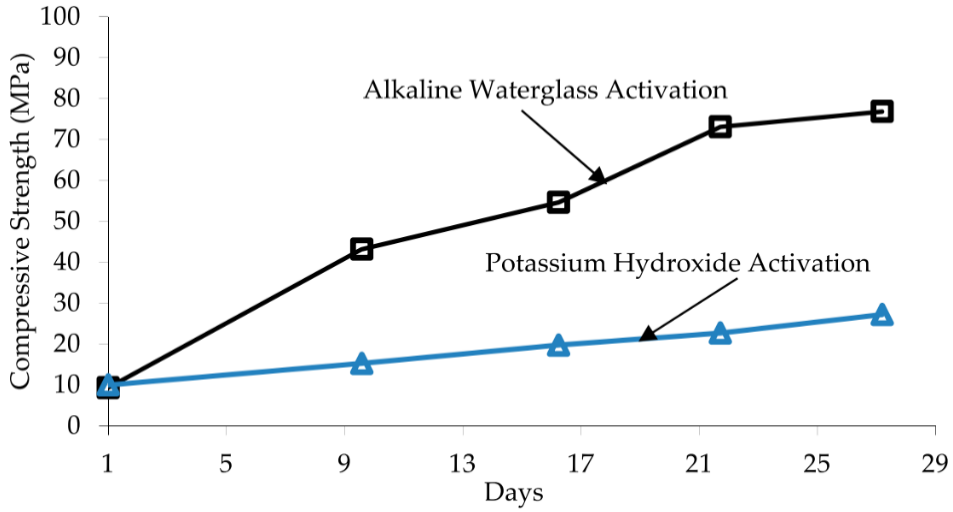

Figure I-34. Evolution of compressive strength for alkali-activated slag mortars activated by alkaline waterglass (sodium silicate) and potassium hydroxide [128,129]

Finally, Figure I-35 presents a comparison between different activators (sodium sulfate, sodium hydroxide, sodium carbonate and sodium silicate). Waterglass activation seemed to offer better mechanical properties for alkali-activated slag based materials than the use of sodium sulfate, sodium hydroxide and sodium carbonate [130]. Therefore, the anionic component of the activator has a significant effect on the properties of the binder. However, the main problem of waterglass activation is the cost and the difficulty of use (viscosity, corrosive properties, etc.), which currently favor the development of sodium carbonate and sodium sulfate but reducing the mechanical strength of the binder in early ages.

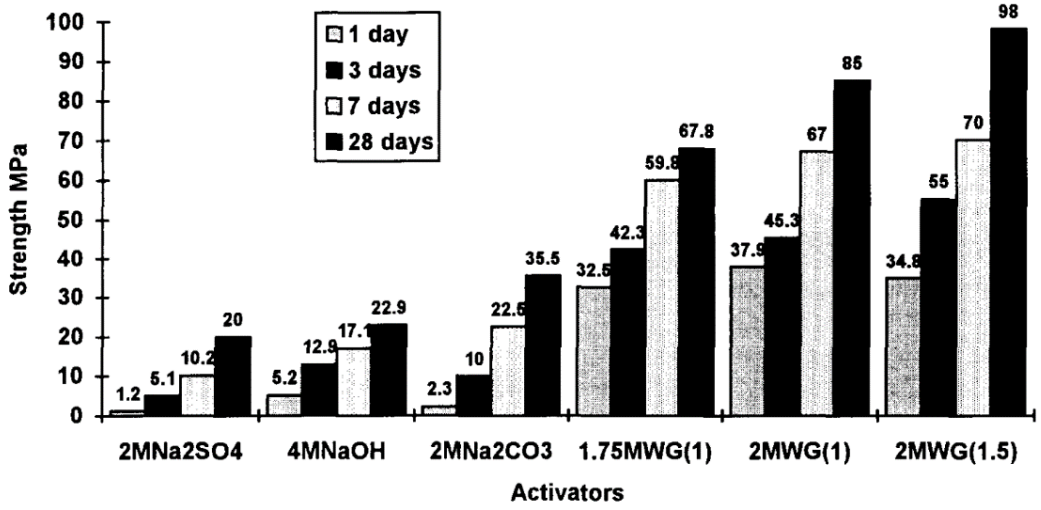

Figure I-35. Comparison of the strength development at 1, 3, 7 and 28 days of slag activated by different activators (sodium sulfate, sodium hydroxide, sodium carbonate and waterglass) [130]

The literature reported that the hydration process of activated slag is carried out by dissolution and precipitation mechanisms at early stages of the hydration [121]. Regardless the nature of the activator, the main hydration product resulting from the alkaline activation of slag is calcium silicate hydrate (C-S-H) [121,131,132]. Such phase is identified by its gel-like form and its lower Ca/Si ratio (typically 0.9-1.2) compared to C-(A)-S-H found in Portland cement [118,132]. Hydrotalcite is also one of the hydrated products issued from the release of magnesium from slag into the pore solution [121].

Generally, slag presents higher aluminum content compared to Portland cement. The presence of high aluminum amounts results in the substitution of bridging silicon by aluminum [62,121,132,133]. In addition, aluminum also could be present in AFm phases (e.g. C_4AH_{13}) intermixed with C-S-H gel [121]. Portlandite was not detected in such binders since its formation participates in the activation of slag and results in the formation of more calcium silicate hydrate [121].

Curing

Several studies were interested in understanding the impact of the type and duration of the curing period on the hydration process of alkali-activated slag and in particular on the development of mechanical strength on the short- and long-terms [121,134–139].

The intermitting curing between air and water was argued to create a denser microstructure and a higher mechanical strength at 28 days than air curing or continuous water curing. Curing AAS pastes in oven with air circulation at 40-50°C led to the loss of bound water and the decomposition of the C-S-H gel.

Another study was carried out on mortars composed of slag and Portland cement and compared to plain Portland mortars in terms of effect of curing temperature on strength development. The results have shown that the increase in curing temperature from 20 to 50°C accelerated the strength development and the setting time of slag-based mortars [137].

Curing AAS concrete at temperatures between 7 and 15°C did not affect the long term strength but reduced the early ages mechanical strength, delayed the setting time and delayed the shrinkage and cracking of the material [136].

A study has shown that, after 3 days of submerging in water, curing AAS specimens at 45°C produced higher mechanical resistance at 28 days compared to specimens cured at ambient temperature (22°C) [138].

A study carried out on AAS with substitution rate of 5, 10 and 15% with SF concrete specimens in order to investigate the impact of curing nature on the properties of the material. Figure I-36 showed that curing the specimens in water significantly improved the mechanical strength of the materials 90 days while no major difference was observed at 28 days [140].

In addition, the increase in temperature for curing AAS materials showed that at 14 days at 80°C the crystallinity of C-S-H was better than at 15 months at 20°C [121].

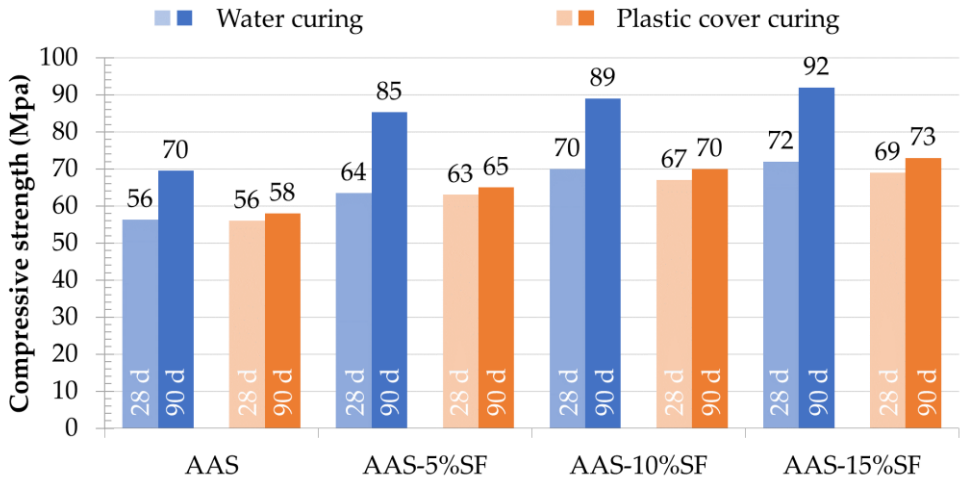

Figure I-36. Effect of type of curing at 28 and 90 days on the compressive strength of plain AAS and AAS substituted with silica fume at the rate of 5, 10 and 15 wt.% [140]

Durability

- **Microstructure and evolution of porosity**

AAS concretes endure autogenous shrinkage (self-desiccation) for longer periods, than OPC concretes, going up to 91 days [141]. Such shrinkage could lead to higher risks of cracks formation which could lead to the penetration of exterior chemical aggressive agents; hence,

lowering the durability of the material. It was proven that adding 15% of SF to AAS concrete decreases the autogenous shrinkage [141]. In addition to SF, fly ash could be used to reduce drying shrinkage, although replacing slag with silica fumes (at 10%) was found to be optimum in terms of shrinkage and compressive strength compared to a replacement by fly ash at 20% or 40%, as shown in Figure I-37 [142].

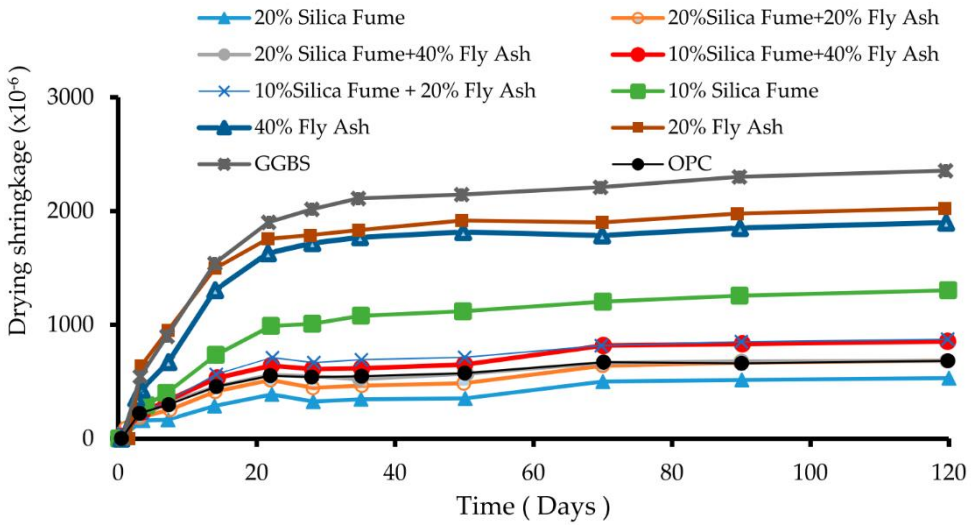

Figure I-37. Evolution of the drying shrinkage over time for simple, binary and ternary alkali-activated materials composed of slag, silica fumes and fly ash [129], adapted from [142]

Another study showed that adding calcium hydroxide to AAS mixture decreases the autogenous and drying shrinkage of the concrete, however, higher hydration rates were observed in the first 120 hours which could lead to increase the plastic shrinkage of the binder [143].

- **Sulfate attack**

A study compared the resistance of alkali-activated slag and Portland concretes to sulfate attack by immersion in 5% of magnesium sulfate and 5% of sodium sulfate [144]. AAS showed a higher resistance in terms of mechanical loss with only 17% and 23% compared to 25% and 37 for OPC in sodium sulfate and magnesium sulfate solutions respectively. In addition, the sulfate reaction with AAS matrix resulted only in the formation of gypsum while it produced gypsum and ettringite in the case of OPC. The absence of secondary precipitation of expansive ettringite in AAS led to decrease the cracking of the material; thus, slowing down the sulfate penetration.

Another study compared the sulfate resistance of sodium silicate activated slag to CEM II (Portland-slag cement) after 28 days of curing [122]. The authors attributed the higher resistance of AAS compared to Portland-based material to: (i) the lower permeability of the AAS microstructure which led to the decrease of the amount of sulfate diffused into the matrix [145]; (ii) the absence of portlandite which dissolves at pH lower than 12 while the pH of the aggressive solution was always kept below 12; (iii) the higher susceptibility of AAS to carbonation which could improve its resistance to sulfate attack by forming a calcium carbonate layer on the surface which limits the ingress of sulfate [146–148]; (iv) the less

availability of aluminum which is bounded in C-(A)-S-H instead of unreacted C_3A in Portland based systems, resulting in the absence of secondary expansive ettringite.

- **Acid attack**

The mechanisms of acid attack are different than sulfate or chloride attack. In an acid attack, both anion and cation have a significant role on the deterioration process, as explained in section 1.5 of this chapter on OPC and CAC materials. The literature paid attention to the durability of AAS in sulfate and acidic (nitric, acetic, and citric) environments separately [123,149]. Very few works were carried out on AAS exposed to sulfuric acid attack, and in particular in sewer conditions.

In the same curing conditions, Madhuri and Rao have concluded that alkali-activated slag concretes exhibited lower deteriorated depth, less mass loss and higher residual mechanical strength after exposure to sulfuric acid attack compared to OPC [150]. However, they highlighted that several parameters are critical in optimizing the mix designs of AAS; such as the curing temperature, activator-to-slag ratio and sodium silicate to sodium hydroxide ratio in the activator.

Xie et al showed that alkali-activated concrete (AAC) (made of 80%-20% slag-FA) had a higher resistance to biogenic sulfuric acid than ordinary Portland concrete [151]. Such performance was attributed mainly to the less deterioration of C-A-S-H compared to portlandite and C-S-H in OPC system which led to lower amount of leached calcium and less overall mass loss of the material, as seen in Figure I-38. Generally, C-S-H or C-(A)-S-H produced in AAS hydration has a lower basicity and a higher degree of crystallinity than C-S-H formed in OPC hydration, which could implies an increase in the chemical resistance of the C-S-H in AAS materials [152]. Moreover, while gypsum was detected in both materials as the main deterioration phase, it was formed in significantly higher amounts in OPC than in AAC.

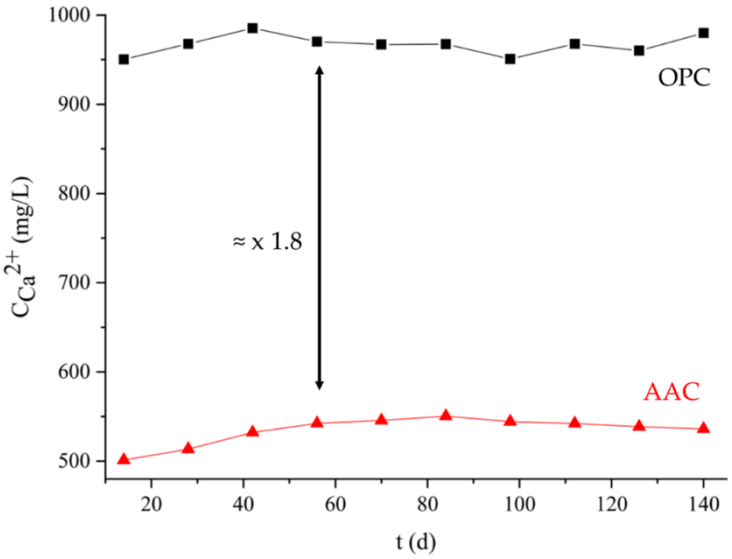

Figure I-38. Evolution of calcium leaching from ordinary Portland concrete (OPC) and alkali-activated concrete (AAC) exposed to biogenic sulfuric acid attack. Note that the first two weeks were not shown due to the low amount of leached calcium (time needed for bacteria to develop on the surface of the materials) [151]

Another study consisted of comparing the behavior of AAS and OPC to various type of acid attack (nitric, chlorohydric, sulfuric and acetic) [153]. Bernal et al showed that the compressive strength of OPC and AAS presented similar behaviors but with different extent. Figure I-39 shows that after 30 days of exposure to sulfuric acid solution (pH maintained at 3), the compressive strength of AAS did not vary much compared to AAS immersed in water. At 90 days of exposure, a slight decrease in the mechanical strength was detected but at 150 days a significant increase of strength was recorded.

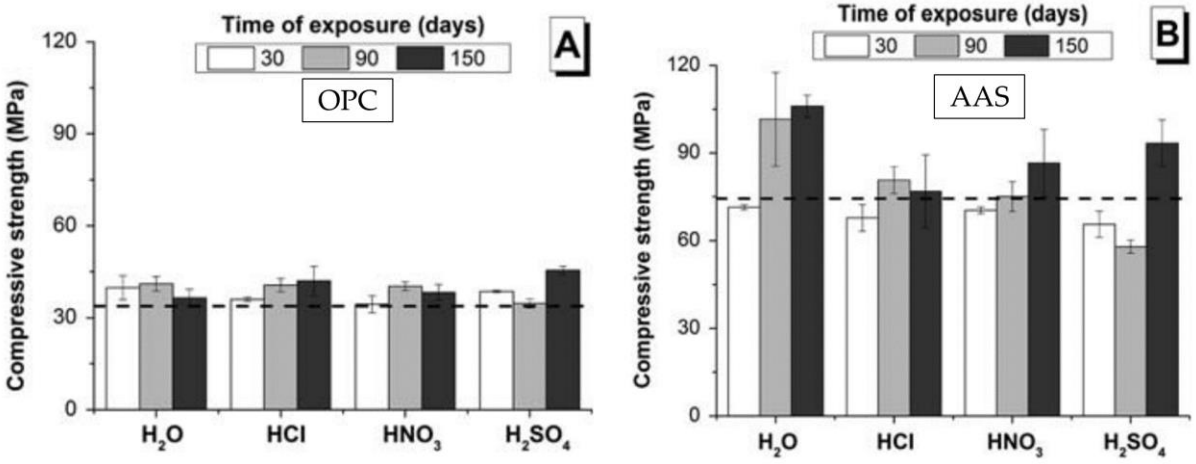

Figure I-39. Compressive strength measured after 30, 90 and 150 days of immersion in H_2O, HCl, HNO_3 and H_2SO_4 of (A) OPC and (B) AAS [153]

Such behavior was correlated to the low concentrations of sulfate (pH 3) and the undersaturation of the pore solution with respect to gypsum precipitation, which led to the leaching of calcium and sodium instead of precipitating expansive products.

1.6.3.2. Geopolymers

Geopolymers (GP), a sub-family of alkali-activated materials, are obtained by activating an aluminosilicate source with a highly alkaline solution to obtain a material with analogous performances to Portland cement binders but with the advantage of reducing greenhouse emissions. However, geopolymers present a completely different chemical and mineralogical composition comparing to cementitious binders. In order to expand their applications, many authors have been interested in geopolymers and several research works were done for the purpose of using geopolymers as an alternative binder to conventional Portland cement.

Geopolymerization and polycondensation

The term "Geopolymer cement" was first used by Davidovits to imply a system which hardens in a room temperature when mixed with water and an alkali hydroxide or silicate solution [154]. Geopolymers are made of a network of $[SiO_4]^{4-}$ and $[AlO_4]^{5-}$ tetrahedral that are linked by sharing oxygen atoms (Figure I-40) which was called poly(sialate), according to Davidovits, with sialate is short for silicon-oxo-aluminate. The negative charge of $[AlO_4]^{5-}$ is compensated by the presence of positive ions – e.g. sodium or potassium – in the framework cavities [155,156].

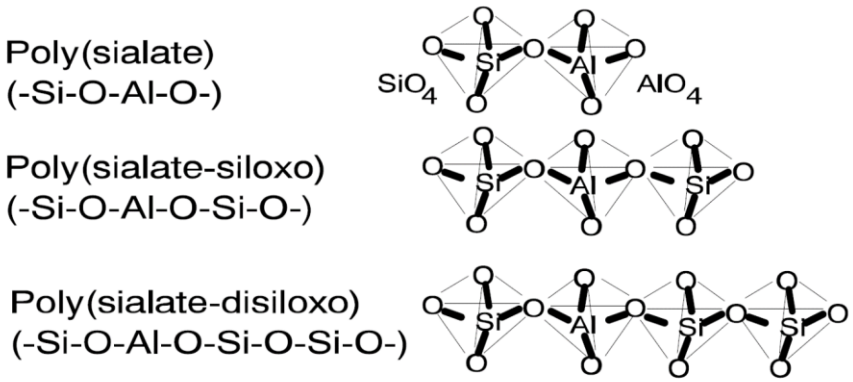

Figure I-40. Polymerization of geopolymers, according to Davidovits [155]

The polymerization mechanisms are still not very well understood. However, Glukhovsky was the first to present a model which based on three steps [157]: (a) destruction-coagulation; (b) coagulation-condensation; (c) condensation-crystallization. Later on, several authors have expanded and improved Glukhovsky theories which led to the highly simplified geopolymerization model proposed by Duxson et al. presented in Figure I-41.

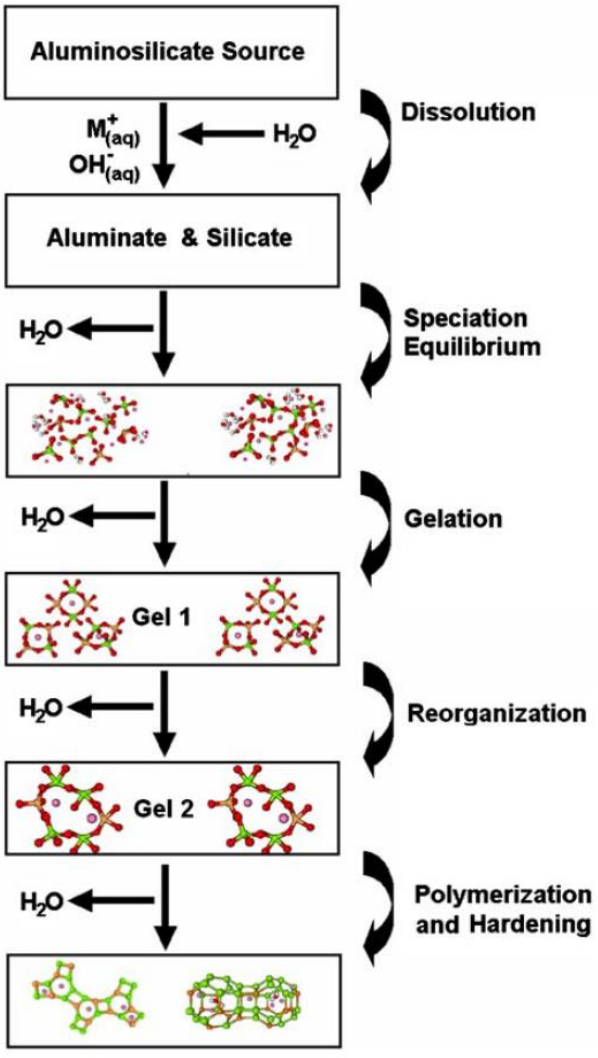

Figure I-41. A simplified conceptual model for the transformation of a solid aluminosilicate source to a synthetic alkali alum inosilicate (geopolymerization) [156]

This model can be summarized in 3 main phases [156]:

- Dissolution of the solid aluminosilicate source to form aluminate $Al(OH)_4$ and silicate $Si(OH)_4$
- Gelation and rearrangement of the aluminate and silicate to a more stable form.
- Polymerization and polycondensation of the system, yielding to form Si-O-Si and Si-O-Al bonds

Geopolymers properties could differ widely (high compressive strength, fast or slow setting, fire resistance and acid resistance). However, these characteristic depend highly on the raw materials and, hence, geopolymers must not be considered as an alternative solution for any problems but more like a solution which could be tailored for a certain application [156].

Durability

Since geopolymers are innovative binders which rely on alumina-silicate instead of calcium silicate hydrates bonds, their nanostructure is very different from ordinary cements. The low calcium content and the absence of conventional phases, such as portlandite and C-S-H, led to different degradation mechanisms compared to OPC. On one hand, OPC's degradation consists of decreasing the pH of the interstitial solution in the concrete resulting in the destabilization of portlandite and C-S-H. The dissolution of such phases generates strength loss and cohesion failure. However, portlandite and C-S-H contains high amounts of calcium which gets leached during the acid attack and could form expansive products, gypsum and/or ettringite with the counter-diffusion of sulfate ions. On the other hand, Geopolymers' degradation mechanisms consist of two steps; the first step is the ion exchange between the acid proton (H^+) from the solution and the charge compensating cations (Na^+ or K^+). This step is also accompanied by an electrophilic attack on the Si-O-Al bonds by the acid leading to the release of Al tetrahedral from the framework. According to the literature, the second step depends highly on the concentration of sulfate – hence, the pH – in the aggressive solution. The leached Ca ions may encounter sulfate ions, coming from the solution, to form gypsum. However, gypsum precipitation has been observed in the degraded zone at high acid concentration (pH ≈ 1), at the degradation front at moderate acid concentration (pH ≈ 2) and no gypsum formation was observed at low acid concentration (pH ≈ 3) [158].

The resistance of different geopolymers to acid attack – and in particular sulfuric acid attack – have been studied in the literature. For instance, Davidovits reported that rock-based geopolymers – made of metakaolin, slag and volcanic tuffs – suffered from a mass loss of only 0.1% per day when immersed in 10%H_2SO_4 solution [154]. Bakharev compared OPC, OPC+FA and FA-based geopolymers with different activators (NaOH, mix of NaOH and KOH, Na_2SiO_2) using an immersion test for 150 days with a sulfuric acid solution at pH ≈ 0.8. The results showed that geopolymers based binders had a better resistance than OPC and OPC+FA which suffered from severe deterioration after only 1 month of exposure [159]. Figure I-42 shows the weight changes of the OPC, OPC+FA and the different geopolymers after 150 days

of immersion into a 5% sulfuric acid solution. The deterioration of these geopolymers was linked to the depolymerization of the alumina-silicate and the formation of new amorphous/crystallized phase depending on the nature of the geopolymer formulation.

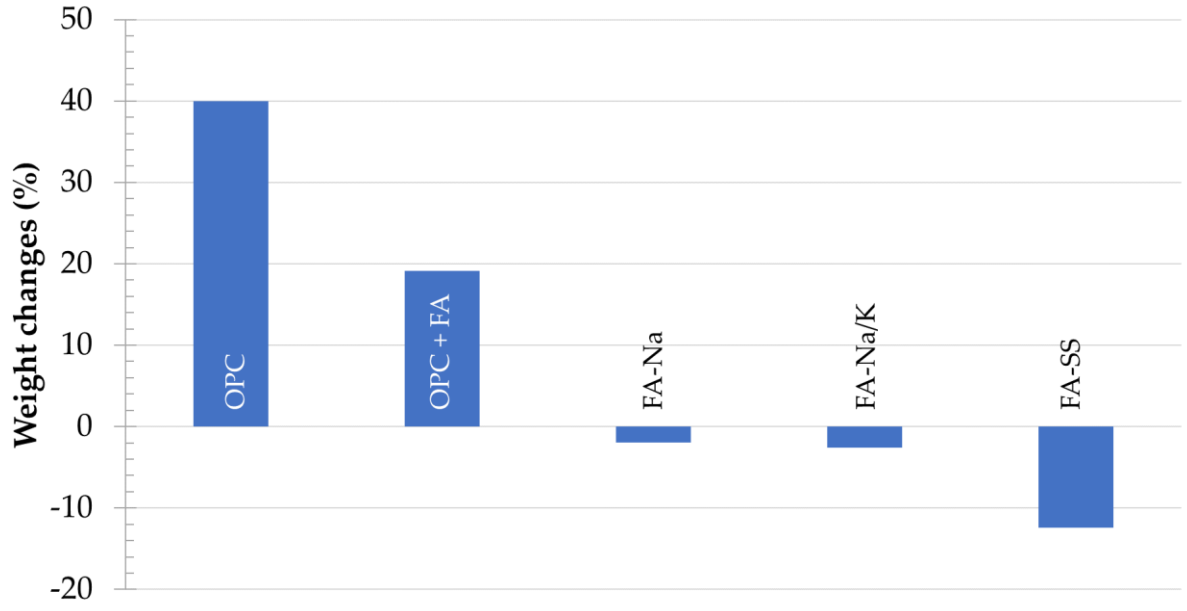

Figure I-42. Weight changes of different binders immersed into 5% sulfuric acid solution [159]. OPC: ordinary Portland cement; FA: fly ash; FA-Na: fly ash-based geopolymer activated by NaOH; FA-Na/K: fly ash-based geopolymer activated by a mix of NaOH and KOH; FA-SS: fly ash-based geopolymer activated by sodium silicate

Song et al. exposed fly-ash based geopolymers concrete and an OPC-based control concrete to a 10%H_2SO_4 solution. Figure I-43 shows that, only after 28 days, the control specimen has suffered from intense degradation while the geopolymer-based concretes were remained structurally intact in a 10% H_2SO_4 solution after 56 days [160].

Figure I-43. The concrete specimens exposed to 10% H_2SO_4 (Left: Control concrete after 28 days; Middle and Right : FA-based geopolymer concretes after 56 days) [160]

Moreover, the mass loss recorded for geopolymer concretes and the control specimen is shown on Figure I-44. Geopolymer concretes had a very low mass loss (less than 3%) while the OPC-based concrete has suffered from a significant mass loss up to 41% only after 28 days of immersion into sulfuric acid.

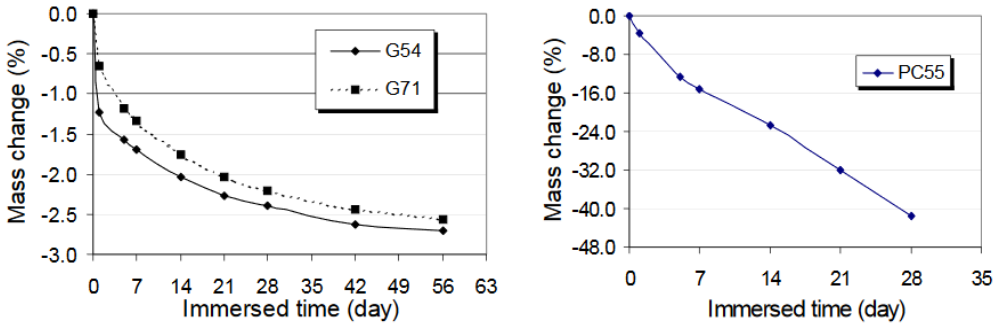

Figure I-44. Mass loss of concrete specimens exposed to 10% H_2SO_4; Left: Geopolymers concretes; Right: OPC concrete [160]

More data were published on gypsum precipitation during a sulfuric acid attack at different pH (1, 2 and 3) on fly ash and slag based geopolymer [161]. At pH 1, first signs of degradation were significant expansive of the specimens with a hard corroded layer. Gypsum was observed in the degraded layer but it was not considered as the main responsible of the specimens' swelling. After 90 days of exposure to the aggressive solution, the total expansion was only 7%. It was proposed that the hard – and difficult to remove – corroded zone could provide a protective layer which might result in an inhibition of the acid attack. At pH 2, gypsum deposition was observed only in cracks in the deteriorated zone. The mechanisms, proposed by Allahverdi and Skvara, consisted of the leaching of soluble elements and the removal of tetrahedral aluminum until the formation of shrinkage cracks. When the cracks are wide enough, sulfate ions diffuse into the cracks and encounter the leaching calcium ions to form gypsum. It was suggested that gypsum deposition in the cracks might slow down the sulfuric acid attack. At pH 3, after 90 days of exposure, SEM observations coupled with EDS analysis showed no gypsum precipitation. However, the authors linked the attack mechanism to just the leaching of charge compensating cation (Ca or Na) and to the removal of tetrahedral aluminum. Figure I-45 shows SEM observations for the same geopolymer under sulfuric acid attack at pH 1,2 and 3, showing the presence of gypsum in the degraded zone for pH 1, in the microcracks for pH 2 and the absence of gypsum deposition for pH 3.

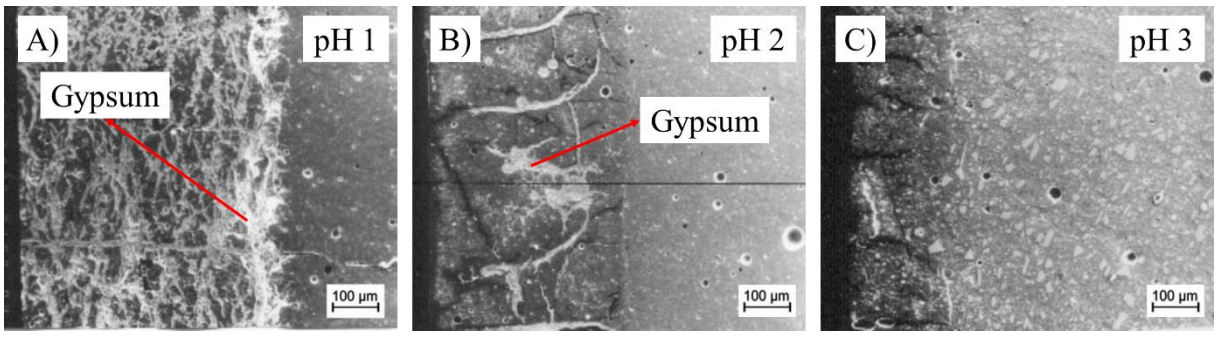

Figure I-45. Corroded layer and gypsum precipitation after 60 days of exposure to sulfuric acid solution at (A) pH 1 (B) pH 2 (C) pH 3 [161]

In the end, geopolymer-based binders had a better resistance to sulfuric acid compared to classic ordinary cements. The better performance is related to the different nanostructure of the geopolymers and the degradation mechanisms. However, the data in the literature were

always based on chemical immersion tests using sulfuric acid and, thus, the potential interaction between geopolymers and microorganisms is neglected.

1.7. SUMMARY OF THE BEHAVIOR OF VARIOUS BINDERS IN ACIDIC ENVIRONMENTS

The previous part has discussed the performance of cementitious materials against sulfuric acid. Portland cement and calcium aluminate cement have been studied in both chemical and biological conditions using in-situ experiments and laboratory tests. CAC binders have proved their higher resistance to biogenic sulfuric attack in sewer conditions. It was suggested that the higher performance of CAC is due to its chemical and microstructural compositions and to its stifling impact on the microorganisms' activity. On the other hand, ordinary Portland cement has suffered from severe physical and chemical deteriorations based on the results obtained in different campaigns. Expansion and change in length of ordinary Portland cement specimens were observed in addition to microcracks that are principally due to precipitation of secondary expansive products such as gypsum and ettringite.

However, Portland cements blended with supplementary cementitious materials – slag, metakaolin, silica fume and fly ash – present a positive effect on the durability of the mix. The main impact of SCM was the decrease in calcium hydroxide content which is the most reactive phase of the Portland cement matrix. Moreover, denser structure and chemical and microstructural modifications were observed as well. Blended cements with SCM are known to resist better than plain Portland cement to sulfate attack but, on the other hand, their resistance against sulfuric acid is still debatable. Nevertheless, the majority of the authors in the literature [95,96,109–111,162,163] confirmed the better behavior of Portland cement when mixed with SCM against sulfuric acid. Nevertheless, the results obtained by these authors were based only on measurements of weight loss. Despite the positive impact on the durability of the OPC-SCM binders, their performance in sewer conditions was scarcely discussed in the literature with no solid results on their behavior or their alteration mechanisms as they incorporate a non-negligible amount of aluminum which was suggested to contribute to the stifling effect on the microorganisms.

Alkali-activated slag materials showed promising properties in terms of raw materials, hydration and durability. The low carbon footprint and reuse of industrial by-products are two essential parameters proving the environmental impact of implementing AAS in construction. The hydration of such binder is known to give high early mechanical strength by the early development of C-S-H and C-A-S-H. The incorporation of aluminum in C-A-S-H gives the mineralogical phases a slightly higher chemical resistance while reducing the amount of aluminum available for reaction with sulfate to form destructive expansive products, in the case of sulfate or sulfuric acid attack. Although the literature presented AAS as a material with a better resistance to sulfuric acid attack compared to Portland cement, several parameters must be considered in order to achieve such resistance, in particular the

curing period and temperature, the nature of the activator and the activator-to-slag ratio. The resistance of AAS to sewer conditions was not sufficiently tested in order to draw a clear conclusion regarding its resistance to such environments.

Furthermore, geopolymers industry showed great potential in terms of durability against sulfuric acid attack. Several tests were carried out and the results indicate the better performance of geopolymers in acidic environments [154,158–160]. Still, the durability tests consisted mainly of weight loss measurements and visual degradation, only few information were available on the degradation mechanisms at microscopic level. Moreover, the attack mechanisms of sulfuric acid on geopolymers were found depending on the concentration of sulfate in the aggressive solution as gypsum and/or other expansive products might precipitate in the binder's degraded zone due to the high concentration of sulfate in the solution.

Therefore, further chemical and microstructural analyses are needed to characterize the alteration mechanisms of these alternative cementitious matrixes under sulfuric acid attack (chemical and biological) and to understand the interaction mechanisms between the cementitious matrix and the microorganisms.

1.8. MODELING OF THE BIODETERIORATION OF CEMENTITIOUS MATERIALS IN SEWER CONDITIONS

The previous parts of the literature review showed the complexity of the biological attack on the cementitious materials in the sewer systems. Several parameters have key-roles in the deterioration of concrete; for instance, the environmental conditions, the microbial growth, the bio-chemical oxidation of sulfur (and/or other elements), the pH of the medium, the diffusion mechanisms of the acid, the dissolution/precipitation of cementitious phases, etc. All these parameters made it difficult to propose a simple model to represent the attack phenomena.

However, several authors worked on developing simple semi-empirical models to represent the biodeterioration phenomena [164–168]. Although these models offer an easy-to-use feature because of their simple mathematical equations, their application is mainly limited to very few types of materials (mainly PC and CAC) due to the high diversity in the properties of other materials and the different deterioration mechanisms which are difficult to model using simple equations.

In order to reconcile with the variability of the composition of the materials, chemical models were developed to reproduce the deterioration of the cementitious materials using reactive-transport modeling with chemical H_2SO_4 [169–171]. Such models were developed to include different complex phenomena, such as the evolution of the effective diffusion coefficient as function of the porosity and the evolution of the cementitious phases during the aggressive attack. Nevertheless, the results of such models, in some cases, underestimated the deterioration due to the differences in the production of sulfuric acid biologically (pH, acid

concentrations, acid neutralization, etc.). Hence, the interactions between the microorganisms and the cementitious materials should be considered.

Other authors worked on developing biological models including the evolution of the biofilm during the attack process [172]. The particularity of these models is the incorporation of additional parameters concerning the biofilm, such as the consumption rate of sulfur and the presence of oxygen and nutriments in the medium.

This section presents some of the numerical tools used to simulate the exposure of cement-based materials to sewer conditions. The advantages and disadvantages of the different models are also discussed with, if applicable, propositions for improvements.

1.8.1.Mathematical modeling

The prediction of the service life or the rate of the deterioration of concrete-based structures was a subject of interest for several mathematical models [164–168]. The mathematical models were mainly based on fitting mathematical equations to the observations and the results obtained from experimental works.

One mathematical model, called Life Factor Method (LFM), was used at the university of Cape-Town to link the production of hydrogen sulfide in the sewers to the deterioration of the cementitious material by implementing a consumption rate of H_2S by concrete surface and by the equivalent alkalinity of the concrete (expressed as calcium carbonate) [164,165]. The original version of the LFM for biogenic acid attack on concrete in sewer networks was based on the semi-empirical approach proposed by Pomeroy [173] and is presented in **Eq.I-30** [164].

$$c = 11.4 \times k \times \frac{\emptyset_{sw}}{A} \quad \textbf{Eq.I-30}$$

With c: annual corrosion rate (mm/year); k: efficiency factor (<1); $\emptyset_{sw}$: rate of H_2S absorption in the water film at the concrete surface ($gH_2S\text{-}S/m^2/h$); A: equivalent alkalinity of the concrete material, expressed as calcium carbonate ($gCaCO_3$/gConcrete).

Such model was improved over the years to extend its use for materials other than Portland cement by including other factors, such as alkalinity parameters other than $CaCO_3$: portlandite(CH), aluminum hydroxide (AH_3) and iron oxyhydroxide (FeO(OH)) and aluminum and iron relative contents to calcium [174]. The new and improved version of the model is presented in **Eq.I-31** and **Eq.I-32**.

$$C_{avg,t} = \frac{0.57}{(RC_{eff})^{1.49}} \quad \textbf{Eq.I-31}$$

$$RC_{eff} = CaCO_{3\,eq,agg} + CH_{eq,CAC} + \frac{CH_{eq,PC}^{-1}}{100} + AH_{3\,eq,binder} + FeO(OH)_{eq,binder} + \frac{Al}{Ca} + \frac{Fe}{Ca} \quad \textbf{Eq.I-32}$$

Note that $CH_{eq,PC}^{-1}$ is inversed due to the inverse proportionality between the amount of portlandite and the deterioration rate in Portland cement.

Another model was developed by a research team at the University of Newcastle in Australia to predict the loss of concrete due to deterioration by exposure to sewer conditions [166,167]. This model was even simpler than the LFM model and was based mainly on two parameters:

(i) t_i: initial time at which the deterioration of concrete starts

(ii) r: a deterioration rate

The initial time and the corrosion rate were determined based on experimental findings carried out on new and old (70 years) concrete specimens in aggressive sewer environments. The experimental results showed three stages of deterioration as function of the exposure time, the evolution of pH and the deterioration rate. During these 3 stages, the authors have determined two behaviors of the material. Initially, the material does not suffer from any significant mass loss, while starting from a certain point where the pH decreases into acidic values, a constant deterioration rate was detected. The values of the two parameters were then determined and were as follows: t_i: 0.9 years and the r = 12 mm/year. Figure I-46 shows the bilinear behavior of the material as a function of exposure time and an example of the application of this bilinear model on concrete with a cover thickness of 100 mm.

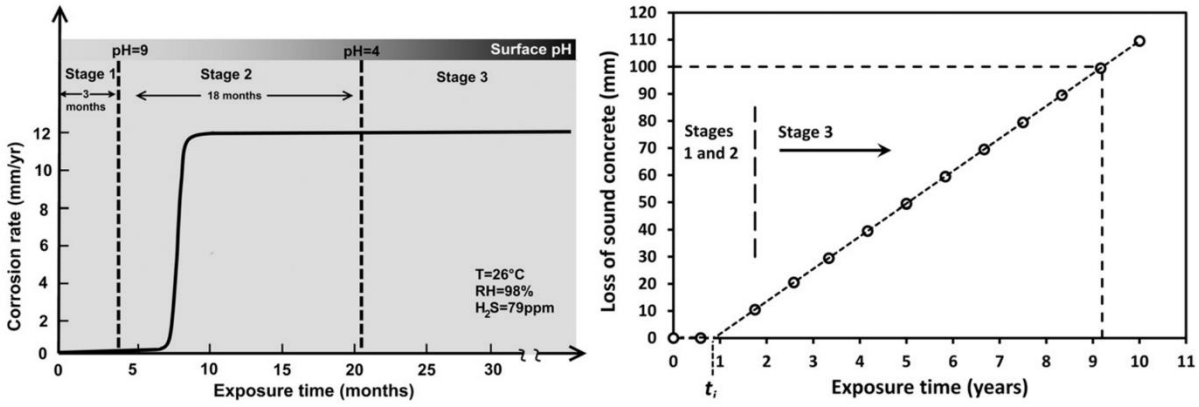

Figure I-46. Left: Bilinear approach to represent the corrosion rate of concrete in highly aggressive exposure conditions as function of exposure time; Right: Prediction of the service life of a concrete-based sewer pipe with a concrete cover of 100mm-thick using the proposed bilinear model in [166]

Lastly, a single model was used to represent the experimental deteriorated depth of concrete specimens composed of calcium aluminate cement with CAC clinker aggregate [168]. The concrete specimens were exposed into two different sewer sites with different aggressive conditions in terms of H_2S concentrations (0-650 ppm), temperature (17-30°C) and RH (85-99 %). The depth of deterioration was obtained from the difference between the initial thickness of the specimens and the thickness after deterioration. While the environmental conditions (H_2S concentration, temperature and RH) did not present a clear and direct correlation to the deterioration depth, the authors found that the concentration of the acid was in accordance with the aggressiveness of the sewers and with the deterioration depth. A model was developed to consider such parameter in the prediction of the deterioration depth and is presented in **Eq.I-33**.

$$D = 0.19 \times [H^+]^{0.21} \times t^{0.37} \qquad \textbf{Eq.I-33}$$

With D: predicted deteriorated depth (mm); [H^+]: concentration of acid (mmoles/gConcrete); t: time of exposure (days).

Figure I-47 shows that the fitting of the predicted and measured deterioration depths resulted in a regression correlation (R^2) of 0.84. However, this model was developed based only on calcium aluminate cement. The chemical and mineralogical nature of the materials could have an impact on the production of the acid, which was not taken into account by this model. Moreover, as presented in section 1.6.2.2, sulfuric acid could be produced inside the cementitious matrix and resulting into more severe deterioration. Such model shows a promising results but still further improvements are to be done in order to obtain a more complete model which considers both the aggressive environment and the material.

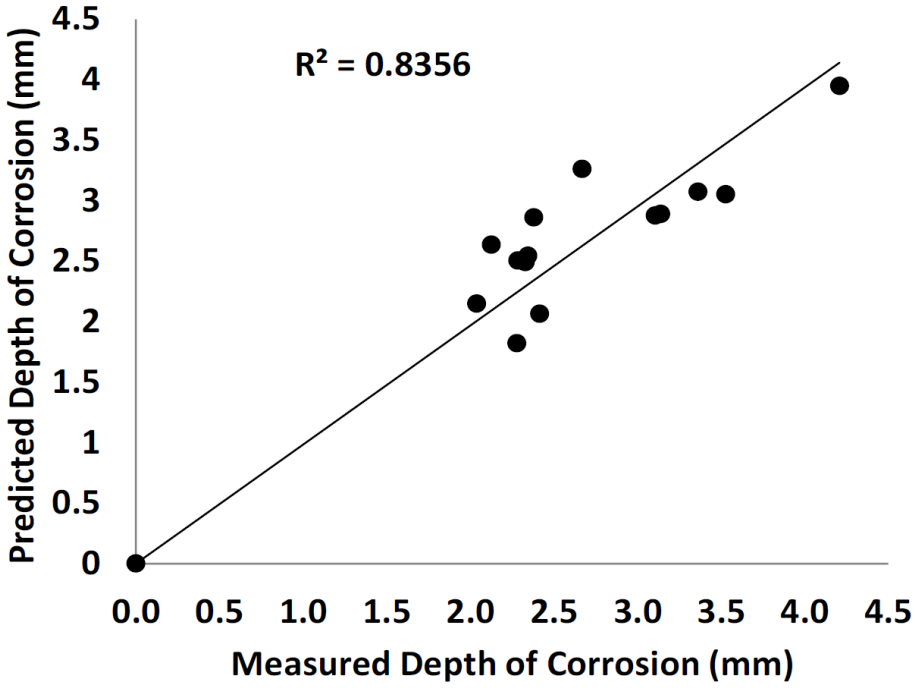

Figure I-47. Comparison between the predicted depth of deterioration and the experimentally measured depth of deterioration in order to evaluate the representativeness of the model [168]

1.8.2.Chemical modeling

Different models were proposed in the literature to simulate a sulfuric acid attack in the sewer conditions on cementitious materials. One of these models was based mainly on the kinetics and stoichiometry of sulfide oxidation by the biofilm in aerobic/anaerobic conditions [175]. A rate equation was developed to estimate the sulfide production by the biofilms as a function of the temperature. However, this model did not tackle the attack on the cementitious materials but highlighted the importance of several parameters linked to the biofilm evolution in the attack process.

A reactive-transport model (HYTEC) was used in previous studies to establish numerical modeling of acid attack on concrete. De Windt and Devillers have simulated a bioleaching test where ordinary Portland cement pastes were exposed to organic acids (acetic, butyric, lactic

and oxalic) [176]. Figure I-48 shows the complexation of calcium and aluminum by organic acids was proposed in the study based on the pH evolution. Since the chemical and thermodynamic stability of the phases – Al-bearing phases in particular – might be a key factor in the resistance of the different binders to biogenic acid attack, these results could be reproduced using sulfuric acid instead of organic acids in order to evaluate the complexation of calcium and aluminum in sewer conditions. However, the equilibrium between the solid phases and the diffusion of the different species were not studied in particular.

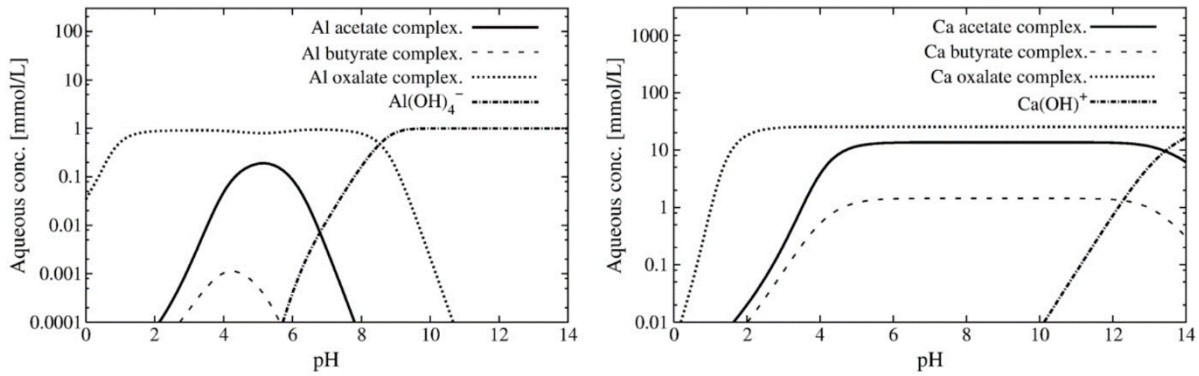

Figure I-48. Aluminum complexation by organic acids as a function of pH at 25°C [176]

Yuan et al. adapted a model, which answered these two specific points by including the transport of aqueous species. Also, the swelling of gypsum has been modeled by a change in porosity during the degradation. The model was used firstly to predict the behavior of Portland cement mortars subjected to H_2SO_4 solution, then extended to predict the degraded depth of several cementitious formulation – such as CEM I, CEM III, CEM IV, CEM V and CAC – as carried out by Grandclerc et al. [170,171].

One dimensional model was used to simulate the attack process in sewer conditions with a concentration of sulfuric acid of 10^{-1} mol/L. The porosity in this model was calculated from the evolution of the volume of the solid phases during the attack, following **Eq.I-34**.

$$\Delta\emptyset = -\Delta \boldsymbol{V}_{\boldsymbol{solid}} \qquad \textbf{Eq.I-34}$$

The model, coupling the chemical equilibrium with the transport of aqueous species, was governed by a global mass balance equation and electeroneutrality equation. However, the stability of the solid phase was described by a dependence of the saturation index of the phase to the saturation indexes of portlandite and gibbsite and to the activity of the sulfuric acid (equal to its concentration). This dependence was considered since portlandite, gibbsite and sulfuric acid were considered as primary variables, following the Gibbs phase rule [171].

The results obtained on OPC and CAC are shown on Figure I-49. The profiles of the solid phases evolved during the attack and after a simulation of 1 year of exposure to H_2SO_4 at extreme conditions; the graphs show a more severe deterioration for CAC compared to OPC. The deterioration of OPC led the dissolution of the matrix and the precipitation of gypsum on the surface with a very low amount of ettringite precipitated at the interface between the

degraded and the sound zones. On the other hand, the precipitation of ettringite was significantly higher in the case of CAC. Furthermore, AH_3 was found at the surface.

The released calcium ions during the attack shows a better resistance of CAC. Moreover, the porosity for CAC was completely filled in in the area where ettringite was precipitated (due to its high molar volume). Nevertheless, the experimental investigations showed that the precipitation of ettringite leads to micro-cracks in the cementitious matrix and hence, a higher porosity in such area.

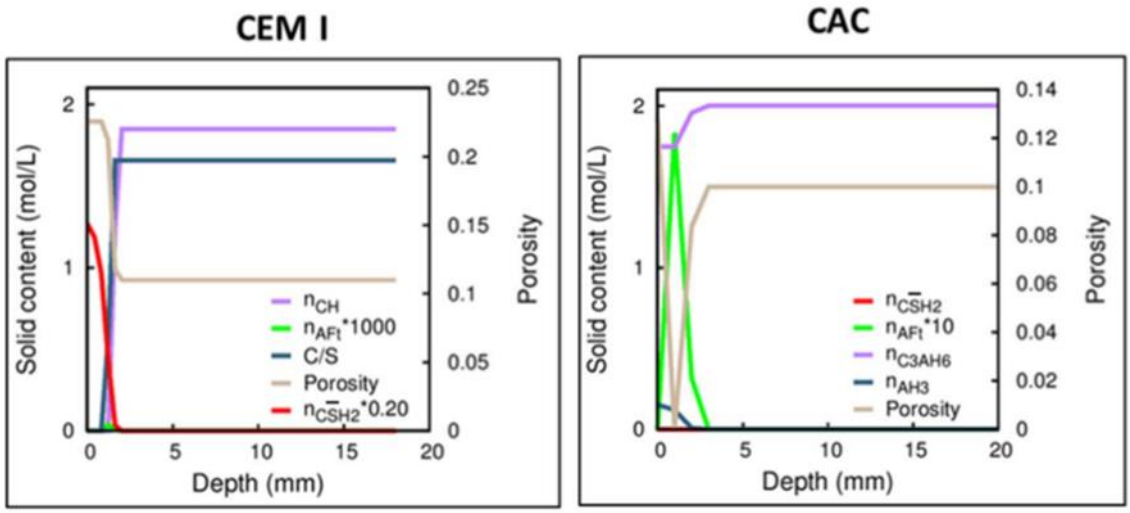

Figure I-49. Evolution of the solid phases for OPC and CAC after 1 year of exposure to acid attack using Grandclerc et al. model [171]

The model presented in Grandclerc et al. was a first step to propose a chemical model to reproduce the sulfuric acid attack in the sewer networks. However, the investigations demonstrate the better resistance of CAC compared to OPC, which is not the case in a purely chemical attack. Moreover, the swelling and cracking (mechanical model) should be taken into account to better represent the actual phenomena inside the cementitious matrix. Furthermore, the biofilm should be implemented in such models. The biofilm creates a different local conditions which are different from the conditions produced by a simple chemical attack. In addition, the biofilm evolves over time and in a heterogeneous way. One should know that the implementation of a bio-mechanical model in a reactive-transport model is not an easy task.

1.8.3.Biochemical modeling

A 1D numerical model was develop using Aquasim software to simulate the deterioration of cementitious materials exposed to sewer conditions [172]. This model considered two microbial populations (neutrophil and acidophil) responsible for acid production, acid/base kinetics reactions, diffusion of aqueous species based on modified Fick's law, dissolution and precipitation of cementitious phases and evolution of the local porosity. The development of this model was based on experimental results obtained from PC and CAC mortars exposed to a laboratory testing protocol aimed at reproducing sewer conditions.

Figure I-50 presents a schematic representation of the 1D biochemical model. The aggressive solution was composed of tetrathionate (a reduced sulfur source) which is oxidized by the sulfur-oxidizing activity, presented by a biofilm layer, to produce sulfuric acid.

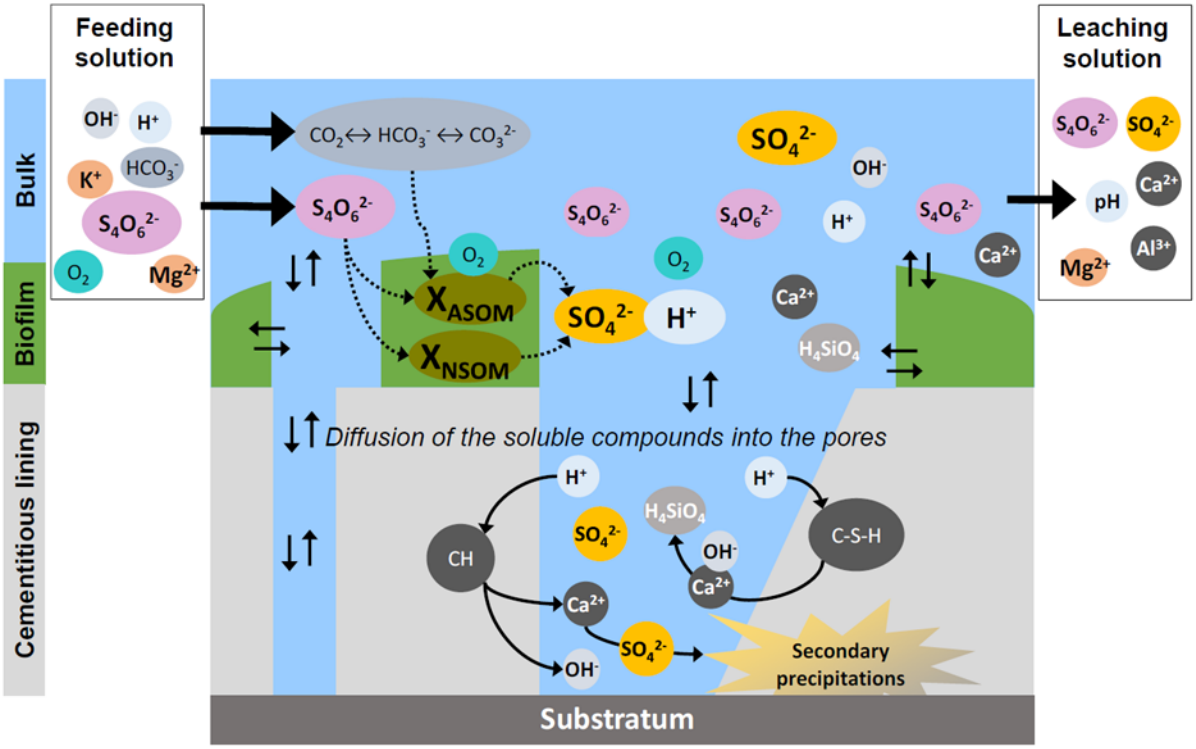

Figure I-50. The biochemical model considering the aggressive solution, a biofilm layer representing the sulfur-oxidizing activity and the cementitious materials [172]

This model reproduced the biological acid production and allowed the quantification of the composition of the leached solution and the evaluation of the mineralogical composition inside the cement matrix (Figure I-51). Moreover, the impact of the materials in terms of pH evolution on the microbial activity was highlighted.

Finally, an underestimation of the total leached amounts of calcium and aluminum was observed and was due to the consideration of anhydrous phases as inert. In addition, the absence of the possibility to couple the Aquasim model with a robust thermodynamic database made the work carried out to enter manually all the data very laborious and would need to be updated regularly.

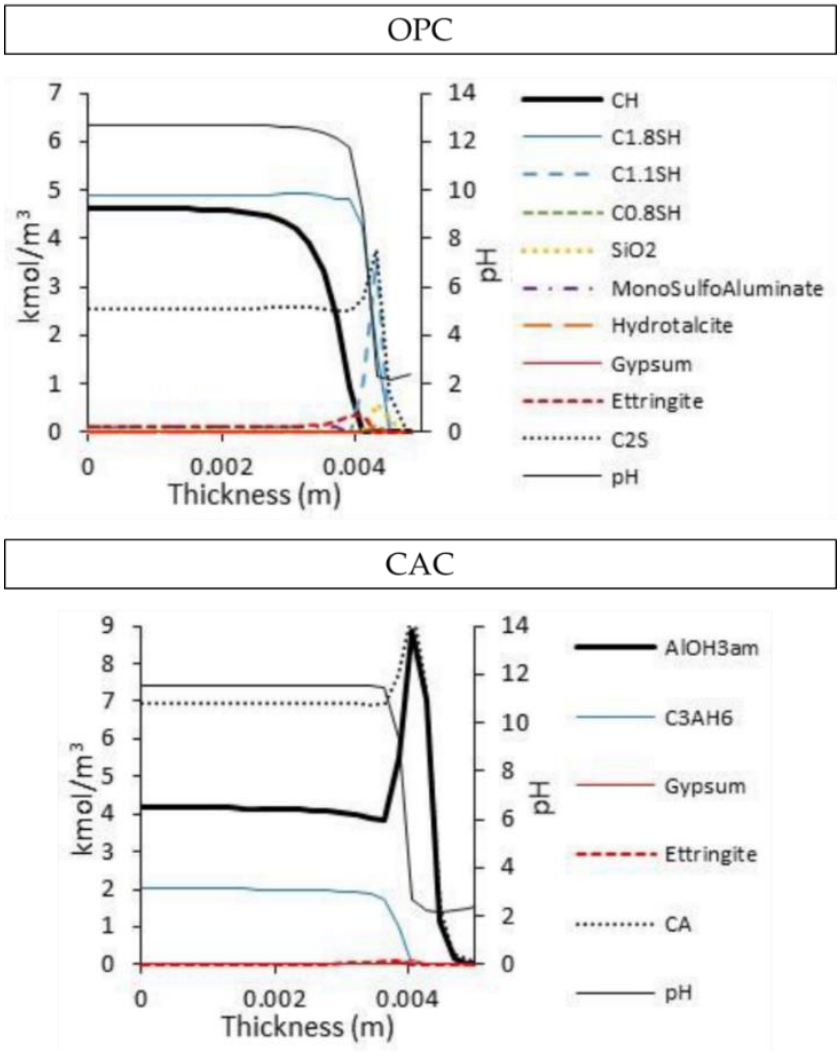

Figure I-51. Simulation results showing the profile of the solid phases for OPC and CAC after 100 days of exposure to biogenic sulfuric acid using the biochemical model by [172]

1.9. CONCLUSION

The sewer environment is known to be aggressive to cementitious materials used in the construction of pipes. The biodegradation constitutes about 10% of the deterioration and leads to the loss of mechanical strength and, in some cases, the collapse of the structure. The deterioration mechanisms are a combination of chemical and biological attacks on the concrete. At first, an abiotic attack is initiated by H_2S and CO_2 leading to a drop in the pH to the limits allowing the development of microorganisms. Thereafter, bacterium growth takes place and start oxidizing the sulfur species and producing sulfuric acid that starts to attack the cementitious matrix.

In-situ experimental campaigns in different countries and in different conditions showed that calcium aluminate cements had a better resistance than Portland cements to biogenic sulfuric acid attacks. Nevertheless, these results were based mainly on weight loss measurements which can sometimes not be adequate as secondary phases – such as gypsum and/or ettringite

– might precipitate leading to an increase in specimens' weight. Moreover, siliceous aggregates resisted to the acid attack while calcareous aggregates were dissolved.

The degradation mechanisms of ordinary Portland cement by sulfuric acid can be resumed into 2 steps. The first step consists of the penetration of acid ions inside the cementitious matrix leading to a decrease in the pH. Calcium hydroxide (portlandite) starts to dissolve, followed by calcium silicate hydrates (C-S-H) and calcium monosulfoaluminate (AFm) leading to a release of Ca^{2+} and Al^{3+} ions. The second step is where the interstitial solution is rich in Ca^{2+}, Al^{3+} (from the matrix) and SO_4^{2-} (from the acid), expansive products such as gypsum and ettringite start to precipitate (oversaturation conditions). The formation of such products could generate microcracks leading to a deeper penetration of the sulfuric acid.

On the other hand, calcium aluminate cements showed a better performance against biogenic sulfuric acid due to mainly their chemical and microstructural compositions. However, an interaction between the cementitious material and the biofilm was observed. The number of cells measured on CAC specimens in live conditions was found to be lower than OPC specimens. Several authors have attributed this behavior to the buffer effect of AH_3 gel formed during the acidic attack and to the stifling effect coming from Al^{3+} on the microorganisms leading to a less production of sulfuric acid and a more durable material.

In order to find alternative solutions to Portland cement for this field of application, blended cements with supplementary cementitious materials were studied as they are known to have a better resistance than Portland cements in acidic environments. The better performance of these blended cements can be attributed to (i) the decrease in calcium hydroxide content which is the most reactive phase of Portland cement; (ii) the decrease in the pores' size and hence reducing the transportation of aggressive ions into the cementitious matrix; (iii) the formation of additional C-S-H phases with low C/S, favoring the incorporation of Al in the C-S-H systems; (iv) in the case of Al-rich SCM , the formation of calcium aluminate hydrates which are believed to be the reason behind the performance of CAC binders in sewerage conditions; (v) generally, lower diffusion properties.

Innovative materials could also be potentially resistant to acidic attacks, such as alkali-activated slag and geopolymers. The literature confirms the better resistance of geopolymers compared to OPC and OPC with SCM against sulfuric acid attack due to their different nanostructure and the absence of certain easily leached phases, such as portlandite. Alkali-activated slag is made mainly from slag activated by an alkaline solution. The main hydrated phases, C-A-S-H and hydrotalcite, presented higher chemical resistance in acidic environments compared to portlandite and C-S-H found in OPC. While the few studies carried out on AAS exposed to sulfuric acid attack showed a higher performance of AAS compared to OPC, further investigations are needed in order to evaluate the behavior of AAS exposed to sewer-like conditions.

This state-of-the-art report summarizes the actual knowledge on the behavior of ordinary Portland cements and calcium aluminate cements subjected to biodegradation phenomena in

sewer networks. Also, it emphasizes the lack of information about the performance of Portland cements blended with supplementary cementitious materials, which could provide more economical, environmental-friendly and durable solutions than ordinary Portland cements, in these conditions. Hence, there is a necessity of testing such materials to improve the understanding of the bio-physico-chemical mechanisms taking place in the biodeterioration process as well as to progress in the comprehension of microorganisms-cementitious materials interaction mechanisms.

Chapter II

Materials and Methods

2. CHAPTER II – MATERIALS AND METHODS

Table of contents

2.1. INTRODUCTION

The literature review has highlighted the behavior of mainly two binders – Portland cement and calcium aluminate cement – in sewer environments. The attack by the microorganisms, developed on the surface of the materials, leads to severe and differentiated alteration depending on the nature of the cementitious matrices. While the deterioration mechanisms of PC and CAC were reported in the literature, little or no information concerning the performance of non-conventional binders – calcium sulfoaluminate, alkali-activated and others… – in such conditions were to be found. In addition, such innovative binders present low carbon footprint with different chemical and mineralogical composition as well as different physical properties compared to conventional materials.

Aluminum and iron were reported to play a potential key role in the deterioration processes of the cement-based materials. On the one hand, the influence of aluminum, present in CAC cements, is still not clear. The resistance of CAC was attributed mainly to its high aluminum content and to the resistance of the aluminum-bearing phases to the acid attack. Moreover, a potential inhibitory impact of aluminum on microbial activity has also been suggested. On the other hand, the resistance of iron-bearing phases was also suggested to be higher than conventional calcium-based phases, such as portlandite and calcium silicate hydrate. In addition, iron has been reported to be implicated in the microbial activities, in particular with *Acidithiobacciullus ferrooxidans* bacteria. Therefore, the behavior of aluminum and iron is still to be further investigated in order to better describe their influence on the deterioration processes.

This chapter presents the methods used to characterize the cementitious matrix before and after deterioration. The different studied materials are presented as well as the chemical and mineralogical composition of each material. Afterwards, the experimental protocol to evaluate the performance of the cement-based binders is presented from the casting process to the durability testing. Finally, the analytical methods used to monitor the materials' behavior during the testing period are presented at the end of this chapter.

2.2. CEMENTITIOUS MATERIALS

2.2.1. Composition of binders and mixture designs

Cementitious materials are widely employed in the sewer networks structure as they represent nearly 50% of materials used for canalization systems [4]. Cement-based materials can be categorized into 3 groups: cement paste (made of cement and water), mortars (cement, water and sand) and concrete (cement, water, sand and coarser aggregates).

Mortars present the advantage of studying, at the same time, the behavior of the cement matrix and sand, which allows the study of several physico-chemical properties, e.g. the transfer

phenomena and the interface transition zone. Moreover, while concrete is the most widely used form of cementitious materials in the sewers, the large amount and size of the aggregates as well as the possible disparities in the properties of the specimens could create a bias in the results, in particular for the study of the behavior of the binder. In this work, cement pastes were considered to focus mainly on the chemical resistance of the cementitious phases. The study of cement pastes facilitates the identification of different properties of the cementitious binders – for instance, the reactivity of the phases, the phase assemblage… – which could not be easily studied in mortar nor in concrete. However, an optimization of the mix designs for mortars/concrete using the studied cements will be necessary for applications in sewer networks.

Eleven binders were considered for testing their resistance against biodeterioration. The binders were categorized into 4 groups (Table II-1):

- Reference materials: Portland cement (PC) and calcium aluminate cement (CAC), the behavior of which has already been thoroughly studied in the literature
- Portland (PC)-based materials
- Calcium sulfoaluminate (CSA)-based materials
- Alkali-activated slag (AAS)-based materials

Six of the studied materials were composed of only one type of hydraulic binder (i.e. clinker, cement or slag). These materials were: Portland cement (PC), calcium aluminate cement (CAC), two sulfate-resistant PC (SR0 and SR3), calcium sulfoaluminate clinker (CSAC) and an alkali-activated slag (AAS). The other materials were composed of a mixture of a hydraulic binder (PC, CSAC or AAS) with mineral additives, such as: HardCem (noted H), bauxite (noted B), anhydrite (noted A) and gypsum (noted G); to form five additional binders: PCH, CSAA, CSAG, AASB and AASH.

Table II-1. Summary of the binders used in this study

Category	Reference materials	PC-based materials	CSA-based materials	AAS-based materials
Binder's reference	CAC PC	PCH SR0 SR3	CSAC CSAA CSAG	AAS AASB AASH

Table II-2 and Table II-3 present the chemical compositions of the binders and the mineral additives used in this study. The chemical compositions were determined by ICP-OES technique (**Appendix II-A**) at LMDC.

Table II-2. Chemical composition of the studied binders (in weight %)

		CAC	PC	PCH	SR0	SR3	CSAC	CSAA	CSAG	AAS	AASB	AASH
Oxides (wt.%)	SiO_2	5.37	20.00	21.98	21.30	20.47	7.86	6.60	6.40	34.68	28.55	34.32
	CaO	38.10	66.20	58.22	64.95	65.05	42.69	41.57	40.69	41.54	34.48	39.13
	Al_2O_3	51.20	4.85	4.89	3.62	3.57	29.26	24.46	23.33	9.83	18.04	9.34
	Fe_2O_3	1.88	2.64	8.84	5.80	4.88	11.31	9.37	9.29	0.28	4.21	4.21
	K_2O	0.32	0.00	0.19	0.67	0.65	0.18	0.15	0.14	0.35	0.31	0.43
	Na_2O	0.06	0.14	0.27	0.12	0.13	0.12	0.11	0.10	0.23	0.20	0.30
	MgO	0.52	1.06	1.08	0.82	0.73	0.61	0.63	0.51	6.09	4.90	5.59
	Mn_2O_3	0.04	0.03	0.22	0.07	0.08	0.06	0.05	0.05	0.27	0.22	0.36
	TiO_2	2.21	0.27	0.28	0.17	0.19	1.32	1.12	1.07	0.62	0.98	0.59
	SO_3	0.02	3.01	2.54	1.69	2.79	5.86	15.79	13.70	0.60	0.57	0.55
	P_2O_5	0.13	0.06	0.10	0.17	0.35	0.11	0.10	0.09	0.04	0.04	0.06
	Cr_2O_3	0.04	0.01	0.02	0.03	0.01	0.01	0.01	0.01	0.00	0.02	0.01
Ignition loss (%)		1.03	1.64	1.37	0.60	1.08	0.60	0.05	4.62	0.10	3.27	0.10

Table II-3. Chemical composition of additives (in weight %)

		H - HardCem	G - Gypsum	B - Bauxite
Oxides (wt.%)	SiO_2	31.1	0.36	4.01
	CaO	16.4	32.73	6.23
	Al_2O_3	4.92	0.19	50.90
	Fe_2O_3	39.6	0.01	19.90
	K_2O	1.13	0.02	0.14
	Na_2O	0.93	0.04	0.08
	MgO	1.16	0.04	0.18
	Mn_2O_3	1.12	0.00	0.02
	TiO_2	0.30	0.01	2.39
	SO_3	0.10	44.43	0.45
	P_2O_5	0.29	0.02	0.07
	Cr_2O_3	0.07	0.00	0.11
Ignition loss (%)		0.00	21.26	15.90

In the aim of studying the resistance of different compositions of calcium sulfoaluminate binders to biogenic acid attack, anhydrite and gypsum (calcium sulfate sources) were mixed with the CSA clinker (CSAC) in order to form ettringite (instead of monosulfoaluminate in the case of CSAC) as a main hydrated phase with aluminum hydroxide (AH_3). The use of two different natures of calcium sulfate allowed to obtain different ratios of ettringite/monosulfoaluminate ratio according to the reactivity of the added calcium sulfate. The ratios of anhydrite and gypsum (18 and 20 wt.% respectively) in the binder (CSAA and CSAC respectively) were obtained from previous studies on the optimization of such mixtures.

The study of the impact of iron on the deterioration processes of the binders in such environments was carried out using SR0 and SR3 binders due to their high initial iron content (mainly in C_4AF form) compared to the reference material. In addition, HardCem, an iron-rich material, was added to the reference Portland material (PCH) and to an alkali-activated slag (AASH) binders in order to study the impact of a different form of iron in different matrices. Finally, in the aim of investigating the role of aluminum in the binders, bauxite, which contained 50 wt.% of aluminum oxide, was added to an alkali-activated slag binder (AASB) in order to increase the initial aluminum content of the binder and to study its behavior against biogenic sulfuric acid attack in sewer conditions.

2.2.2. Description of the binders

2.2.2.1. Reference materials

Portland cement (PC)

The Portland cement, which was used as a reference material with low resistance to biodeterioration, was a CEM I 52.5 R CE CP2 NF. The XRD pattern of the anhydrous cement is presented in Figure II-1 and its main components were tricalcium silicate (C_3S), dicalcium silicate (C_2S), tricalcium aluminate (C_3A), tetracalcium ferroaluminate (C_4AF) and anhydrite ($C\check{S}$). Gypsum was also identified but in a very low quantity.

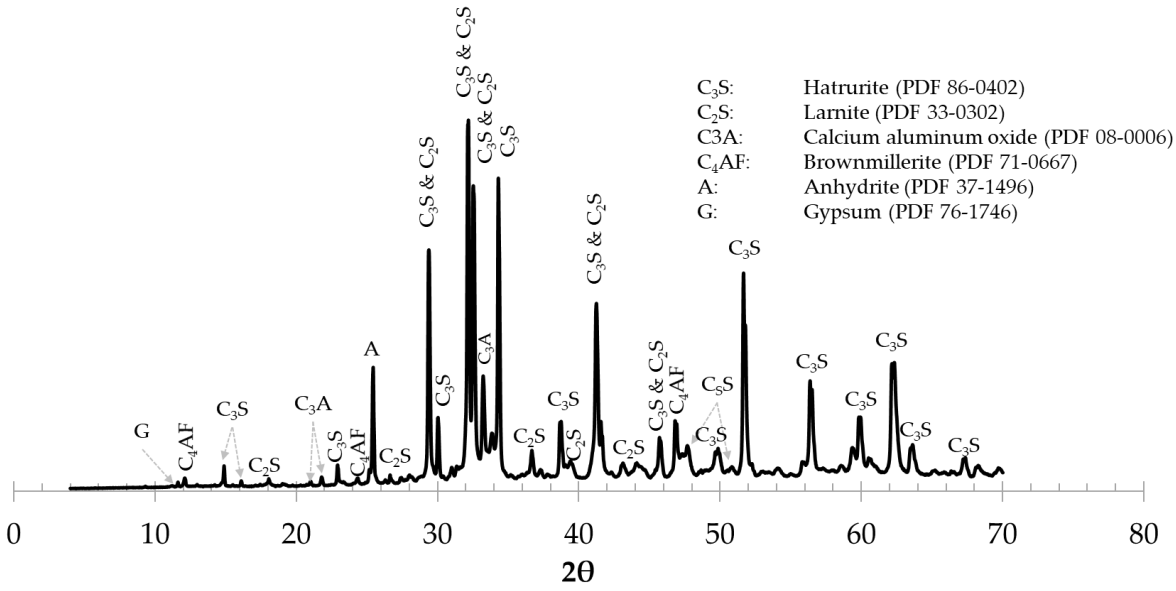

Figure II-1. XRD pattern of anhydrous PC cement

Calcium aluminate cement (CAC)

Calcium aluminate cement was used as a reference material with high resistance to biodeterioration. The XRD pattern of the anhydrous cement is presented in Figure II-2. The main anhydrous phases are monocalcium aluminate (CA), gehlenite (C_2AS) and perovskite (CT). Typically, the main hydrated phases are calcium aluminate hydrates (C_3AH_6, CAH_{10} and C_2AH_8) and aluminum hydroxide (AH_3) [62,64,177].

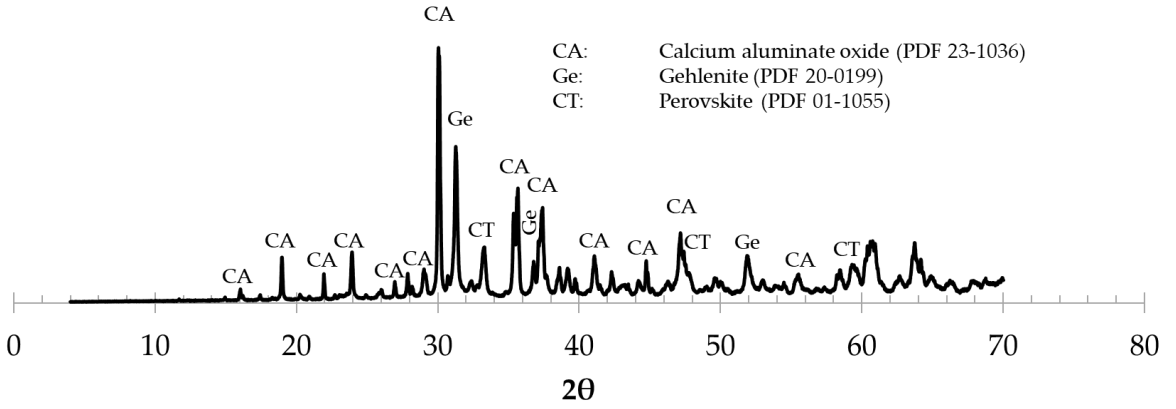

Figure II-2. XRD pattern of anhydrous CAC cement

2.2.2.2. PC-based materials

Portland cement + HardCem (PCH):

PCH binder was composed of 80 wt.% of PC and 20 wt.% of HardCem. The XRD pattern of HardCem is presented in Figure II-3. HardCem was composed essentially of amorphous phases rich in silicon and iron, as seen in Table II-3.

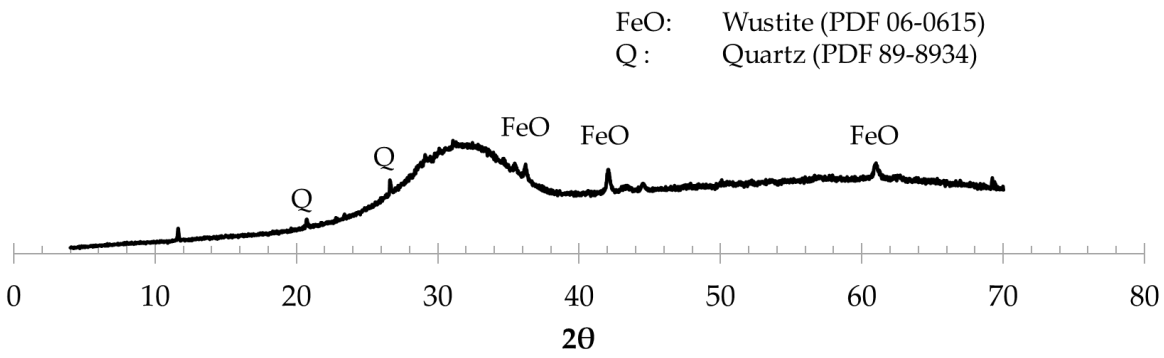

Figure II-3. XRD pattern of anhydrous HardCem

Portland cement – Sulfate Resistant type 0 (SR0):

SR0 is a CEM I 52.5 N SR0 CE PM-CP2 NF with no C_3A and a higher C_4AF (17 wt.%) content than ordinary Portland cement [178]. The XRD pattern of the anhydrous cement is presented in Figure II-4. The main anhydrous phases were C_3S, C_2S and C_4AF. The main hydrates of such cement are portlandite, C-S-H, AFt and AFm phases [62].

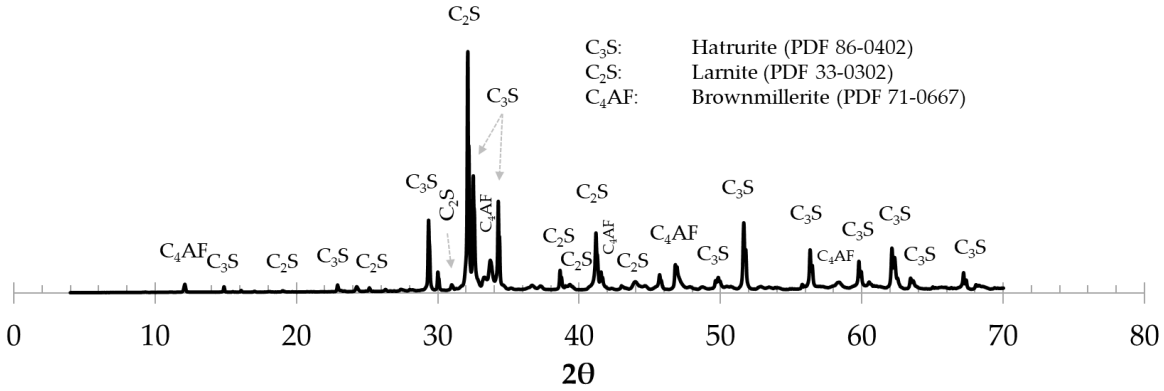

Figure II-4. XRD pattern of anhydrous SR0 cement

Portland cement – Sulfate Resistant type 3 (SR3):

SR3 is a CEM I 52.5 N SR3 CE PM-CP2 NF with low C_3A (< 3%) and low sulfate (as SO_3) (< 3%) content [178]. SR3 is recommended for aggressive conditions, such as seawater, agriculture environments, high sulfate environments, etc. The XRD patterns of the anhydrous cement is presented in Figure II-5. The main anhydrous phases are C_3S, C_2S, C_3A, C_4AF and anhydrite. The main hydrates are similar to those of SR0: portlandite, C-S-H, AFt and AFm phases [62].

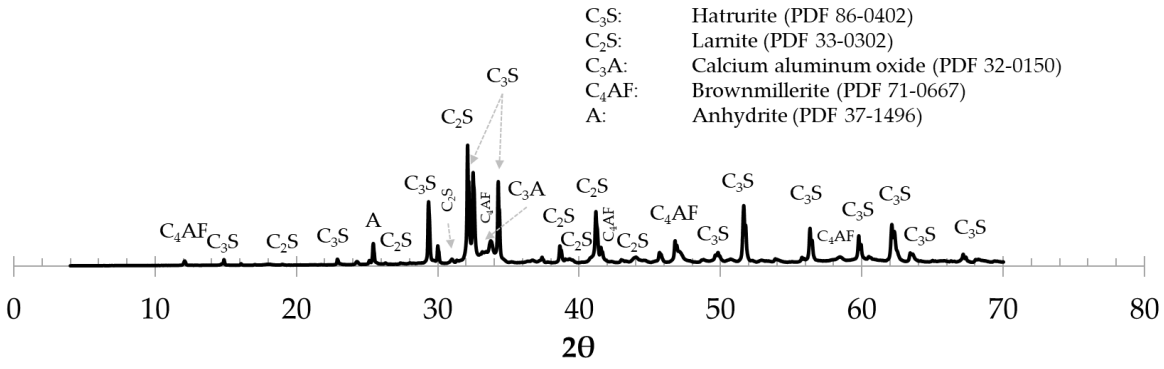

Figure II-5. XRD pattern of anhydrous SR3 cement

2.2.2.3. CSA-based materials

Calcium sulfoaluminate clinker (CSAC):

CSAC binder was obtained from the hydration of pure calcium sulfoaluminate clinker with no addition of calcium sulfate. The XRD pattern of the anhydrous CSA clinker is presented in Figure II-6. The main anhydrous phases are ye'elimite ($C_4A\check{S}$), C_2S, gehlenite (C_2AS), C_4AF and a very small amount of anhydrite. The main hydrates are AFm phases (Calcium monosulfoaluminate hydrate, calcium monocarboaluminate hydrate, calcium hemicarboaluminate hydrate, etc.) and aluminum hydroxide [76,179]. Minor phases may form depending on the content of ye'elimite and secondary phases in the clinker [76,179–181].

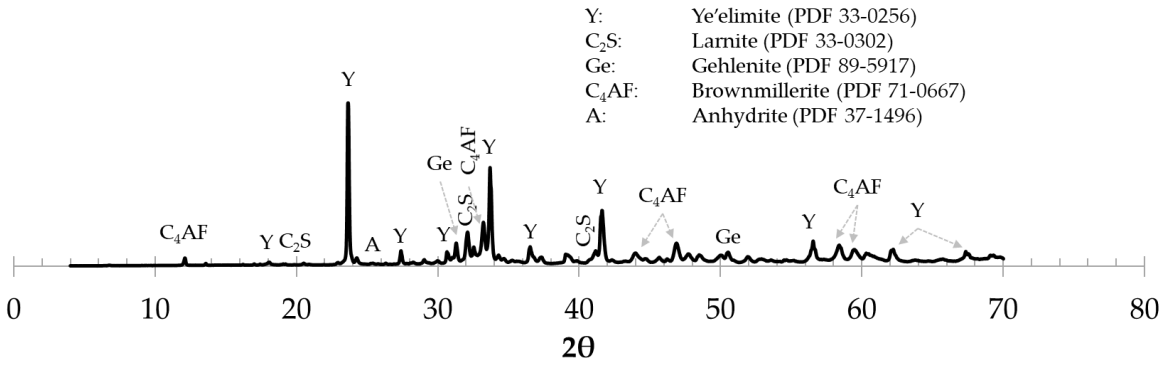

Figure II-6. XRD pattern of anhydrous CSA clinker

Calcium sulfoaluminate clinker + anhydrite (CSAA):

CSAA binder was composed of 82 wt.% of CSA clinker and 18 wt.% of anhydrite. The XRD pattern of the anhydrous cement is presented in Figure II-7. The main anhydrous phases are the same as those of the CSA clinker to which anhydrite was added. The main hydrates are AFm phases, ettringite and aluminum hydroxide [76,77,180,182–184].

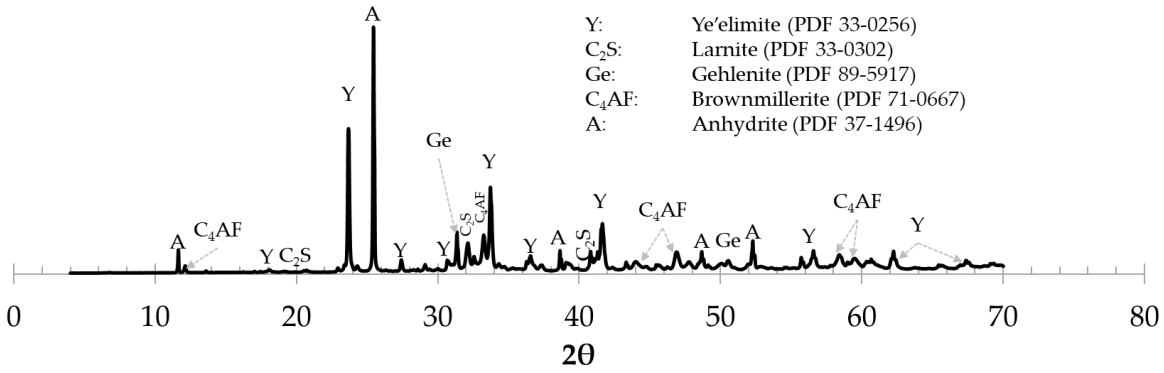

Figure II-7. XRD pattern of anhydrous CSA clinker mixed with anhydrite

Calcium sulfoaluminate clinker + gypsum (CSAG):

CSAG was composed of 80 wt.% of CSA clinker and 20 wt.% of gypsum. The XRD pattern of the anhydrous cement is presented in Figure II-8. The main anhydrous phases are the same as those of the CSA clinker to which gypsum was added. The main hydrates are AFm phases,

ettringite and aluminum hydroxide [76,77,180,182–184]. The ratio of AFm/ettringite formation depends on the ratio of ye'elimite/calcium sulfate during the hydration process [180,181,184].

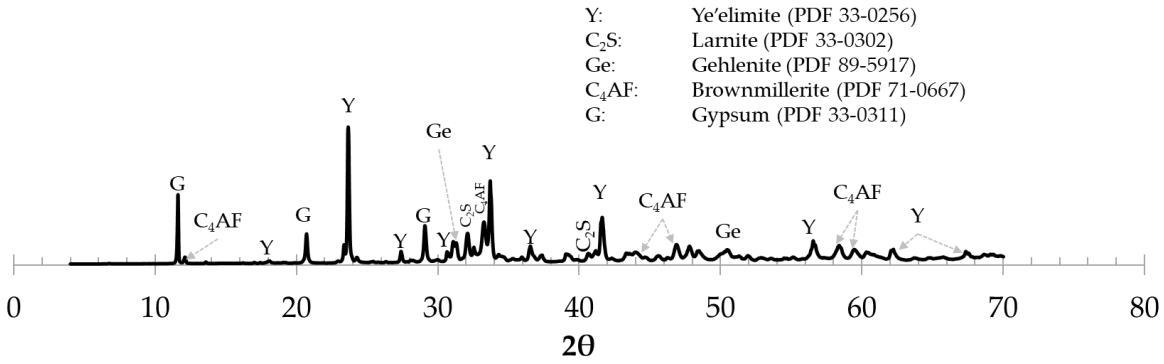

Figure II-8. XRD pattern of anhydrous CSA clinker mixed with gypsum

2.2.2.4. AAS-based materials

Alkali-activated slag (AAS):

The alkali-activated material used in this study was based on the activation of slag by sodium carbonate (4 wt.% of slag) and lime (1 wt.% of slag). The XRD pattern of the anhydrous slag is presented in Figure II-9. The anhydrous slag was composed mainly of amorphous phases. The main hydrated phases are C-A-S-H and hydrotalcite [62,76,121].

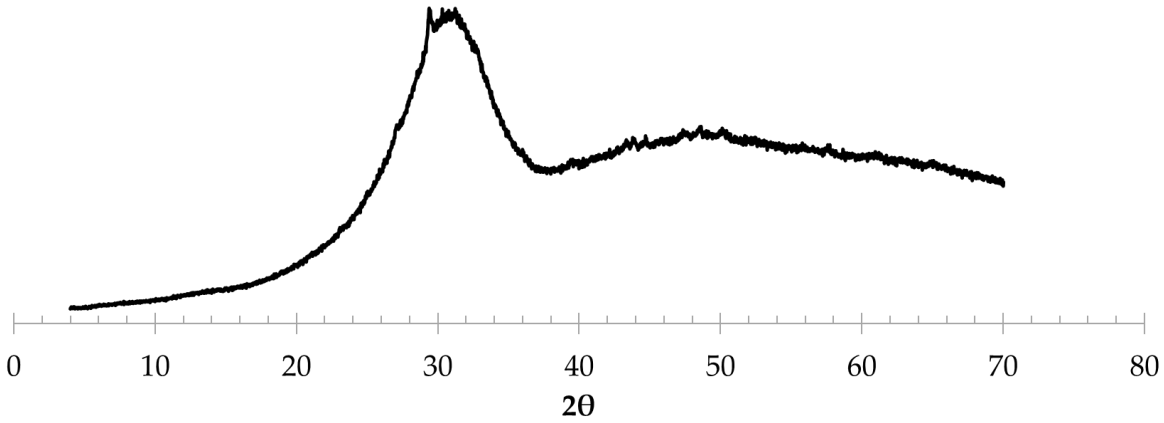

Figure II-9. XRD pattern of anhydrous slag

Alkali-activated slag + bauxite (AASB):

AASB was composed of 90 wt.% of slag and 10 wt.% of bauxite. The activation of this binder was carried out using the same activator as for AAS; i.e. sodium carbonate at 4 wt.% of the slag and lime at 1 wt.% of slag. The XRD pattern of anhydrous bauxite is presented Figure II-10. The main anhydrous phases were diaspore, boehmite, hematite, goethite, calcite, quartz and anatase.

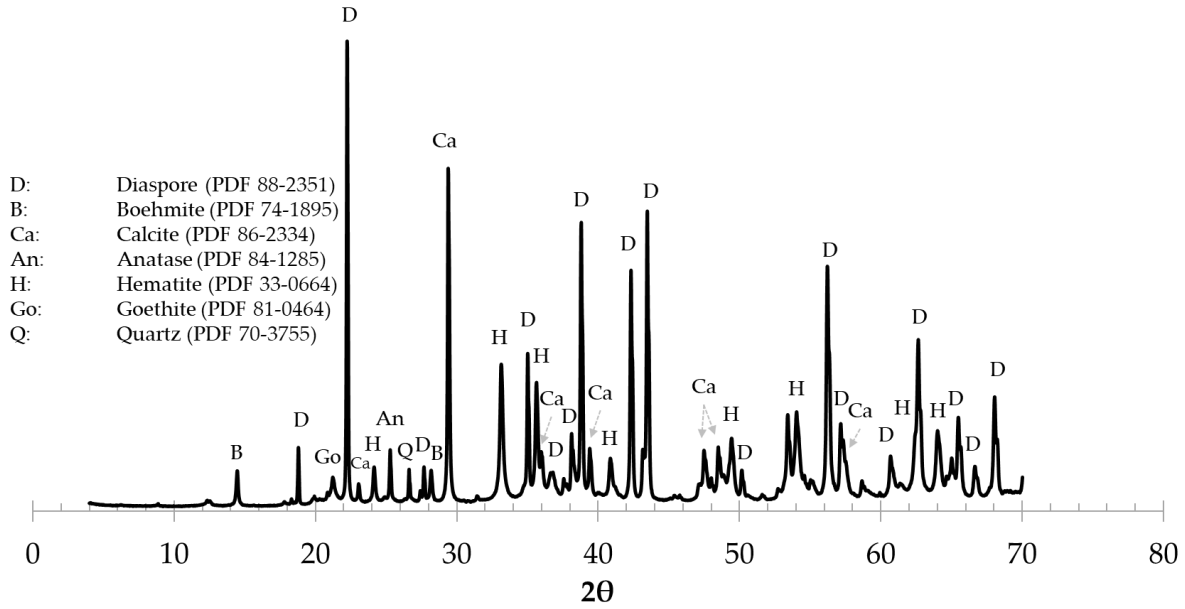

Figure II-10. XRD pattern of anhydrous bauxite

Alkali-activated slag + HardCem (AASH):

AASH was composed of 90 wt.% of slag and 10 wt.% of HardCem. The activation of this binder was carried out using the same activator as for AAS; sodium carbonate at 4 wt.% of the slag and lime at 1 wt.% of slag.

2.2.3.Hydration conditions of cementitious materials

2.2.3.1. Water/binder ratio

Since the present study is mainly focused on the chemical resistance of cement pastes, the water/binder ratio (w/b) should supply enough water to insure appropriate hydration of the binders. However, while a certain amount of water is needed to obtain sufficient rheology properties, too much water can increase the initial porosity of the materials.

The four categories of cement materials, in Table II-1, required different w/b ratio depending on the reactivity of the used cement and the potential hydrated phases. For example, a material composed mainly of ettringite would require more water than a material composed of portlandite or katoite since ettringite contains 32 moles of water while portlandite and katoite contain 1 and 6 moles of water respectively.

Fixing a w/b for all materials seemed a solution to reduce the impact of water on the evolution of the microstructure of the hydrated pastes as well as on the transfer properties of the binders. The selected w/b ratio was set to 0.4 for all materials except for CAC which was set to 0.3 due to problems with its rheological properties.

2.2.3.2. Curing

Curing has the role to offer good maturing conditions for the specimens by protecting the latter from water evaporation which could result in the risk of shrinkage and/or poor hydration process. All the specimens were cured directly after being demolded for at least 28 days before being tested with the durability tests. All the materials in this work were cured in a 20°C room after being sealed with a plastic film. However, CAC underwent a thermal curing process in order to favor the formation of stable hydrated phases (e.g. C_3AH_6) instead of metastable hydrated phases (e.g. CAH_{10} and C_2AH_8) [64]. Figure II-11 presents the evolution of the temperature as a function of thermal curing time as well as the relative humidity (RH). The climatic chamber was pre-set to a temperature of 20°C and a RH of 95%.

The CAC specimens were introduced into the chamber directly after inserting the binder into the molds. The temperature increased progressively with a step of 0.42°C/min until reaching 70°C. After three hours of thermal curing at 70°C, the temperature decreased with the same rate (0.42°C/min) until reaching the ambient temperature of 20°C. During the whole process of thermal curing of CAC, the relative humidity was fixed at 95% to limit any shrinkage, in particular at the surface, of the specimens due to water evaporation. At the end of the curing process, the specimens were collected and were put into the same curing conditions as the rest of the materials.

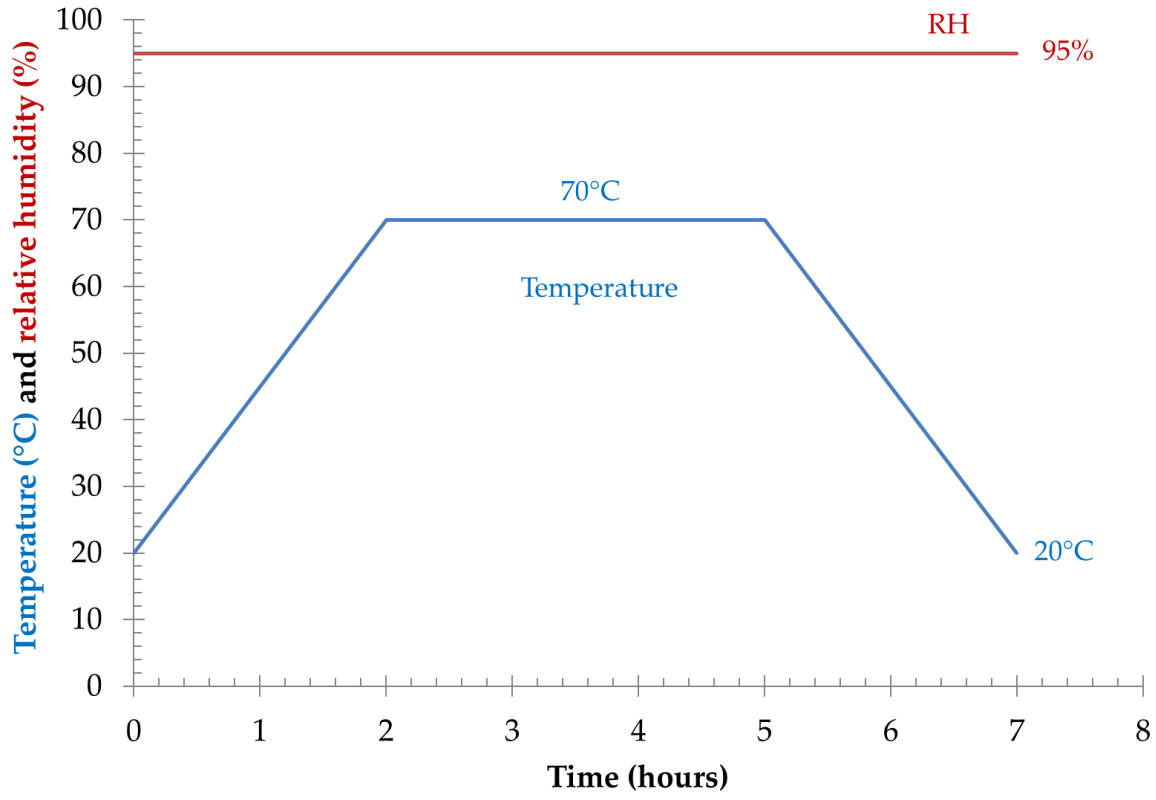

Figure II-11. Thermal curing of CAC specimens showing the evolution of the temperature as a function of time while fixing the relative humidity at 95%

2.2.3.3. PC-based materials

Figure II-12 presents the microstructure observations of the hydrated cement paste for PC, PCH, SR0 and SR3. The anhydrous grains of HardCem were easily identified due to their particular shape and size and to their intense brightness translating their high density. The shapes of HardCem grains were much more angular than C_3S and C_2S, which were more rounded. Moreover, HardCem showed large size grains (75-135 µm) and small size grains (20-40 µm). The microstructure of SR0 and SR3 were similar with lower density of anhydrous phases compared to PC and PCH. This might be due to a slightly higher hydration degree leading to a consumption of more anhydrous phases.

The chemical analyses by EDS, presented in Figure II-13, were carried out only on the hydrated part of the cement pastes. The ratio Al/Ca as a function of (Si+Al)/Ca suggested the presence of portlandite and C-S-H with Ca/Si ratio close to 1.8 as the two main phases. PC and PCH presented higher aluminum content with the possible incorporation of aluminum within the C-S-H and the potential formation of small amounts of hydrogarnet (C_3AH_6) along with ettringite and AFm phases. Moreover, the incorporation of HardCem in the cement matrix did not show any significant impact on the hydrated products for PC-based materials.

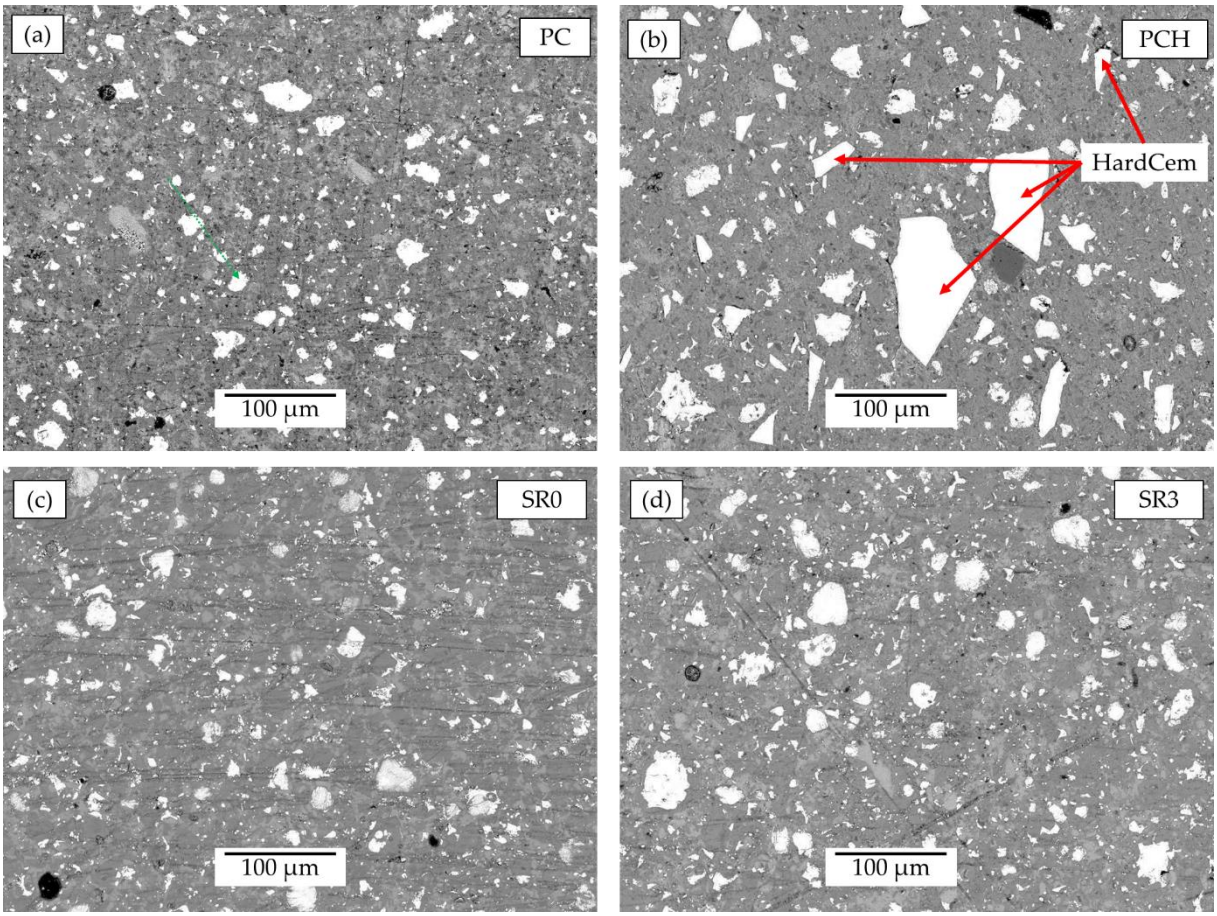

Figure II-12. SEM observations (in BSE mode) of the microstructure of hydrated cement pastes of (a) PC (b) PCH (c) SR0 (d) SR3 after 135 days of hydration

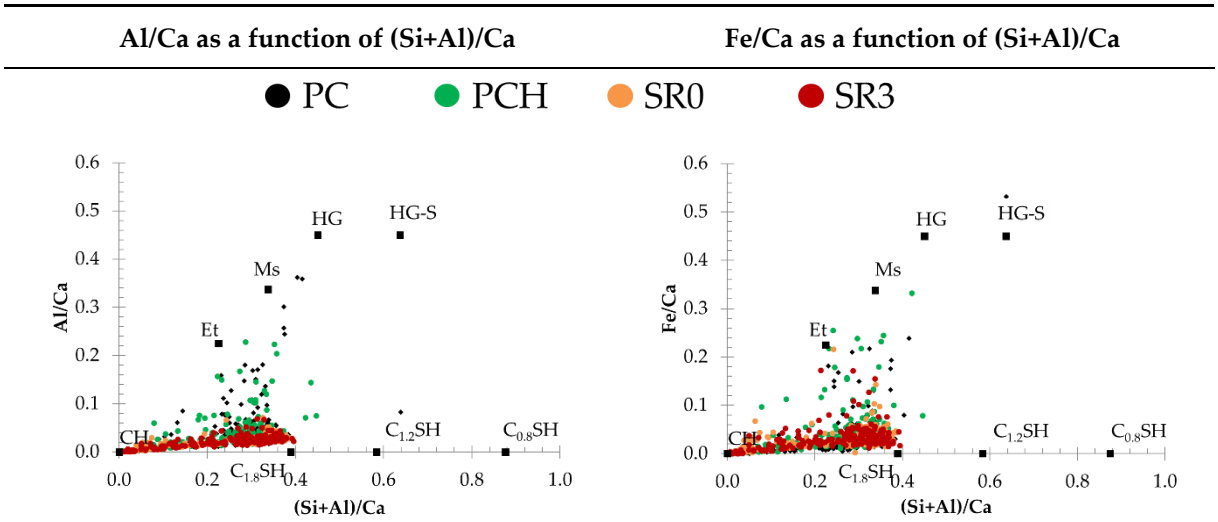

Figure II-13. Chemical analyses by EDS presenting Al/Ca and Fe/Ca ratios as a function of (Si+Al)/Ca to investigate the aluminum and iron incorporation in the hydrated paste for PC-based materials after 135 days of hydration

The XRD patterns of the four PC-based binders are compared in Figure II-14. The results showed portlandite formation in all four materials. The absence of C_3A in SR0 and the its lower content in SR3 led to a lower incorporation of aluminum in the hydrated paste due to the slower dissolution of C_4AF compared to C_3A [62]. Thus, the lower Al/Ca in the hydrated paste and the lower intensity of the peaks of ettringite compared to PC, PCH. C_4AF peaks were still visible in the hydrated cement pastes for all materials with more intense peaks for SR0 and SR3. In the case of SR0, higher amounts of C4AF are typically found to compensate for the aluminum content due to the absence of C3A phase. Gypsum was identified only for PC and PCH. Other residual anhydrous phases (C_3S, C_2S and C_3A) were also detected.

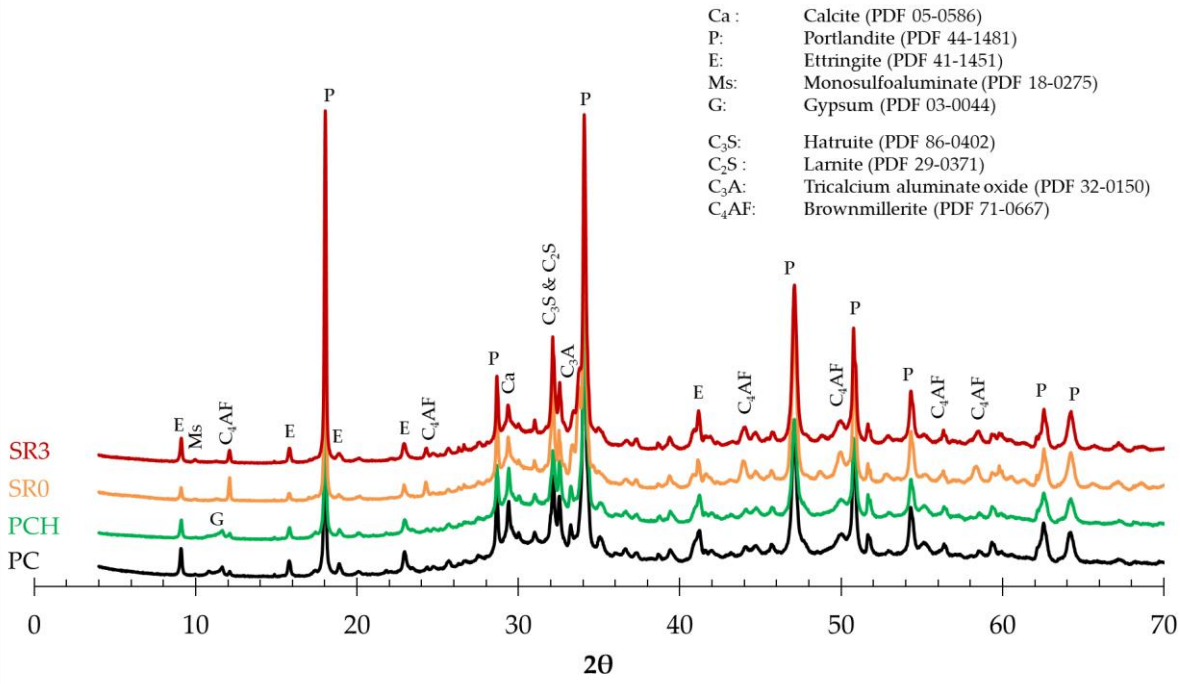

Figure II-14. XRD patterns of PC, PCH, SR0 and SR3 hydrated cement pastes after 140 days of hydration

2.2.3.4. CSA-based materials

The evolution of the microstructure of CSA cement-based materials after 28 days of curing was studied. The three materials did not produce the same phases during the hydration process. Microstructure, chemical and mineralogical analyses were carried out before the exposure to the durability test in order to highlight the differences associated with the nature of each binder.

Figure II-15 presents the SEM observations of the microstructure for the various CSA-based materials and the plot of S/Ca ratio as function of Al/Ca ratio of the hydrated cement paste. The microcracks (drying shrinkage due to SEM vacuum conditions) were clearly visible in the hydrated paste of CSAA and CSAG indicating the abundant precipitation of primary ettringite. Smaller and finer microcracks were observed in CSAC specimen which was probably due to the formation of calcium monosulfoaluminate rather than ettringite. The brighter grains (white) were residual anhydrous grains of gehlenite (C_2AS). Such phase was found in the three different mixtures and it showed a very low hydration reactivity.

The results of the chemical analyses by EDS suggested that CSAC mainly formed AFm phases. The lower S/Ca ratio indicated the possible formation of monocarboaluminate by substitution of sulfate by carbonate [185]. Moreover, the hydration of CSAA and CSAG produced ettringite and monosulfoaluminate with CSAG having a higher Al/Ca ratio.

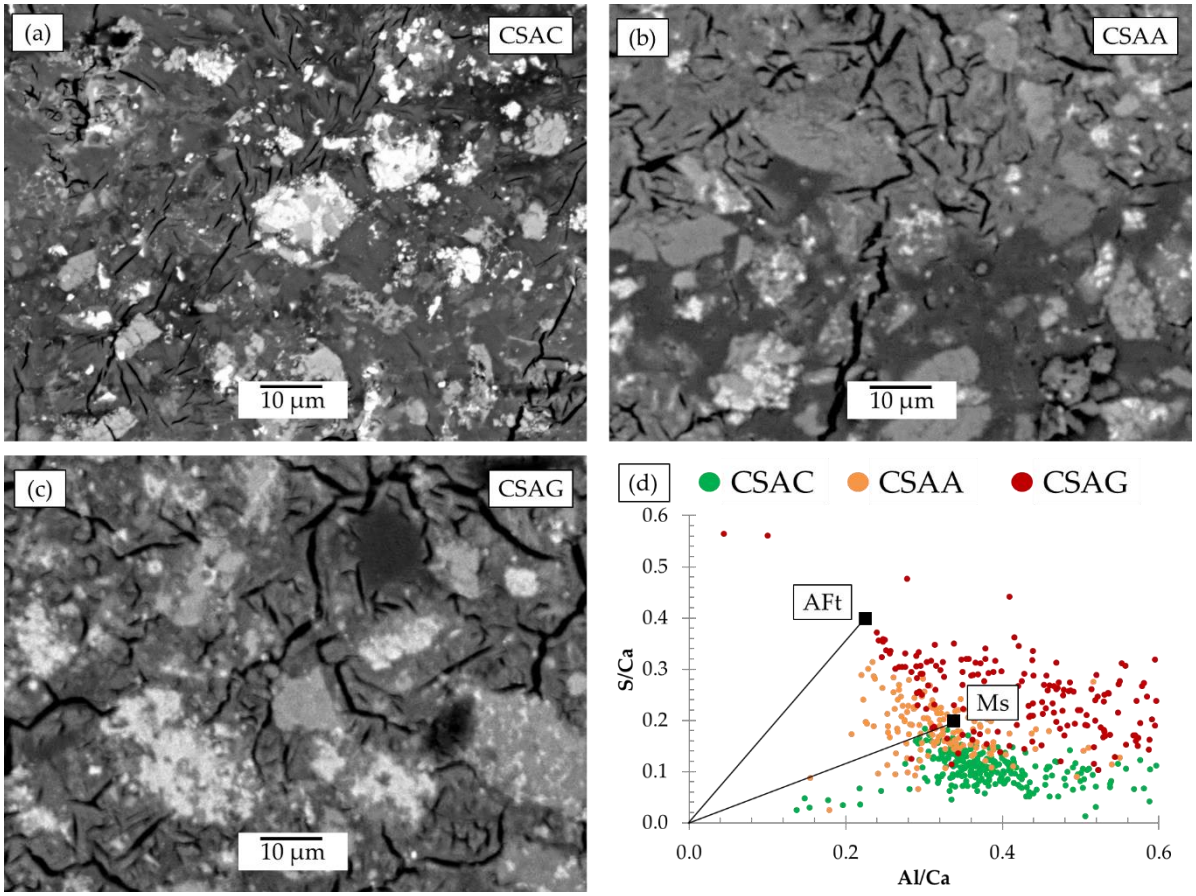

Figure II-15. SEM observations (in BSE mode) of (a) CSAC (b) CSAA (c) CSAG; and (d) EDS plot of S/Ca versus Al/Ca after 138 days of hydration

Figure II-16 presents the distribution of the chemical composition of the dark gray areas in CSAA specimen. Such areas were composed mainly of aluminum, indicating the presence of aluminum hydroxide [44,64,67,68,186], with small amounts of calcium.

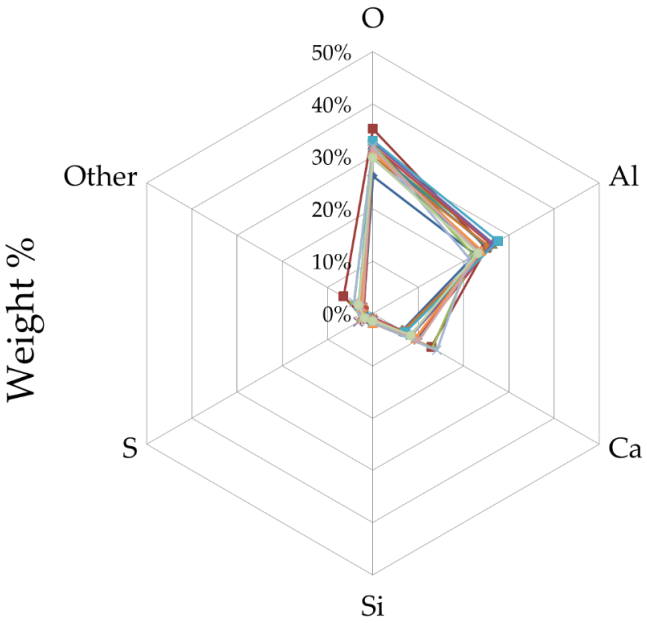

Figure II-16. Distribution of chemical elements (by weight %) obtained from EDS analyses of the dark areas of the microstructure image of CSAA

Figure II-17 presents the XRD patterns of the hydrated cement paste for CSAC, CSAA and CSAG materials at specific angle ranges: 8-13°, 18-19.5° and 23-26°.

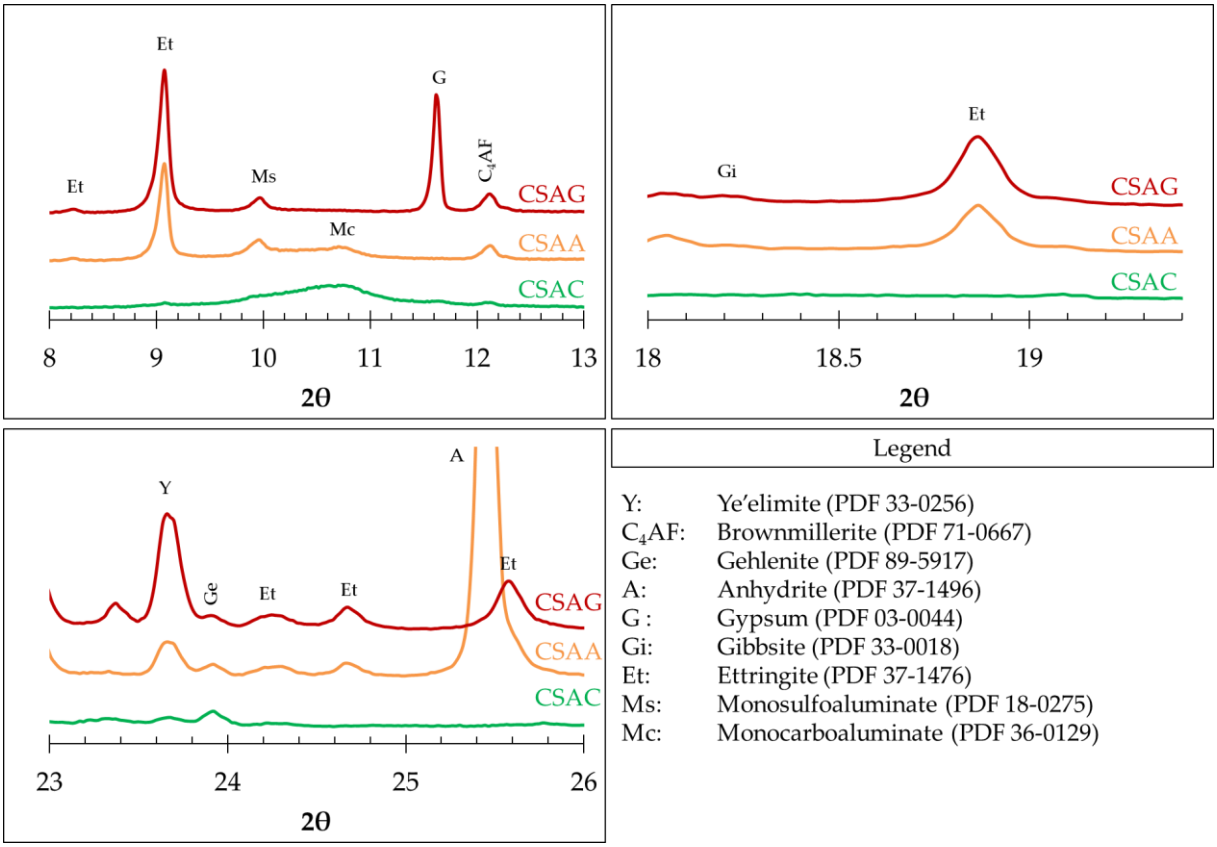

Figure II-17. XRD patterns of CSAC, CSAA and CSAG hydrated cement pastes after 142 days of exposure

Ettringite was clearly visible in CSAA and CSAG with the latter having higher intensity of the peaks. Moreover, crystallized monosulfoaluminate was detected in all three binders with CSAC and CSAA showing the formation of monocarboaluminate in addition to monosulfoaluminate. A very small peak of gibbsite was identified in hydrated systems with calcium sulfate (CSAA and CSAG). CSAC material did not show any peaks for possible crystallized polymorphs of AH_3 (gibbsite, bayerite or nordstrandite). The peak at 11.6° was attributed to the residual gypsum while the peak at 25.4° was linked to the unreacted anhydrite. Finally, anhydrous residual phases were detected such as ye'elimite, gehlenite and C_4AF.

Figure II-18 presents the TGA (in mass loss and the 1st derivative) of hydrated cement pastes for CSAC, CSAA and CSAG compared to CAC. The range of the temperature (X-axis) in the presented graph goes only to a maximum of 550°C as there was no major weight loss above this temperature.

In the temperature range of 100-200°C, the peaks for the CSA materials were very wide and covering the whole temperature range. While it was very difficult to differentiate the phases in such range of temperature, the mass loss was the highest for CSAG followed by CSAA while the lowest weight loss in this temperature range was for CSAC. This could indicate that higher hydration degree for CSAG compared to CSAA which resulted in the formation of higher amounts of ettringite and monosulfoaluminate.

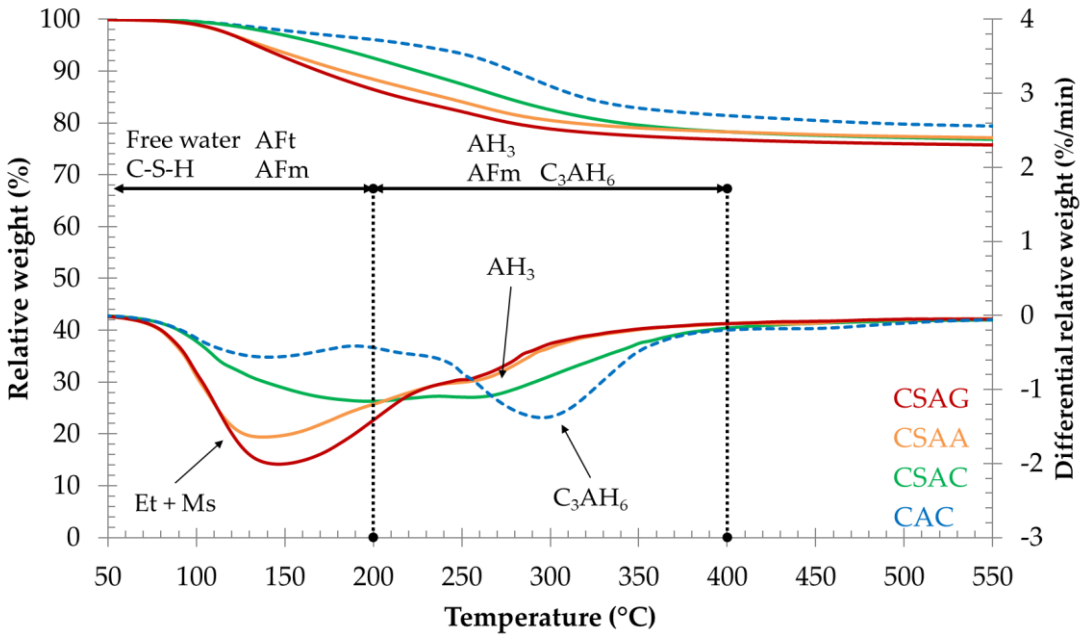

Figure II-18. TGA-DTG thermograms of hydrated CAC, CSAC, CSAA and CSAG after 140 days of hydration

The mass loss due to the departure of water from ettringite was reported to be around 100°C, confirming the absence of ettringite in CSAC material. The weight loss for AFm phases depends on the nature of the anion [187]. The loss of interlayer water molecules from monosulfoaluminate was identified between 100 and 200°C while the dehydroxylation from the octahedral layers occurred at temperature between 250 and 350°C. Monocarboaluminate

presented similar temperature ranges (100-300°C) for the loss of interlayer water molecules and the dehydroxylation of the octahedral layers.

The dehydroxylation of $[Al(OH)_6]^{3-}$ occurs between 200 and 400°C with a main peak at 270°C [187,188]. The mass loss around 270°C could be attributed to AH_3, monosulfoaluminate and monocarboaluminate; hence, due to the intermixing of the temperature ranges for the different phases (ettringite, monosulfoaluminate, monocarboaluminate, katoite and AH_3), it was quite complex to estimate the exact amount of each phase. Although, it could be suggested that CSAG material had a slightly higher AH_3 content compared to CSAA because of the formation of AFm phases during the hydration of the latter (monosulfoaluminate and monocarboaluminate). The higher solubility of gypsum, compared to anhydrite, could be the reason for the formation of higher amounts of AH_3.

2.2.3.5. AAS-based materials

A brief study of the hydration of the different AAS-based materials was carried out to highlight the differences in the cement paste and the impact of the mineral additions to the hydrated phases. SEM observations of the microstructure and chemical and mineralogical analyses of the cement paste are presented in Figure II-19 and Figure II-20.

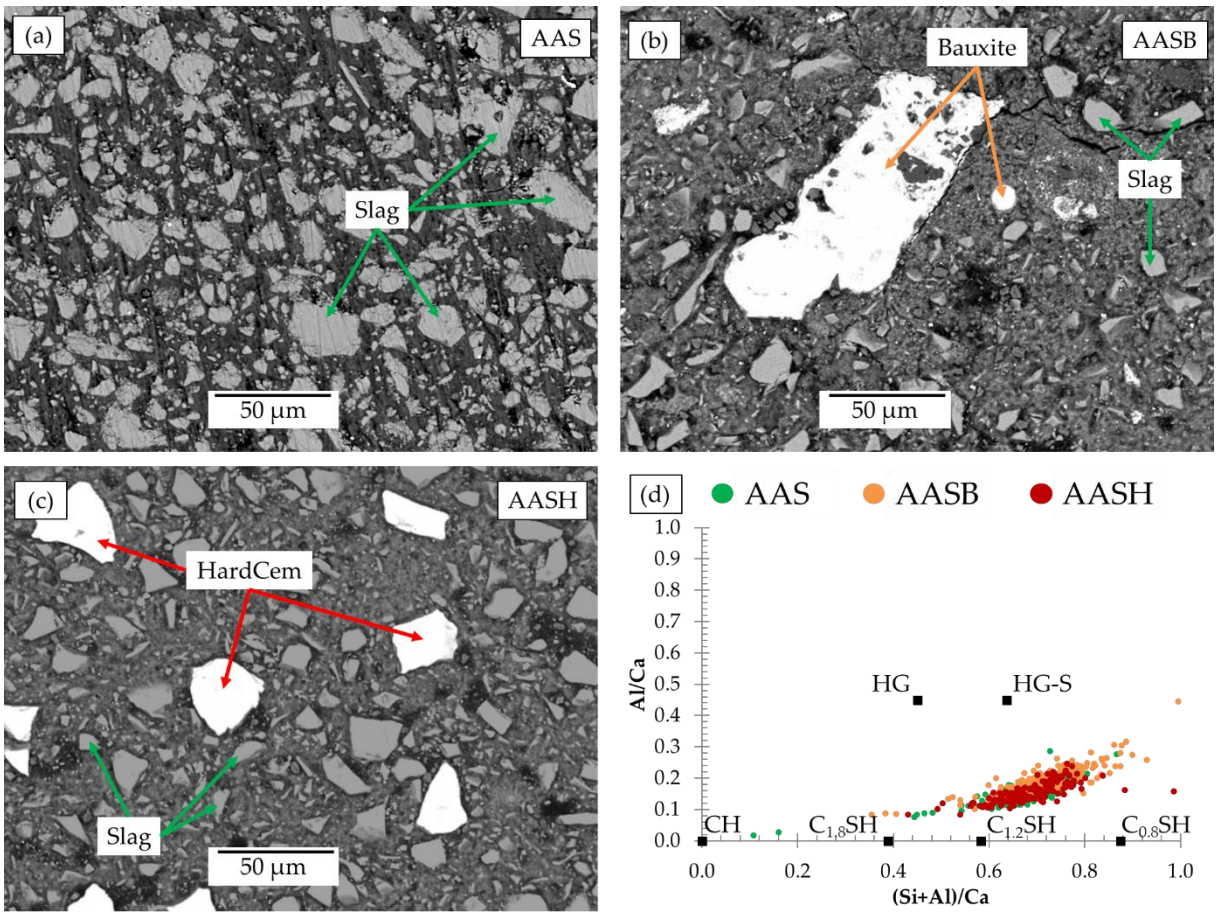

Figure II-19. SEM observations (in BSE mode) of (a) AAS (b) AASB (c) AASH; and (d) EDS plot of Al/Ca versus (Si+Al)/Ca after 150 days of hydration

The SEM images showed high amounts of residual anhydrous slag in the hydrated materials. Bauxite and HardCem grains were easy to identify due to their high density (rich in iron). Moreover, the plot of Al/Ca against (Si+Al)/Ca showed that the incorporation of the mineral additives did not have any impact on the hydrated phases. Mainly C-A-S-H with Ca/Si ratio around 1.1-1.2 was formed and Al/Ca ratio of approximately 0.1-0.2 compared to C-S-H in the PC materials with Ca/Si ratio of 1.8. Nevertheless, no significant higher aluminum content was detected in the AASB material, indicating the very low participation of bauxite to the hydration process.

The XRD patterns of the hydrated AAS-based materials showed that AAS and AASH had very similar patterns with mainly amorphous phases. C-A-S-H, hydrotalcite and calcite were the main identified crystalline phases. AASB showed a similar pattern to AAS and AASB; however, the crystalline phases of anhydrous bauxite were clearly detected.

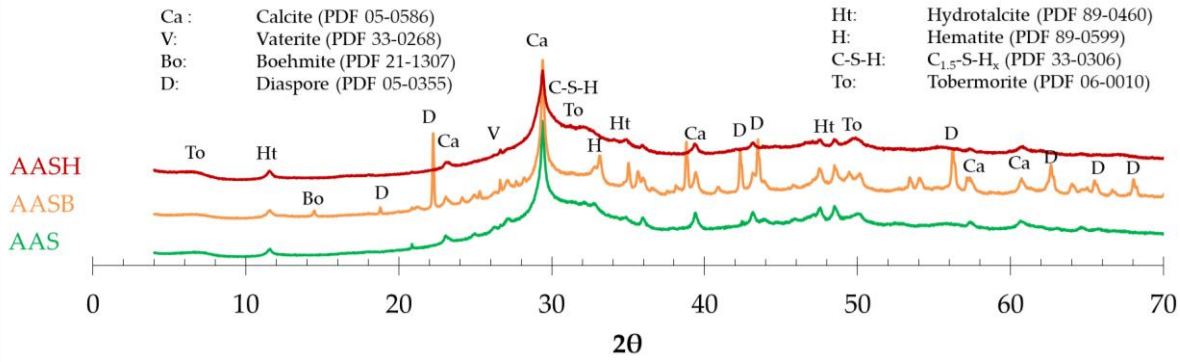

Figure II-20. XRD patterns of AAS, AASB and AASH hydrated cement pastes after 152 days of hydration

2.2.4.Physical and mechanical properties

2.2.4.1.Porosity

A total of three specimens per material, of 1 cm^3, were used to evaluate the porosity of the cement pastes following the recommendations of GranDuBé [189]. The specimens were put in a desiccator under vacuum conditions for 4 hours to eliminate the air entrapped inside the pores. Water was introduced into the desiccator – still maintained under vacuum conditions – until all specimens were submerged of at least 2 cm from the water surface. After 48 hours, the specimens were removed and hydrostatically weighed before being dried. While the French Standard (NF P18-459) requires a drying process of the specimens at 105°C for conventional cements, i.e. Portland-based materials [190], temperatures higher than 45°C leads to the dehydration of ettringite [191]. The loss of water from ettringite results in the change in its molar volume; hence, changing the density of the hydrated paste, in particular for ettringite-rich materials, e.g. CSA-based materials. Therefore, the evaluation of porosity by water intrusion (WIP) was carried out on all studied hydrated cement pastes at two drying temperatures: 105° and 40°C.

Daily weighing was carried out until the relative difference between two successive weighings, 24 hours apart, was less than 0.05 %. The porosity (Φ) was obtained using **Eq.II-1**:

$$\Phi = 100 \times (M_{air} - M_{dry}) / (M_{air} - M_{water}) \quad \text{, expressed in \%} \qquad \textbf{Eq.II-1}$$

Table II-4 presents the results for the eleven studied binders. Significant difference was found between the porosity of all materials at 40 and 105°C. This difference was estimated up to 130% in the case of CSAG material, which is composed mainly of ettringite. The difference was estimated between 30 and 40% for PC-based materials and 10 and 20% for AAS-based materials. CAC showed a difference of porosity of 20% between the two temperatures. For the rest of this study, only porosity at 40°C was considered in order to be able to compare the CSA binders with the rest of the materials. However, the values of the porosity obtained at 40°C were underestimated since the materials were still partially saturated with free water.

At 40 °C, the lowest porosity was attributed to CAC and CSA-based materials, which showed similar porosity between 19 and 24%. For CSA materials, the formation of expansive products, such as ettringite and monosulfoaluminate, at early ages is known to reduce the porosity at the hardened state of the materials. For CAC, the transformation of metastable phases (CAH_{10} and C_2AH_8) into C_3AH_6 and AH_3 leads to the densification of the matrix and the release of available water for the hydration of more anhydrous phases [64].

Table II-4. Water intrusion porosity (WIP) of the hydrated cement paste specimens

Materials	40 °C	105 °C
CAC	19.4	23.1
PC	29.8	40.8
PCH	25.1	35.4
SR0	30.4	39.6
SR3	28.5	38.9
CSAC	23.3	35.9
CSAA	20.8	41.3
CSAG	21.1	48.1
AAS	37.9	46.0
AASB	40.5	47.9
AASH	40.0	44.4

2.2.4.2. Mechanical strength

The mechanical strength of the cement specimens was evaluated after 28 days of curing (except for AAS, AASB and AASH specimens, which was carried out after 315 days). The results of flexure and compressive strengths are presented in Table II-5.

PC-based materials exhibited high mechanical strength as expected despite the w/b ratio of 0.4. SR0 and SR3 had lower compressive strength compared to PC and PCH. Moreover, the difference between PC and PCH could be explained by the incorporation of HardCem which could have acted as "aggregates" due to the large size of its grains. Regarding CSA-based materials, the lack of ettringite formation in CSAC might be the reason for the low compressive strength compared to CSAA and CSAG [74,192]. CAC material presented similar compressive strength as CSA binders but showed slightly higher flexure strength.

Table II-5. Flexure and compressive strengths of the different cement specimens used in this study after 28 days of hydration, except AAS, AASB and AASH which was after 315 days of hydration; *: specimen was "broken" instantly

Materials	Flexure strength (MPa)	Compressive strength (MPa)
CAC	11.05	61.50 ± 5.66
PC	11.35	70.70 ± 1.70
PCH	11.84	78.40 ± 2.83
SR0	-*	62.78 ± 0.31
SR3	9.91	68.05 ± 1.06
CSAC	7.88	46.97 ± 0.66
CSAA	7.95	62.94 ± 1.50
CSAG	8.72	60.16 ± 0.31
AAS	5.50	54.10 ± 0.05
AASB	7.35	51.60 ± 0.30
AASH	8.27	67.67 ± 4.57

Figure II-21 presents the compressive strengths of the different materials as a function of the porosity. CAC showed the lowest porosity (19.4%) with a mechanical strength (61.5 MPa) similar to SR0, CSAA and CSAC. The addition of HardCem to PC increased the mechanical resistance by 8 MPa and decreased the initial porosity of the material by 4%. The porosity of PC-based materials was between 25% and 30% while the compressive strength varied greatly between the different materials and ranged between 62 and 78 MPa. The porosity of SR0 was similar to that of PC while its mechanical strength was lower than PC by 8 MPa. CSAA and CSAG showed very similar porosity (20.8% and 21.1% respectively) and compressive strengths (62.94 and 60.16 MPa respectively); however, CSAC showed comparable porosity

(23%) with a very low mechanical resistance (46.97 MPa). The previous section concerning the hydration of the materials showed that ye'elimite was completely depleted from the material which should indicate a good hydration of the material.

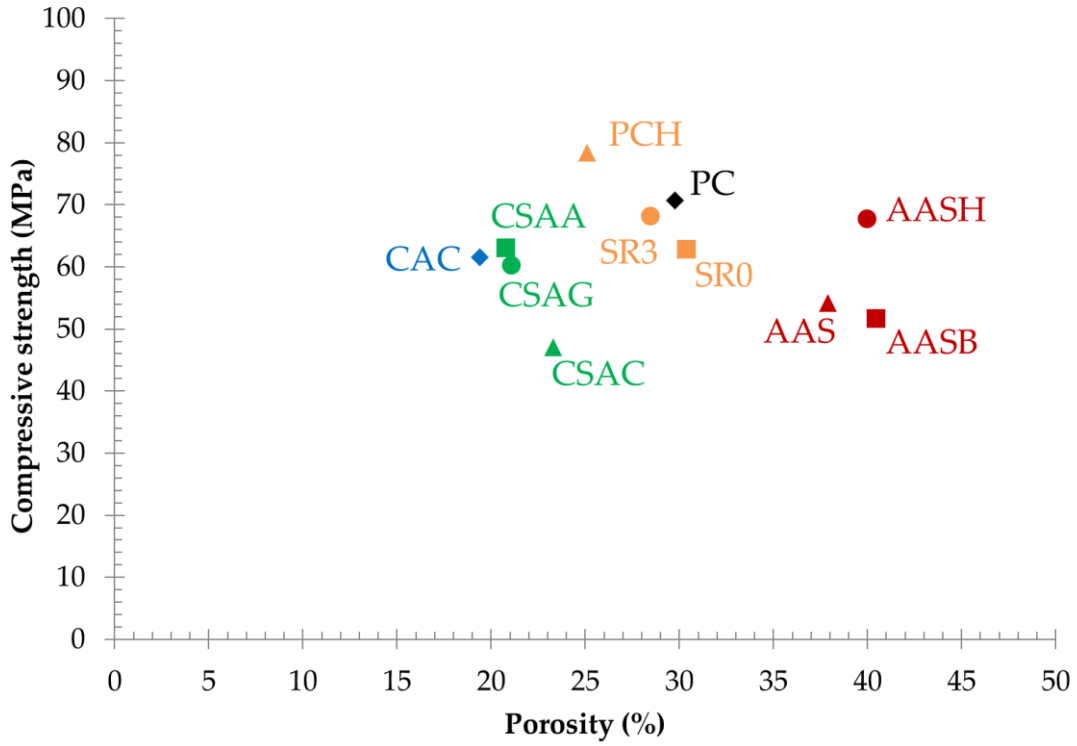

Figure II-21. The compressive strength of the different studied binders as a function of the porosity (evaluated at 40°C as drying temperature)

Using the same water-to-binder ratio of 0.40 still generated variabilities in the physical properties of the materials which emphasizes the difficulty in determining a comparative mix design criterion for all the studied materials.

2.3. EXPOSURE OF CEMENTITIOUS MATERIALS TO BIOGENIC ACID ATTACK IN LABORATORY CONDITIONS

2.3.1. Experimental campaigns

During this study, four experimental campaigns were carried out to expose cement-based materials to an accelerated biodeterioration test in laboratory conditions. The summary of the materials used in each campaign is presented in Table II-6.

Table II-6. The distribution of the materials over the four experimental campaigns

Campaigns	C1	C2	C3	C4
Cement paste	PC CAC OFH CSA	OF CSA	PC OF OFH CSA	PC CAC PCH SR0 SR3 CSAC CSAA CSAG AAS AASB AASH
Mortars	OF-S OFH-S CSA-S	CAC-C OF-C OFH-C CSA-C	-	-

In terms of cement pastes, every experimental campaign exhibited a Portland-based cement paste (PC) as a reference material, except campaign C2. The exposed cement pastes from campaigns C1 to C3 were:

- OF: Sulfate-resistance Portland cement + fly ash
- OFH: Sulfate-resistance Portland cement + fly ash + HardCem
- CSA: Calcium sulfoaluminate cement

In terms of mortars, in addition to testing the performance of the several mortars, the nature of the sand (inert and reactive) was evaluated as well. The exposed mortars from campaigns C1 and C2 were:

- OF-S: Sulfate-resistance Portland cement + fly ash + silica-based sand
- OFH-S: Sulfate-resistance Portland cement + fly ash + HardCem + silica-based sand
- CSA-S: Calcium sulfoaluminate cement + silica-based sand
- CAC-C: Calcium aluminate cement + calcium-based sand
- OF-C: Sulfate-resistance Portland cement + fly ash + calcium-based sand
- OFH-C: Sulfate-resistance Portland cement + fly ash + HardCem + calcium-based sand
- CSA-C: Calcium sulfoaluminate cement + calcium-based sand

The objectives of the experimental campaigns were different and were as follows:

- **1st campaign**: The main objective of this campaign was to compare the reactivity of a CSA binder to that of PC and CAC and to investigate the potential impact of adding HardCem to a mixture of ordinary Portland cement and fly ash at 10 wt.% of the binder.

Moreover, a secondary objective of this campaign was to test the resistance of three mortars with silica-based sand.

- **2nd campaign**: The main objective of this campaign was to reproduce the same results obtained from the 1st campaign on CSA and to test a mixture of ordinary Portland cement and fly ash. A secondary objective was to highlight the differences in substituting silica-based sand by calcite-based sand on the durability of four materials (CAC, OF, OFH and CSA).
- **3rd campaign**: The main objective of this campaign was to test four cement paste materials, previously tested in 1st and 2nd campaign, in less aggressive conditions. These materials served as a testing benchmark for the optimizing of the BAC test to reproduce less aggressive conditions, i.e. pH 3-4.
- **4th campaign**: After compiling all the results from the previous campaigns, the fourth and final campaign was focused on evaluating the resistance of materials with different chemistry and mineralogy in order to investigate further the resistance of CSA materials, the impact of aluminum and iron on the deterioration process.

The results presented in this work were mainly from the 4th campaign. However, the previous campaigns served as: (i) trials for different materials; (ii) comparison with the results from the other campaigns to ensure good reproducibility; and (iii) a base for complementary studies, such as mortar resistance and advanced analyses techniques, such as ^{27}Al NMR analyses and nanoindentation, which are not presented in this document.

2.3.2. Preparation of cementitious specimens and measurements before the test

The recommended size of specimens is 2 cm x 4 cm x 8 cm, typically obtained by sawing 4 cm x 4 cm x 16 cm mortar specimens into 4 equal parts. The dimensions (thickness (th), width (w), and length (L)). An epoxy resin, EUROKOTE 48-20, was applied to the cementitious specimens to cover 5 of the 6 surfaces, leaving only the top surface (corresponding to the surface from the core of the original 4 cm x 4 cm x 16 cm specimen) exposed to the biodeterioration test as shown in Figure II-22.

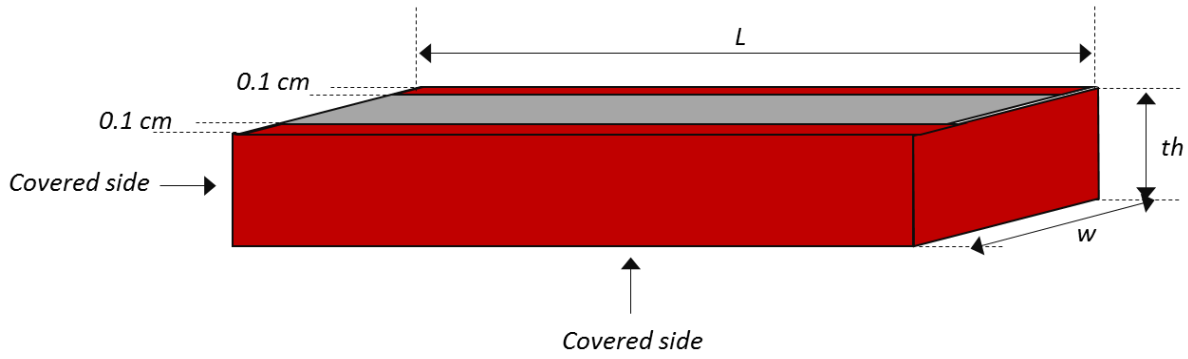

Figure II-22. Scheme of the sawn cementitious specimen with the side covered with an epoxy resin

Two thin lines (1 mm) of resin were also applied to the edges of the exposed surface in order to delimit the solution flow from upstream of the specimen to downstream and to preserve a reference of the initial thickness for further observations, by SEM for example.

2.3.3.Preparation of the feeding solution

The feeding solution contains a reduced sulfur source as well as the nutrients necessary for the development of microorganisms. Potassium tetrathionate ($K_2S_4O_6$) is the reduced sulfur source used in the BAC test. Table II-7 and Table II-8 present the composition of the mineral solution and the trace compounds solution respectively. The composition of the trace compound solution was not analyzed (nor measured). It was prepared manually by adding the different compounds to 1 L of deionized water. It was used as part of the feeding solution for microorganisms and the trace compounds were not monitored over time. The trace compounds solution was added as 5 mL for every 100 L of feeding solution.

Table II-7. Composition of the feeding solution

Compound	Concentration	Unit	Salt
$S_4O_6^{2-}$	158.86	mgS-$S_4O_6^{2-}$/L	$K_2S_4O_6$
N-$NH4^+$	3.93	mgN-NH_4^+/L	NH_4Cl
P	1.71	mgP/L	$(Na(PO_3))_3$
Mg^{2+}	0.18	mgMg^{2+}/L	$MgCl_2$, $6H_2O$
Mn^{2+}	0.03	mgMn^{2+}/L	$MnCl_2$
Fe^{3+}	0.02	mgFe^{3+}/L	$FeCl_3$, $6H_2O$

Deionized water – or water of equivalent purity (pH 5-7.5) and conductivity < 0.1 $mS.m^{-1}$ – was used to fill a thermostatic tank with a minimum volume of 100 liters, containing a mixing system. The nutrients were dissolved salts prepared and stored in separate glass bottles at 4°C to prevent any microbial growth. The nutrient salts and the reduced sulfur source were then added to the deionized water in the tank.

Table II-8. Composition of the trace compounds solution

Compound	Concentration (g/L)
H_3BO_3	0.30
$CoCl_2$, $6H_2O$	0.20
$ZnSO_4$, $7H_2O$	0.10
Na_2MoO_4, $2H_2O$	0.03
$CuSO_4$, $5H_2O$	0.01
$NiCl_2$, $6H_2O$	0.02

2.3.4. Inoculum

Throughout the different testing campaigns, various activated sludges were used to inoculate the surface of the cementitious specimens. They were collected from different wastewater treatment plants at different times and were composed of diversified microbial populations. The surface of the specimens was inoculated only once, at the beginning of each experiment.

Activated sludges were collected from the sanitation system with solid particles in suspension in liquid solution. The centrifugation of 500 mL at 4000 rpm provided sufficient solid phase, corresponding to the suspended organic matter of the activated sludge containing the microorganisms.

The repeatability of the results obtained with different sludges was validated in a previous study [20]. After the end of the testing period, samples of the biofilm were collected from the two CAC specimens that had been inoculated with two different activated sludges. The microbial populations in those biofilms were compared with another biofilm obtained from BFSC material inoculated with one of the activated sludges previously used for CAC as well as the initial consortium.

The analyses showed that all initial inocula were composed mainly of heterotrophic (92%) and nitrifying (8%) bacteria, showing that sulfur-oxidizing bacteria were not detectable initially in the inoculum. After the testing period, the biofilm analyses showed that sulfur-oxidizing bacteria were detected in the biofilm whatever the material or the activated sludge used. Heterotrophic bacteria were still identified in the biofilm at the end of the experiments but in a smaller quantity than in the initial consortium. This was in good agreement with the data reported for deteriorated concrete in sewer networks [193–195].

2.4. BAC TEST EXPERIMENTAL SETUP AND TESTING PROCEDURES

The biodeterioration test is suited to sewer environments where H_2S is present and is applicable to any cementitious material (concrete for construction, mortars for rehabilitation of canalization systems and cement paste for studying the physico-chemical properties of the binders), with or without admixtures (chemicals, biocide, etc.). Cementitious samples are first inoculated with a consortium (an activated sludge) and are then exposed to the trickling of a feeding solution containing a reduced sulfur source, tetrathionate ($S_4O_6^{2-}$), and nutrients. In presence of oxygen, sulfur-oxidizing bacteria in the consortium oxidize tetrathionate ($S_4O_6^{2-}$) into sulfuric acid on the surface of the exposed cementitious samples.

The duration of exposure of the samples to the trickling solution is 3 months. The trickling solution is collected weekly downstream of each sample to analyze the concentration of various cementitious cations (calcium, aluminum, iron, magnesium, potassium and sodium) and to measure the pH. The same leached solutions were also used for analyzing the different

sulfur species, sulfate, sulfite and polythionates (thiosulfate, tetrathionate, pentathionate and hexathionate).

The optimization of the durability test and the acquired experience and knowledge about the relative performances of a wide range of conventional materials has been published in Aboulela et al. 2021 [26]. Moreover, following round robin tests carried out as part of the national project *Perfdub*, the BAC test is now one of the two referenced tests for characterizing the performance of cementitious materials exposed to biodeterioration. Additionally, the BAC test is in the process of standardization at European level within the framework of the standard *CEN TC 165-WG13 Mortars for rehabilitation of sewer networks*.

2.4.1.Architecture of the test

The apparatus, presented in Figure II-23, consisted of a feeding solution in a 100-liter thermostatic (4°C) tank (1), connected to the specimens by plastic tubes (PTFE natural tube 0.5-1.0 mm) that transported the solution from the tank via flow pumps (regulated at 20 ±5 mL/h) (2) and dropped it onto the top of the specimens (3). The specimens were placed on supports set at an angle of 5° to the horizontal in order to optimize the flow of the solution over the surface of the specimens. During the exposure period, samples of the leaching solutions were punctually collected downstream of the cementitious specimens and filtered immediately at 0.2 µm.

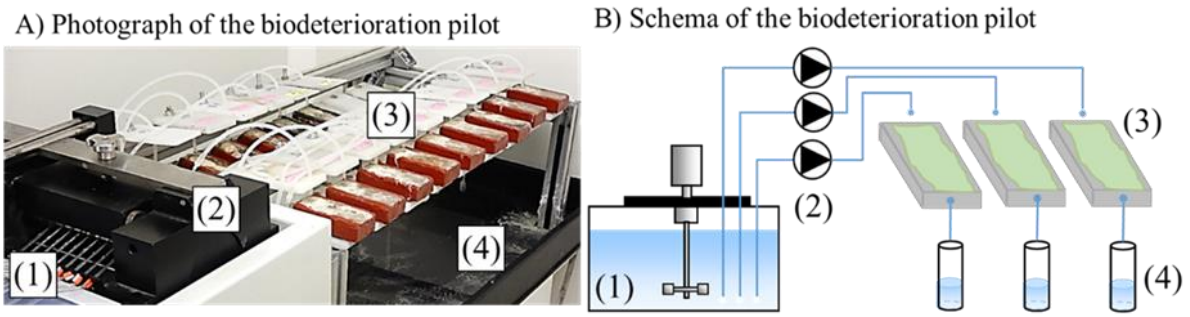

Figure II-23. A) BAC test pilot; B) Schematic diagram of the BAC test [67]

2.4.2.Exposure procedures

The first step of the exposure procedure was to inoculate the surface of the material with a microbial consortium collected from a wastewater treatment plant. This type of microbial consortium is known to be very diverse in terms of microbial population. Controlling the environment (feeding solution, exposed surface of the material, temperature and relative humidity) encouraged natural selection of the microbial activity and its adaptation to the surface of the material as in sewer environments [24,67]. The sludge was deposited delicately on the exposed surface of the cementitious materials using a brush and left to dry for 1 hour so that it adhered well to the surface of the material.

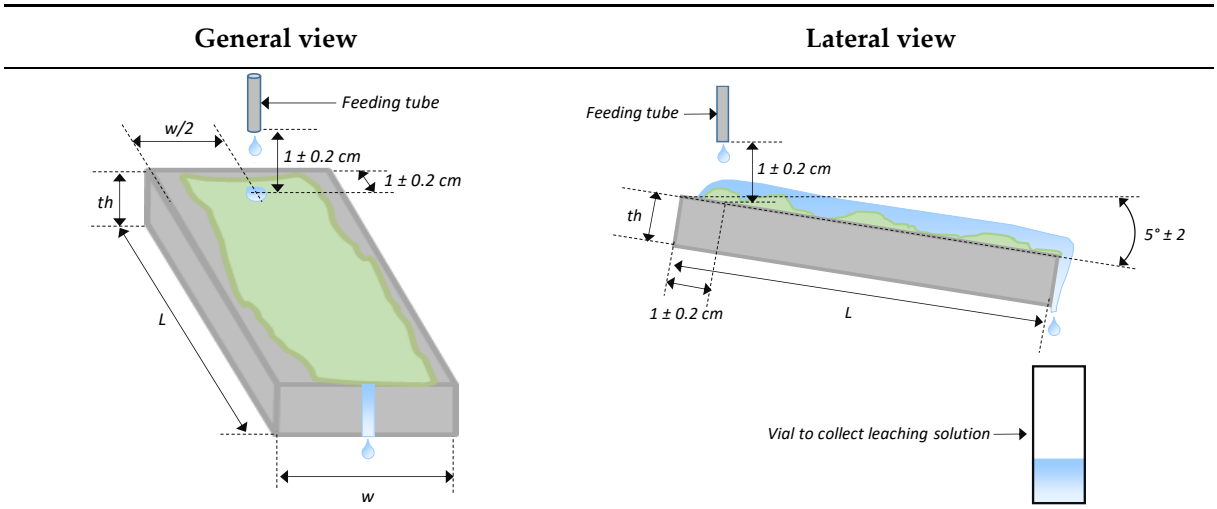

Figure II-24. Scheme of one exposed cementitious specimen with the location of the feeding tubes and the collection tube for the leaching solution sample

The second step consisted in placing the cement samples on the supports while ensuring that the feeding solution droplets fell onto the exposed surface as described in Figure II-24. The feeding tubes were placed 1 cm above the specimens to avoid contamination of the tubes by the biofilm. When the flow pumps were started, the first solution droplets were monitored until they fell off the material downstream. If it did not cover the entire surface of the material, the liquid film was gently spread over the surface with a brush (The biofilm was not yet developed at this stage, so there was no risk of distributing it). The pH of the solution was first measured for each specimen one hour after the beginning of the testing period.

2.4.3. Collecting of the leached solution

Collecting the leached solution at the downstream end of the specimen over a given time duration made it possible to verify the solution flow over the specimens, to monitor the pH evolution of the trickling solution during the exposure period and to quantify the concentrations of leached cementitious cations and leached sulfate (produced by microorganisms).

The flow pumps were then stopped and empty collection tubes (30 mL), previously weighed, were placed downstream of the specimens. The pumps were restarted for a sampling time of 60 ± 5 min. At the end of this time, the flow was cut off to take out the collection tubes before restarting it again. The exact leached solution flow over the exposed surface of the material at day "d_n" (in mL/h) was obtained by equation (**Eq.II-2**):

$$Q_{dn} = (m_{cn} - m_{c0})/d_w) / t_n \qquad \textbf{Eq.II-2}$$

with Q_{dn}: flow of the leached solution at day "d_n", expressed in mL/h; m_{cn}: weight of the collection tubes filled with the leached solution, expressed in g; m_{c0}: weight of the empty collection tubes, expressed in g; d_w: water density, expressed in g/L; t_n: collection time, expressed in hours.

2.4.4.Presentation of the leaching results of the BAC test

The concentration of sulfate in the leached solution is an indicator of the biogenic production of sulfuric acid over the exposed surface of the cementitious materials. Therefore, the objective here was to express the cumulative leached cementitious ion per the initial content of the cementitious ion in the exposed material per square meter of exposed surface as function of the cumulative amount of sulfate produced. In what follows, leaching of calcium will be used as an example, however, the same method was adapted for the rest of the cementitious cations (aluminum, iron and magnesium).

The analyses of the leached solutions provided the calcium concentration during the period of exposure to the BAC test of the different materials. Thus, the flux of leached calcium for each specimen could be calculated following equation (**Eq.II-3**):

$$F(Ca^{2+})_{dn} = Q_{dn} \times [Ca^{2+}]_{dn} \times 10^{-3} \quad \textbf{Eq.II-3}$$

with $F(Ca^{2+})_{dn}$: flux of leached calcium ions at day d_n (in mol/h); Q_{dn}: flow of leached solution at day d_n (in mL/h); $[Ca^{2+}]_{dn}$: concentration of leached calcium measured in the leached solution at day d_n (in mol/L).

The same calculation was carried out at day d_{n+1} to obtain $F(Ca^{2+})_{dn+1}$ using the amount of calcium leached between day d_n and day d_{n+1}, calculated following equation (**Eq.II-4**):

$$Tot(Ca^{2+})_{dn+1 - dn} = ((F(Ca^{2+})_{dn+1} + F(Ca^{2+})_{dn})/2) \times (d_{n+1} - d_n) \quad \textbf{Eq.II-4}$$

with $Tot(Ca^{2+})_{dn+1 - dn}$: cumulative leached calcium between day d_{n+1} and day d_n, expressed in mole; $(d_{n+1} - d_n)$: the time between day d_{n+1} and day d_n, expressed in days.

Finally, the results of the cumulative cementitious calcium were standardized by the initial content of calcium in the exposed material and the exposed surface. Thus, the exposed surface was evaluated based on the dimensions (section 2.3.2) measured prior to the exposure of the specimens to the BAC test. The exposed area was calculated using equation (**Eq.II-5**):

$$S = L \times w \quad \textbf{Eq.II-5}$$

with L: the length of the exposed specimen, expressed in m; w: the width of the exposed specimen, expressed in m.

The initial total calcium ($Tot^{init}(Ca^{2+})$) content – expressed in mole – in the materials was obtained by chemical analyses of the cementitious binders (section 2.2.1). The standardized cumulative leached Ca per total initial Ca per unit of exposed surface could be evaluated as follows (**Eq.II-6**):

$$STot(Ca^{2+}) = Tot(Ca^{2+})_{dn+1 - dn} / Tot^{init}(Ca^{2+}) / S, \text{ expressed in molCa/molCa.m}^2 \quad \textbf{Eq.II-6}$$

Finally, the performance indicator (PI) translates the resistance of material "X" to biogenic acid attack in sewer conditions compared to the resistance of ordinary Portland cement mortar (OPC). However, in order to compare the resistance of a material to that of the reference material, the ratio should be calculated for the same amount of measured sulfate. Thus, a linear model was fitted to the experimental results, with the equation (**Eq.II-7**):

$$STot_x = A \times [SO_4^{2-}] + B \qquad \textbf{Eq.II-7}$$

where A and B are constants calculated by the least-squares method. Then, the model was applied to a wide range of sulfate concentration for the different materials. Consequently, the PI is calculated as follows (**Eq.II-8**):

$$PI_x = 100 \times (STot_x / STot_{OPC}) \text{ expressed in \%} \qquad \textbf{Eq.II-8}$$

The purpose of using the reference material was to classify the performance of the tested materials independently of the considered campaign. For a given campaign, **the PI (performance indicator) of each material was calculated as the standardized cumulative leached calcium values divided by the standardized cumulative leached calcium of the control material (PC).**

PI was used as the performance indicator of the BAC test in the literature [26]. This criterion was developed based on materials relatively rich in calcium (i.e. Portland cement and calcium aluminate cement), although low-calcium materials and materials rich in other chemical elements, such as iron, magnesium and sulfate which are susceptible of getting leached during the biodeterioration phenomena, were considered in this work. **Therefore, the optimization of the PI was necessary to consider the various nature of the cementitious binders. A new criterion, called "PIeqOH" was developed and presented in section 4.2 of chapter IV.**

In the conditions of the BAC test, the sulfate content in the previously studied materials in the literature was very low (< 3%) [20,26,67]; hence, the cumulative measured sulfate was used as a stoichiometric indicator of the amount of acid produced by the microorganisms on the exposed surface of the materials. However, in this study, introducing calcium sulfoaluminate materials (CSA), which contain up to 18 wt.% of sulfur in the form of SO_3, made it difficult to separate the amount of sulfate leached from the material and the amount of sulfate produced biologically. **Thus, the method of presenting the results of the BAC test was further improved by directly estimating the amount of acid produced by the bacteria using a developed model and is detailed in chapter III.**

2.4.5. Maintenance of the BAC test pilot during the exposure period

The feeding solution passes through the connecting plastic tubes before falling off on top of the material. Such tubes are not sterile; hence the risk of developing a biofilm inside the plastic

tubes –which could go up to the feeding solution tank – is not null. The colonization of the tubes could result in the production of acid not in contact with the material, and thus bias the results of the test. In order to prevent microorganisms flourishing in the tubes, the feeding solution was renewed and the tank containing it was cleaned using bleach every 2 weeks. Before the tank was cleaned, 5 liters of the feeding solution were collected in an adequate clean container and the tubes were put into the newly filled container to ensure continuous supply of the solution to the exposed materials during the cleaning of the feeding tank. The plastic tubes were renewed regularly, typically every 2 weeks, to stop any microbial growth outside the exposed surface of the material.

2.5. ANALYSES OF AGGRESSIVE SOLUTIONS DURING EXPOSURE TO THE BAC TEST

2.5.1. pH measurements

The pH was measured with a pH meter directly after collection of the leached solutions downstream of the specimens with a precision of 0.01 pH unit for each sample. The solutions were then filtered to 0.2 μm to eliminate all parts of biofilm, microorganisms and particles that could have fallen into the tubes during the collection period. The liquid samples were stored at 4°C to avoid proliferation.

2.5.2. Chemical analyses of the leaching solutions

2.5.2.1. Cementitious cations (Ca, Al, Fe, Mg, Na, K)

The concentrations of the cementitious cations (Ca, Al, Fe, Mg, Na, K) in the leached solutions were determined using Inductively Coupled Plasma with Optical Emission Spectrometry (ICP-OES) [196–198]. The used ICP-OES equipment was an Optima 7000 DV, with a Meinhart nebulizer. The generator power was 1450 W. The flows of argon and air (auxiliary gas) were 15 L/min and 0.2 L/min, respectively. The flow at the entry of the nebulizer was 0.6 L/min. Finally, the obtained results were processed using treatment and acquisition software (WinLab32).

Firstly, standards of the different chemical elements (Ca, Al, Fe, Mg, Na, K) were prepared and the concentrations (in mg/L) are presented in Table II-9. Secondly, the solution samples were diluted with a factor of 10 to reduce the concentrations in the leached solutions into the standards concentration range. ICP-OES is more stable when the analyzed liquid matrices are acid; hence, the standards and the diluted leached solutions were prepared using ultrapure water with 2 vol.% of nitric acid.

Table II-9. Concentrations of the standards for different chemical elements used in calibrating the analyses by ICP-OES

Chemical elements	Standards concentrations (mg/L)									
Ca	-	-	-	-	1.00	5.00	10.0	20.0	50.0	-
Al	0.01	0.05	0.10	0.50	1.00	5.00	10.0	20.0	-	-
Fe	0.01	0.05	0.10	0.50	1.00	5.00	10.0	-	-	-
Mg	0.01	0.05	0.10	0.50	1.00	5.00	10.0	-	-	-
Na	-	-	0.10	0.50	1.00	5.00	10.0	-	-	-
K	-	-	-	-	-	-	10.0	20.0	50.0	100.0

2.5.2.2. Sulfur compounds

2.5.2.2.1. Sulfite (SO_3^{2-}) and sulfate (SO_4^{2-}) quantification

The concentrations of sulfate in the leached solutions were measured using High-Performance Ionic Chromatograph (HPIC) (Dionex ICS-3000). In our conditions, because of the microbial sulfur-oxidizing activity in the biofilm on the surface of the materials, the leached solutions contained different types of polythionates, which disturbed the identification and the quantification by usual techniques of the amount of produced sulfate. A dedicated method was thus developed to measure the sulfate concentrations after separating the sulfate from the other polythionates. In particular, the pre-column and column were a Dionex AG11 and an IonPac AS11-HC, respectively. The column flow was of 1.5 ml/min. The gradient of eluent (KOH) was between 1 and 60 mM, and the column temperature was of 30°C. A suppression system (AERS 500 4 mm) was used to increase the sensitiveness and to reduce the background conductivity of the eluent.

Sulfate standards were prepared at 0.1, 0.5, 1.0, 5.0, 10.0, 20.0, 50.0 and 100.0 mg/L. The leached solution samples were diluted with different factors during the testing period. In the early stages of the test, the concentration of sulfate was known to be very low; therefore, the dilution factor was 5. However, as the intensification of the attack was observed via the pH evolution of the leached solution, the dilution factor increased up to 20.

The sulfite concentrations were determined following the exact same protocol for sulfate but with changing the sulfate standards to sulfite standards with the same concentration range (0.1 to 100.0 mg/L).

2.5.2.2.2. Polythionates quantification

The analyses of the different polythionates in the leached solutions were carried out using High Performance Liquid Chromatography (HPLC) (Ultimate 3000) with an ultra-violet (UV) detector. Pressure of 69 psi was used to ensure reasonable flow rates. The mobile phase was

injected with a flow of 0.6 ml/min. A 10-µl sample of the leached solution was injected into the separating column (regulated temperature at 23°C). Ultra-violet component was used to analyze the solution at four wavelengths: 220, 225, 230 and 235 nm. Only the results obtained using wavelength of 220 nm are presented in this paper since they had the best separation/intensity ratio of the peaks.

The mobile phase was a solvent of constant composition and was adapted from Miura and Kawaoi [199]. A water-acetonitrile (75:25 vol.%) containing 15 mM of tetrapropylammonium hydroxide (TPA) was prepared in a 1 L recipient. Acetic acid was added at 1.5 mL to adjust the pH of the mobile phase to 5.0.

Commercially obtained salts, potassium tetrathionate ($K_2S_4O_6$) (P2926, CAS 13932-13-3, Sigma-Aldrich, Saint Louis, MO, USA) and sodium thiosulfate ($Na_2S_2O_3$) (202875000, CAS 7772-98-7, Arcos Organics, Fair Lawn, NJ, USA), were used as sources for tetrathionate and thiosulfate. The polythionate salts were dissolved in ultra-pure water to obtain the main standard solution (Std 0) which contained tetrathionate and thiosulfate with the concentrations of 1.5 and 3 mM respectively. The rest of the standard solutions (Std 1 to Std 4) were obtained by suitable dilution of the main standard solution as presented in Table II-10.

Table II-10. Preparation of the standard solutions for tetrathionate and thiosulfate

	Std 0	**Std 1**	**Std 2**	**Std 3**	**Std 4**
Dilution factor	1.0000	0.5000	0.2500	0.1250	0.0625
$[S_4O_6^{2-}]$ in mM	1.523179	0.761589	0.380795	0.190397	0.095199
$[S_2O_3^{2-}]$ in mM	3.184810	1.592405	0.796203	0.398101	0.199051

2.6. MICROBIOLOGICAL ANALYSES

2.6.1. DNA extraction and sequencing

At the end of the exposure period, firstly, 600 mg of the developed cultures on the surface of the materials were collected for each exposed material, using sterile nozzles, and was labelled "Surface". Once the first collection of biofilm was done, the deteriorated layers were grinded, using sterile nozzles, to collect any possible developed biomass and the samples were labelled "Deep". For each type of collected biomass "Surface" and "Deep", the biomass samples were divided into 3 separate tubes in order to triplicate the results.

DNA was extracted from the cells using DNeasy PowerBiofilm kit following the manufacturer's (Qiagen, Germantown, Maryland, USA) recommended protocol. Agarose gel at 0.7% was used to validate the quality of the DNA samples and a nanodrop dosage was carried out to ensure the quantity and the quality of the DNA samples.

The sequencing was carried out by the platform GeT-Biopuces. The sequencing was processed using the protocol recommended by the developers of the DADA2 package [200–205]. The main processing steps are as follows:

- Sequences filtering.
- Elimination of sequences which are shorter than 100nt.
- Reducing the sequences in 5′ and 3′ over 20 nucleotides to eliminate the primers.
- Dereplication of the sequences to obtain unique sequences with the abundance of each sequence.
- Learning of the DADA2 algorithm from the sequencing error rate to determine the Amplicon Sequence Variants (ASV).
- Chimera filtering, which are sequences resulting from the hybridization of 2 parent-sequences, often during PCR.

2.6.2. Microbial fluorescent imaging

A fluorescent dye was used to highlight the bacterial activity on the surface and inside the cement matrix. The dye consisted of SYTO™ 61 red fluorescent nucleic acid stain (Ref: S11343, Thermo Fisher Scientific, 5mM in DMSO) which is the component of a Live/Dead BackLight bacterial viability kit L7012 (Molecular probe kit).

40 µl of SYTO™ 61 was diluted in 5ml of sterile distilled water. The cementitious specimen was then covered with the solution and kept in the dark for 30 min. Afterwards, the specimen's surface was carefully rinsed with distilled water several times then dried. The microbial fluorescence was visualized using Axio Zoom.V16 from ZEISS in white light and fluorescence modes.

2.7. ANALYSES METHODS FOR CHARACTERIZING CEMENTITIOUS MATERIALS

Some of the methods presented in this section are commonly used for the characterization of cementitious materials. The chemical composition of the cement was carried out using Inductively Coupled Plasma coupled with Optical Emission Spectroscopy (ICP-OES) and High Performance Ionic Chromatography (HPIC). Thermal Gravimetric Analyses (TGA), Scanning Electron Microscope (SEM) and X-ray diffraction (XRD) techniques were also used to evaluate the microstructure and the chemical/mineralogical composition of cementitious materials. Finally, the water porosity and the mechanical strength of the materials were carried out to complete the characterization of the sound materials.

2.7.1.Mineralogical analyses by X-ray diffraction

Figure II-25 presents the schematic representation of the X-ray diffraction (XRD) techniques carried out on sound and deteriorated samples. XRD diffraction data were collected using a Brucker D8 diffractometer in θ-θ configuration using a monochromator incident beam and CuKα radiation (λ = 1.54 Å) with a rotating sample holder. The mineralogical phases were identified using the EVA software.

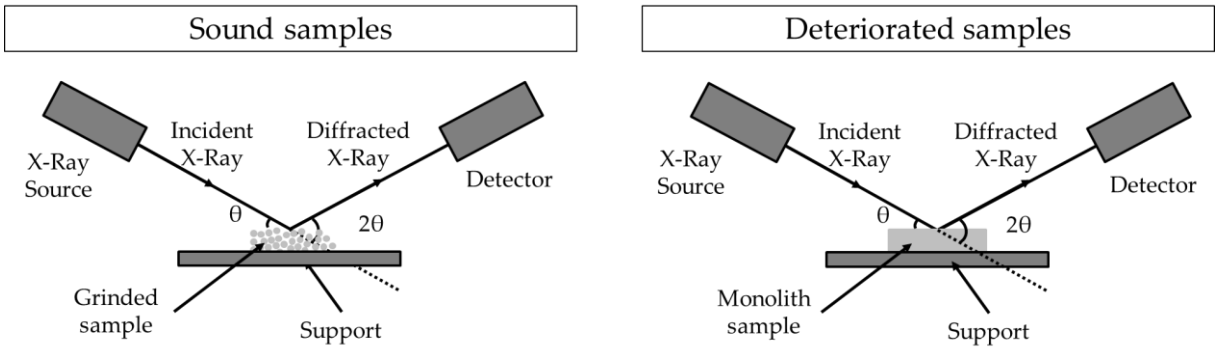

Figure II-25. Schematic representation of the principle of X-ray diffraction carried out on two types of samples: grinded for sound material and monolith for deteriorated material

Sound samples: The hydrated cement paste specimens were grinded and sieved at 80 μm. The analyses were carried out over 2h. The acquisition was performed with a step of 0.02 ° and 2.50 s per step in an angle range of 4 to 70 ° (2 theta). The samples were prepared with particular precautions using backloaded samples techniques to avoid preferential orientations of mineralogical phases.

Deteriorated samples: After exposure to durability tests, the deteriorated specimens were cut into cubes of ~ 1 cm^3 and were analyzed as a massive (or monolith) sample (not grinded). The external surface was analyzed firstly then successive abrasion of the surface was carried out to characterize the different depths of the material until reaching the sound zone. Likewise, the sound zones of the deteriorated samples were analyzed using the monolith. The acquisition was performed with a step of 0.02 ° and 0.25 s per step in an angle range of 4 to 70 ° (2 theta). The abrasion of the surface was done using abrasive disc of size 1200 μm to remove a thin layer of 100 μm. However, such conditions were not optimal for quantitative analyses but sufficient for identifying the phases. The analyses were carried out over 15 mins per surface.

2.7.2.Thermogravimetric analyses

The thermogravimetric analyses (TGA) were carried out to identify cementitious crystalline and amorphous phases. The weight loss of the sample is measured continuously while increasing the temperature at a determined rate. The selected heating rate was 10°C/min and the temperature range was between 40 and 1050°C which corresponds to the dehydroxylation and decarbonation of the cementitious phases [187]. Around 300 mg samples were powder,

crushed and sieved at 80 µm. TGA analyses was carried out using the Netzsch instruments: STA 449 F3 Jupiter® coupled with the QMS 403 Aëolos for mass spectrometry analyses.

2.7.3. Microstructural and chemical analyses of cementitious materials

Microstructural and chemical analyses were carried out using scanning electron microscope coupled with energy dispersive spectrometer (EDS). The combination of the results from SEM (in backscattered electron mode) and EDS provides detailed information about the evolution of the microstructure of the cementitious specimens, in particular the evolution of the mineralogical phases during the external attack with a combined chemical composition of the paste.

The gray levels in BSE imaging relies on the atomic number of the elements constituting the mineralogical phase. The higher the atomic number, the higher the number of generated BSE, which leads to a brighter phase appearing in the BSE image. Since the volume of X-ray generated from the backscattered electrons is relatively large (~1 μm^3), EDS analyses might include spectra from different intermixed mineralogical phases.

In this view, the analyses were carried out in two stages. The first stage concerned the characterization of the sound sample and the second stage concerned the characterization of the deteriorated sample. Figure II-26 shows the preparation steps of the deteriorated specimen to be analyzed by SEM/EDS. The deteriorated specimens were put into a resin (MA2+, 04040, PRESI, Eybens, France) with the appropriate catalyst for 48 hours. The resin was used to protect the specimen during the preparation of the samples since the cementitious matrix is very fragile after deterioration, in particular the deteriorated zones. The specimens were collected and flat sections were sawn at 4 cm from the outlet edge of the specimens.

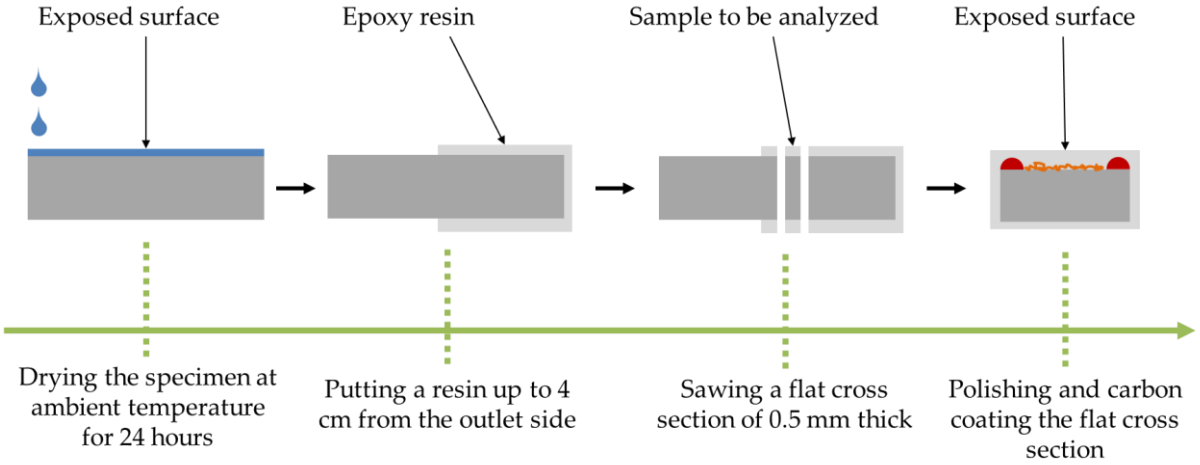

Figure II-26. Preparation of the deteriorated cementitious paste samples for microstructural observations and analyses using SEM coupled with EDS

Before coating the specimens with a carbon film, the polishing of the samples embedded in resin was carried out manually as follows :

- Polishing disc of 800 μm: the necessary time to obtain a homogenous flat section.
- Polishing disc of 1200 μm: 20 min.
- Polishing disc of 4000 μm: 20 min.

The observations were performed using a scanning electron microscope (JEOL JSM-6380LV with accelerating voltage 15kV) in backscatter electrons (BSE) mode and were completed with punctual analyses using energy dispersive spectroscopy (Rontec XFLASH 3001).

2.8. REACTIVE-TRANSPORT MODELS

The evolution of cementitious mineral phases in time and space due to leaching phenomena involved the coupling processes of chemistry and species migration. Several models have been developed in the literature to solve chemical and migration processes. However, this study focuses mainly on two models: HYTEC and Aquasim.

2.8.1. HYTEC®

HYTEC is a reactive transport model developed since 2003 [206]. If HYTEC was originally designed for the coupling of chemical reactions with flow for hydrogeological and water saturated applications, it has been recently extended to multiphase flow for CO_2 storage [207] and to reactive multiphase flow with variable porosity [208].

HYTEC is based on an iterative and staggered solver efficient in propagating reactive front in pure diffusive problems and in adapting mass transfer properties with porosity. Moreover, the model presented in this study assumes thermodynamic equilibrium when the chemical reactions are calculated, which means, compared to the diffusion, the chemical reactions were instantaneous. Furthermore, the effective diffusion coefficient (De) in saturated conditions is controlled by Archie's modified law which is function of the porosity ω, as shown in **Eq.II-9**:

$$D_e(\omega) = D_e(\omega_0)\left(\frac{\omega - \omega_c}{\omega_0 - \omega_c}\right)^{\alpha} \qquad \textbf{Eq.II-9}$$

Where ωc is the critical porosity below which diffusive transfer is negligible, ω_0 is the initial porosity of the cement paste and α is Archie's empirical coefficient. In absence of enough data in the literature on the evolution of the diffusion coefficient on local scale, α was considered equal to unity.

Thermodynamic equilibrium was controlled by Thermoddem, a database for thermochemical, mineralogical and geochemical modeling. Thermoddem was developed by the French national geological service BRGM to assemble thermodynamic properties of mineral phases, aqueous species and gases [209]. The version used in this study was Thermoddem v1.10, adapted for CHESS software. Thermoddem is an open access database and can be accessed through: https://thermoddem.brgm.fr/databases/chess

2.8.2.Aquasim®

A dynamic model was developed using the modeling software Aquasim® using the "Biofilm compartment" [210]. This compartment represents transport-reaction in a porous medium with or without running solution at the surface of the porous medium. Thermodynamic equilibrium was represented by kinetic processes to couple the microbial activity on the material surface with the reactive-transport phenomena inside the cementitious matrix [172]. The 1D model considered: 1) the biological activity; 2) the pH and the salinity impact on the activity of sulfur-oxidizing bacteria; 3) the acid-base and ionic equilibrium. Moreover, only kinetic processes were described in 1D model. Thus, dissolution/precipitation phenomena were chemically represented by a thermodynamic equilibrium, which is function of the rate of a dissolution/precipitation process [172].

In addition, the transport of soluble compounds through the porous medium was represented by Fick's law, where the diffusion of each soluble compound was dependent on the local concentration but independent of the concentrations of the other ionic compounds. Nevertheless, in the case of cementitious materials, the influence of the other soluble species could not be neglected (defined by the Nernst-Planck equation). In Aquasim software, since the transport equations could not be modified; therefore, to respect the charge balance in time and space, the definition of the diffusion was adapted using the Nernst-Planck derivation for the diffusion of salts and ion exchange transport (two or three species) [211]

Aquasim's model considered that the pore solution in cementitious materials was defined by the local concentrations of $[Ca^{2+}]$ and $[OH^-]$, and that the diffusion of all the soluble compounds was driven by the same diffusion coefficient. Moreover, in a porous medium, the structure of the pores influenced the effective diffusion of soluble compounds. Because of the lack of data concerning the porous medium, a simple influence of the porosity was considered in the global effective diffusivity of soluble compounds, as shown in **Eq.II-10** and **Eq.II-11**:

$$D = \frac{(Z_{Ca^{2+}}.[Ca^{2+}] + Z_{OH^-}.[OH^-]) \times (D_{Ca^{2+}}.D_{OH^-})}{(Z_{Ca^{2+}}.[Ca^{2+}].D_{Ca^{2+}} + Z_{OH^-}.[OH^-].D_{OH^-})} \quad \textbf{Eq.II-10}$$

$$D_e = \frac{D}{T_f} \times (\omega(t))^2 \quad \textbf{Eq.II-11}$$

Where D is the diffusion coefficient of all the soluble compounds (m^2/d); $Z_{Ca^{2+}}$ and Z_{OH^-} are the charges of Ca^{2+} and OH^-, respectively (2 and 1); $D_{Ca^{2+}}$ and D_{OH^-} are the diffusion coefficients of Ca^{2+} and OH^- respectively (in m^2/d); D_e is the effective diffusivity in the porous medium (m^2/d); $\omega(t)$ is the local porosity of the porous medium at time t and T_f is the tortuosity factor arbitrarily fixed at 4.

2.9. CONCLUSION

The study was carried out on cement paste specimens made of conventional cements and innovative low-carbon binders (Portland cement, calcium aluminate cement, calcium sulfoaluminate cement and alkali-activated slag) of which the properties and the durability were highlighted in the literature review (Chapter I). Several mineral additives were used to modify the physico-chemical properties of the binders in the aim of improving their performances in sewers environments. Bauxite (high aluminum content) and HardCem (high iron content) was the two main mineral additives used in this study. Bauxite was added to an alkali-activated slag binder in order to provide more aluminum while HardCem was added to a Portland cement and to an alkali-activated slag in order to enrich the two matrices with iron.

The different natures of the studied binders presented a difficulty in determining a criterion for their mix design; however, water to binder ratio was selected as such criterion and was determined at 0.40 for all binders, except for CAC which was at 0.30.

The studied binders presented different physical, chemical and mineralogical characteristics. The hydration of CSA clinker (CSAC) resulted in the total consumption of ye'elimite and the formation of mainly AFm (monosulfoaluminate and monocarboaluminate) and AH_3 phases. Adding calcium sulfate resulted in the formation of mainly ettringite along with monosulfoaluminate and AH_3. The AH_3 phase in CSA-based binders was mainly amorphous while gibbsite and bayerite were the main crystallin form of AH_3 found in CAC binder. Additionally, the porosity and the compressive strengths of CSA-binders were very similar to that of CAC, except the CSAC which presented very low compressive strength compared to the rest of the materials.

The physico-chemical properties of SR0 and SR3 were very similar in terms of hydration products. While SR0 exhibited no C3A, the availability of aluminum was bound to the reactivity of C_4AF, which was the main source of aluminum in such binder. However, the reactivity of C4AF was found to be very slow compared to other anhydrous phases (e.g. C_3S, C_2S and C_3A) and relatively high amounts of anhydrous C4AF were found in the hydrated cement paste, even after 140 days of hydration.

The incorporation of mineral additives (i.e. HardCem and bauxite) had very low influence on the chemical composition of the binders. Both HardCem and bauxite showed no formation of new phases compared to the same materials without the mineral additives. However, the particular size and shape of the mineral additives could have an influence on the transfer properties of the binders. Furthermore, the addition of HardCem to a PC-based material increased its compressive strength and reduced its porosity. Nevertheless, it was not the case when HardCem was added to an AAS-based material where it decreased its compressive strength and increased its initial porosity.

The resistance of such materials to biodeterioration was evaluated in laboratory conditions using the Biogenic Acid Concrete (BAC) test, developed at INSA Toulouse. The testing protocol aimed to represent the deterioration of cementitious materials exposed to sewer conditions by using a soluble reduced sulfur source ($S_4O_6^{2-}$) instead of toxic H_2S. The development of microbial activity on the surface of the material was carried out naturally and the production of biogenic sulfuric acid was monitored by regularly evaluating the evolution of the pH and the sulfate concentrations.

The performance indicators for materials exposed to the BAC test was based on the leaching of calcium from the cementitious materials. However, by including innovative binders in this study (e.g. calcium sulfoaluminate and alkali-activated slag), the performance indicator was optimized to consider other main elements/compounds such as aluminum, iron, magnesium and sulfate (detailed in chapter IV). Moreover, while sulfate can be considered as an indicator of the microbial activity on the surface of materials containing very low sulfate initially, it can not be the case with CSA-based materials. Therefore, a method was developed and optimized to present the results of the performance indicator as a function of the amount of acid produced by the microorganisms (detailed in chapter III).

In the different experimental campaigns, the leached solutions were monitored over the 3-months of testing period in order to (i) investigate the possible interactions between the cement-based materials and the microorganisms by analyzing the different sulfur species; (ii) evaluate the performances of the materials using the developed performance indicator based on the leaching of cementitious cations. At the end of the testing period, the cementitious specimens were collected to identify the evolution of the microstructure and the modification of the chemical and mineralogical composition using different techniques (XRD, SEM-EDS, TGA, etc.). Finally, the compilation of all previous results was used as database for the development of the reactive-transport model.

Chapter III

Investigation of the transformation of tetrathionate during acid production by sulfur-oxidizing microorganisms

3. CHAPTER III – INVESTIGATION OF THE TRANSFORMATION OF TETRATHIONATE DURING ACID PRODUCTION BY SULFUR-OXIDIZING MICROORGANISMS

Table of contents

3.1. INTRODUCTION

The chemistry of sulfur is studied in many different contexts, going from coal mining to the treatment of wastewater in sewage plants [212–216]. The identification of the different redox pathways of sulfur led to progress in the understanding of the different mechanisms as well as the development of new techniques to improve industrial processes, such as the extraction of carbonate-associated sulfate in seawater by pyrite oxidation [217] or the use of sulfur from the biogas industry as a fertilizer [218].

In the context of sewer networks, hydrogen sulfide (H_2S) is present in the gas phase, on the aerial walls of canalizations and on effluent collection structures where sulfur-oxidizing bacteria (SOB) are able to develop and oxidize sulfur compounds into polythionic and sulfuric acids [5,6,9,10]. The production of different acids on the surface of materials leads to severe deterioration of the hydraulic cement-based binders.

In the conditions of the BAC test, the reduced sulfur source used was soluble tetrathionate ($S_4O_6^{2-}$) instead of hydrogen sulfide. During the process of sulfate production, tetrathionate was transformed into different sulfur species through abiotic and biotic reactions. In addition, the presence of a mineral-based medium containing sulfate might influence the different transformations of tetrathionate. Therefore, studying the different alteration mechanisms of cementitious materials in sewage conditions required a thorough understanding of the mechanisms of interaction between the cementitious material and the microorganisms. Moreover, determining the different sulfur reaction pathways was essential for understanding the complete mechanisms of concrete's attack in such environments.

In the perspective of investigating and describing the fate of tetrathionate and other polythionates as well as their transformation in the context of biodeterioration of cementitious materials in sewer conditions, a method was developed and optimized based on the identification and quantification of different polythionates (thiosulfate, tetrathionate, pentathionate and hexathionate), sulfite (SO_3^{2-}) and sulfate (SO_4^{2-}) by coupling High-Performance Liquid Chromatography (HPLC) and High-Performance Ion Chromatography (HPIC) analyses. Currently, the quantification can only be carried out for thiosulfate, tetrathionate sulfite and sulfate, commercially available salts; the method allows only the identification of the other polythionates. Different pathways (biological and chemical) for tetrathionate and intermediate polythionates conversion into sulfuric acid were proposed and analyzed depending on the different exposed cement materials.

3.2. MATERIALS AND REMINDER ABOUT TESTING PROTOCOL

In this part of the study, one material of each different nature of binders (CAC-based, CSA-based and AAS-based materials) was selected except for PC-based materials where two materials were selected. The selected materials were as follows:

- **CAC-based materials**: CAC
- **PC-based materials**: SR0 and SR3
- **CSA-based materials**: CSAA
- **AAS-based materials**: AAS

These materials were exposed to the BAC-test (during campaign n°4) for 3 months. Figure III-1 presents a scheme of the BAC-test with the associated experimental data. The BAC-test consisted of exposing hydrated cement-based binders inoculated with activated sludge to a feeding solution containing tetrathionate ($[S_4O_6^{2-}]_{in}$) as a reduced sulfur source. The feeding solution was trickled on the surface of the exposed materials using a flow pump to regulate the flow rate at 25 ml/h. Through the development of the biofilm, the microorganisms oxidize the tetrathionate and produces several sulfur species (e.g. polythionates, sulfate, elemental sulfur) along with acid production. The inclination of the specimens ensures that the flow of the leached solutions goes from the upstream to the downstream of the specimens and into the collection tube. These tubes are then collected to analyze the pH (acid concentration) and the different sulfur species.

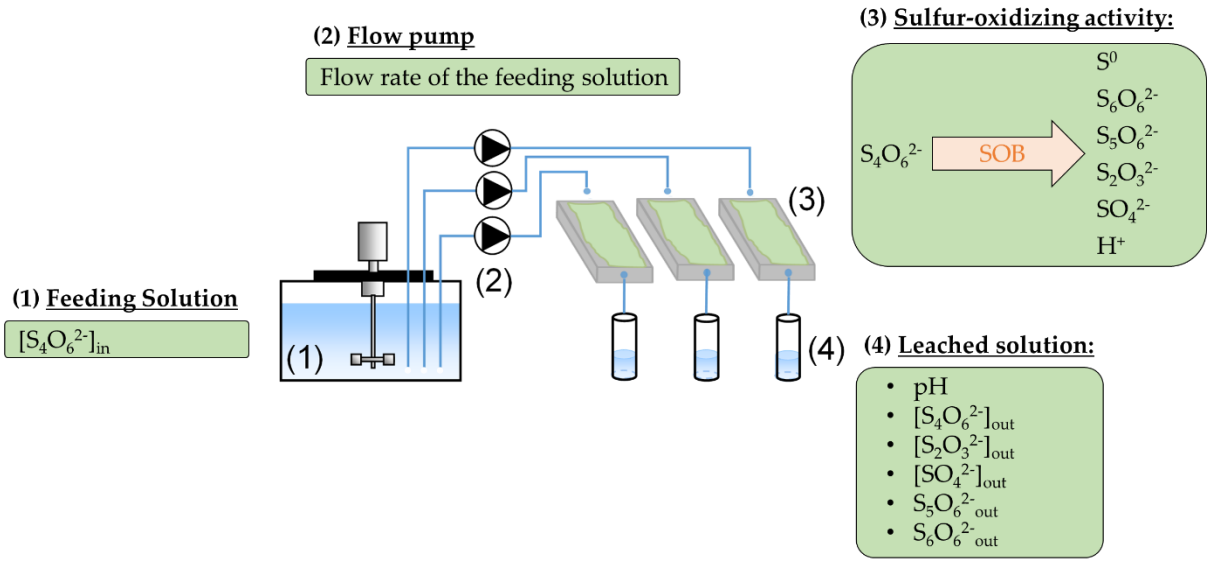

Figure III-1. Scheme of the BAC-test showing the inlet and outlet experimental data

Table III-1 presents the initial SO_3^{2-} content (in wt.%) for all five studied materials. The SO_3^{2-} content shows clearly that CAC and AAS have very low amounts of sulfur, followed by OC-based materials (SR0 and SR3) and finally, CSAA that contains around 14 wt.% of SO_3^{2-}. During the biodeterioration phenomena, the microbial activity produces sulfate among other sulfur

species. However, simple analyses using HPIC can not differentiate the amount of sulfate produced by the microorganisms and the amount of sulfate released by the material. While sulfur content can be considered insignificant compared to calcium or aluminum content for some materials (e.g. CAC and AAS), CSA-based materials contained significant amounts of sulfur which could not be neglected; hence, the need to develop a method allowing to quantify the amount of acid produced at each step of the biochemical redox reactions of tetrathionate.

Table III-1. The initial SO_3^{2-} content in the studied binders

Materials	CAC	SR0	SR3	CSAA	AAS
Initial SO_3^{2-} content (wt.%)	0.02	1.69	2.79	13.70	0.64

3.3. DATA PROCESSING, pH DEPENDENCY AND ESTIMATION OF PARAMETERS

A protocol was developed to study the fate of tetrathionate during biodeterioration of cementitious materials in sewer-like conditions. Figure III-2 presents a summary of this protocol which is detailed in this section.

The first step of the procedure consisted in collecting experimental data: the pH, the flow rate of the feeding solution, the concentrations of tetrathionate entering the system, the concentrations of tetrathionate, thiosulfate and sulfate leaving the system and finally the areas of the peaks in chromatogram results for tetrathionate, pentathionate and hexathionate. The areas of such species were determined because for some species (pentathionate and hexathionate), calibration solutions which should normally be used in chromatography for quantification, were not commercially available. In this case, the concentrations were deduced from the areas of the peaks using tetrathionate as an intermediate mean of calibration.

The second step was to calculate the converted part of the tetrathionate, by the difference between the inlet flux and the outlet flux for each sample collected from the leached solutions, as well as the area ratios between the tetrathionate and the compounds of which the concentration could not be obtained (pentathionate and hexathionate). Afterwards, based on the experimental results and a literature review, stoichiometric reactions were proposed to describe the redox phenomena of tetrathionate during biogenic acid production. In order to link these stoichiometric reactions to the evolution of pH, different factors were attributed to each one of the equations allowing to control their participation rate.

This step was carried out for all materials except CSAA due to its high initial sulfate content. The sulfate measured in the leached solutions for CSAA was coming from the biological oxidation of tetrathionate and the dissolution of the sulfate-bearing phases inside its cementitious matrix. However, CSAA material was used to validate the method for estimating the part of sulfate produced biologically and the part coming from the material itself.

Two of these reactions were dependent and described the conversion of tetrathionate in alkaline and acid environments. Hence, the sum of their respective factors equals one. The three other reactions which described the total oxidation of other species were independent of these equations and, consequently, their factors were independent. The difference between the experimental data and the estimated results from the proposed reaction pathways was reduced by the least-of-squares method applied only to thiosulfate and sulfate concentrations since the concentrations of pentathionate and hexathionate could not be determined.

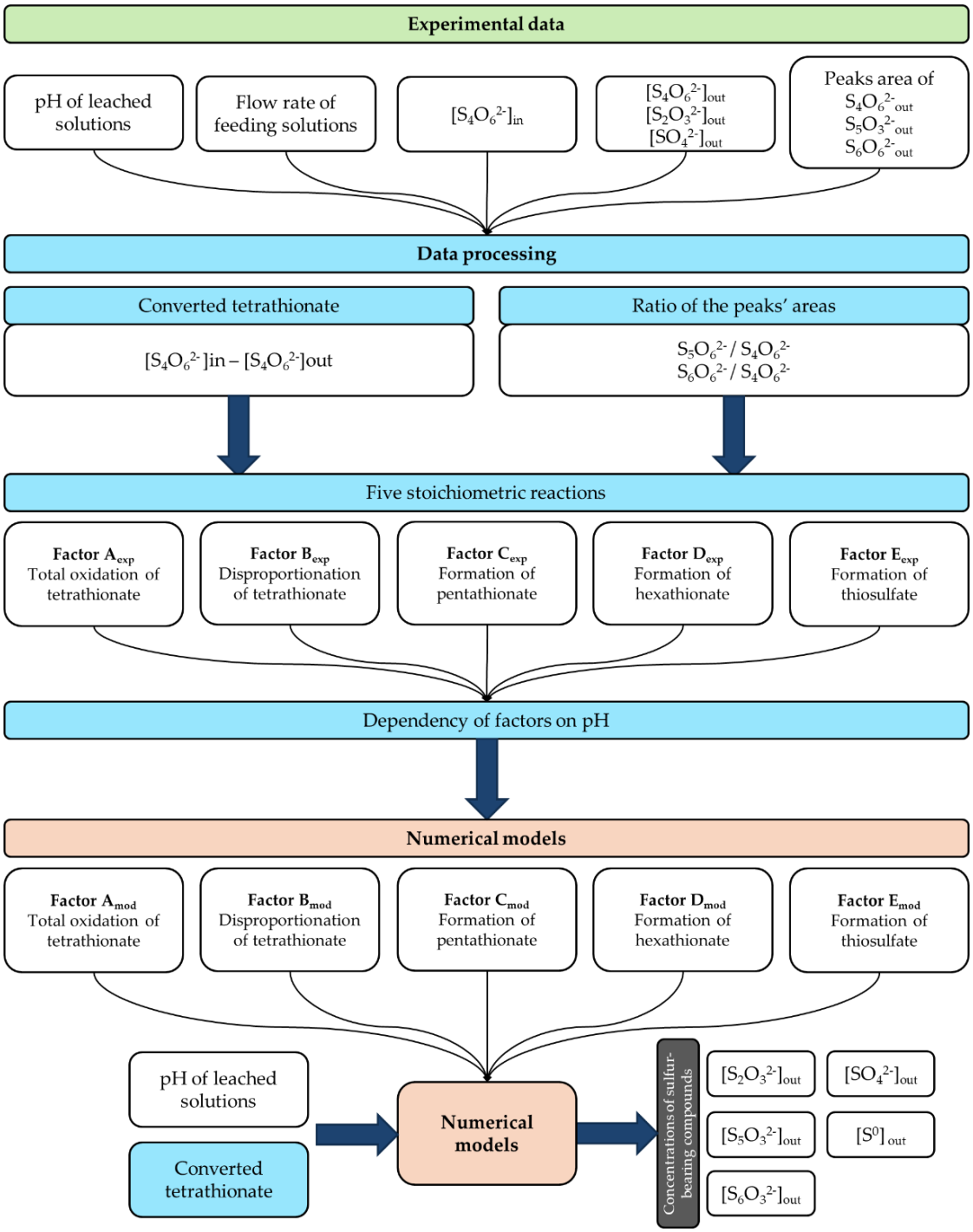

Figure III-2. Summary of the protocol for studying the fate of tetrathionate and the development of numerical models for estimating the production of sulfate, elemental sulfur and intermediate polythionates by using the pH of the leached solutions and the converted tetrathionate

Finally, the evolution of the factors as a function of the pH made it possible to establish mathematical equations describing the dependency of such reaction pathways to the pH evolution. Therefore, the mathematical models represented the evolution of sulfur species using the concentrations of converted tetrathionate in the system and the pH. The various parameters of the mathematical models, considering the pH, were calibrated by the method of least squares between the experimental data and the numerical results.

3.4. EXPERIMENTAL OBSERVATIONS AND ANALYSES

3.4.1.pH evolution and microbial activities

The pH of the leached solutions and the concentration of sulfate were measured at the outlet of the specimens to monitor the biogenic acid production linked to the microbial activity. Figure III-3 presents the evolution of the pH and Figure III-4 presents the cumulative measured sulfate for cement pastes during the exposure period to the BAC test.

The biodeterioration attack in sewer conditions could be categorized into 3 phases (Figure III-3) depending on the pH of the surface of the exposed materials [5,6,9,10]:

i. Abiotic attack: carbonation and hydrogen sulfide attack on the cementitious materials inducing the decrease of pH from 12 to 9.
ii. Biotic attack: development of neutrophilic sulfur-oxidizing bacteria (NSOB) accompanied with the oxidation of sulfur substrate into sulfuric acid, leading the decrease of pH from 9 to 4.
iii. Active biotic attack: development of acidophilic sulfur-oxidizing bacteria (ASOB) generating significant amounts of sulfuric acid and causing severe deterioration to the cement-based materials.

At the early days of the testing period, the pH of the leached solutions for all five materials was relatively high (around 11 for Portland-based materials (SR0 and SR3) and alkali-activated slag (AAS) and around 10 for calcium aluminate (CAC) and calcium sulfoaluminate (CSAA) materials). Three different behaviors were observed for the evolution of the pH. Firstly, SR0 and SR3 started at pH around 11 and decreased progressively down to 9 over 4 weeks. The pH continued to decrease from 9 to 4 over 3 weeks followed by 3 more weeks between 3.5 and 4. Finally, the pH was stabilized until the end of the test at pH around 3. Secondly, CAC and CSAA started with a lower pH of 10 and a shorter period (3 weeks) for the progressive decrease of pH down to 9. Like PC-based materials, the pH continued to decrease for 1 week until reaching pH 4, followed by 3 weeks of pH ranging between 3.5 and 4. After then, the pH was stabilized around pH 3 until the end of the test. Thirdly, the pH of AAS started as high as for PC-binders (around 11) while it decreased rapidly as for CAC and CSAA. The rest of the evolution of pH for AAS was similar to that of CAC and CSAA. The sudden increase in pH for AAS at 35 days was due to a problem with the pump of the feeding solution, resulted in drying the specimen for 24 hours.

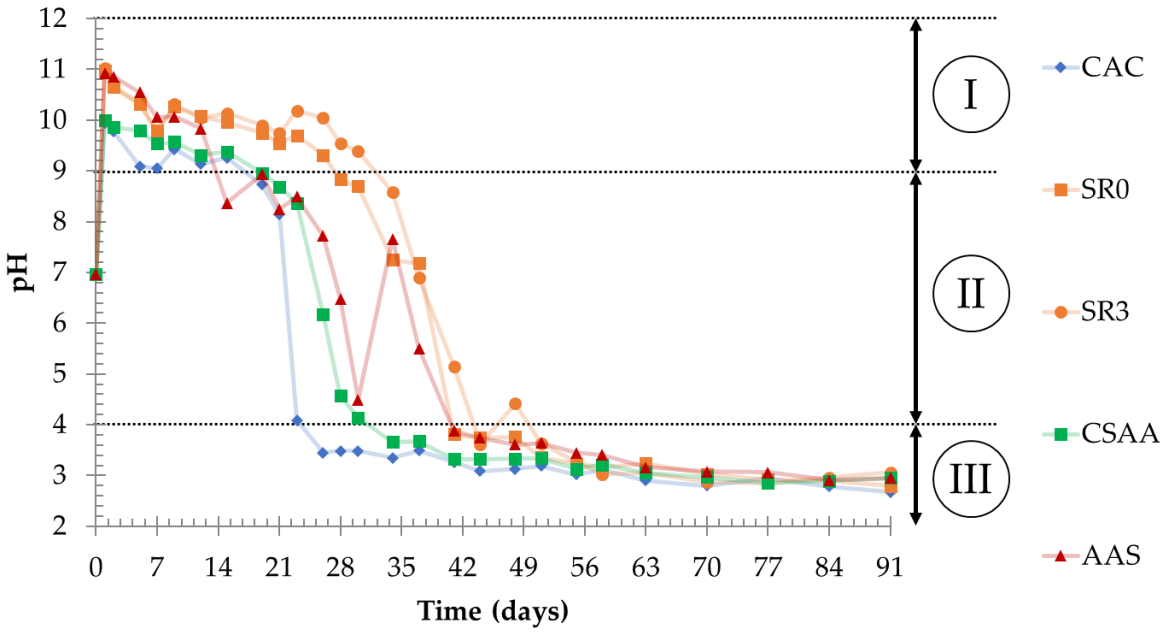

Figure III-3. Evolution of the pH measured in the leached solutions for CAC, SR0, SR3, CSAA and AAS materials during the exposure to the BAC test

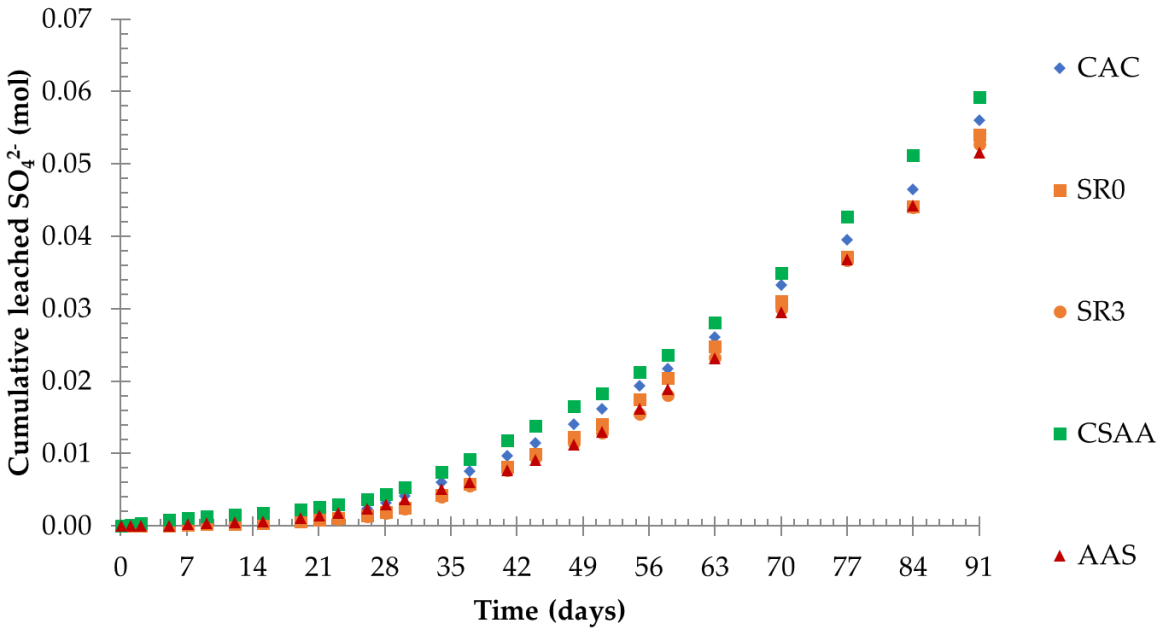

Figure III-4. The cumulative measured SO_4^{2-} (in moles) for CAC, SR0, SR3, CSAA and AAS materials during the 3-months exposure period to the BAC test

The difference in the initial pH and the decrease of pH between CAC and CSAA from one side and SR0 and SR3 from the other side was linked to the depletion of the neutralization capacity of the exposed surface of the material [67,68]. The neutralization capacity of such materials at high pH values was mainly due to the dissolution of calcium-based phases ($Ca(OH)_2$ for PC-binders, $Ca_3Al_2(OH)_{12}$ for CAC and ettringite/AFm for CSAA), leading to the release of OH^- ions. However, in the case of AAS, the higher initial pH was attributed to the hydrolysis of sodium carbonate – used as an activator for the slag – to form carbonic acid and sodium hydroxide, which has a high alkalizing property.

The cumulative leached sulfate as a function of time was in accordance with the pH profiles for the cement pastes. For early periods of the test, where the pH of the leached solutions for all materials was relatively high, only CSAA (material initially rich in SO_4^{2-}) leachate showed an increase in sulfate concentrations, which could be linked to the release of SO_4^{2-} from the cementitious matrix. However, between 21 and 35 days, SO_4^{2-} concentrations in the leached solution increased for all materials. Such period corresponded to the time when the pH of the leached solutions decreased from alkaline to acidic values. This period is known in the literature as the transition period where the number of neutrophilic bacteria decreases and the number of acidophilic bacteria increases [9,10,219]. Starting from 49 days, the kinetics of SO_4^{2-} leaching increased for all materials due to the activity of SOB. At the end of the test, the cumulative measured SO_4^{2-} ranged between 0.05 and 0.06 mole for all materials. The lowest value was recorded for AAS at 0.052 mole, followed by PC-based binders SR3 and SR0 with 0.053 and 0.054 mole respectively. CAC material had 0.056 mole of cumulative measured sulfate whilst the highest value was for CSAA at 0.059 mole, which was expected since the material contained high initial sulfate, as seen in Table III-1, susceptible of being released in an acid attack.

3.4.2. Sulfur precipitation during the exposure to the SOB attack

The exposure of different cementitious materials to the accelerated biodeterioration test (BAC test) for 3 months resulted in the formation of a yellowish-whitish layer on the exposed surfaces, as seen in Figure III-5. The formation of such precipitates did not occur at the same time for all the exposed materials. For instance, CAC, CSAA and AAS materials showed earlier precipitations (after approximately 1 month of exposure) compared to PC-based materials. Such precipitations were strongly accumulated when the pH of the leached solutions was acidic (< 4). At the end of the test, all the materials were covered with such precipitates, which were collected, grinded to < 80 μm and analyzed by X-ray diffraction (Figure III-6).

Days	1	30	55	91
CAC				
pH (CAC)	9.94	3.48	3.02	2.67
SR0				
pH (SR0)	10.98	8.70	3.23	2.79
SR3				
pH (SR3)	11.03	9.39	3.26	3.06
CSAA				
pH (CSAA)	10.00	4.14	3.13	2.95
AAS				
pH (AAS)	10.93	4.49	3.45	2.95

Figure III-5. Evolution of the precipitations on the surface of the cement pastes at different days with the correspondent pH of the leached solutions

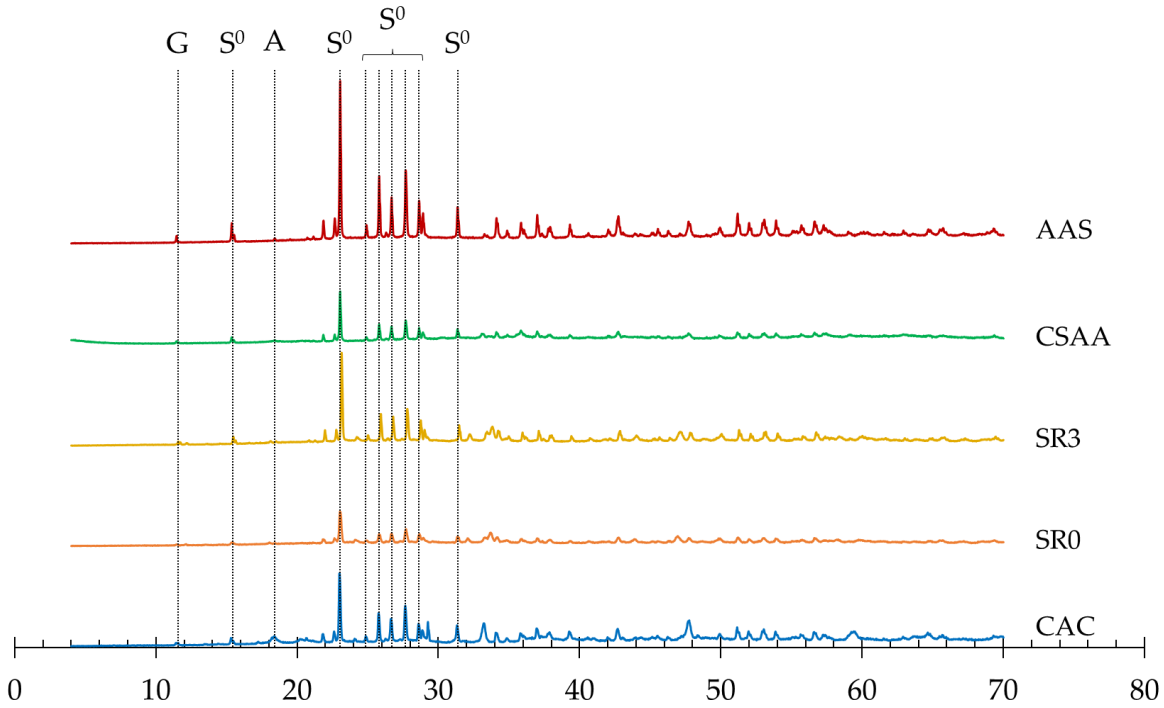

Figure III-6. X-ray patterns of the precipitation on the surface for CAC, SR0, SR3, CSAA and AAS cement pastes; S0: elemental sulfur, G: gypsum, A: aluminum hydroxide

For all materials, elemental sulfur (S^0), which was often detected on the surface of concrete exposed in sewer networks resulting from the oxidation of H_2S [5,9,10,220], was identified as the major phase in the precipitates along with other phases such as gypsum and aluminum hydroxide.

Elemental sulfur is a more reduced form of sulfur compared to tetrathionate. Hence, since the only source of sulfur introduced into the system was tetrathionate (from the feeding solution), a disproportionation of tetrathionate has occurred and is a possible pathway for tetrathionate conversion in the conditions of the BAC test.

3.4.3.Quantification of sulfur compounds

In the frame of the investigation of the sulfur cycle and the determination of the possible biochemical pathways in sewer conditions, analyses of the leached solutions were carried out to identify and quantify, if possible, the sulfur compounds. The leached solutions were analyzed by HPLC (protocol detailed in section 2.5.2.2.2 of chapter II) and an example of the results, obtained for CSAA specimen at 48 days, is reported in Figure III-7.

The chromatogram of the leached solution of the CSAA cement paste shows that not all of the tetrathionate initially present in the feeding solution was converted during the run-off on the specimen surface and that various sulfur compounds other than sulfate were formed, such as thiosulfate, pentathionate and hexathionate. Moreover, the comparison between the chromatograms during the experiment showed that the formation of the different polythionates depended highly on the pH of the leached solutions.

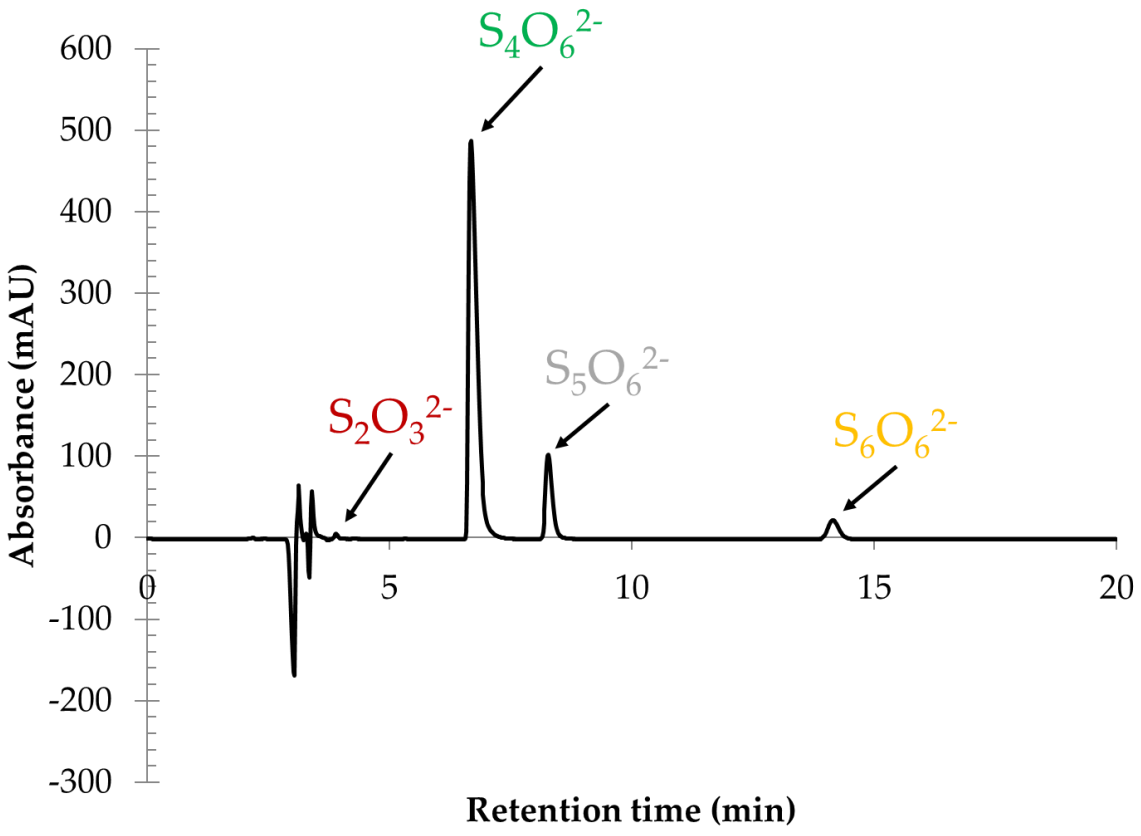

Figure III-7. Chromatogram of the leached solution of CSAA at 48 days of exposure to the BAC test

The quantification of the amount of tetrathionate and thiosulfate in the leached solutions was carried out using a prepared series of standards; however, the quantification of pentathionate and hexathionate was not possible as these products are not commercially available. Consequently, a method was used to quantify $S_5O_6^{2-}$ and $S_6O_6^{2-}$ based on their areas of the peaks compared to the area of the peak for $S_4O_6^{2-}$ on the chromatograms.

For every sample of the leached solutions collected at the outlet of the specimens, the concentrations of sulfate ($[SO_4^{2-}]_{out}$) and thiosulfate ($[S_2O_3^{2-}]_{out}$) were measured and the peak areas of tetrathionate ($S_4O_6^{2-}{}_{out}$), pentathionate ($S_5O_6^{2-}{}_{out}$) and hexathionate ($S_6O_6^{2-}{}_{out}$) were evaluated. Moreover, the peak areas of tetrathionate in the feeding solution ($S_4O_6^{2-}{}_{in}$), which was trickled on the materials surface at the inlet of the specimens, were also measured. These results are reported in Figure III-8 for the five materials.

Vertical dotted lines were reported on Figure III-8 to delimit the three different phases (I, II and III) corresponding to the three different inlet tetrathionate concentrations. The concentrations of tetrathionate at the inlet were increased progressively to accommodate the consumption rate of tetrathionate, which was low at the early days of the test and increased with the development of the microbial activity.

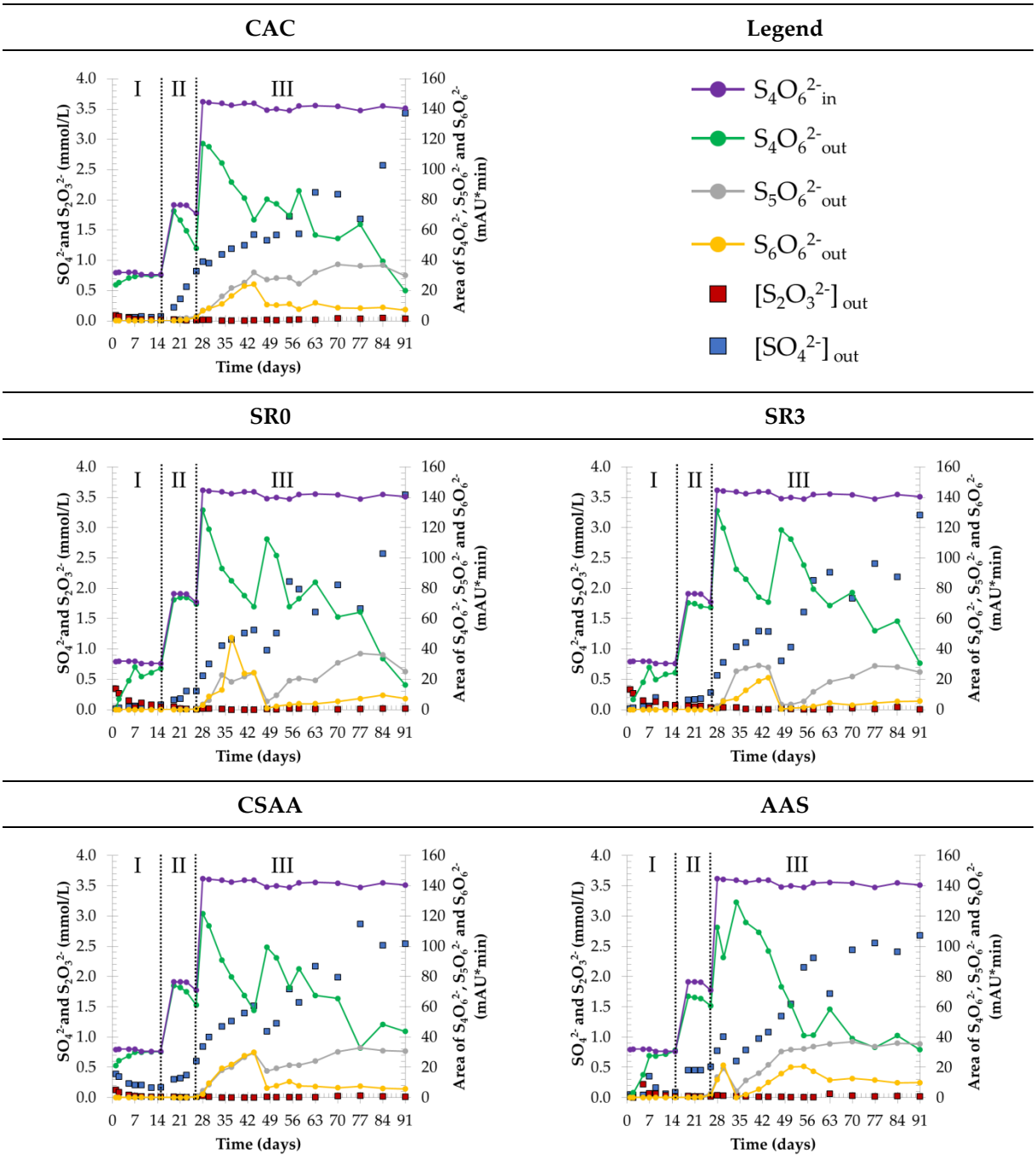

Figure III-8. Evolution of the concentrations of sulfate and thiosulfate (in mmol/L) and the area of peaks for tetrathionate, pentathionate and hexathionate (in mAU*min) obtained from the leached solutions for cement paste specimens

At the early days of the test, the conversion of tetrathionate into sulfate and thiosulfate was observed for all materials. CSAA showed relatively high sulfate concentrations, which are likely to correspond to the amount of sulfate released by the material itself because of the neutral/acidic conditions the material is exposed to, leading to the dissolution of sulfate-bearing hydrated compounds (ettringite, monosulfoaluminate, monocarboaluminate, etc). The conversion of tetrathionate was low over the first two weeks of exposure compared to the rest of the experiment for all materials, leading to low production of sulfate and thiosulfate (in particular for CAC, CSAA and AAS). The concentrations of sulfate started to increase

significantly for CAC, CSAA and AAS after 21 days of exposure compared to 28 days for PC-based materials (SR0 and SR3). The increase in sulfate concentrations was consistent with the evolution of pH (Figure III-3) where the pH decreased from alkaline to acid starting from 21 days for CAC, CSAA and AAS and starting from 28 days for SR0 and SR3.

After 28 days of exposure, pentathionate and hexathionate were firstly observed, corresponding to the period when the pH of the leached solutions was lower than 9. At such pH, the elemental sulfur started to be observed on the specimens' surfaces (Figure III-5), showing a correlation between the formation of polythionates and elemental sulfur and the decrease in pH. The concentration of pentathionate and hexathionate continued to increase until 49 days (except for AAS which was around 35 days because of a drying period of 24h leading to a punctual decrease of the microbial activity with no further consequences). The sudden decrease in pentathionate and hexathionate corresponded to the date at which the flow pumps were changed. Afterwards, from day 49 to day 91, sulfate production (thus acid production) increased with the increase in tetrathionate and hexathionate consumption and the stabilization of pentathionate. The period of high tetrathionate consumption with high rate of sulfate production corresponded to the period with low pH for the leached solutions of all materials.

3.5. MODELING APPROACH TO SIMULATE THE TRANSFORMATION OF TETRATHIONATE BY SULFUR-OXIDIZING ACTIVITIES

3.5.1. Proposed reactions to describe the oxidation of polythionates

Based on experimental observations and the literature review, for a mass balance approach, five stoichiometric reactions (**Eq.III-1** to **Eq.III-5**) were proposed to represent the different pathways and the different observed sulfur-based intermediates. Only sulfate, thiosulfate, tetrathionate, pentathionate, hexathionate and elemental sulfur were considered due to no detection of other sulfur compounds in the experimental conditions.

$S_4O_6^{2-} + 0.5\ O_2 + 1.5\ H_2O \rightarrow 1\ SO_4^{2-} + 1.5\ S_2O_3^{2-} + 3\ H^+$ **Eq.III-1**

$S_4O_6^{2-} + 0.05\ O_2 + 0.65\ H_2O \rightarrow 0.75\ SO_4^{2-} + 0.55\ S_2O_3^{2-} + 0.25\ S_5O_6^{2-} + 0.1\ S_6O_6^{2-} + 0.3\ S^0 + 1.3\ H^+$ **Eq.III-2**

$S_5O_6^{2-} + 5\ O_2 + 4\ H_2O \rightarrow 5\ SO_4^{2-} + 8\ H^+$ **Eq.III-3**

$S_6O_6^{2-} + 6.5\ O_2 + 5\ H_2O \rightarrow 6\ SO_4^{2-} + 10\ H^+$ **Eq.III-4**

$S_2O_3^{2-} + 2\ O_2 + H_2O \rightarrow 2\ SO_4^{2-} + 2\ H^+$ **Eq.III-5**

Reaction (**Eq.III-1**) corresponds to the disproportionation of tetrathionate, in alkaline environments, into sulfate with intermediate production of thiosulfate (due to experimental observations in early steps of tetrathionate conversion) [221]. Reaction **Eq.III-3** corresponds to the total oxidation of pentathionate into sulfate. Reaction **Eq.III-4** corresponds to the total oxidation of hexathionate into sulfate. Reaction **Eq.III-5** corresponds to the total oxidation of thiosulfate into sulfate. Finally, based on experimental results and literature observations, reaction **Eq.III-2** was proposed as a global reaction of tetrathionate disproportionation in acid environments. This reaction led to the production of sulfate, thiosulfate, pentathionate, hexathionate and elemental sulfur as described for the last period of the experimental data (day 49 to day 91). This reaction produces less acid per mole of converted tetrathionate compared to reaction **Eq.III-1**. The part of tetrathionate, which was oxidized directly into sulfate, was obtained by the combination of reactions **Eq.III-1** and **Eq.III-2**.

In the BAC test conditions, since the acid production is the key parameter of the biochemical aggressiveness of the environment, the oxidation of tetrathionate into sulfite or sulfate leads, from a stoichiometric viewpoint, to the same production of H^+ (as presented in equations **Eq.I-2** and **Eq.I-3**, in chapter I and **Eq.III-6**. The only difference is the oxygen consumption; thus, the little amount of sulfite formed were considered as sulfate:

$$S_4O_6^{2-} + 3.5\ O_2 + 3\ H_2O \rightarrow 4\ SO_4^{2-} + 6\ H^+ \qquad \textbf{Eq.III-6}$$

3.5.2. Evolution of the proposed pathways over time for cement-based materials exposed to the BAC test

For each leached solution, since the area of the tetrathionate peak is proportional to its concentration, the amount of converted tetrathionate was calculated from the difference between the inlet flux and the outlet flux of tetrathionate, obtained after calibrating the HPLC equipment with the tetrathionate standards. An Excel solver was used to determine the applied percentage of each proposed pathway (reactions **Eq.III-1**, **Eq.III-2**, **Eq.III-3**, **Eq.III-4** and **Eq.III-5**), using corresponding factors A_{exp}, B_{exp}, C_{exp}, D_{exp} and E_{exp} respectively, at each time step. The aim of using such factors was to minimize the difference between the amount of measured and estimated sulfate, the amount of measured and estimated thiosulfate, the ratio of peaks' area of the measured pentathionate and tetrathionate and the ratio of their estimated concentrations, and finally the ratio of peaks' area of the measured hexathionate and tetrathionate and the ratio of their estimated concentrations.

The evolution of the factors, obtained from experimental data, considering the five proposed reaction pathways are presented Figure III-9. The results showed different evolution over time for each factor. However, each factor presented the same trends for all materials. At the beginning of the testing period, since only sulfate, thiosulfate and tetrathionate were detected, reaction **Eq.III-1** was considered as the only pathway for the transformation of tetrathionates. Hence, factor A_{exp} was at its highest rate (=1). However, as the pH decreased, the impact of

reaction **Eq.III-1** decreased progressively – indicating that factor A_{exp} followed similar trends to that of the evolution of the pH (Figure III-3) – and reaction **Eq.III-2** took place in acidic environments. Correspondingly, factor A_{exp} decreased and factor B_{exp} increased following the equation $B_{exp} = 1 - A_{exp}$ since reactions **Eq.III-1** and **Eq.III-2** are complementary and describe the fate of tetrathionate.

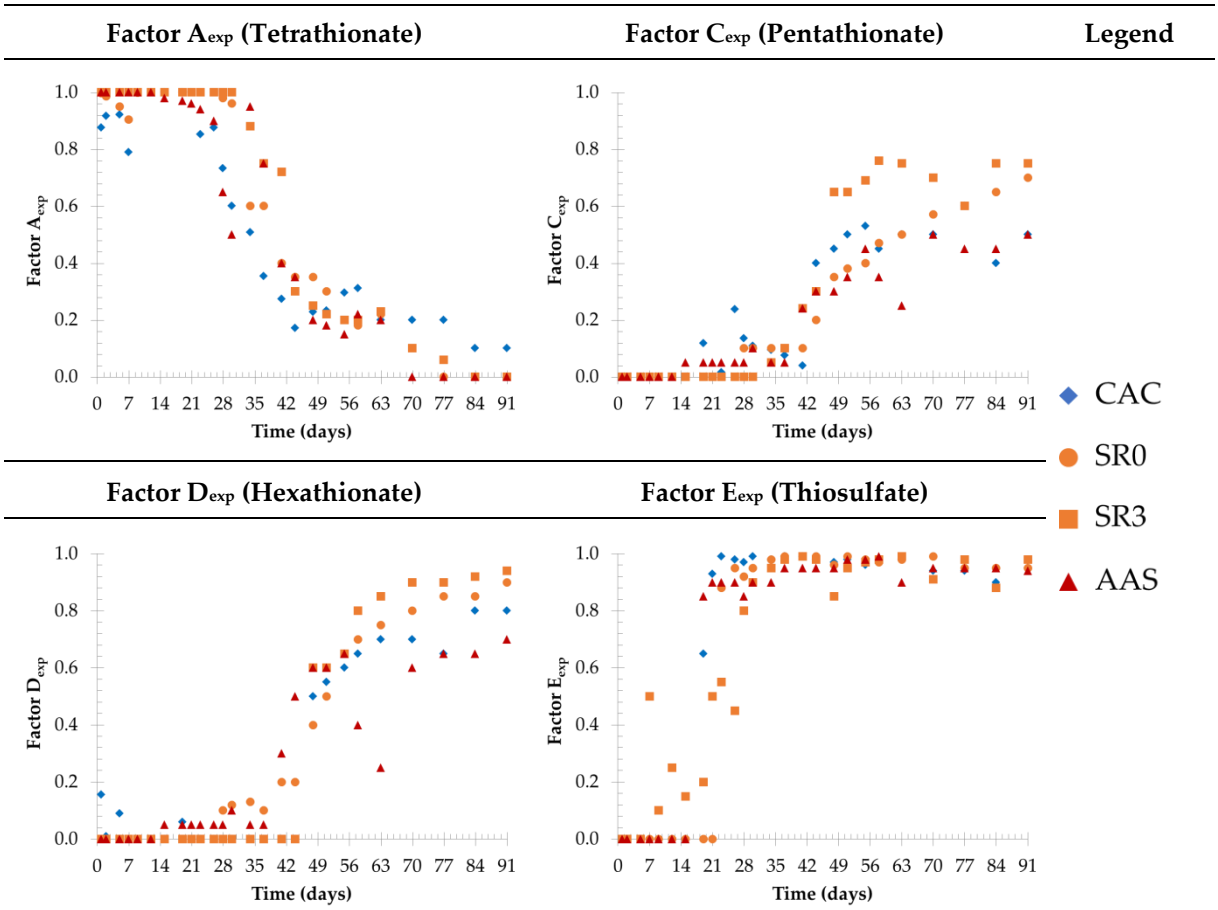

Figure III-9. Estimation values for factors (A_{exp}, C_{exp}, D_{exp} and E_{exp}), obtained from experimental data, for the exposed materials

For factors C_{exp} and D_{exp}, corresponding to the complete oxidation of pentathionate and hexathionate into sulfate respectively, their evolutions were similar and seemed to be correlated to the pH, with no activity at alkaline pH and maximal activity at low pH. In fact, reactions **Eq.III-3**, **Eq.III-4** and **Eq.III-5** are secondary reactions and dependent on reactions **Eq.III-1** and **Eq.III-2**. The reactants are the products of the latter reactions; thus, since neither pentathionate nor hexathionate were produced by the reaction **Eq.III-1**, the factors C_{exp} and D_{exp} were equal to zero in the very first steps of the conversion of tetrathionate. For factor E_{exp}, corresponding to the complete oxidation of thiosulfate, the trend was slightly different with very low activity at high alkaline pH; however, the activity increased sooner at relative neutral pH compared to factors C_{exp} and D_{exp}.

Based on the values of the factors for each sample, reactions **Eq.III-1** to **Eq.III-5** were used to estimate the yield of the different pathways, thus the production of sulfate, thiosulfate,

pentathionate, hexathionate and elemental sulfur with the known amount of converted tetrathionate. The results issued from these calculations are presented in Figure III-10.

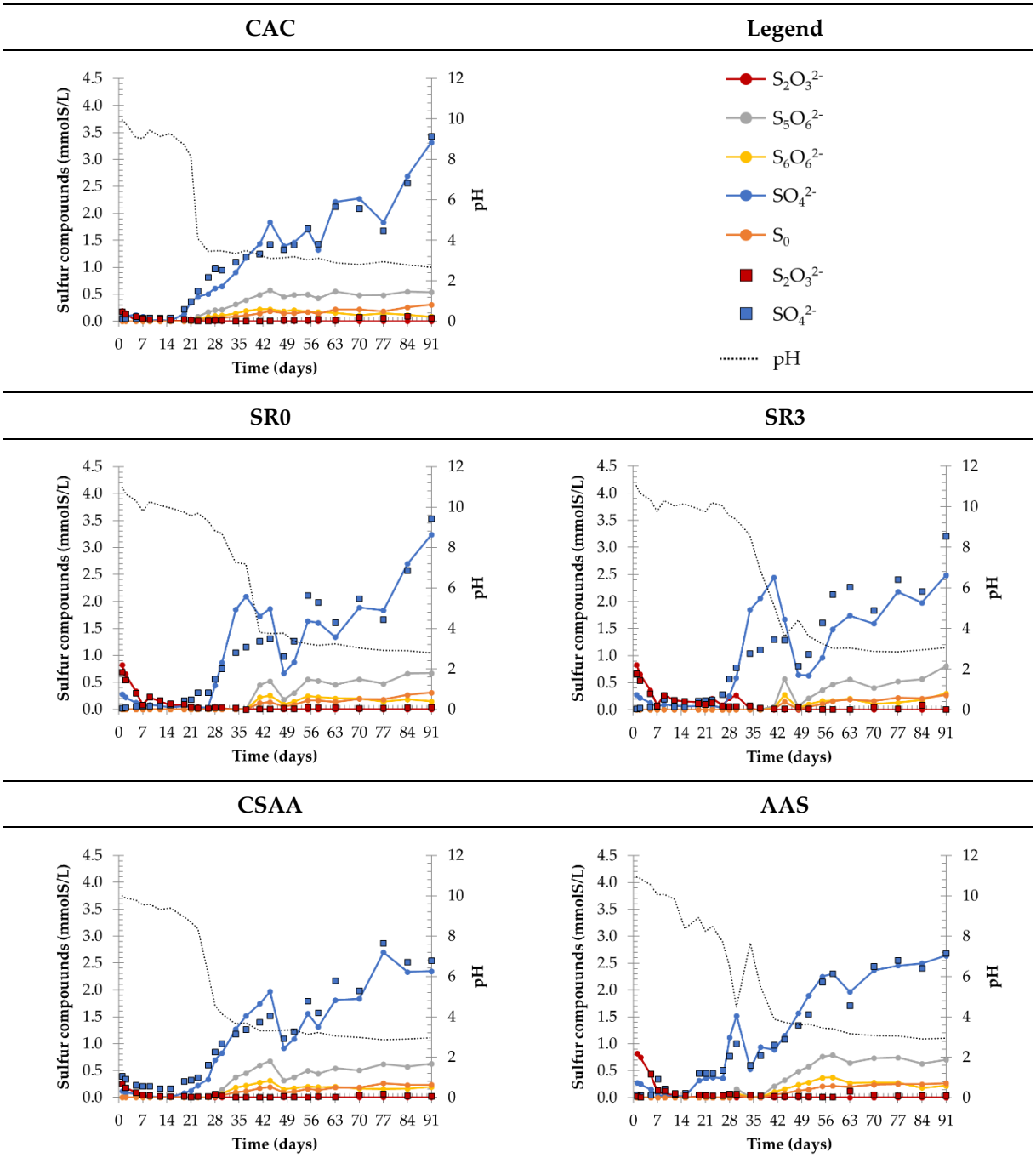

Figure III-10. Conversion of tetrathionate into polythionates; elemental sulfur and sulfate for the cement specimens

The proposed stoichiometric biochemical pathways for tetrathionate conversion showed good representation of the production of sulfate and the formation of the different sulfur compounds ($S_2O_3^{2-}$, $S_5O_6^{2-}$, $S_6O_6^{2-}$ and S^0). At the initial periods of the test, the pH was relatively high for all materials, the oxidation of thiosulfate was not activated which resulted in the oxidation of tetrathionate into sulfate and thiosulfate as the main pathway. However, in acidic environments, the disproportionation of tetrathionate seemed to be the main pathway with

the formation of mainly sulfate, thiosulfate, pentathionate and elemental sulfur with little amounts of hexathionate.

3.6. BIOLOGICALLY PRODUCED POLYTHIONATES AND SULFATE

3.6.1. Influence of pH on the reaction pathways taken by microorganisms and the consequences on polythionates' transformation

In the previous section, each proposed pathway (reactions **Eq.III-1**, **Eq.III-2**, **Eq.III-3, Eq.III-4** and **Eq.III-5**) was attributed a factor determining its applied percentage following the experimental results of the sulfur analyses.

Since the pH was identified to be the main influential factor of the different pathways, five mathematical equations, representing modeled factors for the five stoichiometric reactions, were proposed to represent the influence of the pH on the active pathways for the reactions of tetrathionate and sulfur intermediates. These factors were called A_{mod}, B_{mod}, C_{mod}, D_{mod} and E_{mod}.

Table III-2 presents the numerical models, except factor B_{mod} since it is linked to factor A_{mod} by the same equation as in experimental results, i.e. $B_{mod} = 1 - A_{mod}$. The different parameters (μ, pH_{opt}, α, γ, δ and ε) were estimated using an excel solver and the least squares method between the experimental and the modeled factors.

Table III-2. Mathematical equations representing the influence of pH on the sulfur reaction pathways

Associated Species	Model factor	Parameters					
		μ	pH_{opt}	α	γ	δ	ε
Tetrathionate	$A_{mod} = pH^{\alpha} / (pH_{opt}^{\alpha} + pH^{\alpha})$	-	4.02	8	-	-	-
Pentathionate	$C_{mod} = pH / (pH + (pH/\mu)^{\gamma})$	2.50	-	-	10	-	-
Hexathionate	$D_{mod} = pH / (pH + (pH/\mu)^{\delta})$	2.81	-	-	-	16	-
Thiosulfate	$E_{mod} = (1.6\ pH) / (pH + (pH/\mu)^{\varepsilon})$	9.00	-	-	-	-	45

Figure III-11 presents the obtained results for the different experimental factors (A_{exp}, C_{exp}, D_{exp} and E_{exp}) and the corresponding modeled factors (A_{mod}, C_{mod}, D_{mod} and E_{mod}) for all exposed materials, except CSAA, as a function of the pH. CSAA was excluded from the data set to avoid disturbing the calibration of the models by the very high initial SO_4^{2-} content of the material.

The estimated A_{mod} showed very good representation at high pH (> 10) of the experimental factor A_{exp}. Around neutral pH (7-5), A_{mod} slightly overestimated the part of reaction **Eq.III-1** in the transformation of tetrathionate. This was due to the quick decrease of pH of the materials over relatively short period. However, the developed factor A_{mod} was overall

successful in reproducing the trend of A_{exp} with high values in alkaline conditions and a progressive decrease in values moving toward acidic conditions. Factors C_{mod} and D_{mod} showed similar trends and a very good representation of the experimental factors C_{exp} and D_{exp}. Both factors remained very low until pH 4, below which pH their values increased exponentially. The last phase corresponds to the transformation of pentathionate and hexathionate into sulfate. Finally, factor E_{mod} increased progressively starting from pH 10 to represent the transformation of thiosulfate into sulfate, observed previously in Figure III-9. Moreover, factor E_{mod} reached its maximum value (=1) starting from pH around 8, which corresponded to the disappearance of thiosulfate in the leached solutions.

The different nature of the studied materials did not seem to have any significant impact on the transformation of tetrathionate. The different pathways were mainly controlled by the evolution of the pH of the leached solutions.

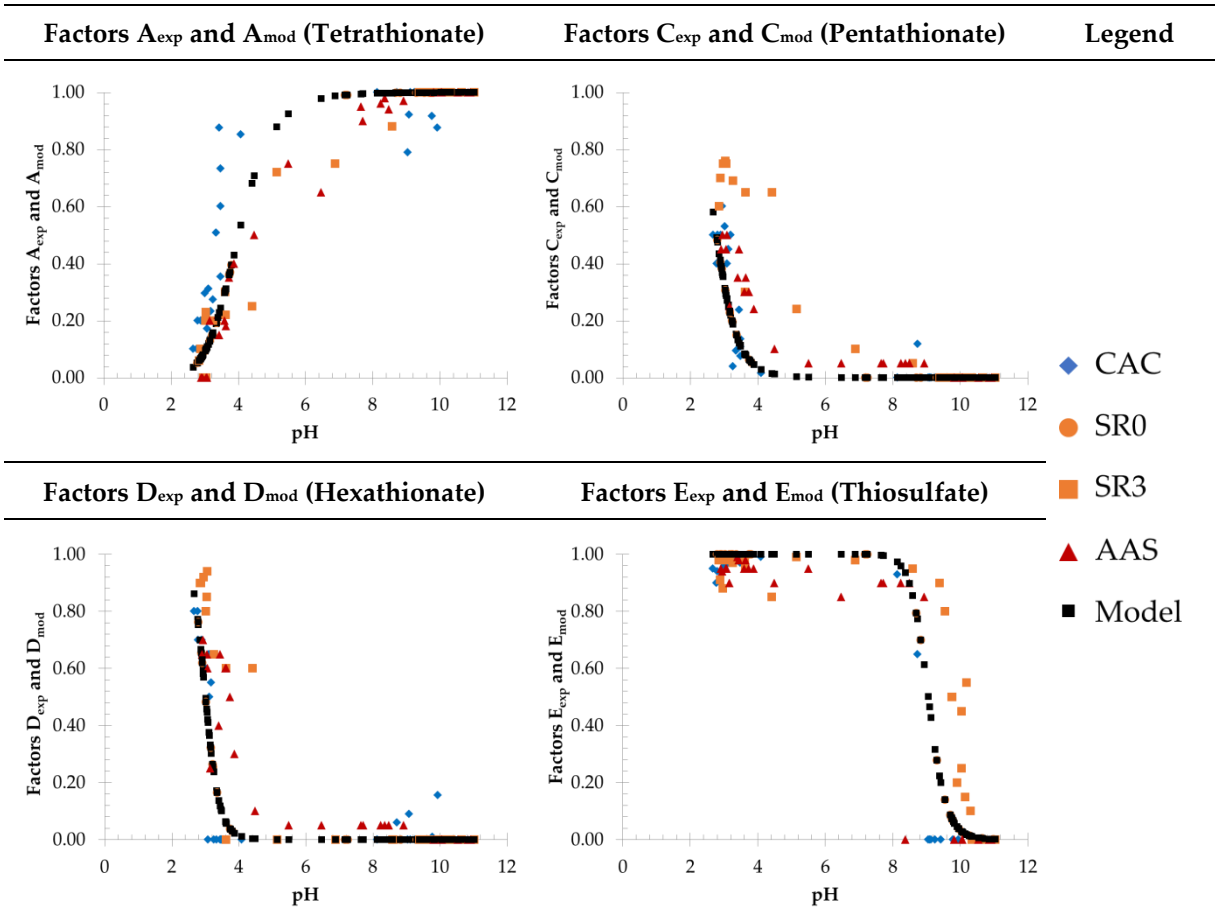

Figure III-11. Evolution of the factors A_{mod}, C_{mod}, D_{mod} and E_{mod} compared to the experimental factors A_{exp}, C_{exp}, D_{exp} and E_{exp} for the different pathways as a function of pH

3.6.2. Estimation of biologically produced sulfate and thiosulfate

Figure III-12 presents the results of the cumulative sulfate and thiosulfate measured experimentally and the estimated amounts of the different polythionates, elemental sulfur and sulfate (in mmolS) identified in the corresponding leached solutions for cement materials.

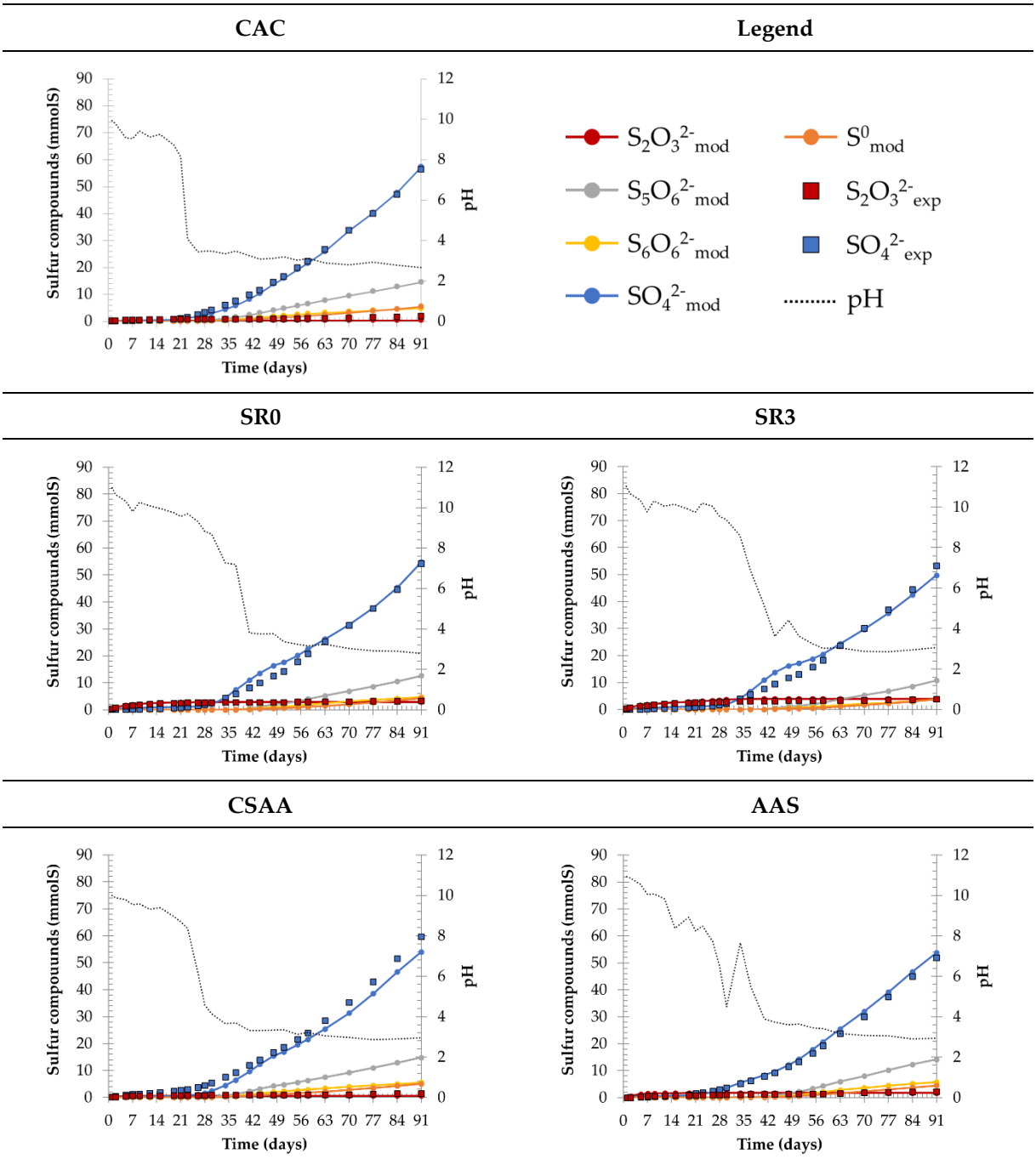

Figure III-12. Cumulative sulfur compounds (in mmolS) comparing measured experimentally and calculated using the proposed model for cement paste specimens

For all materials, the developed models have successfully represented the experimental results in terms of amount and kinetics of sulfate production using the amount of converted tetrathionate and the evolution of pH. Moreover, the formation and quantification of the observed polythionates (pentathionate, hexathionate and thiosulfate) in the leached solutions

and the elemental sulfur on the surface of the materials became possible by using the model equations linking these sulfur species to the pH.

The study of the fate of tetrathionate in biodeterioration conditions highlighted the difference in the part of sulfate produced biologically and the part of sulfate released from the materials. Table III-3 shows the comparison between the total amounts of cumulative sulfate measured experimentally and the total amounts of biologically produced sulfate estimated using the mathematical functions.

Overall, the amount of leached sulfate estimated by the models was lower than the amount measured experimentally for all materials. Such difference was observed for all materials with different extent and depended strongly on the amount of initial sulfur in the cementitious matrix as well as on the chemical stability of the mineralogical phases.

For materials with very low initial amount of sulfate in the cementitious matrix (CAC and AAS), the models showed that nearly 99 and 98%, respectively, of sulfate came originally from the biochemical oxidation of tetrathionate (either direct oxidation from tetrathionate or by passing through the sulfur intermediates). 96% of sulfate for SR0 material were identified to come from the biochemical oxidation of tetrathionate while only 4% were coming from the material itself which contained initially 2.86% of sulfur in the form of SO_3^{2-}. Although SR3 had slightly higher amount of initial sulfur compared to SR0, the results showed that at the end of the testing period, around 10% of the experimentally measured sulfate was released from the material itself. The increase in measured sulfate seemed to occur during the pH transition period from alkaline to acid. Finally, CSAA, as a sulfate-rich material, showed that 87% of sulfate came from microorganisms' activities while 13% was released from the material.

Table III-3 shows a comparison between the cumulative amount of acid estimated from the literature using **Eq.III-6** and the cumulative amount of acid estimated using the developed numerical model.

Table III-3. The total amount of cumulative sulfate (in mmolS) measured experimentally and estimated using the numerical model (five stoichiometric reactions) after 91 days of exposure highlighting the part of the sulfate released from the materials

Materials	Cumulative SO_4^{2-} (mmolS)				Initial SO_3^{2-} content (wt.%)	Cumulative H^+ (mmolH)	
	Exp.	Model	Estimated biologically produced SO_4^{2-} (%)	SO_4^{2-} released from the material (%)		Estimated from **Eq.III-6**	Estimated using the model
CAC	56.38	55.96	99.26	0.74	0.02	84.08	79.29
SR0	54.35	52.26	96.15	3.85	1.69	81.03	75.12
SR3	53.27	47.52	89.21	10.79	2.79	79.09	69.16
CSAA	59.62	51.93	87.10	12.90	13.70	88.83	73.17
AAS	51.93	50.83	97.88	2.12	0.64	77.42	71.99

The estimation of acid using stoichiometric equations from the literature was based on the total amount of measured sulfate. For each mole of sulfate produced, 1.5 moles of acid were produced. However, the estimation of acid using the model for all materials did not seem to correlate only to the amount of sulfate measured experimentally, which confirmed the importance of taking into account the sulfur intermediate compounds. The lowest estimated amount of acid was obtained for SR3 and the highest was obtained for CAC. Surprisingly, CAC has very low amount of initial sulfur in the cementitious matrix. However, its early drop in pH allowed bacteria to develop earlier than other materials and to produce more acid. Although measured sulfate concentrations were higher for CSAA, CAC showed more acid production by the bacteria on its surface, which is in accordance with the pH decrease of CAC. Moreover, the measured sulfate for CSAA contained the amount of sulfate produced biologically as well as the amount of mineral sulfate released by the material itself. Hence, the amount of estimated acid based on the measured sulfate was not adequate in the case of CSAA. Therefore, the amount of acid estimated by the model was more representative of the real amount of acid produced on the surface of the material.

Figure III-13 shows the experimental measurements of cumulative thiosulfate (in mmolS) compared to the cumulative estimated thiosulfate (in mmolS) using the proposed models.

In the first 14 days of the test, the pH of CAC and CSAA was between 10 and 9 and the pH of AAS was between 11 and 10. While the main pathway for thiosulfate production was still reaction **Eq.III-1** for the three materials, Figure III-11 showed that between pH 10 and 9, up to 50% of the thiosulfate formed via reaction **Eq.III-1** was oxidized to form sulfate. Contrarily, at pH > 10, the factor E_{mod} indicated only 5% of thiosulfate was oxidized, resulting in the high accumulation and overestimation of thiosulfate formation using the modeled equations for AAS.

As PC-based materials showed pH between 11 and 9 for 28 days, the kinetics of thiosulfate oxidation to form sulfate were very low and the model represented very well the tendency of the production of thiosulfate using reaction **Eq.III-1** in alkaline conditions. However, in acidic conditions, the results of the model showed constant values for all materials, which was due to the constraints linked to reaction **Eq.III-5** and to pH. Nevertheless, the amount of thiosulfate measured experimentally remained very small compared to the amount of sulfate or other sulfur species as shown in Figure III-12.

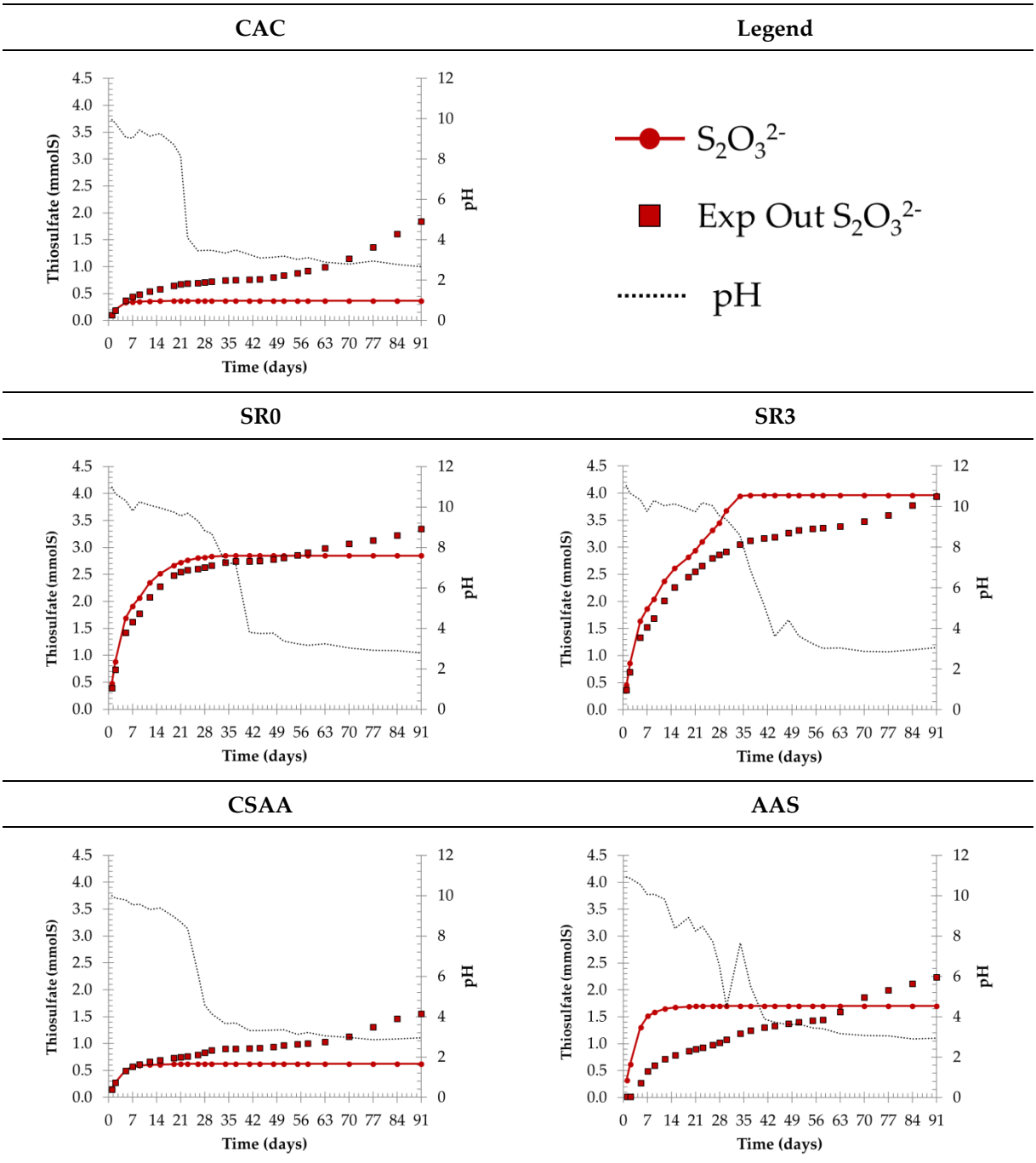

Figure III-13. Comparison between experimental measurements of thiosulfate (in mmolS) and estimated amount of thiosulfate (in mmolS) using the proposed model for cement paste specimens

3.6.3. Influence of the materials on tetrathionate conversion and sulfuric acid production

Figure III-14 presents the cumulative leached sulfate for each material after the 3-month exposure to the BAC test. Except CSA materials (CSAC, CSAA and CSAG), the initial amount of sulfur in the materials were very low (Table II-2); therefore, the measured leached sulfate for these materials could be directly correlated to the biological conversion of the tetrathionate

and to the sulfuric acid produced. The quantity of produced sulfate was different from one material to another and the values ranged between 52 mmolS to 68 mmolS.

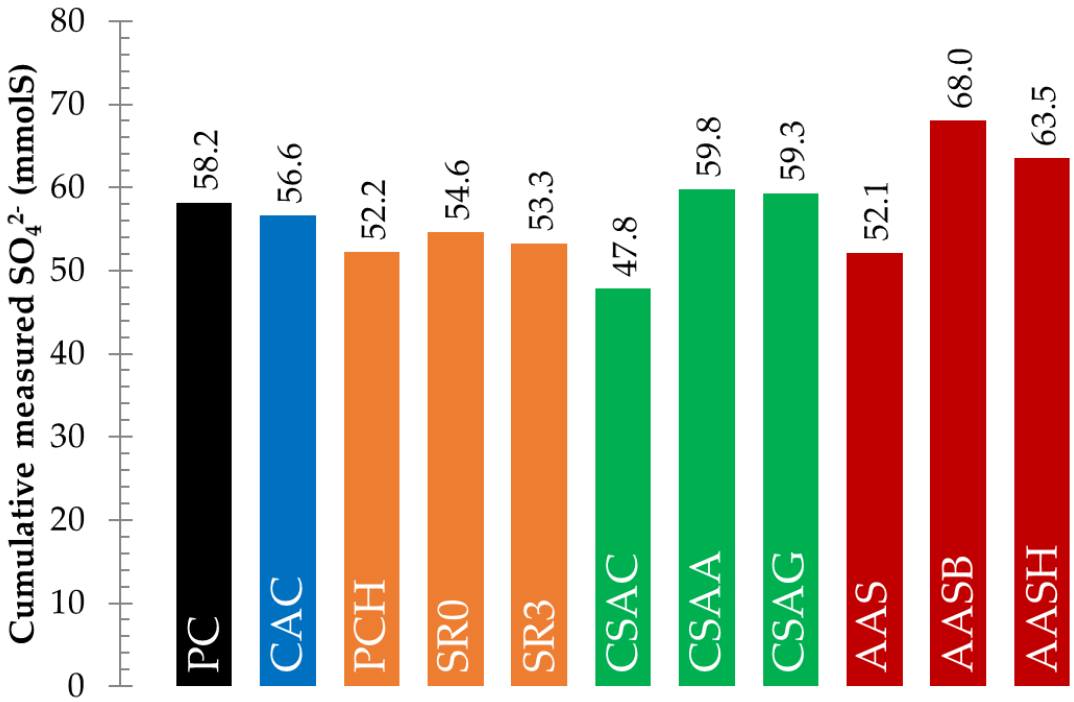

Figure III-14. Cumulative leached sulfate for all exposed materials after 3 months

Regarding the impact of HardCem, while PCH (containing 20 wt.% of HardCem) had a lower cumulative sulfate than PC which could indicate that HardCem limited the sulfate production, AASH (containing 10 wt.% of HardCem) showed higher cumulative sulfate than AAS (without HardCem), indicating that the influence of HardCem did not follow the same trend. The cumulative measured sulfate for the CAC (56.6 mmolS) material was in the same magnitude as that of the PC material (58.2 mmolS). SR0 and SR3 presented also similar values; i.e. 54.2 and 53.3 mmolS, respectively. AASB showed the highest quantity of cumulative sulfate measured at 68 mmolS.

Several parameters, such as the average pH, the calcium, aluminum or iron content, were investigated in order to explain the differences; however, no clear correlation was found. As a matter of fact, the microbial activity under such complex and highly heterogeneous conditions is not fully controllable. **Thus, the evaluation of the reactivity of the materials was carried out, in the rest of this document, as function of the cumulative produced acid rather than the cumulative produced sulfate.**

3.7. IDENTIFICATION OF MICROBIAL POPULATIONS COLONIZING THE MATERIALS

The analyses of the conversion of tetrathionate and the associated sulfuric acid production showed that the materials have no clear impact, in the experimental conditions, on the sulfur-oxidizing activities, except a pH influence dependent on the material reactivity.

However, while the fate of the tetrathionate conversion was only pH dependent, with no significant impact of the material except the resulting pH, the selected microbial populations could vary depending on the nature of the exposed material. The variation in the microbial populations could result from an influence of the materials with no consequences on the tetrathionate conversion nor the acid production, in our experimental conditions.

In the objective of investigating such aspect, biomass samples were collected at the end of campaign 3 (for PC and CAC materials) and at the end of campaign 4 for all the materials. For campaign 4, two different types of samples for each materials were carried out:

(i) Surface: samples of biomass corresponding to the biofilm developed at the exposed surface of the cementitious specimens.
(ii) Deep: samples of biomass obtained by grinding the totality of the deteriorated zones; thus, considering the possible biomass developed inside the material.

3.7.1.Relative abundance and diversity of selected consortium

Figure III-15 presents the relative abundance of the selected bacterial species for each tested material, from two different campaign (C3 and C4), with different types of samples (Surface and Deep). For a better readability, species found below 2% were associated to the category Others. In order to ease the readability of the figure, the sulfur-oxidizing bacteria and bacteria from the genus *Acidophilium* were represented in black boxes while the bacteria involved in the sulfur cycle (other than sulfur-oxidizing bacteria) were represented in black dotted boxes. The bacteria involved in the iron cycle were represented in white and the species represented by a white rectangle framed in black is *Acidithiobacciullus Ferrooxidans*, a sulfur-oxidizing species capable of growing on iron.

Major remarks: The presented results are not quantitative; they represent only relative abundance and index diversity. Only known bacteria are identified since the analysis of the data was based on the main biological activity or the specific environment, such as sulfur-oxidizing bacteria, or acidophilic bacteria, etc. The analysis focused only on bacteria (major microorganisms developed) whilst other sulfur oxidizing microorganisms could be present, such as archaea [222].

The data analyses showed that :

(1) Compared to the initial consortium (activated sludge, labelled ASludge-Inoc) used as inoculum, the selected consortium for all materials were completely different at the end of the experiment. However, the very significant diversity of bacteria in the initial activated sludge could indicate a technical problem with the sample analysis.
(2) For all the materials, mainly acidophilic and sulfur-oxidizing bacteria were selected (with *Thiomonas* and *Acidithiobacillus* as the major identified species),

confirming the presence of acidophilic sulfur-oxidizing activity. Moreover, *Thiomonas Intermedia* (*a Thiomonas* species) is known to be able to disproportionate tetrathionate in the absence of oxygen, which could explain some of the fate of tetrathionate during the conversion [223].

(3) The consortia for the PC, exposed in campaigns C3 and C4, were similar: same dominant species *Acidiphilum Rubrum*, *Thiomonas* and *Acidithiobacillus* species, representing more than 40% of the total population identified.

(4) For the CAC, the selected consortium in campaign C3 was different from that of campaign C4. An over-representation of *Acidiphilum* species was observed in campaign C3. In campaign C4, the amount of sulfur-oxidizing bacteria was lower than for the other materials of the same campaign. A high proportion of the category Others could indicate some problems with these samples. In a previous study, no difference was observed in terms of microbial diversity between BFSC and CAC mortars exposed to similar conditions [24].

(5) For the PC based materials (PC, PCH, SR0 and SR3), no significant difference in the selected consortia was detected. The addition of Hardcem did not influence the selected population. Only one sample seemed different (SR0-Deep (C4)); however, like the CAC C4, the category of Others was over-represented indicating a possible problem with the analysis of this sample.

(6) The AAS consortium was similar to that of PC-based materials. The addition of bauxite led to an over-selection of *Acidithiobacillus ferrooxidans*, which could indicate a specific impact of iron provided by the bauxite in such materials. The addition of HardCem led also, but to a lower extent, to an over-selection of *Acidithiobacillus ferrooxidans*, which could indicate a difference in the mobility of iron between HardCem and bauxite. The mineral additives seemed to contribute to the reactivity of the material in acidic conditions and to influence the selected consortia.

(7) On the one hand, for CSAC and CSAG, the selected consortia were similar to the consortia selected on PC-based materials. On the other hand, for CSAA, a high proportion of *Acidithiobacillus ferrooxidans* was observed indicating a particular fate of iron in such material.

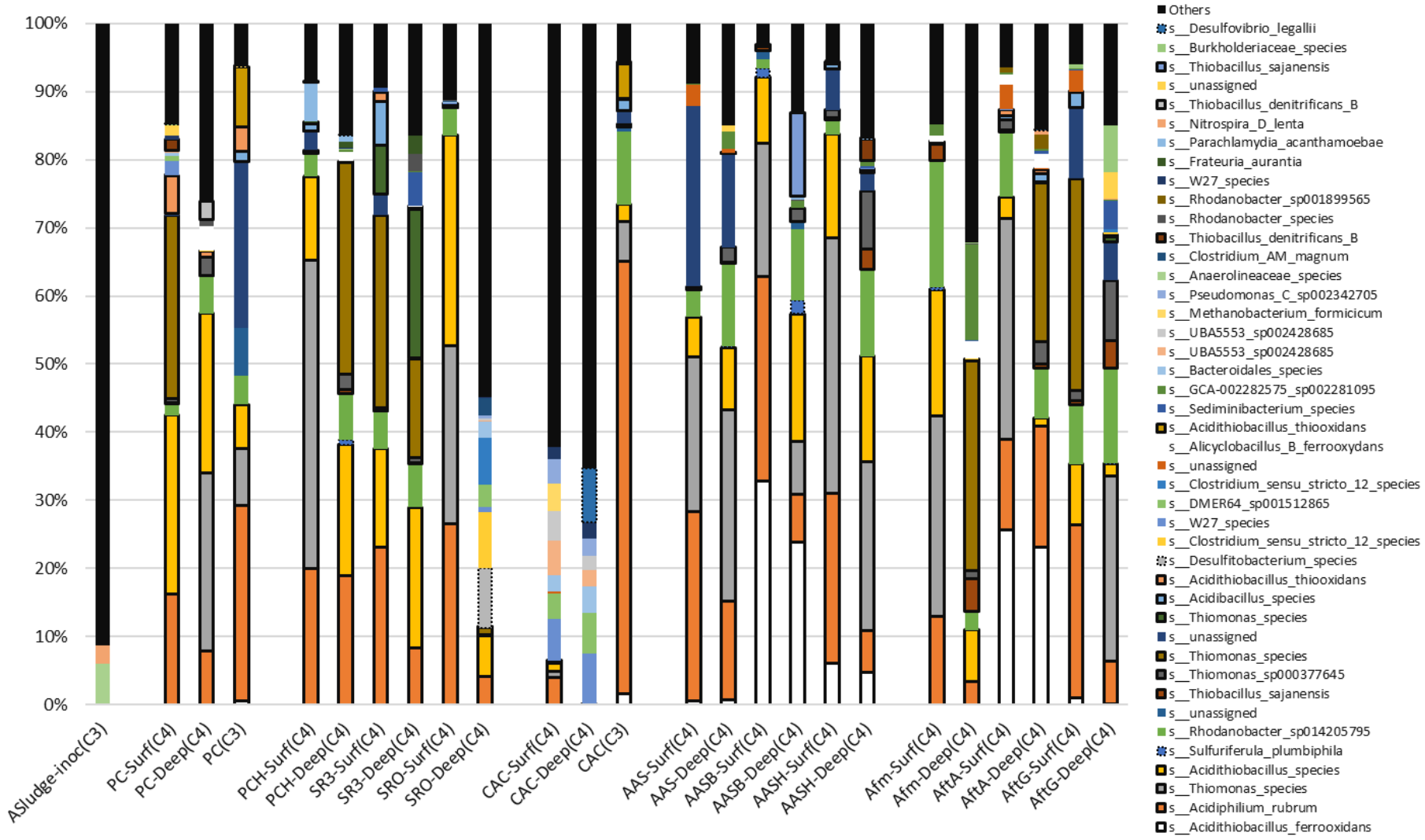

Figure III-15. Identification of the microbial populations developed on the exposed surface of the specimens (Surf) and possibly inside the deteriorated zones (Deep) for various cementitious materials after 3-months of exposure to the BAC test compared to the initial activated sludge (ASludge-inoc) from two different campaigns

3.8. DISCUSSION

3.8.1. Influence of pH on the determination of reaction pathways for tetrathionate transformation during sulfur-oxidizing process

The different natures of cementitious materials did not have a direct impact on the transformations of tetrathionate, although it did on the evolution of the pH. During the development of sulfur-oxidizing activities on mineral substrate in sulfide environments, stages of attack and their mechanisms have been identified and documented in the literature [5,6,9,10,15]. Bacterial activities result in the production of polythionate and sulfuric acids on the surface of mineral materials. As the pH of the medium decreases, the deterioration process of the materials progresses, leading to the dissolution of mineralogical phases. Such dissolution releases hydroxide ions (OH^-) which are the responsible for neutralization of the acid (H^+).

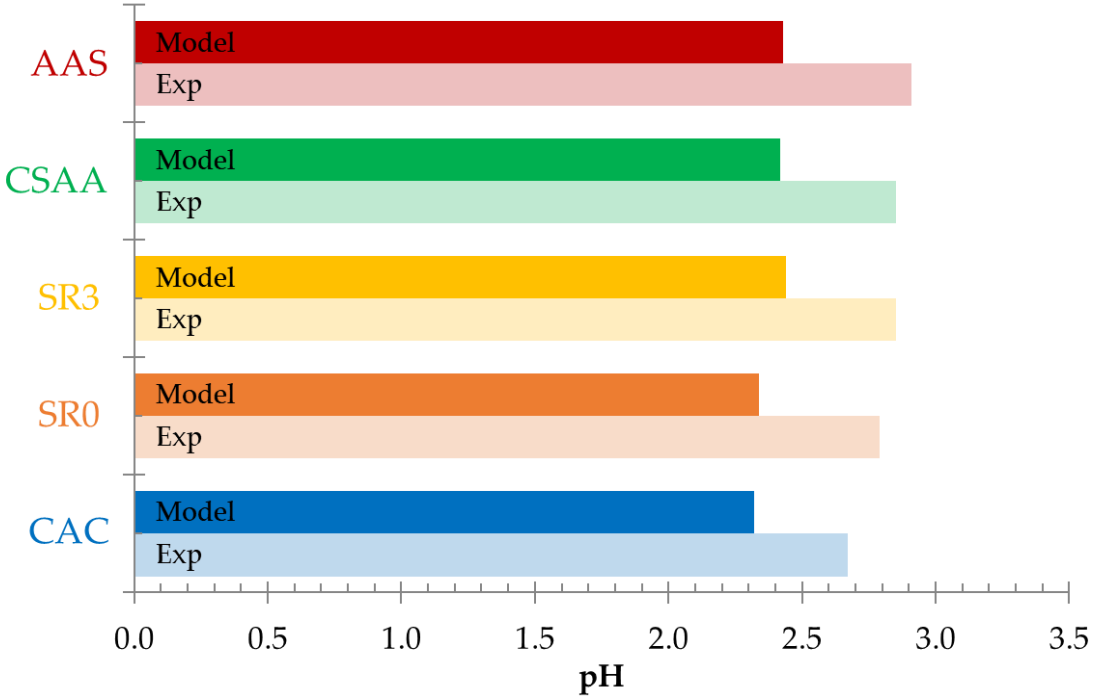

Figure III-16. Comparison between the experimental measured pH and the estimated theoretical pH (not taking into account the neutralization capacity of the materials) using the amount of acid estimated from the model

Figure III-16 shows a comparison between the lowest pH measured experimentally and the corresponding theoretical pH (without taking into account the buffer effect of the materials) using the amount of estimated acid by the developed model.

The theoretical values of pH were lower than the experimental pH, showing an alkalization of the medium due to the release of OH^- ions. These results were in accordance with the literature

showing the impact of different cementitious phases on the evolution of the pH on the surface and the calculation of the neutralization capacity of different cement materials [67,68].

The impact of the dissolution of the matrix was different depending on the composition of the material. For instance, calcium-bearing phases, in materials such as SR0 and SR3, are known to be less stable phases to acid attack than Al-bearing phases composing Al-rich systems (e.g. CAC) [44,64,67,68,186]. The rapid dissolution of calcium-bearing phases and the release of a significant amount of hydroxide ions contributed to maintaining higher pH conditions; thus, extending the period of tetrathionate degradation in alkaline medium into thiosulfate and sulfate. This was observed and validated by the formation of higher amounts of thiosulfate in PC-based materials than in the rest of the materials.

However, when the pH reached acidic conditions, no significant difference was observed between the materials in terms of formation of sulfur compounds. All materials showed the formation of the same sulfur species issued from the disproportionation of tetrathionate, indicating that the pH controlled the phenomena of tetrathionate transformation and not the nature of the materials.

3.8.2.Determination of reaction pathway for sulfur cycle

In alkaline conditions, the formation of thiosulfate and sulfate was the main pathway for tetrathionate transformation [221]. In acidic conditions, in the experimental conditions with biofilm development, biological disproportionation of tetrathionate seemed to represent better the phenomena.

Elemental sulfur is one of the products of tetrathionate disproportionation, in particular in highly acidic environments [30,224]. While the other sulfur compounds produced during this disproportionation were partly re-consumed to produce sulfate, elemental sulfur precipitated in a solid form. A hypothesis related the precipitation of elemental sulfur to its high required energy for oxidation. In the conditions of the BAC-test, the biofilm developed on the surface of cement-based materials at ambient temperature (20°C). In such temperature, the activation energy to oxidize elemental sulfur is higher than that needed to oxidize tetrathionate [225]. Moreover, the feeding solution ensured an unlimited tetrathionate environment (residual unconsumed tetrathionate was always found in the leached solutions). Thus, more and more elemental sulfur was formed and assumed not to be consumed during the deterioration process.

3.8.3.Disproportionation of tetrathionate

During the period when the pH was relatively high (alkaline conditions), a natural selection of sulfur-oxidizing bacteria was carried out to progressively develop a biofilm using tetrathionate as a reduced sulfur source. The development of such biofilm was dependent on bacterial consumption of oxygen and reduced sulfur source (tetrathionate). The conditions of

the BAC test created a complex microbial system where aerobic and anaerobic zones could potentially form within the biofilm with different local pH.

In our conditions, the source of oxygen was the atmospheric air and therefore oxygen was abundant. However, the growth of bacteria increases the kinetics of oxygen uptake until reaching yielding point, which should be equivalent to the kinetics of oxygen diffusion from air to water layers on the top of the specimens. Moreover, while the biofilm grew and got thicker, it is possible that the diffusion of oxygen from the air to the water film above the biofilm and then the diffusion of soluble oxygen through the biofilm layers became slower than the reaction of oxidation of tetrathionate [226].

Furthermore, the conditions of the BAC test created a complex microbial system where aerobic and anerobic zones could potentially form within the biofilm with different local pH. In order for bacteria to survive without oxygen in such zones, they could reduce some tetrathionate to oxidize other tetrathionate to generate the necessary energy to survive [34]. Hence, tetrathionate could act as both donor and acceptor of electron, leading to the disproportionation of tetrathionate. Similar behavior was reported in the literature for the disproportionation of sulfur species (thiosulfate, sulfite and elemental sulfur) in oxygen-free conditions [34,227–229]. In this process, the electrons are redistributed internally among the sulfur atoms to produce oxidized and reduced sulfur species.

3.8.4. Comparison between the biomass at the surface of the materials and inside the cementitious matrices

Figure III-17 and Figure III-18 present the results of the diversity indexes (Shannon and Simpson respectively) obtained from the previous results of the microbial populations carried out on the samples only from campaign C4. The data compare the samples of the biomass collected at the surface of the materials (Surf) to that collected within the deteriorated zones of the cementitious matrices (Deep).

The Shannon index is used to express the specific diversity of a consortium. This index indicates roughly the number of species present in a consortium. If only one population is represented in the consortium, the Shannon index is equal to zero. The more different species constitute the consortium, the more Shannon index is high.

The Simpson index is used to calculate the probability of having two random individuals belong to the same species. The closer this index to 1, the higher the homogeneity of the sample. However, in our case, the Simpson diversity index was used for simplification of the readability and the correlation with the Shannon index. The Simpson diversity index represents the difference between the unit and the Simpson index; thus, the value 1 indicates a high diversity in the sample.

For all the materials, the diversity of the sample was confirmed using Shannon and Simpson indexes. No significant difference between the tested materials could be observed from these

results. Concerning the comparison between the consortia developed at the surface of the exposed materials (with low pH) and inside the matrix (with higher pH than the surface due to the reactivity of the cementitious matrices), the results from Shannon index and Simpson Diversity index did not show any differences.

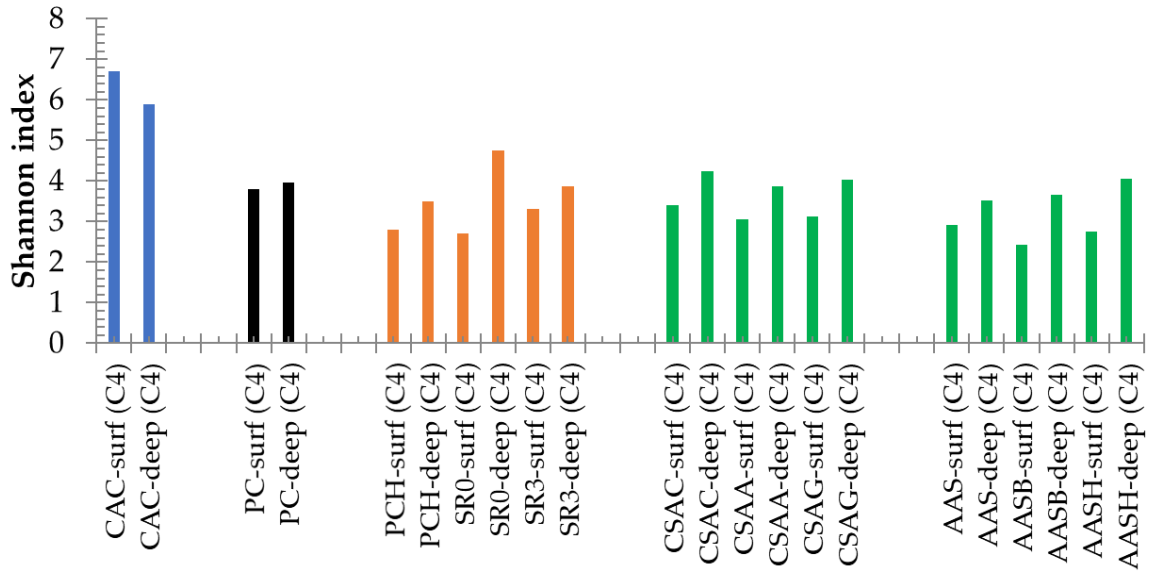

Figure III-17. Shannon index for the different cementitious materials

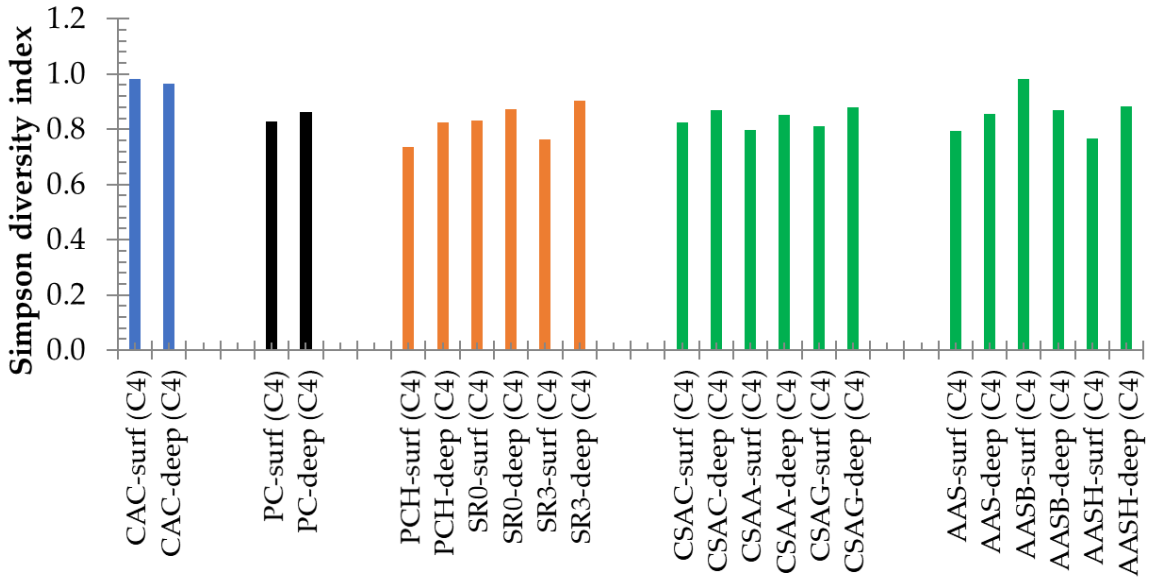

Figure III-18. Simpson index for the different cementitious materials

3.9. CONCLUSION

Tetrathionate and/or polythionates are intermediate compounds observed in sulfur environments, such as sulfidic oceanic sediments, acid mine drainage and H_2S sewer environments. Understanding the fate of tetrathionate conversion to sulfuric acid was an important question to address in order to understand the mechanisms of interactions between

the medium and the microorganisms. In the context of the selection of acidophilic sulfur-oxidizing bacteria on several cementitious materials, the investigation of the different sulfur species involved in the sulfur cycle led to propose possible stoichiometric reaction pathways based on a literature review with experimental data.

Samples of cement pastes, inoculated by activated sludge consortium, were exposed to a feeding solution composed of tetrathionate and nutrients, leading to the selection of a sulfur-oxidizing activity at the surface of the cement materials and to the reproduction of biological colonization and biodeterioration phenomena in sewage environments. During the exposure period of 3 months, the leached solutions on the surface of the materials showed the presence of thiosulfate, pentathionate, hexathionate and sulfates as well as an excess of tetrathionate. In addition, the precipitation of elemental sulfur was observed on the surface of the materials.

The experimental results from different types of cementitious materials (Portland cement, calcium aluminate cement, calcium sulfoaluminate cement and alkali-activated material) showed that the materials did not have a direct impact on the transformation of tetrathionate. The measurements of pH allowed the establishment of a relationship between the formation of different sulfur species and the evolution of the pH of the leached solutions. In alkaline conditions, the degradation of tetrathionate produced thiosulfate and sulfate while in acidic conditions, the disproportionation of tetrathionate produced thiosulfate, pentathionate, hexathionate, sulfate and elemental sulfur.

This experimental work resulted in the development of mathematical models. These models were used to estimate the amount of sulfate biologically produced by the biofilm, which was in direct contact with the surface of the materials, from the evolution of pH and the amount of converted tetrathionate the system. Moreover, by estimating the amount of sulfate produced biologically, the quantification of the sulfate released from the material became possible and will be used to improve the understanding of the biodeterioration mechanisms on sulfate-rich materials.

The process of trickling a feeding solution containing a reduced sulfur source (tetrathionate) resulted in the natural selection of mainly sulfur-oxidizing bacteria and/or acidophilic bacteria. No clear influence of the cementitious materials on the selected population, confirming the previous results concerning the impact of the materials on the selected reaction pathways for tetrathionate transformation.

For all exposed materials, *Thiomonas* species were detected. While the specific species of *Thiomonas Intermedia* was not identified, such species is known to be capable of disproportionate the tetrathionate. The identification of Thiomonas species supported the previously proposed reaction pathways and explained the formation of elemental sulfur during the biological conversion of tetrathionate.

The addition of bauxite and HardCem for AAS induced the selection of a specific population capable of developing using iron: *Acidithiobacillus ferrooxidans*. The incorporation of HardCem in the PC-based material (PCH) did not lead to the selection of such species. Furthermore,

Acidithiobacillus ferrooxidans was identified in the sample of CSAA whilst it was not detected in the CSAC nor in the CSAG samples.

Two hypotheses were proposed to explain these phenomena: (i) the reactivity of HardCem could be different depending on the environment created by the reactive matrix; (ii) the mineralogical form of iron could influence its reactivity. These remarks could be linked to a particular behavior of these materials in the experimental conditions.

Chapter IV

Performance of innovative cement-based materials in sewer conditions: analyses of the leached solutions

4. CHAPTER IV – PERFORMANCE OF INNOVATIVE CEMENT-BASED MATERIALS IN SEWER CONDITIONS: ANALYSES OF THE LEACHED SOLUTIONS

Table of contents

4.1. INTRODUCTION

Cementitious materials are widely used in the construction of sewer pipes. Many degradations in such environments are associated to the presence of acidophilic bacteria producing sulfuric acid on the surface of the materials [6,9]. The deterioration process of cement-based materials in sewer networks generally takes place over several months or even years, depending on the environmental conditions (H_2S concentrations, flow rate, temperature, etc.). The need to evaluate the performance of materials in reasonable time of experiments (accelerated test) has led to the use of the BAC test. The performance and classification of materials (CEM I, CEM III and CAC) were obtained in previous campaigns and were in accordance with the results obtained in field conditions [20,26].

In this work, cement pastes were exposed to very favorable conditions, using the BAC test (presented in section 2.4 of chapter II), for the development of microbial activity. During the exposure period, the leached solutions were collected regularly in order to analyze the liquid phase over time (pH, sulfate, calcium, aluminum, iron and magnesium concentrations).

Moreover, works have been done for defining a performance indicator, based on chemical analyses of the leached solutions, capable of capturing with the best efficiency the general deterioration of the materials. First quantifications of the performance of materials were mainly based on calcium leaching since the studies were carried out on Portland and Calcium aluminate cements which the decalcification is known to be the main process of the deterioration with secondary precipitations. However, this criterion was suitable for cementitious matrices with different compositions than that of PC and CAC. A recent work was carried out on a large set of materials to optimize the durability criterion for classifying cementitious materials according to their performances. The new criterion, called performance indicator (PI), was based on the total amounts of OH^- likely to be released in the leached solutions following the deterioration of the cementitious matrices.

In this chapter, the behavior of different cementitious materials with respect to the composition of the leachates in the liquid phase issued from the BAC test was studied and the performance indicator was improved to better represent the performances of non-conventional cementitious binders, such as calcium sulfoaluminate materials, Fe- and Al- rich materials and alkali-activated materials.

The main objectives of this chapter were to (i) improve the performance indicator allowing to classify non-conventional materials; (ii) compare the performances of cement-based materials with different chemical and mineralogical composition, and (iii) evaluate the role of different forms of aluminum and iron in various cementitious matrices in relation to the biological activity and the resistance of the binders.

In order to characterize the sulfur-oxidizing activity, analyses of the leached solutions were carried out to evaluate the amount of acid produced by the biofilm (chapter III). In chapter IV,

the analyses of the leached solutions and the measurements of the leached mineral elements allowed the evaluation of the reactivity of the binders with respect to the biological attack.

During these experiments, two reference materials (PC and CAC) were systematically tested to represent a highly resistant material (CAC) and a conventional material (PC). The studied alternative materials are presented in Table IV-1.

Table IV-1. Summary of the different tested materials

Category	Control materials	PC-based materials	CSA-based materials	AAS-based materials
Binder's reference	CAC	PCH	CSAC	AAS
	PC	SR0	CSAA	AASB
		SR3	CSAG	AASH

The analyses of the liquid phase served as a first step in evaluating the mechanisms of alteration of the cement matrix as well as in understanding the mechanisms of interactions between microorganisms and cementitious materials. This part will be followed by an extensive study of the alteration of the microstructure, which will be presented in chapter V.

4.2. PERFORMANCE OF CEMENT-BASED MATERIALS EXPOSED TO BIODETERIORATION IN SEWER-LIKE ENVIRONMENT

Portland-based materials are mainly composed of calcium oxide. Calcium is found in the main phases such as portlandite, C-S-H, AFt and AFm [62]. During an acid attack, the progressive dissolution of these phases occurs and calcium ions are released from the cementitious matrix [14,49,67,68]. Therefore, calcium was considered to be a key element in the evaluation of the resistance of cementitious materials in these conditions.

However, the use of unconventional and innovative materials, such as calcium aluminate cement, calcium sulfoaluminate cement and alkali-activated cement, in sewage environments is of particular interest due to their different physico-chemical properties compared to Portland cement. These materials contain, in addition to calcium, significant amounts of other elements such as aluminum, iron, magnesium and sulfur. Moreover, the mineralogical phases, formed during hydration, are very different from those of Portland cement [62]. These phases can also have different chemical resistance to acid attacks, as it is the case with AH_3 for example [44,67,68,186]. It has become necessary to take into account the influence of these chemical elements (and their corresponding mineralogical phases) in order to better represent the performance of cementitious materials.

The performance indicator was developed to classify cementitious materials according to their resistance to biogenic sulfuric acid attack in sewer conditions. This indicator was based on the

release of the main cementitious cations by the cement matrices as a function of the corresponding quantity of sulfuric acid produced by the microorganisms. The details of the calculation of the performance indicator have been presented in section 2.4.4 of chapter II.

4.2.1.Standardized leached eqOH

In order to consider the impact of the different chemical elements (as well as the mineralogical phases) on the resistance of materials, a common parameter to all these elements had to be found. The parameter equivalent OH (eqOH) was developed to consider the five major ions susceptible to be leached from the cement matrix, calcium, aluminum, iron, magnesium and sulfur.

The equivalent OH represents the total amount of OH^- to be released from the dissolution of the main oxides in a cementitious matrix (CaO, Al_2O_3, Fe_2O_3 and MgO). Table IV-2 presents the dissolution reactions which were considered for the total dissolution of cementitious oxides and the corresponding eqOH per mole of ion released from the cement matrix.

Table IV-2. Respective dissolution reaction considered for the main oxides of a cement-based material

Oxide	Dissolution reaction	eqOH (in moles) for 1 mole of the corresponding ions	
CaO	$CaO + H_2O \rightarrow Ca^{2+} + 2\ OH^-$	2	**Eq.IV-1**
SiO_2	$SiO_2 + H_2O \rightarrow H_4SiO_4$	0	**Eq.IV-2**
Al_2O_3	$Al_2O_3 + 3\ H_2O \rightarrow 2\ Al^{3+} + 6\ OH^-$	3	**Eq.IV-3**
Fe_2O_3	$Fe_2O_3 + 3\ H_2O \rightarrow 2\ Fe^{3+} + 6\ OH^-$	3	**Eq.IV-4**
MgO	$MgO + H_2O \rightarrow Mg^{2+} + 2\ OH^-$	2	**Eq.IV-5**
SO_3	$SO_3 + 2\ OH^- \rightarrow SO_4^{2-} + H_2O$	-2	**Eq.IV-6**

In addition, the impact of SO_3 on the consumption of OH^- was considered following reaction **Eq.IV-6**. The total dissolution of SO_3 was reported to consume 2 moles of hydroxide. For sulfate rich materials, the release of sulfate was correlated to the leaching of calcium and aluminum, in particular for ettringite and monosulfoaluminate phases. Therefore, the eqOH linked to calcium and aluminum was calculated after linking all sulfate to leached calcium and aluminum.

Furthermore, silicon was not taken into account in the calculations of the equivalent OH as its dissolution is very low in the conditions of the BAC test. The approach of using the equivalent OH enabled to consider the hydrated and anhydrous phases of the material, since both forms of phases are dissolved during biologic sulfuric acid attack on cementitious materials.

The calculations for the eqOH were similar to that of the standardization of the leached calcium per initial total calcium in the materials per exposed surface (presented section 2.4.4

of chapter II). The same calculations for the calcium were carried out for aluminum, iron, magnesium and sulfate in order to obtain the cumulative leached amount of these ions. Afterwards, the Tot(OH^-) was calculated as the equivalent amount of hydroxide ions obtained from the dissolution of corresponding oxides between day d_{n+1} and day d_n. The $Tot^{init}(OH^-)$ represents the initial amount of equivalent OH obtained from the chemical composition of the different binders, presented in Table II-2 in chapter II. **Eq.IV-7** presents the eqOH as the standardization of the total amount of equivalent OH leached from the cementitious matrix per the initial amount of equivalent OH in the binders per exposed surface (S: previously defined section 2.4.4 of chapter II).

$$eqOH = Tot(OH^-)_{dn+1\,-\,dn} / Tot^{init}(OH^-) / S \quad \text{, expressed in molOH/molOH.m}^2 \qquad \textbf{Eq.IV-7}$$

Figure IV-1 shows the evolution of the standardized $eqOH^-$ parameter as a function of the amount of acid to which the different materials were in contact.

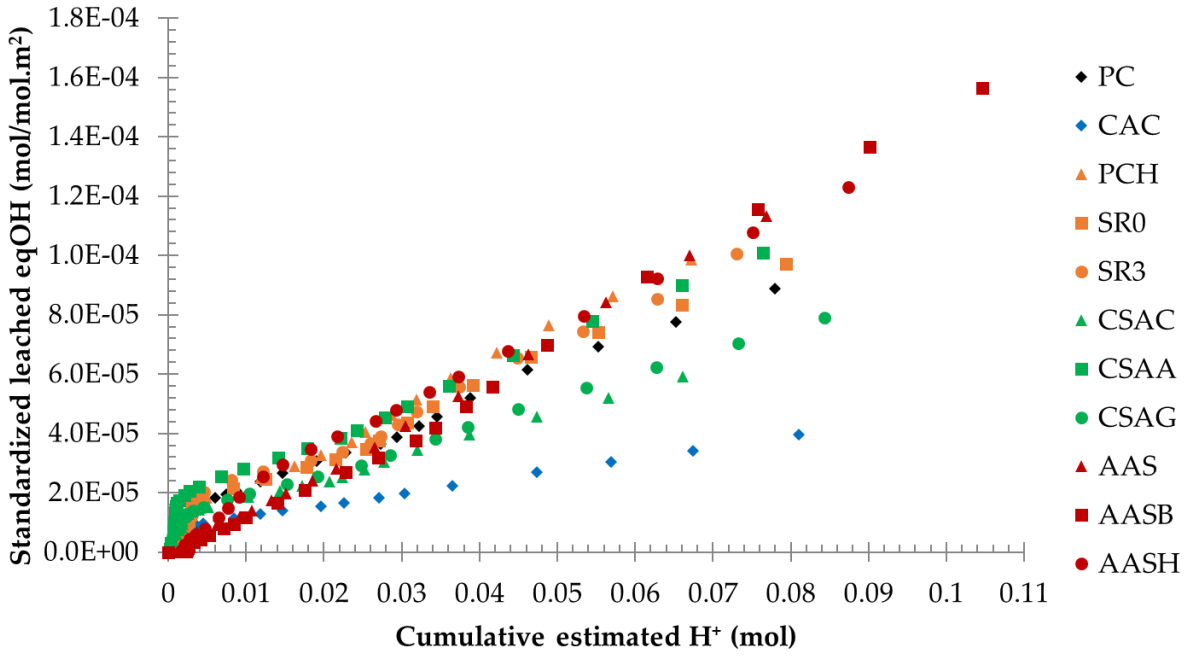

Figure IV-1. Standardized leached eqOH (mol/mol.m²) as a function of cumulative estimated H^+ (in moles) for all materials

In early days of the test, the cumulative amount of acid was very low, however, the exposure of the materials' surface to a run-off solution at pH 7 induced a destabilization of the mineralogical phases leading to their dissolution and the release of the cementitious cations. A particular behavior was observed for AAS-based materials, which will be discussed in section 4.5 of this chapter.

Calcium aluminate cement showed very good performance in accordance with the literature [49,64,67,68,230]. CAC released low amounts of calcium and aluminum compared to the high initial content of both elements (40 and 50% of calcium and aluminum oxides respectively).

The main hydrates in such system seemed to have higher resistance against sulfuric acid attack compared to Portland cement.

Calcium sulfoaluminate cement have a similar composition to CAC in terms of calcium oxide (40%) and slightly lower aluminum oxide (20-30%). In addition, CSA matrix have higher resistance to external sulfate attack than Portland cement due to the absence of C_3A, absence or very low amount of portlandite, non-reactivity of ettringite with sulfate and a denser microstructure [74,179,231]. Two CSA binders showed a better resistance to biogenic attack than Portland cement while the third material had slightly poorer performance. The nature of the added calcium sulfate (gypsum or anhydrite) to the CSA clinker might have had a great influence on the durability of the material, this aspect will be discussed in the section 4.3.2.1 of this chapter. AASB material showed very similar behavior compared to plain AAS (without any addition), indicating that simply increasing the initial aluminum content was not sufficient to improve the resistance of the material to the attack. Similar results were obtained in a previous study on Portland cement partially substituted with slag from 0 to 95% of the binder [67]. The substitution enabled to increase the aluminum content in the binder, however, it did not improve its resistance to the attack. This behavior suggested that the nature of the mineralogical phases and their corresponding stability in acidic environments would be the key factor in improving the resistance of cement materials.

All PC-based materials, with high and low iron content, showed very similar performance. An initial higher iron content did not seem to increase the resistance of the material. On the one hand, sulfate resistant cements (SR) are used mainly when the material is exposed to high sulfate environments due to their lower C_3A content. During external attack, sulfate diffuses into the pores of the material and reacts with C_3A to form secondary ettringite [232,233]. The lower C_3A amount in the binder is often compensated by the increase of the amount of C_4AF [62]. However, the results showed no significant impact of decreasing C_3A amount and increasing C_4AF amount on the eqOH.

Moreover, it seemed that the slightly higher C_4AF amount did not produce more durable phases. The hydration of cement leads in a high alkaline environment where the main form of Fe(III) complex, results from C_4AF hydration, would be $Fe(OH)_4^-$ [234]. The literature reported that iron does not migrate and can precipitate either as ferrihydrite ($Fe(OH)_3(s)$) or bound to hydrotalcite ($M_3F_{0.5}\check{C}_{0.5}H_6$), hydrogarnet ($C_3(A,F)S_yH_{6-2y}$ or $C_3FS_yH_{6-2y}$), C-S-H or partially substituting aluminum in ettringite and/or monosulfoaluminate, depending on the concentration of iron in the pore solution [62,235–242]. Additionally, hydrogarnet and Fe-containing AFm phases were reported as the main iron-bearing phases observed in Portland cement [62,238,239]. The former is mainly formed in an SO_3 deficit condition within the cement matrix while the latter is often poorly crystallized and formed in very low amounts [243]. Such phases have slightly higher resistance to acid attack compared to portlandite and calcium silicate; however, the amount of iron in Portland cement are typically very low and the reactivity of C_4AF is very slow compared to that of the other constituents of Portland cement (C_3S, C_2S and C_3A) to form any significant amounts of hydrated Fe-bearing phases [114].

In addition, incorporating HardCem additives increased the total iron content in the binder, however, it seemed that the performance of the material slightly decreased. An absence of reactivity of the mineral addition could explain the particular behavior of such material. The details of the impact of HardCem on the deterioration mechanisms of the microstructure is detailed in chapter V.

Overall, PC-based materials showed very similar performances, indicating that mainly calcium-bearing hydrated phases were responsible for the chemical resistance of these materials.

Finally, the studied alkali-activated materials were based on slag, which increased the initial aluminum content of the binders compared to PC. However, the amount of aluminum was still very low compared to CAC and CSA materials. The low eqOH^- in the early days of the test was due to the high pH and the low acid concentrations in the leaching solution. However, with the increase of the intensity of the attack, AAS-based materials showed a significant increase in the eqOH^-, corresponding to a very high release of calcium, aluminum and magnesium. The hydration of alkali-activated slag produces C-A-S-H with a Ca/Si ratio typically around 1.1-1.2 and Al/Ca around 0.19 [62]. These phases are composed of tetrahedron $[SiO_4]^{4-}$ and $[AlO_4]^{5-}$, increasing their durability against acid attack compared to hydrated calcium silicates in the Si-O-Al system [158,161,244]. However, the acid attack on C-A-S-H induces firstly the release of calcium followed by the ejection of tetrahedral aluminum from the aluminosilicate system due to the electrophilic attack of the acid on Si-O-Al polymers, as presented in the literature [161,244].

4.2.2. Equivalent OH Performance indicator (PIeqOH)

The equivalent OH performance indicator (PIeqOH) is an indicator that assesses the resistance of cementitious materials tested in the BAC test compared to the reference material. Such indicator allows a classification of cementitious materials according to their resistance to biological attack in sewer conditions assimilated by the accelerated laboratory test.

The development of the PIeqOH was based on the calculations from the eqOH in the previous section (4.2.1) and it is expressed for a material "X" in **Eq.IV-8**:

$$PIeqOH_x = 100 \times (eqOH_x / eqOH_{PC}) \quad \text{,expressed in \%} \qquad \textbf{Eq.IV-8}$$

In addition, in laboratory conditions, the evaluation of the performance of the materials could be influenced by the nature of the used activated sludge, in particular the presence of sulfur oxidizing microorganisms. An acceleration or a delay in the development of the microbial activity could bias the results; hence, modifying the performances of the materials. Therefore, the equivalent OH performance indicator was implemented to standardize the results by the same reference material (PC) and made it possible to compare all the materials regardless of the experimental campaign.

Figure IV-2 presents the classification of materials according to their PIeqOH. The control material (PC) of each campaign had a PI of 100%, which means that materials with PIeqOH above 100% performed better than the PC and materials with PIeqOH lower than 100% did not perform as well as the PC.

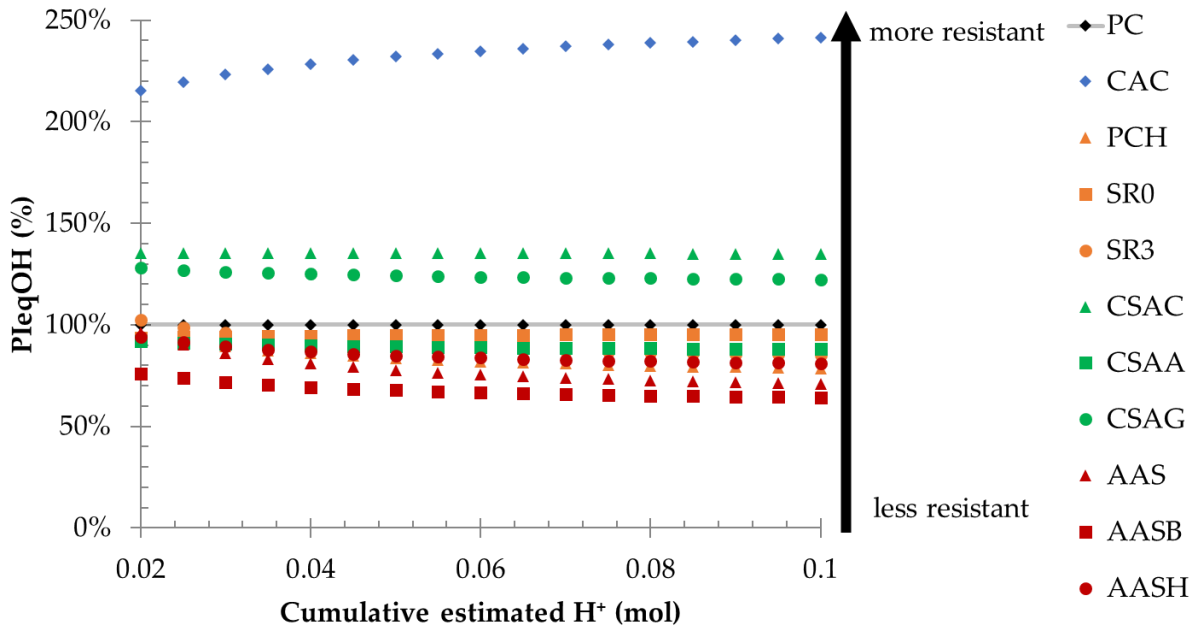

Figure IV-2. The eqOH Performance indicator (PIeqOH) of the different binders as a function of the cumulative leached sulfated in the leached solution

Firstly, CAC material showed an average PIeqOH of 233%, which was slightly more than double of the reference cement. This behavior was not very surprising given the results in the literature indicating the very good resistance of calcium aluminate cement to biogenic sulfuric acid attack [41,64,67,121,186,230,245]. Secondly, all PC-based materials were between 84-95% of PIeqOH. The addition of HardCem to Portland cement (20 wt.%) did not improve the performance of the binder, with a PIeqOH of 83% for PCH. SR0 and SR3 had average PIeqOH of 95 and 90% respectively. Thirdly, two CSA-based binders (CSAC and CSAG) showed better overall performances compared to Portland cement. The average PIeqOH were 135, 124 and 89% for CSAC, CSAG and CSAA respectively. The performance of CSA was not as good as that of CAC but was still an increase up to 30% (for CSAC) in the resistance of the binders compared to PC. Anhydrite-based CSA (CSAA) seemed to perform less well than gypsum-based CSA (CSAG) and CSA clinker (CSAC). This may be due to the reactivity of calcium sulfate and the presence of excess unreacted calcium sulfate and ye'elimite which could act as a supplementary source of calcium in these materials [74,79]. Fourthly, binders based on alkali-activated slag performed the poorest in these conditions, with PIeqOH ranging between 68 and 85% compared to Portland cement. Adding bauxite to the alkali-activated mixture showed no improvement despite the high aluminum content. However, the addition of HardCem to the AAS at 10 wt.% slightly improved its resistance to sulfuric acid compared to plain AAS material.

The average PIeqOH of materials was calculated between 0.02 and 0.08 moles of measured sulfate and presented in Figure IV-3.

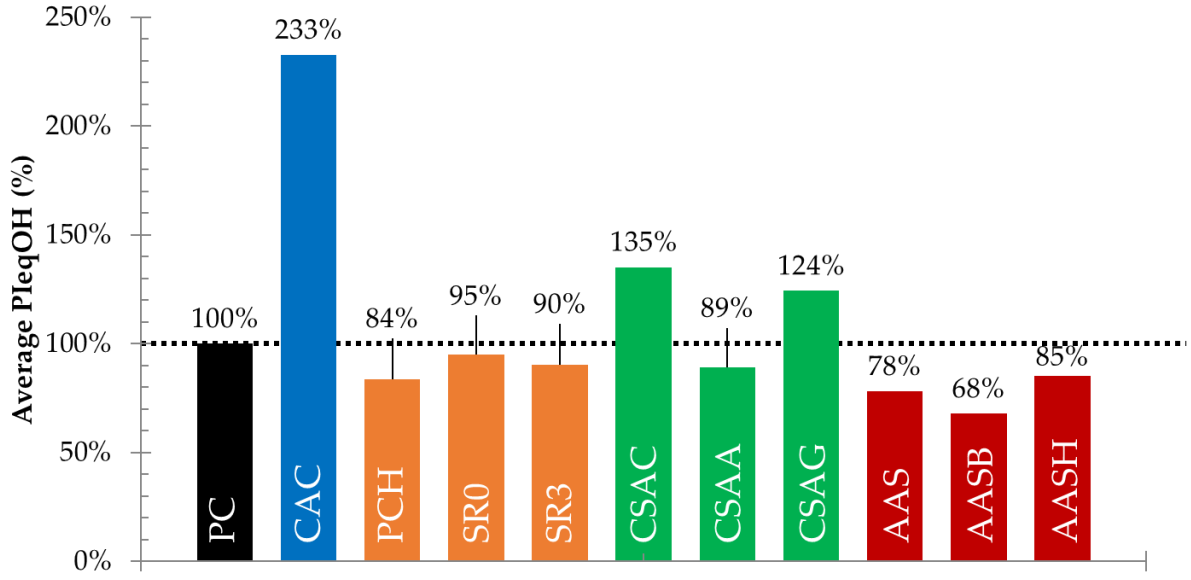

Figure IV-3. Average PIeqOH values for the exposed cementitious materials

4.3. BEHAVIOR OF ALUMINUM-RICH MATERIALS EXPOSED TO BIODETERIORATION TEST IN LABORATORY CONDITIONS

The better resistance of CAC-based cement materials in the literature has been attributed to its high aluminum content generally and to the resistance of the gibbsite phase in particular [20,44,49,64,67,68,230]. On the one hand, the high aluminum content might have an inhibitory effect on bacteria but different studies have shown that this impact was short-lived and the bacteria were able to adapt to the new environment [68,230,246]. On the other hand, the high chemical resistance of the aluminum-bearing phases and in particular gibbsite (AH_3) allowed a better resistance to acid attack [44,49,67,68]. CSA-based materials are rich in aluminum compared to Portland cement, as shown in Table IV-3.

Table IV-3. Aluminum content (Al_2O_3) in the different binders (in wt.%)

Weight %	PC	CAC	CSAC	CSAA	CSAG	AAS	AASB
Al_2O_3	4.85	51.20	29.26	24.46	23.33	10.38	18.83

In addition, AH_3 phase was a main phase resulting from the hydration of this type of cement [179,181,247,248] and could potentially form from the decomposition of other phases, such as C_3AH_6 in CAC materials [68]. In the previous section, it was shown that the performance of some CSA-based materials was between CAC and PC, which might be linked to the presence of AH_3 phases in the cement matrix. However, in this section we will study the potential impact of aluminum-rich materials (CSAC, CSAA , CSAG and AASB) on bacterial activity as

well as the evolution of aluminum in the liquid phase, in particular as a function of the pH (the analyses of the evolution of the mineral phases will be presented in chapter V).

4.3.1.Evolution of pH and microbial activity

Figure IV-4 presents the evolution of the pH of the leached solutions of reference materials (PC and CAC), CSA-based materials (CSAC, CSAA and CSAG), AAS and AASB materials as a function of the exposure time to the BAC test. One should note that the evolution of the pH of PC was not usual as the pH decreased rapidly compared to previous another PC specimen exposed to the same condition at the same time (**Appendix IV-A**).

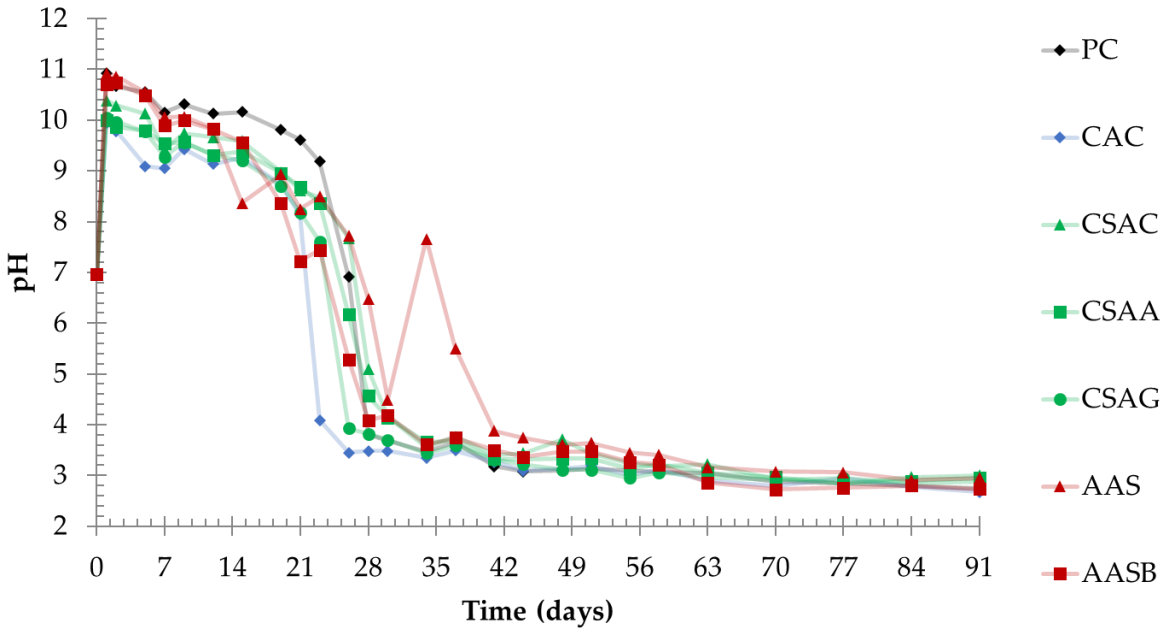

Figure IV-4. Evolution of the pH of the leached solutions for CSA-based binders

The pH evolution of CSA-based materials was similar to that of CAC. During biodeterioration attack, the calcium-bearing phases are the phases responsible for the buffering capacity of the binder [64,68,246]. Since CSA cement contained lower amounts of calcium compared to Portland cement, its buffering capacity at the beginning of the test was lower than that of PC cement. Moreover, the main phases of such materials were calcium trisulfoaluminate (AFt) and/or calcium monosulfoaluminate (AFm) with aluminum hydroxide (AH_3). AFt/AFm phases are slightly more resistant to acid attack than portlandite and C-S-H, which constitute roughly 50 wt.% PC-based cements [62,64].

The participation of AH_3 in the neutralizing capacity only occurred once the surface pH has exceeded the chemical stability threshold of such phase, which is estimated between 3 and 4 [64,186,249]. The dissolution of one mole of AH_3 neutralizes 3 moles of H^+ according to equation **Eq.IV-9**. However, around the same pH threshold of AH_3 dissolution, acidophilic sulfur-oxidizing bacteria developed with a significant increase in sulfuric acid production [9,10,24]. In the conditions of BAC test, at pH values < 4, the amount of sulfuric acid produced at the surface of the cementitious materials was significantly higher than the amount of OH^-

ions released by the materials, which meant that the kinetics of the acid neutralization by the different materials was significantly slower than the acid production by the bacteria, when the pH of the leached solutions reached acidic values.

$$Al(OH)_3 \rightarrow Al^{3+} + 3\ OH^- \qquad \textbf{Eq.IV-9}$$

The evolution of pH for AAS and AASB was slightly different compared to CSA materials. The pH increased as high as PC material before decreasing rapidly following the same trends as CAC and CSA. Such behavior will be thoroughly discussed in section 4.5.1.

4.3.2.Reactivity of cementitious phases to biogenic acid attack

4.3.2.1. Sulfate-bearing phases

Figure IV-5 shows the evolution of the cumulative sulfate in the leached solutions for CSA-based, AAS and AASB materials compared to PC and CAC materials in the first three weeks of exposure to the BAC test while Figure IV-6 shows the cumulative leached sulfate for the same materials during the total exposure period of 3 months.

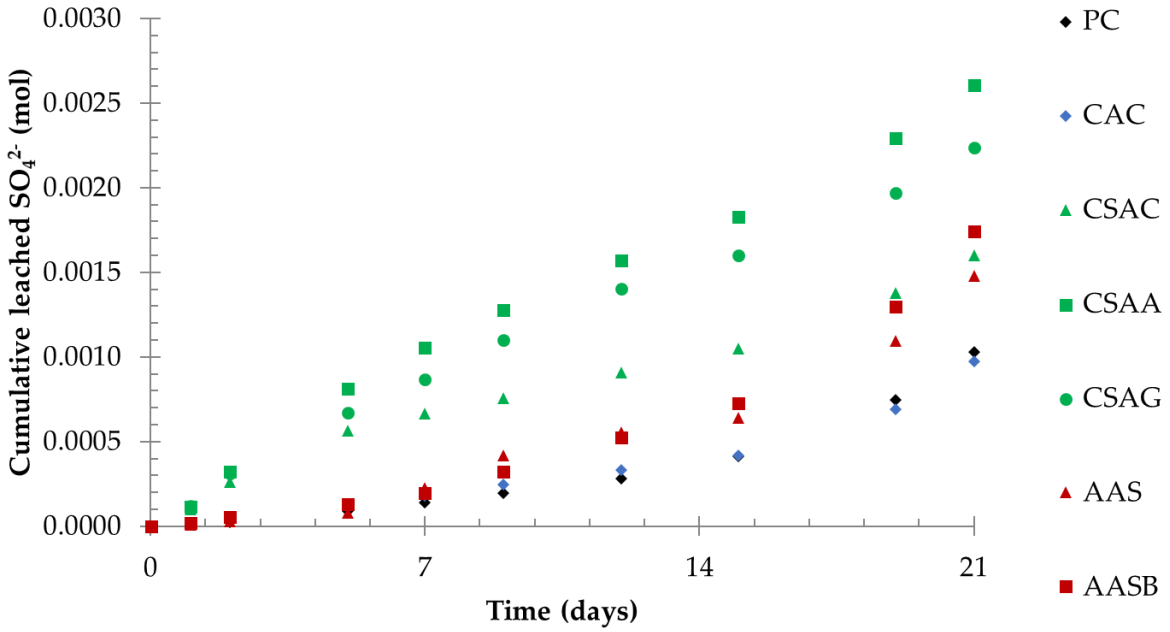

Figure IV-5. Total measured sulfate (mole) in the leached solutions, collected downstream of the BAC test, on the first 3 weeks of exposure time (days) for CSA-based, AAS and AASB materials compared to PC and CAC

In the first three weeks, a significant difference was observed between CSA-based materials and the other materials. Higher amounts of sulfate were measured in the leached solutions for CSA-based materials starting from 1 day of exposure to the accelerated test. The gap between CSA-based and the rest of the materials continued to increase over the next two weeks. However, kinetics of sulfate leaching from CSAC decreased after only one week compared to CSAA and CSAG. AAS and AASB showed relatively low sulfate concentrations while PC and CAC presented similar tendencies for the first 3 weeks. Nevertheless, the cumulative amount

of sulfate released by all materials were substantially low (< 0.003 moles) compared to the amount at the end of the testing period (0.47-0.68 moles), as seen on Figure IV-6.

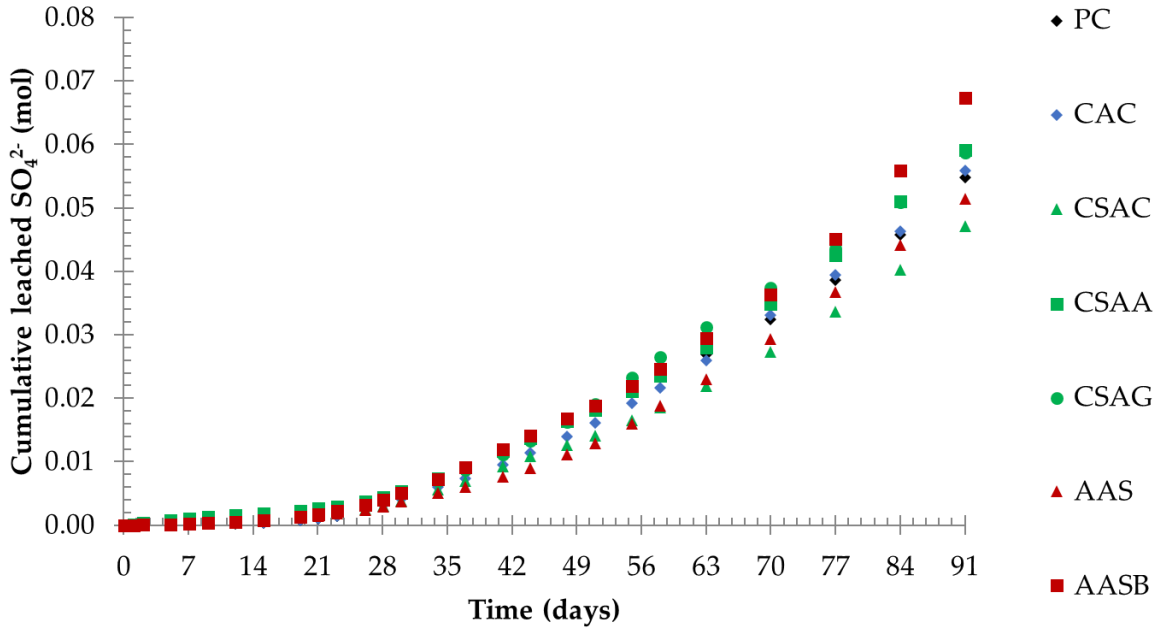

Figure IV-6. Total measured sulfate (mole) as a function of the exposure time (days) for CSA-based, AAS and AASB materials compared to PC and CAC

After laying the activated sludge of the exposed surfaces of the materials, a flow of reduced sulfur (tetrathionate) was run-off on these surfaces. At the early stages of the test, the sulfur oxidizing metabolism was not yet developed. The transformation of tetrathionate into sulfate by sulfur-oxidizing bacteria could not occur at the high pH values observed in the leached solutions [6,9]. Thus, the concentrations of sulfate in the leached solutions were attributed to the release of sulfate from the cementitious matrix.

CSA-based materials contained significant amount of sulfate initially in the binder in different forms. For instance, hydrated calcium sulfoaluminate phases (ettringite, monosulfoaluminate, monocarboaluminate,…), calcium sulfate phases (gypsum, anhydrite) and residual sulfate-bearing anhydrous phases (ye'elimite) [62,76]. The exposition of such phases on the surface of the material to the feeding solution (pH ≈ 7) resulted in the release of sulfate in the leached solutions. Similar behavior was reported in the literature by exposing CSA material to leaching by water at pH regulated at 7 [84]. Moreover, since CSAC (6%) contained less amount of SO_3 compared to CSAA and CSAG (14% and 16% respectively), the decrease in the leaching kinetics may be linked to the lower abundance of sulfate in the exposed surface of the material. Additionally, the presence of unreacted calcium sulfate phases in the matrix of CSAA and CSAG could be the main responsible for the excess sulfate in the leached solutions.

After about 21 days, the pH of all materials started to decrease to acidic values, following the development of microbial activity on the surface of the materials [6,9]. Sulfate concentrations in the leached solutions were mainly issued from the biofilm and potentially from the cement matrix. However, the difference observed during the first three weeks between CSA materials

and the other materials was no longer attributed to the initial sulfate as the part of the released sulfate was considered very low compared to the part of sulfate produced biologically on the materials' surface by microorganisms.

4.3.2.2. Calcium-bearing phases

In conventional cements, calcium oxide is the major oxide and represents more than 50 wt.% of the cement matrix. The reactivity of cement phases to sulfuric acid differs from one phase to another according to complex processes taking into account several factors, such as the equilibrium constant of the phase, the pH of the medium, the concentration of acid, etc.

By measuring the concentrations of calcium in the leached solutions at the outlet of the various materials, the cumulative released calcium was calculated. Figure IV-7 presents the cumulative leached calcium for PC, CAC, CSA-based, AAS and AASB materials as a function of the cumulative estimated acid to which each material was exposed.

PC materials showed the highest leached calcium amount among all materials. However, it also contained the highest amount of calcium oxide initially in the binder (66%) compared to CSA-based and CAC materials (about 40%). Therefore, the results were standardized by the initial amount of calcium in the binders (Figure IV-8).

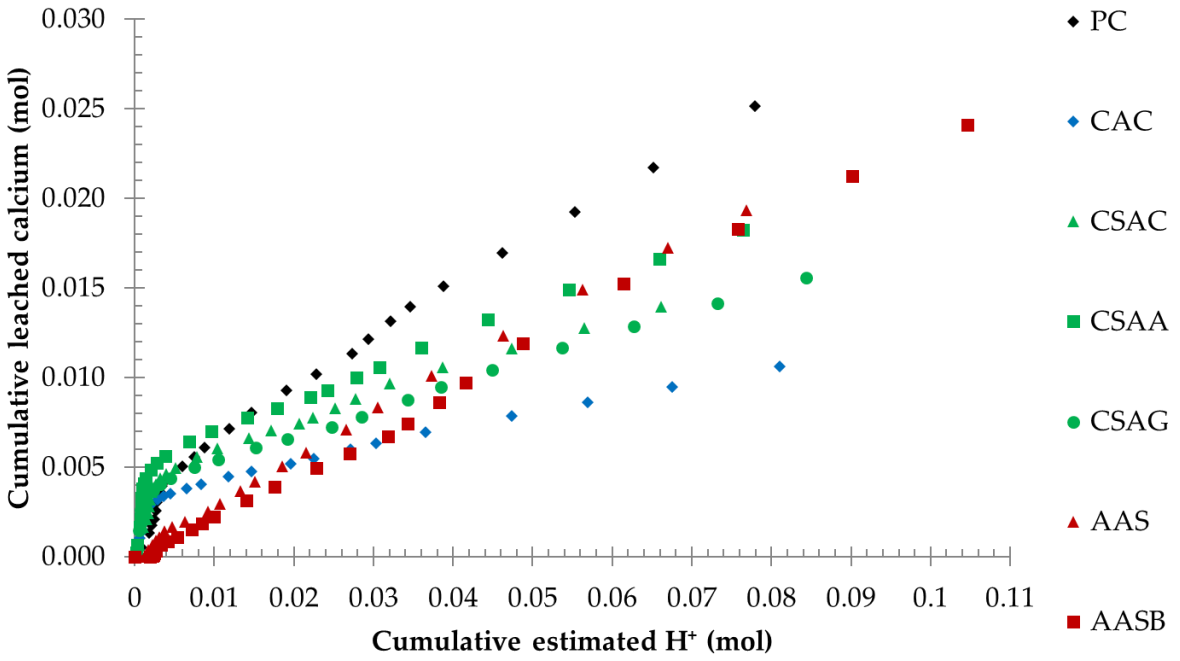

Figure IV-7. Total leached calcium (mol) as a function of cumulative estimated acid (mol) for CSA-based, AAS and AASB materials compared to PC and CAC

For very low acid concentrations (and sulfate concentrations), significant amount of calcium was released from all materials except AAS and AASB. This high calcium content in the leached solutions was linked to the destabilization of the mineralogical phases on the surface of the exposed material to the leaching solution [26]. AAS and AASB showed very low calcium leaching due to the release of sodium, used as activator for the slag, instead of calcium. The

particular behavior of AAS-based materials regarding calcium and sodium is discussed in section 4.5 of this chapter.

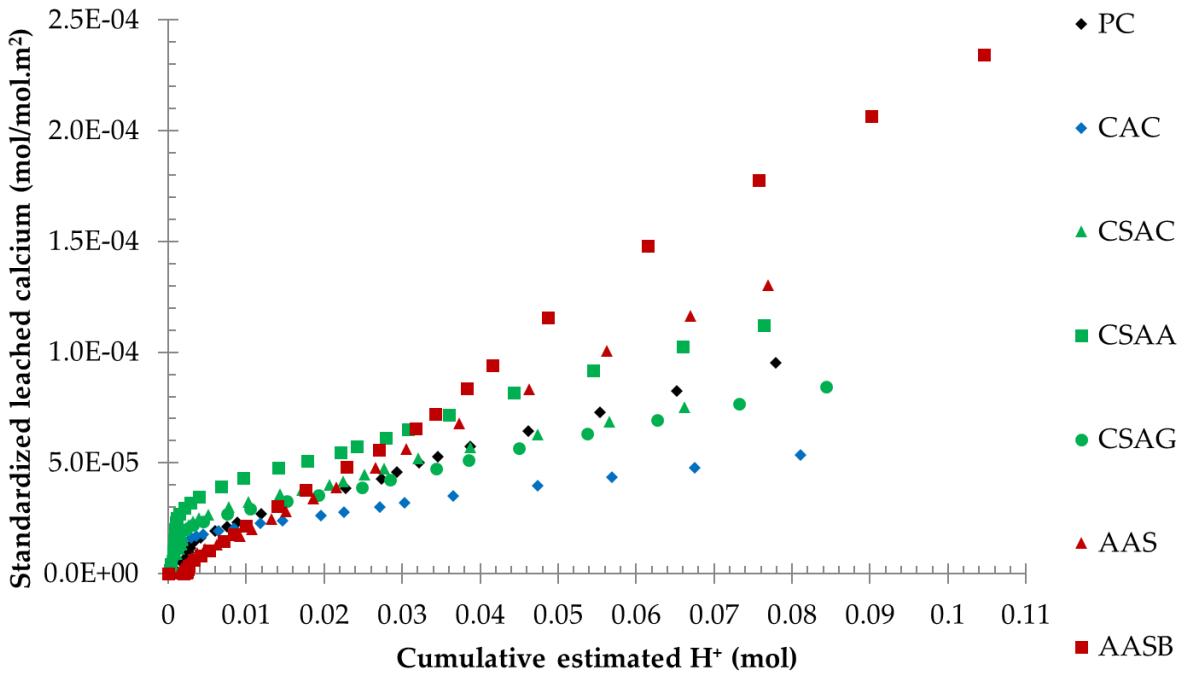

Figure IV-8. Standardized leached calcium as a function of cumulative estimated acid for CSA-based, AAS and AASB materials compared to PC and CAC

PC is composed essentially of portlandite and C-S-H with lower content of ettringite and monosulfoaluminate [62]. Portlandite dissolution and decalcification of C-S-H were reported in the literature as the main phenomena responsible for calcium release from Portland-based materials [67,68]. Calcium-bearing phases in CSA-based materials seemed to have similar reactivity against biogenic sulfuric acid attack.

Moreover, the nature of the added calcium sulfate seemed to influence the calcium leaching. The literature reported that the reactivity of anhydrite and gypsum was not the same during the hydration process of calcium sulfoaluminate cements [77,250]. On the one hand, the reactivity of gypsum is higher than that of anhydrite, which leads to the formation of ettringite rapidly. On the other hand, the slow dissolution of anhydrite leads to the formation of monosulfoaluminate from partial hydration of ye'elimite at early stages of the hydration process. Additionally, the slower dissolution of anhydrite compared to gypsum results in the presence of higher amounts of unreacted calcium sulfate in the materials with anhydrite than in materials with gypsum [181,250].

4.3.2.3. Aluminum-bearing phases

Aluminum concentrations in leached solutions were measured during the exposure period of the materials to the accelerated test. These concentrations were processed to obtain the cumulative leached aluminum depending on the amount of acid seen by the materials. Figure IV-9 presents the evolution of the cumulative leached of aluminum as a function of the

cumulative estimated acid for the reference materials (PC and CAC), the CSA-based materials (CSAC, CSAA and CSAG) and alkali-activated slag-based materials (AAS and AASB).

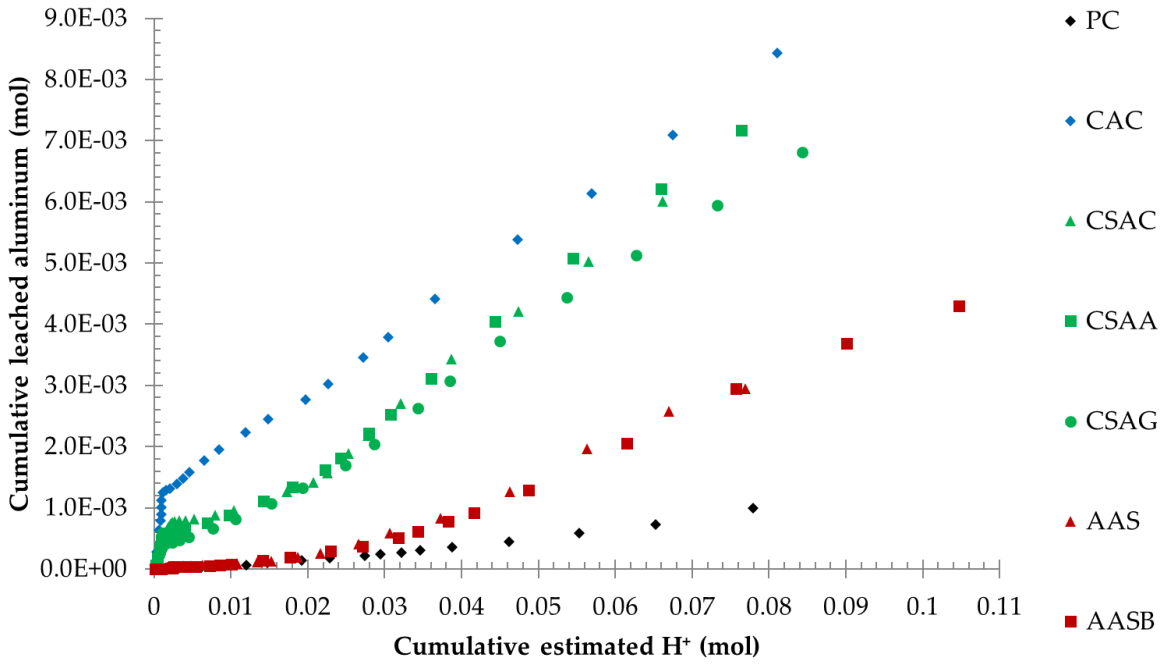

Figure IV-9. Total leached aluminum (mole) as a function of cumulative estimated acid (mole) for CSA-based, AAS and AASB materials compared to PC and CAC

As expected, CSA and CAC materials released more aluminum compared to the rest of the materials. Moreover, the total aluminum leached from CSA and CAC was comparable. The leaching kinetics were different at the beginning of the test when the amount of acid was relatively low (< 0.02 molH^+). However, exceeding this threshold (which corresponded to an acidic environment with a pH < 4.0), the kinetics of aluminum leaching in CSA materials increased to become similar to that of CAC. AAS and AASB exhibited the same trends in terms of leaching kinetics and total leached aluminum. Finally, since PC contained very low amounts of aluminum oxide, the kinetics and the total leached aluminum was the lowest.

Although, in order to compare the different materials, the total leached aluminum was standardized by the initial aluminum content in the binder. Figure IV-10 presents the results of the standardized leached aluminum as a function of the estimated cumulative acid for the same materials as in Figure IV-9. CSA binders contained relatively high initial aluminum amounts compared to PC. However, the standardized leached aluminum for CSAC and CSAG were slightly higher than for PC. While aluminum in PC-based materials is mainly incorporated in ettringite and C-A-S-H as hydrated mineralogical phases, in CSA-based materials, the main aluminum content was distributed between ettringite/AFm phases and AH_3 [76]. The higher stability of AH_3 over a wide range of pH (between 8 and 4) slowed down the release of aluminum from CSA binders, which consequently, decreased slightly the slope of the CSA-based materials aluminum leaching plots. Although, unlike CAC, the phenomenology of secondary products formation, resulting from the deterioration of Al-

bearing phases in CSA in such environments, is not known, in particular it is so far not known if more AH_3 is formed after deterioration.

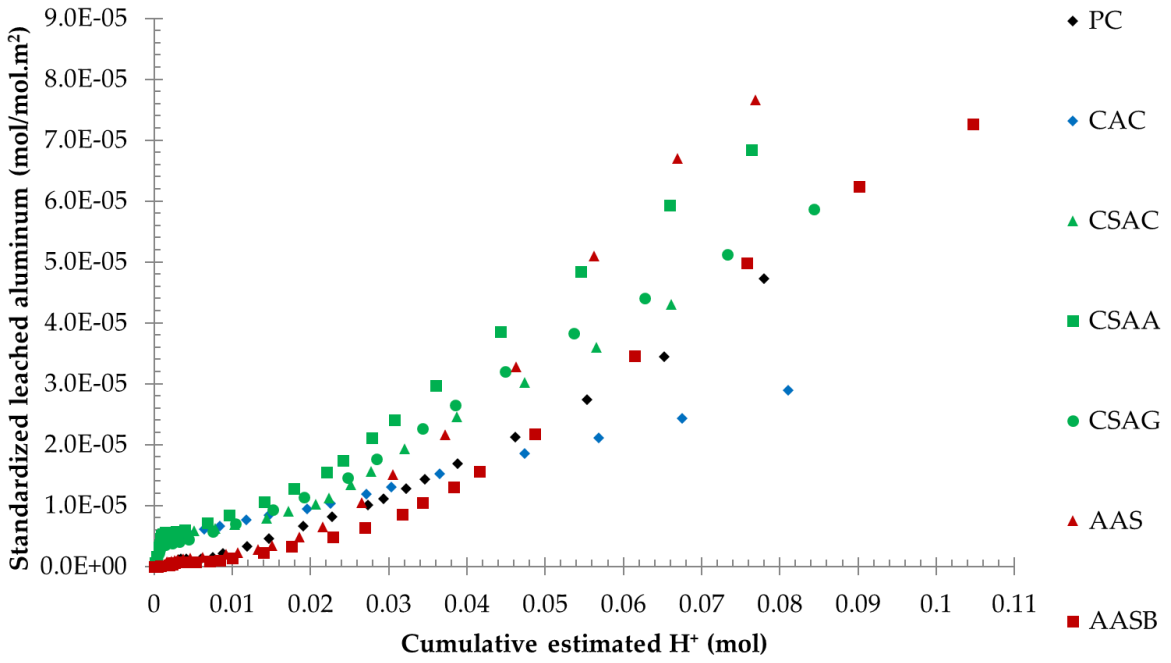

Figure IV-10. Standardized leached calcium as a function of cumulative estimated acid for CSA-based, AAS and AASB materials compared to PC and CAC

The aluminum content in the CAC is higher than in any of the materials tested with the main aluminum-bearing phases being katoite (C_3AH_6) and gibbsite (AH_3). Although CAC material was composed of high aluminum and high AH_3 content initially, the standardized leached aluminum was very low compared to CSA binders and to PC. Besides the chemical stability, the dissolution of one mole of C_3AH_6 leads to the release of 6 moles of OH^- and the formation of 2 moles of AH_3 in the deteriorated part, according to **Eq.IV-10**. The OH^- ions react with the acid in the neutralization reaction, which leads to the increase in pH of the solution. Therefore, the dissolution of C_3AH_6 delayed the pH from crossing the threshold of AH_3 dissolution, which kept the aluminum from getting leached.

$$Ca_3Al_2(OH)_{12} \rightarrow 3\ Ca^{2+} + 2\ Al(OH)_3 + 6\ OH^- \qquad \textbf{Eq.IV-10}$$

Moreover, over the deterioration period, the formation of an excess of AH_3 in the deteriorated zones might have led to a decrease in the porosity, which consequently, slowed down the diffusion of the acid into the cementitious matrix as suggested in the literature [44]. The difficulty of the acid to penetrate into deeper zones of the cement matrix suggested that the attack on such materials became more of a surface attack by the acid rather than a diffusion phenomenon when the pH reached acidic conditions.

By comparing CSA and CAC materials, it seemed that aluminum was more stable in CAC systems. Several hypotheses could explain this behavior: (i) the amount of AH_3 formed during hydration was higher for CAC; (ii) the mineralogical nature of AH_3 was different in the two

systems, in particular for AH_3 formed from the deterioration reactions; (iii) the chemical stability of aluminum-bearing phases (other than AH_3) could be different in CAC and in CSA. These hypotheses will be discussed further in chapter V on the basis of the analyses of the materials' microstructures before and after deterioration.

The aluminum in AAS is mainly contained in slag and its hydrated phases. However, since the literature indicated that high aluminum content in CAC was one of the main reasons for its high resistance to acid attacks, bauxite was added to AAS to increase the aluminum content in the binder. Despite the high aluminum content of AASB which is about twice as much as in AAS, no difference between AAS and AASB in terms of leached aluminum was observed, implying that the aluminum was mainly leached from the hydrated matrix of the slag as well as from the dissolution of slag anhydrous grains [67]. Moreover, AAS contained higher aluminum amount compared to PC. The standardized leached aluminum curves showed that more aluminum was leached from AAS than from PC, probably resulting from the deterioration of C-A-S-H (high slopes for calcium leaching) and the release of aluminum in the pore solution.

Furthermore, bauxite dissolution is often carried out at relatively high temperature (> 60°C) using strong acid, e.g. hydrochloric acid, with relatively high concentrations [251–254]. These conditions were somewhat different from the conditions of the BAC test, which suggested that bauxite was not attacked by the acid in the exposure conditions of the test. The lower amount of leached aluminum from AASB compared to AAS (after standardization of the results) in Figure IV-10 was linked to the increase in the initial aluminum content and not to the reactivity of the material. Finally, the amount of aluminum leached from AAS-based materials and CAC- and CSA-based materials was completely different, highlighting the significant impact of the nature of the aluminum-bearing phases.

In order to understand the reasons behind such difference in the behavior of the materials, the evolution of the aluminum concentration in the leached solutions as a function of the pH of the same solutions was studied and the results are presented in Figure IV-11. For alkaline conditions, CAC and CSA released aluminum ions while AAS-based materials hardly leached any aluminum in these conditions. Between pH 8 and 4, very little aluminum leaching was detected for all materials. It was only from pH 4 that an exponential increase in aluminum concentration was observed for all materials at different rates. For example, the PC material released the lowest amount of aluminum considering that its aluminum content was initially very low. CAC and CSA materials released the highest amount of aluminum and they had very similar evolution of aluminum concentrations in the leached solutions as a function of the pH. Such behavior suggests that the aluminum-bearing phases in these 2 materials were very similar, and that AH_3 was the phase mainly responsible for aluminum leaching in acid conditions. The difference between CAC and CSA respective behaviors at alkaline pH might come from the difference in the stability of calcium aluminate and calcium sulfoaluminate phases in these matrices, respectively [67,68].

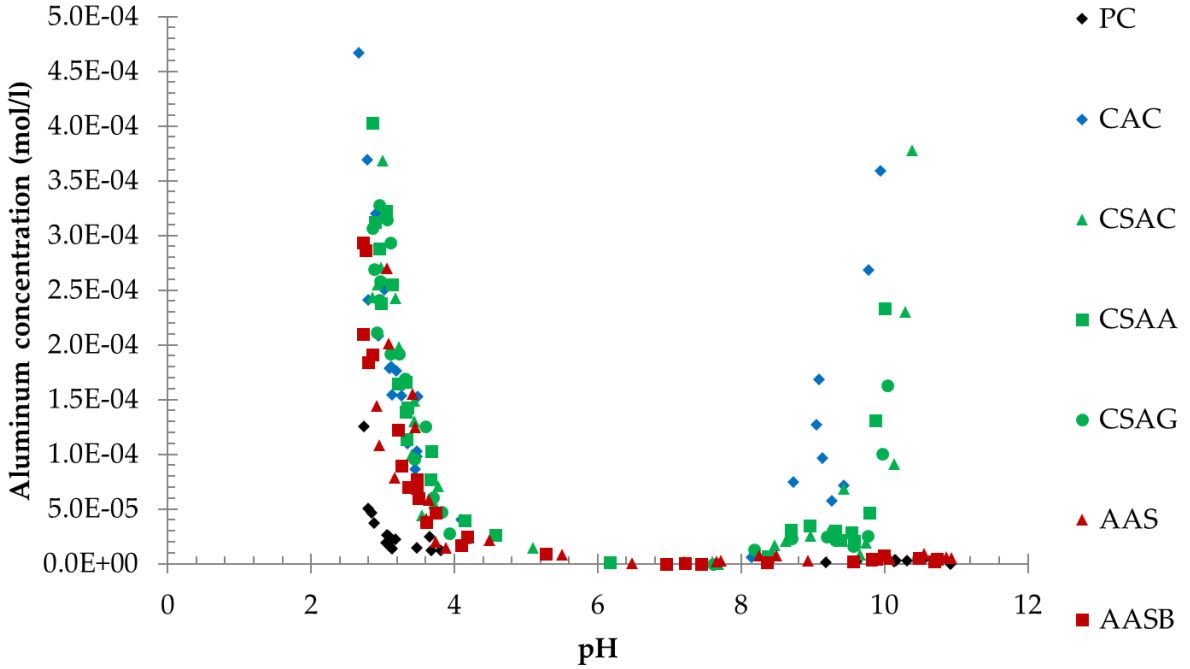

Figure IV-11. The evolution of the aluminum concentration in the leached solutions as a function of the pH for the different materials during their exposure to the BAC test

Finally, the aluminum concentrations for AAS and AASB were found between the CAC/CSA and the PC. This behavior could be related to the difference in the reactivity of the Al-bearing phases in the AAS system and the CAC and CSA systems. In addition, just increasing the aluminum content in the material (in this case by adding bauxite) did not necessarily increase its resistance. The incorporation of bauxite in the cementitious matrix in terms of hydration, mineralogical phases and reactivity with the acid will be discussed in chapter V.

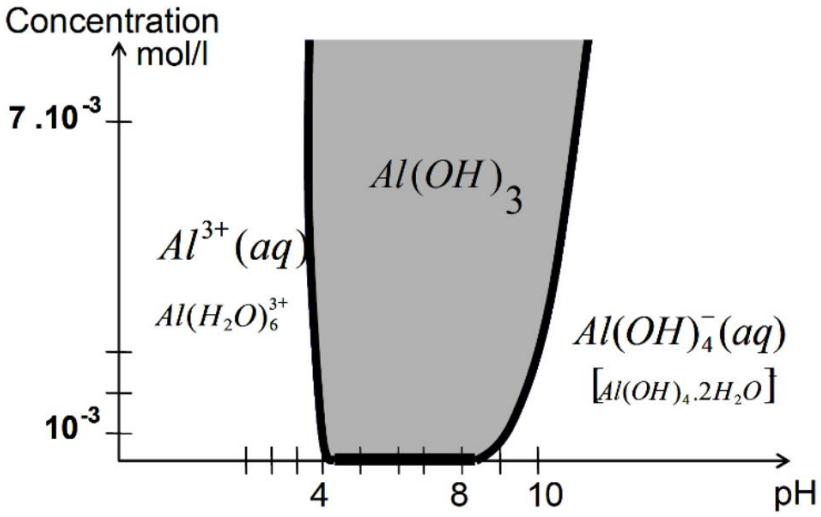

Figure IV-12. Stability domain of AH_3 as a function of pH [186]

The concentrations of aluminum in the leached solutions of CAC and CSA materials were consistent with the literature for aqueous aluminum forms as a function of pH, as seen in Figure IV-12. The presence of AH_3 phases in such materials released aluminum ions at high alkaline environment (supposedly in the form of aqueous $Al(OH)_4^-$). However, with the

decrease of pH to the range of AH_3 stability, very low aluminum was observed in the leached solutions. Once crossing the threshold of AH_3 stability in acidic environments, aluminum was once again observed in the leached solutions. The difference in the amount of aqueous aluminum between alkaline and acidic pH values was due to the period to which the material was exposed to the leached solution. CAC and CSA were exposed to alkaline solution for 2 weeks and to acidic solution for 8 weeks.

4.4. IMPACT OF FE-RICH MATRIX ON THE REACTIVITY OF THE MATERIAL

The impact of iron-rich matrices on the surface pH of cementitious materials exposed to sulfuric acid has recently been discussed in the literature [18,71,115,255]. Iron salt ($FeCl_2$) was added into sewers to limit H_2S formation by precipitating iron sulfides such as pyrite (FeS_2) and ironmonosulfide (FeS) [18,255]. Meanwhile, ferric iron could be used as an electron acceptor in anoxic conditions by *A. ferrooxidans* bacteria to produce sulfuric acid in deeper zones of the concrete [18,256]. Moreover, in chemical conditions, the incorporation of iron (i.e. in the form of hematite) increased the buffering capacity of alkali-activated materials, in particular for high alkali content (Na: Al = 1.39) [115]. In biological conditions, the use of a geopolymer rich in iron (~ 4.5 wt.% Fe_2O_3) seemed to improve the performance of the material after an exposure of 18 months in a sewer network, although the role of iron in improving the performance was confirmed [71]. In this part, the iron behavior in the leached solutions of binders with different iron contents as well as different mineralogical forms of the ferrous phases was studied. Table IV-4 presents the iron content in the different studied binders.

Table IV-4. Iron content (Fe_2O_3) in the different binders (in wt.%)

Weight %	PC	PCH	SR0	SR3	AAS	AASH
Fe_2O_3	2.64	8.84	5.80	4.88	0.30	4.43

4.4.1. The evolution of the pH of the leached solutions

Figure IV-13 shows the evolution of the pH of the leached solutions resulting from the exposure of cementitious specimens containing different amounts of iron. The sudden increase in pH of AAS at 35 days was due to a single problem with the feed pump, which led the specimen to dry for less than 24 hours (with no consequences on the long-term experiment).

In the BAC test conditions, the pH of PC and the AAS was disturbed by the development of the biofilm on the exposed surface. While the biofilm developed earlier than in previous experimental campaigns for PC material, it developed relatively late on AAS. This was due to a technical problem leading to a slightly lower flow of the feeding solution for AAS material between 14 and 28 days. Since the BAC test was developed to represent sewer conditions, all processes were carried out naturally without any exterior interferences.

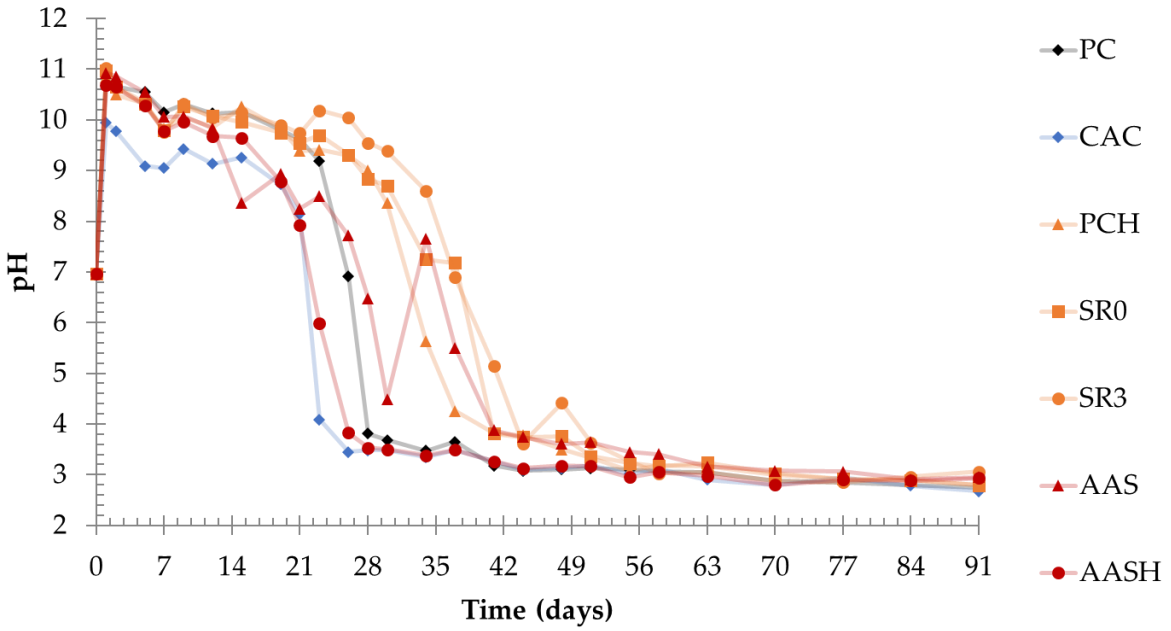

Figure IV-13. pH evolution of the leached solutions for PC, CAC, PCH, SR0, SR3, AAS and AASH during their exposure to the BAC test

The incorporation of HardCem in mixture based on Portland cement (PCH at 20 wt.%) did not show any significant influence on the evolution of the surface pH compared to other PC-based materials. In addition, by enriching the alkali-activated binder matrix with HardCem (10 wt.%), the iron content increased from 0.30 to 4.43 wt.%. However, such enrichment also showed no impact on the evolution of pH during the deterioration process.

Similarly, the presence of Fe in the form of C_4AF with different content (SR0 at 5.80 wt.% and SR3 at 4.88 wt.%) did not show any significant influence, compared to the PC (control specimen) on the capability of the materials to neutralize acid.

4.4.2. Impact of iron on the bacterial activity

The HardCem was added in two different binders (Portland-based and alkali-activated slag-based). The HardCem content in the mixtures was 20 and 10 wt.% for PCH and AASH, respectively. Control samples (AAS and PC) were studied in parallel in order to highlight the impact of the added HardCem. SR0 and SR3 were also studied as two materials containing higher iron content than the reference material with a different mineralogical form compared to HardCem.

Figure IV-14 presents the evolution in the amount of cumulative measured sulfate for the exposed materials as a function of the duration of exposure period to the BAC test. The main results showed no significant impact of iron on the production of sulfate by microorganisms. Moreover, the difference observed between AAS and AASH was linked to a technical problem during the exposure period, which was explained in the previous section (4.4.1).

The kinetics of leached sulfate were similar between the control material and the materials containing high amounts of iron. Moreover, the total cumulative amount of sulfate was very

much alike. The higher total measured sulfate between AASH and PC materials concentrations could be explained by the earlier decrease in pH for AASH and was not linked to the amount of iron in the binder.

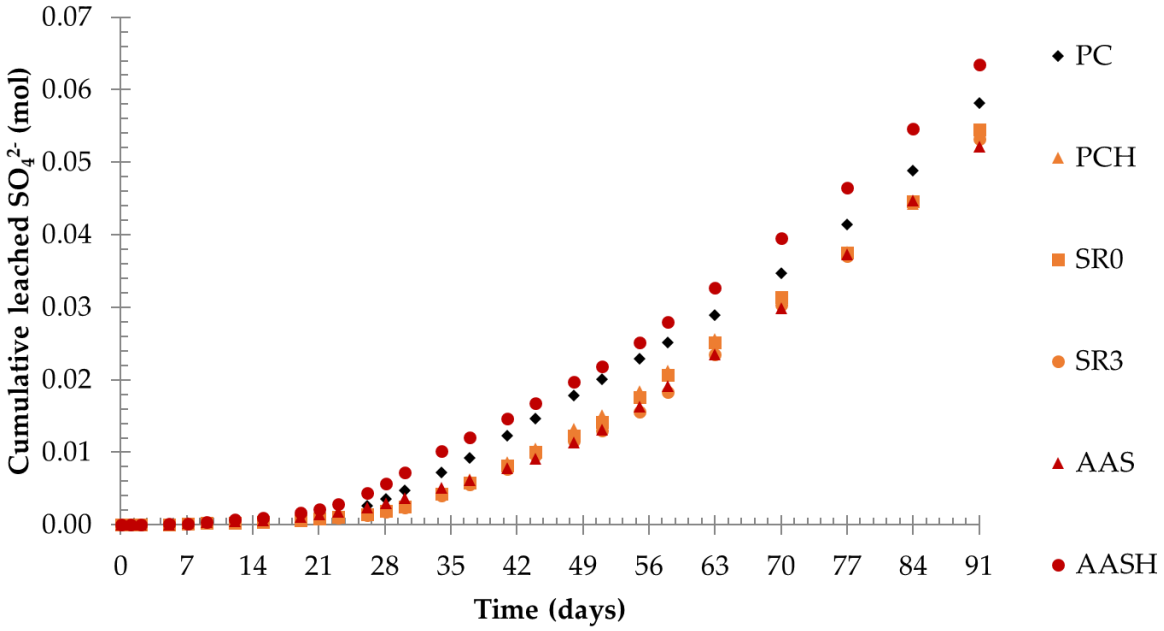

Figure IV-14. Cumulative leached sulfate (in mol) measured in the leached solutions of PC, PCH, AAS, AASH, SR0 and SR3 during the exposure of the specimens to the BAC test

4.4.3. Iron phases' stability and iron leaching

The behavior of the ferrous phases against biologic sulfuric acid attack was monitored by measuring the amount of iron released by the materials in the leached solutions. Figure IV-15 presents the concentrations of iron in the leached solution as a function of pH for PCH and AASH compared to their respective control materials PC and AAS as well as SR0 and SR3. Firstly, iron was not detected at high pH in the leached solutions. Secondly, starting around pH 5, materials containing HardCem (PCH and AASH) showed an increase in iron concentrations. Thirdly, iron concentrations increased exponentially for all materials when the pH decreased below 4.

The soluble iron measured using ICP-OES is the total iron (Fe^{2+} and Fe^{3+}) in the leached solution. Since the BAC test provided oxidizing conditions (oxygen is present in the atmosphere), iron is mostly present at its highest oxidation degree, i.e. Fe^{3+}. The Pourbaix diagram for iron in Figure IV-16 shows the possible forms of iron (solid or soluble) as a function of pH. The threshold for Fe^{3+} was set around pH 4, which corresponded to the results from the analyses of the leached solutions. However, it seemed that the low threshold for iron dissolution was not sufficient to increase the durability of the material, since iron oxide content was still limited to less than 9% of the chemical composition of the material.

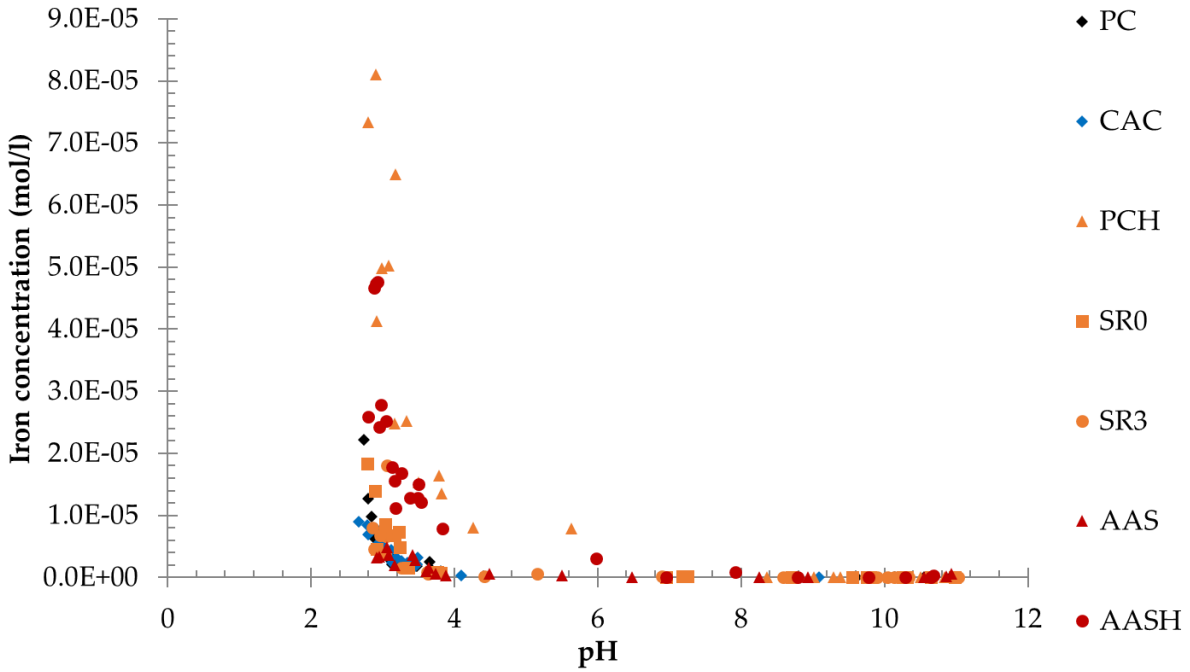

Figure IV-15. Fe concentrations (in mol/l) as a function of pH of the leached solutions

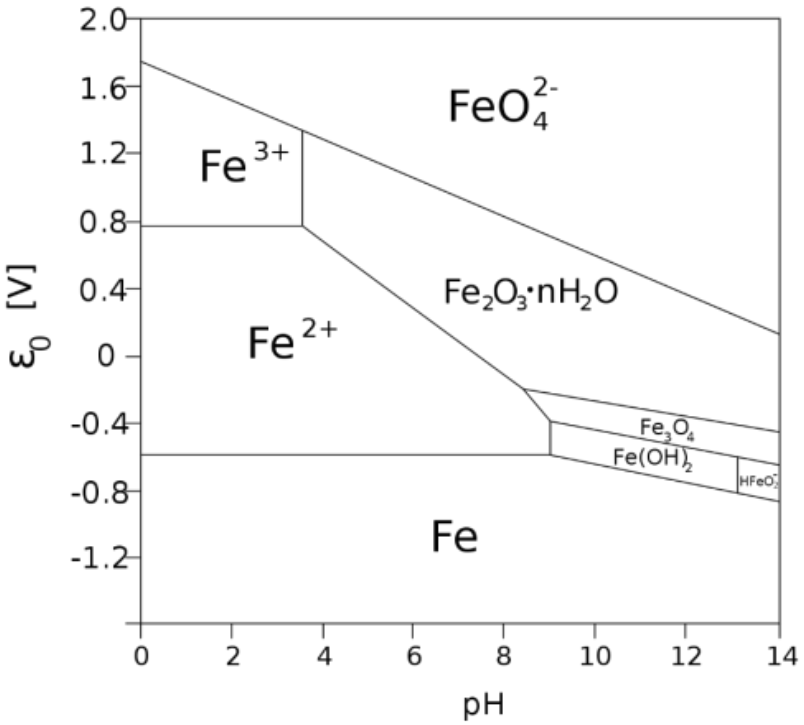

Figure IV-16. Simplified Pourbaix diagram for iron at 1M at 25°C, after [257]

Figure IV-17 shows the standardized cumulative leached iron as a function of the estimated cumulative acid. The results showed negative values for the cumulative iron for acid concentrations lower than 0.01 moles. The difference in iron concentrations between the cement matrix and the feeding solution resulted in a diffusion of iron towards the cement material. However, as the pH continued to decrease with the increase of the acid concentrations, the phases containing iron started to dissolve, and releasing iron in the interstitial solution. The migration of iron shifted towards the solution.

Moreover, two distinctive behaviors were observed for materials containing HardCem. One the one hand, PCH showed high standardized leaching of iron compared to respective control material (PC). One the other hand, AASH showed lower standardized leaching of iron compared to respective control material (AAS). The difference lies in the amount of initial iron in the control materials. AAS contained very low amount of iron in the matrix compared to PC with 0.28 and 2.64 respectively. The leaching of little amount of iron would have a higher impact on AAS than on PC when the results are standardized (ratio between leached iron and initial iron concentrations). Nevertheless, it seemed that iron in the form of HardCem is reactive with acid at low pH conditions.

While SR0 and SR3 contained higher iron amount than PC, they showed lower release of standardized iron. Such behavior could be linked to the initial mineralogical form of iron (mainly C_4AF). The reactivity of C_4AF is known to be slower than the other anhydrous phases of the cement; thus, iron is often found in anhydrous form surrounded by a small layer of hydrated paste [62]. In order to release high amounts of iron, the acid must dissolve the hydrated phases before attacking C_4AF grains.

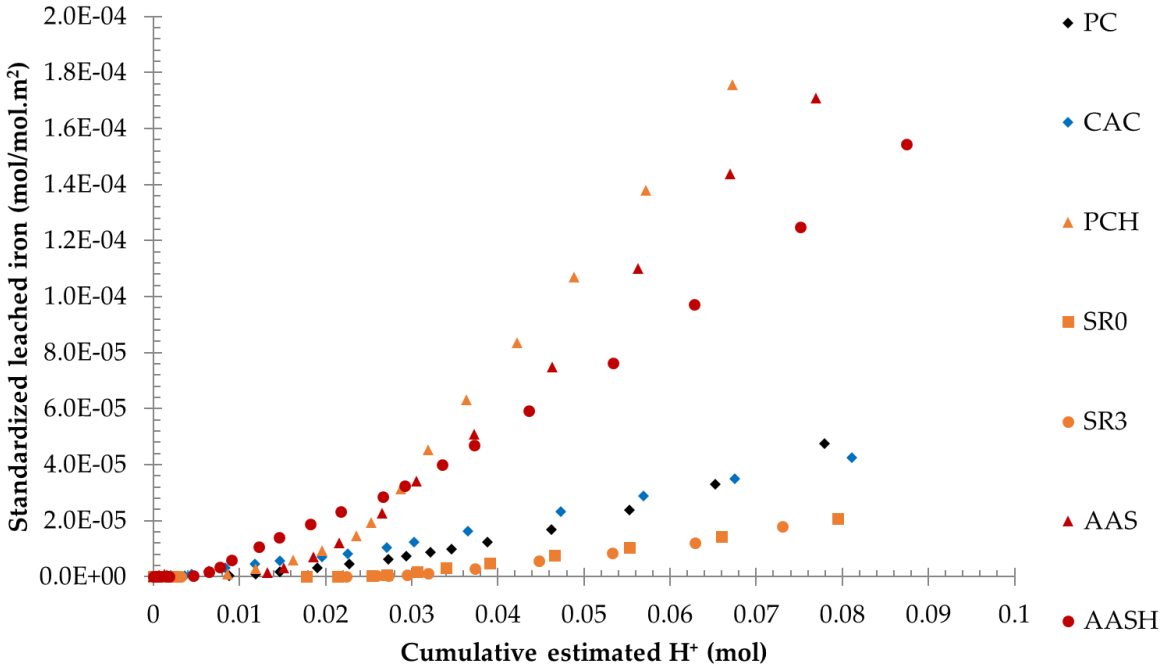

Figure IV-17. Cumulative leached Fe (in mol/mol.m²) as a function of cumulative estimated H^+ (in moles) for the different materials exposed to the BAC test

4.5. REACTIVITY OF ALKALI-ACTIVATED MATERIALS TO BIOGENIC SULFURIC ACID ATTACK IN SEWER CONDITIONS

4.5.1. Particular behavior of pH evolution of AAS materials

Figure IV-18 presents the evolution of the pH of the leached solutions for AAS-based materials as a function of the exposure time of these materials to the BAC test. AAS materials showed a particular behavior. In the early days of the test, the pH profiles were as high as for the PC-based materials, around 11. However, as the testing period progressed, the pH decreased more rapidly than PC and reached acidic conditions earlier. The evolution of pH for AAS materials could be divided into four phases: (i) phase 1 which lasted 2 weeks; (ii) phase 2 started from day 14 until day 28, (iii) phase 3 started from day 28 until day 63; (iv) phase 4 lasted from day 63 until the end of the testing period.

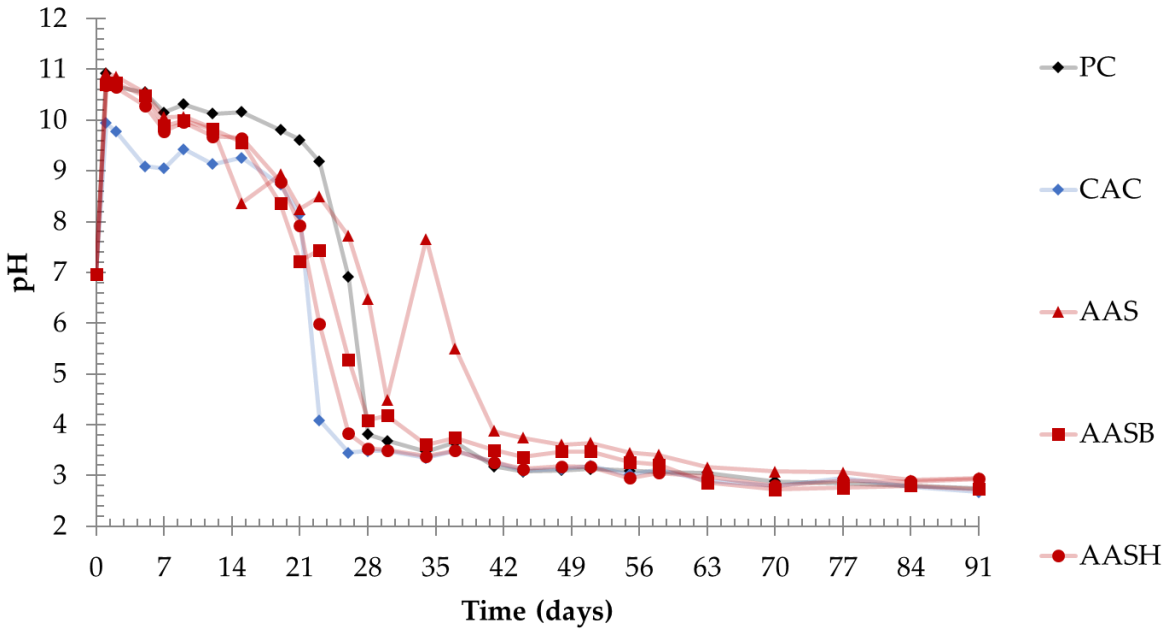

Figure IV-18. Evolution of the pH of the leached solutions for AAS-based binders

Regarding phase 1, the high pH of the leached solutions for PC materials was linked to the dissolution of calcium-bearing phases, such as portlandite and calcium silicate hydrates [14,49,67,68]. The dissolution of such phases releases hydroxide ions which neutralize the acid. However, for alkali-activated slag, portlandite was not present. Nevertheless, the high pH in the earlier days of the test was related to a different species which neutralized the acid. The analyses of the leached solutions showed high concentrations of sodium released from the binders in the same period of time (first 14 days). While sodium carbonate was added to activate the hydration processes of slag, the feeding solution contained very low concentrations of sodium and carbonate. Thus, the amount of sodium carbonate which did not react with slag (form calcium carbonate for example) got diffused into the leached solution. The neutralization capacity of sodium carbonate could be explained by equations **Eq.IV-11**, **Eq.IV-12** and **Eq.IV-13**. Firstly, the hydrolysis of sodium carbonate takes place followed by a reaction between carbonate ions and the acid as a function of the pH of the solution.

$$Na_2CO_3 + 2\,H_2O \rightarrow 2\,Na^{+}_{(aq)} + CO_3^{2-}{}_{(aq)} \qquad \textbf{Eq.IV-11}$$

$$CO_3^{2-}{}_{(aq)} + H^{+} \rightarrow HCO_3^{-} \qquad pH > 6 \qquad \textbf{Eq.IV-12}$$

$HCO_3^- + H^+ \rightarrow H_2CO_3$ pH < 6 **Eq.IV-13**

Therefore, the leaching of sodium could be used to evaluate the neutralizing capacity of the AAS binders. The concentrations of sodium in the leached solutions as a function of exposure period and as a function of the pH are presented in Figure IV-19 and Figure IV-20 respectively.

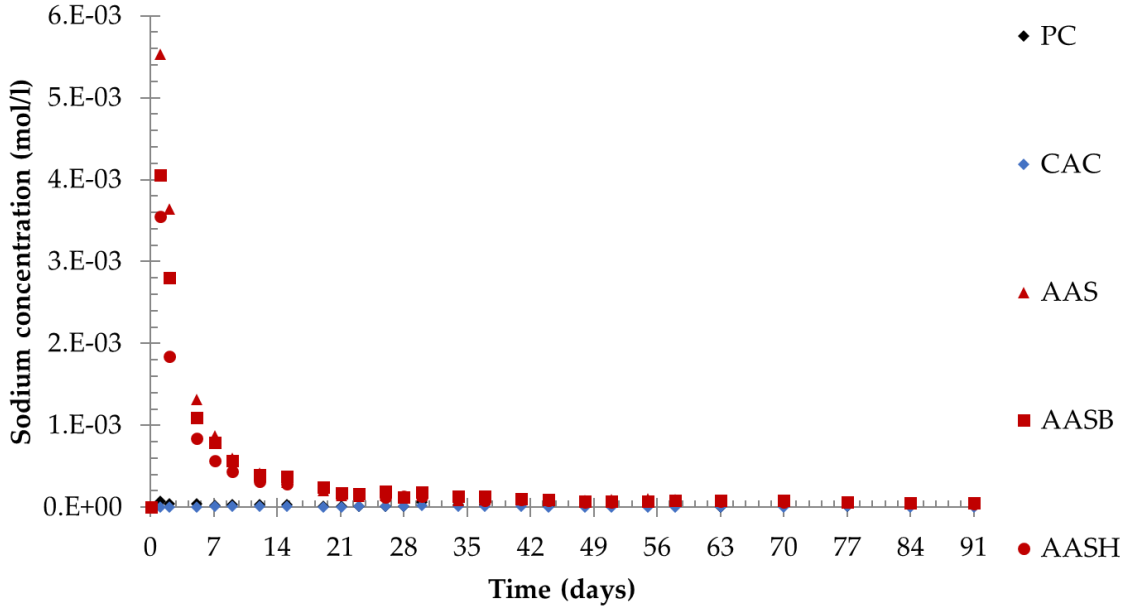

Figure IV-19. Evolution of the concentration of sodium in the leached solutions for PC, CAC, AAS, AASB and AASH

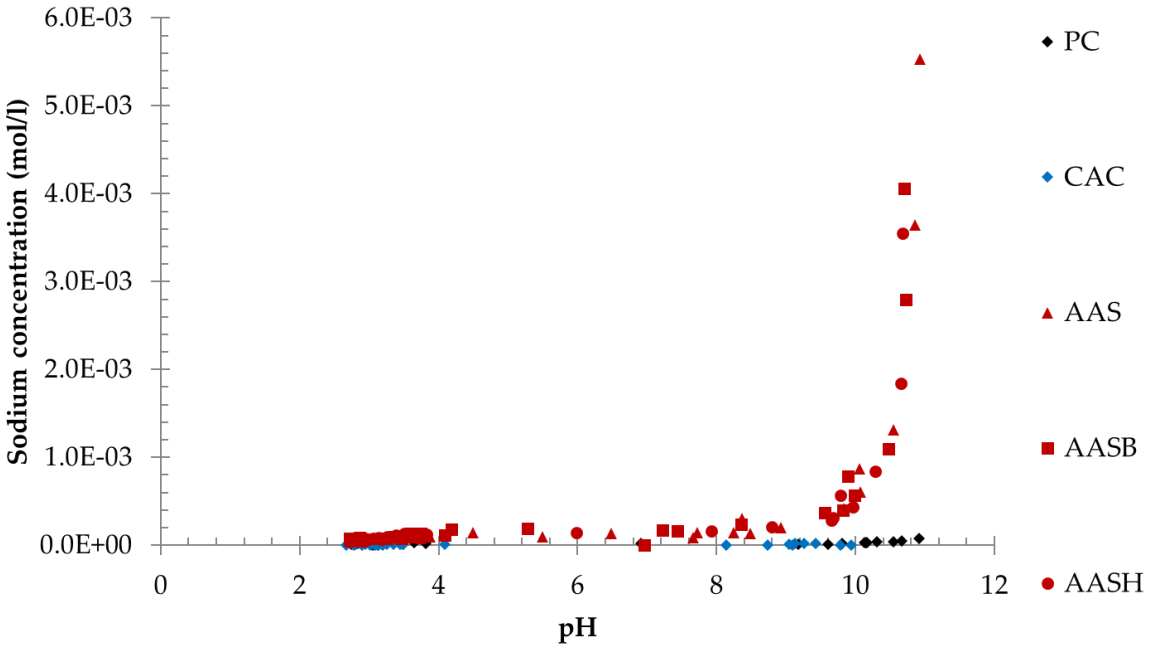

Figure IV-20. Sodium concentrations in the leached solutions for PC, CAC and AAS-based materials

High concentrations of sodium were observed only for AAS-based materials. Moreover, high concentrations were observed mainly for the first 14 days, when pH was of about 9.5. Since the major amount of sodium was present in the pore solution of the alkali-activated materials,

the kinetics of sodium leaching was very high and the major portion of sodium was leached in the first 14 days [121,122,128]. However, after 14 days when the pH dropped to acidic conditions, very low concentrations of sodium were measured for AAS-based materials, which demonstrated the relationship between the leaching of sodium and the evolution of the pH of the leached solutions.

Phase 2 consisted of the decrease of pH from alkaline to acidic conditions. The distribution of the sludge on the surface of the specimens as well as the preferential pathways created by the feeding solution can influence (accelerate/delay) the development of the biofilm, thus impacting the pH of the solution. The slower decrease in pH for AAS during phase 2 has been linked to the delay in biofilm development on the material. This behavior is not intrinsic to the material but rather linked to random phenomena impacting the biological activity.

Phase 3 was the period where the pH was between 4 and 3, mentioned in the literature as the transition period where acidophilic bacteria start to grow to replace neutrophilic bacteria. At day 35, the pH of AAS increased significantly from 4 to 8 before decreasing again to 4. Such sudden increase was due to a technical problem with the flow pump which resulted in the drying of the specimen for at most 24 hours. The drying of the surface of the specimen disturbed the microbial activity by cutting out the inlet of the reduced sulfur, leading to less production of sulfuric acid and an increase in pH. However, once the problem was solved, the pH decreased to join the other materials. In phase 4, like the other exposed materials, the pH stabilized between 2.5 and 3.

4.5.2.Sulfate concentration in the leached solutions

Figure IV-21 presents the cumulative leached sulfate measured experimentally in the leached solutions for PC, CAC, AAS, AASB and AASH during their exposure to the BAC test.

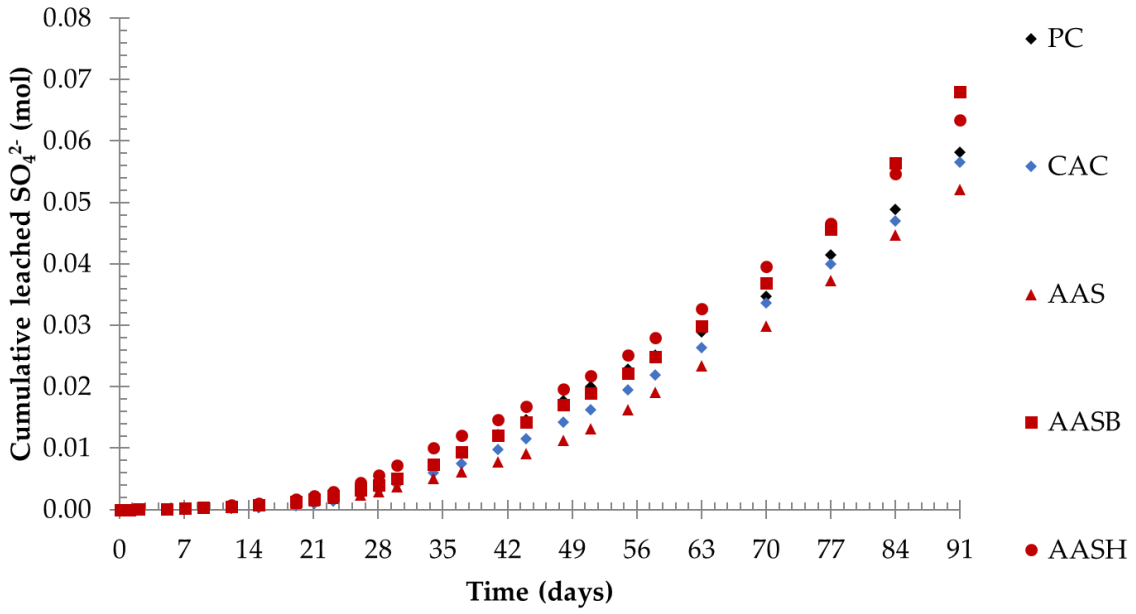

Figure IV-21. Cumulative leached sulfate measured for PC, CAC, AAS, AASB and AASH materials

The pH evolution of AASB and AASH were very similar and this was also observed on the evolution of the sulfate concentrations. However, a difference in sulfate production between AAS and AASB/AASH was observed at 35 days, which corresponded to the time where the pH increased due to the problem in the pump. Moreover, the flow of the feeding solution was slightly lower for AAS, which, on the long term, might have supplied less sulfur substrate for sulfur-oxidizing bacteria and have led to lower amount of sulfate biologically produced.

4.5.3.Calcium leaching

The hydration of alkali-activated slag resulted mainly in the formation of calcium (aluminate) silicate hydrates (C-S-H and/or C-(A)-S-H depending on the amount of aluminum in the slag) [258,259]. Therefore, calcium-based phases represented the main phases of these binders. The sulfuric acid attack on such materials led to the release of calcium ions in the leached solutions. Monitoring the leached calcium in terms of amount and kinetics was carried out to evaluate the reactivity of the calcic-phases to the biological sulfuric acid attack. The curves of the total leached calcium and the standardized leached calcium as a function of the estimated acid produced by microorganisms are presented in Figure IV-22 and in Figure IV-23 respectively.

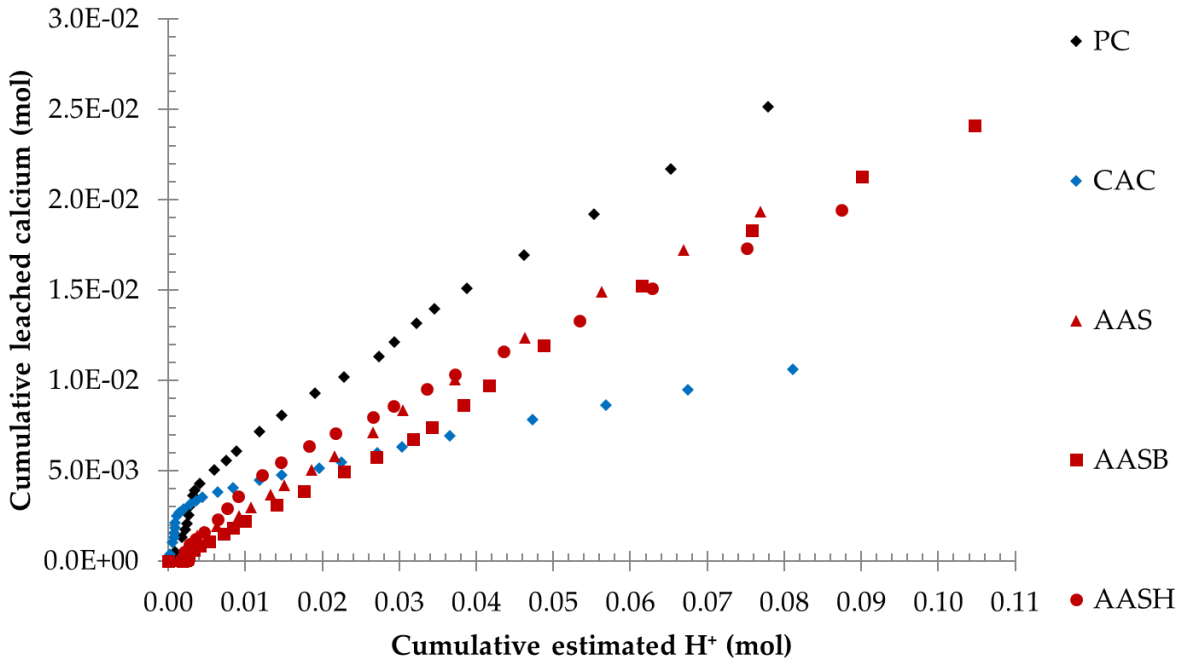

Figure IV-22. Cumulative leached calcium (mole) as a function of cumulative estimated acid (mole) for AAS-based materials (AAS, AASB and AASH) compared to PC and CAC

The behavior of AAS materials regarding calcium leaching was quite atypical compared to other cementitious materials. Typically, two phases of calcium leaching were observed during the deterioration process using the BAC test, as observed for PC and CAC materials [26,67]: (i) fast kinetics of calcium leaching at the start of the test; (ii) slower leaching kinetics in acidic conditions. However, the two phases corresponded to different behavior for AAS materials. In the first phase, instead of having fast kinetics of calcium leaching, the measured calcium in

the leached solutions was lower than the amount of calcium in the feeding solution (< 1.25×10^{-5} mol/l). The calcium seemed to be bounded inside the matrix; thus, negative values were observed in the first phase of calcium leaching for AAS materials. The second phase consisted of calcium leaching with much greater kinetics compared to PC and CAC. Such behavior could be the result of (i) the rapid decalcification of C-A-S-H from ion exchange with the acid leading to the release of high amounts of calcium; and (ii) having more porosity and cracks inside the matrix for sulfuric acid to reach deeper unaltered zones more rapidly compared to the reference materials.

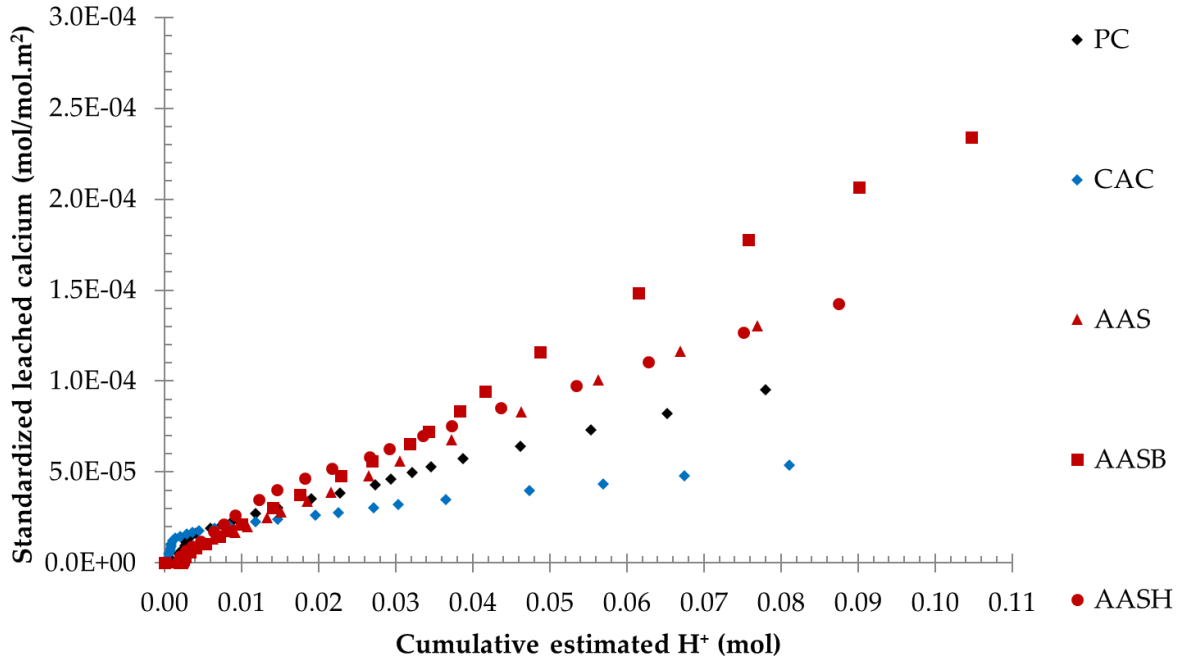

Figure IV-23. Standardized leached Ca (mol/mol.m²) as a function of cumulative estimated H^+ (mol) for AAS-based materials (AAS, AASB and AASH) compared to PC and CAC

Nevertheless, the three AAS-based materials showed very similar kinetics of calcium, suggesting that calcium was mainly leached from hydrated phases of slag. AAS materials released lower total calcium compared to PC and higher total calcium compared to CAC. Although, by standardizing the results of calcium leaching, AAS materials have leached calcium up to 5 times higher than the amount of standardized calcium for CAC. Moreover, by having higher slopes for AAS materials compared to PC and CAC, the resistance of AAS's mineralogical phases seemed to be lower against biological sulfuric acid attack when compared to PC and CAC. Finally, no difference was observed in the reactivity of calcium-bearing phases when HardCem was added to the binder, indicating again the non-improvement of the performance of materials with the addition of HardCem. However, by incorporating bauxite, high calcium amounts were leached with much higher kinetics compared to AAS. The behavior of such additions will be studied in terms of microstructural evolution in chapter V in order to understand their particular behavior.

4.6. CONCLUSIONS

This chapter was focused on the study of the leached solutions from different cementitious materials obtained from an accelerated laboratory test for biodeterioration phenomena. The liquid phase was monitored over the exposure period (3 months) in order to evaluate the behavior of the cement matrices against biogenic sulfuric acid attack.

Firstly, the performance of the different materials was compared to the reference material (Portland cement) using an optimized performance indicator. The equivalent hydroxide performance indicator (PIeqOH) was based on the amount of hydroxide ions potentially released from the dissolution of the corresponding mineralogical phases. The evaluation of OH^- quantity was linked to five major elements/compounds constituting the cement matrix, calcium, aluminum, iron, magnesium and sulfate. By using the amount of acid produced and the PIeqOH, a performance ranking for all materials was obtained.

CAC was found to provide the best performance, with a performance indicator equivalent to 2.3 times the reference material. CSA materials showed promising performances with PIeqOH varying between 0.9 and 1.3 times the performance of the PC material. All PC-based materials (with and without mineral additives) presented very similar performances. Finally, the resistance of alkali-activated slag materials was lower than that of Portland cement, indicating a very poor performance of such materials in the sewer conditions.

Secondly, the study of the liquid phase for CSA showed similar behavior to CAC in terms of pH evolution and in aluminum leaching. However, it seemed that the stability of aluminum-containing phases was the main criterion of the better durability of the materials while increasing the aluminum content by non-reactive phases seemed to not improve the resistance of the materials. The chemical stability of major aluminum-bearing phases could be key factor to optimize the formulation of CSA binders.

Thirdly, incorporating iron as a mineral additive to the binder or using high-iron Portland-based materials showed no impact on the behavior of the materials. In the conditions of the BAC test, the sulfate measurements and the estimation of acid showed that iron did not have any influence on the microbial activity. Nevertheless, the evolution of iron inside the cement matrix will be studied in the next chapter.

Fourthly, alkali-activated slag binders presented a particular behavior regarding calcium leaching. Sodium leaching maintained a high pH, consequently, the calcium-bearing phases were not dissolved. The sharp drop in pH was accompanied by very high concentrations of calcium in the leached solutions, suggesting that the anhydrous and hydrated phases suffered from severe attack from biological sulfuric acid.

Chapter V

Alteration mechanisms of the cementitious binders exposed to sewer environments

5. CHAPTER V – ALTERATION MECHANISMS OF THE CEMENTITIOUS BINDERS EXPOSED TO SEWER ENVIRONMENTS

Tables of Contents

5.1. INTRODUCTION

The literature review showed that the biodeterioration of cement-based materials in sewer environments could be categorized into three phases. The first phase consists in the carbonation and the abiotic attack by H_2S leading to the decrease of pH to around pH 9. Neutrophilic microorganisms start to develop and colonize the surface of the material. Such microorganisms produce sulfuric acid which reduces the pH of the medium to approximately 4. Acidophilic microorganisms colonize the surface of the material and produce high amounts of sulfuric acid which causes a progressive local dissolution of the cementitious matrix and the formation of secondary expansive phases, e.g. gypsum and ettringite [5,6,9,10,49,230].

The previous chapter (chapter IV) showed that the reactivity and the resistance of the materials differed greatly depending on their chemical and mineralogical compositions. In BAC test, the evaluation of the resistance of the cementitious materials to biogenic acid attack was based on the leaching of the cement cations (calcium, aluminum, iron and magnesium) in standardized concentrations, i.e. ratio of the leached element per initial total content of the element in the binder per exposed surface. In the experimental conditions, the CAC-based material appeared to be more resistant than CSA-based materials. Even within the three CSA-based materials, two materials, CSAC (calcium sulfoaluminate clinker) and CSAG (calcium sulfoaluminate clinker with gypsum) showed similar performances while CSAA (calcium sulfoaluminate clinker with anhydrite) presented a lower performance which was equivalent to the reference PC material. The addition of mineral additives rich in iron did not seem to improve the resistance of the cement pastes.

Furthermore, although the sulfur-oxidizing activity seemed to be the same from a material to another, the reactivity of the cementitious materials to the biogenic acid attack was different. Some specificities appeared in the selected microbial populations, in particular for CSAA (with anhydrite), AASB (with addition of bauxite), and AASH (with addition of Fe-rich mineral) materials, which showed a microbial selection of the species *Acidithiobacillus ferrooxidans* on their surfaces.

Therefore, in the objective of understanding the differences in the performance of the exposed materials and of establishing the corresponding alteration mechanisms, the analyses of the microstructure of the cement specimens after deterioration were carried out.

This chapter is focused on:

i. The characterization of the evolution of the microstructure as well as the changes in the chemistry and the mineralogy of the different cementitious materials after a 3-month exposure to the BAC test.
ii. The microbial colonization of the surface of the materials and their penetration inside the cementitious matrix
iii. The study of the impact of the amount and the mineralogical form of iron in the mix designs on the resistance of the cement matrix.

iv. The comparative study between CSA- and CAC-based materials in order to highlight the difference in the evolution of their respective hydrated phases, in particular the aluminum hydroxide, during the deterioration process as well as to establish a complete description of the deterioration mechanisms of different CSA formulations.

v. The investigation of the performance of alkali-activated slag materials as well as the establishment of their deterioration mechanisms in these environments.

5.2. MACROSCOPIC AND MICROSCOPIC OBSERVATIONS

5.2.1. Visual observations of the surface of the materials after 3-months exposure to the BAC test

At the end of the 3-month exposure period of the specimens to the BAC test, the cement materials were collected and sawn into two halves. The upper half was used for microscopic analyses and the lower half was used for microbiological analyses. Figure V-1 presents the photographs of the surface of the halves of the specimens used for microscopic analyses.

All specimens' surfaces showed severe deterioration and a yellow-whitish layer likely composed of mineral/organic precipitates and biofilm. Moreover, this layer presented cracks which were mainly attributed to the drying of the specimens at 20°C for 24 hours after 3 months in saturated conditions. Nevertheless, these cracks were not detected in the CAC specimens. The deteriorated layers were not very cohesive with the sound core of the specimens, especially for the CSAA, with the matter partly lost during the sample handling.

The surface layer of PC-based materials showed slightly more cohesion with the sound matrix compared to the rest of the materials. The surface layer of CSA-based materials was highly cracked layer due to the self-desiccation of the deteriorated zone [74]. During the preparation of the specimens for further analyses, the outer layers of the CSA materials were detached from the specimens, as seen on the image of the CSAA specimen. The deteriorated layers of AAS-based materials showed the same behavior as those of CSA materials, although with a slightly higher cohesion with the sound zones. The CAC, nonetheless, presented a degraded layer with a pasty consistency. This layer was homogenous all over the surface of the CAC specimens.

Different colorations have been observed on the surface depending on the nature of the materials. For instance, PC and AAS materials showed a dark brown color, which was mainly related to the decalcification of the matrices; thus, highlighting the color of iron oxides. CAC, having the deteriorated layer composed mainly of aluminum hydroxide, exhibited a light gray color relatively close to the color of the precipitations on its surface. Finally, CSA materials had a rather dark orange (or light brown) color. This tint, located between dark brown and light gray, suggested the presence of oxidized Fe-bearing phases embedded in the outer deteriorated layer.

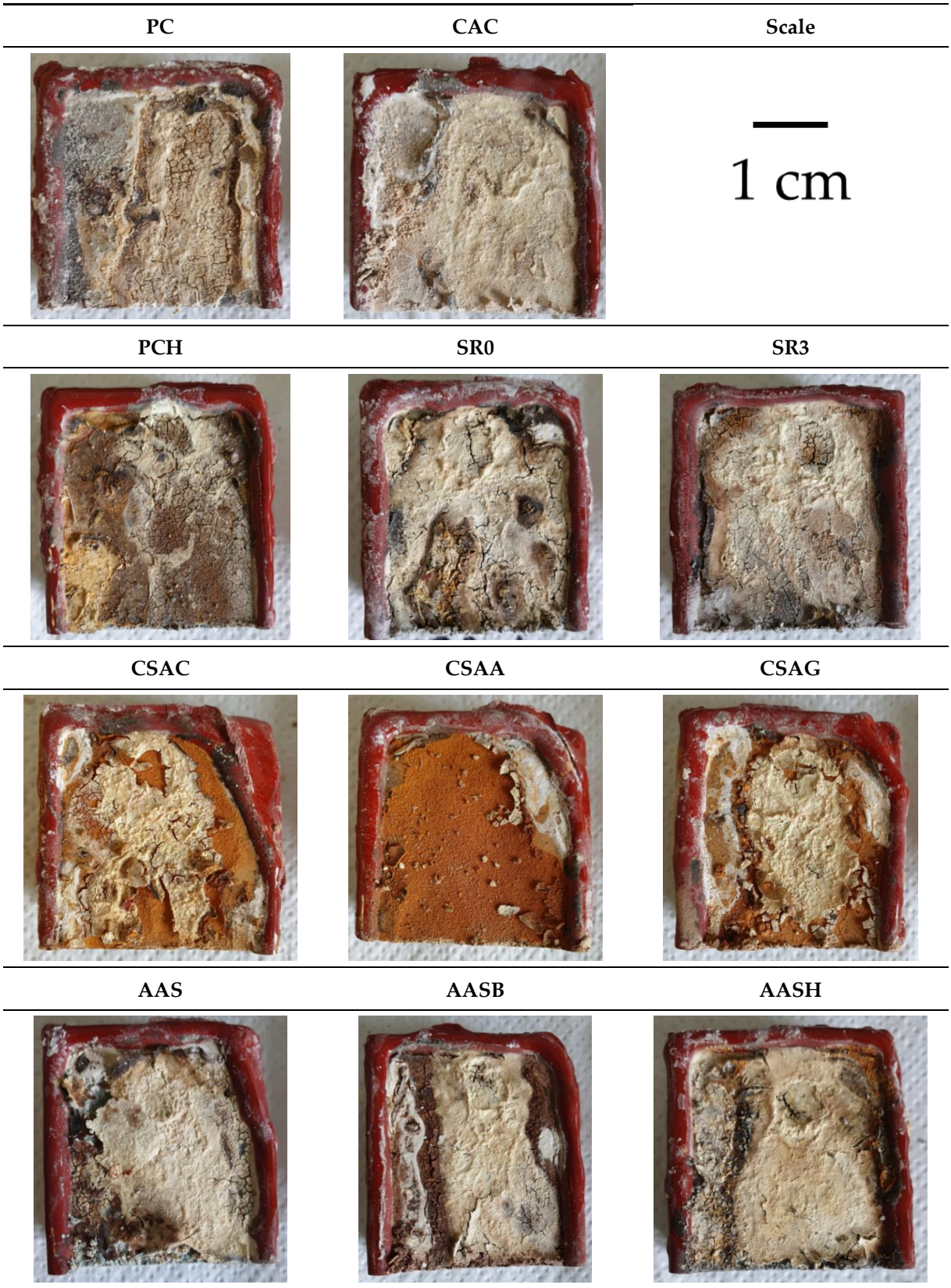

Figure V-1. Visual observations of the deteriorated surface of the different specimens at the end of the exposure period (3 months) to the BAC test

In the BAC test, the cementitious specimens were inoculated with activated sludge then were exposed to a trickling solution containing tetrathionate as a reduced sulfur source. The run-off of the solution on the surface of the specimens was carried out naturally and without any

exterior intervene. Therefore, preferential pathways of the run-off solution might have occurred on the surface of the materials. In addition, the outer layers (colonized and/or deteriorated) were not homogenous on the surface of the specimens, and local accumulation of precipitates and biofilm in the width and the length of the materials were observed.

5.2.2. Microscopic observations of the materials after 3 months of exposure to the BAC test

SEM microstructural observations of the cross-sections of the specimens after their exposure to the BAC test for 3 months are presented in Figure V-2 (PC-based materials), in Figure V-3 (CAC- and CSA-based materials) and in Figure V-4 (AAS-based materials). These images show the entire width of the specimens and the two edges covered with epoxy resin.

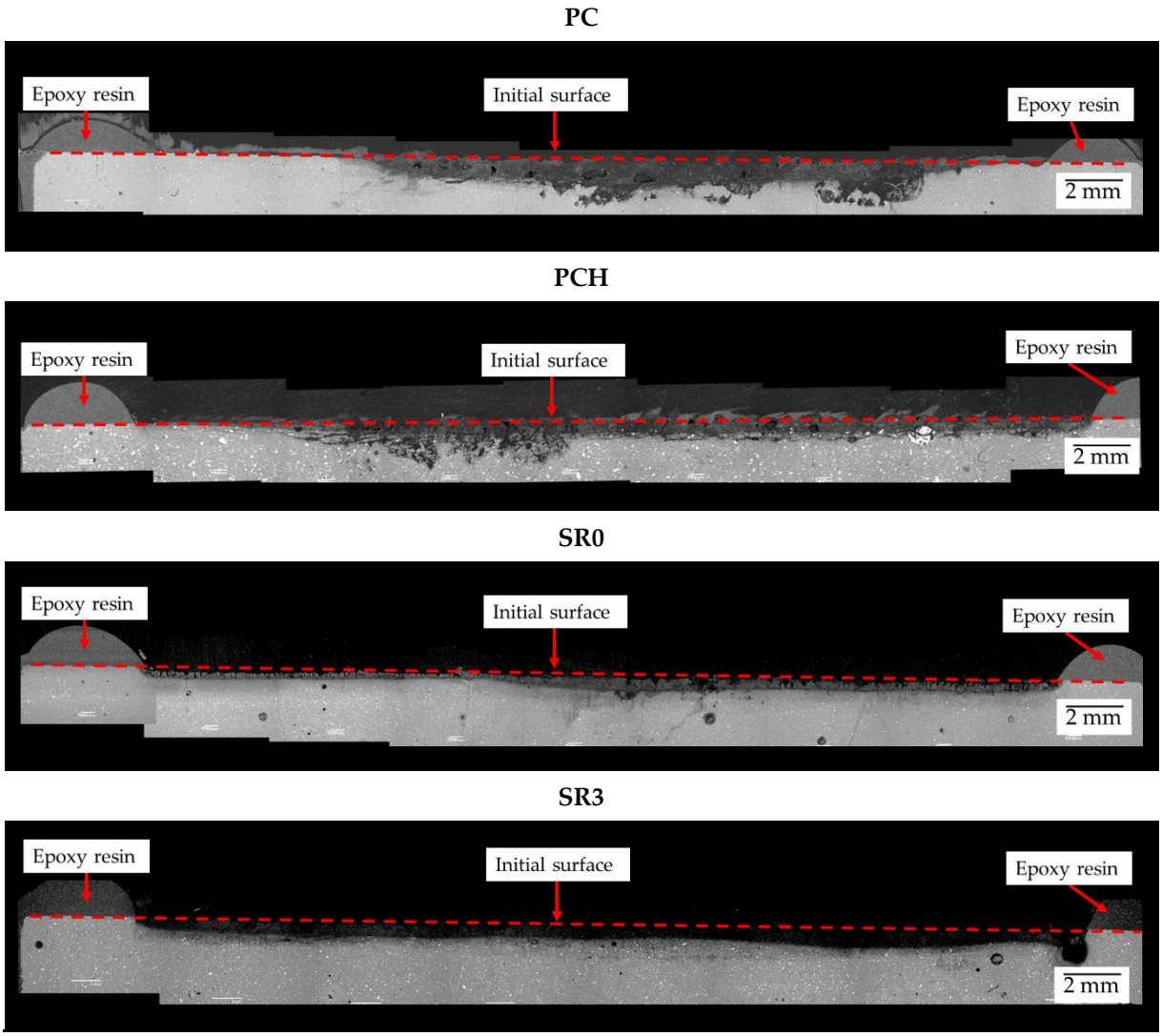

Figure V-2. Microstructure observations of the cross-section of PC, PCH, SR0 and SR3 pastes after 3 months of exposure to the biodeterioration test

For PC-based materials, the cross-sections showed relatively small deteriorated depths. However, as mentioned in the previous section, due to the preferential pathways of the run-

off solutions, local zones were created where the deterioration was not very severe, as it was the case for all four PC-based materials.

The SEM observations of the cross-sections of PC and PCH materials showed several similarities. The deteriorated part appeared to be very local with a dissolution of the outer layer of the matrix and severe deteriorations of the inner deteriorated zones. The SR0 and SR3 materials showed more homogeneous attack and lower deterioration depth compared to PC and PCH. The deteriorated zones of SR0 and SR3 presented a complete dissolution of the outer part of the matrix and a layer of lower density of the inner deteriorated zones. Precipitates were found on the surface of both materials.

The CAC-based material had a very homogeneous deteriorated surface. No total dissolution of the paste on the surface was observed and the deteriorated zone seemed to be a composed of a single layer.

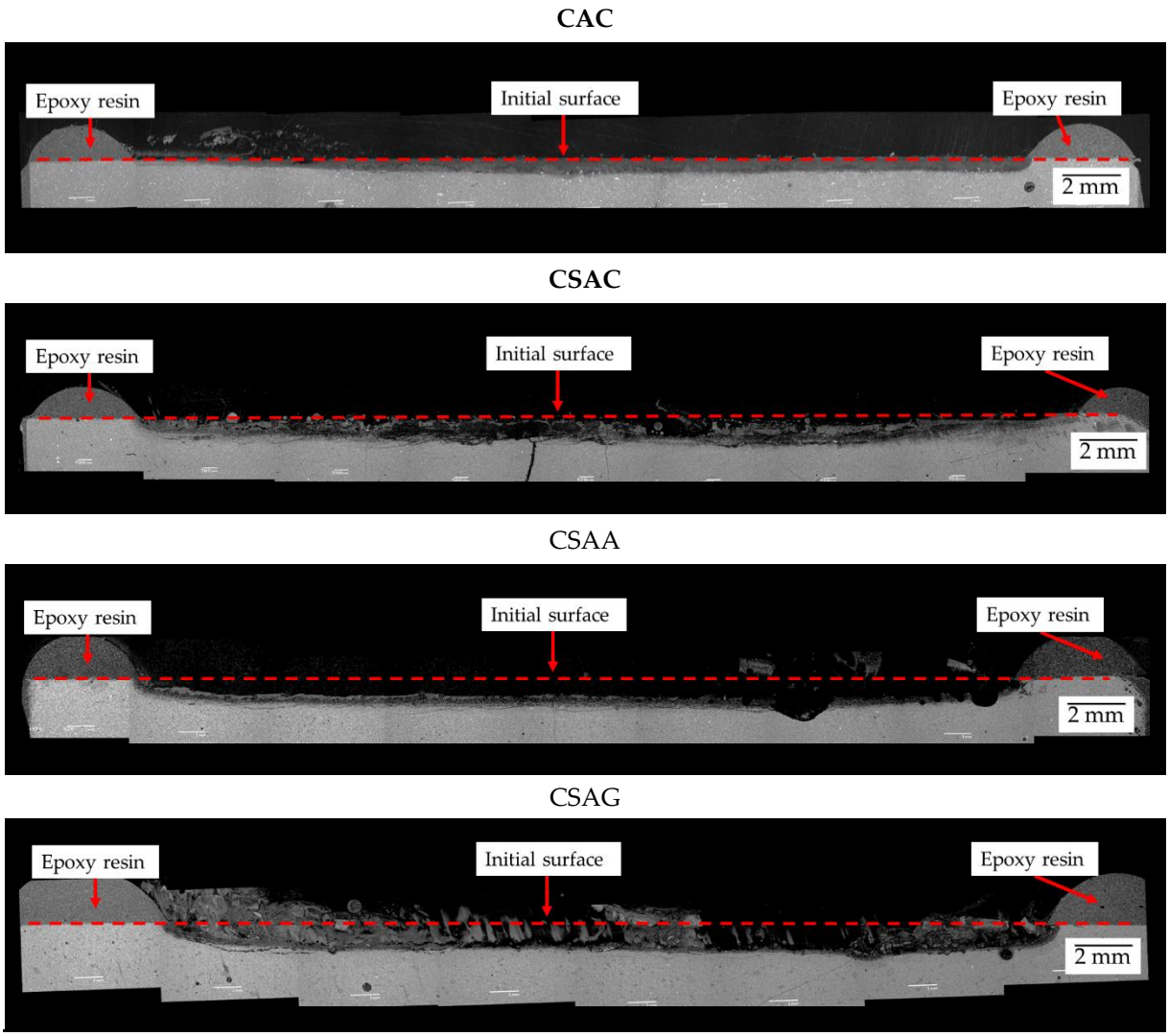

Figure V-3. Microstructure observations of the cross-section of CAC, CSAC, CSAA and CSAG pastes after 3 months of exposure to the biodeterioration test

CSA-based materials were quite different. While the deteriorated zones were very fragile, the deteriorated part of CSAA specimen detached during the preparation of the sample for the

analyses; thus, the less precipitates observed on its surface. CSAC and CSAG presented a complete dissolution of the cement matrix outer layer. More heterogeneous precipitates were observed on CSA materials compared to CAC. The deteriorated zones of CSA materials did not form a cohesive layer as observed for the CAC material. One should note that surface precipitates were very mobile, and during preparation of polished section, due to the viscosity of the resin, these precipitates could shift easily as was the case for CSAG.

Finally, AAS-based materials showed a very different behavior depending on the mixtures. However, the three materials exhibited very large vertical cracks that started from the exposed surface and went up to 5 mm within the cementitious matrix. The control samples of AAS-based materials exhibited smaller and shorter cracks, mainly attributed to shrinkage of the paste [141,260]; however, the relatively deep cracks could result from a specific behavior of the hydrated phases, in particular C-A-S-H, when attacked by sulfuric acid.

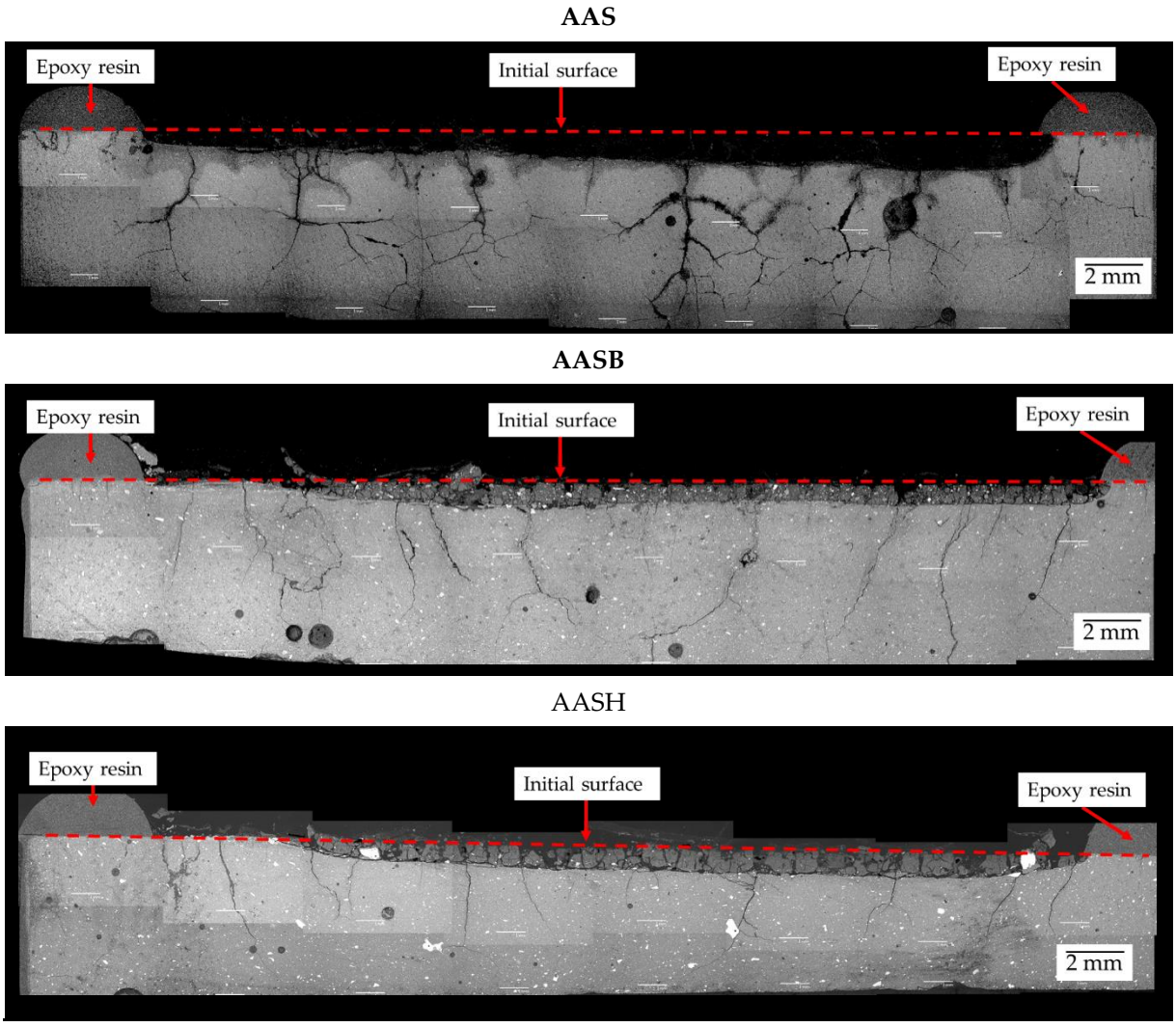

Figure V-4. Microstructure observations of the cross-section of AAS, AASB and AASH pastes after 3 months of exposure to the biodeterioration test

The AAS material showed complete dissolution at the surface of the material and strongly deteriorated zones, highlighted by the difference in density observed on the SEM images. In addition, the immediate vicinity of all the large cracks within the cementitious matrix

appeared to have a lower density than that of the sound paste. AASB and AASH presented local dissolution at the level of the highly deteriorated zone. In this zone, a low-density layer which contained residual unreacted grains of the mineral additives, bauxite and HardCem, was observed.

5.3. CHEMICAL AND MINERALOGICAL ALTERATION OF THE CEMENT PASTES EXPOSED TO THE BAC TEST

5.3.1. Reference materials

5.3.1.1. Portland cement (PC)

Figure V-5 presents the EDS chemical composition profile of PC paste specimen (wt.%) exposed to the BAC test for 3 months as a function of the distance to the surface in contact with biofilm. Figure V-6 presents the evolution of the mineralogical composition at several depths within the PC material.

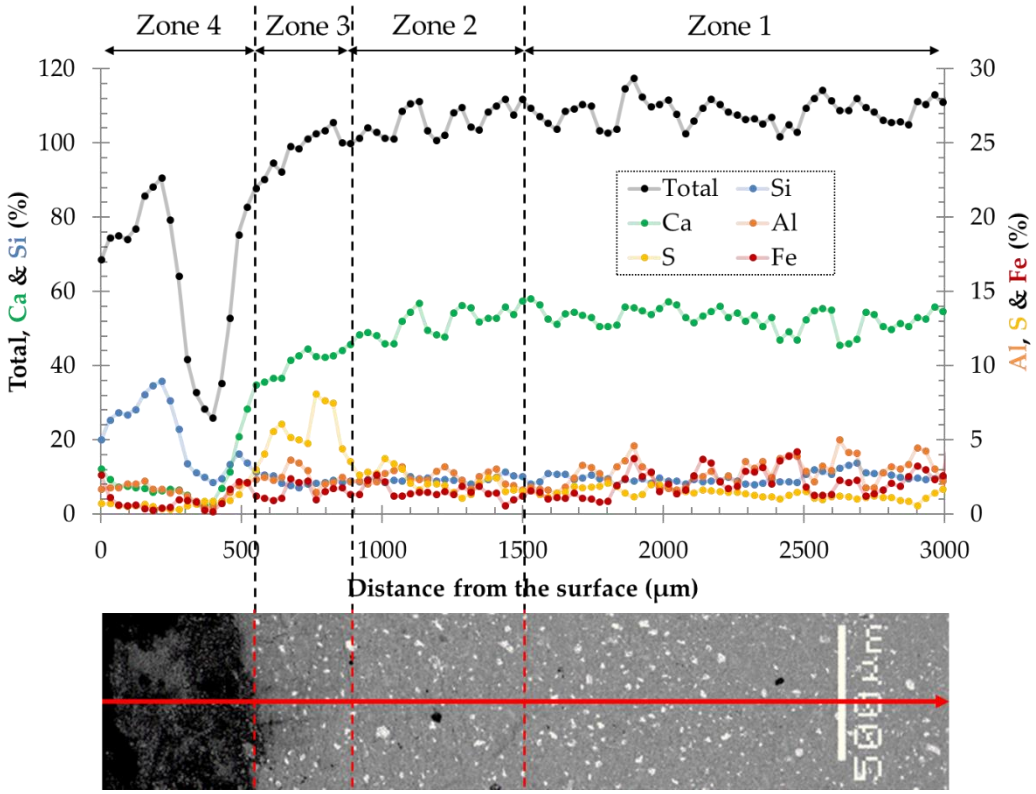

Figure V-5. Evolution of the chemical composition of the PC material exposed to the BAC test for 3 months as a function of the distance from the initial surface of the specimen (at 0 µm) and the SEM observation of the microstructure of the cross-section in BSE mode

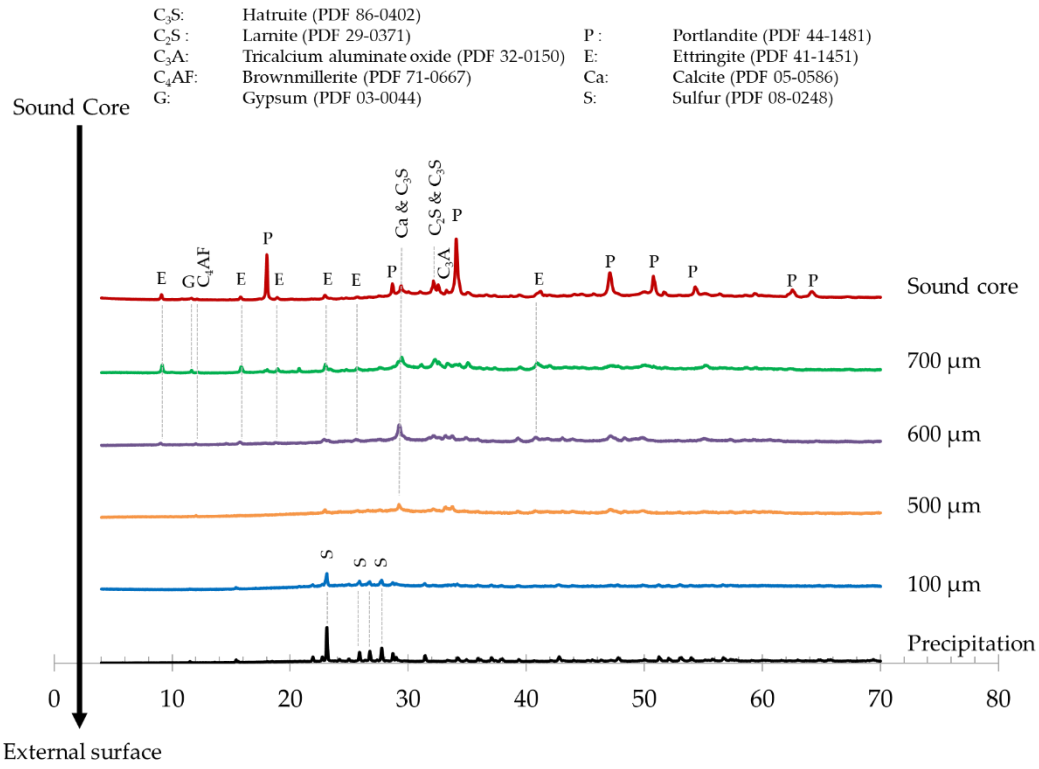

Figure V-6. Evolution of the mineralogical composition of the PC material exposed to the BAC test for 3 months as a function of the distance from the surface of the specimen

Five altered zones were identified from the sound zone or the core of the material (zone 1) to the surface exposed directly to the biofilm (zone 5).

- Zone 1 corresponded to the unaltered core of the material, characterized by the presence of high calcium content (~50 %). The amount of silicon in the PC material was relatively low compared to ordinary Portland cement, with an average of 10 %, resulting of a Ca/Si ratio of 5.53. The Ca/Si ratio was slightly higher than that of the control material of 4.75. The difference in the Ca/Si. The mineralogical analyses showed the presence of hydrated and anhydrous crystallized phases, such as: portlandite, ettringite, C_3S, C_2S and gypsum in this zone.
- Zone 2, having a thickness of 600 µm, showed a slight decrease in calcium content with the other elements being stable.
- Zone 3, with a thickness of 350 µm, was characterized by the sudden increase in sulfur concentration. The calcium content continued to decrease and the rest of the elements remained unchanged. The disappearance of portlandite peaks corresponded to the decrease of calcium while a slight intensification in ettringite peaks explained the increase in sulfur by precipitation of secondary ettringite. The microstructure observation showed microcracks in this zone, which could be correlated to the formation of secondary expansive ettringite.
- Zone 4, with a thickness of approximately 550 µm, showed severe deterioration of the matrix. The total amounts of elements dropped significantly from 80 to 25 %. The microstructure observation showed a very low density which corresponded to a high

decalcification of the matrix. However, silicon was still present in this zone which suggested the complete decalcification of the C-S-H, leaving a hydrogel composed mainly of silicon and aluminum [67,68,230,261,262]. The XRD patterns at 500 µm showed the precipitation of calcium carbonate (calcite) which was a result of the carbonation of the zone. The decalcification of the matrix in a high porous zone released calcium in the pore solution where it reacted with carbonate from the passage of carbon dioxide (CO_2) from the air into the pore solution. The silica gel was not detected as it precipitated mainly in amorphous form. Elemental sulfur was identified and linked to precipitations in the biofilm (on the specimen surface) due to bio-chemical reactions as explained in section 3.4.2 of chapter III.

The general deterioration mechanisms described corresponded to previous deterioration observed for such material [44,49,67].

5.3.1.2. Calcium aluminate cement (CAC)

Figure V-7 presents the EDS chemical composition profile of CAC paste specimen (wt.%) exposed to the BAC test for 3 months as a function of the distance to the surface in contact with biofilm along with the microstructure observation of the specimen in BSE mode. Figure V-8 presents the evolution of the mineralogical composition at several depths within the CAC material.

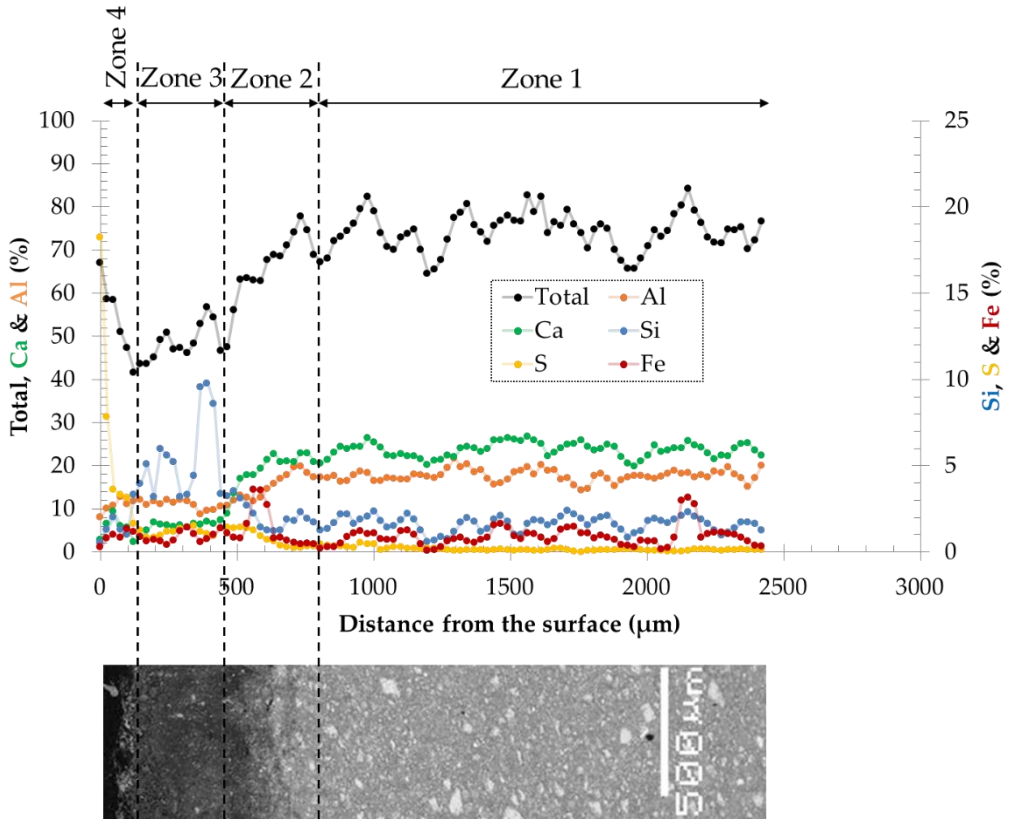

Figure V-7. Evolution of the chemical composition of the CAC material exposed to the BAC test for 3 months as a function of the distance from the initial surface of the specimen (at 0 µm) and the SEM observation of the microstructure of the cross-section in BSE mode

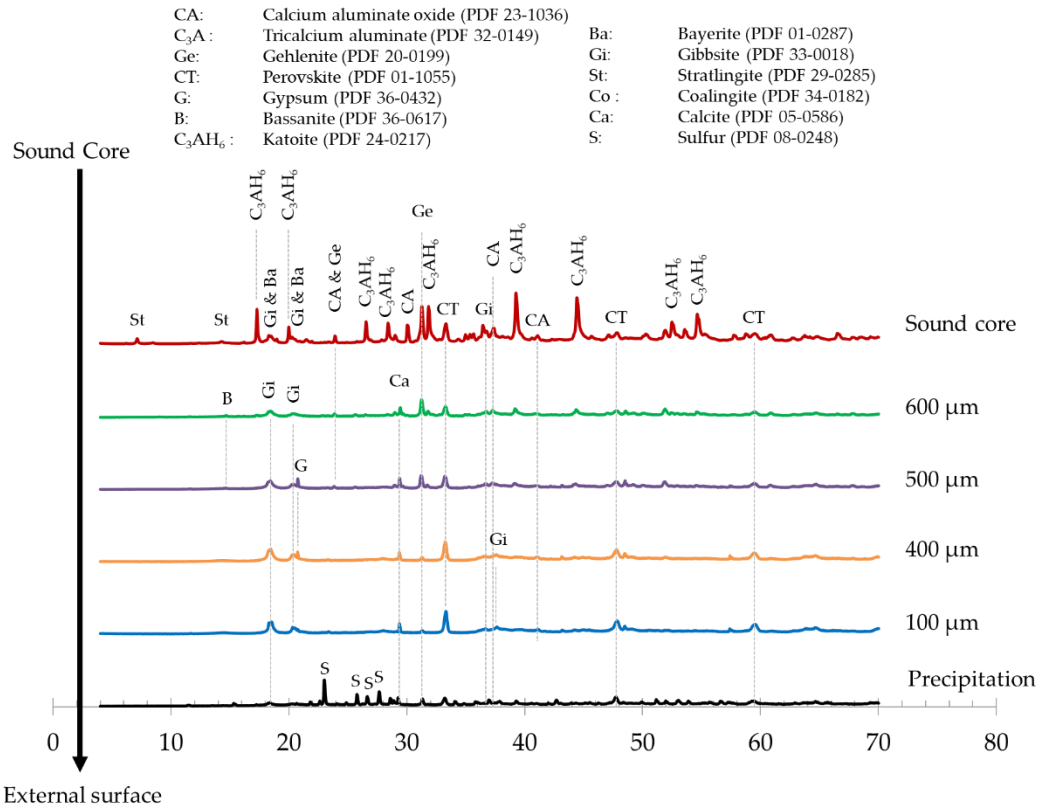

Figure V-8. Evolution of the mineralogical composition of the CAC material exposed to the BAC test for 3 months as a function of the distance from the surface of the specimen

Figure V-7 shows 3 altered zones:

- Zone 1 was considered as the sound zone and was composed of calcium and aluminum as the two main chemical elements and silicon and iron as secondary elements. The main mineralogical phases were katoite and AH_3 (gibbsite and bayerite). Stratlingite (C_2ASH_8) was the main phase containing silicon and it resulted from the hydration of gehlenite (C_2AS).
- Zone 2 of 350 µm of thickness was mildly deteriorated and showed a decrease of calcium and aluminum contents from around 20 to 10% which was likely linked to the dissolution of katoite (C_3AH_6). The increase in sulfur was linked to the diffusion of sulfur-bearing species towards the unaltered zone via the high porous deteriorated area since the material did not contain any sulfur initially. Bassanite was detected in this zone as the sulfate phase.
- Zone 3 was a very low dense and homogenous 400-µm zone which has a gel-like texture from the microstructural observations. The chemical composition profile showed mainly aluminum and silicon. Fewer amounts of calcium and iron were also observed and were attributed to the remaining anhydrous grains. Sulfur in zone 3 was considered to be exogenous (in the form of sulfuric acid, produced by the SOB). The XRD patterns showed an increase in gibbsite and bayerite peaks' intensity. Gypsum was identified as the sulfate bearing phase instead of bassanite. The peak of perovskite (CT) seemed to not change.

- Zone 4 was the outer zone and was identified up to 150 μm. The mineralogical phases in this zone were similar to zone 3. AH_3 was the main phase with lesser amounts of residual resistant anhydrous phases, e.g. perovskite. The chemical analyses showed high sulfur concentrations. Elemental sulfur was the main sulfur-bearing solid precipitate identified in this zone.

The overall deterioration mechanisms corresponded to previous studies in the literature for such materials [44,49,64,67,186]. The identification of bassanite confirmed the penetration of sulfate inside the matrix. The reactivity and the dissolution of the hydrated phases in CAC resulted in the formation of AH_3 phase and the formation of slightly denser deteriorated zones, probably limiting the diffusion of sulfate, compared to PC. This particular behavior of CAC material resulted in a low aluminum concentration in the pore solution; hence, the absence of secondary ettringite formation.

5.3.2.PC-based materials

Figure V-9 presents a summary of the evolution of the chemical and mineralogical composition profiles for PC-based materials, based on the experimental analyses carried out on specimens after 3 months of exposure to the BAC test. The experimental results (SEM observations, EDS and XRD analyses) are presented in **Appendix V-A**. The three PC-based materials were:

- **PCH**: Portland cement (as the reference material) + HardCem
- **SR0**: Portland cement – sulfate resistant Type 0
- **SR3**: Portland cement – sulfate resistant Type 3

PCH was composed of 80% of PC and 20% of HardCem. HardCem is an iron-rich mineral additive which was added to the mixture to increase its initial iron content. The chemical composition of PCH (Table V-1) showed that the iron oxide content in PCH (8.84%) was 3 times higher than that in PC (2.64%). SR0 and SR3 cements are two types of cement which are recommended by the French Standard for structures exposed to aggressive chemical environments due to their low initial C_3A content (< 3%). However, the aluminum content is often compensated by increase the amount of C_4AF, which explains the higher iron oxide content for SR0 (5.80%) and SR3 (4.88%).

Table V-1. Iron oxide content (in weight %) for the studied PC-based materials

Wt.%	PC	PCH	SR0	SR3
Fe_2O_3	2.64	8.84	5.80	4.88

Therefore, the investigation of the impact of the iron on the microstructure evolution was carried out on these three PC-based binders which present different iron oxide contents and different mineralogical forms (C_4AF for SR0 and SR3 and amorphous inert phase for HardCem).

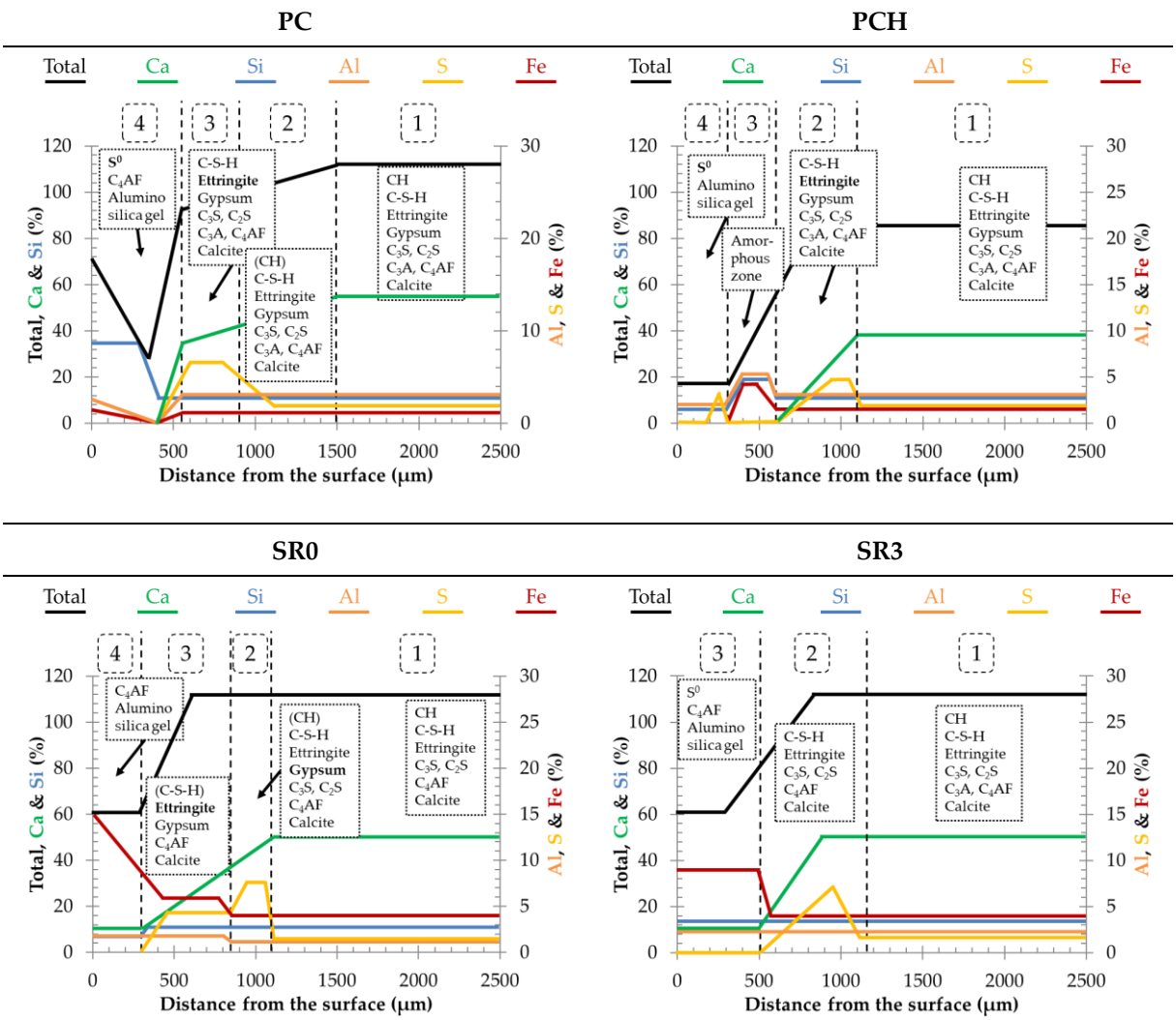

Figure V-9. Summary of the evolution of the chemical and mineralogical composition of PC, PCH, SR0 and SR3 pastes exposed to the BAC test for 3 months as a function of the distance from the initial surface of the specimen (at 0 µm).

The evolution of the chemical composition profiles of PC-based materials was correlated to the changes in the mineralogical composition after exposure to the BAC test for 3 months.

- The sound zone of these materials was mainly composed of typical hydrated phases of Portland cement (e.g. portlandite and ettringite) and anhydrous phases (e.g. C_3S, C_2S and C_4AF). The iron content was higher for SR0 and SR3 than for PC and PCH since they contain very low amount of C_3A and higher amount of C_4AF than PC and PCH.
- In zone 2, the decalcification of the matrices was observed and was correlated to the dissolution of portlandite and a part of C-S-H and to the precipitation of calcite. Sulfur enrichment was detected and linked to the presence of expansive ettringite and gypsum in this zone (presence of microcracks on the BSE images). In addition, the iron content seemed to be stable.
- In zone 3, the decalcification of the matrix became more severe and the materials PCH, SR0 and SR3 showed a relative enrichment in iron. However, no iron-containing

crystalline phases were detected by XRD for PCH while the iron enrichment for SR0 and SR3 was correlated to the presence of C_4AF.

- The outer area of PC-based materials was mainly composed of silicon with lesser amount of aluminum and calcium. The absence of the crystalline phases containing silica and aluminum suggested the precipitation of aluminosilicate gel. The iron content in this zone significantly increased for the SR0 and SR3 materials while PC and PCH presented little or no iron. This suggested that the C_4AF phase (detected in the SR0 and SR3 matrices) seemed to be more resistant to the acid attack than HardCem. Finally, the precipitation of elemental sulfur, resulting from the biochemical reactions taking place in the biofilm, was linked to the sulfur content in this zone.

The results obtained on PC-based cement pastes were consistent with the studies carried out in the literature [12,43,49,67,263,264]. Decalcification of the matrix and precipitation of sulfur-bearing phases (mainly ettringite and gypsum) were the main deterioration mechanisms of these materials. However, the behavior of ferrous phases and their evolution in the cementitious matrix after exposure to biogenic sulfuric acid attack in sewer conditions were little or not studied. The increase in the relative iron content in the severely deteriorated layers could indicate a higher stability of the iron-bearing phases than the calcium-bearing phases in PC-based materials when exposed to such environment. In addition, although HardCem did not participate in the hydration process, the high acidic conditions, generated by the acid attack, resulted in its dissolution, in particular in the outer layer which was exposed directly to the biofilm. In contrast, residual C_4AF anhydrous phase was identified in the outer layer of SR0 and SR3, which could indicate a different behavior than HardCem regarding the acid attack.

5.3.3.CSA-based materials

The literature review attributed the better resistance of CAC binders compared to PC binders to the high stability of AH_3 in acidic environments (down to pH 3-4). The hydration of CAC results in the formation of AH_3 and its exposure to biogenic sulfuric acid attack leads to the dissolution of C_3AH_6 and the precipitation of more AH_3. While the hydration of CSA binders leads to the formation of AH_3 phase, the behavior of the other main phases, such as ettringite and/or AFm phases, in sewer conditions is still not very well documented.

Figure V-10 presents a summary of the evolution of the chemical and mineralogical composition profiles for CAC and CSA-based materials, based on the experimental analyses carried out on specimens after 3 months of exposure to the BAC test. The experimental results (SEM observations, EDS and XRD analyses) are presented in **Appendix V-B**. The three CSA-based materials were:

- **CSAC**: CSA clinker
- **CSAA**: CSA clinker + anhydrite
- **CSAG**: CSA clinker + gypsum

Since CSA-based materials are mainly composed of calcium and aluminum instead of calcium and silicon as previously seen for PC-based binders, the main Y-axis in the chemical profile figures presented the evolution of calcium and aluminum (along with the total element content).

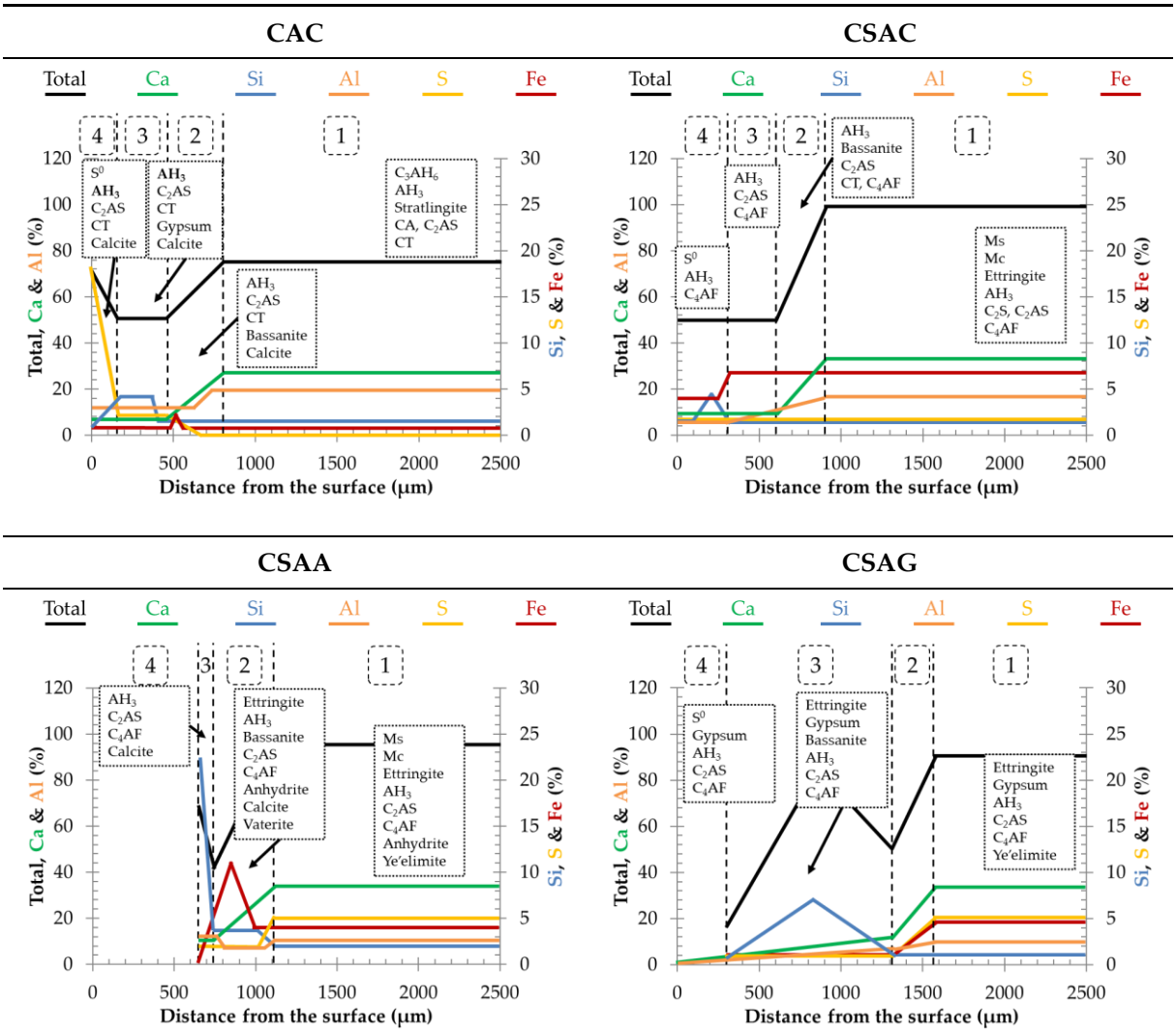

Figure V-10. Summary of the evolution of the chemical and mineralogical composition of CAC, CSAA, CSAA and CSAG pastes exposed to the BAC test for 3 months as a function of the distance from the initial surface of the specimen (at 0 µm). Ms: monosulfoaluminate, Mc: monocarboaluminate, C_2AS: gehlenite, S^0: elemental sulfur, CA: calcium aluminate, CT: perovskite

Four altered zones were identified from the sound zone or the core of the material (zone 1) to the surface exposed directly to the biofilm (zone 4).

- The composition of the sound zone of CSA-based materials was different as a function of the binder's nature. The absence of calcium sulfate in the CSA binder resulted in the total consumption of ye'elimite and in the formation of mainly AFm phases (monosulfoaluminate and monocarboaluminate) and poorly crystallized AH_3. The addition of calcium sulfate to the binder led to the formation of only ettringite when gypsum was added (CSAG) and of ettringite and AFm phases when anhydrite was added (CSAA). However, both binders formed poorly crystallized AH_3 and residual

ye'elimite was detected. The hydration of silicon-bearing phases (C_2S and C_2AS) could have formed C-S-H phases; however, these phases are mainly amorphous and therefore they could not be detected by XRD. The sound zone of CAC was mainly composed of katoite (C_3AH_6) and crystallized AH_3 (gibbsite and bayerite). Few amounts of stratlingite were identified and residual anhydrous grains (CA, C_2AS and CT) were detected.

- Zone 2 was characterized by the decalcification of the matrix for CAC and CSA-based materials. The decalcification of the CAC paste was linked to the dissolution of the C_3AH_6 phase while for CSA-based materials it was linked to the dissolution of AFm phases. Ettringite was still identified in this zone, however, it was not possible to define if it was primary or secondary ettringite. Gypsum and bassanite was the two main forms of calcium sulfate identified in this zone. The aluminum content decreased about the half of the aluminum content in the sound zone for CAC and CSA materials
- In zone 3, the aluminum content in CAC material did not change and was linked to the formation of a deteriorated layer composed mainly of crystallized AH_3 (gibbsite). For CSA-based materials, the aluminum content continued to decrease, except for CSAA which slightly increased. However, the XRD patterns showed crystallized AH_3 (gibbsite) instead of the amorphous/poorly crystallized AH_3 present in the sound zone. The silicon content in CSAA significantly increased (up to 23%) with only C_2AS detected as crystallized phase. Since this zone was severely deteriorated in CSA materials, the chemical composition suggested the presence of an aluminosilicate gel.
- The outer zone for CSAA was detached during the preparation of the specimen for the analyses; therefore, the chemical and mineralogical analyses were not carried out in this zone. Precipitation of elemental sulfur (S^0) was identified for all materials. This zone was composed of mainly AH_3 for CAC and of AH_3 and potentially aluminosilicate gel for CSA materials.

5.3.4.AAS-based materials

The studied AAS-based materials were prepared in the laboratory and were subject to the same preparation protocol as the other cementitious binders, in particular the curing period. While the required curing time for optimized hydration processes was 3 months, only one month of curing was carried out for time-constraint reasons. Therefore, in this study, these materials were mainly used to evaluate the differences in the reactivity of their hydrated phases as well as the particularities of this type of material (high slag content, activation by alkalis, etc.). Moreover, mineral additives (bauxite and HardCem) were incorporated to increase aluminum and iron content respectively and to study the chemical aspect of their reactivity in such matrices.

Figure V-11 presents a summary of the evolution of the chemical and mineralogical composition profiles for AAS-based materials, based on the experimental analyses carried out

on specimens after 3 months of exposure to the BAC test. The experimental results (SEM observations, EDS and XRD analyses) are presented in **Appendix V-C**. The three AAS-based materials were:

- **AAS**: Slag
- **AASB**: Slag + bauxite
- **AASH**: Slag + HardCem

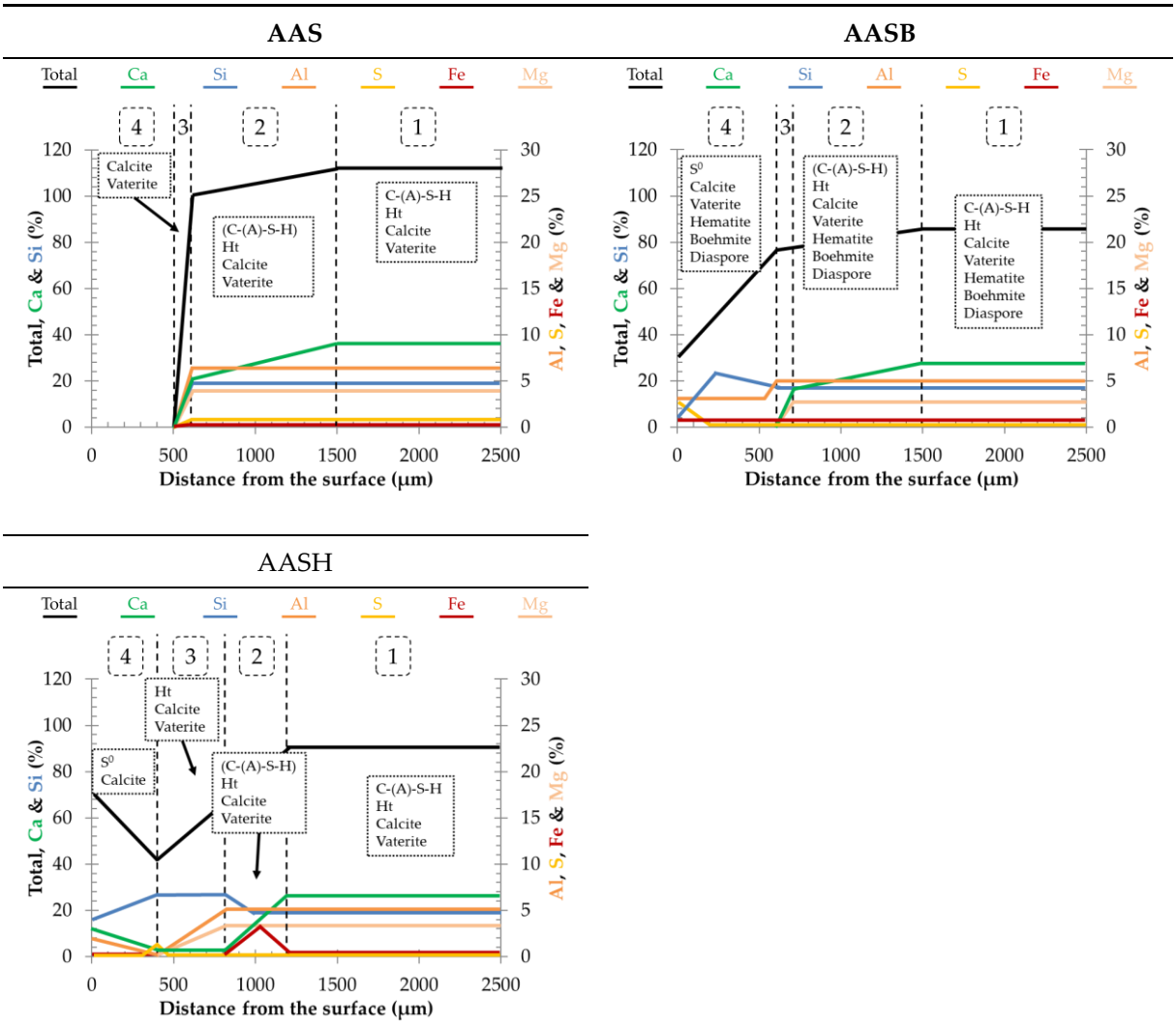

Figure V-11. Summary of the evolution of the chemical and mineralogical composition of AAS, AASB and AASH pastes exposed to the BAC test for 3 months as a function of the distance from the initial surface of the specimen (at 0 µm). Ht: hydrotalcite, S^0: elemental sulfur

Four altered zones were identified from the sound zone or the core of the material (zone 1) to the surface exposed directly to the biofilm (zone 4).

- The sound zone (zone 1) was very similar between the 3 AAS-based materials. C-S-H (tobermorite), Hydrotalcite, calcite and vaterite was the main crystallized phases identified in this zone and amorphous C-(A)-S-H was identified, as seen previously in section 2.2.3.5 of chapter II. However, while the addition of HardCem did not form any crystallized phases, the addition of bauxite showed the presence of ferric oxide (e.g.

hematite) and aluminum oxide-hydroxides (e.g. diaspore and boehmite). Although, these phases were linked to the anhydrous bauxite grains. Furthermore, the amount of iron was relatively low (< 1%) for all AAS-based pastes

- Zone 2 was characterized by a progressive decalcification of C-A-S-H for the 3 materials. In addition, AASH showed an increase in iron but without identifying any crystallized iron-bearing phases. This behavior could be correlated with the diffusion of iron from external zones (zones 3 and 4) and the precipitation of amorphous iron-bearing phases. The iron content for AAS and AASB, in this zone, remained unchanged.
- Zone 3 for AAS showed very severe deteriorations which led to the total dissolution of the cementitious matrix at the limit with zone 4. However, AASB and AASH presented a zone composed of silicon and aluminum with a residual amount hydrotalcite. The presence of silicon and aluminum was likely to indicate the formation of aluminosilicate gel, resulting from the dissolution of C-A-S-H. Moreover, the iron content remained very low for AASB and AASH (< 1%).
- The outer zone (zone 4) was completely dissolved for AAS while it was composed of aluminosilicate gel, elemental sulfur and calcite for AASB and AASH. Moreover, the crystallized phases of bauxite (hematite, boehmite and diaspore) were still detected in this zone.

Figure V-12 presents the SEM observations of the microstructure and chemical analyses of the outer deteriorated layer of AAS-based materials after 3 months of exposure to the BAC test. One should note that the outer layer of AASB and AASH was not dissolved while the outer layer for AAS was completely dissolved. Therefore, the chemical analyses were carried out in zone 4 for AASB and AASH and in zone 3 for AAS (identified in Figure V-11).

The density of the outer layer of AAS was very low compared to AASB and AASH. Anhydrous slag grains were identified in the deteriorated zone of AAS. The deteriorated paste of AASB and AASH was mainly composed of silicon and aluminum while the outer deteriorated paste of AAS still contained significant amount of calcium (~20 wt.%). In addition, the Al/Ca ratio in the deteriorated zone was slightly higher for AASB although the initial chemical composition (Figure II-19) showed that AASB and AASH exhibited very similar Al/Ca ratio in the hydrated sound paste. Moreover, the AAS material showed very strong decalcification of the matrix around the vertical cracks as shown in Figure V-13.

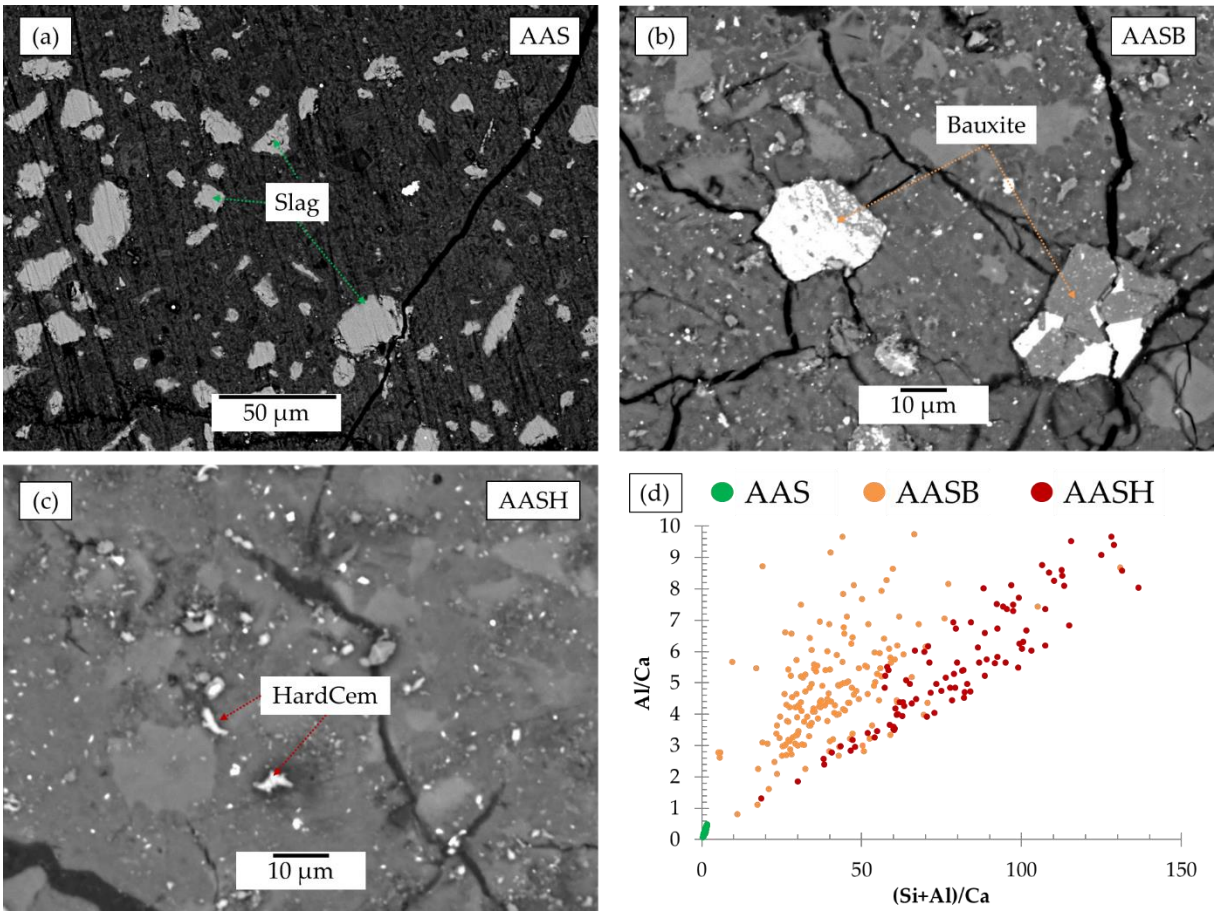

Figure V-12. SEM/EDS analyses of the outer layer of (a) AAS (b) AASB (c) AASH (d) EDS plot of Al/Ca versus (Si+Al)/Ca after 3 months of exposure to the BAC test

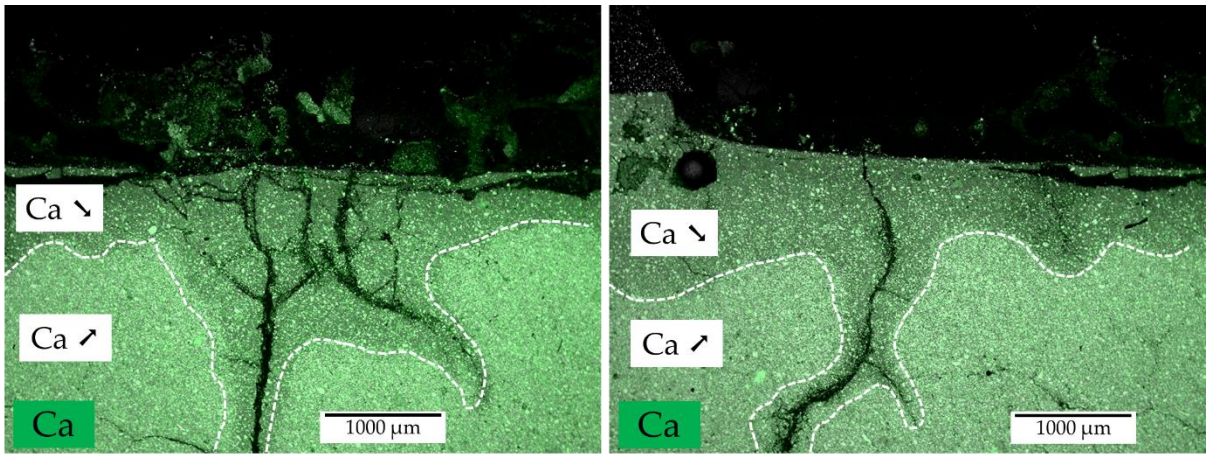

Figure V-13. Calcium mapping for AAS microstructural images showing the decalcification of the matrix around the vertical cracks

5.3.5. Impact of HardCem on the deterioration mechanisms of the binders exposed to biogenic acid attack

Microstructural and chemical analyses were carried out to highlight the impact of HardCem on the deterioration mechanisms of AASH after 3 months of exposure to the BAC test. Figure V-14 presents an SEM image coupled with EDS analyses for deteriorated and sound zones of

AASH. The deteriorated layer showed that iron was mainly found in the residual HardCem grains which were located in the lower part of the deteriorated layers (at the interface with the sound zone).

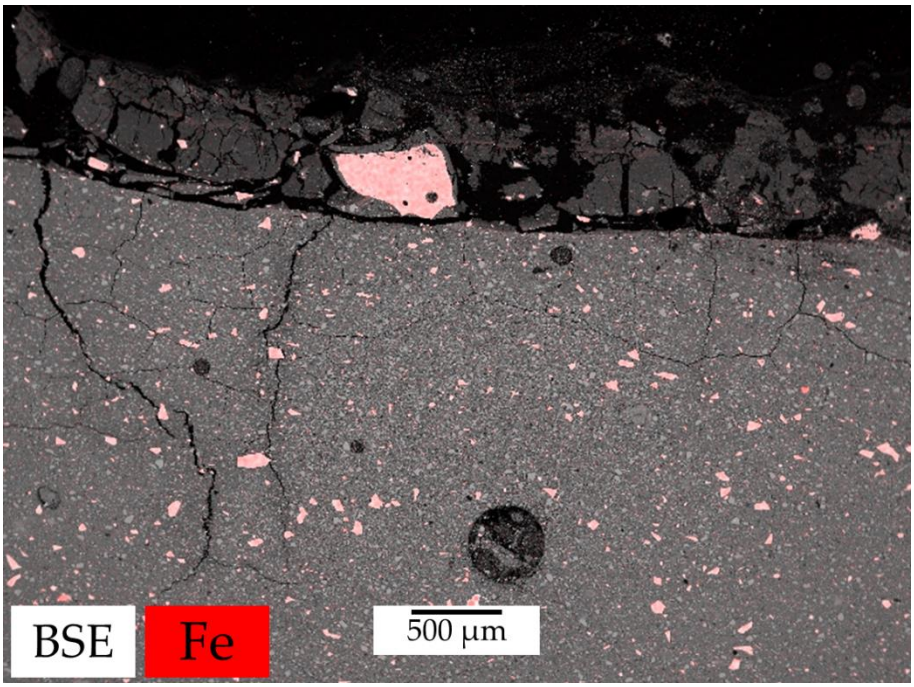

Figure V-14. SEM image and EDS analyses (for iron) for deteriorated and sound zones of AASH material

Figure V-15 presents Fe/Al as a function of Si/Al in the outer deteriorated zone observed by SEM analyses for AAS-based materials. The ratio of Fe/Al for AASH was lower than for AASB, which indicated that iron released from HardCem dissolution was leached from the matrix. Moreover, the ratio of Si/Al was higher for AASH than for AASB, which might be linked to the dissolution of HardCem grains that are rich in silicon.

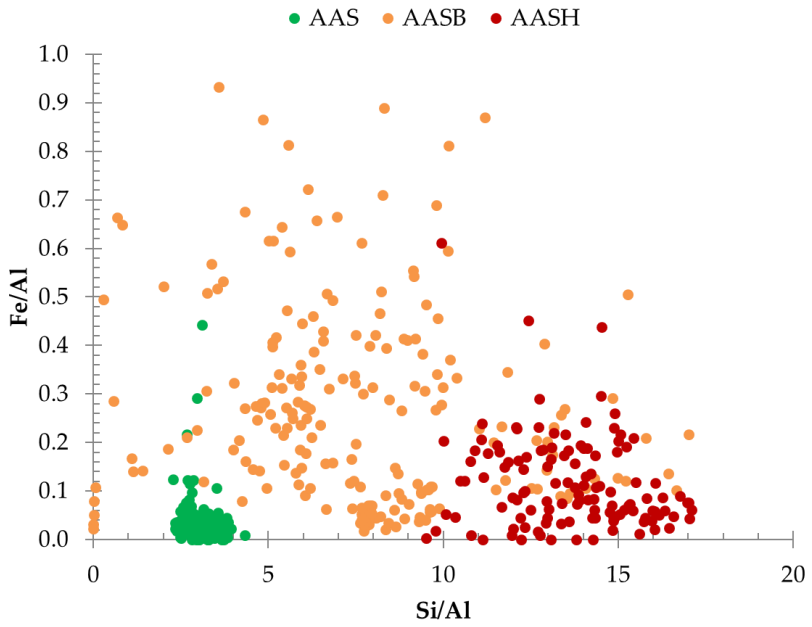

Figure V-15. Fe/Al ratio as a function of Si/Al of the outer deteriorated layer for AAS, AASB and AASH

Furthermore, the dissolution of HardCem grains seemed to alter the physical properties of the deteriorated layers in terms of porosity. In Figure V-16, the deteriorated layer of AASH appeared to form blocks of aluminosilicate gel and presented lots of voids in contrast with the deteriorated layer of AASB which appeared to form one deteriorated layer despite the heterogeneity within it in terms of the chemical composition (deteriorated paste, residual bauxite grains).

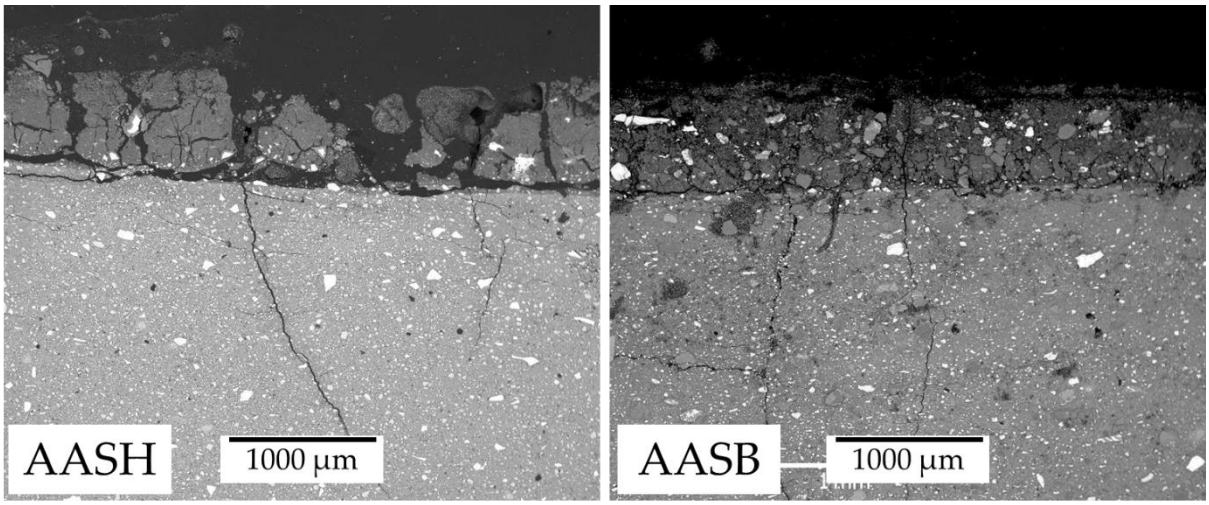

Figure V-16. BSE images of the microstructure of AASH and AASB showing the higher porous deteriorated layers of AASH

The reactivity of HardCem with sulfuric acid was investigated independently from the cementitious matrix. 5g of HardCem grains were introduced gradually into a hermetically sealed reactor containing 2 liters of sulfuric acid solution (0.17 M H_2SO_4) at pH 2.7 (Figure V-17). The pH of the solution was measured continuously and reported in Figure V-18. After the last addition of the 5g of HardCem, the solution was filtered and the precipitates were analyzed by XRD and compared to the XRD patterns of initial HardCem (Figure V-19). The method of exposing HardCem to chemical sulfuric acid is further detailed in **Appendix V-D**.

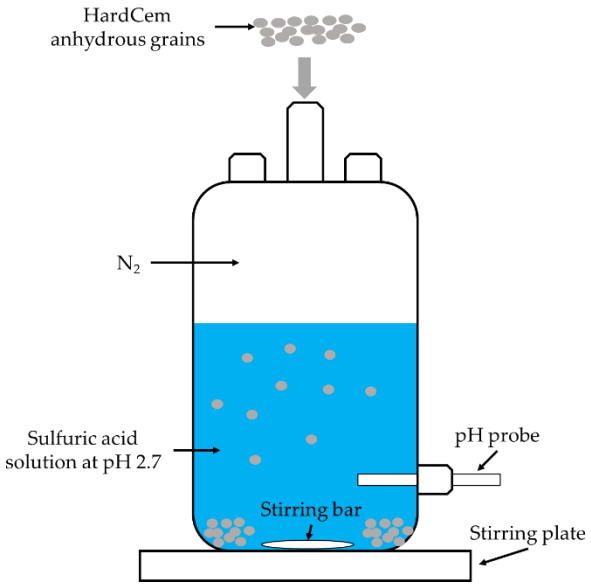

Figure V-17. Schematic representation of the different parts of the testing pilot

The results showed that a very rapid dissolution of HardCem occurred at pH lower than 5 and a slow dissolution occurred at pH higher than 5. The XRD patterns showed no significant transformation in the mineralogical forms of HardCem before and after exposure to sulfuric acid with the exception of the disappearance of quartz and the formation of silicon.

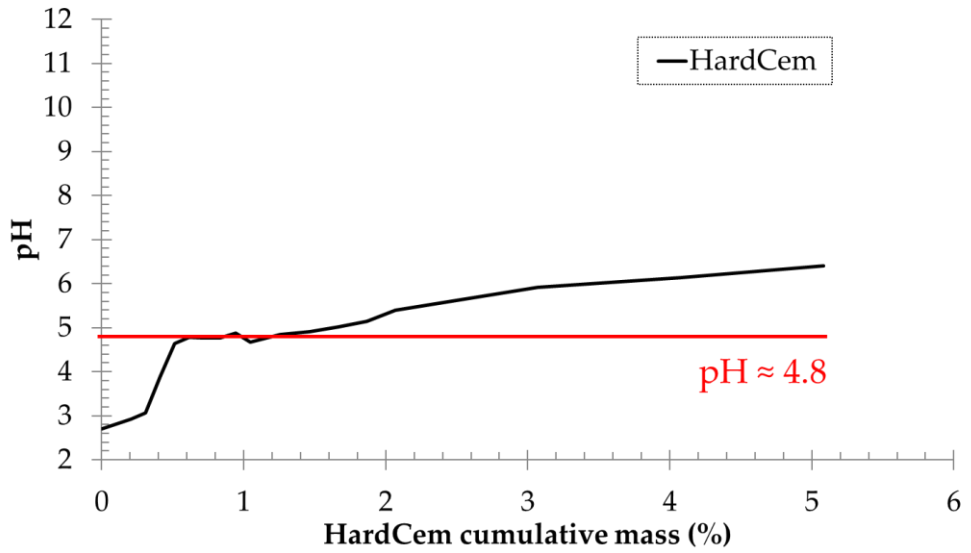

Figure V-18. Evolution of the pH of the solution as a function of the cumulative added mass of HardCem

FeO: Wustite (PDF 06-0615)
Q : Quartz (PDF 89-8934)
Si: Silicon (PDF 75-0589)

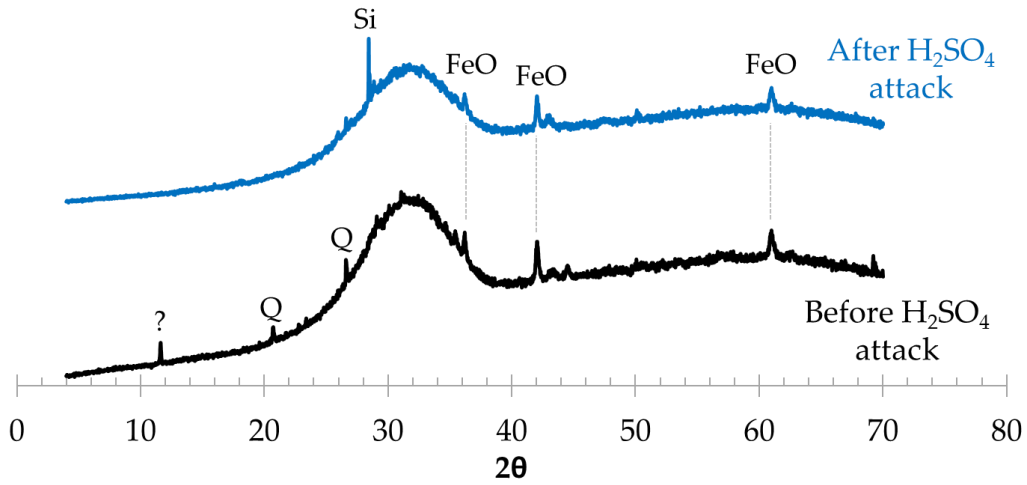

Figure V-19. XRD patterns before and after H_2SO_4 attack on HardCem

5.3.6. Impact of bauxite on the deterioration mechanisms of the binders exposed to biogenic acid attack

Figure V-20 shows the microstructural images of bauxite grains in the sound zone of the AASB material. The SEM observation (in BSE mode) allowed the identification of two groups of grains according to their gray level: high density (brighter) and lower density grains. Figure

V-21 presents the chemical composition corresponding to the numbered grains in Figure V-20. The high density grains were mainly composed of iron and the low density grains were mainly composed of aluminum.

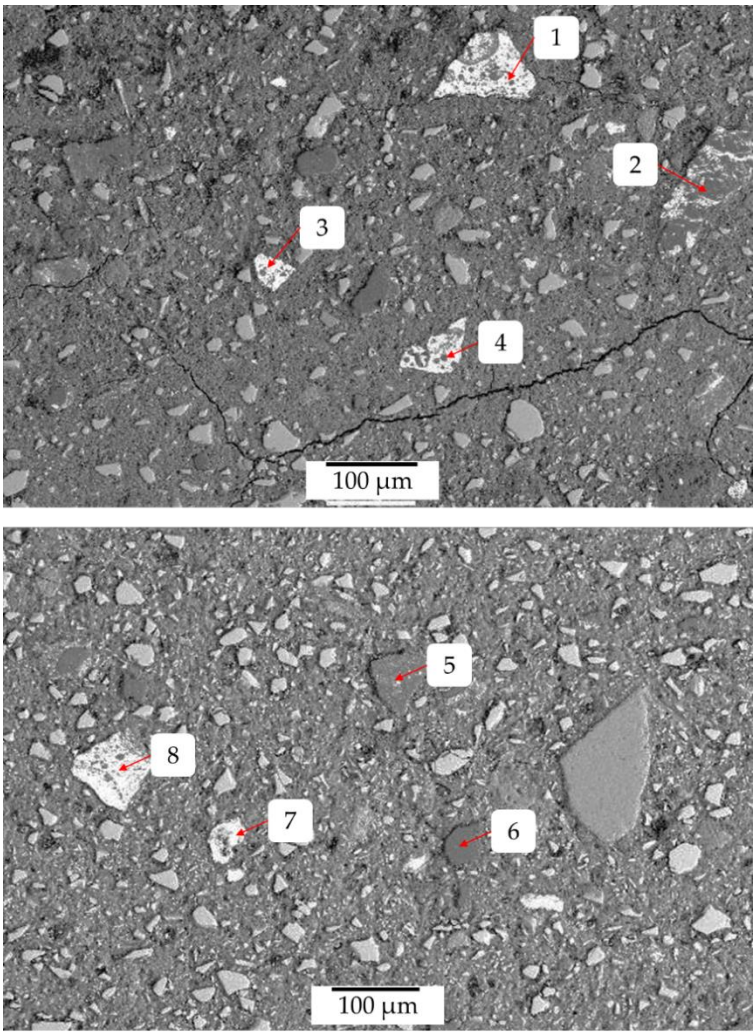

Figure V-20. Microstructural image showing bauxite grains in different sound zone of AASB material

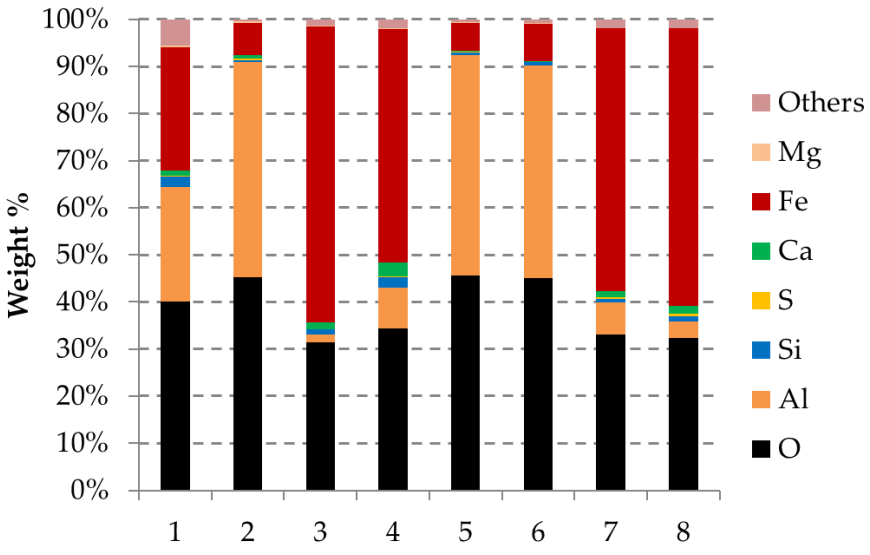

Figure V-21. Chemical composition of bauxite grains identified in Figure V-20 (standardized to 100%)

Figure V-22 presents microstructural images of bauxite grains in the deteriorated layers of AASB material (red circled for high density grains and orange circled for low density grains) and the EDS chemical analyses for aluminum and iron.

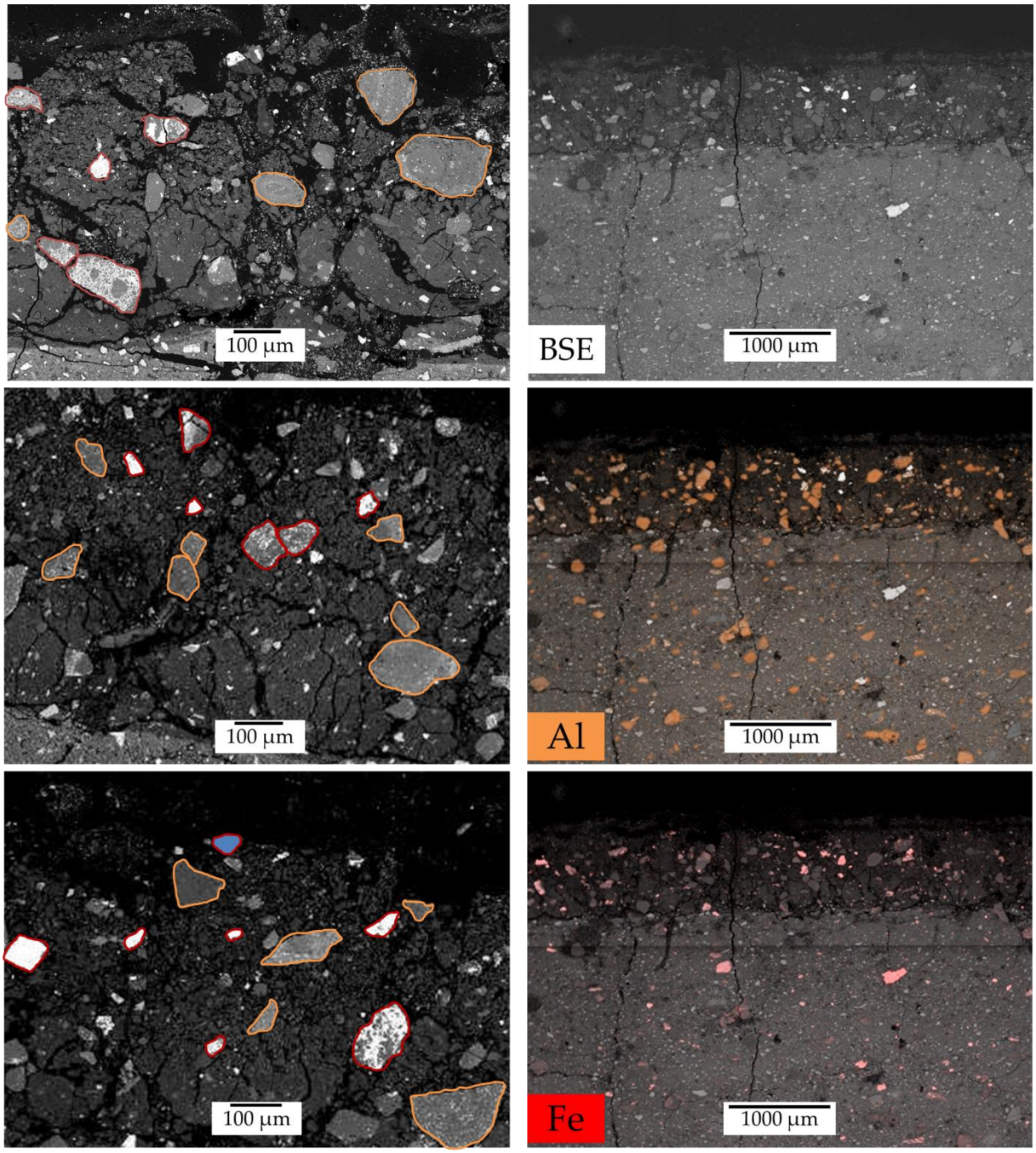

Figure V-22. LEFT: Microstructural image of residual grains in the deteriorated layer (zone 4) of AASB material; RIGHT: BSE image of the deterioration layer showing that the majority of bauxite grains were mainly composed of aluminum with only few and smaller grains containing iron.

The EDS elemental mapping showed that higher amounts of bauxite grains, identified in the deteriorated zones, were composed of aluminum compared to the amount of bauxite grains composed of iron. In addition, the overall size of the red circled bauxite grains seemed to be smaller compared to orange circled grains. This could suggest the progressive dissolution of

iron-based bauxite grains in the deteriorated zones in contrast with aluminum-based bauxite grains.

Figure V-23 shows that the chemical composition of bauxite grains did not change between the sound and the deteriorated zones. The high density grains were composed of iron and the low density grains were composed mainly of aluminum.

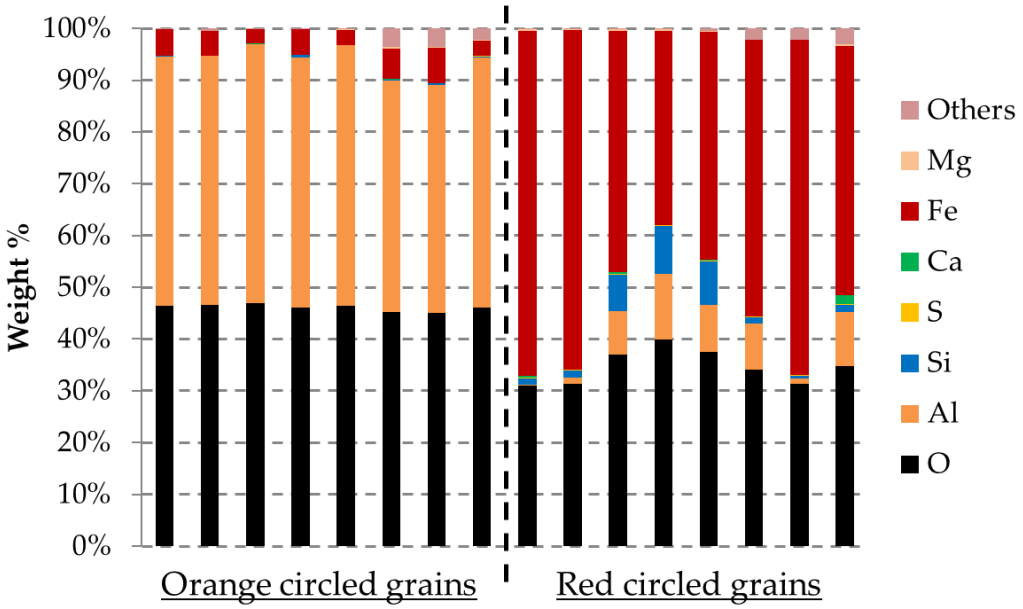

Figure V-23. Chemical composition of the bauxite grains in the deteriorated layers (standardized to 100%)

5.4. MICROBIAL DISTRIBUTION IN THE DETERIORATED LAYERS OF THE EXPOSED MATERIALS TO THE BAC TEST

In the literature, a recent study reported the presence of microbial activity, in particular *A. ferrooxidans*, at the interface between deteriorated zones and the sound core of a geopolymer-based concrete exposed in field to sewer conditions [48]. The presence of such bacteria in this zone was correlated to an accumulation of iron and, assuming anaerobic conditions considering the distance to the surface, ferric iron can be used by *A. ferrooxidans* to oxidize reduced sulfur species. The ferric iron is used as an electron acceptor and gets reduced into ferrous iron (Fe^{2+}). Thus, a possible production of sulfuric acid directly at the interface with the sound zone would accelerate the deterioration of the cementitious materials.

The results in chapter III showed the presence of *A. ferrooxidans* on the surface and in the deteriorated layers of CSAA, AASB and AASH. Moreover, the observations of the microstructure of AASB and AASH presented high amounts of cracks which suggested that bacteria might have penetrated inside the cementitious matrix through these cracks. Therefore, in the aim of investigating this phenomena, flat cross-sections of the deteriorated cementitious specimens were analyzed using optical microscopy coupled with a fluorescent nucleic acid stain to highlight in red the presence of bacteria (live or dead). Figure V-24 presents optical microscope and scanning electron microscope observations with the images indicating the

penetration depth of bacteria using the red fluorescence dye for AAS, AASB and AASH pastes after 3 months of exposure to the BAC test.

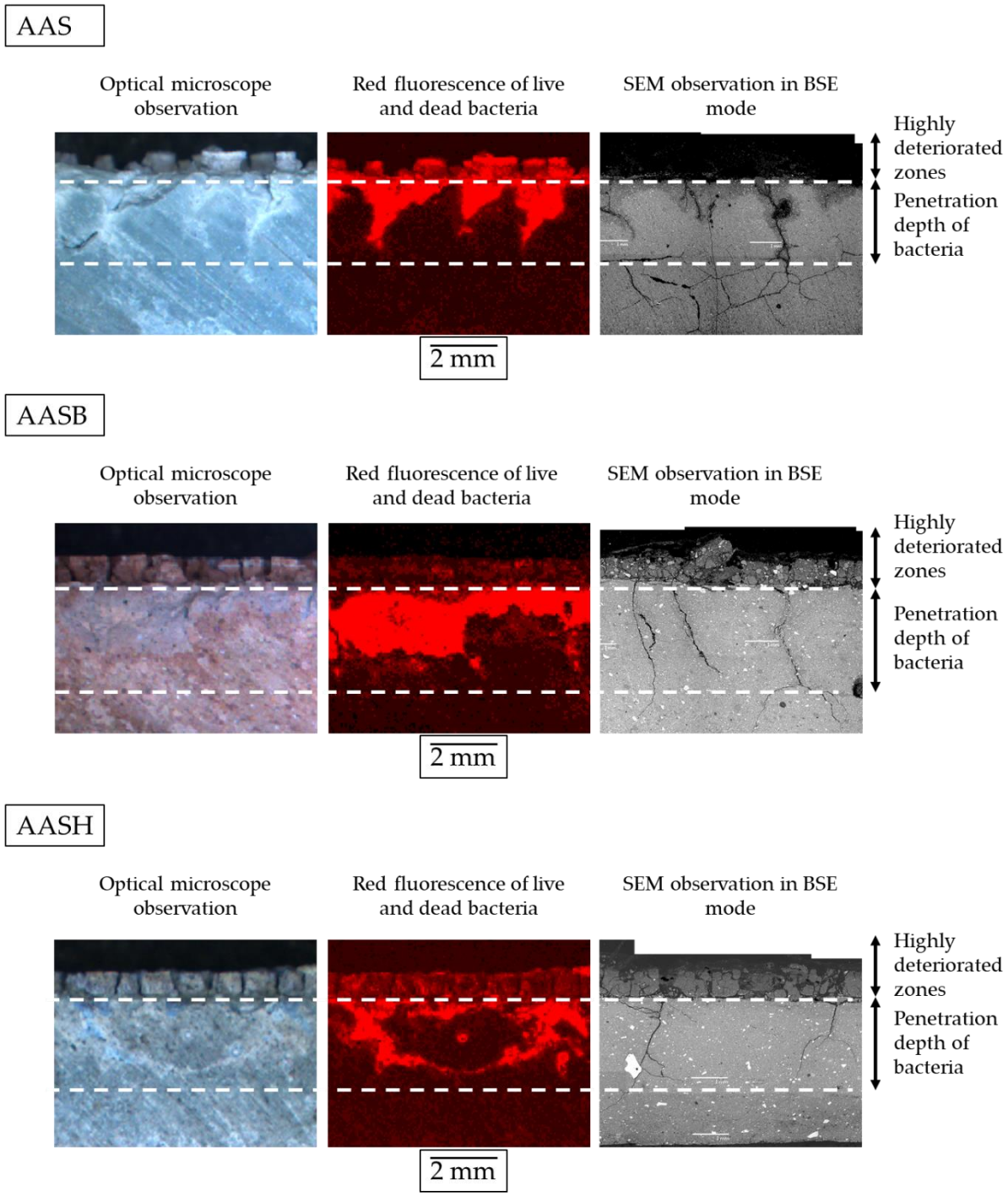

Figure V-24. Optical microscope and SEM observations showing the cracks in the cement paste which were correlated with the penetration of bacteria inside the cementitious matrix using the red fluorescence dye (for live and dead bacteria) for AAS, AASB and AASH pastes after exposure to the BAC test for 3 months

The results for AAS-based materials (AAS, AASB and AASH) showed that bacteria penetrated inside the cementitious matrix through the large vertical cracks, previously identified in Figure V-4. The microscopic observations as well as the chemical analyses showed that the cement pastes of AAS materials were severely deteriorated around these cracks. Bacteria were

detected on the surface and within the cementitious matrix for AAS while for AASB and AASH, bacteria were mainly identified inside the cementitious matrix (lower intensity of the red fluorescence in the highly deteriorated zones). The penetration of bacteria seemed to be carried out through the interconnected cracks with the exterior surface of the specimens. Furthermore, the presence of bacteria inside the cementitious matrix was linked to more severe deterioration than observed on specimens where bacteria was identified only on the surface (e.g. PC and PCH). The cement pastes in the vicinity of the cracks showed very low density than that of the sound paste, indicating the high decalcification of these zones. The presence of large cracks in alkali-activated materials exposed to sulfuric acid attack at low pH (≈2) was attributed to a shrinkage of the matrix following the release of aluminum ions [161]. As the deterioration progresses, these cracks become wide enough for aggressive agents to diffuse more easily into the material; thus resulting in secondary precipitations often expansive and harmful to cementitious materials. In addition, these cracks ease the leaching cementitious cations, such as calcium and aluminum; hence contributing to the acceleration of the deterioration of the material. This behavior might explain the lower performance indicator (PIeqOH) for AAS-based materials compared to other studied materials which did not present such cracks.

The precipitation of gypsum was systematically identified in these cracks [67,161,265]. While gypsum was often considered to create a protective layer against the diffusion of acid in the case of a chemical attack, such layer could create a suitable environment for bacterial growth [44]. Moreover, if the cracks were wide enough, bacteria could penetrate inside the matrix and produce sulfuric acid close to the sound paste. While the cracks were identified up to 2 cm (e.g. AAS), the highest penetration depth of bacteria within the cement paste was estimated at about 3 mm from the outer surface of the specimen. Although a study, which compared an attack of chemical and biological sulfuric acid, concluded that the presence of bacteria accelerate the attack by their presence only on the exposed surface [266], another study identified bacteria present in deteriorated areas of concrete exposed to natural conditions [48]. The results from this study came to confirm the possible penetration of bacteria inside the binder's matrix and the severe consequences of such penetration on the deterioration of the materials.

Figure V-25 presents the optical microscope observations and the presence of bacteria (red fluorescence) over the width (4 cm) of PC, PCH, AAS, AASB and AASH specimens. Although PC and PCH have both presented microcracks due to precipitation of ettringite near the exposed surface, the presence of bacteria was found to be only on the surface. The cracks, correlated with ettringite's precipitation, in PC and PCH were smaller and narrower than the cracks observed for AAS-based materials. Bacteria seemed to not get through these cracks and the acid production on PC and PCH was mainly produced on the surface.

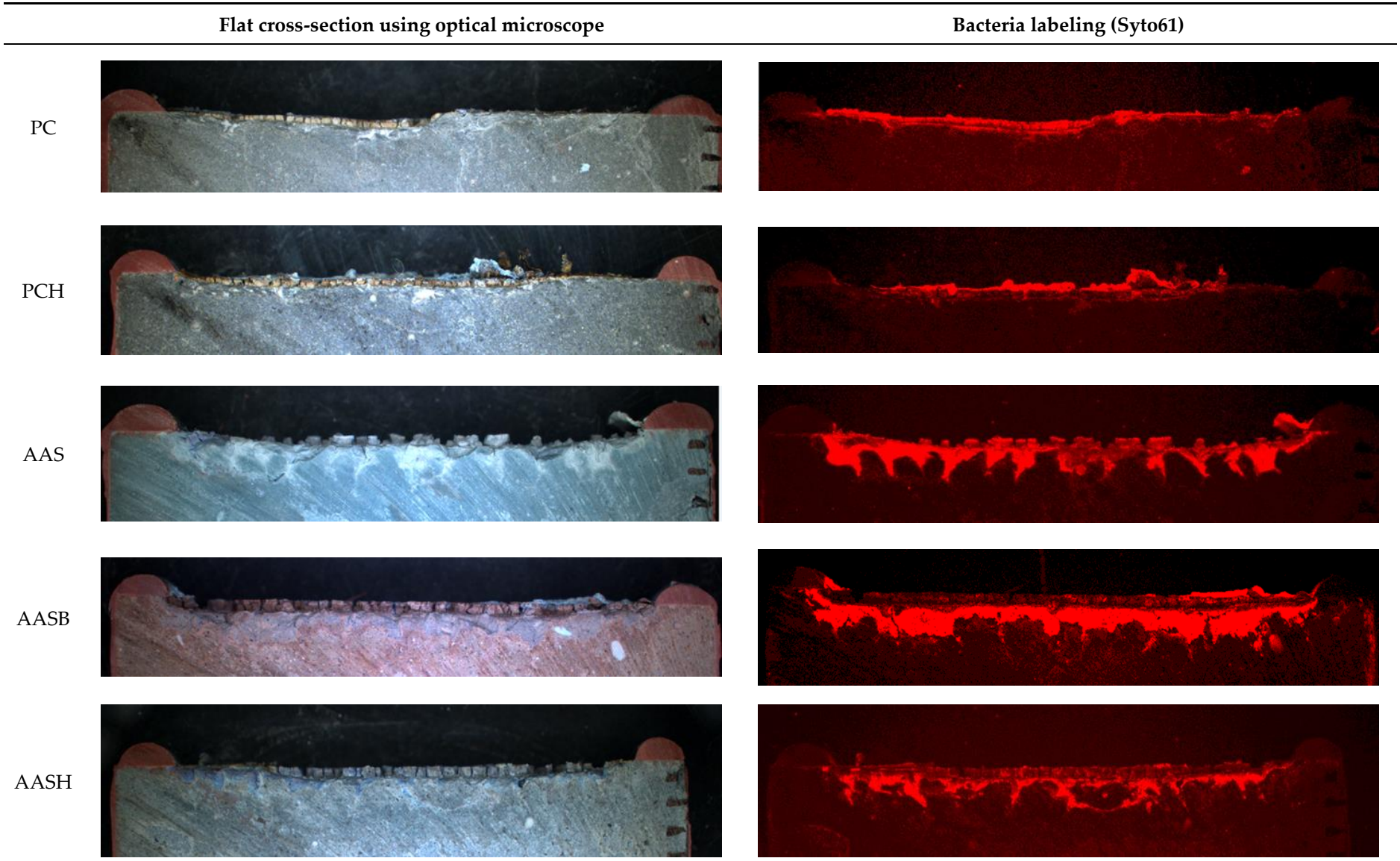

Figure V-25. Flat cross-sections of cement specimens and the labeling of the presence of bacteria (Live and Dead labeling) using Syto61

5.5. SUMMARY OF THE MICROSTRUCTURAL, CHEMICAL AND MINERALOGICAL MODIFICATIONS OF THE DIFFERENT CEMENTITIOUS MATRICES.

The four PC-based materials showed very similar behavior when exposed to biogenic sulfuric acid attack. The main deterioration mechanisms could be summed up in the severe decalcification of the matrix which led to the formation of a totally amorphous zone composed of silica gel. In addition, gypsum and secondary ettringite were identified in the deteriorated zones as products from the sulfate penetration inside the matrices. SR0 and SR3 materials showed the presence of C_4AF, which showed low reactivity with the acid, in the highly deteriorated zones [262].

CSA-based materials showed that monosulfoaluminate and primary ettringite were not stable in the conditions created by the biogenic attack. While the pH of the surface, generated by the sulfuric acid, was relatively low for ettringite and monosulfoaluminate to precipitate, gypsum and bassanite were detected as two mineralogical forms of calcium sulfate resulted from the sulfate penetration. These two phases were observed mainly closer to the surface compared to ettringite. Poorly crystallized gibbsite was identified in the highly deteriorated zones of all three tested CSA binders. The amount of AH_3 were relatively lower compared to CAC which showed a strong presence of gibbsite in the deteriorated zones. Residual anhydrous phases, C_2AS and C_4AF, were also detected in the deteriorated zones due to their low reactivity with the acid [74].

AAS-based materials showed completely different behavior compared to PC and CSA binders. Their microstructural exhibited high amounts of cracks connected to the external surface which facilitated not only the diffusion of sulfuric acid towards the inside of the matrix but also the leaching of the cementitious ions. Moreover, microbial activity was detected inside these cracks, indicating the presence of bacteria in deeper zones of the matrix and in contact with more sound zones. The main mechanism of deteriorated of such binders was the decalcification of the matrix. The release of calcium was often detected at the interface between the highly deteriorated zones, composed mainly of silica and aluminum, and the sound zone. The presence of unreacted slag might have contributed to the resistance of the material; however, its impact was insignificant compared to the severity of the attack. As the AAS-based materials were composed mainly of amorphous C-S-H and C-A-S-H, the modification of the mineralogical composition revealed only the presence of calcium carbonates, resulting from the reaction of leached calcium and CO_2 from the atmosphere. No gypsum nor ettringite were detected in the deteriorated zones.

The presence of bauxite modified the response of the matrix to the sulfuric acid attack. Instead of having a highly deteriorated zone with very low density, the external zone showed the presence of hydration products, such as hydrotalcite, and residual bauxite grains. Moreover,

the microstructure of such zone showed more matter compared to the external zone in plain AAS. Similarly, HardCem incorporation in the AAS matrix have modified the general aspect of the deteriorated zones. Highly deteriorated gel-like zones with slightly more cohesion were detected in the AASH. Residual anhydrous grains of HardCem were also identified in the deteriorated zones.

5.6. DISCUSSION

5.6.1. Correlation between the deteriorated depths and the performance indicator (PIeqOH)

The measurement of deteriorated depths highly depends on the location where the analyses were carried out. At the start of the test, activated sludge was installed evenly over the entire exposed surface of the cement samples. As discussed for Figure V-1, during the test, the development of the biofilm was not homogeneous on the surface, probably due to (i) the roughness of the exposed surface which was different from one material to another, and which could facilitate/complicate the attachment of bacteria on the surface; (ii) the preferential paths of the feeding solution containing the source of reduced sulfur necessary for the development of the biofilm.

For microstructural observations, the analyzed cross-sections were all cut in the same place, corresponding to half the length (8 cm) of the sample. This was arbitrarily chosen in order to avoid cutting out a highly deteriorated zone (upstream of the sample) where the droplets of the feeding solution fell. Two factors were to be considered for this zone; (i) the mechanical impact of the fall of the droplets could contribute to the deterioration of the matrix; (ii) the more favorable conditions for bacterial growth as the feeding solution, at this place, was very rich in reduced sulfur, allowing quicker development of the biofilm than on the rest of the surface of the materials. At the downstream of the specimens, although the biofilm was nearly developed on the whole surface of the sample and the microbial activity was present, the inclination of the specimens, in order to optimize the exposure time of the specimens to the feeding solution, could create stagnation conditions for the solution containing tetrathionate; thus, intensifying the attack at this location.

Table V-2 presents a summary of the maximum total deteriorated depths from microscopic observations by SEM and EDS analyses and the PIeqOH values (obtained in section 4.2.2 of chapter IV). For all materials, the deteriorated depths were measured from the initial surface preserved by the resin on both sides of the cross-sections (Figures Figure V-2, Figure V-3 and Figure V-4). The deteriorated depths consisted of the totally dissolved layer, the severely and mildly deteriorated zones identified in the previous section of results.

The PIeqOH were used to estimate equivalent deteriorated depths for all exposed materials by considering the deteriorated depth for PC (reference) material at 1 500 μm (equivalent to the deteriorated depth from experimental measurements). Table V-2 presents the results of the

estimated PIeqOH equivalent deteriorated depths and Figure V-26 shows a visual comparison of the experimental and estimated deteriorated depths.

Table V-2. Summary of the measured deteriorated depth, the relative deteriorated depth to PC material, the PIeqOH (from chapter IV) and the deteriorated depth per moles of acid per exposed surface.

	Experimental	Relative deteriorated depths / PC (%)	PIeqOH (%) (Chapter IV)	Estimated
	Total deteriorated depths (µm)			PIeqOH equivalent deteriorated depths (µm)
PC	1 500	100	100	1 500
CAC	800	188	233	644
PCH	1 100	136	84	1 786
SR0	1 100	136	95	1 579
SR3	1 150	130	90	1 667
CSAC	900	167	135	1 111
CSAA	1 100	136	89	1 685
CSAG	1 550	97	124	1 210
AAS	1 500	100	78	1 923
AASB	1 500	100	68	2 206
AASH	1 150	130	85	1 765

The performance indicators, presented in the previous chapter, showed that the resistance of CAC, CSAC and CSAG was higher than the reference material (PC) with CAC having the highest resistance (233%) followed by CSAC (135%) and CSAG (124%). While the experimental measurements showed lower deteriorated depths for these materials, it was not the case for the other materials. CSAA presented a lower deteriorated depth than that of PC material while it had a slightly lower PIeqOH. The deteriorated depths measured for PC-based materials (PCH, SR0 and SR3) was lower than that of the control material (PC) despite having lower performance indicators (PIeqOH). The same applies to materials based on alkali-activated slag (AAS, AASB and AASH) which had lower performance indicators than the control material but showed deteriorated depths similar to PC or even slightly lower in the case of AASH. Therefore, measuring the deteriorated depth alone is not a reliable indicator.

Finally, depending on where the cross-section was cut (as shown in Figure V-2, Figure V-3 and Figure V-4), in particular for PC materials, more or less deteriorated areas could be observed. Therefore, evaluating the performance of materials by only observing the deterioration depths should not be carried out. The approach of using the analyses of the leached solutions to evaluate the reactivity of the phases exposed to the acid presented a better indicator for the resistance of cementitious materials.

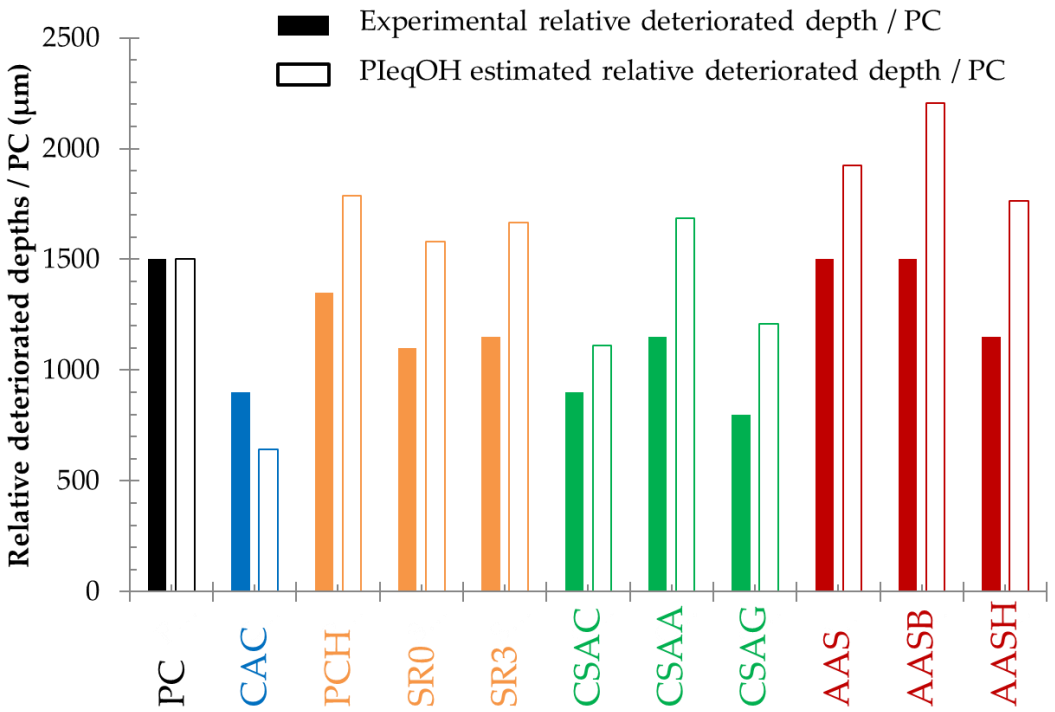

Figure V-26. Comparison between the experimentally measured relative maximum deteriorated depths of the exposed materials to PC material (%) and the estimated relative deteriorated depths from PIeqOH measurements, previously evaluated in chapter IV

5.6.2. Influence of aluminum on the alteration mechanisms of the cement matrix

In the literature, CAC-based materials have a good durability in sewer networks (H_2S environments) [44,49,64,68]. Our previous study, carried out in laboratory conditions, showed that aluminum content is not the only parameter but the nature of the hydrated phases, such as C_3AH_6 and AH_3, plays a key role in improving the resistance of the materials [67]. In this context, the study of the influence of aluminum concentration on the deterioration mechanisms of cement-based materials in sewer conditions was carried out by considering two types of materials: (i) matrices initially rich in aluminum, such as calcium aluminate and calcium sulfoaluminate cements with different amounts of aluminum oxide; (ii) cement matrices (AAS-based materials) with mineral additives rich in aluminum (Bauxite)

The results in the previous chapter showed that CAC, CSAC and CSAG materials had a higher performance indicator compared to PC. Moreover, despite using the same clinker for all CSA materials and changing only the nature of the added calcium sulfate, CSAA (CSA with anhydrite) showed lower performance than CSAC (CSA clinker) and CSAG (CSA with gypsum). The standardization of the amount of leached aluminum by the initial content in the different binders showed that the aluminum from CSA was more mobile compared to CAC. This behavior could be linked to the accessibility, the availability and the stability of the reactive phases in the CSA matrix. Finally, the impact of bauxite was not significant as AAS and AASB showed exactly the same behavior in terms of kinetics and total cumulative

amounts of aluminum leached. The general analyses of the microstructure suggested very low participation of bauxite to the deterioration mechanisms.

5.6.2.1. Aluminum concentration

Matrices with highly initial reactive aluminum-bearing phases showed mainly a good performance in sewer conditions compared to PC materials. The external deteriorated zones of CAC and CSA materials were made of an alumina and aluminosilicate gel-like layer, respectively. AH_3 was the main identified aluminum phase in the deteriorated zones in these materials. Moreover, the AH_3 rich zone was reported to influence the kinetics of the attack by slowing down the diffusion of the acid due to its relatively denser microstructure [44,267]. Thus, increasing reactive aluminum-bearing phases to form AH_3 would be beneficial in terms of resistance against biogenic sulfuric acid attack.

However, the simple increase of aluminum content by incorporating non-reactive mineral additives (bauxite) did not improve the chemical resistance of the binder since bauxite did not react with the matrix of the alkali-activated material. Despite the initial difference in aluminum oxide content between AAS and AASB (9.83 and 18.04% respectively), total cumulative aluminum leaching curves showed that both materials released the same amount of aluminum. These results highlighted the non-implication of bauxite in the physico-chemical resistance of the binder.

5.6.2.2. The differences in the AH_3 between CAC and CSA

The aluminum hydroxide (AH_3) phase, both as the original hydrate and as the newly formed phase during the attack, is known in the literature to be one of the key factors explaining the better resistance of calcium aluminous cements (CAC) compared to Portland cement in sewer conditions [20,44,49,64,67,68]. The hydration of CAC and CSA resulted in the formation of AH_3 in different quantity and different natures. Gibbsite and bayerite were identified as the main forms in CAC while CSA-based matrices often produce amorphous AH_3 [76,84,180,182,188,268]. Different mineralogical natures of AH_3 were reported in the literature as a function of the pH. In alkaline conditions, bayerite was more prone to precipitate while gibbsite is more favorable to form in acidic conditions [269]. Nordstrandite was also identified as the main form of AH_3 in neutral conditions [270]. In addition, the formation of bayerite and gibbsite was observed in a medium with neutral pH with the transformation of gibbsite into bayerite with the aging of the material [269].

The biogenic sulfuric acid attack created acidic conditions on the surface of the cementitious materials. In such conditions, gibbsite was the only AH_3-type identified on the surface of the CAC material. The disappearance of bayerite was consistent with the literature as the pH of the surface was be relatively low considering the amount of acid produced on the surface and the dissolution of C_3AH_6 phases [12]. On the other hand, the nature of AH_3 in CSA materials was quite different. First of all, the chemical and mineralogical analyses have showed little

presence of aluminum hydroxide in the deteriorated zones of CSA-based materials. Moreover, the broad and very weak peaks of gibbsite indicated a very poor crystal structure of gibbsite on the surface of the materials [76,81,179,188,271,272].

Furthermore, the solubility of the different mineralogical forms of aluminum hydroxide (amorphous and crystalline) was evaluated in the literature [273]. For instance, while the results from Cemdata18 database showed that the three types of AH_3, amorphous, microcrystalline and gibbsite, have the same chemical composition and the same dissolution equation, they did not have the same dissolution constants. Amorphous AH_3 (0.24) had the highest solubility followed by AH_3 microcrystalline (-0.67) and gibbsite (-1.12)

The thermogravimetric analyses, presented in Figure V-27, carried out on the deteriorated zones of CAC and CSA materials showed that the intensity of the peak at 270°C was higher for CAC than for the CSA-based materials, indicating the formation of higher amounts of AH_3 in the deteriorated zone of CAC.

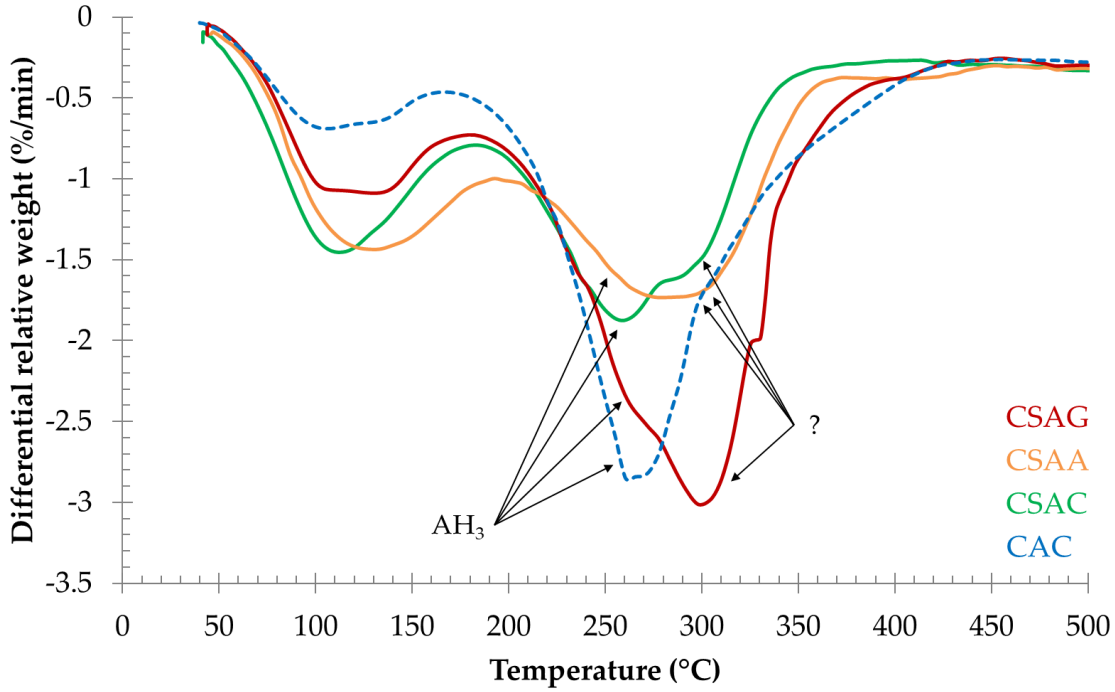

Figure V-27. DTG curves of the deteriorated zone for CAC, CSAC, CSAA and CSAG

A second peak was detected at around 300°C for all four materials. Several studies attributed this peak to monosulfoaluminate phases, however, it is highly unlikely to have such phase in the deteriorated zone exposed to very acidic conditions [274]. However, other studies showed a weight loss for gibbsite exhibiting nanostructures at around 310°C [275–277]. While the formation of nanocrystalline gibbsite is more favorable with the conditions of exposure of the BAC test, it was not detected using the XRD analyses. The collection of samples from deteriorated zones was carried out by gently scratching the surface of the materials. Therefore, it is possible that monosulfoaluminate (or C_3AH_6 in the case of CAC) was present in the analyzed samples and that it was collected from deeper less deteriorated zones.

CSAG showed higher resistance than CSAA which could be linked to the presence of higher amounts of AH_3 phase (peak of thermograms at 270°C) in the deteriorated zone for the former compared to the latter. CSAC material showed the highest resistance of all CSA materials while it exhibited the highest quantity of AH_3 in the hydrated paste (Figure II-18). However, the amount of AH_3 in the deteriorated layer of CSAC seemed to be lower than that of CSAG. Both materials had the same mineralogical form of AH_3 in the hydrated paste (amorphous and/or poorly crystallized, Figure II-17) and in the deteriorated layers (Figure V-B-2 and Figure V-B-6), it seemed that the initial amount of AH_3 could have an important influence on the resistance of the material to the acid attack and/or that AFm phases (monosulfoaluminate and monocarboaluminate) could positively improve the durability of the materials. However, these hypotheses need further investigation, in particular for comparing the deterioration mechanisms of ettringite and AFm phases.

In conclusion, the mineralogical form and the quantity of AH_3 phase in the hydrated matrix could play an important role in the resistance of cementitious binders to biogenic sulfuric acid attack. The lower resistance of CSA-based materials might be linked to the lower initial amount of AH_3 and to the higher solubility of the amorphous AH_3. Moreover, the dissolution of ettringite and monosulfoaluminate did not seem to produce as much aluminum hydroxide as it is the case for C_3AH_6 in CAC matrix [12,64,68].

5.6.3.The behavior of iron during the biodeterioration attack and its impact on the resistance of the materials

The study of the potential influence of iron consisted of studying 2 different ways in which iron might be involved in the deterioration process. The first by using cements with higher quantities of C_4AF than the reference cement, sulfate-resisting cements SR0 and SR3 containing lower quantities of C_3A, 0 or 3% maximum respectively, and higher quantity of C_4AF. The second by adding a mineral product rich in iron to the mixture. The mineralogical form of the iron-containing phases was predominantly amorphous. The purpose of this mixture was to incorporate iron into the hydrated phases of Portland cement thus aiming to increase their resistance.

For all PC-based materials, decalcification of the matrix was the main identified mechanism of deterioration as a response to the severe microbial attack. As seen on the chemical profiles, the decalcification was carried out progressively in the different deteriorated zones. The decalcification of PC binders concerned mainly portlandite and C-S-H phases. However, not all the calcium was leached out of the matrix as secondary phases, such as gypsum and calcite, precipitated as a result from the reaction of the mobile calcium with exogenous sulfate and carbonate respectively. Furthermore, like the PC material, all three PC-based materials showed cracks in inner zones where secondary precipitation of ettringite was identified by SEM/EDS and analyzed by XRD. This is in accordance with the literature [110,263,265,278]. The outer layer of the exposed surface was composed mainly of silica gel following the total

decalcification of C-S-H. Similar behavior has been reported in the literature on field and laboratory studies carried out on Portland cement-based materials [20,49,67,94,230,245,279–281].

The chemical composition profiles of the specimens showed different deterioration patterns between AAS and AASH. The response of the matrix of AASH was different from AAS despite having similar results in terms of the performance indicator (presented in chapter IV). The outer layer was not completely dissolved and was composed of silicon and aluminum. In addition, the dissolution of HardCem due to the acid attack might have enriched the outer layer with additional silicon released from its grains.

The incorporation of HardCem was tested to evaluate its potential positive influence on the resistance of the materials to the biogenic acid attack. The absence of the hydration phenomena of HardCem particles led to the entrapment of the iron inside the anhydrous grains. Furthermore, the results from the previous chapter showed that PCH and AASH materials presented 4 to 5 times higher cumulative concentrations of iron in the leached solutions compared to PC and AAS respectively when the pH of the leached solution decreased below 5. However, the release of such high amounts of iron did not favor the development of specific types of bacteria (in particular, *Acidithiobacillus Ferrooxidans*).

The proposed attack mechanism is that the acid firstly attacks the hydrated paste all around the anhydrous grains and then attacks the HardCem by dissolution mechanisms. The dissolution of HardCem grains, that are relatively larger than conventional cement anhydrous grains, created a lot of porosity, thus facilitating and accelerating the diffusion of acid towards the inside of the material. Iron was expected to migrate into the material and precipitate in zones where the pH is relatively high, as has been seen in the literature [48]. However, this phenomenon was not observed neither for PCH (20 wt.% HC) nor AASH (10 wt.% HC).

SR0 and SR3 materials had very similar behavior to each other which came in accordance with the results obtained from the performance indicator in the previous chapter. Like PCH, iron was not incorporated into the hydrated paste but rather stayed in the form of C_4AF (section 2.2.3.3 of chapter II). Studies have shown that the reactivity of C_4AF is considerably slow comparing to the other clinker phases during the cement hydration process [282]. Thus, increasing the C_4AF content could have led to slowing down the formation of calcium aluminate or calcium-ferro-aluminate phases (ettringite, AFm phases) and favoring the formation of calcium silicate phases (CH, C-S-H). In addition, due to the low reactivity of C_4AF, iron was not as available as calcium and aluminum in the pore solution [62]. Ettringite and monosulfoaluminate are more susceptible to precipitate than iron-bearing hydrated phases (e.g. Fe-ettringite, Fe-monosulfoaluminate, C_3FH_6, etc.). The non-detection of iron-based ettringite and AFm phases indicated either (i) the mobility of iron was very low resulting in formation of insufficient amount of these phases to be detected; or (ii) the amount of iron was very low in the pore solution to reach the oversaturation of these phases.

5.6.4. Reactivity of HardCem and its contribution to the resistance of the binder to acid attack

While HardCem additive did not participate in the hydration process of the cementitious binders, it reacted with sulfuric acid in acid conditions. The chemical and mineralogical analyses did not show any particular phases rich in iron formed during the hydration for PCH (chapter II, section 2.2.3.3) and for AASH (chapter II, section 2.2.3.5). Moreover, the Ca/Si ratio of C-S-H did not change with the incorporation of HardCem in the matrix. The portlandite content seemed to be lower in the material containing HardCem which could be due to the filler effect of HardCem grains limiting available nucleus locations for precipitation of high portlandite amounts.

The reactivity of HardCem was linked to the pH of the medium. During the acidification of the surface of the exposed materials, materials containing HardCem showed release of iron starting from pH 6 whilst the other materials started to release iron around pH 4 (Figure IV-5). The HardCem, containing high iron content in the form of mainly amorphous iron-bearing phases, presented a lower stability in acidic environments compared to C_4AF which was the main iron-bearing phase in the tested materials. Furthermore, with the absence of detected iron-bearing phases in deteriorated layers of PCH and AASH, it was assumed that the HardCem was dissolved and the iron was totally leached from the cementitious matrix. Such dissolution could have a negative impact on the deterioration of the material by creating porosity and allowing the acid to penetrate the deteriorated zone more easily.

From another point of view, the dissolution of the iron-containing phases also contributes to the increase in the acid neutralizing capacity. During the dissolution of these phases, OH^- ions are released and react with the acid causing pH buffering. By comparing HardCem to calcium-bearing phases (such as CH), HardCem (and ferrous phases in general) could have a positive impact since they have a higher chemical stability to acid attack going down to pH of the order of 5.

5.6.5. Reactivity of bauxite and its contribution to the resistance of the binder to acid attack

The chemical composition profiles showed different evolution in the deteriorated zones between AAS and AASB despite having similar results in terms of performance indicator (presented in section 4.2.2 of chapter IV). The addition of bauxite (at 10 wt.% of slag) influenced the evolution of the matrix (the outer part of AAS was completely dissolved while it was composed of aluminosilicate gel for AASB and the presence of partially deteriorated bauxite grains in the deteriorated zones); however, this influence could be due to its high aluminum content, its neutralization capacity, its reactivity with acid or to a physical effect (granular arrangement and compactness of the mixture) influencing the transfer properties.

The bauxite did not seem to show any significant participation in the hydration process. The anhydrous phases of bauxite were mainly found in the XRD patterns of hydrated paste. The very low reactivity of bauxite (see chapter II, section 2.2.3.5) indicated that the aluminum added to the material was therefore not mobilized to form additional aluminum-bearing hydrates, in particular AH_3.

Unlike CAC and CSA-based materials, at alkaline pH AASB material, like AAS, did not release aluminum and the dissolution of bauxite appeared to occur in acidic conditions. These observations are consistent with several studies in the literature aimed at assessing the leaching of metal oxides from bauxite [251–254,283]. The process of refining bauxite to produce alumina is called Bayer process. In this process, the dissolution of bauxite in alkaline conditions is carried out by heating the bauxite along with sodium hydroxide at a high temperature (100-250°C) and a high pressure ranging between 1-6 atm [284]. Such conditions are totally different from the conditions of the BAC test which explains the absence of aluminum in the leached solutions at high pH. Even in acidic conditions, bauxite leaching requires high temperature < 60 ° C [254,283]. Furthermore, one study showed that the release of aluminum from bauxite was lower than the release of calcium and iron at different acid concentrations (1-5 M of HCl) [254]. Another study, focused mainly on aluminum leaching from calcined kaolinite using sulfuric acid, showed that the appropriate temperature tange for a high degree of reactivity of kaolinite with acid was 80-95°C [251]. At a lower temperature (60°C), the reactivity degree of the kaolinite was estimated at around 20%, emphasizing the significant role of high temperatures in aluminum leaching from such materials.

The analyses of the sound zone of AASB showed bauxite exhibited either high amounts of iron or high amounts of aluminum in its grains. The chemical analyses of the deteriorated layers of AASB showed that mainly the aluminum-based bauxite grains were present while very few quantities of iron-based bauxite grains were identified. In addition to the higher chemical stability of aluminum-based phases (such as AH_3) to acid attack compared to iron-based phases [Ref], it seemed that Fe-based grains of bauxite progressively dissolved when the pH became acid while the Al-based grains resisted to this attack. This hypothesis was in agreement with the study showing the release of more iron compared to aluminum when bauxite was exposed to hydrochloric acid [254].

Moreover, at the surface of the specimens, very local conditions could have led to a partial dissolution of bauxite grains, leading to its participation in acid neutralization phenomena. The contribution to the buffer effect by bauxite could slightly decrease the amount of acid seen by the hydrated matrix itself; hence, explaining the differences in the profiles between AAS and AASB.

In conclusion, the impact of incorporating bauxite inside the cement-based materials could be summed up into four points: (i) the chemical resistance of the material was not improved; (ii) bauxite, which could be considered as very low reactive material to acid attack, could potentially have an influence on the transfer properties; (iii) the addition of bauxite increased

indeed the total aluminum content in the binder, however, not all the aluminum was available during neither the hydration nor the acid attack; (iv) the presence of bauxite, rich in iron, resulted in the selection of *Acidithiobacillus Ferrooxidans*.

5.6.6. The resistance of calcium sulfoaluminate materials to biogenic sulfuric acid attack

5.6.6.1. Influence of the nature of phases in the system $CaO-Al_2O_3-SO_3$ on the durability of the materials

The presence of ettringite or monosulfoaluminate (or both at the same time) did not seem to be the factor controlling the resistance of CSA-based materials. The results from the previous chapter on materials' resistance indicated an improvement in performance for a CSA-binder without ettringite and another CSA-binder composed mainly of ettringite with lower amounts of monosulfoaluminate.

Such phases are reported to have a poor resistance to acid attack as monosulfoaluminate is stable at pH > 11.6 and ettringite is stable at pH > 10.6 [80]. The environmental conditions in sewers expose the materials to pH much lower than the pH stability limits of these phases. Thus, increasing ettringite content in the material would not necessarily going to improve the durability of the materials as it is the case for sulfate attack [89,231].

Producing ettringite in early stages of the hydration (before hardening of the material) has two advantages in the case of a sulfate attack: (i) aluminum is already bound to sulfate-rich phases; thus not available to form secondary ettringite [85]; (ii) the production of high-volume phases in early ages of the hydration allows to have room for delayed ettringite formation, hence, lowering the impact of the internal stress and minimizing the possible microcracks [74,76]. However, in the case of no addition of calcium sulfate and monosulfoaluminate was formed instead of ettringite, the material might be susceptible to secondary expansive precipitation of ettringite, leading to expansion and cracking of the material [285]. In the BAC test conditions, the deterioration process was mainly controlled by the reactivity of the phases leading to decreasing the impact of diffusion properties [67]. Hence, low amount of secondary expansive products was detected.

5.6.6.2. Calcium sulfate impact on the chemical resistance of the binder

The nature of the added calcium sulfate had an influence on the hydration products of CSAA and CSAG materials (Figure II-15 and Figure II-17). The consumption of gypsum during hydration seemed higher than anhydrite's consumption, indicating a better and faster reactivity of the former [181]. In addition, the higher solubility of gypsum compared to anhydrite favored the formation of higher ettringite content, in particular in the first hours of hydration [250,286]. In contrast, the slower dissolution of anhydrite gave time for ye'elimite to react with firstly water and form monosulfoaluminate [184].

The presence of both ettringite and monosulfoaluminate in CSAA and CSAG materials indicated that the ratio of ye'elimite and calcium sulfate was at least equal to 0.5 [81]. Moreover, during the hydration, the accessibility to calcium sulfate source (gypsum or anhydrite) decreases with the formation of hydrated paste which could result in the transformation of monosulfoaluminate into ettringite and aluminum hydroxide [79,81,287].

Furthermore, the CSA materials seemed to be exposed to carbonation, as calcite was often detected in the XRD patterns. The lower S/Ca ratio also indicated the formation of monocarboaluminate, resulting from the transformation of monosulfoaluminate into monocarboaluminate as a result of the exchange of SO_4^{2-} with CO_3^{2-} [185].

The literature reported that introducing calcium sulfate into the system should accelerate the reactivity of ye'elimite, however, in both systems with calcium sulfate (CSAA and CSAG), ye'elimite was not completely consumed as it was the case in the system without calcium sulfate (CSAC) [77]. It seemed that water deficiency was the reason behind this behavior. CSA systems have a high chemical water demand, estimated with a water to binder ratio between 0.45-0.50, depending on the assumptions made for their hydration [248]. The water to binder ratio used in this study was 0.40, which created a water deficiency leading to lower hydration effectiveness and, if possible, the cease completely of the hydration process. Although, the difference between CSAA and CSAG in terms of ye'elimite consumption could be linked to the amount of ettringite. As ettringite consumes big quantity of free water, the rapid formation of high amounts of ettringite in CSAG might have led to the decrease of water available for hydration.

5.6.7. Durability of alkali-activated slag in sewer-like environment

The mineralogical phases of AAS-based materials seemed to be very unstable under the exposure conditions. A significant release of cementitious cations (calcium in particular) was observed with the drop in pH from alkaline to acidic conditions. The partial substitution of silicon by aluminum in the structure of C-S-H led to the formation of C-A-S-H, which was identified as the main phase of this system. The Ca/Si ratio in C-A-S-H resulting from the hydration of slag was of the order of 1.88, which remained relatively high compared to the values in the literature, generally around 1.1-1.2 [62]. The fact that there was more silicon in C-A-S-H also made the Al/Ca ratio relatively low at 0.16.

Generally, alkali-activated slag materials suffer from volume instability due to shrinkage phenomena (drying and/or autogenous). Since AAS specimens were sealed immediately after being demolded, i.e. 24 hours after casting, the drying shrinkage was very limited. However, with sufficient autogenous shrinkage, cracks occur within the hydrated paste and impact the physico-chemical properties of the materials, in particular the transport properties [288]. In addition, the absence of thermal curing and the relatively short period of curing (1 month)

contrarily to the recommended period of 90 days did not result in optimized materials with higher density (i.e. less porous) and more complete hydration [141,289].

The results from the previous chapter (chapter IV, section 4.2.2) showed the poor performance of the studied AAS-based materials compared to the reference material (PC). Such poor behavior was explained by the evolution of the matrix during the deterioration process. Observations of the microstructure by SEM analyses showed a very clear decrease in the cohesion of the binders' matrices. Cracks up to a depth of 2 mm were observed. These cracks were large enough to allow the penetration of bacteria to deeper zones; thus, accelerating the deterioration process. This bacterial penetration has been observed in other studies of geopolymer-based materials exposed to wastewater [48,290]. In addition, the chemical analyses of the AAS matrix showed a very strong decalcification along the cracks. This behavior suggested that the attack was not only coming from the surface, but also that bacteria generated acid inside the material itself increasing the severity of the attack.

The non-hydrated residual slag didn't seem to resist such a severe attack. Magnesium, which was the cursor of the presence of mainly slag and other hydrated phases such as hydrotalcite, has almost all disappeared in the outer areas. Calcite was the main crystalline phase detected in the deteriorated zones.

The precipitation of ettringite or gypsum was not detected, probably due to the large cracks which facilitated the transport of calcium towards the outside of the matrix rapidly, thus keeping the pore solution under-saturated with respect to the precipitation of these two phases. Moreover, the acid penetration via such cracks decreased the pH of the deteriorated zones, probably below the minimum pH required for the precipitation of ettringite (10.6) [80].

The relatively large cracks in alkali-activated materials (based on fly ash and fly ash/slag) was reported in the literature to ease the penetration of sulfate towards the inside of the matrix during a sulfuric acid attack at pH 2 [161]. While gypsum was observed at pH 2, having an aggressive solution of sulfuric acid at pH 3 seemed to create under-saturation conditions in respect with the precipitation of gypsum. The combination of the large cracks, the pH of the leached solutions which was closer to 3 than to 2 and the flow of the solution on the materials surface could make it possible to reduce the concentration of calcium; hence, prevent gypsum formation.

5.7. CONCLUSION

This chapter investigated the modifications of the microstructure as well as the evolution of the chemical and mineralogical composition of the studied binders after 3 months of exposure to the accelerated BAC test. The development of the biofilm on the surface of the exposed materials was not homogenous and led to a heterogenous attack of the surface. Therefore, the measurements of deteriorated depths were not a reliable indicator to evaluate the performance of materials in such conditions.

The sample increase of aluminum by incorporating low-reactive bauxite did not show any significant improvement in terms of resistance to the acid attack. Bauxite did not participate to the hydration of the binder and the aluminum remained unavailable for the formation of AH_3 during the hydration. However, the acid attack on bauxite grains consisted of leaching iron firstly followed a progressive dissolution of the bauxite grains.

The hydration of calcium sulfoaluminate clinker and cement resulted in the formation of lower amounts of AH_3 than in calcium aluminate cement. In addition, amorphous AH_3 was formed in CSA compared to well crystallized gibbsite and bayerite in CAC. Finally, the lower resistance of CSA to biogenic acid attack could be partially linked to the absence of a cohesive, homogenous and dense deteriorated layer composed of AH_3 as it was the case with CAC. This was probably due to the higher solubility of amorphous AH_3 compared to crystallized forms of AH_3.

The role of iron in the deterioration mechanisms of cementitious materials was investigated by testing the resistance of PC-based materials containing slightly higher C_4AF than the reference material (PC) and by incorporating Fe-rich mineral additive (HardCem) in the mix design using a PC cement. Due to its low reactivity, C_4AF anhydrous phase were detected in highly deteriorated zones and showed relatively good resistance to the acid attack. However, no specific influence of the presence of iron was to be concluded. HardCem did not participate in the formation of new Fe-rich phases and remained inactive vis-à-vis the hydration of the binder. However, at the encounter with the sulfuric acid, HardCem grains were dissolved in high acidic conditions ($pH < 5$) and led to the release of high amounts of iron. Nevertheless, the leaching of iron did not favor the development of the microbial species, *Acidithiobacillus Ferrooxidans*. Finally, the dissolution of iron-phases was found to highly participate in the overall neutralizing capacity of the material; thus, reducing the severity of the attack.

The microstructure of the alkali-activated slag after exposure to the BAC test showed that residual anhydrous slag was dissolved and calcite was the main crystalline phase detected in the deteriorated zones. The formation of large vertical cracks created a pathway for bacteria to penetrate inside the hydrated matrix; hence, increase the intensity and the severity of the attack. In addition, the production of sulfuric acid inside the matrix led to the dissolution of higher amounts of hydrated phases. The presence of the large cracks eased the exit of the leached cations (mainly calcium and aluminum) from the matrix; thus, keeping the pore solution under-saturated with respect to the precipitation of gypsum and ettringite.

Chapter VI

Contribution to the modeling of the biodeterioration of cement-based materials in sewer conditions

6. CHAPTER VI – CONTRIBUTION TO THE MODELING OF THE BIODETERIORATION OF CEMENT-BASED MATERIALS IN SEWER CONDITIONS

Table of contents

6.1. INTRODUCTION

The biodeterioration mechanisms of cementitious materials in sewage networks are due to the microbial reduction of sulfate compounds – present in the wastewater stream – to hydrogen sulfide (H_2S) by anaerobic microorganisms called sulfate-reducing bacteria (SRB). The hydrogen sulfide, degassed in the air above the water surface, gets in contact with the cementitious matrix where other microorganisms, sulfur-oxidizing bacteria (SOB), develop. H_2S is used, by SOB, as sources of energy and electrons by oxidizing it into several sulfur species, in particular the formation of sulfuric acid (H_2SO_4) as a final product [5,6,9,10,13].

As shown in chapter III, the conversion of reduced sulfur compounds into sulfuric acid is a complex phenomenon, involving several intermediates depending on the chemical conditions. Over the different stages of oxidation of the reduced sulfur, acid was produced. Moreover, the structure of the biofilm, the oxygen diffusion and the developed microbial populations can lead to particular reactions. The development of a biofilm – and the production of H_2SO_4 – on the surface of the cement-based materials, and possibly the penetration of microorganisms inside the cementitious matrix, as seen in chapter V, generates a severe attack on the cementitious material [48]. The deterioration phenomenon is due to the progressive dissolution of the cementitious matrix and to the precipitation of secondary phases, such as gypsum and/or ettringite. Hence, implementing a biological aspect to a reactive-transport model is a key step in further understanding the biodeterioration of sewer pipes.

As presented in the previous chapters, several experimental studies were carried out and many laboratory tests were developed in the literature aiming to reproduce the biochemical deterioration of cementitious materials in sewer networks [16,20,24,27,94,281]. These accelerated tests have shortened the testing period from years to several months.

However, as rapid and efficient are the laboratory tests, many impacting factors – such as the increase in the acidity of the aggressive solution, the porosity of the cement paste, etc. – would require multiplying the experiments in order to be able to analyze the influence of each parameter. Therefore, information about the evolution of the microstructure during the attack is still missing to understand and to explain the behavior and the performances of mineral materials in such environment.

In the aim of improving the understanding of the reactivity of different cementitious materials in controlled biodeterioration conditions (adapted to our experimental results), numerical tools must be developed and adapted to use complex thermodynamic databases coupled with reactive-transport calculations. Moreover, the results obtained in chapter III concerning tetrathionate conversion showed that in order to better reproduce the biodeterioration phenomena in terms of sulfuric acid production, the dependency of the biochemical transformation of sulfur compounds and formation of the different polythionates, should be considered.

Hence, this study presents two specific sections:

i. The development of a chemical reactive-transport model (using HYTEC® software) representing a sulfuric acid attack on the solid phases of PC and CAC. In addition, a brief comparison between two numerical approaches to solve reactive-transport problems is presented, including the geometry (1D or 2D) and the boundary conditions.

ii. The development of kinetics equations to represent the transformation of tetrathionate as presented in chapter III. The software Aquasim® was used to estimate the kinetics parameters and evaluate the simulation.

6.2. CHEMICAL REACTIVE-TRANSPORT MODEL (HYTEC®)

6.2.1. Model configuration and initial conditions

The experimental configuration of the BAC test allowed the establishment of a 2D-modelling design (Figure VI-1). The cement paste thickness was 5 mm, discretized into grids of 100 µm-thick. The length of the cement paste was 80 mm (grids of 8 mm-thick), which corresponded to the experimental specimens. The leaching solution consisted of sulfuric acid (H_2SO_4) where [SO_4^{2-}] was adjusted in order to obtain 2 case-scenarios: pH 3 and pH 1. The leached cementitious cations were measured at the outlet of the solution.

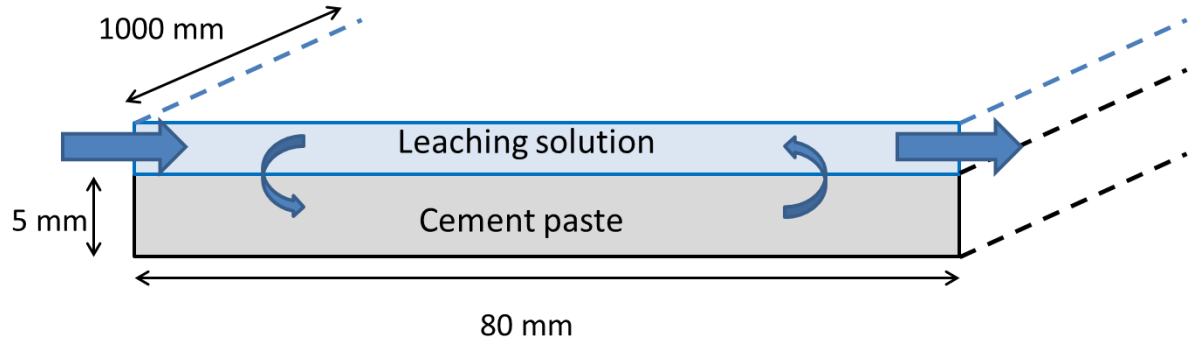

Figure VI-1. 2D-modelling design of a 5mm-deep cement paste exposed to a flow of a H_2SO_4 leaching solution at 25 ml/h

The 1D-model was represented by a thickness of 5 mm and was discretized into 100 µm-thick grids. The length of the modeled cement paste was 1 mm and was discretized into two 500 µm-thick grids. The conditions of flow and of sulfuric acid concentrations in the aggressive solution were the same as in the 2D-model.

6.2.2. Choice of the studied binders

Cement pastes were considered in this part in order to evaluate the reactivity and the resistance of the cementitious phases to the sulfuric acid attack. Two cement pastes (PC and CAC) with completely different chemical and mineralogical compositions were tested. Table VI-1 provides the cement paste initial compositions, where anhydrous phases were considered as inert. In Aquasim modeling, the concentration of the anhydrous phases was entered as an

input, however, in HYTEC simulation, only the concentrations of the hydrated phases were entered as the model takes automatically into account the inert phases. In addition, 20 vol.% of initial porosity was applied to both cementitious pastes in order to study the differences in the behavior of the cementitious mineral phases in regards with the acid attack. For both pastes, the initial diffusivity of the paste was 10^{-10} $m^2.s^{-1}$. The thermodynamic constant values were obtained from the database (THERMODDEM 2011) for HYTEC.

Table VI-1. Initial composition of PC and CAC pastes in mol/L. Et: Ettringite; Ms: Calcium monosulfoaluminate hydrate

	CH	CSH (1.6)	Et*	Ms*	C_3AH_6	Gibbsite	Anhydrous phases
PC	4.636	4.887	0.104	0.105	-	-	2.56
CAC	-	-	-	-	2.011	4.179	6.96

6.3. RESULTS OF THE CHEMICAL MODEL: COMPARISON BETWEEN 2D AND 1D MODELS

The experimental configuration consisted of an aggressive solution injected on the upstream part of the specimen with a regulated flow (25 ml/h) then collected at the downstream of the specimen for the chemical analyses. Figure VI-2 presents the two configurations (2D and 1D) which were adapted to model the sulfuric acid attack on the cement paste specimens.

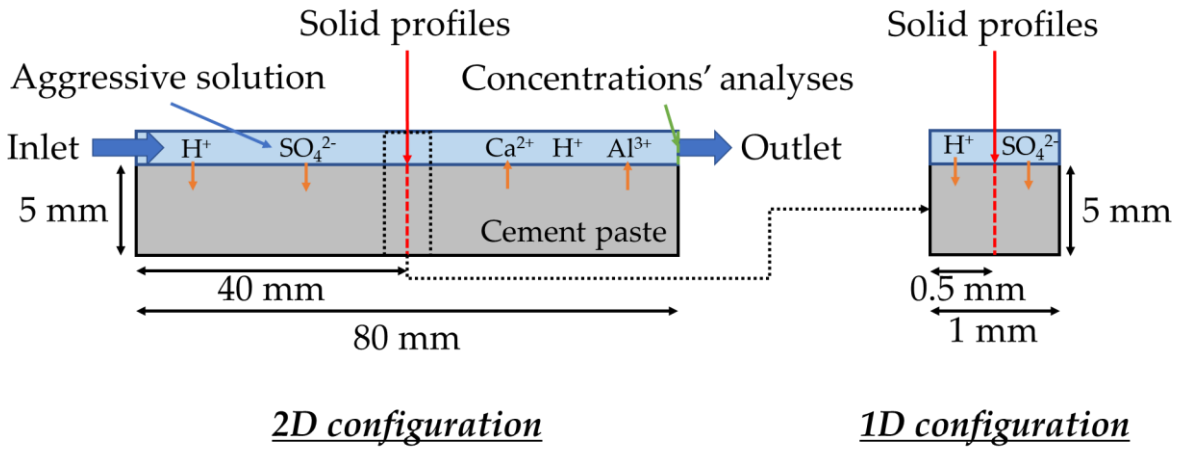

Figure VI-2. The two configurations (2D and 1D) used to model the attack of a sulfuric acid solution of cement paste specimens.

The 2D configuration allowed to couple the flow of the aggressive solution with the reaction of the cement paste with the attack. The concentrations of the sulfate and the leached cations (calcium and aluminum) were evaluated at the downstream of the solution (at 80 mm on the x-axis) while the solid profiles of the cement pastes were evaluated at the middle of the specimen (at 40 mm on the x-axis). The 2D configuration of HYTEC simulation reproduced the same configuration used in the BAC test.

The 1D configuration was developed to accelerate the duration of the simulation from several hours to several minutes. The 1D configuration simulates the zone at the middle of the specimen (at 40 mm on the x-axis). In such configuration, the aggressive solution was considered to be renewed instantly and the flow of the solution was not simulated.

6.3.1.2D model with continuous inlet flow

6.3.1.1. Leaching of cementitious cations

Figure VI-3 presents the cumulative leached calcium and aluminum ions from the cementitious matrix standardized to the initial calcium and aluminum contents of PC and CAC pastes after 100 days of exposure to H_2SO_4 solution.

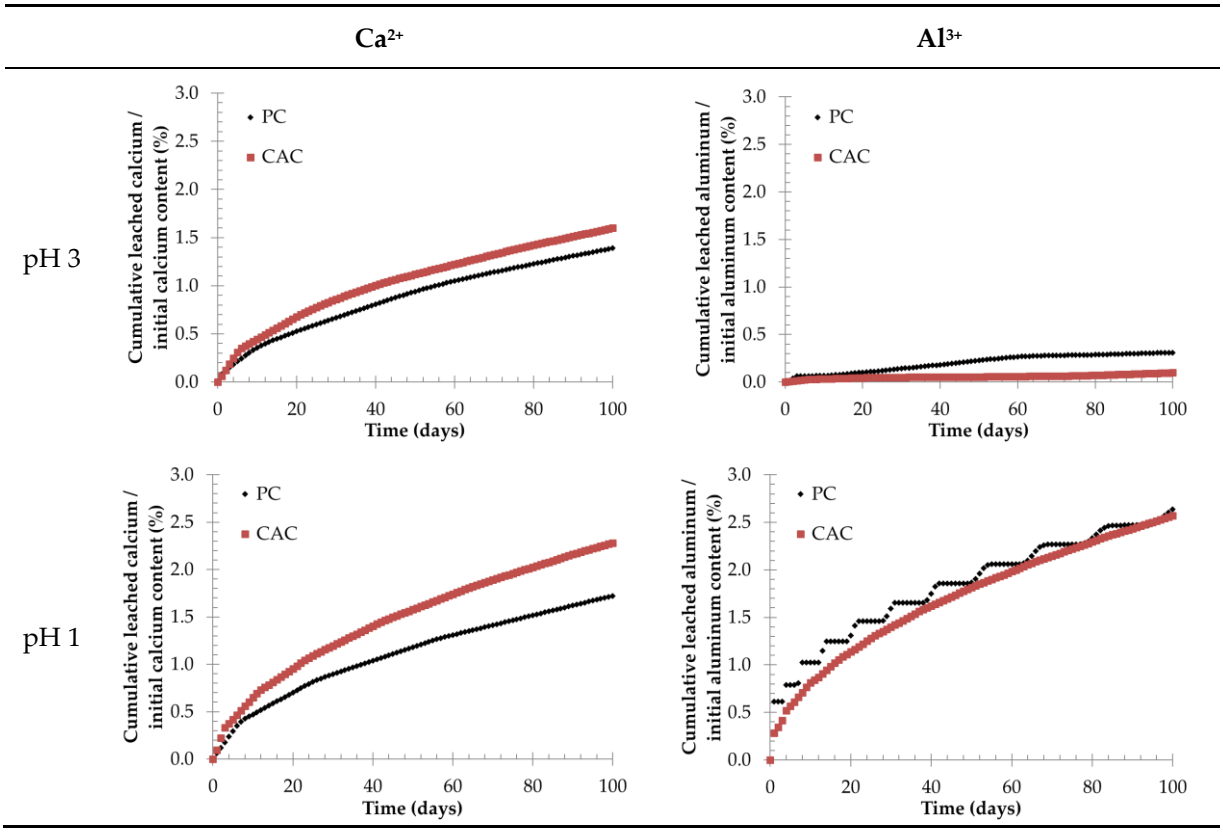

Figure VI-3. Standardized cumulative leached Ca^{2+} and Al^{3+} (in %) for PC and CAC exposed to sulfuric acid solution

At pH 3, the standardized cumulative leached calcium of CAC paste was slightly higher than for that of PC paste, which was not consistent with experimental data. In the experiment where pH ranged between 3 and 2.5 for the last 2 months of exposure, a lower amount of standardized calcium was observed for the CAC paste compared to PC paste. The cumulative aluminum ions leached from CAC were 3 times lower than from PC despite that a higher initial aluminum content for CAC. The lower release of aluminum from CAC specimen is likely linked to the thermodynamic stability of AH_3 down to pH 3 – 4 [186].

At pH 1, the standardized calcium released by CAC paste was higher than by PC paste. Nevertheless, the cumulative aluminum released by CAC and PC were very similar although

the pH of the aggressive solution was below the threshold of the stability of AH_3 and more aluminum should have leached from CAC than from PC. In the next section, investigations of the microstructure and the evolution of the mineralogical phases were carried out in order to understand the differences between the experimental and the modeled data, in particular the aluminum role.

6.3.1.2. Evolution of the porosity, pH and mineralogical phases in the cementitious matrices in the 2D configuration

The evolution of the mineralogical phases, pH and porosity of PC and CAC pastes after 100 days of exposure to chemical sulfuric acid at the center of the specimen (40 mm away from the inlet point) at pH 3 is presented in Figure VI-4.

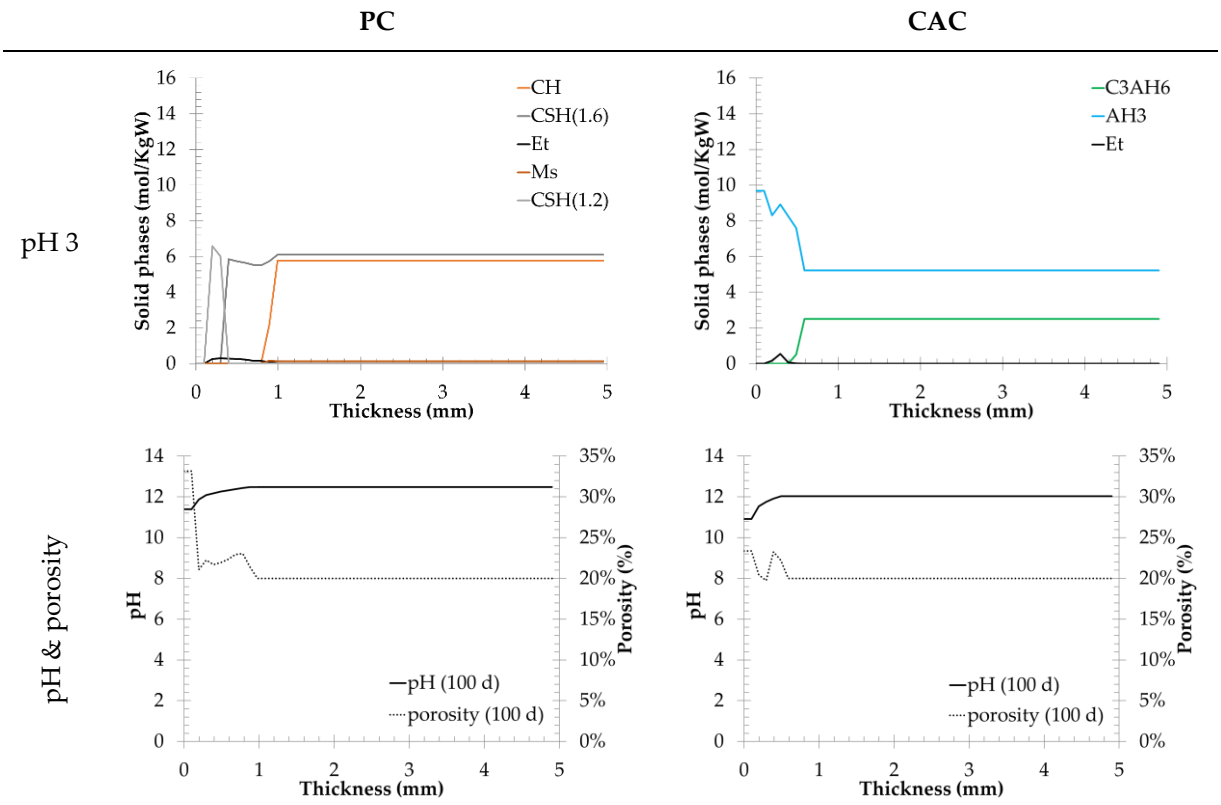

Figure VI-4. The profiles of the solid phases for PC and CAC after 100 days of exposure to a sulfuric acid solution at pH 3 (CH: portlandite; CSH: calcium silicate hydrates; Et: Ettringite; Ms: Monosulfoaluminate; C_3AH_6: Katoite; AH_3: Aluminum hydroxide)

Regarding PC paste, portlandite total dissolution was observed up to 0.8 mm (at pH 3) and up to 1.5 mm (at pH 1) from the exposed surface. The decalcification of C-S-H was progressive and led to the formation of C-S-H with lower C/S ratio ($C_{1.2}SH$). Moreover, the dissolution front of monosulfoaluminate (Ms) phase corresponded to the depth of penetration of sulfate (data not shown). The dissolution of Ms was observed at about 1 mm from the surface at pH 3 and was linked to the penetration of sulfate inside the cementitious matrix, which led to the transformation of Ms into ettringite.

The presence of low Ca/Si C-S-H near the surface was linked to the relatively high pH (11.4), although such pH was unexpected. It seemed that the hydroxide ions released from portlandite, and possibly from the $C_{1.6}SH$, had locally neutralized the acid. Moreover, the flow of the aggressive solution at the surface led to the leaching of the different released cementitious cations, in particular calcium, towards the outside of the system. Additionally, the penetration of sulfate allowed the formation of ettringite in deep zones of the cementitious matrix while gypsum was not detected. This might be due to the relatively low amount of sulfate in the aggressive solution, compared to the solution at pH 1 for example, and to the leaching of the calcium ions; hence, the undersaturation conditions of the pore solution in respect with gypsum formation. The outer layer of the PC paste was considered completely dissolved; however, it showed a maximum porosity of 33%. The 67% of the remaining volume was attributed to anhydrous grains which were considered inert in HYTEC simulations.

Regarding CAC paste, the decalcification front corresponded to the depth where C_3AH_6 was dissolved, which was around 0.5 mm at pH 3. The dissolution of C_3AH_6 likely led to the precipitation of additional AH_3 gel. Calcium and aluminum ions, released from the dissolution of C_3AH_6, reacted with sulfate – brought by sulfuric acid – resulted in the precipitation of ettringite in high pH zones. Like for PC, gypsum was not detected for CAC paste at pH 3.

The evolution of the pH of CAC paste was similar to that of PC and showed a pH of 10.9 at the surface of the specimen. The relatively high value of the pH was likely due to the dissolution of C_3AH_6 and the release of hydroxide ions, which are responsible of neutralizing the acid. The absence of gypsum was probably due to the same conditions as for PC (flow of the solution, leaching of calcium and low amount sulfate in the solution). The porosity at the surface of the CAC specimen was estimated at 23%, which was significantly lower than for PC (33%). The absence of a completely dissolved layer and the formation of additional AH_3 at the surface were the two main reasons to explain the lower porosity of CAC paste.

The evolution of the mineralogical phases, pH and porosity of PC and CAC pastes after 100 days of exposure to chemical sulfuric acid at the center of the specimen (40 mm away from the inlet point) at pH 1 is presented in Figure VI-5.

The deterioration of the PC paste was very severe at pH 1 compared to at pH 3. Portlandite was completely dissolved up to 1.5 mm while the decalcification of CSH led to the formation of $C_{1.2}SH$ and $C_{0.8}SH$. Additionally, silica gel was formed near the surface and resulted from the total decalcification of CSH phases. The penetration of sulfate up to 4 mm inside the PC matrix resulted in the transformation of Ms into ettringite. Moreover, small amounts of secondary ettringite and AH_3 were formed at 1.1 mm from the surface and resulted in a significant decrease in the porosity down to 12%. Unlike at pH 3, high amounts of gypsum were formed near the surface and was probably due to the presence of high amounts of sulfate brought by the solution at pH 1 and the to the high amounts of calcium resulting from the dissolution of CH and CSH. The precipitation of gypsum showed also an impact on the porosity (≈ 9%) while no impact was detected on the evolution of the pH. The pH was

relatively high at the sound part of the matrix and dropped to about 2 following the total dissolution of CSH and the formation of silica gel.

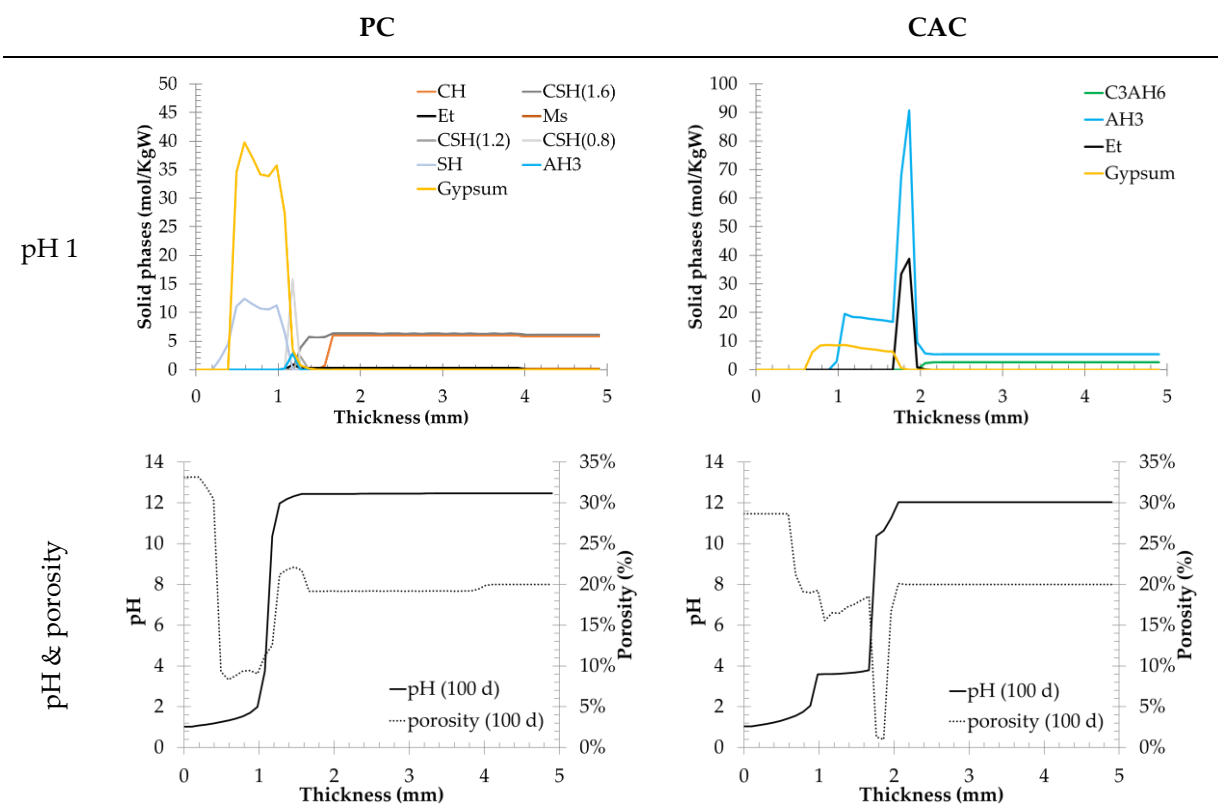

Figure VI-5. The profiles of the solid phases for PC and CAC after 100 days of exposure to a sulfuric acid solution at pH 1 (CH: portlandite; CSH: calcium silicate hydrates; Et: Ettringite; Ms: Monosulfoaluminate; SH: Silica gel; C_3AH_6: Katoite; AH_3: Aluminum)

The behavior of CAC paste in regard to the aggressive solution at pH 1 was different from that at pH 3. A completely dissolved layer of 0.6 mm from the surface was detected and the decalcification of the matrix was observed at 2 mm from the surface. Gypsum was identified in high amounts at the surface, which was not the case at pH 3. In addition, very high amounts of ettringite and AH_3 were formed and resulted in the reduction of the porosity to the lowest possible value, which was fixed at 1%. Furthermore, unlike gypsum, the precipitation of AH_3 influenced the pH of the deteriorated zone and maintained it between 3 and 4, which corresponds to the domain of the stability of AH_3.

6.3.2.1D model with constant concentration at the boundary

The first developed configuration was a 2D-model where coupling the chemical reactions and the transport phenomena generated highly time-consuming simulations. Moreover, at a flow rate of 25 ml/h, the mineralogical phases and aqueous species profiles were the same at every point of the length (80 mm) of the cement paste specimens, potentially due to a low hydraulic retention time. To confirm this hypothesis, the calculation was carried out at a flow rate decreased by about two orders of magnitude. In this case, a significant difference between the mineralogical composition profiles at the inlet and at the outlet point was observed.

Therefore, in order to optimize the calculation time, a 1D-model was developed to calculate the mineralogical and chemical alteration of the specimen without considering the flow of the solution on the specimen's surface. Hence, the boundary conditions of the second configuration consisted of a constant concentration of sulfuric acid (regulated at pH 3 and pH 1), which was renewed at every time-step of the simulations.

6.3.2.1. Evolution of the mineralogical phases in the cementitious matrices in the 1D configuration

Figure VI-6 presents the evolution of the solid phases as a function of the distance to the surface of PC and CAC matrices after 100 days of exposure to sulfuric acid at pH 3 using the 1D-model.

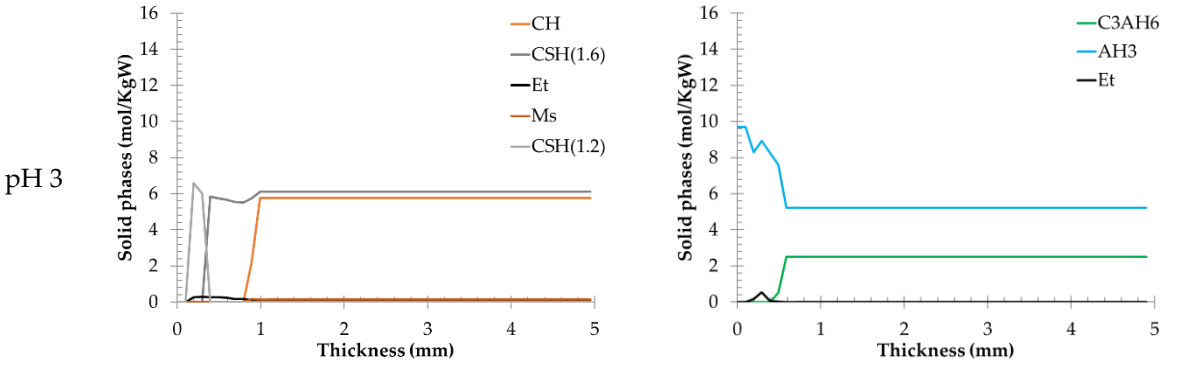

Figure VI-6. The profiles of the solid phases for PC and CAC pastes after 100 days of exposure to sulfuric acid solutions at pH 3

The results for the PC paste indicated the dissolution of portlandite occurred at distance of 1 mm from the surface with a decrease of C/S ratio of the C-S-H from 1.6 to 1.2 near the surface. Moreover, precipitation of ettringite was detected in zones with relatively high pH. Likewise, the CAC matrix suffered from decalcification and dissolution of C_3AH_6, leading the precipitation of additional AH_3 gel on the surface. In addition, a minor ettringite formation was observed at the dissolution front of the C_3AH_6. Due to the low residence time of the acid solution at the surface of the material in the 2D-model, the 1D model gave the very similar results in terms of deteriorated depths and mineralogical transformations in relatively short time.

6.3.2.2. Buildup of AH_3 layer

The buildup of AH_3 rich layer for PC and CAC systems is shown in Figure VI-7 displaying Al^{3+} and AH_3 profiles for both cement pastes at 10 and 100 days of exposure to sulfuric acid solution at pH 1.

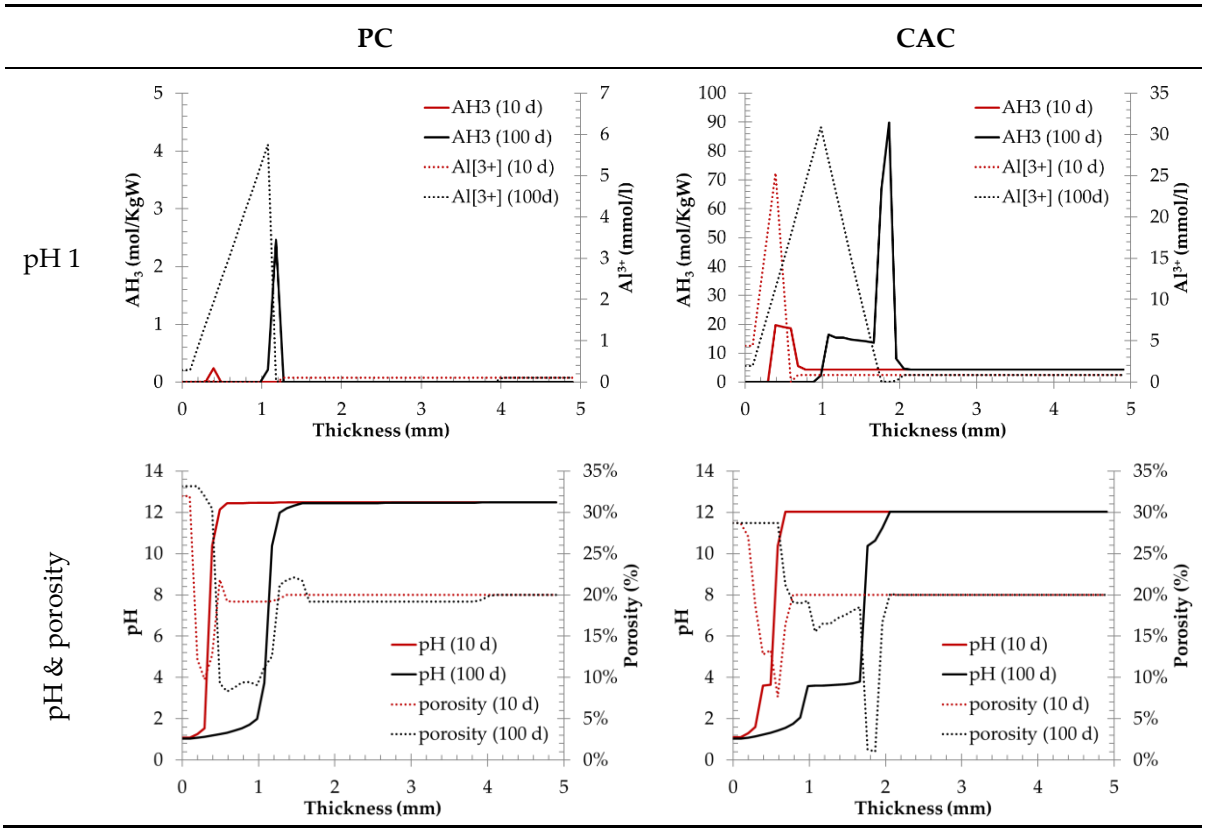

Figure VI-7. AH_3, Al^{3+}, pH and porosity profiles after 10 and 100 days of exposure to sulfuric acid solution at pH 1

The Al^{3+} profiles for PC and CAC suggested that leaching and diffusion towards the inside of the matrix were the main mechanisms for the aqueous aluminum. In addition, the concentration of aluminum in the pore solution for CAC paste was 5 times higher than for PC paste. Furthermore, for CAC, the Al^{3+} concentration profile showed a significant decrease in the zone where AH_3 precipitated in higher quantity. This specific zone presented a very low porosity (< 1%) due to AH_3 and ettringite precipitation (see Figure VI-4). The increase in Al^{3+} in the solution was likely due to the dissolution of Al-bearing phases (mainly AH_3 and ettringite) due to the highly severe conditions. Moreover, while the amount of newly-precipitated AH_3 and ettringite was much lower for PC than for CAC, a filling effect of the porosity was observed in the zone where gypsum precipitated. However, the lowest value of porosity for PC was detected at around 10%.

6.3.3. Discussion

6.3.3.1. Analyses of boundary conditions choices

In the 2D configuration, the flow, which was regulated at 25 ml/h, was injected on a specimen with a length of 80 mm. Hence, the residence time of the solution on the specimen surface was very short and the renewal of the solution could be considered as almost instantaneous. By comparing the results obtained from sections 6.3.1.2 and 6.3.2.1, the 1D-model has represented efficiently the phenomena observed in the 2D model.

6.3.3.2. Degradation mechanisms

The results of this study indicated that the performances of PC and CAC pastes were strongly influenced by the aggressiveness of the attack. The analyses of the solid profiles of the cementitious matrices confirmed the conclusion that the chemical and mineralogical composition of the cement was a key factor in the resistance of a material against sulfuric acid.

The exposure of PC and CAC pastes to sulfuric acid solutions at pH 3 and pH 1 allowed the evaluation of the decalcified depths, the completely dissolved zones, the total degraded depths and the chemical/mineralogical alterations for both PC and CAC materials.

At pH 3, CAC paste showed higher resistance than PC paste. However, by investigating a more severe condition (pH 1), it seemed that the CAC suffered from more deterioration compared to PC which was in accordance with the results obtained from experimental chemical tests [49]. The differences in the performances between PC and CAC pastes was likely explained by the reactivity and the thermodynamic stability of CAC phases. During the acid attack, C_3AH_6 phase reacts with the acid to form an alumina gel (AH_3) which is stable between pH 9 and 3-4 [186]. The wide stability range of this alumina gel ensured a higher acid neutralization capacity, hence, a better performance of CAC at pH 3. However, when CAC paste was exposed to pH 1, the dissolution of AH_3 occurred and resulted in the opening of the porosity, leading to more penetration of the acid. For PC paste, the formation of significant amounts of gypsum contributed to the decrease in the porosity in the deteriorated layers; hence reducing the penetration depth of the acid.

In the case of chemical sulfuric acid attack, in very severe conditions, the performance of the PC paste was better than that of CAC. However, in sewer conditions, PC-based materials showed lower resistance to biogenic acid attack than CAC-based materials [26,44,49,67,245]. Moreover, the results obtained for PC and CAC at pH 3 were similar to the results obtained from several studies carried out in sewer conditions (in field and laboratory) [20,44,67,174,245]. However, ettringite was little or not detected in CAC matrices exposed to these conditions while it was observed in the chemical model. This indicates that chemical models do not quite represent the biological attack in sewer conditions and that the impact of the biofilm on the deterioration phenomena was not considered.

In addition, in a chemical attack, the diffusion of the aggressive agents and reactivity of the cementitious phases are likely to control the mechanisms of the attack, while, in a biological attack, there are interactions between the cementitious matrix and the microbial activity. Therefore, an optimization of the model in terms of representativity (variable pH, oxidation of sulfur species and acid production) and attacking mechanisms (diffusion or surface attack) should be carried out to improve the modeling of the phenomena.

6.3.3.3. Barrier effect of phases' assemblage

In a sulfuric acid attack, although the formation of gypsum layer near the surface of the material has been often reported in the literature to create swelling and cracking of the material leading to a deeper penetration of the acid [158]. Moreover, several authors reported the capacity of the aluminum gel in CAC systems to create a physical barrier against sulfate penetration [44,177].

The results of the numerical modeling showed a decrease of the penetration of the sulfate species into the cementitious matrix for PC and CAC pastes in highly severe conditions. As for PC, the highly deteriorated zone was mainly composed of gypsum and silica gel, and for CAC, it was composed of gypsum and aluminum gel. Moreover, the barrier effect was more pronounced in the zone where the ettringite was formed. This was likely due to the high molar volume of the ettringite phase which could fill the pores. However, since the damage due to swelling and cracking from gypsum/ettringite precipitations was not implemented in this model, they were of course considered as barriers for the species' diffusion.

6.3.3.4. Chemical and biological acid attacks

The presented model simulated chemical sulfuric acid attack with a continuous flow at the surface of cementitious (PC and CAC) pastes to reproduce the exposure conditions of the BAC test. During the last two months of exposure, the pH ranged between 3 and 2.5 in the experimental conditions and the results of the leached calcium differed significantly between the chemical model and the experimental results. Moreover, the literature showed that chemical tests were inefficient to represent biodeterioration processes in sewer-like environment, in particular by comparing PC-based and CAC-based materials [49,69,291].

The previous chapters showed that specific transformations of reduced sulfur compounds led to the production of acid in contact with the cementitious pastes. A first approach, presented in chapter III, was developed to represent the transformation of tetrathionate during time using successive stoichiometric chemical reactions to reproduce the biological phenomena.

The next section presents the numerical model proposed to represent the tetrathionate conversion in the experimental conditions of the BAC test to reproduce biodeterioration processes due to biogenic sulfuric acid production. This proposed model, could be developed in HYTEC, with the reactive-transport model proposed in the previous section.

6.4. MATHEMATICAL REPRESENTATION OF TETRATHIONATE CONVERSION IN CONTACT WITH CEMENTITIOUS MATERIALS (pH DEPENDENCY)

In chapter III, the analyses of the leaching solution in terms of sulfur compounds showed that the materials did not have a direct impact on the transformation of tetrathionate and the

production of the different intermediate sulfur species. The reactivity of the materials to the acid attack determined the evolution of the pH on the surface of the materials and consequently influenced the reaction pathways for tetrathionate conversion.

Five stoichiometric reactions were proposed to represent the evolution of the different intermediate sulfur compounds, previously identified in the experimental results as a function of the pH conditions of the liquid sample (the pH of the leached solution) and of the measured consumed tetrathionate.

In the objective of representing numerically the BAC test, the tetrathionate consumption over time should be estimated using a dynamic model. This part of the study focuses on the definition of the consumption of tetrathionate and the production of the different intermediate including thiosulfate, pentathionate, hexathionate, elemental sulfur and sulfate.

The software Aquasim, developed to simulate biological processes in environmental water, was firstly used to evaluate and calibrate the proposed model by estimating the different parameters. However, the proposed equations should be adapted to be implemented in HYTEC.

6.4.1. Mathematical equations to represent dynamic conversion of reduced sulfur compounds into sulfate

In steady state conditions, biofilm culture in continuous reactors leads to biomass production associated with the consumption of a stable flux of substrate (tetrathionate is the initial substrate in this study). In order to reach steady state conditions, microbial populations must colonize the exposed surface and grow. Such process, dependent on environmental conditions, is time dependent, i.e. depends on the accumulation of active biomass. Therefore, kinetic equations were developed to include the time dependency to model the different reactions pathways. The pH dependencies and the stoichiometry proposed in chapter III were used to represent the reaction pathways and the quantity of consumed and/or produced compounds.

Eq.VI-1 was proposed to represent the consumption of tetrathionate during time. This equation is based on **Eq.III-1** (chapter III).

$$\frac{d[S_4O_6^{2-}]}{dt}.V = -b.[S_4O_6^{2-}].V - k.t.A_{mod}.[S_4O_6^{2-}].\frac{[S_4O_6^{2-}]}{K_{S_4O_6^{2-}} + [S_4O_6^{2-}]}.V \qquad \textbf{Eq.VI-1}$$

Where,

- $[S_4O_6^{2-}]$: local concentration of tetrathionate (mol/L).
- t: time (d).
- V: volume of liquid film (L).
- b: minimal rate corresponding to a minimal and constant tetrathionate consumption rate (d^{-1}).
- k: rate of tetrathionate consumption over time (d^{-2}).

- A_{mod}: pH-dependent factor for **Eq.III-1** proposed in chapter III.
- K_{S4O62-}: half-saturation constant for tetrathionate (mol/L).

Eq.VI-2 was proposed to represent the consumption of tetrathionate during time. This equation is based on **Eq.III-2** (chapter III).

$$\frac{d[S_4O_6^{2-}]}{dt}.V = -k.t.(1-A_{mod}).[S_4O_6^{2-}].\frac{[S_4O_6^{2-}]}{K_{S_4O_6^{2-}}+[S_4O_6^{2-}]}.V \qquad \textbf{Eq.VI-2}$$

Where,

- $[S_4O_6^{2-}]$: local concentration of tetrathionate (mol/L).
- t: time (d).
- V: volume of liquid film (L).
- k: rate of tetrathionate consumption over time (d^{-2}).
- $(1-A_{mod})$: pH-dependent factor for **Eq.III-2** proposed in chapter III.
- K_{S4O62-}: half-saturation constant for tetrathionate (mol/L).

Eq.VI-3 was proposed to represent the consumption of pentathionate during time. This equation is based on **Eq.III-3** (chapter III).

$$\frac{d[S_5O_6^{2-}]}{dt}.V = -k.t.(1-A_{mod}).C_{mod}.[S_5O_6^{2-}].\frac{[S_4O_6^{2-}]}{K_{S_4O_6^{2-}}+[S_4O_6^{2-}]}.\frac{[S_5O_6^{2-}]}{K_{S_5O_6^{2-}}+[S_5O_6^{2-}]}.V \qquad \textbf{Eq.VI-3}$$

Where,

- $[S_5O_6^{2-}]$: local concentration of pentathionate (mol/L).
- $[S_4O_6^{2-}]$: local concentration of tetrathionate (mol/L).
- t: time (d).
- V: volume of liquid film (L).
- k: rate of tetrathionate consumption over time (d^{-2}).
- $(1-A_{mod})$: pH-dependent factor for **Eq.III-2** proposed in chapter III.
- C_{mod}: pH-dependent factor for **Eq.III-3** proposed in chapter III.
- K_{S4O62-}: half-saturation constant for tetrathionate (mol/L).
- K_{S5O62-}: half-saturation constant for pentathionate (mol/L).

Eq.VI-4 was proposed to represent the consumption of hexathionate during time. This equation is based on **Eq.III-4** (chapter III).

$$\frac{d[S_6O_6^{2-}]}{dt}.V = -k.t.(1-A_{mod}).D_{mod}.[S_6O_6^{2-}].\frac{[S_4O_6^{2-}]}{K_{S_4O_6^{2-}}+[S_4O_6^{2-}]}.\frac{[S_6O_6^{2-}]}{K_{S_6O_6^{2-}}+[S_6O_6^{2-}]}.V \qquad \textbf{Eq.VI-4}$$

Where,

- $[S_6O_6^{2-}]$: local concentration of hexathionate (mol/L).
- $[S_4O_6^{2-}]$: local concentration of tetrathionate (mol/L).
- t: time (d).
- V: volume of liquid film (L).

- k: rate of tetrathionate consumption over time (d^{-2}).
- ($1-A_{mod}$): pH-dependent factor for **Eq.III-2** proposed in chapter III.
- D_{mod}: pH-dependent factor for **Eq.III-4** proposed in chapter III.
- K_{S4O62-}: half-saturation constant for tetrathionate (mol/L).
- K_{S6O62-}: half-saturation constant for hexathionate (mol/L).

Eq.VI-5 was proposed to represent the consumption of thiosulfate during time. This equation is based on **Eq.III-5** (chapter III).

$$\frac{d[S_2O_3^{2-}]}{dt}.V = -k.t.(1-A_{mod}).E_{mod}.[S_2O_3^{2-}].\frac{[S_4O_6^{2-}]}{K_{S_4O_6^{2-}}+[S_4O_6^{2-}]}.\frac{[S_2O_3^{2-}]}{K_{S_2O_3^{2-}}+[S_2O_3^{2-}]}.V \qquad \textbf{Eq.VI-5}$$

Where,

- $[S_2O_3^{2-}]$: local concentration of thiosulfate (mol/L).
- $[S_4O_6^{2-}]$: local concentration of tetrathionate (mol/L).
- t: time (d).
- V: volume of liquid film (L).
- k: rate of tetrathionate consumption over time (d^{-2}).
- ($1-A_{mod}$): pH-dependent factor for **Eq.III-2** proposed in chapter III.
- E_{mod}: pH-dependent factor for **Eq.III-5** proposed in chapter III.
- K_{S4O62-}: half-saturation constant for tetrathionate (mol/L).
- K_{S2O32-}: half-saturation constant for thiosulfate (mol/L).

The half-saturation values (K) for all intermediate sulfur species (pentathionate, hexathionate and thiosulfate) were set at very low value (1.10^{-7} mol/L). This value was only set to avoid numerical problems and limit the consumption rate of the specific compounds when concentrations were close to zero.

6.4.2.Results and discussions

6.4.2.1. Estimation of k and K_{S4O62-}

In this part of the study, Aquasim software was used to estimate k and K_{S4O62-}, using as input parameters: the liquid volume V (L), the pH of the leaching solution during time for all the exposed materials, the water inlet flows during time for each exposed materials, and the inlet tetrathionate concentrations. These parameters were calibrated to fit the experimental tetrathionate outlet concentrations. The estimated values for k and K_{S4O62-} were 11.5 d^{-2} and 1.39×10^{-6} mol/L, respectively.

The liquid film was considered as a perfectly mixed reactor (PMR), with a fixed volume of 0.74 mL corresponding to a liquid volume for a film of 8 cm long, 3.7 cm wide and 0.25 mm thick. Such volume was calculated to represent the liquid film at the surface of the cementitious materials. One should note that since the liquid volume is part of the kinetic equations, the value of k was dependent on the liquid volume; hence, k values were only applicable to this

specific volume. If the liquid volume changes, k values should be recalculated, however, the factor k.V remains constant.

6.4.2.2. Concentrations of sulfur compounds

Figure VI-8 presents the evolution of the concentrations of tetrathionate, thiosulfate, pentathionate, hexathionate, elemental sulfur and sulfate estimated in the liquid volume using the kinetic models and compared to the experimental data for tetrathionate, thiosulfate and sulfate for CAC material (lowest amount of initial sulfur content of all tested materials in this study, ~ 0.02 wt.% SO_3).

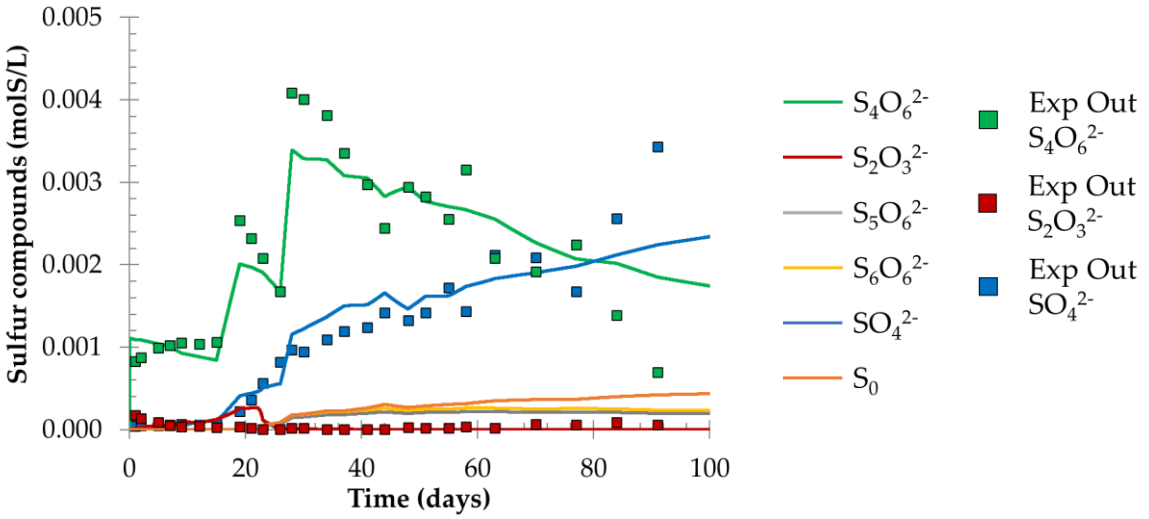

Figure VI-8. Evolution of sulfur compounds in the liquid volume using the kinetic models (solid lines) in comparison to the experimental results (marks) for CAC material

The results showed that the overall trends of the estimated concentrations of the sulfur species by the models were in accordance with the evolution of the sulfur species' concentrations measured experimentally. In the first stages of the colonization, a low consumption of tetrathionate and a low production of sulfate were observed. In addition, very low concentrations of thiosulfate were detected due to the use of a kinetic law with a time dependency for the consumption of tetrathionate. The decomposition of tetrathionate into thiosulfate in alkaline conditions was not very well represented by the model; hence, the delay in the accumulation of thiosulfate observed when the pH decreased. At around 20 days, the acceleration in the sulfate production was linked to the increase in the microbial activity and to the complete consumption of thiosulfate. The decrease in the pH, due to the increase in the production of sulfuric acid by the microorganisms, led to the disproportionation of tetrathionate and the production of pentathionate, hexathionate and elemental sulfur as described in chapter III. The same trends were observed for all exposed materials. The results are presented in **Appendix VI-B**.

6.4.2.3. Accumulation of sulfate and thiosulfate

The main objectives of the model were, on the one hand, to describe the transformation of the sulfur compounds, and on the other hand to estimate the amount of acid and sulfate produced in contact with the exposed material. Figure VI-9 presents the comparison between the modeled (using the estimated values of k and K_{S4O62-}) and the experimental data of the cumulative amount of sulfate and thiosulfate in the liquid volume for CAC material as a function of the time of exposure.

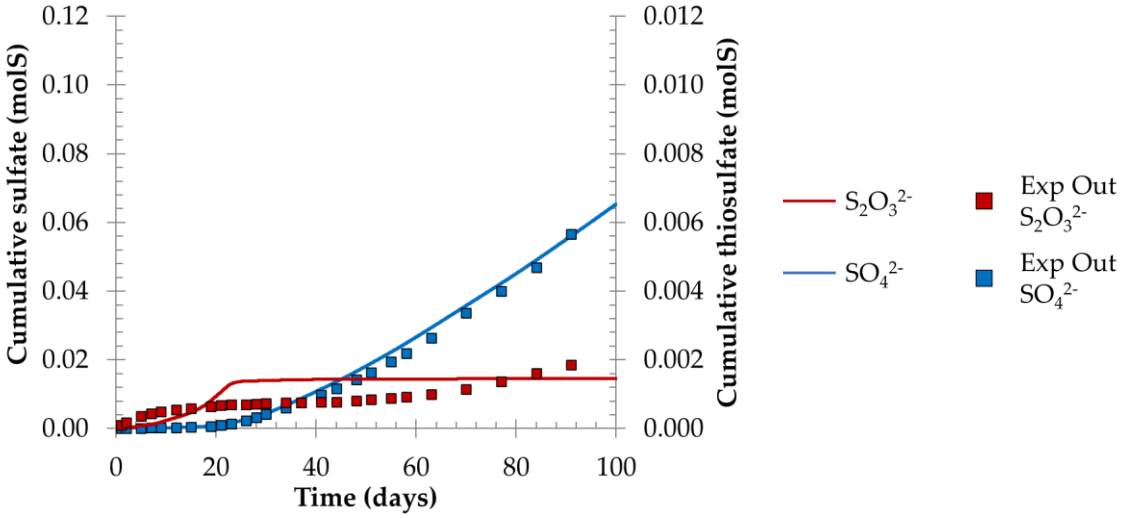

Figure VI-9. Cumulative amount of sulfate and thiosulfate in the liquid volume using the kinetic models (solid lines) in comparison to the experimental results (marks) for CAC material

The trends of the sulfate and thiosulfate modeled curves were very similar to the experimental results, confirming the estimation of k and K_{S4O62-} values. The delay in the accumulation of thiosulfate was linked to the pH factor as explained in the previous section.

Figure VI-10 presents the cumulative amount of sulfate and thiosulfate in the liquid solution for AAS, which another low sulfur material (~ 0.64 wt.% SO_3). While the cumulative amount of sulfate was similar to the experimental data, the modeled thiosulfate cumulative amount was slightly higher than the amount found experimentally. Nevertheless, thiosulfate accumulation accounts for only ~ 3 % of the sulfur mass balance at the end of the experiment.

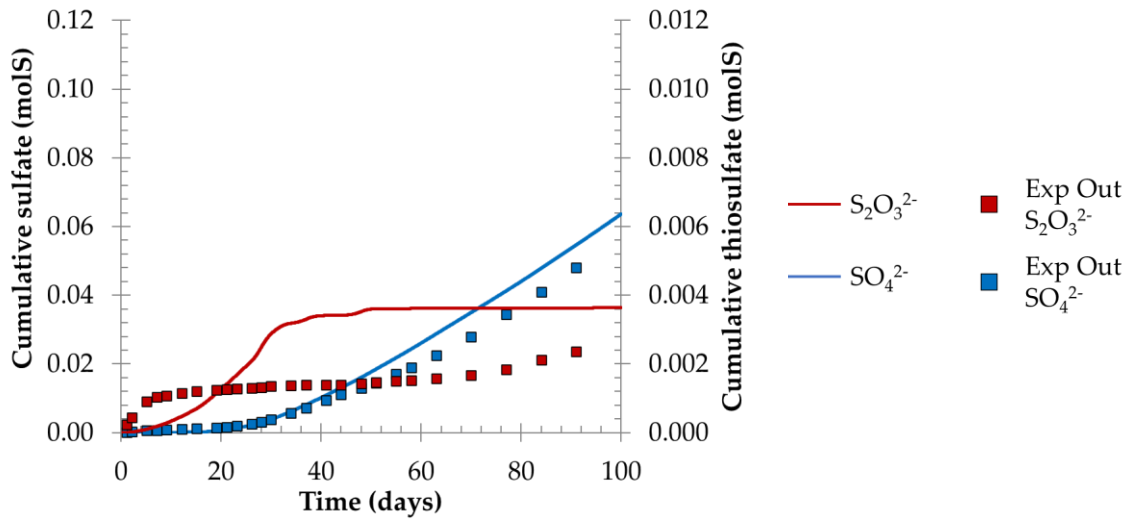

Figure VI-10. Cumulative amount of sulfate and thiosulfate in the liquid volume using the kinetic models (solid lines) in comparison with the experimental results (marks) for AAS material

Figure VI-11 presents the modeled and experimental cumulative amounts of sulfate and thiosulfate in the liquid solution for high sulfur material CSAG (~ 13.70 wt.% SO_3).

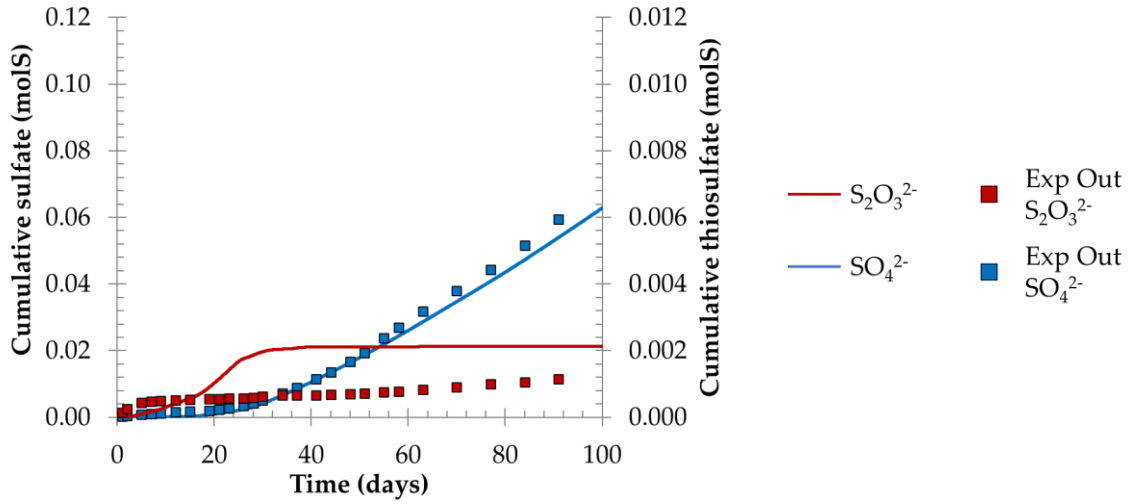

Figure VI-11. Cumulative amount of sulfate and thiosulfate in the liquid volume using the kinetic models (solid lines) in comparison with the experimental results (marks) for CSAG material

The modelling of the evolution of cumulative sulfate was very similar to the experimental results (Figure VI-11). However, starting from 60 days, the experimental data showed slightly higher amounts of sulfate in the solution, which could represent a part of sulfate provided by the dissolution of sulfate-bearing phases from the cementitious matrix during the biodeterioration phenomena.

In the next section, a focus on the contribution of the initial sulfur, present inside the cement materials, to the sulfate concentration in the solution, in particular in the early days of the exposure of CSA-based materials to the BAC test. The cumulative amount of sulfate and thiosulfate for the other tested materials are presented in **Appendix VI-C**.

6.4.2.4. Cumulative amount of sulfate in the first days of exposure, bioproduction of sulfate and sulfate released from the cementitious materials

Figure VI-12 presents the experimental and modeled cumulative amount of sulfate for CAC and CSA materials (CSAC, CSAA and CSAG) during the first 20 days of exposure.

As described in chapter IV (section 4.3.2.1), the sulfate concentrations were higher for CSA materials than for CAC material during the first days of exposure. Such behavior was probably due to the high initial sulfur amount in CSA materials and the reactivity of mineralogical phases, e.g. AFt, AFm, gypsum and anhydrite, while CAC material contained very low initial sulfur (< 1 wt.% of SO_3). Therefore, since the amount of sulfur was negligeable in CAC, the sulfate concentrations in the early days of exposure of CAC could be linked to the development of biological activities on its surface.

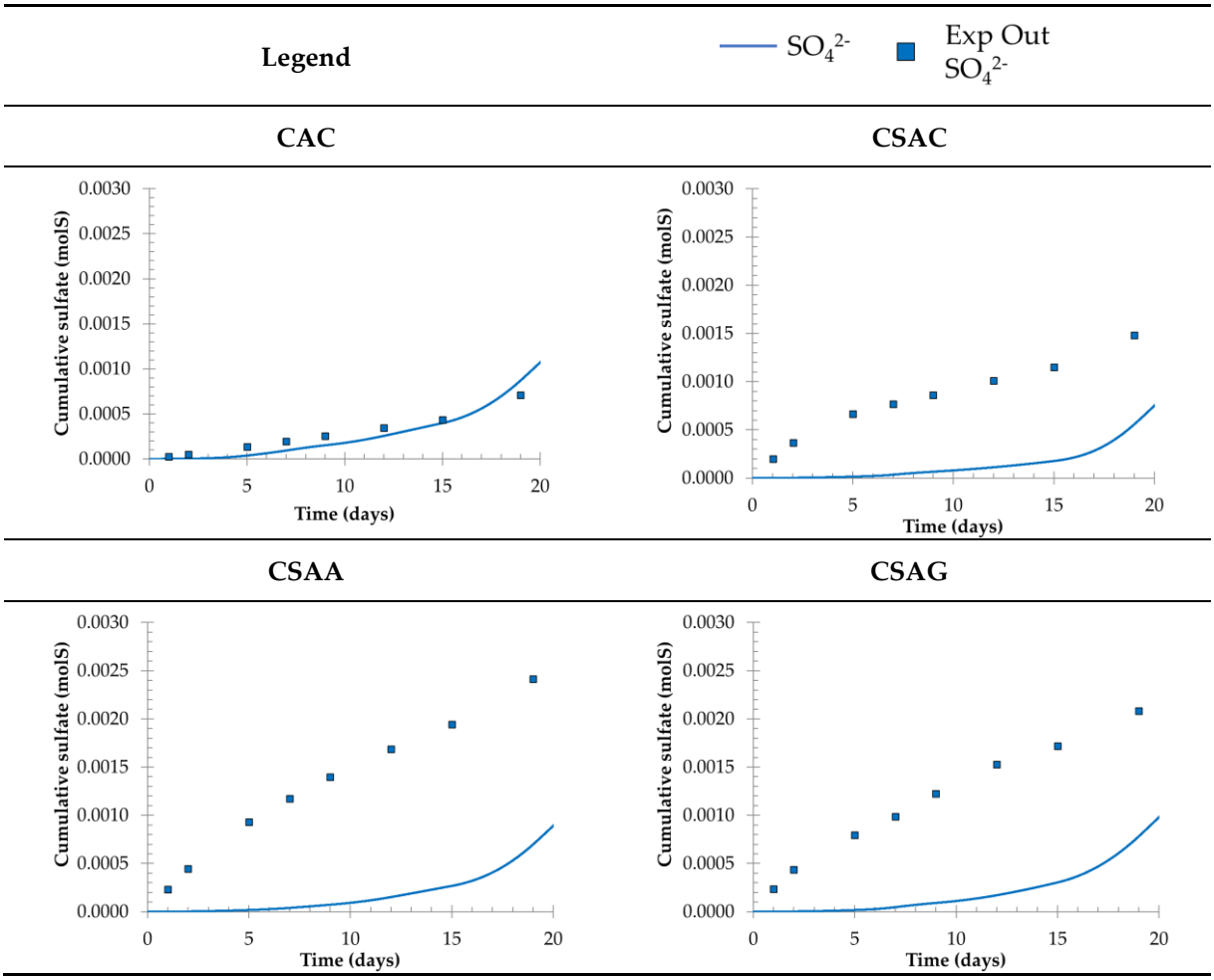

Figure VI-12. Cumulative amount of sulfate in the liquid volume using the kinetic models (solid lines) in comparison to the experimental results (marks) for CAC, CSAC CSAA and CSAG materials for the first 20 days

The proposed kinetic model estimated accurately the cumulative amount of sulfate biologically produced in the leached solution for CAC material. However, by comparing the experimental data and the kinetic models for CSA materials in the first 20 days, a significant

difference was observed. It was linked to the amount of sulfate released from the different cementitious matrices. Moreover, since the amount of sulfate biologically produced in the early days of the test was very similar for all materials (depending on the evolution of pH), the cumulative amount of sulfate was slightly different for the CSA materials and was correlated to their initial sulfur content. For instance, CSAC contained the lowest amount of sulfur among the CSA materials and also showed the lowest amount of cumulative sulfate at 20 days (1.5 mmolS-SO_4). CSAA presented slightly higher cumulative sulfate (2.4 mmolS-SO_4) compared to CSAG (2.1 mmolS-SO_4) since it contained slightly higher initial sulfur content.

In addition, on the one hand, the sulfur in CSAC was mainly bound to hydrated phases, principally monosulfoaluminate, with no residual anhydrous phases containing sulfur. On the other hand, residual ye'elimite ($C_4A_3\check{S}$), anhydrite ($C\check{S}$) and gypsum ($C\check{S}H_2$) were detected in CSAA and CSAG and are susceptible to release sulfate in the pore solution during the biodeterioration phenomena in saturated conditions.

Figure VI-13 presents the difference between the experimental and the modeled cumulative amount of sulfate after 19 days of exposure as a function of the initial SO_3 content for all exposed materials during campaign n°4. This difference, corresponding the estimated amount of cumulative sulfate released from the different materials, was clearly linked to the initial sulfur content in the materials, except for AASB and AASH.

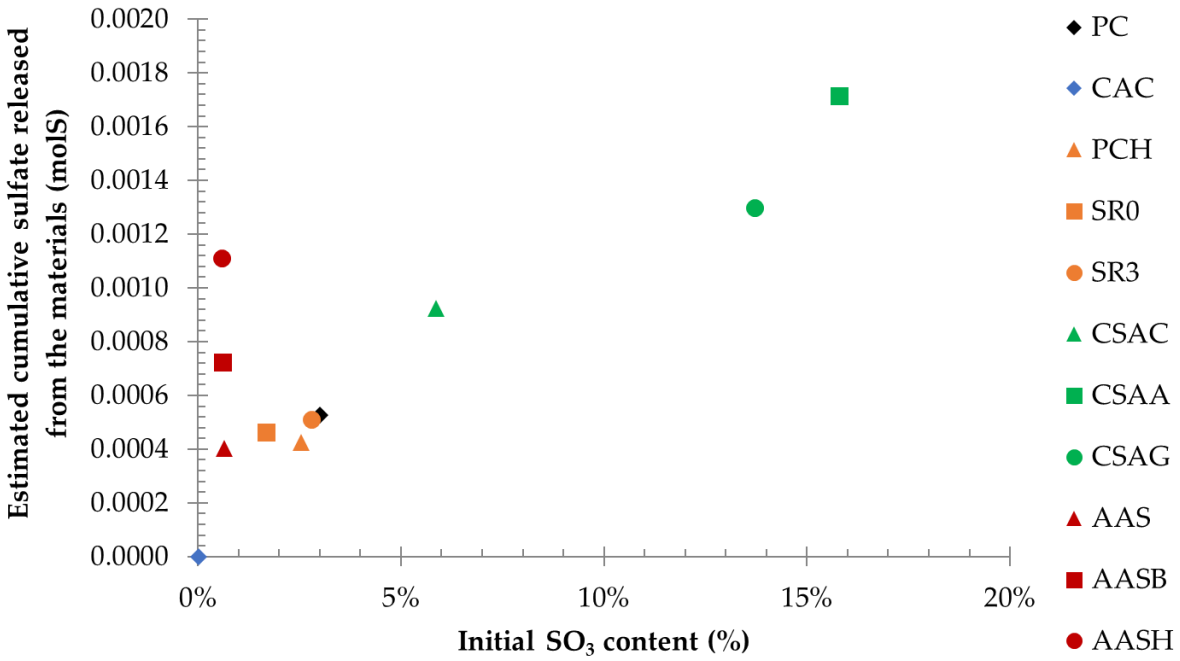

Figure VI-13. Estimated cumulative sulfate released from the materials at day 19 for all materials exposed to the BAC test in campaign n°4 as a function of their initial SO_3 content

Except for AASB and AASH, the kinetics models seemed to represent efficiently the transformation of sulfur species on the surface of the materials, confirming the non-influence of the nature of the material (except on the evolution of pH) on the biological activities, in particular sulfur-oxidizing ones.

In the case of AASB and AASH, such materials, which contained specific mineral additives (bauxite and HardCem, respectively), showed high amounts of sulfate in the leached solutions with low amount of initial sulfur content. While there is still no clear conclusion on the particular behavior, some hypothesis could be drawn:

- In chapter III, the results of the identification of the microbial populations at the end of the exposure period showed the presence of specific microbial species (*Acidithiobacillus Ferrooxidans)* on AASB and AASH materials. However, such species were also detected on CSAC materials. The incorporation of bauxite and HardCem (both rich in iron) might have influenced the selection of the consortia and led to higher production of sulfuric acid compared to the other materials.
- In chapter V, the microstructure observations showed the relatively bigger and rougher aspect of the mineral additives (bauxite and HardCem). Moreover, the chemical analyses showed very little, if no, participation of bauxite and HardCem to the hydration of the binder. Therefore, these properties could have led to less cohesion between the additives aggregates and the hydrated paste, easing the propagation of cracks within the matrix. Such cracks, combined with the cracks resulting from the shrinkage of the hydrated paste due to the severe attack, were relatively large; thus, facilitating the diffusion of sulfate from deeper zones to the outside of the matrix.
- In chapter II, the measurement of the physical properties of AAS-based materials showed that the initial porosity was significantly higher than that of the other materials (up to twice as high as that of the CAC material). The high porosity of the matrix leads to different diffusion properties which contribute greatly to the biodeterioration in the BAC test conditions in the early days of the testing period when the biological acid production was still relatively low [67].

6.4.2.5. Conclusion on the model of the sulfur transformation and the sulfuric acid biologically produced

A simple kinetic model composed of five reactions was proposed to represent the fate of sulfur compounds during the transformation of tetrathionate in a liquid medium in contact with cementitious materials. The model, which only depended on the time of exposure, pH and concentrations of the different sulfur species allowed simulating the evolution and the production of sulfuric acid within a complex biofilm.

The proposed model, validated on various cement materials with different chemical and mineralogical nature, seemed to represent fairly well the biochemical conversion of tetrathionate and the production of sulfuric acid. While the amount of thiosulfate is insignificant in the final mass balance of tetrathionate conversion, its representation by the model needs to be further improved, in particular in the first few days of the exposure. Moreover, the model allowed to estimate the amount of sulfate biologically produced; thus,

identifying the amount of sulfate released by the materials, especially in the first days of the exposure period.

The fate of sulfur for materials with additions of bauxite and HardCem was not clear, with pending questions regarding the specific selected microbial populations, the chemistry of the materials and the initial porosity and/or the high cracking potential of the matrix.

In the end, the proposed model based on chemical kinetic equations with specific conditions of pH and concentrations could be adapted for HYTEC® software to obtain a more complete model representing the biological phenomena on the surface of the materials as well as the evolution of the chemical and mineralogical composition of the cementitious binders during the biodeterioration phenomena.

6.5. CONCLUSION

The construction of a 1D numerical tool permitted to save considerable time of calculation while representing the same phenomena as observed in a 2D configuration. This was essentially due to the very short residence time of the solution on the surface of the simulated materials and the attack of cementitious materials by chemical sulfuric acid can be considered the same at all points on the surface of the material; therefore, the attack can be considered unidirectional towards the core of the specimen because of the flow gradient in the attack with respect to the specimen's length.

Coupling the transport phenomena with a geochemistry model, based on a robust thermodynamic database, allowed evaluating the evolution of the mineralogical phases of these materials during the attack. Moreover, the quantification of the leached cations (calcium and aluminum) at the outlet of the simulated specimens led to identify the leaching kinetics of the materials.

In both conditions (pH 3 and 1), the relative amount of calcium leached from CAC was higher than from PC, which was not in accordance with the experimental results, obtained in field and in laboratory conditions. This behavior might be linked to the particular interactions of CAC matrices with the biofilm in sewer conditions.

Under moderately acidic conditions (pH 3), the simulations showed a very good representation of sulfuric acid attacks on CAC and PC materials. Dissolution of calcium-bearing phases, such as CH and C-S-H for PC paste and C_3AH_6 for CAC paste, has been identified as the predominant mechanism during the attack at pH 3. Ettringite has been detected in deteriorated areas near the surface of the two materials and the absence of gypsum formation under these conditions has been noted. Although, ettringite was little or not observed in experimental conditions which raised questions about the attacking mode and the representativeness of the model.

In addition, for CAC material, the attack at pH 3 resulted in favorable conditions for the precipitation of AH_3 from dissolution of C_3AH_6. The chemical stability of AH_3 at this pH

protected the material by reducing the porosity of the deteriorated areas, thus reducing the penetration of sulfuric acid, decreasing the intensity of the attack and improving the resistance to sulfuric acid attack.

Under highly acidic conditions (pH 1), Both materials suffered from very severe deteriorations, leading to the total dissolution of the cement paste on thickness of 200 μm for PC and 600 μm for CAC. For CAC, these conditions led to the dissolution of AH_3 in the outer part of the deteriorated zones which was not enough to neutralize the acid over 100 days of exposure. Moreover, the dissolution of AH_3 led to a significant release of aluminum compared to the exposure conditions at pH 3. The PC paste has suffered from of the dissolution of CH and C-S-H leading to the complete leaching of calcium and the formation of a silica gel in the outer layer which was also systematically found on PC cement in sewer conditions [49,67,68].

Additionally, high amounts of gypsum and ettringite were detected for CAC while gypsum was the main mineralogical form in which sulfate precipitated for PC. For both materials, the amounts of precipitated ettringite were correlated to the concentration of aluminum in the interstitial solutions, to the migration of the aqueous aluminum through the porosity towards the inner or the outer part of the specimen and to the pH conditions which needed to be relatively high (> 10.6) for ettringite precipitation. The high amounts of ettringite in CAC was essentially due to its very high initial amounts of aluminum compared to PC and to the dissolution of AH_3 which created more porosity in the severely deteriorated zones.

In terms of porosity, gypsum formation has been correlated with decreased porosity of deteriorated areas in PC cement. Similarly, AH_3 and ettringite had the same effect but with more impact on porosity (complete clogging of porosity). However, in experimental conditions, the precipitation of ettringite is accompanied by the formation of cracks (the mechanical aspect was not taken into account in this model), which increases the porosity and allows the acid to penetrate more deeply.

The pH conditions at the inner parts of the deteriorated zones were between 3 and 4 which permitted the precipitation of AH_3 in CAC material. However, as the deterioration progressed, the pH decreased below 3 and the AH_3 was dissolved. Three zones were identified as a function of the pH for CAC: sound zone with relatively high pH, moderately deteriorated zone with pH between 3 and 4 and highly deteriorated zone with pH < 3. Contrarily to AH_3, precipitations of gypsum were not linked to pH conditions (related only to the oversaturation of the pore solution with calcium and sulfate in respect with gypsum formation). Therefore, the sharp drop in pH observed between the sound zone (relatively alkaline pH) and the deterioration zone (< 3) for PC material.

Finally, the chemical model could not represent the attack by biogenic sulfuric acid on PC and CAC as identified in this work and as reported in the literature. In experimental conditions, PC-based materials suffered more deterioration than CAC ones in terms of calcium release and in terms of microstructure changes. Hence, in order to better represent these phenomena,

it was necessary to reproduce the same attack conditions encountered in the networks (evolution in pH, change in the concentration of acid and sulfate).

The results from Chapter III of this work have identified five chemical reactions capable of representing the impact of the evolution of a biofilm on the surface of the material in terms of transformation of sulfur species and acid production. These reactions evolve over time (kinetic equations) and are a function of the pH evolution. Thus, they mimic the production of sulfuric acid by the SOBs (neutrophil and acidophil).

The validation of the pseudo-biological model was carried out using Aquasim software in which the incorporation of such equations was easier. The first results validated the model on PC and CAC materials which are simple (without mineral additives) and conventional (well-studied cement phases) materials. The model represented very well the transformation of tetrathionate (with a little less precision on the evolution of thiosulfate) as well as the production of biogenic sulfuric acid. In addition, the estimation of the amount of sulfate resulting from microbial activity allowed the evaluation of the amounts of sulfate released from the cementitious matrix, in particular for materials initially rich in sulfate such as calcium sulfoaluminate cement and supersulfated cement.

General conclusions and perspectives

General conclusions and perspectives

During the service life of concrete structures in sewer networks, concrete undergoes both chemical and biological deteriorations. The cementitious material is exposed to the atmospheric air, containing carbon dioxide and hydrogen sulfide. These two compounds react with the cement matrix to induce a decrease in pH. Microorganisms capable of growing on the sulfur substrate develop and produce sulfuric acid on the surface of the cementitious material, causing severe deterioration of the matrix and, in some cases, its complete disintegration.

The main objectives of this study were:

(i) Developing an overall performance indicator allowing the comparison of a wide variety of binders, exposed to biogenic acid attack in laboratory conditions using a biological test (the BAC test).

(ii) Studying the behavior and the deterioration mechanisms of various low-CO_2 cementitious materials (calcium sulfoaluminate cement and alkali-activated slag) exposed to microbial attack in sewer conditions.

(iii) Assessing the impact of partially substituting Portland cement with mineral additives, rich in aluminum and/or iron, on the durability of the materials.

(iv) Understanding the interaction mechanisms between the cement matrix and the microorganisms.

(v) Optimizing a numerical model, based on coupling the chemistry of materials and the transport of species in solution, by including the biological transformations of sulfur species.

The literature review has identified several parameters influencing the biodeterioration phenomena of cementitious materials in sewer environments. Among these parameters, the pH of the medium, the temperature, the relative humidity, the wastewater flow and the slope of the structure are critical environmental parameters. However, the physico-chemical characteristics of the cement-based materials were identified as key factors in the durability of concrete-based structure exposed to sewer conditions.

The in-depth review of the reaction pathways of sulfur species redox phenomena highlighted the ability of microorganisms to disproportionate sulfur species depending on the evolution of the environmental conditions, in particular the pH.

A summary of several field studies was carried out in order to assess the performance and the resistance of materials mainly based on Portland cement and calcium aluminate cement against biological attacks in such conditions. The overall conclusion of these studies has attributed the better performance of calcium aluminate cement to: (i) the potential inhibitory effect of aluminum released by the cement matrix on the microbial activity; (ii) the higher chemical stability of AH_3 phase in acidic conditions compared to calcium-bearing phases; (iii) the secondary formation of more AH_3 due to the dissolution of calcium aluminate phases (e.g.

C_3AH_6). In addition, the main durability indicator used in field studies was the mass variations of the specimens; however, mass measurements could be misleading as secondary precipitation could take place, thus masking the real deterioration of samples. Finally, these studies showed that there was a major lack of data on the durability of other types of cementitious binders in such environments.

A thorough investigation was done on the potential characteristics and properties of various binders (calcium aluminate cement, Portland cement, Portland cement with mineral additives, calcium sulfoaluminate cement and alkali-activated materials) which could improve their durability against acid attack. Partially substituting Portland cement with mineral additives (such as blast furnace slag, fly ash or silica fume) appeared to be beneficial to the durability of the materials. Calcium sulfoaluminate cement showed good resistance, in particular through its aluminum-bearing phases, to sulfate attacks and to certain acid attacks. Finally, alkali-activated materials were reported to have a very good resistance to sulfuric acid attack, considering their different chemical and mineralogical composition, in particular the slightly higher resistance of C-A-S-H and to the absence of C_3A, susceptible to react with sulfate to form expansive secondary phases, e.g. gypsum and/or ettringite.

Finally, due to the relatively long time associated with experiments, carried out in field conditions (several years) and in laboratory conditions (several months to several years), the modeling of the biodeterioration phenomena was a subject of interest of several studies. However, the major obstacle remained in having a model incorporating transfer phenomena in a porous medium, a complete and robust database on the different mineralogical phases of a cementitious material, the evolution of the chemistry of the medium (aggressive solution and material) and finally, a representation of a biofilm evolving over time.

The literature review has raised some points which were further be investigated in this study:

(i) The need for a reliable and robust durability indicator which considers the different physico-chemical characteristics of the cement-based materials and which allows to compare different materials in terms of performance.

(ii) The behavior and the deterioration mechanisms of calcium sulfoaluminate cement and alkali-activated slag in sewer conditions are not very well documented in the literature.

(iii) The nature of the impact of aluminum on the durability of materials (aluminum mobility in solution, inhibitory effect on microbial activity, chemical resistance of the aluminous phases to acid attack) is still not very well understood.

(iv) The role of iron in the behavior of cementitious materials and the influence of the chemical resistance of iron-bearing phases in the overall durability of the materials, knowing that these phases favor the growth of other types of bacteria capable of accelerating the deterioration process.

(v) The absence of a biochemical reactive-transport model considering the biological component and its evolution over time.

A study strategy was established in order to answer the questions raised by the literature review. Thus, this work was based on a multidisciplinary investigation of a large panel of cementitious materials exposed to biodeterioration in laboratory conditions.

Studied materials and protocol of biodeterioration testing

These selected materials were:

(i) Two reference cements: Portland cement (PC) and calcium aluminate cement (CAC).
(ii) A Portland cement with Fe-rich mineral additives (PCH).
(iii) Two Portland cements recommended in the European Standard for the exposure of structures in environments with chemical aggression: SR0 and SR3.
(iv) Three types of calcium sulfoaluminate binders: calcium sulfoaluminate clinker (CSAC), calcium sulfoaluminate clinker with anhydrite (CSAA) and calcium sulfoaluminate clinker with gypsum (CSAG)
(v) Three types of calcium sulfoaluminate binders: alkali-activated slag (AAS), alkali-activated slag with bauxite (AASB) and alkali-activated slag with Fe-rich mineral additives (AASH)

The cementitious specimens were inoculated with activated sludge, and then were exposed to a continuous solution containing tetrathionate ($S_4O_6^{2-}$) as a reduced sulfur source and nutrients which were necessary for the development of the biofilm. The selection of sulfur-oxidizing bacteria occurred naturally and the microbial activity were developed on the exposed surface of the cementitious materials. During the 3 months of exposure of each experimental campaign, the leached solutions downstream of the samples were collected and analyzed in terms of pH, concentrations of sulfates and polythionates, and concentrations of leached cementitious cations, such as calcium, aluminum, iron, magnesium, sodium and potassium.

The study of the behavior of the different materials was carried out in 2 stages: (i) monitoring of the liquid phase (leached solutions) during exposure to the BAC test; and (ii) analysis of the microstructure of the cementitious materials, as well as identification and location of microbial population developed on the samples, after exposure.

The analyses of the leached solutions made it possible to compare the performance of the studied materials to those of the reference material (PC). This comparison was made using the optimized performance indicator (PIeqOH) which was based on the amount of hydroxide ions linked to the leaching of the five major elements of a cement matrix (calcium, aluminum, iron, magnesium and sulfate) which are released by the dissolution of the mineralogical phases during the biogenic acid attack process.

Transformations of tetrathionate by sulfur-oxidizing bacteria in sewer conditions

The study of the transformation of tetrathionate in sewer conditions was carried out by investigating the different reaction pathways of tetrathionate conversion. Moreover, this study investigated the influence of the nature of different types of cementitious materials (SR0, SR3, CAC, CSAA and AAS) on the transformation of tetrathionate. The results showed that the cementitious materials did not have a direct influence on these transformations other than their participation in the evolution of the pH of the leached solution. Tetrathionate was converted into thiosulfate and sulfate in alkaline conditions while in acidic conditions, tetrathionate was disproportionated and produced thiosulfate, pentathionate, hexathionate, sulfate and elemental sulfur. In addition, the study of tetrathionate transformation led to the development of an empirical model to quantify the amount of sulfate and acid, produced by the microbial activity, which were in direct contact with the exposed surface of the material. Thus, this model made it possible to separate the sulfate released from the material (especially from sulfate-rich materials, such as CSA-based materials) and the sulfate produced from the biological transformation of the tetrathionate. Furthermore, DNA sequencing of the biofilm, collected after 3 months of exposure of the specimens to the accelerated biodeterioration test, highlighted the presence of mainly *Acidithiobacillus* and *Thiomonas* species. *Acidithiobacillus* species are sulfur-oxidizing species found systematically in the sewer while *Thiomonas* species are known for their ability to disproportionate tetrathionates.

Performance of calcium sulfoaluminate cement in sewer-like environments

CSA-based materials showed equivalent or even slightly better performance than Portland cement. The PIeqOH for CSAC, CSAA and CSAG were 135, 89 and 124% respectively while it was 100 and 233% for PC and CAC respectively. The study of the leached solutions showed that the evolution of the aluminum concentrations was similar to that of CAC in alkaline and in acidic conditions. However, by standardizing the aluminum concentrations to the initial amount of aluminum in the binder, CSA materials released 2 to 3 times more aluminum than CAC.

Overall, the dissolution of ettringite and/or AFm phases (monosulfoaluminate and monocarboaluminate) and the formation of aluminosilicate and AH_3 gel on the surface were the two main deterioration mechanisms of CSA-based materials. Moreover, the addition of gypsum instead of anhydrite to the calcium aluminate clinker seemed to improve its resistance. However, while the absence of calcium sulfate led to the formation of only AFm phases, higher amounts of AH_3 was formed in CSAC than in CSAA and CSAG. This could be linked to a better hydration process as the ye'elimite was totally consumed during hydration.

The comparison of the deteriorated layers of CSA and of CAC materials showed that the precipitation of high-resistant aluminum-bearing phases, i.e. AH_3, for both systems, was in the form of gibbsite despite that AH_3 was initially amorphous in the CSA hydrated binders. The mineralogical nature of AH_3 could partially account for the difference in performance between these two materials, in particular with respect to the chemical stability which was relatively

lower for amorphous AH_3 than for crystallized AH_3. Moreover, higher quantities of AH_3 were formed in the deteriorated layers of CAC material than in those of CSA-based materials, which could also explain the lower performance of CSA materials compared to CAC.

- **Perspectives**

The results of this work and the literature showed that a high initial concentration of AH_3 is favorable to the resistance of cement-based materials to a biogenic acid attack in sewer conditions. The initial amount of AH_3 and the possibility of its formation during the attack for CAC can partially explain its higher resistance than CSA. However, despite the lower performance of CSA compared to CAC, CSA binders present interesting durability performances. Industrially, a life-cycle assessment should be performed for CSA, and compared to that of CAC, in order to evaluate its applicability and the potential gain of its use. Scientifically, it is important to note that different forms of AH_3 can be produced during biodeterioration phenomena. Today, the role and the reasons for the formation of different polymorphs of AH_3 is still to be fully understood.

Moreover, the studied CSA binders were prepared with a relatively low w/b ratio for such materials, which might have led to non-optimized hydration conditions, in particular for binders with calcium sulfate (CSAA and CSAG). Additionally, a poor hydration process could lead to higher porosity and, thus, increase the diffusivity of the material, which in turn could accelerate the deterioration process. In this perspective, the necessity of optimizing the hydration process of these binders in terms of w/b ratio, percentage of added calcium sulfate and curing protocol is stressed here

On the other hand, few information was found in the literature about the transformation of ettringite and monosulfoaluminate, in particular the mechanisms of their dissolution in sewer conditions. The formation of additional AH_3 was identified in this study; however, the mechanism of its formation and the quantification of the precipitated amount, relatively to the dissolution of ettringite and monosulfoaluminate, still need to be further investigated. Therefore, studying the deterioration of synthetic ettringite and AFm phases by biogenic sulfuric acid would be an interesting brick in the understanding of their behavior.

Resistance of alkali-activated slag to biogenic sulfuric acid attack

Alkali-activated materials (AAS, AASB and AASH) showed a strong alkalization of the leached solution, which was linked to the release of the alkalis used for the activation of the slag. Upon the total leaching of the alkalis from the pore solution, the drop of the pH from alkaline to acid conditions induced higher kinetics of calcium release into the leaching solution than the other materials. The PIeqOH for AAS, AASB and AASH were 78, 68 and 85% respectively.

The microstructure of alkali-activated slag materials showed wide vertical cracks, connected to the exposed surface. These cracks were linked to the strong decalcification and the release

of aluminum from the C-A-S-H phases which caused a significant shrinkage in the cementitious matrix. Moreover, the penetration of bacteria through the cracks and the severe decalcification of the matrix around these cracks suggested that acid was also produced inside the matrix by the microbial activity. The residual anhydrous slag did not resist to the acid attack. In contrast with PC-based materials, the precipitation of ettringite or gypsum was not observed, probably due to the wide cracks which might have facilitated the leaching of the cementitious cations outside the matrix and kept the poral solution undersaturated in regard to the precipitation of these two phases.

- **Perspectives**

The curing of AAS-based materials is very important to achieve a proper hydration process. While the curing period was set at 1 months for all materials in this study, AAS-based materials need at least 2 more months to obtain comparable mechanical strength to PC material. In addition, the absence of a thermal curing also slowed down the hydration of the slag and resulted in high amounts of anhydrous slag in the hydrated paste.

Moreover, tests on mortars/concretes would be interesting for all materials, and for the AAS-based materials in particular, to evaluate the performances of such mix designs in terms of rheology, shrinkage/expansion, mechanical resistance, porosity and the nature of the aggregates and their reactivity with the acid, and particle size distribution.

Furthermore, AAS materials contain higher amounts of aluminum than in PC materials. The aluminum is mainly incorporated in C-A-S-H phases. However, the dissolution of C-A-S-H does not form any AH_3. Therefore, there is a need to unveil the fate of aluminum released from C-A-S-H in AAS systems. The investigation could be carried out using μ-Raman technique to determine the possible evolution of the Al-bearing mineralogical phases and by aluminum (^{27}Al) Nuclear Magnetic Resonance (NMR) to study the environment of aluminum in the deteriorated layers.

Aluminum and iron influence on the deterioration mechanisms of cementitious materials exposed to sewer conditions

The study of the evolution of aluminum concentrations in the leached solutions for CAC, CSAC, CSAA, CSAG and AASB showed that the resistance of the materials to the biogenic acid attack was not improved by increasing the initial aluminum content with non-reactive aluminum rich additives, which confirmed previous results in the literature. The use of a non-reactive aluminum source, such as bauxite, did not improve the resistance of the material since aluminum remained unavailable to form hydrated aluminum-bearing phases, e.g. AH_3. However, microstructural analyses showed that the majority of bauxite grains in the deteriorated layers of AASB was mainly composed of aluminum. This suggested that the acid attack on bauxite grains consisted of leaching iron firstly followed by a progressive dissolution of the grains.

Iron (in the form of HardCem or C_4AF) was shown to remain inert during the hydration of the cementitious materials. The study of the evolution of iron concentrations in the leached solutions for PCH, SR0, SR3 and AASH showed that iron did not have a significant influence on the microbial activity. Moreover, HardCem was dissolved in high acidic conditions (pH < 5) and led to the release of high amounts of iron in the leached solution. However, the high quantities of iron did not densify the deteriorated layers.

The dissolution of HardCem did not result in the formation of Fe-rich phases in the deteriorated zones. Residual C_4AF was often found in the highly deteriorated zones, which confirmed its good resistance to the acid attack. However, no specific influence of the presence of iron was to be concluded.

- **Perspectives**

While the increase in the aluminum content by inert mineral additives did not seem to improve the resistance of the materials to the biogenic attack, other sources of aluminum could be considered (e.g. metakaolin). There is little information about the attack of acid-activated metakaolin, especially on the transport properties and the life-cycle assessment. Even if the application of such material today is not considered, the study of the resistance of its hydration products could be of interest in the understanding of the deterioration mechanisms of aluminum-bearing phases.

The results of this thesis did not show any significant increase in the durability of the materials that could be linked to iron. Today, the literature is still unclear about the role of iron. Iron was linked to improved durability through a negative impact on the microbial activity [174] while a decrease in the durability was also reported to be linked to an influence of iron on certain microbial metabolisms [48]. The experiments in this project showed the development of specific populations on certain materials, without major impact on the production of acid and/or on the deterioration of cement matrices, in the experimental conditions.

Further experiments could be performed on materials enriched in iron (different contents and different mineralogical forms) to investigate the development of specific populations inside the materials. To carry out this type of study and to clearly investigate the possibilities of iron enrichment on the performance of materials, it seems important to analyze the incorporation of iron and its participation to the hydration process of the cementitious materials.

Modeling of the biodeterioration phenomena

A reactive-transport model (using HYTEC software) was used to simulate, in the BAC test configuration, the attack by sulfuric acid (at pH 3 and at pH 1) on PC and CAC pastes without considering the microbial activity. This model presented several drawbacks by comparing its results with the experimental results from the BAC test campaigns. The model showed that the standardized leached calcium of CAC paste was higher than that of PC paste at pH 3 and 1 while the experimental results showed the opposite. Moreover, at pH 3, the deterioration of

PC paste was less aggressive than that observed in real conditions, particularly the absence of gypsum and silica gel precipitates on the surface. Additionally, the formation of ettringite that was observed in the CAC simulations was not identified during microstructural observations on samples exposed to the BAC test. Furthermore, at pH 1, CAC showed more severe deteriorations than that observed for PC, including precipitation of very high amounts of ettringite and AH_3 at the interface between sound core and deteriorated zones. Such precipitates completely clogged the porosity, thus stopped the diffusion of sulfuric acid to deeper zones. In the objective of improving the modeling of biodeterioration phenomena, a model based on kinetic equations was developed and was validated on cementitious materials of different compositions (using Aquasim software) to integrate a part simulating the influence of the bacterial activity on the deterioration process into a reactive-transport model. This model was based on the study of the transformation of tetrathionate which established a relationship between the change in pH and the amount of sulfuric acid produced, thus evolving the severity of the attack over the exposure time.

- **Perspectives**

The modeling of a biological attack by sulfuric acid on cementitious materials in sewer conditions is far from complete. The work carried out in this project added a significant step towards the construction of a full bio-chemical model. However, several points were identified during this work that require specific attention in order to optimize the model. These points were:

- The modeling in this work was limited to well-known phases, mainly based on calcium and aluminum. However, as the experimental work has shown in the previous chapters, other chemical elements could have an impact, in particular iron, and should be taken into account in the simulations. For example, iron could be found in several mineralogical forms (with different solubility) in a cementitious material or as a mineral additive. Recently, work on improving databases has enriched them with more iron-containing phases, for example 17 phases for the CEMDATA 18 database compared to 9 only for the CEMDATA 14 database [273].
- The simulation of mineral additives was not considered in this work as well. These additives could not only have an impact on the chemical and mineralogical changes of the materials but also on the transport phenomena, through the influence on the evolution of the porosity and/or the apparent diffusion coefficient of the materials.
- The five kinetic reactions, which were developed to represent the transformations of sulfur species during a biological attack on a cementitious material, were tested using the Aquasim software only. Although Aquasim is a robust and proven modeling tool for simulations in aquatic environments, the lack of a coupling with a geochemical database makes it less efficient to model very complex systems in the desired conditions. Therefore, adapting these reaction pathways in the language of HYTEC

could provide a very powerful numerical tool to model the deterioration of cementitious materials in sewer environments.

- Coupling a reactive-transport model with a mechanical model to consider the impact of expansive secondary precipitations on the hardened cement matrix is a way of optimizing further the model. The mechanical model can simulate the cracks which will impact the porosity and the pathways for acid penetration inside the cementitious matrix.
- Finally, the formation of a biofilm on the surface of cementitious materials is not homogeneous and depends on many factors, such as the roughness of the surface, the surface conditions, the preferential pathways of the trickling solutions, the concentration of reduced species and nutrients…etc. The model in its current state simulates the development of the biofilm as a whole and considers it to be homogeneous on the surface. Further work should be carried out to optimize these factors to get even closer to the real the phenomena

Appendices

Appendices

Appendix II-A: Chemical composition of the cement

An adapted protocol from the European standard NF EN 196-2 was used for chemical analyses of cements [292]. The analyses had 3 components: the first component concerned the total elements' content (Si, Al, Ca, Mg, Mn, Fe, Na, K, Ti, P, Cr, Sr, etc.) which was assessed via the fused cast-bead method followed by an acid attack and an analysis by wet chemistry. The concentration of elements was further quantified by ICP-OES. The anhydrous cement was slightly crushed to < 80 µm, and 0.2 g of the powder was put into a vitrified graphite crucible. 1.2 g of lithium borates (25% metaborate – 75% tetraborate) was added to the cement powder and mixed homogenously. The graphite crucible was inserted into a graphite sheath with a cover and was put into a muffle furnace at 1100°C for 30 minutes. The graphite crucible was taken out of the furnace and was put aside for 5 minutes to cool down before inserting a magnetic bar into the crucible. Consequently, the set (crucible + magnetic bar) was put into a solution made of 100 mL of ultrapure water + 5 mL of nitric acid (HNO_3 plasma pure). A continuous stirring using the magnetic bar was carried out until the total dissolution of the beads. Once the beads were completely dissolved, the liquid solutions were filtered, using quantitative adequate filters, into a vial and the volume of solution was completed with ultrapure water until 250 ml. The second component concerned the quantification of oxyanions fluoride, sulfate, nitrate and phosphate in the cementitious matrix, which were quantified via High-Performance Ionic Chromatography (HPIC) in a solution prepared via an acid attack of the cement powder sample, since the analysis of the solution issued from the fused cast-bead attack was too concentrated in lithium. The cement was slightly crushed to < 80 µm and 1 g of the powder was put into a hydrochloric acid solution (95 mL of ultrapure water + 5 mL of HCl Plasma Pure). The mix was boiled during 2 minutes with a continuous stirring using glass spatula. The liquid mix was filtered, using quantitative adequate filters, into a vial and the volume of solution was completed with ultrapure water until 250 ml. The third component concerns the ignition loss, which was carried out following the European Standard NF EN 196-2 (ranking index: P 15-471-2).

Moreover, a reference cement, provided by the Bureau of Analysed Samples LTD (BCS-CRM No.353), the composition of which is certified (British chemical standard certified reference materials), was used systematically to calibrate the analyses. The chemical composition of this reference cement was obtained from 9 independent analysts [293].

Appendix IV-A: Evolution of the pH of two PC specimens from the same experimental campaigns

Figure IV-A-1 presents the evolution of the pH of two specimens made of PC and were exposed to the same conditions of the BAC test at the same time. The acidification time of the leached solution was determined at the day when the measured pH was below pH 4 for the first time. The acidification time of PC-1 was recorded at 28 days compared to 42 days for PC-2. The significant difference (14 days) in acidification time was linked to the development of the microbial activity on the exposed surface. While both specimens were issued from the same formulation batch and were prepared in the same exact conditions, several parameters could be present and impact the growth of the biofilm. For instance, the physical aspect and the roughness degree of the exposed surface have a high influence on the adhesion of the activated sludge. Moreover, the trickling solution on the upstream of the specimens might lead to preferential pathways due to the presence of relatively large fragments of sludge. Such pathways could concentrate the solution in specific directions where the local neutralizing capacity of the material was exhausted; therefore, accelerating the acidification and the development of microbial activities.

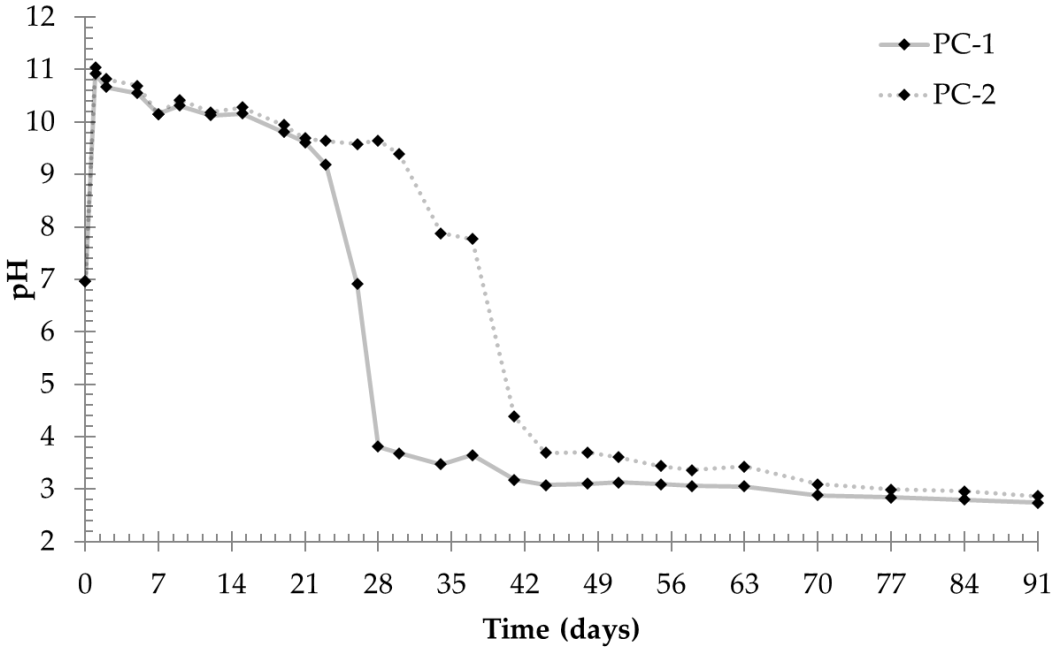

Figure IV-A-1. The evolution of the pH showing the differences between two PC specimens exposed to the same conditions and at the same time in terms of time before acidification

From a technical point of view, the analyses of the leached solutions for specimen PC-1 started before any differences were observed. Therefore, due to the high number of samples to be analyzed using the different techniques, the specimen PC-1 was considered for the rest of the study.

Appendix V-A: Description of the evolution of the chemical and mineralogical composition of PC-based materials exposed to the BAC test for 3 months

Portland Cement + HardCem (PCH)

Figure V-A-1 presents the EDS chemical composition profile of PCH paste specimen (wt.%) exposed to the BAC test for 3 months as a function of the distance to the surface in contact with biofilm, along with the microstructure observation of the specimen in BSE mode. Figure V-A-2 presents the evolution of the mineralogical composition at several depths within the PCH material.

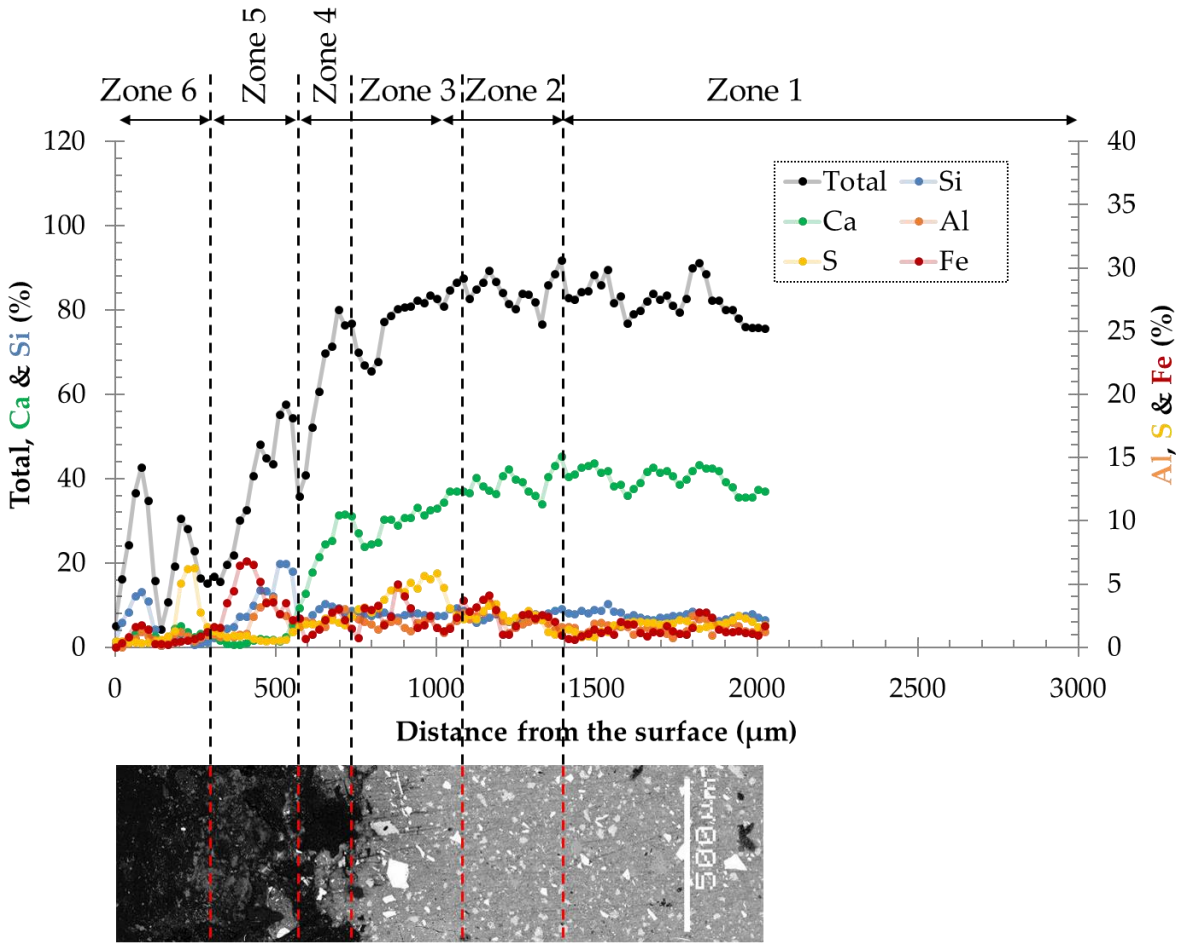

Figure V-A-1. Evolution of the chemical composition of the PCH material exposed to the BAC test for 3 months as a function of the distance from the initial surface of the specimen (at 0 µm) and the SEM observation of the microstructure of the cross-section in BSE mode

The evolution of the chemical composition profile within the PCH cement matrix allowed the identification of five altered zones. The borders of each zone are reported in Figure V-A-1.

- Zone 1 or the sound zone (observed from 1 400 deep) had a Ca/Si ratio similar to that of the PC paste: around 5.32. The XRD analyses did not show any difference in the mineralogical patterns between the PC and the PCH materials in terms of hydrated

crystallized phases. Nevertheless, the HardCem were clearly visible on the microstructure image as large high density (high brightness) grains.

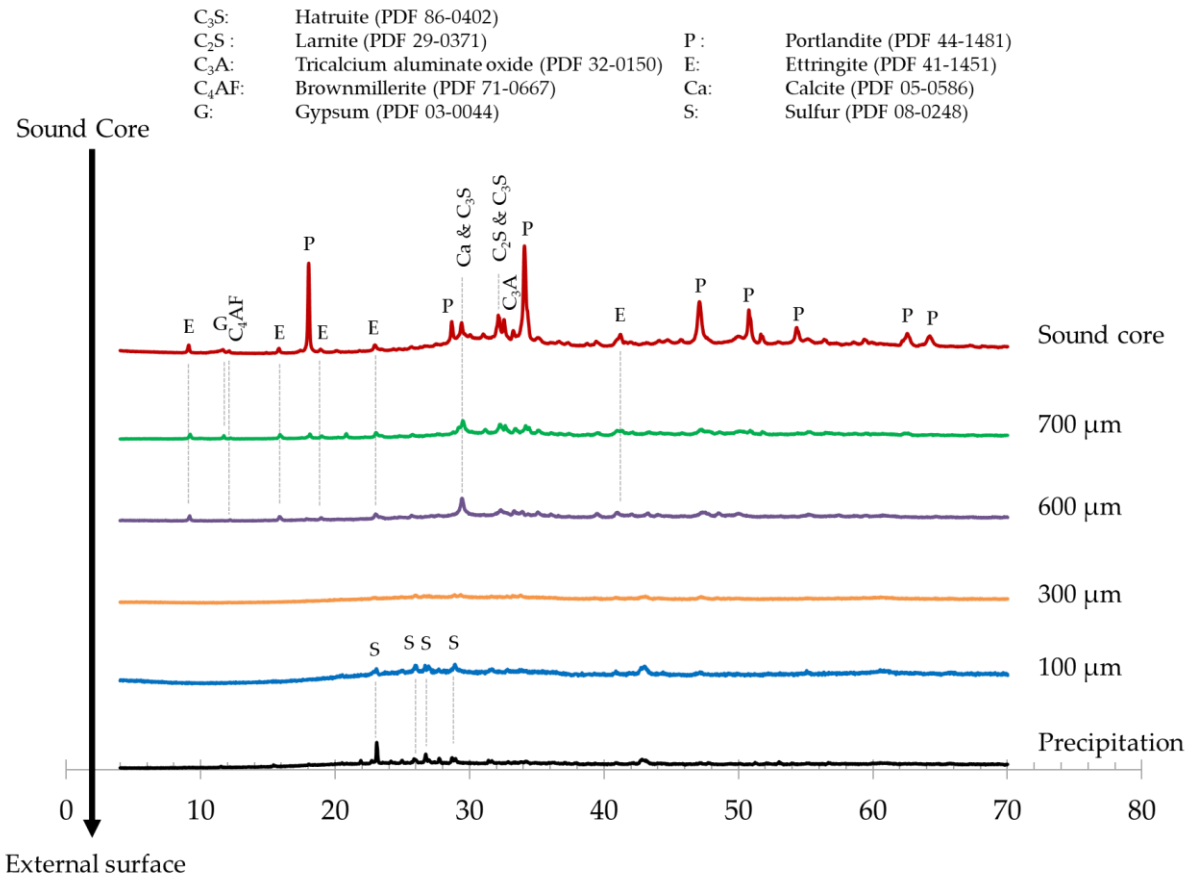

Figure V-A-2. Evolution of the mineralogical composition of the PCH material exposed to the BAC test for 3 months as a function of the distance from the surface of the specimen

- Zone 2, approximately 300 µm of thickness, presents a slight decalcification of the matrix from 45% at the limit with zone 1, to 36%. At the limit with zone 3.
- Zone 3, having a width of 450 µm, showed a higher decalcification of the matrix than in zone 2 with an increase in the sulfur content. The SEM BSE image showed the presence of microcracks in this zone, which could be linked to the precipitation of secondary expansive ettringite. Residual anhydrous grains of the cement and of HardCem were still observed.
- Zone 4, 100 µm-thick of thickness, presented lower density of the cement paste than the previous zones, resulting from the severe decalcification of the matrix (from 30 to 12%). Moreover, the microstructure of the zone was heterogeneous and with high porosity, due to the complete dissolution of the matrix.
- Zone 5 was observed between 300 to 600 µm inside the matrix and presented an increase in silicon (from 5 to 20%) and in iron (from 2 to 7%). The silicon content decreased to 8% and the iron content decreased to 2% at the limit with zone 6. The XRD analyses at 300 µm did not show any crystallized phases, which could suggest a dissolution and precipitation of amorphous iron- and silicon-bearing phases.

- The outer layer, zone 7, was a 300 µm-thick zone with very low density and composed of sulfur and silicon. The XRD analyses indicated the formation of elemental sulfur while the silicon in this zone could be linked to amorphous silica-gel, which was very similar to PC results.

SR0

Figure V-A-3 presents the EDS chemical composition profile of SR0 paste specimen (wt.%) exposed to the BAC test for 3 months as a function of the distance to the surface in contact with biofilm, along with the microstructure observation of the specimen in BSE mode. Figure V-A-4 presents the evolution of the mineralogical composition at several depths within the SR0 material.

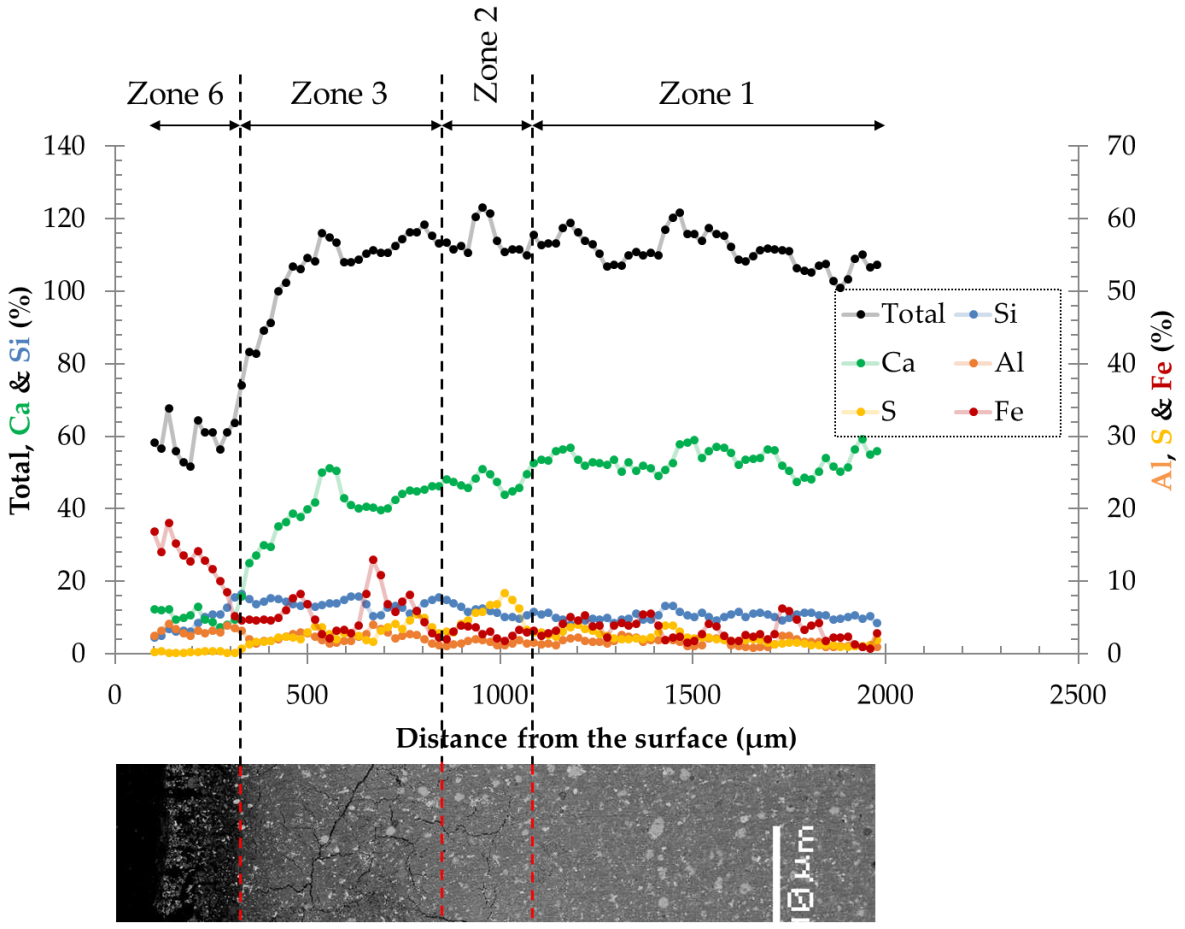

Figure V-A-3. Evolution of the chemical composition of the SR0 material exposed to the BAC test for 3 months as a function of the distance from the initial surface of the specimen (at 0 µm) and the SEM observation of the microstructure of the cross-section in BSE mode

The chemical analyses allowed the identification of three deteriorated zones, which are presented on the elemental profile.

- The sound zone (zone 1) was characterized by the presence of high calcium content (54 %) and lower amounts of silicon (10%), iron (4%), sulfur (2%) and aluminum (2%). The microstructure showed homogenous hydrated cement paste with the presence of

remaining anhydrous particles. The main crystallized phases were portlandite, ettringite, C_3S, C_2S, C_3A and C_4AF.

- A slightly deteriorated zone (zone 2) of 250 µm of thickness, starts at about 1100 µm deep within the cementitious matrix. Zone 2 was slightly decalcified (calcium content dropped from 54 to 48 %) and enriched in sulfur (up to 9%). The decrease in calcium was consistent with the decrease in the intensity of portlandite peaks. Ettringite and gypsum were detected in this zone, explaining the increase in sulfur and the microcracks observed on the microstructure image.

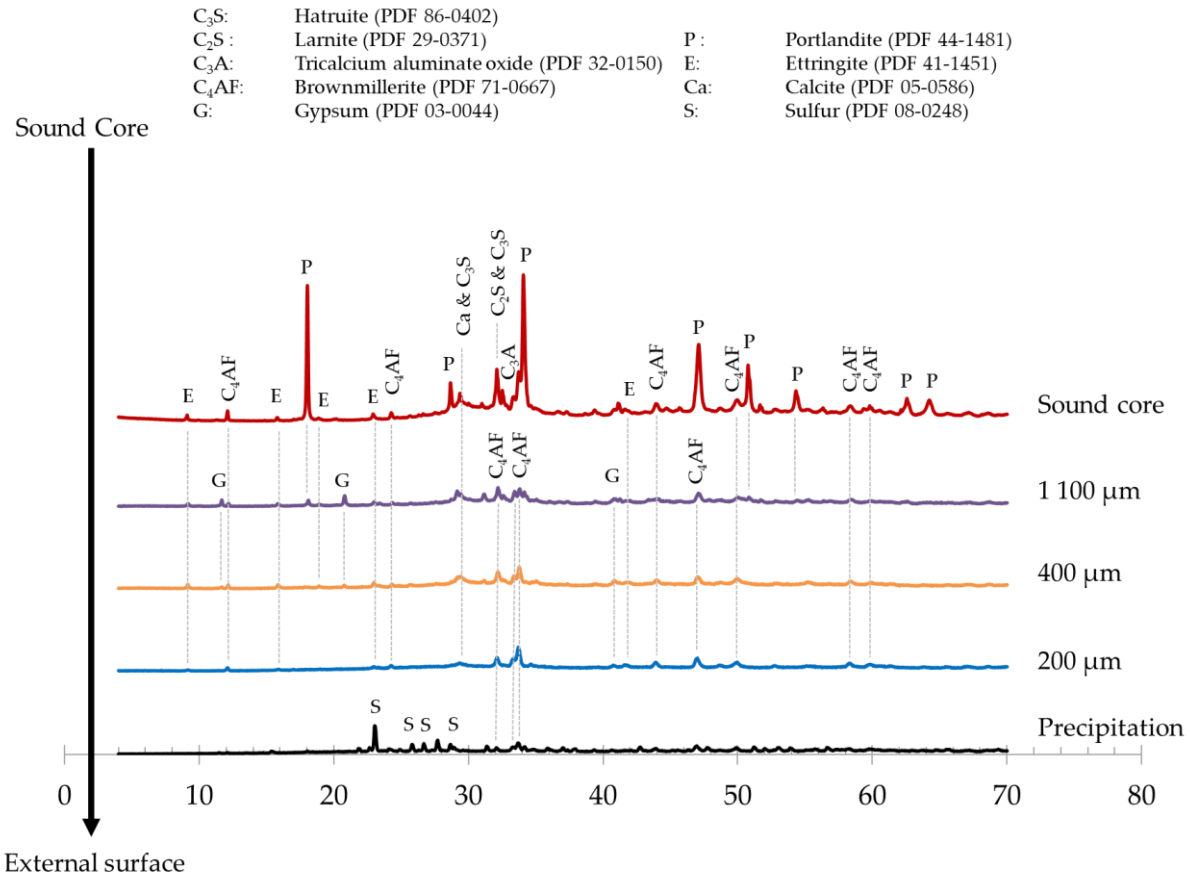

Figure V-A-4. Evolution of the mineralogical composition of the SR0 material exposed to the BAC test for 3 months as a function of the distance from the surface of the specimen

- Zone 3 was identified between a distance of 300 and 850 µm from the initial surface of the material. This zone presented a severe decalcification of the matrix (calcium content dropped from 46 to 10%). The iron content increase from 2 to 13% while silicon and aluminum remained unchanged. Sulfur seemed to decrease going towards the outer part of the zone. The XRD analyses showed the complete disappearance of portlandite. However, ettringite and gypsum were still detected and explained the microcracks as well as the relatively high calcium content.
- Zone 6, 200 µm thick, was a relatively homogenous layer with very low density and presented residual high density (high brightness) anhydrous grains. The chemical composition profile showed high iron content with calcium, aluminum and silica.

While the main crystallized phase identified was C_4AF, the residual anhydrous grains were mainly trapped inside the silica hydrogel.

- Finally, the first 100 µm of the material was completely dissolved and was not observed using the SEM. The microstructural images allowed the estimation of such depth by using the edges (protected with the epoxy resin) as a reference for the initial surface.

SR3

Figure V-A-5 presents the EDS chemical composition profile of SR3 paste specimen (wt.%) exposed to the BAC test for 3 months as a function of the distance to the surface in contact with biofilm, along with the microstructure observation of the specimen in BSE mode. Figure V-A-6 presents the evolution of the mineralogical composition at several depths within the SR3 material.

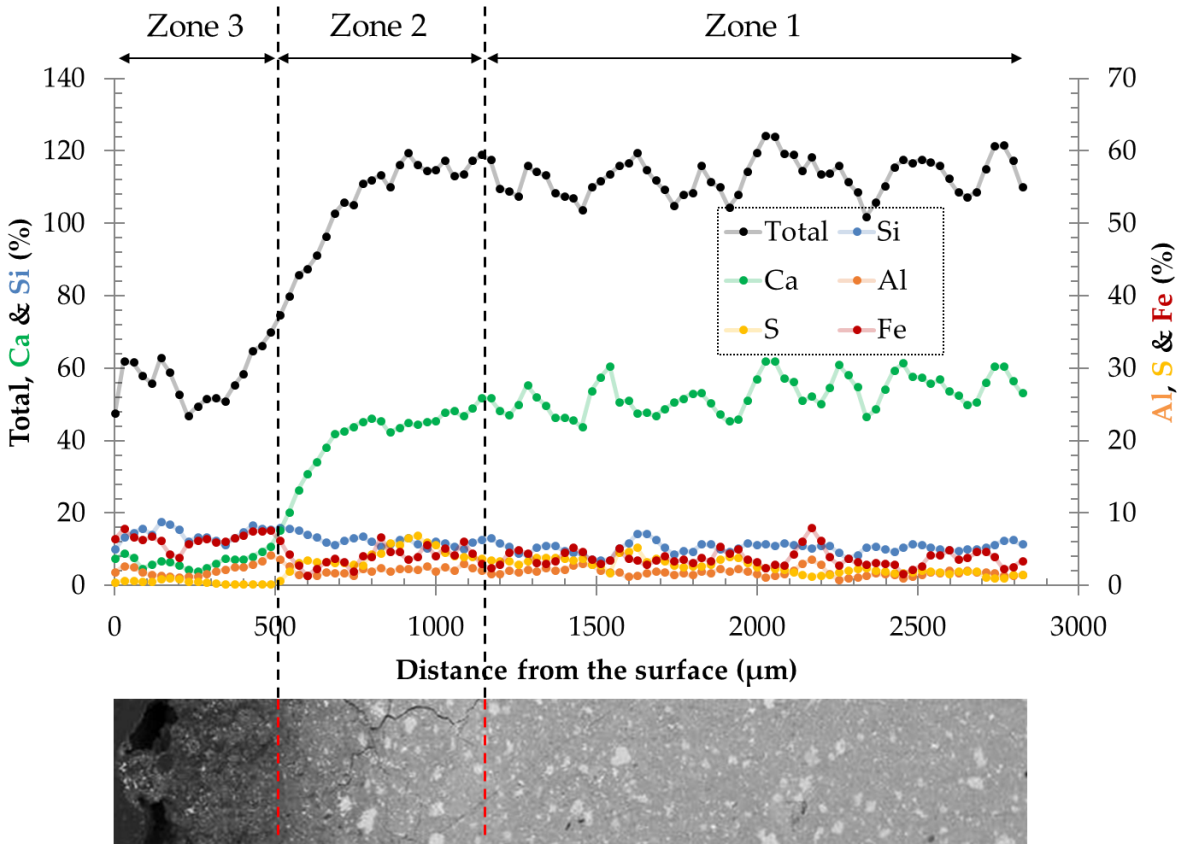

Figure V-A-5. Evolution of the chemical composition of the SR3 material exposed to the BAC test for 3 months as a function of the distance from the initial surface of the specimen (at 0 µm) and the SEM observation of the microstructure of the cross-section in BSE mode

Two deteriorated zones were identified and are reported on the figure with the chemical profile.

- Zone 1, the sound zone, was characterized by the high calcium content (54 %). Silicon was the second main element with an average of 10 %. Iron, sulfur and aluminum were present with less quantity, 4, 2.5 and 1.7 % respectively.

- Zone 2, consisted of 650 µm of thickness, showed severe decalcification of the matrix (calcium content dropped from 54 to 10%). The sulfur content increased gradually towards the surface. The microstructure of the zone showed microcracks where the sulfur was present. Ettringite was identified in the XRD patterns in this zone and could be linked to the formation of the microcracks.
- Zone 3, consisted of 500 µm of thickness, was the outer layer which was directly exposed to the biofilm. This zone showed lower density compared to the two previous zones and was mainly composed of silicon (15%), calcium (6%) and iron (6%).

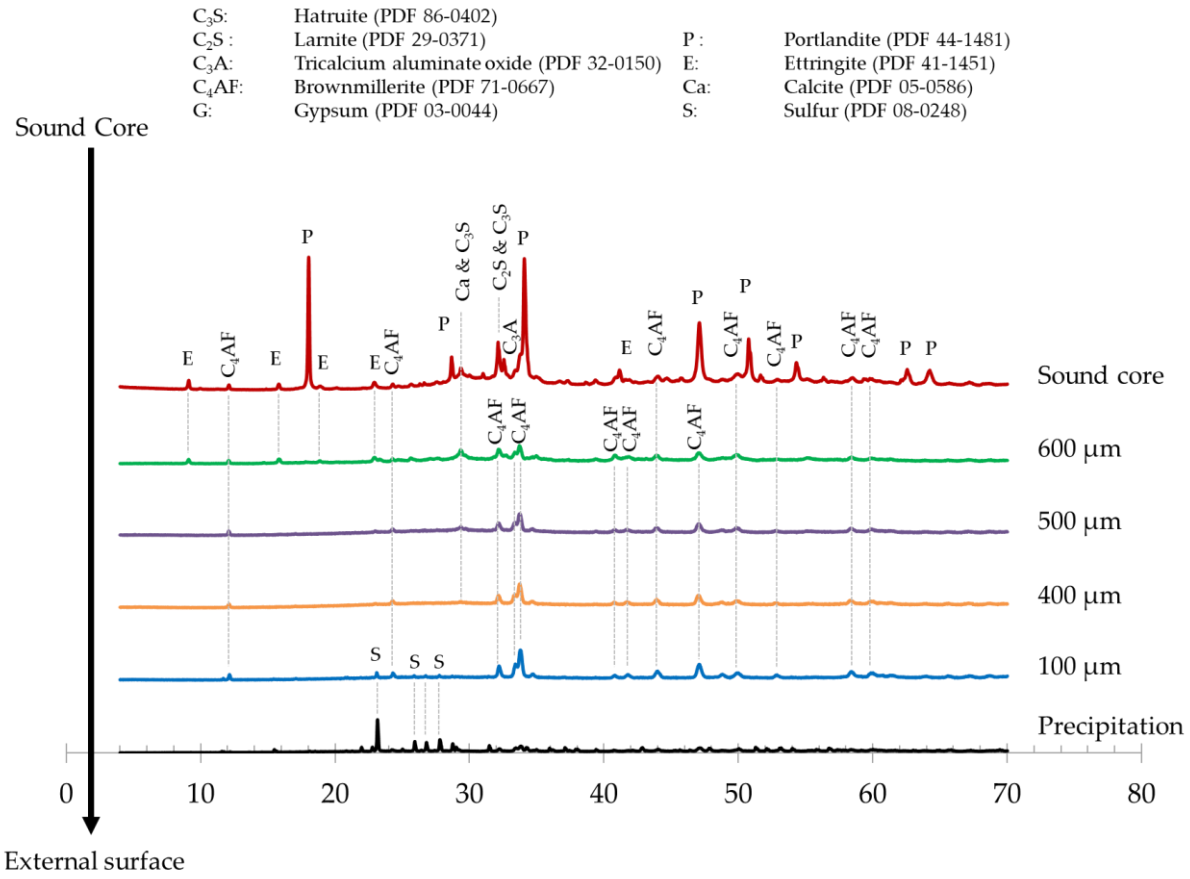

Figure V-A-6. Evolution of the mineralogical composition of the SR0 material exposed to the BAC test for 3 months as a function of the distance from the surface of the specimen

Appendix V-B: Description of the evolution of the chemical and mineralogical composition of CSA-based materials exposed to the BAC test for 3 months

Calcium sulfoaluminate clinker (CSAC)

Figure V-B-1 presents the EDS chemical composition profile of CSAC paste specimen (wt.%) exposed to the BAC test for 3 months as a function of the distance to the surface in contact with biofilm, along with the microstructure observation of the specimen in BSE mode. Figure V-B-2 presents the evolution of the mineralogical composition at several depths within the CSAC material.

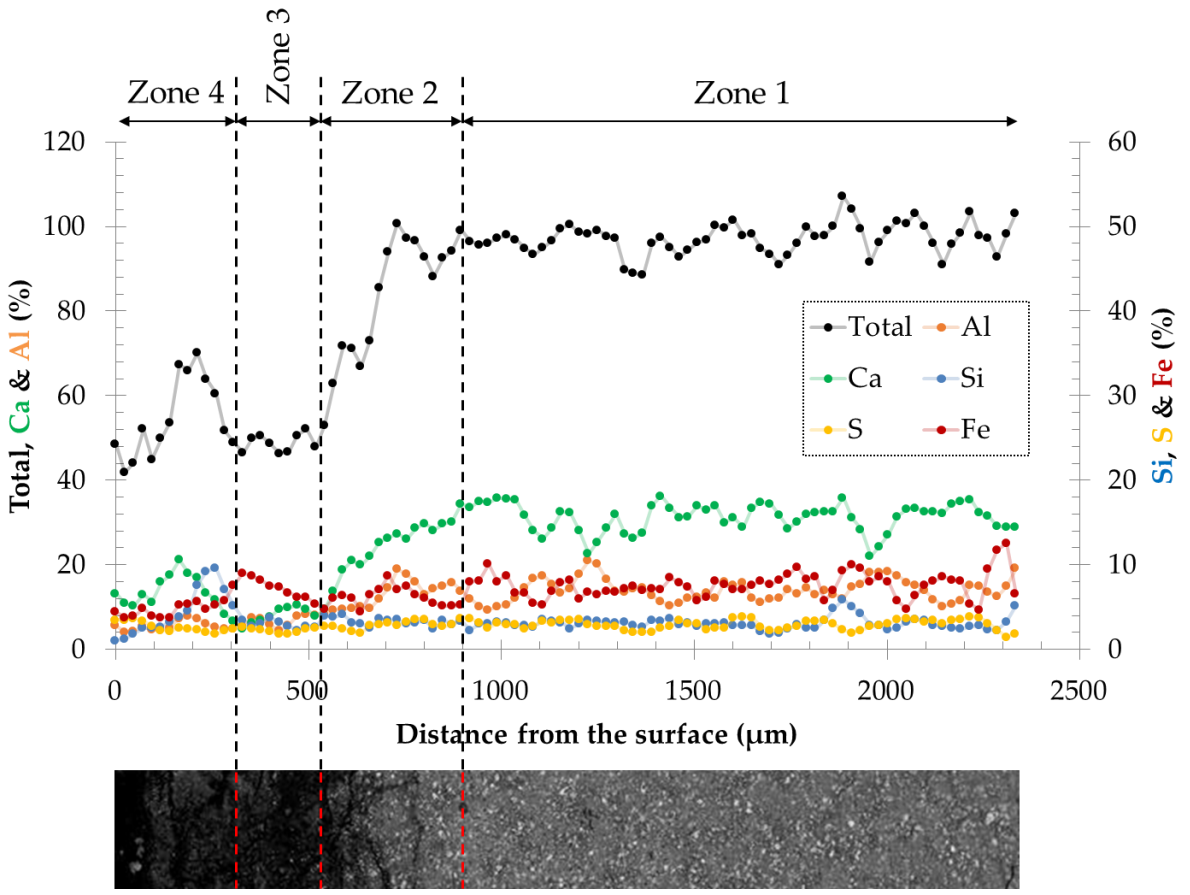

Figure V-B-1. Evolution of the chemical composition of the CSAC material exposed to the BAC test for 3 months as a function of the distance from the initial surface of the specimen (at 0 µm) and the SEM observation of the microstructure of the cross-section in BSE mode

- Zone 1 was detected at 900 µm of depth inside the cement matrix. The average composition of the sound zone was made of 31% of calcium, 14% of aluminum, 7.6% of iron, 3% of sulfur and 3% of silicon. Zone 1 was composed mainly of AFm phases (monosulfoaluminate and monocarboaluminate), aluminum hydroxide and residual anhydrous grains (gehlenite, C_2S, C_4AF). No residual ye'elimite was detected in this zone.

- Zone 2 (thickness of 400 µm) showed a lower density than zone and a decalcification of the matrix (from 31 to 10%). Moreover, large microcracks were observed in this zone. Bassanite was identified as the main calcium sulfate form in the deteriorated zone.
- Zone 3 (thickness of 200 µm) showed a particular behavior of iron which increase up to 9% and decreased brutally in zone 4. The XRD pattern of this zone shows the presence of mainly aluminum hydroxide, C_4AF and gehlenite. The disappearance of the other phases could explain the sudden relative increase in the iron content.
- Zone 4 (thickness of 300 µm) was the most deteriorated zone as it was in direct contact with the biofilm. The microstructural observations showed low density with the presence of very low amounts of calcium, aluminum, iron, sulfur and silicon. Aluminum hydroxide and residual non-hydrated gehlenite and C4AF were the main mineralogical phases.

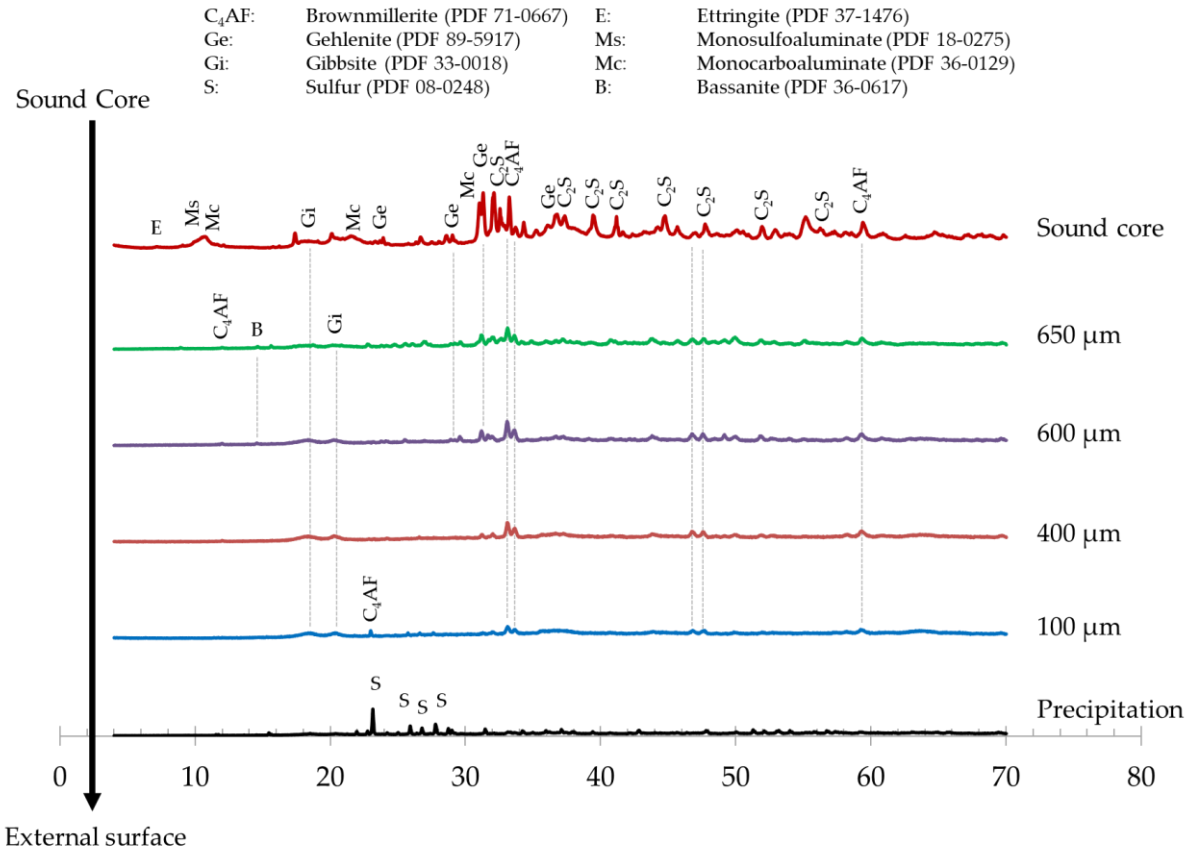

Figure V-B-2. Evolution of the mineralogical composition of the CSAC material exposed to the BAC test for 3 months as a function of the distance from the surface of the specimen

Calcium sulfoaluminate clinker + anhydrite (CSAA)

Figure V-B-3 presents the EDS chemical composition profile of CSAA paste specimen (wt.%) exposed to the BAC test for 3 months as a function of the distance to the surface in contact with biofilm, along with the microstructure observation of the specimen in BSE mode. Figure V-B-4 presents the evolution of the mineralogical composition at several depths within the CSAA material.

During the preparation of the specimen for the SEM observations (as described in 5.2.2), a very large portion of the deteriorated layers fell off with a thickness estimated at 650 µm. It seemed that the deteriorated zone was less cohesive with the sound zone compared to the other two CSA-based materials. Such layer was described as zone 5 in the chemical profile figure; however, three more deteriorated zones were identified.

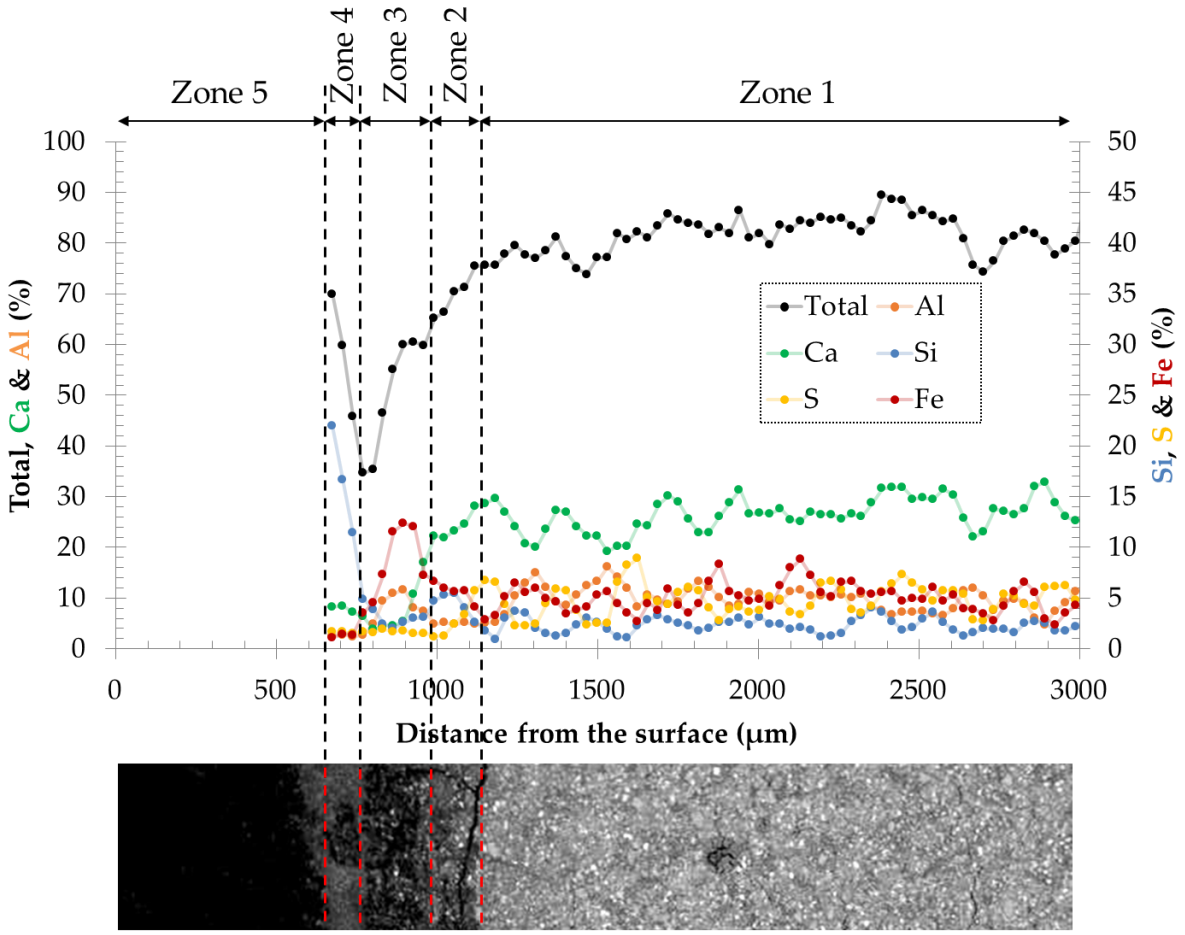

Figure V-B-3. Evolution of the chemical composition of the CSAA material exposed to the BAC test for 3 months as a function of the distance from the initial surface of the specimen (at 0 µm) and the SEM observation of the microstructure of the cross-section in BSE mode

- Zone 1 corresponded to the sound core of the material, which presented anhydrous grains in white due to their high density with the hydrated cement paste around them. Microcracks were also observed in the sound core due to the drying of ettringite in high vacuum conditions of the SEM. The cement paste in the sound zone was mainly composed of calcium and aluminum with fewer amounts of sulfur and iron. The XRD analyses in the sound zone revealed the presence of ettringite and calcium monosulfoaluminate (Ms), which are characteristics of this binder. Moreover, it showed that anhydrite was not completely consumed in the hydration reaction due to its slower reaction kinetics compared to gypsum [184]. The large and very small peaks of gibbsite and bayerite indicated the formation of few amounts of poorly crystallized AH_3.

- Zone 2 was of 150 µm of thickness and showed a decrease in the total elements' content. The relative concentration calcium and sulfur decreased (from 29 and 7 to 22 and 1.5% respectively). Moreover, iron and silicon content increased in such area from 3 and 2 to 7 and 5% respectively. The low density of this zone indicated a high porosity which facilitated the movement of different species in and out of the matrix. For instance, vaterite was detected following the possible penetration of CO_2. Ms disappeared while ettringite peaks decreased significantly. Similarly, anhydrite peaks decreased with no identification of gypsum, which means that the sulfate mainly exited in the pore solution.

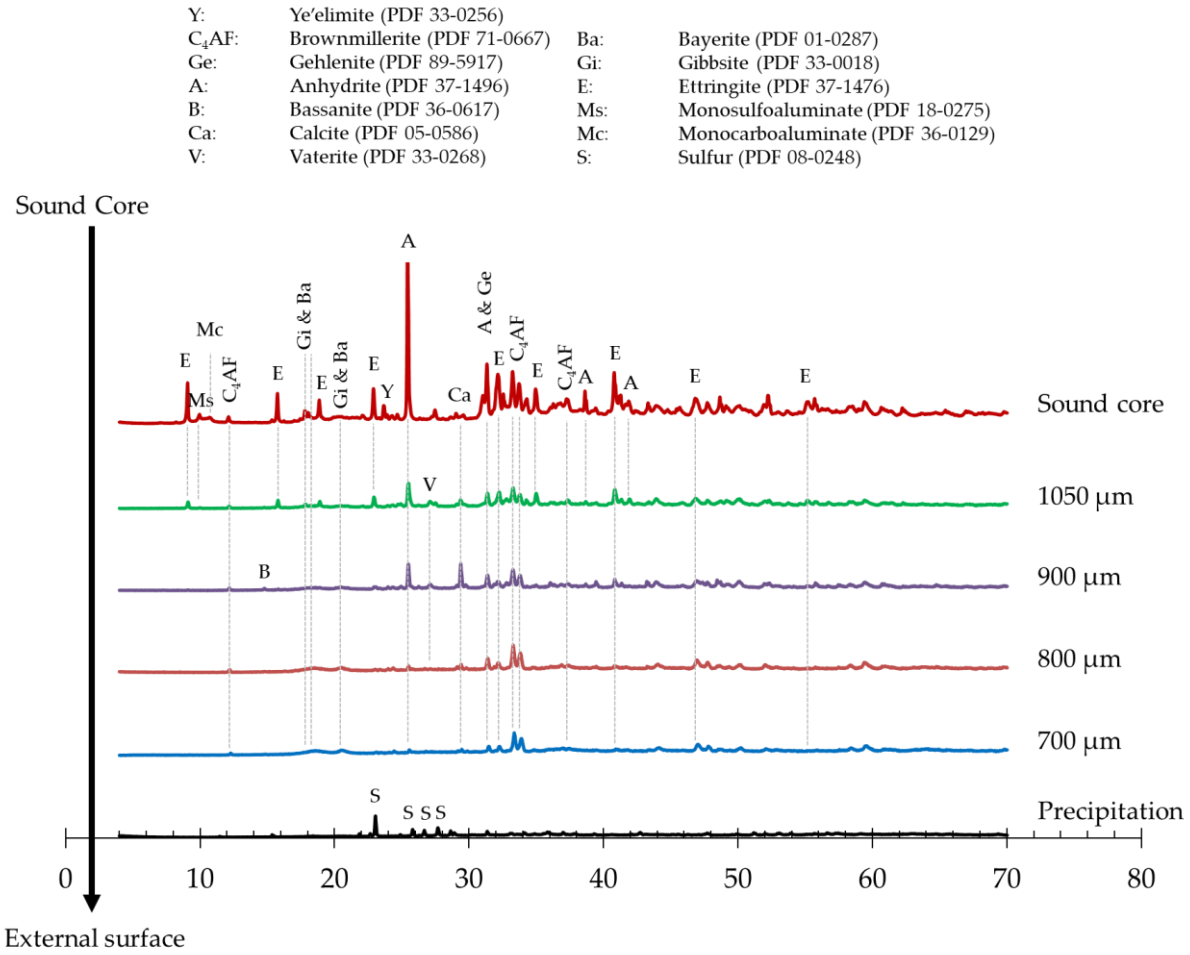

Figure V-B-4. Evolution of the mineralogical composition of the CSAA material exposed to the BAC test for 3 months as a function of the distance from the surface of the specimen

- Zone 3 was of 250 µm of thickness and presented a severe decalcification of the matrix. The calcium content dropped from 22 to 4%. The aluminum content was relatively high (ranging between 7.5 and 11%) before decreasing at the interface between zone 3 and zone 4. The microstructure observation showed a very low dense area, which corresponded to the decrease of the total element content (from 60 to 35%). C_4AF was the main identified mineralogical phase explaining the high iron content. While C_4AF is considered inert during the hydration of CSA [74], iron could still be leached from the attack of the mineralogical phase by sulfuric acid in very acidic conditions.

Ettringite disappeared completely from this zone while anhydrite content was similar to the previous zone. Vaterite and calcite was the two identified calcium carbonate. A wide peak regrouping gibbsite and bayerite was observed, contrary to the narrower peaks in the sound zone.

- Zone 4 was of 100 µm of thickness and it was composed mainly of silicon. Calcium was still detected in this zone but with an average of 8%. Aluminum, iron and sulfur were also present in content less than 5%. Residual grains of C_4AF were still detected, however, the iron content was relatively low. No crystallized silicon-bearing phases were identified which leads to the hypothesis of having a silica hydrogel coming from the decalcification of amorphous C-S-H.

Calcium sulfoaluminate clinker + gypsum (CSAG)

Figure V-B-5 presents the EDS chemical composition profile of CSAG paste specimen (wt.%) exposed to the BAC test for 3 months as a function of the distance to the surface in contact with biofilm, along with the microstructure observation of the specimen in BSE mode. Figure V-B-6 presents the evolution of the mineralogical composition at several depths within the CSAG material.

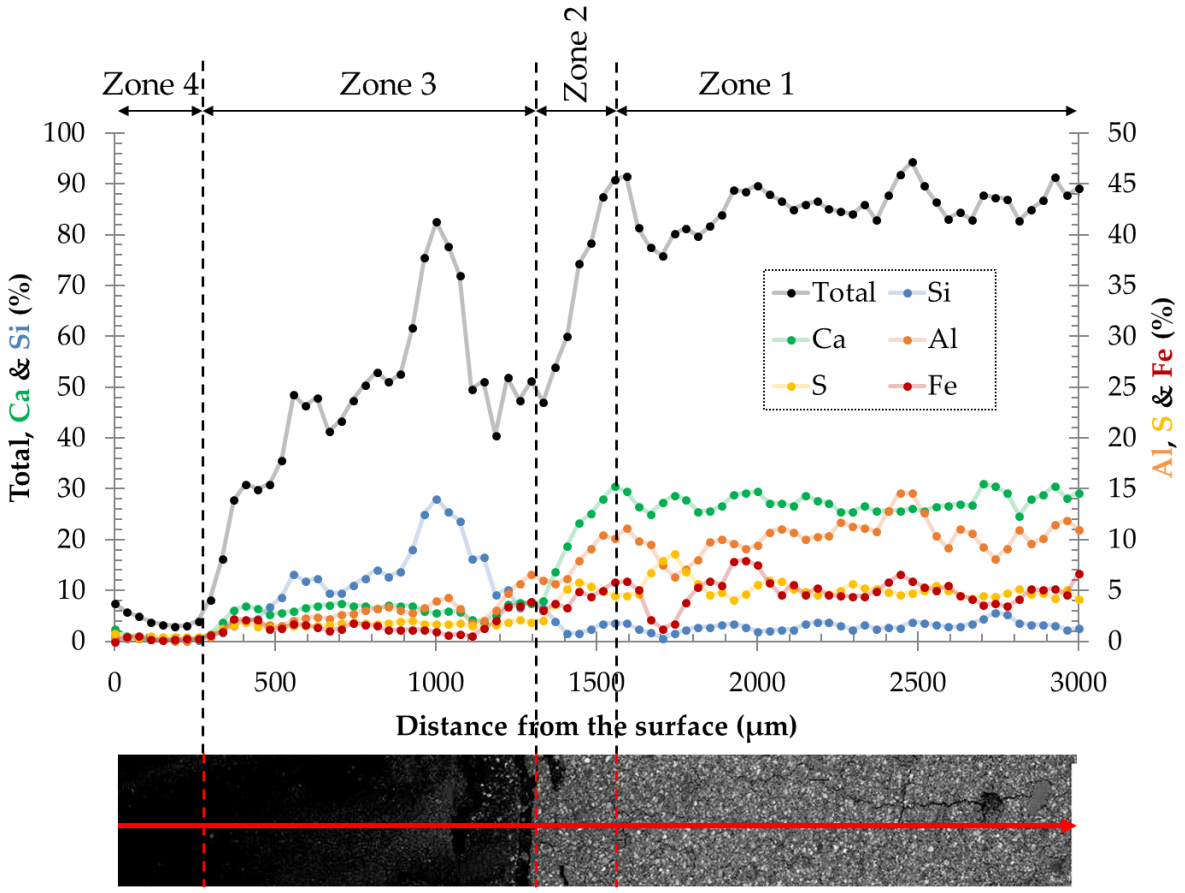

Figure V-B-5. Evolution of the chemical composition of the CSAG material exposed to the BAC test for 3 months as a function of the distance from the initial surface of the specimen (at 0 µm) and the SEM observation of the microstructure of the cross-section in BSE mode

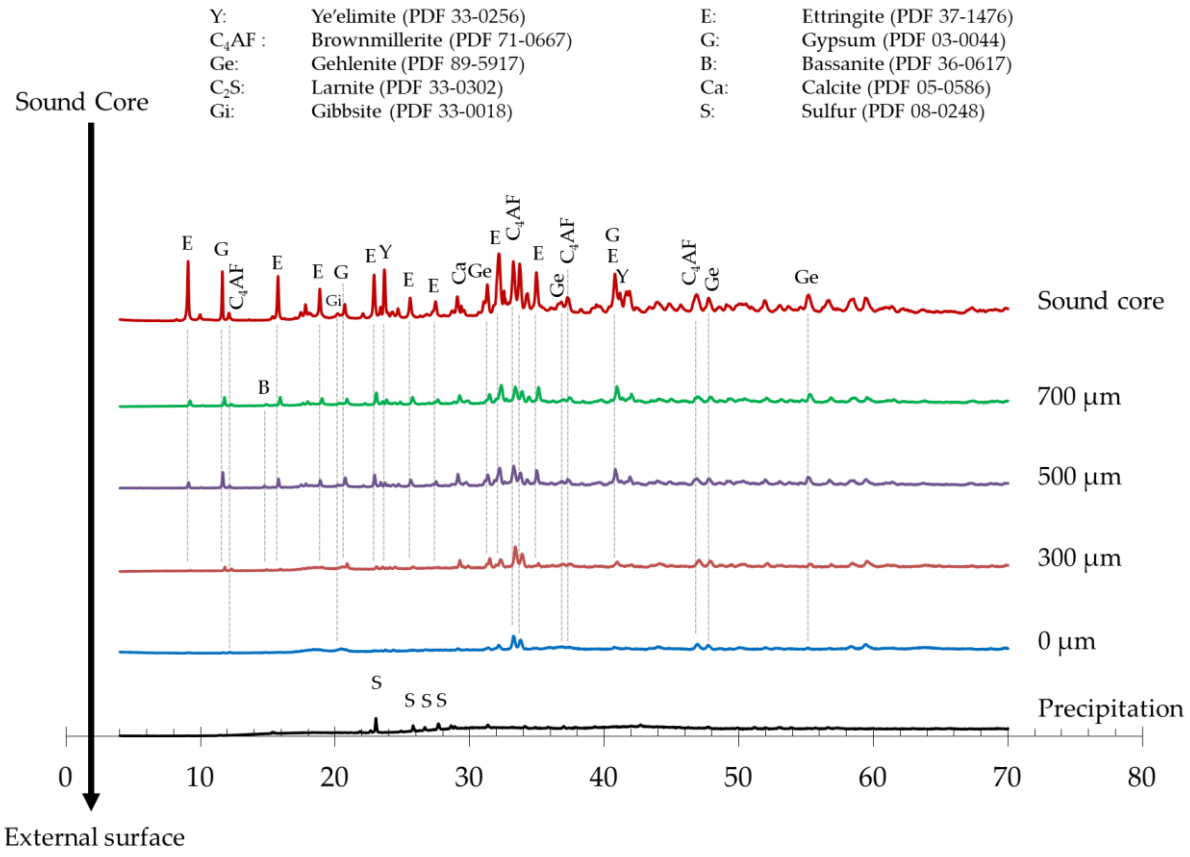

Figure V-B-6. Evolution of the mineralogical composition of the CSAG material exposed to the BAC test for 3 months as a function of the distance from the surface of the specimen

The chemical analyses by EDS allowed the identification of three deteriorated zones. The description of the zones is as follows:

- Zone 1 was identified as the sound zone and was detected at approximately 800 µm deep inside the cement matrix. This zone was characterized by the presence of high amounts of dense anhydrous grains (bright points on the SEM image). Moreover, microcracks were also observed, however, they were attributed to the formation of ettringite, which is unstable in vacuum conditions of the SEM. The XRD patterns showed intense peaks for ettringite, gypsum and ye'elimite. Gibbsite was also identified but in very low amount (small peaks). Residual anhydrous grains from the clinker were detected such as gehlenite and C_4AF. Calcite formed in the sound zone; however, it might have formed during the preparation of the specimen for the analyses.
- Zone 2 was the first deteriorated zone going from inside the material towards its surface. It was of 250 µm of thickness and showed large cracks inside the matrix near the interface with zone 3. The total elemental content decreases (from 81 to 54%), mainly due to the decalcification of the matrix (from 26 to 14%). A slight decrease in aluminum content was detected (from 10 to 5%) while the remaining elements stayed relatively stable. Gypsum and bassanite was the two forms of calcium sulfate detected in this zone. Peaks of ettringite and ye'elimite decreased significantly while the anhydrous C4AF and gehlenite were still identified.

- Zone 3 was of 150 μm of thickness and showed larger cracks in the matrix. The calcium content was relatively low while sulfur, aluminum and iron were still detected. Silicon content seemed to increase from less than 5% to around 10%. To the exception of gehlenite, no silicon-bearing crystalline phases were detected. The intensity of the gypsum peaks increased slightly.
- Zone 4, thickness of 400 μm, showed very low density and was composed mainly of silicon. Calcium, aluminum, sulfur and iron contents were very low. The gypsum peaks decreased until its total disappearance at the surface of the material. Moreover, gibbsite was detected as the crystalline form of AH_3 in the severely deteriorated zone. Residual anhydrous gehlenite and C_4AF was detected as well.

Appendix V-C: Description of the evolution of the chemical and mineralogical composition of AAS-based materials exposed to the BAC test for 3 months

Alkali-activated slag (AAS)

Figure V-C-1 presents the EDS chemical composition profile of AAS paste specimen (wt.%) exposed to the BAC test for 3 months as a function of the distance to the surface in contact with biofilm, along with the microstructure observation of the specimen in BSE mode. Figure V-C-2 presents the evolution of the mineralogical composition at several depths within the AAS material.

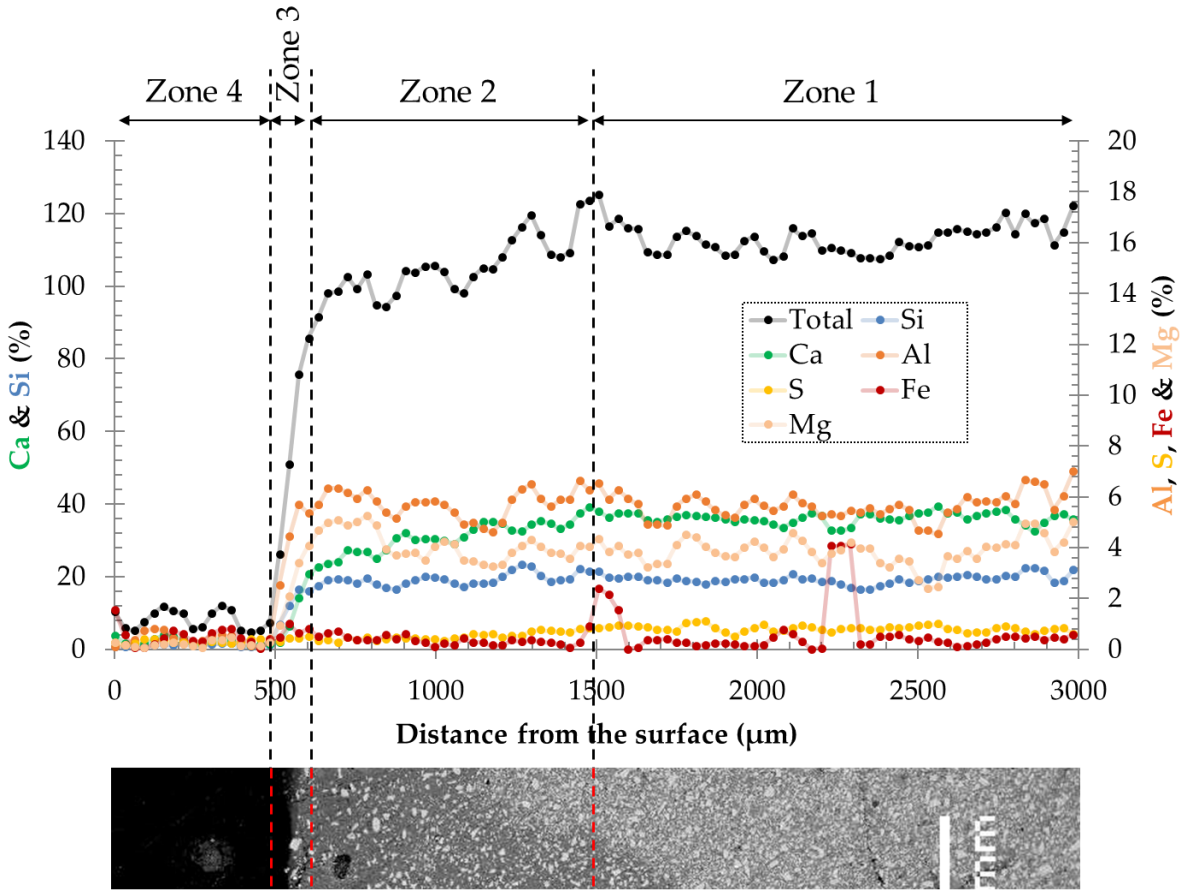

Figure V-C-1. Evolution of the chemical composition of the AAS material exposed to the BAC test for 3 months as a function of the distance from the initial surface of the specimen (at 0 µm) and the SEM observation of the microstructure of the cross-section in BSE mode

Three deteriorated zones were identified in addition to the sound zone:

- Zone 1 was identified as the sound zone where the chemical profile corresponded to the core of the specimen. The major identified elements were Ca and Si with an average of 40 and 20 wt.% respectively. Other elements were present, however, in much less amounts, such as aluminum, sulfur, iron and magnesium. Aluminum and magnesium content was between 2.5 and 7% and sulfur and iron content were around 1%. Iron content was higher at two different spots (2200-2300 and 1500-1600 µm), which seemed

to be attributed to Fe-containing anhydrous grains, since the iron content was very low in the hydrated part of the sound zone (less than 1%). As expected, the XRD patterns of the hydrated paste revealed that the matrix was mainly amorphous with the exception of calcium carbonates (calcite and vaterite), hydrotalcite and C-S-H, which the majority was also amorphous.

- Zone 2 (thickness: 900 µm) was characterized by the progressive decalcification of the matrix. Calcium content went from 40 to 20% from the inner to the outer part of this zone. However, the content of rest of the elements did not vary much between zone 1 and zone 2. The paste was composed mainly of calcium carbonate.
- Zone 3 (thickness: 100 µm) was 100 µm, was marked by the significate decrease in all chemical elements. All elements were detected at less than 2% at the interface of zone 3 and zone 4. The mineralogical analyses showed traces of calcite in this zone.
- Zone 4 (thickness: 500 µm) was identified as the severely deteriorated zone. Such zone was not completely dissolved but had a very low density.

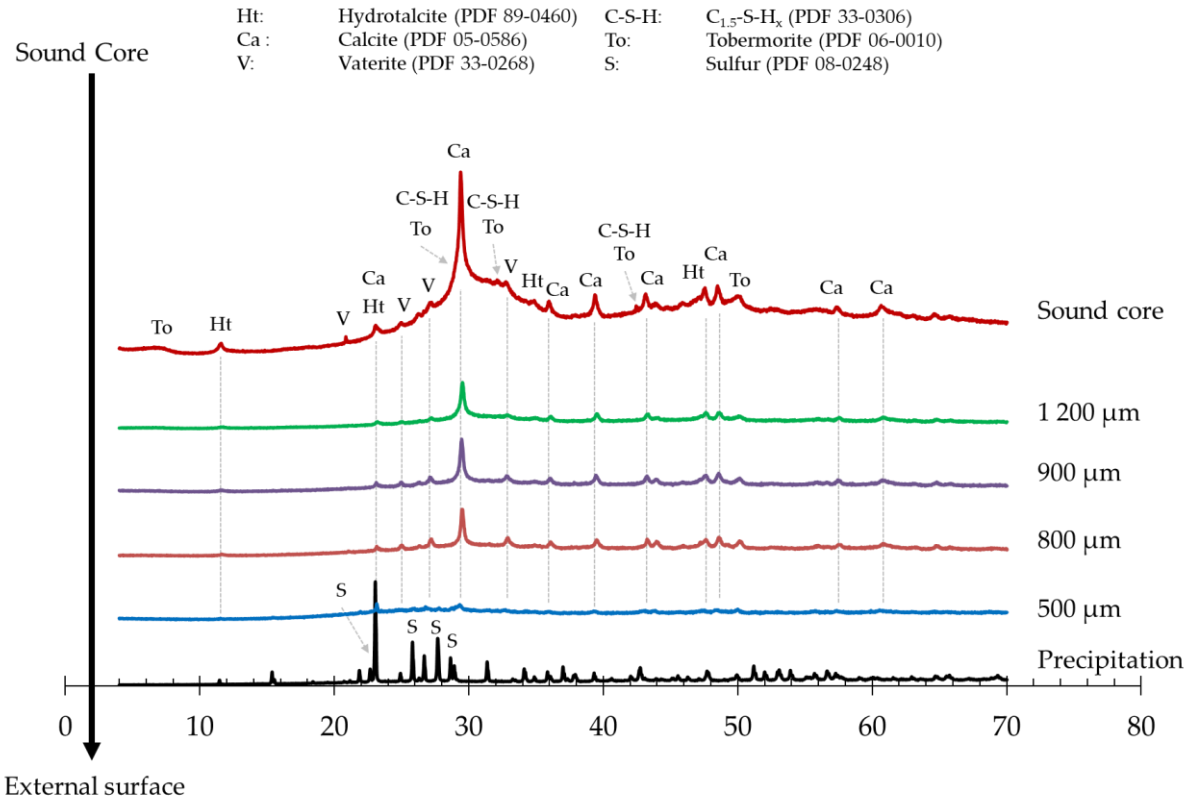

Figure V-C-2. Evolution of the mineralogical composition of the AAS material exposed to the BAC test for 3 months as a function of the distance from the surface of the specimen

Figure V-C-3 shows an image of the sound zone and an image of the deteriorated zone, previously identified as zone 2. The sound area showed a very large number of anhydrous grains, identified as anhydrous slag grains. The deteriorated zone showed the disappearance of many of the slag anhydrous grains.

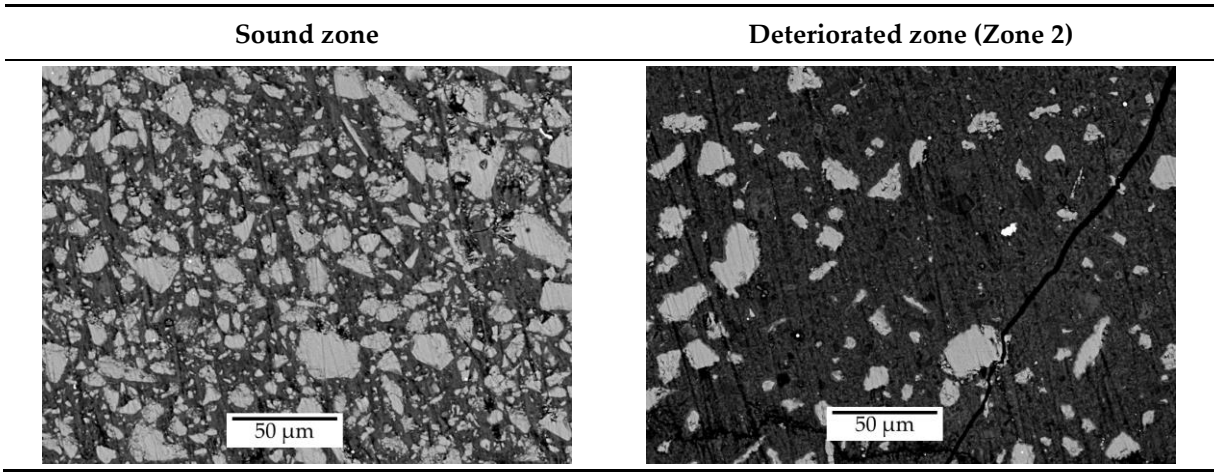

Figure V-C-3. SEM observations showing the difference between a sound zone and a deteriorated zone (zone 2)

Figure V-C-4 presents the chemical analyses carried out on the hydrated paste in the sound zone and the deteriorated zone in order to compare their respective chemical compositions. The mass ratio of Al/Ca as a function of Si/Ca showed a significant decrease of calcium in the deteriorated zone, indicating the decalcification of this zone compared to the sound zone. In addition, the evolution of Al/Ca ratio in the deteriorated zone seemed linear as a function of the Si/Ca, showing that, possibly, the leaching concerned only the calcium and not the aluminum nor the silica. The Al/Si mass ratio as a function of Si/Ca showed that the Al/Si ratio in the deteriorated zone was between 0.25 and 0.4 compared to 0.2 and 0.4 for the sound zone. This mechanism seemed to show a progressive decalcification of the C-(A)-S-H phases of the AAS matrix.

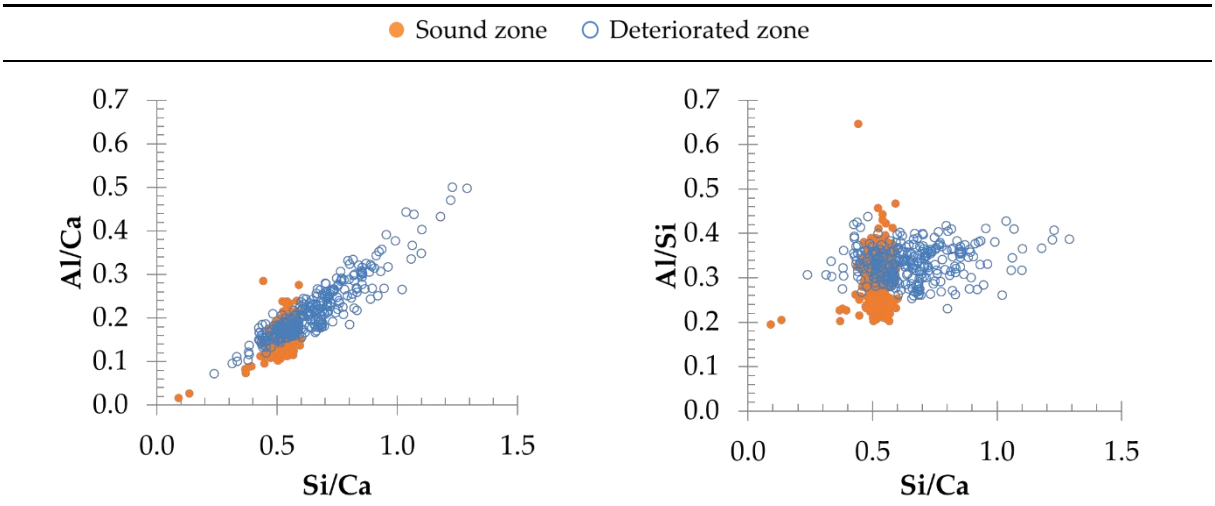

Figure V-C-4. Al/Ca and Al/Si ratio as a function of Si/Ca for sound zone and deteriorated zone (zone 2)

Alkali-activated slag + bauxite (AASB)

The evolution of the chemical profile of the AASB materials as a function of the thickness of the specimen is shown on Figure V-C-5. The mineralogical analyses at different depth are shown in Figure V-C-6. Three deteriorated zones were identified in addition to the sound zone.

- Zone 1 was considered as the sound zone. This zone was mainly composed of calcium and silica (33 and 17% respectively). Aluminum content averaged around 5.5%, except for two sites where the aluminum increased suddenly before decreasing again. This was mainly due to the presence of anhydrous bauxite grains. Like AAS, the sound zone was mainly amorphous. Diaspore, hematite and boehmite were identified by XRD and were linked to the presence of bauxite in the matrix since these phases were not present in AAS binder.

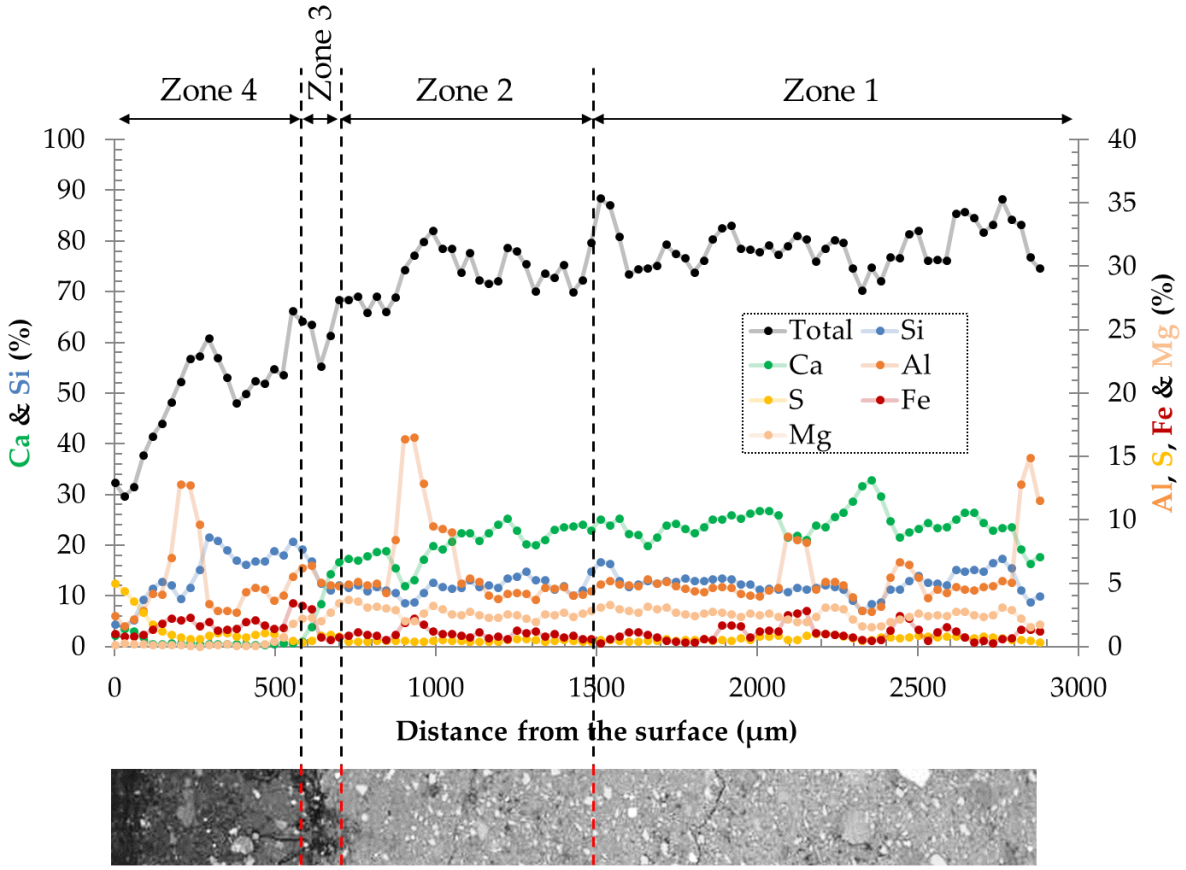

Figure V-C-5. Evolution of the chemical composition of the AASB material exposed to the BAC test for 3 months as a function of the distance from the initial surface of the specimen (at 0 µm) and the SEM observation of the microstructure of the cross-section in BSE mode

- Zone 2 (thickness: 800 µm) was the zone where the decalcification of the matrix started to be observed progressively down to 16%. Again, the high sudden increase in aluminum was attributed to the presence of bauxite grains. Silica, magnesium iron and sulfur seemed to not vary significantly compared to zone 1. C-S-H peaks disappeared with a general decrease in the intensity of all peaks. Calcium carbonate and bauxite composed mainly this zone.
- Zone 3 (thickness: 100 µm) showed a brutal decalcification of the cement matrix. Calcium content went from 16 to less than 1%. Unlike AAS, silica content increased from 11 to 19% and iron content increased from less than 1% to 3%. The microstructure of this zone showed a very low density, suggesting a gel-like zone (similar to zone 5

observed in PC specimen). Calcite peaks decreased significantly compared to the previous zone. However, peaks of diaspore, boehmite and hematite were still detected.

- Zone 4 (thickness: 600 µm) was composed mainly from silica, aluminum and iron contrarily to AAS which showed a severely deteriorated zone with a total of elements presence less than 10%. The microstructure showed the presence of residual grains with different forms and sizes. The chemical composition showed that the residual grains were composed mainly of aluminum and iron. The mineralogical composition revealed the presence of diaspore, hematite and boehmite, indicating the presence of bauxite in the severely deteriorated zone.

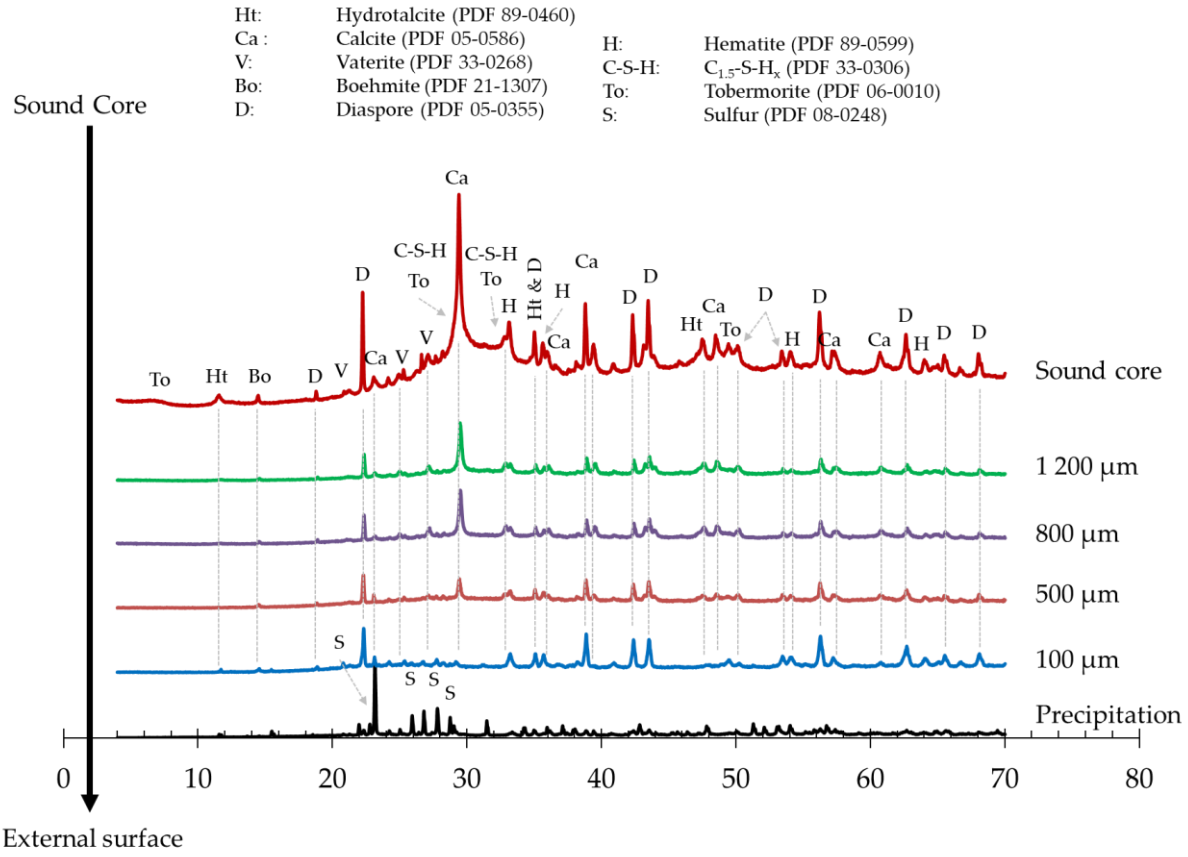

Figure V-C-6. Evolution of the mineralogical composition of the AASB material exposed to the BAC test for 3 months as a function of the distance from the surface of the specimen

Alkali-activated slag + HardCem (AASH)

The evolution of the chemical profile of the AASH materials as a function of the thickness of the specimen is shown in Figure V-C-7. The mineralogical analyses at different depth are shown in Figure V-C-8. Five deteriorated zones were identified in addition to the sound zone.

- Zone 1 was considered as the sound zone and was composed mainly of calcium, silicon, aluminum and magnesium. Although the high iron content in HardCem, very low amount of iron was detected in the hydrated cement paste. No difference was observed between the AAS and AASH mineralogical phases in the sound zone. The

addition of HardCem seemed to not form any crystallized phases when mixed with alkali-activated slag.

- Zone 2 (thickness: 150 µm) showed a decrease in calcium and magnesium content. Iron seemed to increase from less than 1% to 3.5%. The intensity of peaks for hydrotalcite and calcium carbonates (calcite and vaterite) decreased as well. No crystallized phases containing iron were detected, suggesting that iron was coming from anhydrous HardCem grains.

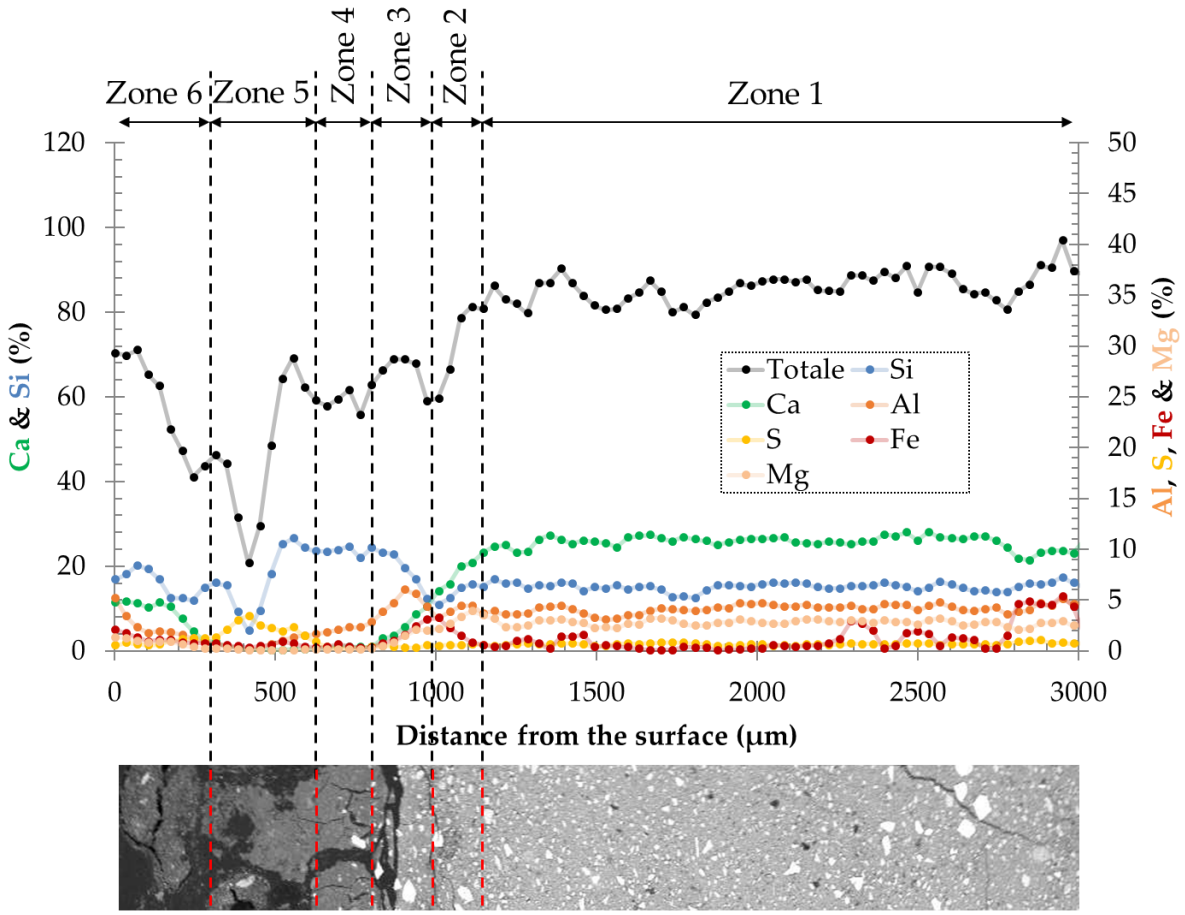

Figure V-C-7. Evolution of the chemical composition of the AASH material exposed to the BAC test for 3 months as a function of the distance from the initial surface of the specimen (at 0 µm) and the SEM observation of the microstructure of the cross-section in BSE mode

- Zone 3 (thickness: 150 µm) presented a decalcification of the cement matrix until the total depletion of calcium. Iron and magnesium continued to decrease while silicon increased from 12 to 23%. Calcium carbonates were the main phase of this zone.
- Zone 4 (thickness: 150 µm) was composed mainly of silicon. Aluminum was detected at low content and continued to decrease.
- Zone 5 (thickness: 300 µm) was highly deteriorated and presented a similar composition as zone 4 with the exception of the presence of sulfur. The low density and the severity of the deterioration might suggest high porosity in such area where sulfuric acid could penetrate easily. The XRD patterns showed very small peaks of calcite.

- Zone 6 (thickness: 300 µm) was the outer layer in contact with the biofilm. Calcium was again detected along with silicon and aluminum. The mineralogical analyses did not reveal any crystallized phases with silicon or aluminum.

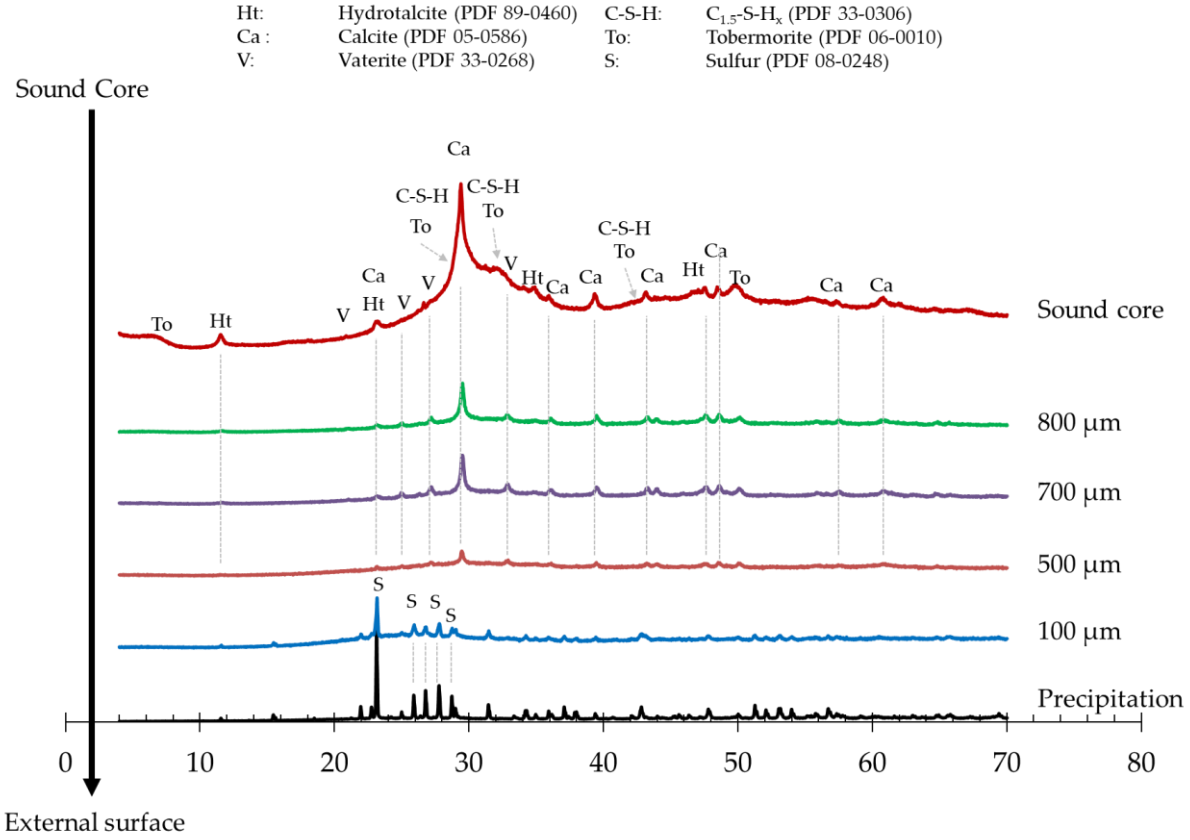

Figure V-C-8. Evolution of the mineralogical composition of the AASB material exposed to the BAC test for 3 months as a function of the distance from the surface of the specimen

Appendix V-D: Reactivity of HardCem grains with chemical sulfuric acid

In order to evaluate the reactivity of HardCem grains with chemical sulfuric acid, HardCem was introduced gradually in a pre-prepared solution of sulfuric acid at pH = 2.7. The choice of such pH was to represent the same pH conditions observed in the BAC test.

170 µl of sulfuric acid was added to two liters of deionized water in order to obtain a pH of 2.7. 5g of HardCem grains were grinded and sieved at 80 µm in order to optimize the exposed surface of the grains. The powder was stored in a desiccator under low vacuum conditions with silica gel and sodium hydroxide to protect the powder from humidity and carbonation.

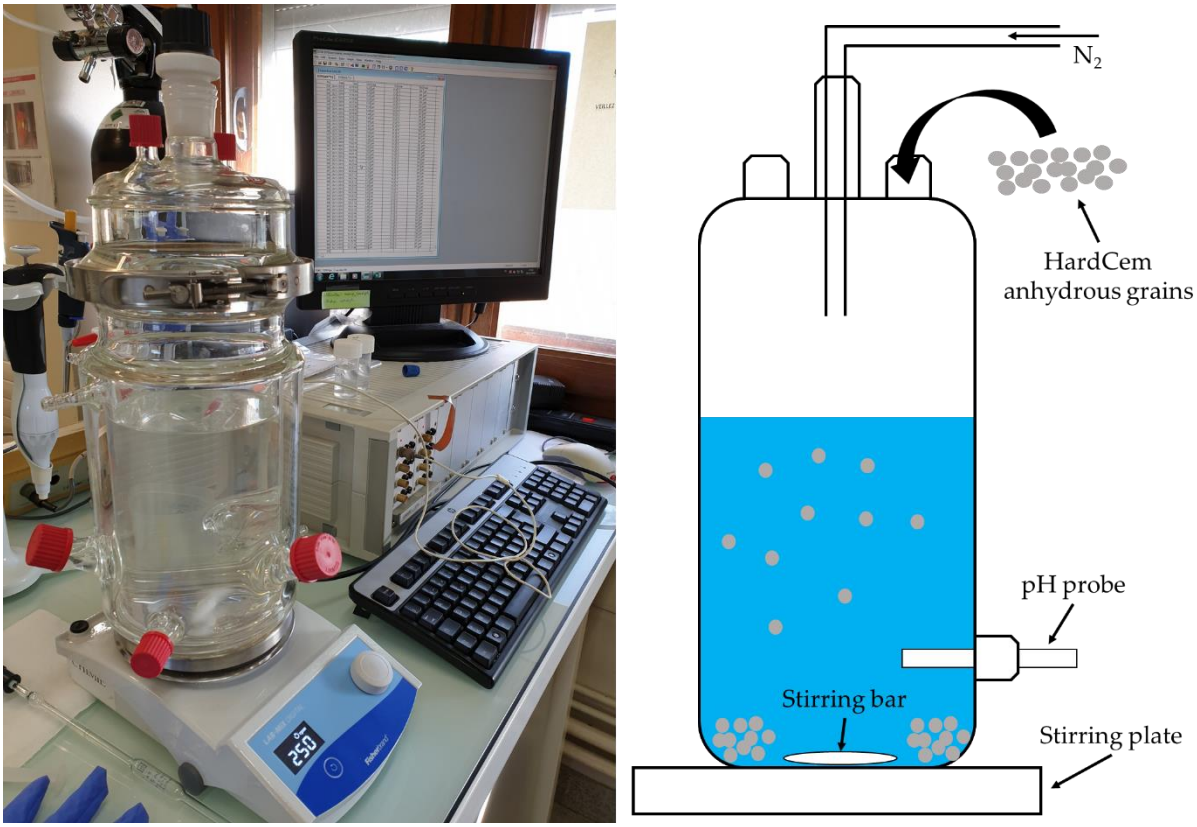

Figure V-D-1. Photograph of the reactor pilot and a schematic representation of the different parts of the pilot

Figure V-D-1 presents the reactor pilot containing the sulfuric acid solution and connected to a pH probe which measures the evolution of the pH continuously. The pH probe was calibrated between 4 and 7 before being inserted in the reactor containing the sulfuric acid solution. The reactor was placed on a stirring plate set up at 200 rpm. The upper part of the reactor was connected to a discrete nitrogen flow ensuring that aerial part inside the reactor is not filled with air to limit the risk of carbonation of HardCem during the experiment. The nitrogen flows for a short period (3 min) after introducing the HardCem grains through the valve to expel the air before closing the valve. The pH probe was connected to the computer which measures and save the pH every 30 seconds. HardCem grains were introduced at the rate of 0.1 g before waiting for the pH to stabilize. The stabilization of the pH was evaluated

over the period of 10 mins. Once the pH is stabilized, 0.1 g of HardCem was introduced and so go on until all the 5 g of HardCem were introduced into the reactor.

At the end of the experiment, the liquid solution was collected and centrifugated at 4000 rpm to separate the liquid phase from the precipitates. The precipitates were then collected and analyzed by XRD to determine the possible modifications of the mineralogical composition.

Appendix VI-A: 1D model HYTEC script for pH 3

PC

```
# Hydrology and geometry
#-----------------------
grid-regime = rectangle
domain = 0.08,10  0.006,60
flow-regime = stationary

# Parameters of simulation:
#--------------------------
duration = 100 d
precision of coupling = 1e-2
maxit of coupling = 5
precision of newton-raphson = 1e-12
maxit of newton-raphson = 1000

timestep = variable {
  start-value = 0.01 s
  minimum-value = 0.001 s
  maximum-value = 10 min
  iteration-threshold = 3
  increment = 3 %
}

porosity   = variable {
  start-value = 0.20
  archie = 1.0
  minimum-value = 0.01
}

courant-factor = 1

samples = 100
# Zones:
#--------------------------
zone BL {
  geometry = rectangle 4.0,5.5 8.0,1.0 mm, nodes = 1,10
  porosity = 1.00
  diffusion-coefficient = 1e-9 m2/s
```

```
  permeability = 1e-6 m/s
  source = 25 ml/h using inlet
}

zone LIQ {
  geometry = rectangle 40.0,5.5 64.0,1 mm, nodes = 8,10
  porosity = 1.00
  diffusion-coefficient = 1e-9 m2/s
  permeability = 1e-6 m/s
  segment seg_in, coordinates = 8,5.0 8,6.0 mm
}

zone BR {
  geometry = rectangle 76.0,5.5 8.0,1 mm, nodes = 1,10
  porosity = 1.00
  diffusion-coefficient = 1e-9 m2/s
  permeability = 1e-6 m/s
  segment seg_out, coordinates = 72.0,5.0 72.0,6.0 mm
}

zone PASTE {
  geometry = rectangle 40.0,2.5 80.0,5.0 mm, nodes = 10,50
  diffusion-coefficient = 1e-11 m2/s
  permeability = 1e-11 m/s
  chemistry = paste
  segment diff, coordinates = 0,5.0 80.,5.0 mm
}

#default database:
#-----------------
database = /home/aaboulela/chess/tdb/brgm_chess.tdb
exclude minerals, colloids, organics, gases
include Portlandite, CSH(1.6), CSH(1.2), CSH(0.8)
#include C3AH6, C4AH13
include Ettringite, Monosulfoaluminate, Monocarboaluminate, Hemicarboaluminate
#include Straetlingite
include Amorphous_silica, Gibbsite, Gibbsite(am), Gypsum
#include Calcite, Magnesite,
#include Fe-Ettringite, C3FH6, Fe-Monosulfoaluminate, C4FH13, Goethite
include Hydrotalcite, Brucite
temperature = 25 C
```

```
unit inlet {
  tot SO4[2-] = 30.0 mmolal
  pH = 3
  balance on SO4[2-]
}

unit paste {
 mineral Portlandite = 4.636  molal
 mineral CSH(1.6) = 4.887 molal
 mineral Ettringite = 0.104 molal
 mineral Monosulfoaluminate = 0.105 molal
 tot Na[+] = 1e-6 mmolal
 tot OH[-] = 1e-6 mmolal
}

# Boundary conditions:
#-------------------------
#boundary LeftBorder {
#   coordinates = -0.4,2 -0.4,2.05 cm
#   flow-condition = constant-flow at 0.5 cm/min
#   transport-condition = flux using inlet
#}

boundary RightBorder {
   coordinates = 80.0,5.0 80.0,6.0 mm
   flow-condition = constant-head at 0 mm
}
verbose = enabled

# Select outputs:
#-------------------------
output = PC_pH3_1D
output-format = vtk, res

select aqueous{SO4[2-]} in mmol/L
select aqueous{Ca[2+]} in mmol/L
select aqueous{Al[3+]} in mmol/L
select aqueous{H4SiO4} in mmol/L
select aqueous{H[+]} in mmol/L
select aqueous{Na[+]} in mmol/L
```

select flowrate in m/d

flux-select aqueous{SO4[2-]} in mmol/d
flux-select aqueous{Ca[2+]} in mmol/d
flux-select aqueous{Al[3+]} in mmol/d
flux-select aqueous{Na[+]} in mmol/d

select minerals in molal
select min-volume in l

select head in m
select porosity
select pH

END :
#-------------------------

CAC

```
# Hydrology and geometry
#------------------------
grid-regime = rectangle
domain = 0.08,10  0.006,60
flow-regime = stationary

# Parameters of simulation:
#-------------------------
duration = 100 d
precision of coupling = 1e-2
maxit of coupling = 5
precision of newton-raphson = 1e-12
maxit of newton-raphson = 1000

timestep = variable {
  start-value = 0.01 s
  minimum-value = 0.001 s
  maximum-value = 10 min
  iteration-threshold = 3
  increment = 3 %
}

porosity   = variable {
  start-value = 0.20
  archie = 1.0
  minimum-value = 0.01
}

courant-factor = 1

samples = 100

# Zones:
#-------------------------
zone BL {
  geometry = rectangle 4.0,5.5 8.0,1.0 mm, nodes = 1,10
  porosity = 1.00
  diffusion-coefficient = 1e-9 m2/s
  permeability = 1e-6 m/s
```

```
  source = 25 ml/h using inlet
}

zone LIQ {
  geometry = rectangle 40.0,5.5 64.0,1 mm, nodes = 8,10
  porosity = 1.00
  diffusion-coefficient = 1e-9 m2/s
  permeability = 1e-6 m/s
  segment seg_in, coordinates = 8,5.0 8,6.0 mm
}

zone BR {
  geometry = rectangle 76.0,5.5 8.0,1 mm, nodes = 1,10
  porosity = 1.00
  diffusion-coefficient = 1e-9 m2/s
  permeability = 1e-6 m/s
  segment seg_out, coordinates = 72.0,5.0 72.0,6.0 mm
}

zone PASTE {
  geometry = rectangle 40.0,2.5 80.0,5.0 mm, nodes = 10,50
  diffusion-coefficient = 1e-11 m2/s
  permeability = 1e-11 m/s
  chemistry = paste
  segment diff, coordinates = 0,5.0 80.,5.0 mm
}

#default database:
#-----------------
database = /home/aaboulela/chess/tdb/brgm_chess.tdb
exclude minerals, colloids, organics, gases
include Portlandite, CSH(1.6), CSH(1.2), CSH(0.8)
include C3AH6, C4AH13
include Ettringite, Monosulfoaluminate, Monocarboaluminate, Hemicarboaluminate
#include Straetlingite
include Amorphous_silica, Gibbsite, Gibbsite(am), Gypsum
#include Calcite, Magnesite,
#include Fe-Ettringite, C3FH6, Fe-Monosulfoaluminate, C4FH13, Goethite
include Hydrotalcite, Brucite
temperature = 25 C
```

```
unit inlet {
  tot SO4[2-] = 30.0 mmolal
  pH = 3
  balance on SO4[2-]
}

unit paste {
 mineral Gibbsite = 4.179  mol/l
 mineral C3AH6 = 2.011 mol/l
 tot Na[+] = 1e-6 mmol/l
 tot OH[-] = 1e-6 mmol/l
}

# Boundary conditions:
#-------------------------
#boundary LeftBorder {
#   coordinates = -0.4,2 -0.4,2.05 cm
#   flow-condition = constant-flow at 0.5 cm/min
#   transport-condition = flux using inlet
#}

boundary RightBorder {
   coordinates = 80.0,5.0 80.0,6.0 mm
   flow-condition = constant-head at 0 mm
}
verbose = enabled

# Select outputs:
#-------------------------
output = CAC_pH3_1D
output-format = vtk, res

select aqueous{SO4[2-]} in mmol/L
select aqueous{Ca[2+]} in mmol/L
select aqueous{Al[3+]} in mmol/L
select aqueous{H[+]} in mmol/L

select flowrate in m/d

flux-select aqueous{SO4[2-]} in mmol/s
flux-select aqueous{Ca[2+]} in mmol/s
```

flux-select aqueous{Na[+]} in mmol/s

select minerals in molal
select min-volume in l

select head in m
select porosity
select pH

END :
#--------------------------

Appendix VI-B: Evolution of the concentrations of the different sulfur species

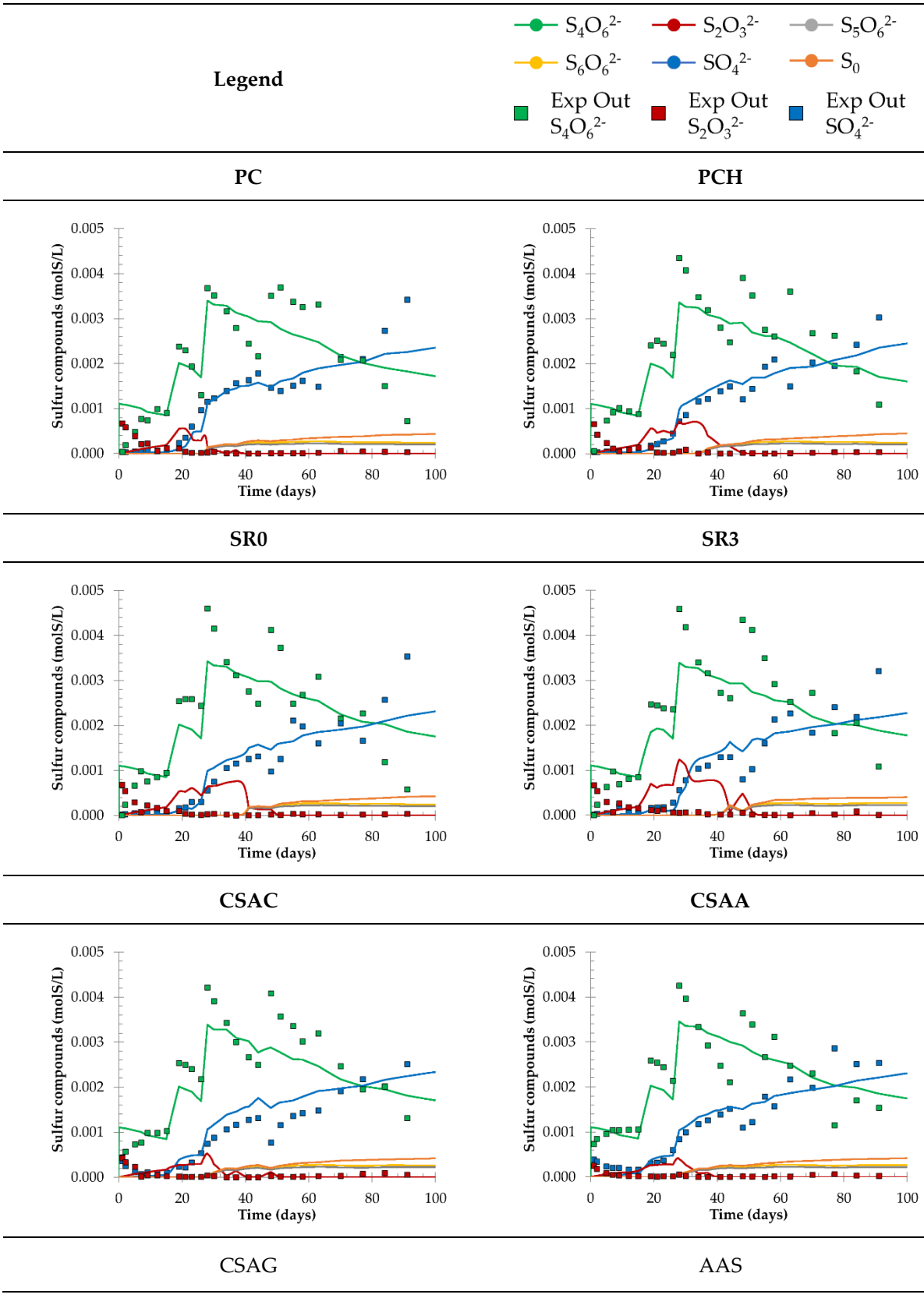

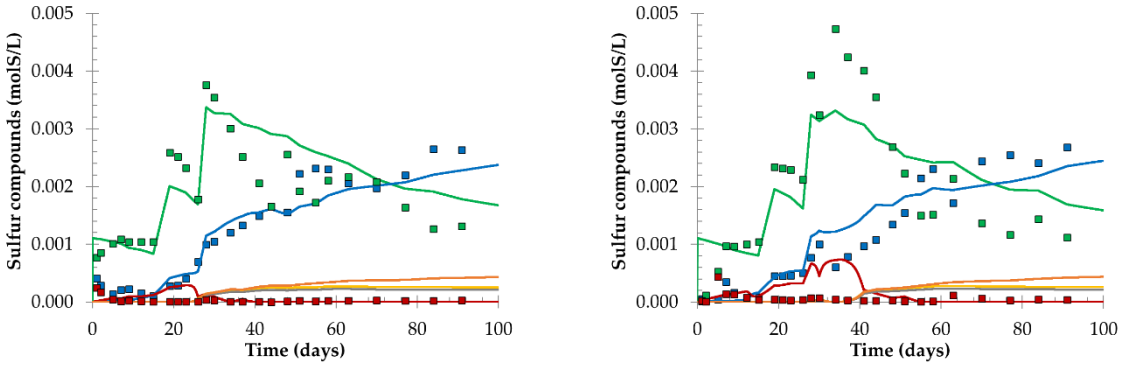

AASB AASH

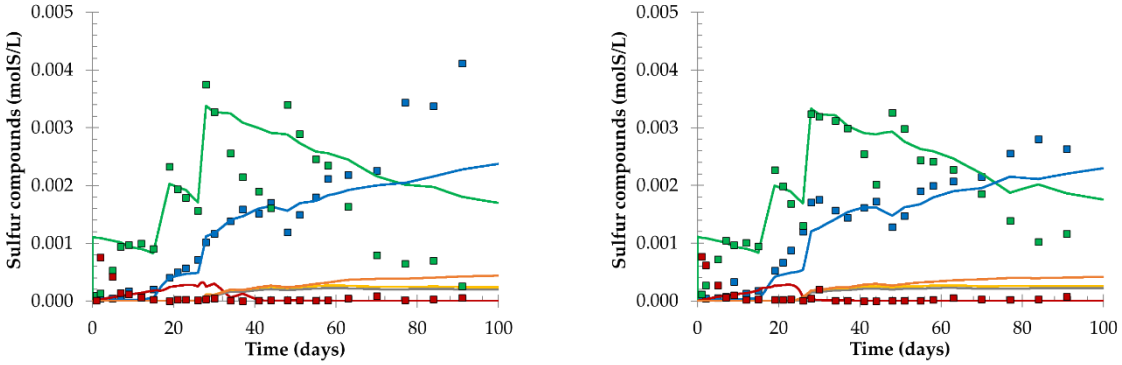

Figure VI-B-1. Evolution of the sulfur compounds in the liquid volume using the kinetic models (solid lines) in comparison with the experimental results (marks) for the different exposed materials

Appendix VI-C: Accumulation of sulfate and thiosulfate in the liquid volume

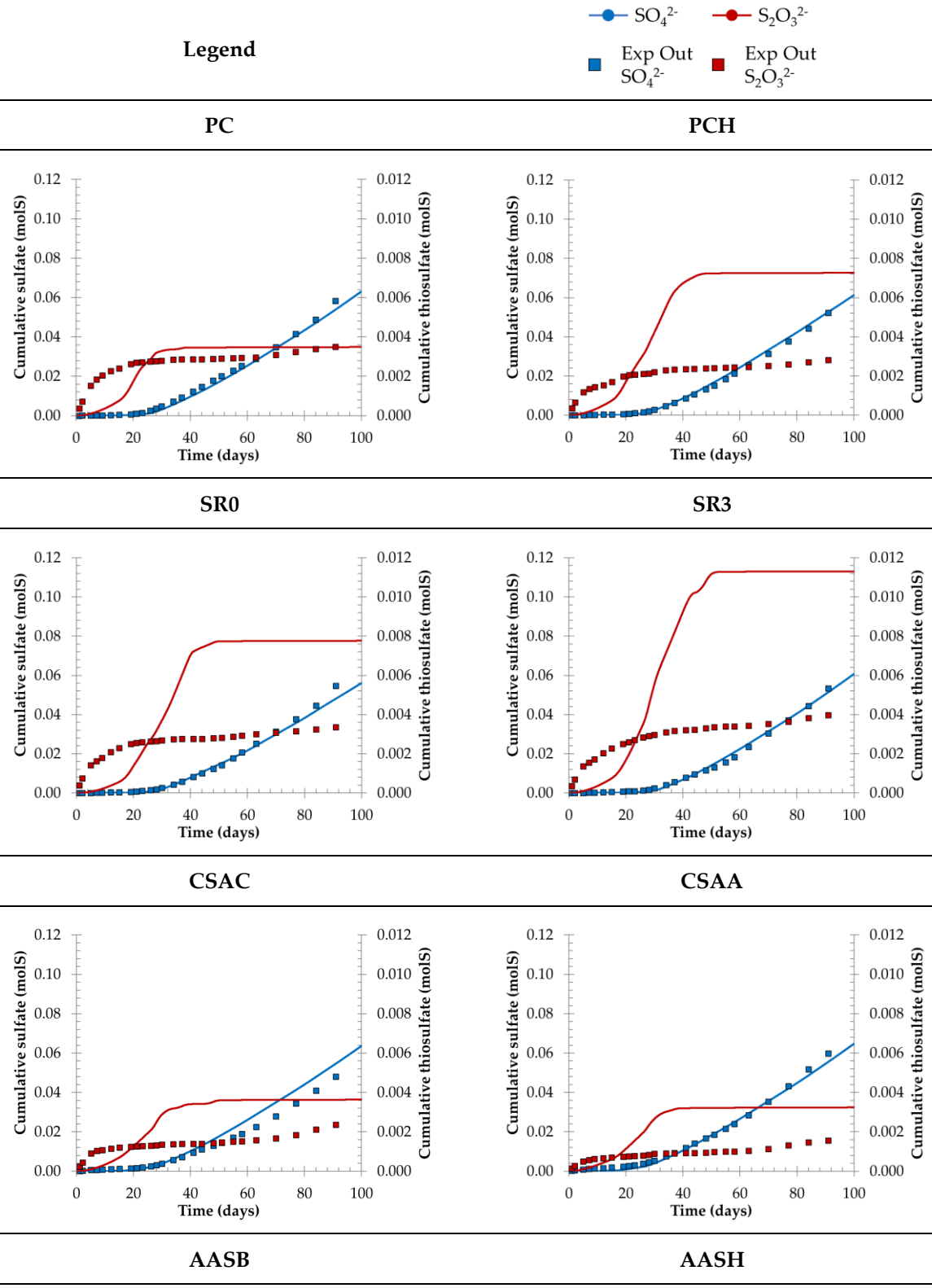

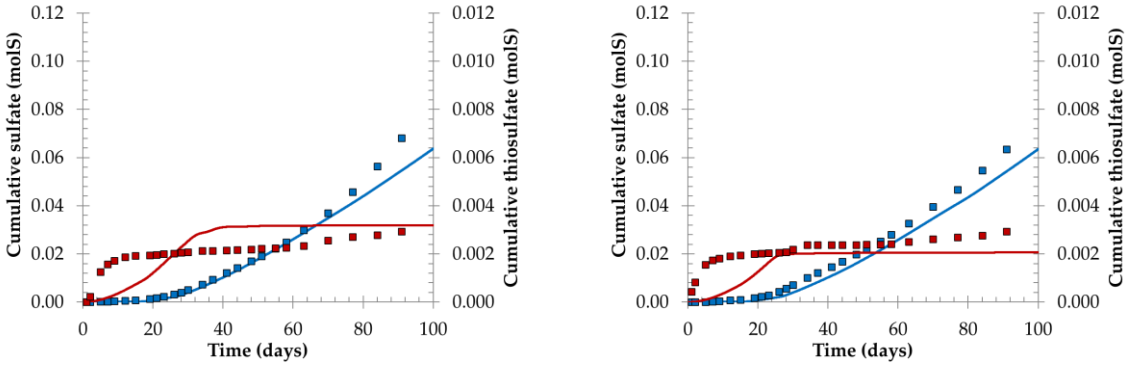

Figure VI-C-1. Cumulative amount of sulfate and thiosulfate in the liquid volume using the kinetic models (solid lines) in comparison with the experimental results (marks) for the different exposed materials

References

References

1. UN-Water. Summary Progress Update 2021 : SDG 6 — water and sanitation for all [Internet]. Geneva, Switzerland; 2021.
2. Gestion patrimoniale des systèmes d'assainissement [Internet]. 1999.
3. Institut Français de L'Environnement. L'environnement en France. 2006.
4. Kaempfer W, Berndt M. Estimation of service life of concrete pipes in sewer networks. Durab Build Mater Components 8. 1999;36–45.
5. Parker CD. Species of sulphur bacteria associated with the corrosion of concrete. Vol. 159, Nature. 1947. p. 439–40.
6. Parker CD. Mechanics of Corrosion of Concrete Sewers by Hydrogen Sulfide. Sewage Ind Waste. 1951;23(12):1477–85.
7. Olmstead WH, Hamlin H. Converting Portions of the Los Angeles Outfall Sewer into a Septic Tank. Eng News Am Railw J. 1900;XLIV(19):317–8.
8. Process design manual for sulfide controle in sanitqry sewerage systems. 1974.
9. Islander BRL, Devinny JS, Member A, Mansfeld F, Postyn A, Shih H. Microbial ecology of crown corrosion in sewers. J Environ Eng. 1992;117(6):751–70.
10. Okabe S, Odagiri M, Ito T, Satoh H. Succession of sulfur-oxidizing bacteria in the microbial community on corroding concrete in sewer systems. Appl Environ Microbiol. 2007 Feb;73(3):971–80.
11. Herisson J. Biodétérioration des matériaux cimentaires dans les ouvrages d'assainissement : étude comparative du ciment d'aluminate de calcium et du ciment Portland [Internet]. Université Paris-Est; 2012.
12. Buvignier A. Caractérisation du rôle de l'aluminium dans les interactions entre les microorganismes et les matériaux cimentaires dans le cadre des réseaux d'assainissement. Université de Toulouse; 2018.
13. Roberts D., Nica D, Zuo G, Davis J. Quantifying microbially induced deterioration of concrete: initial studies. Int Biodeterior Biodegradation. 2002 Jun;49(4):227–34.
14. Joseph AP, Keller J, Bustamante H, Bond PL. Surface neutralization and H2S oxidation at early stages of sewer corrosion: Influence of temperature, relative humidity and H2S concentration. Water Res. 2012;46(13):4235–45.
15. Grengg C, Mittermayr F, Ukrainczyk N, Koraimann G, Kienesberger S, Dietzel M. Advances in concrete materials for sewer systems affected by microbial induced concrete corrosion: A review. Water Res. 2018 May;134:341–52.
16. Vincke E, Verstichel S, Monteny J, Verstraete W. A new test procedure for biogenic sulfuric acid corrosion of concrete. Biodegradation. 1999 Nov;10(6):421–8.
17. Gomez-Alvarez V, Revetta RP, Domingo JWS. Metagenome analyses of corroded concrete wastewater pipe biofilms reveal a complex microbial system. BMC Microbiol. 2012;12.

18. Grengg C, Mittermayr F, Baldermann A, Böttcher ME, Leis A, Koraimann G, et al. Microbiologically induced concrete corrosion: A case study from a combined sewer network. Cem Concr Res. 2015 Nov;77:16–25.

19. Jiang G, Keller J, Bond PL. Determining the long-term effects of H2S concentration, relative humidity and air temperature on concrete sewer corrosion. Water Res. 2014;65:157–69.

20. Lavigne MP, Bertron A, Botanch C, Auer L, Hernandez-Raquet G, Cockx A, et al. Innovative approach to simulating the biodeterioration of industrial cementitious products in sewer environment. Part II: Validation on CAC and BFSC linings. Cem Concr Res. 2016 Jan;79:409–18.

21. Johnson DB, Bridge TAM. Reduction of ferric iron by acidophilic heterotrophic bacteria: Evidence for constitutive and inducible enzyme systems in Acidiphilium spp. J Appl Microbiol. 2002;92(2):315–21.

22. Yamanaka T, Aso I, Togashi S, Tanigawa M, Shoji K, Watanabe T, et al. Corrosion by bacteria of concrete in sewerage systems and inhibitory effects of formates on their growth. Water Res. 2002 May;36(10):2636–42.

23. Jiang G, Zhou M, Chiu TH, Sun X, Keller J, Bond PL. Wastewater-Enhanced Microbial Corrosion of Concrete Sewers. Environ Sci Technol. 2016 Aug 2;50(15):8084–92.

24. Peyre Lavigne M, Bertron A, Auer L, Hernandez-Raquet G, Foussard J-N, Escadeillas G, et al. An innovative approach to reproduce the biodeterioration of industrial cementitious products in a sewer environment. Part I: Test design. Cem Concr Res. 2015 Jul;73:246–56.

25. Sand W, Bock E. Concrete corrosion in the hamburg sewer system. Environ Technol Lett. 1984;5(12):517–28.

26. Aboulela A, Lavigne MP, Buvignier A, Fourré M, Schiettekatte M, Pons T, et al. Laboratory Test to Evaluate the Resistance of Cementitious Materials to Biodeterioration in Sewer Network Conditions. Mater 2021, Vol 14, Page 686. 2021 Feb 2;14(3):686.

27. Sand W, Bock E. Biodeterioration of mineral materials by microorganisms—biogenic sulfuric and nitric acid corrosion of concrete and natural stone. Geomicrobiol J. 1991;9(2–3):129–38.

28. Peyre Lavigne M, Lefebvre X, Patapy C, Bertron A, Paul E. Accelerated test design for biodeterioration of cementitious materials and products in sewer environments. Matériaux Tech. 2015;103(2):204.

29. Kelly DP, Shergill JK, Lu WP, Wood AP. Oxidative metabolism of inorganic sulfur compounds by bacteria. In: Antonie van Leeuwenhoek, International. Kluwer Academic Publishers; 1997. p. 95–107.

30. Balci N, Brunner B, Turchyn A V. Tetrathionate and elemental sulfur shape the isotope composition of sulfate in acid mine drainage. Front Microbiol. 2017 Aug 17;8(AUG):1564.

31. Steudel R, Holdt G, Göbel T, Hazeu W. Chromatographic separation of higher

polythionates SnO62 (n = 3... 22) and their detection in cultures of Thiobacillus ferrooxidans; molecular composition of bacterial sulfur secretions. Angew Chem Int Ed Engl. 1987;26(2):151–3.

32. Schippers A, Jozsa P, Sand W. Sulfur chemistry in bacterial leaching of pyrite. Appl Environ Microbiol. 1996 Sep;62(9):3424–31.

33. Wentzien S, Sand W. Tetrathionate Disproportionation by Thiomonas intermedia K12*. Eng Life Sci. 2004 Feb 5;4(1):25–30.

34. Wentzien S, Sand W. Tetrathionate Disproportionation by Thiomonas intermedia K12**. Eng Life Sci. 2004 Feb 5;4(1):25–30.

35. Wentzien S, Sand W, Albertsen A, Steudel R. Thiosulfate and tetrathionate degradation as well as biofilm generation by Thiobacillus intermedius and Thiobacillus versutus studied by microcalorimetry, HPLC, and ion-pair chromatography. Arch Microbiol. 1994;161(2):116–25.

36. Johnston F, McAmish L. A study of the rates of sulfur production in acid thiosulfate solutions using S-35. J Colloid Interface Sci. 1973 Jan 1;42(1):112–9.

37. Zaiser EM, La Mer VK. The kinetics of the formation and growth of monodispersed sulfur hydrosols. J Colloid Sci. 1948 Dec 1;3(6):571–98.

38. Kelly DP. Thermodynamic aspects of energy conservation by chemolithotrophic sulfur bacteria in relation to the sulfur oxidation pathways. Arch Microbiol. 1999 Mar 22;171(4):219–29.

39. Pan C, Lv F, Kégl T, Horváth AK, Gao Q. Kinetics and Mechanism of the Concurrent Reactions of Hexathionate with S(IV) and Thiosulfate in a Slightly Acidic Medium. J Phys Chem A. 2019 Jul 5;123(26):5418–27.

40. Alexander M, Bertron A, Belie N De. Performance of cement-based materials in aggressive aqueous environments: State-of-the-Art report, RILEM TC 211 - PAE [Internet]. Alexander M, Bertron A, De Belie N, editors. Dordrecht: Springer Netherlands; 2013. 462 p. (RILEM State-of-the-Art Reports; vol. 10).

41. Goyns AM, Alexander MG. Performance of various concretes in the Virginia experimental sewer over 20 years. In: Fentiman CH, Mangabhai RJ, Scrivener KL, editors. Calcium aluminates: Proceedings of the international conference 2014. 2014. p. 573–84.

42. Mori T, Nonaka T, Tazaki K, Koga M, Hikosaka Y, Noda S. Interactions of nutrients, moisture and pH on microbial corrosion of concrete sewer pipes. Water Res. 1992;26(1):29–37.

43. Wells PAT, Melchers RE. Findings of a 4 Year Study of Concrete Sewer Pipe Corrosion. Corros Prev. 2014;(January 2014):1–12.

44. Herisson J, Guéguen-Minerbe M, van Hullebusch ED, Chaussadent T. Behaviour of different cementitious material formulations in sewer networks. Water Sci Technol. 2014 Apr;69(7):1502–8.

45. Munns DN, Keyser HH. Response of Rhizobium strains to acid and aluminium stress. Soil Biol Biochem. 1981;13(2):115–8.

46. Dorea CC, Clarke BA. Effect of aluminium on microbial respiration. Water Air Soil Pollut. 2008;189(1–4):353–8.

47. Saucier F, Lamberet S. Calcium Aluminate Concrete for sewers: Going from qualitative to quantitative evidence of performance. In: Concrete in Aggressive Aqueous Environments, Performance, Testing and Modeling 3-5 June 2009, Toulouse, France. 2009. p. 398–407.

48. Grengg C, Mittermayr F, Koraimann G, Konrad F, Szabó M, Demeny A, et al. The decisive role of acidophilic bacteria in concrete sewer networks: A new model for fast progressing microbial concrete corrosion. Cem Concr Res. 2017 Nov;101(August):93–101.

49. Alexander MG, Fourie C. Performance of sewer pipe concrete mixtures with portland and calcium aluminate cements subject to mineral and biogenic acid attack. Mater Struct Constr. 2011;44(1):313–30.

50. Rozière E, Loukili A, El Hachem R, Grondin F. Durability of concrete exposed to leaching and external sulphate attacks. Cem Concr Res. 2009 Dec;39(12):1188–98.

51. Suraneni P, Azad VJ, Isgor BO, Weiss WJ. Calcium oxychloride formation in pastes containing supplementary cementitious materials: Thoughts on the role of cement and supplementary cementitious materials reactivity. RILEM Tech Lett. 2016;1:24.

52. Santhanam M. Magnesium Attack of Cementitious Materials in Marine Environments. RILEM State-of-the-Art Reports. 2013;10:75–90.

53. Elahi MMA, Shearer CR, Naser Rashid Reza A, Saha AK, Khan MNN, Hossain MM, et al. Improving the sulfate attack resistance of concrete by using supplementary cementitious materials (SCMs): A review. Constr Build Mater. 2021 Apr 26;281:122628.

54. Grengg C. Microbial induced acid corrosion in sewer environments Statutory declaration. 2017;(December).

55. De Belie N, Monteny J, Taerwe L. Apparatus for accelerated degradation testing of concrete specimens. Mater Struct Constr. 2002;35(251):427–33.

56. Sun X, Jiang G, Bond PL, Keller J, Yuan Z. A novel and simple treatment for control of sulfide induced sewer concrete corrosion using free nitrous acid. Water Res. 2015 Mar 1;70:279–87.

57. Kondo R, Daimon M, Akiba T. Mechanism and Kinetics on Carbonation of Hardened Cement, Vol. III. In: 5th International Symposium on Cement Chemistry. Tokyo: The Chemical Society of Japan; 1969. p. 402–9.

58. Moorehead DR. Cementation by the carbonation of hydrated lime. Cem Concr Res. 1986 Sep;16(5):700–8.

59. Morandeau A, Thiéry M, Dangla P. Investigation of the carbonation mechanism of CH and C-S-H in terms of kinetics, microstructure changes and moisture properties. Cem Concr Res. 2014;56:153–70.

60. Zivica V, Bajza A. Acidic attack of cement based materials — a review. Constr Build Mater. 2001 Dec;15(8):331–40.

61. NF EN 14647. Calcium aluminate cement — Composition, specifications and

conformity criteria. 2006.

62. Taylor HFW. Cement Chemistry. 2nd ed. London, UK: Thomas Telford; 1997. 488 p.

63. Yu C, Sun W, Scrivener K. Degradation mechanism of slag blended mortars immersed in sodium sulfate solution. Cem Concr Res. 2015;72:37–47.

64. Scrivener KL, Cabiron J-L, Letourneux R. High-performance concretes from calcium aluminate cements. Cem Concr Res. 1999 Aug;29(8):1215–23.

65. Bertron A. Durabilité des matériaux cimentaires soumis aux acides organiques: Cas particulier des effluents d'élevage. 2004 Jan 1;256.

66. Buvignier A, Peyre-lavigne M, Patapy C, Paul E, Bertron A. Influence de l'aluminium soluble sur les microorganismes sulfo- oxydants : compréhension des mécanismes de résistance des matériaux cimentaires à base de CAC dans les réseaux d ' assainissement. XIIIème Forum Biodétérioration des Matériaux du CEFRACOR. 2016;29–31.

67. Buvignier A, Patapy C, Lavigne MP, Paul E, Bertron A. Resistance to biodeterioration of aluminium-rich binders in sewer network environment: Study of the possible bacteriostatic effect and role of phase reactivity. Cem Concr Res. 2019;123(June):105785.

68. Letourneux R, Scrivener K. The Resistance of Calcium Aluminate Cements To Acid Corrosion in Wastewater Applications. In: Dhir RK, Dyer TD, editors. Modern Concrete Materials: Binders, Additions and Admixtures. Dundee: ICE Publishing; 1999.

69. Herisson J, van Hullebusch ED, Moletta-Denat M, Taquet P, Chaussadent T. Toward an accelerated biodeterioration test to understand the behavior of Portland and calcium aluminate cementitious materials in sewer networks. Int Biodeterior Biodegradation. 2013 Oct;84:236–43.

70. Ehrich S, Helard L, Letourneux R, Willocq J, Bock E. Biogenic and Chemical Sulfuric Acid Corrosion of Mortars. J Mater Civ Eng. 1999 Nov;11(4):340–4.

71. Grengg C, Ukrainczyk N, Koraimann G, Mueller B, Dietzel M, Mittermayr F. Long-term in situ performance of geopolymer, calcium aluminate and Portland cement-based materials exposed to microbially induced acid corrosion. Cem Concr Res. 2020;131(February):106034.

72. Struble LJ, Brown PW. Heats of dehydration and specific heats of compounds found in concrete and their potential for thermal energy storage. Sol Energy Mater. 1986 Aug 1;14(1):1–12.

73. Kasselouri V, Tsakiridis P, Malami C, Georgali B, Alexandridou C. A study on the hydration products of a non-expansive sulfoaluminate cement. Cem Concr Res. 1995 Dec 1;25(8):1726–36.

74. Glasser FP, Zhang L. High-performance cement matrices based on calcium sulfoaluminate-belite compositions. Cem Concr Res. 2001;31(12):1881–6.

75. Zhang L, Su M, Wang Y. Development of the use of sulfo- and ferroaluminate cements in China. Adv Cem Res. 1999 Jan 14;11(1):15–21.

76. Juenger MCG, Winnefeld F, Provis JL, Ideker JH. Advances in alternative cementitious binders. Cem Concr Res. 2011;41(12):1232–43.

77. Winnefeld F, Barlag S. Calorimetric and thermogravimetric study on the influence of calcium sulfate on the hydration of ye'elimite. J Therm Anal Calorim. 2010;101(3):949–57.

78. Hanic F, Kaprálik I, Gabrisová A. Mechanism of hydration reactions in the system C4A3SCSCaOH2O referred to hydration of sulphoaluminate cements. Cem Concr Res. 1989;19(5):671–82.

79. Trauchessec R. Melanges de ciments sulfoalumineux et Portland. Université de Lorraine; 2013.

80. Gabrisová A, Havlica J, Sahu S. Stability of calcium sulphoaluminate hydrates in water solutions with various pH values. Cem Concr Res. 1991;21(6):1023–7.

81. Berger S. Etude des potentialités des ciments sulfo-alumineux bélitique pour le conditionnement du zinc : de l'hydratation à la durabilité. 2009;324.

82. Pelletier-Chaignat L, Winnefeld F, Lothenbach B, Müller CJ. Beneficial use of limestone filler with calcium sulphoaluminate cement. Constr Build Mater. 2012;26(1):619–27.

83. Sudoh G. High strength cement in CaO-Al2O3-SiO2-SO3 system and its application. In: 8th International Congress on the Chemistry of Cement. Paris; 1980.

84. Berger S, Aouad G, Cau Dit Coumes C, Le Bescop P, Damidot D. Leaching of calcium sulfoaluminate cement pastes by water at regulated pH and temperature: Experimental investigation and modeling. Cem Concr Res. 2013;53:211–20.

85. Bescher E, Rice EK, Ramseyer C, Roswurm S. Sulfate resistance of calcium sulphoaluminate cement. J Struct Integr Maint. 2016;1(3):131–9.

86. Dillard R. Comparison of the Resistance of Belitic Calcium Sulfoaluminate Cement and Portland Cement to Sulfate Attack and Sulfuric Acid. University of Arkansas; 2021.

87. Richet C, Le Bescop P, Gallé C, Peycelon H, Bejaoui S, Pointeau I, et al. Synthèse sur le comportement à long terme des colis : Dossier de reference phenomenologique "colis béton" 2004. Gif sur Yvette; 2004.

88. Taylor FW. Microstructural and microanalytical studies of sulfate attack. J Am Ceram Soc. 1990;40:61–78.

89. Quillin K. Performance of belite–sulfoaluminate cements. Cem Concr Res. 2001 Sep;31(9):1341–9.

90. Richardson IG, Groves GW. Microstructure and microanalysis of hardened ordinary Portland cement pastes. J Mater Sci. 1993;28(1):265–77.

91. Lothenbach B, Scrivener K, Hooton RD. Supplementary cementitious materials. Cem Concr Res. 2011;41(12):1244–56.

92. Osborne GJ. Durability of Portland blast-furnace slag cement concrete. Cem Concr Compos. 1999 Jan;21(1):11–21.

93. Abd El.Aziz M, Abd El.Aleem S, Heikal M, El. Didamony H. Hydration and durability of sulphate-resisting and slag cement blends in Caron's Lake water. Cem Concr Res. 2005 Aug 1;35(8):1592–600.

94. De Belie N, Monteny J, Beeldens A, Vincke E, Van Gemert D, Verstraete W.

Experimental research and prediction of the effect of chemical and biogenic sulfuric acid on different types of commercially produced concrete sewer pipes. Cem Concr Res. 2004 Dec;34(12):2223–36.

95. Torii K, Kawamura M. Effects of Fly Ash and Silica Fume on the Resistance. Cem Concr Res. 1994;24(2):361–70.

96. Aydin S, Yazici H, Yiğiter H, Baradan B. Sulfuric acid resistance of high-volume fly ash concrete. Build Environ. 2007 Feb 1;42(2):717–21.

97. Saad MNA, De Andrade WP, Paulon VA. Properties of mass concrete con taining an active pozzolan made from clay. Concr Int. 1982;4(7):59–65.

98. Bucher R. Vers une utilisation rationnelle des métakolins flash : application aux bétons [Internet]. Toulouse 3; 2015.

99. Mielenz RC, Schieltz NC, King ME. Thermogravimetric Analysis of Clay and Clay-Like Minerals. Clays Clay Miner. 1953;2(1):285–314.

100. San Nicolas R. Approche performantielle des bétons avec métakaolins obtenus par calcination flash. Université de Toulouse; 2011.

101. Bishnoi S, Maity S, Mallik A, Joseph S, Krishnan S. Pilot scale manufacture of limestone calcined clay cement : The Indian experience. Indian Concr Journal, Spec issue Futur Cem. 2014;88:22–8.

102. Vizcaíno JL, Sánchez Berriel S, Damas Carrera S, Pérez Hernández A, Scrivener KL, Martirena Hernández JF. Industrial trial to produce a low clinker, low carbon cement. Mater construcción, ISSN 0465-2746, Nº 317, 2015. 2015;(317):5.

103. Sánchez Berriel S, Favier A, Rosa Domínguez E, Sánchez Machado IR, Heierli U, Scrivener K, et al. Assessing the environmental and economic potential of Limestone Calcined Clay Cement in Cuba. J Clean Prod. 2016 Jun 15;124:361–9.

104. Scrivener KL. Options for the future of cement. Indian Concr J. 2014;88(7).

105. Damidot D, Lothenbach B, Herfort D, Glasser FP. Thermodynamics and cement science. Cem Concr Res. 2011 Jul 1;41(7):679–95.

106. Lothenbach B, Le Saout G, Gallucci E, Scrivener K. Influence of limestone on the hydration of Portland cements. Cem Concr Res. 2008;38(6):848–60.

107. Kostuch JA, Walters GV, Jones TR. High Performance concrete incorporating metakaolin - a review. Concr 2000. 1993;2:1799–811.

108. Sabir B, Wild S, Bai J. Metakaolin and calcined clays as pozzolans for concrete: A review. Cem Concr Compos. 2001;23(6):441–54.

109. Roy DM, Arjunan P, Silsbee MR. Effect of silica fume, metakaolin, and low-calcium fly ash on chemical resistance of concrete. Cem Concr Res. 2001;31(12):1809–13.

110. Hewayde E, Nehdi ML, Allouche E, Nakhla G. Using concrete admixtures for sulphuric acid resistance. Proc Inst Civ Eng - Constr Mater. 2007;160(1):25–35.

111. Said-Mansour M, Kadri EH, Kenai S, Ghrici M, Bennaceur R. Influence of calcined kaolin on mortar properties. Constr Build Mater. 2011;25(5):2275–82.

112. Bai J, Kinuthia J, Sabir BB, Wild S. Metakaolin – pulverised fuel ash – Portland cement binders and their role in mortar and concrete. In: Innovations and Developments in Concrete Materials and Construction. Dundee: Thomas Telford; 2002. p. 991.

113. Talero R. Performance of metakaolin and Portland cements in ettringite formation as determined by ASTM C 452-68: kinetic and morphological differences. Cem Concr Res. 2005;35(7):1269–84.

114. Scrivener KL, Pratt PL. Microstructural studies of the hydration of C3A and C4AF independently and in cement paste. In: Glasser FP, editor. Brit Ceram Proc. Stoke-on-Trent: British Ceramic Society; 1984. p. 207–19.

115. Gevaudan JP, Santa-Ana B, Srubar W V. Iron mineral admixtures improve the sulfuric acid resistance of low-calcium alkali-activated cements. Cem Concr Compos. 2021;116(October 2020):103867.

116. Roy D M. Alkali activated cements, opportunities and challenges. Cem Concr Res. 1999;29:249–54.

117. Purdon AO. The action of alkalis on blast-furnace slag. J Soc Chem Ind. 1940;59:191–202.

118. Provis JL, Van Deventer JSJ, editors. Geopolymers: Structure, processing, properties and industrial applications. Woodhead Publishing Limited; 2009.

119. Weil M, Dombrowski K, Buchawald A. Life-cycle analysis of geopolymers. In: Provis JL, Van Deventer JSJ, editors. Geopolymers, structure, processing, properties and applications. 13th ed. Cambridge: Woodhead Publishing Limited; 2009. p. 194–210.

120. McLellan BC, Williams RP, Lay J, Van Riessen A, Corder GD. Costs and carbon emissions for geopolymer pastes in comparison to ordinary portland cement. J Clean Prod. 2011;19(9–10):1080–90.

121. Wang SD, Scrivener KL. Hydration products of alkali activated slag cement. Cem Concr Res. 1995 Apr 1;25(3):561–71.

122. Komljenović M, Baščarević Z, Marjanović N, Nikolić V. External sulfate attack on alkali-activated slag. Constr Build Mater. 2013 Dec;49:31–9.

123. Bakharev T, Sanjayan JG, Cheng YB. Resistance of alkali-activated slag concrete to acid attack. Cem Concr Res. 2003;33(10):1607–11.

124. Bakharev T, Sanjayan JG, Cheng YB. Effect of admixtures on properties of alkali-activated slag concrete. Cem Concr Res. 2000 Sep 1;30(9):1367–74.

125. Glukhovsky VD. Ancient, modern and future concrete. In: First international conference on alkaline cements and concretes. Kiev, Ukraine; 1994. p. 1–8.

126. Krivenko P V. Alkaline cements. In: First international conference on alkaline cements and concretes. Kiev, Ukraine; 1994.

127. Fernández-Jiménez A, Flores E, Maltseva O, Garcia Lodeiro I, Palomo A. Hybrid alkaline cements: Part III. Durability and industrial applications. Rom J Mater. 2013;43:68–73.

128. Brough AR, Atkinson A. Sodium silicate-based, alkali-activated slag mortars - Part I.

Strength, hydration and microstructure. Cem Concr Res. 2002;32(6):865–79.

129. Mohamed OA. A Review of Durability and Strength Characteristics of Alkali-Activated Slag Concrete. Mater 2019, Vol 12, Page 1198. 2019 Apr 12;12(8):1198.

130. Wang SD, Scrivener KL, Pratt PL. Factors affecting the strength of alkali-activated slag. Cem Concr Res. 1994;24(6):1033–43.

131. Gruskovnjak A, Lothenbach B, Holzer L, Figi R, Winnefeld F. Hydration of alkali-activated slag: Comparison with ordinary Portland cement. EMPA Act. 2006;(2006):34.

132. Garcia-Lodeiro I, Palomo A, Fernández-Jiménez A. An overview of the chemistry of alkali-activated cement-based binders. In: Handbook of Alkali-Activated Cements, Mortars and Concretes. Woodhead Publishing; 2015. p. 19–47.

133. Richardson IG, Groves GW. the Incorporation of Minor and Trace Elements Into Calcium Silicate. 1993;23:131–8.

134. El-Hassan H, Shehab E, Al-Sallamin A. Influence of Different Curing Regimes on the Performance and Microstructure of Alkali-Activated Slag Concrete. J Mater Civ Eng. 2018;30(9):04018230.

135. Nasr D, Pakshir AH, Ghayour H. The influence of curing conditions and alkaline activator concentration on elevated temperature behavior of alkali activated slag (AAS) mortars. Constr Build Mater. 2018;190:108–19.

136. Ya-min G, Yong-hao F, Duo Y, Yong-fan G, Chen-hui Z. Properties and microstructure of alkali-activated slag cement cured at below- And about-normal temperature. Constr Build Mater. 2015;79:1–8.

137. Barnett SJ, Soutsos MN, Millard SG, Bungey JH. Strength development of mortars containing ground granulated blast-furnace slag: Effect of curing temperature and determination of apparent activation energies. Cem Concr Res. 2006;36(3):434–40.

138. Mohamed O, Najm O. Effect of Curing Methods on Compressive Strength of Sustainable Self-Consolidated Concrete. IOP Conf Ser Mater Sci Eng. 2019;471(3).

139. Behfarnia K, Shahbaz M. The effect of elevated temperature on the residual tensile strength and physical properties of the alkali-activated slag concrete. J Build Eng. 2018;20(August):442–54.

140. Rostami M, Behfarnia K. The effect of silica fume on durability of alkali activated slag concrete. Constr Build Mater. 2017;134:262–8.

141. Kwon YH, Kang SH, Hong SG, Moon J. Enhancement of material properties of lime-activated slag mortar from intensified pozzolanic reaction and pore filling effect. Sustain. 2018;10(11).

142. Aydin S. A ternary optimisation of mineral additives of alkali activated cement mortars. Constr Build Mater. 2013 Jun 1;43:131–8.

143. Zhu X, Tang D, Yang K, Zhang Z, Li Q, Pan Q, et al. Effect of Ca(OH)2 on shrinkage characteristics and microstructures of alkali-activated slag concrete. Constr Build Mater. 2018;175:467–82.

144. Bakharev T, Sanjayan JG, Cheng YB. Sulfate attack on alkali-activated slag concrete.

Cem Concr Res. 2002 Feb 1;32(2):211–6.

145. Shi C. Strength, pore structure and permeability of alkali-activated slag mortars. Cem Concr Res. 1996 Dec;26(12):1789–99.

146. Higgins DD. Increased sulfate resistance of ggbs concrete in the presence of carbonate. Cem Concr Compos. 2003;25(8):913–9.

147. Bakharev T, Sanjayan JG, Cheng YB. Resistance of alkali-activated slag concrete to carbonation. Cem Concr Res. 2001;31(9):1277–83.

148. Bernal SA, Mejía De Gutiérrez R, Pedraza AL, Provis JL, Rodriguez ED, Delvasto S. Effect of binder content on the performance of alkali-activated slag concretes. Cem Concr Res. 2011;41(1):1–8.

149. Shi C, Stegemann JA. Acid corrosion resistance of different cementing materials. Cem Concr Res. 2000;30(5):803–8.

150. Madhuri G, Srinivasa Rao K. Performance of alkali-activated slag concrete against sulphuric acid attack. Asian J Civ Eng. 2018;19(4):451–61.

151. Xie Y, Lin X, Ji T, Liang Y, Pan W. Comparison of corrosion resistance mechanism between ordinary Portland concrete and alkali-activated concrete subjected to biogenic sulfuric acid attack. Constr Build Mater. 2019 Dec;228:117071.

152. Gifford PM, Gillott JE. Alkali-silica reaction (ASR) and alkali-carbonate reaction (ACR) in activated blast furnace slag cement (ABFSC) concrete. Cem Concr Res. 1996 Jan;26(1):21–6.

153. Bernal SA, Rodrígueza ED, de Gutiérrez RM, Provis JL. Performance of alkali-activated slag mortars exposed to acids. J Sustain Cem Mater. 2012;1(3):138–51.

154. Davidovits J. Eopolymer ement. Inst Geopolymer. 2013;(0):1–11.

155. Davidovits J. Properties of geopolymer cements. Alkaline Cem Concr Kiev, Ukr. 1994;1–19.

156. Duxson P, Fernández-Jiménez A, Provis JL, Lukey GC, Palomo A, Van Deventer JSJ. Geopolymer technology: The current state of the art. J Mater Sci. 2007;42(9):2917–33.

157. Glukhovsky V. Soil silicates. Gostroiizdat Publish, Kiev. Kiev; 1959.

158. Allahverdi A, Škvára F. Sulfuric acid attack on hardened paste of geopolymer cements Part 2. Corrosion mechanism at mild and relatively low concentrations. Ceram - Silikaty. 2006;50(1):1–4.

159. Bakharev T. Resistance of geopolymer materials to acid attack. Cem Concr Res. 2005 Apr 1;35(4):658–70.

160. Song XJ, Marosszeky M, Brungs M, Munn R. Durability of fly ash based Geopolymer concrete against sulphuric acid attack. Int Conf Durab Build Mater Components LYON. 2005;(April):17–20.

161. Allahverdi A, Škvára F. Sulfuric Acid Attack on Hardened Paste of Geopolymer Cements. Part 1. Mechanisms of Corrosion at Relatively High Concentrations. Ceram - Silikáty. 2005;49(4):225–9.

162. Berke NS. Resistance of Microsilica Concrete to Steel Corrosion Erosion and Chemical Attack. Spec Publ. 1989 May 1;114:861–86.

163. Yamato T, Emoto Y. Chemical Resistance of Concrete Containing Condensed Silica Fume. Spec Publ. 1989;114:897–914.

164. Kiliswa MW, Alexander MG, Beushausen HD. Durability design of concrete mixtures for sewer pipe applications: A review of the life factor method. Proc 4th Int Conf Concr Repair, Rehabil Retrofit ICCRRR 2015. 2015;34.

165. Kiliswa MW, Alexander MG, Goyns AM. Extending the Life Factor Method for Predicting Sewer Corrosion to non-Portland-based Cementitious Materials - an Experimental Study. In: Bertron A, Jonkers H, editors. Final Conference of RILEM TC 253-MCI: Microorganisms-Cementitious Materials Interactions. Toulouse: RILEM Publications S.A.R.L; 2018. p. 83–95.

166. Wells T, Melchers RE. An observation-based model for corrosion of concrete sewers under aggressive conditions. Cem Concr Res. 2014;61–62:1–10.

167. Wells T, Melchers RE. Modelling concrete deterioration in sewers using theory and field observations. Cem Concr Res. 2015 Nov 1;77:82–96.

168. Valix M, Bustamante H, Sunarho J. Microbial activity and corrosion of calcium aluminate concrete in sewers. In: Bertron A, Jonkers H, editors. Final Conference of RILEM TC 253-MCI : Microorganisms-Cementitious Materials Interactions. Toulouse: RILEM Publications S.A.R.L; 2018. p. 109–18.

169. Yuan H, Dangla P, Chatellier P, Chaussadent T. Degradation modelling of concrete submitted to sulfuric acid attack. Cem Concr Res. 2013 Nov;53:267–77.

170. Yuan H, Dangla P, Chatellier P, Chaussadent T. Degradation modeling of concrete submitted to biogenic acid attack. Cem Concr Res. 2015;70:29–38.

171. Grandclerc A, Dangla P, Gueguen-Minerbe M, Chaussadent T. Modelling of the sulfuric acid attack on different types of cementitious materials. Cem Concr Res. 2018;105(January):126–33.

172. Lavigne Peyre M, Pechaud Y, Buvignier A, Patapy C, Paul E, Bertron A. 1D Transport reaction model coupling microbial succession of sulfur oxidizing microorganisms and mortar reactivity for OPC-, BFSC- and CAC-based materials. In: Bertron A, Jonkers H, editors. Final Conference of RILEM TC 253-MCI: Microorganisms-Cementitious Materials Interactions. Toulouse: RILEM Publications S.A.R.L; 2018. p. 69–82.

173. Pomeroy RD. Process Design Manual for Sulfide Control in Sanitary Sewerage Systems. United States Environmental Protection Agency,; 1974.

174. Kiliswa MW. Composition and microstructure of concrete mixtures subjected to biogenic acid corrosion and their role in corrosion prediction of concrete outfall sewers [Internet]. PhD thesis, Department of Civil Engineering. University of Cape Town; 2016.

175. Nielsen AH, Hvitved-Jacobsen T, Vollertsen J. Kinetics and stoichiometry of sulfide oxidation by sewer biofilms. Water Res. 2005;39(17):4119–25.

176. De Windt L, Devillers P. Modeling the degradation of Portland cement pastes by biogenic organic acids. Cem Concr Res. 2010 Aug 1;40(8):1165–74.

177. Fryda H, Estival J, Berger S, Bordet F, Andreani PA, Martinet A, et al. Ultra fast hydration opening new application fields: A Comparison of different calcium aluminate technologies. In: Calcium aluminates: Proceedings of the International Conference 2014. 2014. p. 42–53.

178. NF EN 197-1. Cement, Part I: COmposition, specifications and conformity criteria for common cements. 2012.

179. Winnefeld F, Lothenbach B. Hydration of calcium sulfoaluminate cements - Experimental findings and thermodynamic modelling. Cem Concr Res. 2010;40(8):1239–47.

180. Trauchessec R, Mechling J-M, Lecomte A, Roux A, Le Rolland B. Hydration of ordinary Portland cement and calcium sulfoaluminate cement blends. Cem Concr Compos. 2015 Feb;56:106–14.

181. Marchi M, Costa U. Influence of the Calcium Sulphate and W/C Ratio on the Hydration of Calcium Sulfoaluminate Cement. 13th Int Congr Chem Cem. 2011;(January 2011):1–7.

182. Zhang Y, Zhao Q, Gao Z, Chang J. Microstructure Control of AH 3 Gel Formed in Various Calcium Sulfoaluminate Cements as a Function of pH . ACS Sustain Chem Eng. 2021;9(34):11534–47.

183. Gartner GW and EM. Formation and Hydration of Low-CO 2 Cements Based on Belite, Calcium Sulfoaluminate and Calcium Aluminoferrite G. S. Li, G. Walenta and E. M. Gartner Lafarge Central Research, Saint Quentin Fallavier, France. Current.

184. Pelletier-Chaignat L, Winnefeld F, Lothenbach B, Saout G Le, Müller CJ, Famy C. Influence of the calcium sulphate source on the hydration mechanism of Portland cement-calcium sulphoaluminate clinker-calcium sulphate binders. Cem Concr Compos. 2011;33(5):551–61.

185. Lamberet S. Durability of ternary binders based on portland cement, calcium aluminate cement and calcium sulfate, PhD thesis N°3151, Ecole Polytechnique Fédérale de Lausanne. Vol. 3151. 2005.

186. Lamberet S, Guinot D, Lempreur E, Talley J, Alt C. Field Investigations of High Performance Calcium Aluminate Mortar for Wastewater Applications. In: Fentiman CH, Managbhai RJ, Scrivener KL, editors. Calcium aluminates: Proceedings of the Centenary Conference 2008. Avignon, France: IHS BRE Press; 2008. p. 269–77.

187. Scrivener K, Snellings R, Lothenbach B. A practical guide to microstructural analysis of cementitious materials. CRC Press; 2018.

188. Zhang Y, Chang J, Ji J. AH3 phase in the hydration product system of AFt-AFm-AH3 in calcium sulfoaluminate cements: A microstructural study. Constr Build Mater. 2018 Apr 10;167:587–96.

189. Arliguie G, Hornain H, editors. Détermination du dosage en ciment dans un béton durci. In: GranDuBé. Association Française de Génie Civil; 2007. p. 305–14.

190. NF P 18-459. Essai pour béton durci - Essai de porosité et de masse volumique. 2010.

191. Zhou Q, Glasser FP. Thermal stability and decomposition mechanisms of ettringite at

120°C. Cem Concr Res. 2001 Sep 1;31(9):1333–9.

192. Gastaldi D, Paul G, Marchese L, Irico S, Boccaleri E, Mutke S, et al. Hydration products in sulfoaluminate cements: Evaluation of amorphous phases by XRD/solid-state NMR. Cem Concr Res. 2016;90:162–73.

193. Satoh H, Odagiri M, Ito T, Okabe S. Microbial community structures and in situ sulfate-reducing and sulfur-oxidizing activities in biofilms developed on mortar specimens in a corroded sewer system. Water Res. 2009;43(18):4729–39.

194. Vincke E, Boon N, Verstraete W. Analysis of the microbial communities on corroded concrete sewer pipes - A case study. Appl Microbiol Biotechnol. 2001;57(5–6):776–85.

195. Davis JL, Nica D, Shields K, Roberts DJ. Analysis of concrete from corroded sewer pipe. Int Biodeterior Biodegrad. 1998;42(1):75–84.

196. Thompson M, Walsh JN. Inductively Coupled Plasma Spectrometry. Ltd B& S, editor. New York: Blackie & Son Ltd; 1989.

197. Vandecasteele C, Block CB. Modern Methods for Trace Element Determination. John Wiley & Sons Ltd., editor. New York; 1997.

198. Tyler G. ICP-OES , ICP-MS and AAS Techniques Compared. Tech note 05 ICP Opt Spectrosc. 2001;(3):1–11.

199. Miura Y, Kawaoi A. Determination of thiosulfate, thiocyanate and polythionates in a mixture by ion-pair chromatography with ultraviolet absorbance detection. In: Journal of Chromatography A. Elsevier; 2000. p. 81–7.

200. Callahan BJ, McMurdie PJ, Rosen MJ, Han AW, Johnson AJA, Holmes SP. DADA2: High-resolution sample inference from Illumina amplicon data. Nat Methods. 2016 Jul 23;13(7):581–3.

201. Murali A, Bhargava A, Wright ES. IDTAXA: A novel approach for accurate taxonomic classification of microbiome sequences. Microbiome. 2018 Aug 9;6(1):1–14.

202. McMurdie PJ, Holmes S. phyloseq: An R Package for Reproducible Interactive Analysis and Graphics of Microbiome Census Data. Watson M, editor. PLoS One. 2013 Apr 22;8(4):e61217.

203. Quast C, Pruesse E, Yilmaz P, Gerken J, Schweer T, Yarza P, et al. The SILVA ribosomal RNA gene database project: improved data processing and web-based tools. Nucleic Acids Res. 2012 Nov 27;41(D1):D590–6.

204. Rifa E, Theil S. ExploreMetabar: v1.0.0. 2021 Aug 24;

205. Theil S, Rifa E. rANOMALY: AmplicoN wOrkflow for Microbial community AnaLYsis. F1000Research. 2021 Jan 7;10:7.

206. van der Lee J, De Windt L, Lagneau V, Goblet P. Module-oriented modeling of reactive transport with HYTEC. Comput Geosci. 2003;29(3):265–75.

207. Sin I, Lagneau V, Corvisier J. Integrating a compressible multicomponent two-phase flow into an existing reactive transport simulator. Adv Water Resour. 2017;

208. Seigneur N, Lagneau V, Corvisier J, Dauzères A. Recoupling flow and chemistry in variably saturated reactive transport modelling - An algorithm to accurately couple the

feedback of chemistry on water consumption, variable porosity and flow. Adv Water Resour. 2018;122:355–66.

209. Blanc P, Lassin A, Piantone P, Azaroual M, Jacquemet N, Fabbri A, et al. Thermoddem: A geochemical database focused on low temperature water/rock interactions and waste materials. Appl Geochemistry. 2012;27(10):2107–16.

210. Reichert P. AQUASIM A tool for simulation and data analysis of aquatic systems.pdf. Water Sci Technol. 1994;30(2):21–30.

211. Robinson RA, Stokes R. Electrolyte solutions. J Appl Polym Sci. 1959;3(8):255–255.

212. Colmer AR, Temple KL, Hinkle ME. An iron-oxidizing bacterium from the acid drainage of some bituminous coal mines. J Bacteriol. 1950;59(3):317–28.

213. Jorgensen BB, Bak F. Pathways and microbiology of thiosulfate transformations and sulfate reduction in a marine sediment (Kattegat, Denmark). Appl Environ Microbiol. 1991;57(3):847–56.

214. Sievert SM, Kiene RP, Schulz-Vogt HN. The Sulfur Cycle. Oceanography. 2007;20(2):117–23.

215. Janssen AJH, Lens PNL, Stams AJM, Plugge CM, Sorokin DY, Muyzer G, et al. Application of bacteria involved in the biological sulfur cycle for paper mill effluent purification. Sci Total Environ. 2009;407(4):1333–43.

216. Liu LY, Xie GJ, Xing DF, Liu BF, Ding J, Cao GL, et al. Sulfate dependent ammonium oxidation: A microbial process linked nitrogen with sulfur cycle and potential application. Environ Res. 2021;192(October 2020):110282.

217. Marenco PJ, Corsetti FA, Hammond DE, Kaufman AJ, Bottjer DJ. Oxidation of pyrite during extraction of carbonate associated sulfate. Chem Geol. 2008 Jan 15;247(1–2):124–32.

218. Fontaine D, Eriksen J, Sørensen P. Sulfur from biogas desulfurization: Fate of S during storage in manure and after application to plants. Sci Total Environ. 2021 Feb 1;754:142180.

219. Ling AL, Robertson CE, Harris JK, Frank DN, Kotter C V., Stevens MJ, et al. High-Resolution Microbial Community Succession of Microbially Induced Concrete Corrosion in Working Sanitary Manholes. Mormile MR, editor. PLoS One. 2015 Mar 6;10(3).

220. Suzuki I. Oxidation of inorganic sulfur compounds: Chemical and enzymatic reactions [Internet]. Vol. 45, Canadian Journal of Microbiology. National Research Council of Canada; 1999. p. 97–105.

221. Varga D, Horváth AK. Kinetics and mechanism of the decomposition of tetrathionate ion in alkaline medium. Inorg Chem. 2007;46(18):7654–61.

222. Ghosh W, Dam B. Biochemistry and molecular biology of lithotrophic sulfur oxidation by taxonomically and ecologically diverse bacteria and archaea. FEMS Microbiol Rev. 2009;33(6):999–1043.

223. Wentzien S, Sand W. Tetrathionate Disproportionation byThiomonas intermedia K12. Eng Life Sci. 2004 Feb 5;4(1):25–30.

224. Sulonen MLK, Lakaniemi AM, Kokko ME, Puhakka JA. Long-term stability of bioelectricity generation coupled with tetrathionate disproportionation. Bioresour Technol. 2016;216:876–82.

225. Kupka D, Liljeqvist M, Nurmi P, Puhakka JA, Tuovinen OH, Dopson M. Oxidation of elemental sulfur, tetrathionate and ferrous iron by the psychrotolerant Acidithiobacillus strain SS3. Res Microbiol. 2009;160(10):767–74.

226. de Beer D, Stoodley P, Roe F, Lewandowski Z. Effects of biofilm structures on oxygen distribution and mass transport. Biotechnol Bioeng. 1994;43(11):1131–8.

227. Finster K. Microbiological disproportionation of inorganic sulfur compounds. J Sulfur Chem. 2008;29(3–4):281–92.

228. Sinha DB, Walden CC. Formation of polythionates and their interrelationships during oxidation of thiosulfate by Thiobacillus ferrooxidans. Can J Microbiol. 1966;12(5):1041–54.

229. Druschel GK, Hamers RJ, Banfield JF. Kinetics and mechanism of polythionate oxidation to sulfate at low pH by O2 and Fe3+. Geochim Cosmochim Acta. 2003;67(23):4457–69.

230. Herisson J, Guéguen-Minerbe M, van Hullebusch ED, Chaussadent T. Influence of the binder on the behaviour of mortars exposed to H2S in sewer networks: a long-term durability study. Mater Struct. 2017 Feb 4;50(1):8.

231. Guo X, Shi H, Hu W, Wu K. Durability and microstructure of CSA cement-based materials from MSWI fly ash. Cem Concr Compos. 2014;46:26–31.

232. Kurtis KE, Shomglin K, Monteiro PJM, Harvey J, Roesler J. Accelerated Test for Measuring Sulfate Resistance of Calcium Sulfoaluminate, Calcium Aluminate, and Portland Cements. J Mater Civ Eng. 2001 Jun;13(3):216–21.

233. M. Cohen, A. Bentur. Durability of Portland Cement-Silica Fume Pastes in Magnesium Sulfate and Sodium Sulfate Solutions. ACI Mater J. 1988;(May–June):148– 157.

234. Furcas FE, Lothenbach B, Isgor OB, Mundra S, Zhang Z, Angst UM. Solubility and speciation of iron in cementitious systems. Cem Concr Res. 2022 Jan 1;151:106620.

235. Dilnesa BZ, Lothenbach B, Renaudin G, Wichser A, Kulik D. Synthesis and characterization of hydrogarnet Ca3(Al xFe1 - X)2(SiO4)y(OH) 4(3 - y). Cem Concr Res. 2014;59:96–111.

236. Dilnesa BZ, Lothenbach B, Renaudin G, Wichser A, Wieland E. Stability of Monosulfate in the Presence of Iron. Jennings H, editor. J Am Ceram Soc. 2012 Oct 1;95(10):3305–16.

237. Mancini A, Wieland E, Geng G, Lothenbach B, Wehrli B, Dähn R. Fe(II) interaction with cement phases: Method development, wet chemical studies and X-ray absorption spectroscopy. J Colloid Interface Sci. 2021 Apr 15;588:692–704.

238. Taylor HFW, Newbury DE. An electron microprobe study of a mature cement paste. Cem Concr Res. 1984;14(4):565–73.

239. Copeland LE, Kantro DL, Verbeck G. Chemistry of Hydration of Portland cement. In: International Symposium of Chemistry of Cement. 1960. p. 429–65.

240. Mancini A, Wieland E, Geng G, Dähn R, Skibsted J, Wehrli B, et al. Fe(III) uptake by calcium silicate hydrates. Appl Geochemistry. 2020 Feb 1;113:104460.

241. Collepardi M, Monosi S, Moriconi G, Corradi M. Tetracalcium aluminoferrite hydration in the presence of lime and gypsum. Cem Concr Res. 1979 Jul 1;9(4):431–7.

242. Fukuhara M, Goto S, Asaga K, Daimon M, Kondo R. Mechanisms and kinetics of C4AF hydration with gypsum. Cem Concr Res. 1981 May 1;11(3):407–14.

243. Rodger SA, Groves GW. Electron Microscopy Study of Ordinary Portland Cement and Ordinary Portland Cement–Pulverized Fuel Ash Blended Pastes. J Am Ceram Soc. 1989;72(6):1037–9.

244. Allahverdi A, Škvára F. Nitric acid attack on hardened paste of geopolymeric cements, Part 1. Ceram - Silikaty. 2001;45(3):81–8.

245. Grandclerc A. Compréhension des mécanismes de biodétérioration des matériaux cimentaires dans les réseaux d'assainissement : étude expérimentale et modélisation [Internet]. 2017.

246. Buvignier A, Peyre-Lavigne M, Robin O, Bounouba M, Patapy C, Bertron A, et al. Influence of Dissolved-Aluminum Concentration on Sulfur-Oxidizing Bacterial Activity in the Biodeterioration of Concrete. Stams AJM, editor. Appl Environ Microbiol. 2019 May 24;85(15):e00302-19.

247. Huang Y, Pei Y, Qian J, Gao X, Liang J, Duan G, et al. Bauxite free iron rich calcium sulfoaluminate cement: Preparation, hydration and properties. Constr Build Mater. 2020;249:118774.

248. Zhang L, Glasser FP. Hydration of calcium sulfoaluminate cement at less than 24 h. Adv Cem Res. 2002;14(4):141–55.

249. Pina RG, Cervantes C. Microbial interections with aliminium. Bio Met. 1996;9:311–6.

250. Sahu S, Havlica J, Tomková V, Majling J. Hydration behaviour of sulphoaluminate belite cement in the presence op various calcium sulphates. Thermochim Acta. 1991;175(1):45–52.

251. Hulbert SF, Huff DE. Kinetics of Alumina Removal from a Calcined Kaolin with Nitric, Sulphuric and Hydrochloric Acids. Clay Miner. 1970;8(3):337–45.

252. LI X, YE Y, XUE S, JIANG J, WU C, KONG X, et al. Leaching optimization and dissolution behavior of alkaline anions in bauxite residue. Trans Nonferrous Met Soc China. 2018 Jun;28(6):1248–55.

253. Kinnarinen T, Holliday L, Häkkinen A. Dissolution of sodium, aluminum and caustic compounds from bauxite residues. Miner Eng. 2015;79:143–51.

254. Reddy BR, Mishra SK, Banerjee GN. Kinetics of leaching of a gibbsitic bauxite with hydrochloric acid. Hydrometallurgy. 1999;51(1):131–8.

255. Jiang G, Wightman E, Donose BC, Yuan Z, Bond PL, Keller J. The role of iron in sulfide induced corrosion ofsewer concrete. Water Res. 2014;49:166–74.

256. Rawlings DE, Dew D, Du Plessis C. Biomineralization of metal-containing ores and concentrates. Trends Biotechnol. 2003;21(1):38–44.

257. Beverskog B, Puigdomenech I. Revised pourbaix diagrams for iron at 25–300 °C. Corros Sci. 1996 Dec;38(12):2121–35.

258. Brydson R, Richardson IG, McComb DW, Groves GW. Parallel electron energy loss spectroscopy study of al-substituted calcium silicate hydrate (CSH) phases present in hardened cement pastes. Solid State Commun. 1993;88(2):183–7.

259. Richardson IG, Brough AR, Brydson R, Groves GW, Dobson CM. Location of aluminium in substituted calcium silicate hydrate (C-S-H) gels as determined by Si-29 and Al-27 NMR and EELS. J Am Ceram Soc. 1993;76(9):2285–8.

260. Collins F, Sanjayan JG. Effect of pore size distribution on drying shrinkage of alkali-activated slag concrete. Cem Concr Res. 2000;30(9):1401–6.

261. Gruyaert E, Van Den Heede P, Maes M, De Belie N. Investigation of the influence of blast-furnace slag on the resistance of concrete against organic acid or sulphate attack by means of accelerated degradation tests. Cem Concr Res. 2012;42(1):173–85.

262. Bertron A, Duchesne J, Escadeillas G. Accelerated tests of hardened cement pastes alteration by organic acids: analysis of the pH effect. Cem Concr Res. 2005 Jan;35(1):155–66.

263. Kiliswa MW, Scrivener KL, Alexander MG. The corrosion rate and microstructure of Portland cement and calcium aluminate cement-based concrete mixtures in outfall sewers: A comparative study. Cem Concr Res. 2019;124(July):105818.

264. Erbektas AR, Isgor OB, Weiss WJ. An accelerated testing protocol for assessing microbially induced concrete deterioration during the bacterial attachment phase. Cem Concr Compos. 2019;104.

265. Yu C, Sun W, Scrivener K. Mechanism of expansion of mortars immersed in sodium sulfate solutions. Cem Concr Res. 2013;43(1):105–11.

266. Xie Y, Lin X, Pan W, Ji T, Liang Y, Zhang H. Study on corrosion mechanism of alkali-activated concrete with biogenic sulfuric acid. Constr Build Mater. 2018 Nov 10;188:9–16.

267. Fryda H, Saucier F, Lamberet S, Scrivener K. Durabilité des béton d'aluminate de calcium. In: Ollivier J-P, Vichot A, editors. La Durabilité Des Bétons - Bases scientifiques pour la formulation de bétons durables dans leur environnment. Ollivier V. Paris: Presse de l'Ecole Nationale des Ponts et Chaussées; 2010. p. 767–823.

268. Trauchessec R, Mechling JM, Lecomte A, Roux A, Le Rolland B. Impact of anhydrite proportion in a calcium sulfoaluminate cement and Portland cement blend. Adv Cem Res. 2014;26(6):325–33.

269. Schoen R, Roberson CE. Structures of aluminum hydroxide and geochemical implications. Am Mineral. 1970 Feb 1;55(1–2):43–77.

270. Barnhisel RI, Rich CI. Gibbsite, Bayerite, and Nordstrandite Formation as Affected by Anions, pH, and Mineral Surfaces. Soil Sci Soc Am J. 1965;29(5):531–4.

271. Morin V, Termkhajornkit P, Huet B, Pham G. Impact of quantity of anhydrite, water to binder ratio, fineness on kinetics and phase assemblage of belite-ye'elimite-ferrite cement. Cem Concr Res. 2017;99(April):8–17.

272. Chang J, Zhang Y, Shang X, Zhao J, Yu X. Effects of amorphous AH3 phase on mechanical properties and hydration process of C4A3S¯-CS¯H2-CH-H2O system. Constr Build Mater. 2017;133:314–22.

273. Lothenbach B, Kulik DA, Matschei T, Balonis M, Baquerizo L, Dilnesa B, et al. Cemdata18: A chemical thermodynamic database for hydrated Portland cements and alkali-activated materials. Cem Concr Res. 2019 Jan 1;115:472–506.

274. CHITVORANUND N. Stability of hydrate assemblages and properties of cementitious systems with higher alumina content. Ecole Polytechnique Fédérale de Lausanne; 2021.

275. Liu Y, Ma D, Blackley RA, Zhou W, Han X, Bao X. Synthesis and characterization of gibbsite nanostructures. J Phys Chem C. 2008;112(11):4124–8.

276. Filho RWND, De Araujo Rocha G, Montes CR, Vieira-Coelho AC. Synthesis and characterization of boehmites obtained from gibbsite in presence of different environments. Mater Res. 2016;19(3):659–68.

277. Zhang Y, Chang J, Zhao J, Fang Y. Nanostructural characterization of Al(OH)3 formed during the hydration of calcium sulfoaluminate cement. J Am Ceram Soc. 2018;101(9):4262–74.

278. Taylor HFW, Famy C, Scrivener KL. Delayed ettringite formation. Cem Concr Res. 2001 May 1;31(5):683–93.

279. Kiliswa MW, Alexander MG. Biogenic Corrosion of Concrete Sewer Pipes : a Review of the Performance of Cementitious Materials Sao Paulo, Brazil 2-5 September 2014. XIII Conf Durab Build Mater Components, RILEM Proc Pro 96 Sao Paulo, Brazil, 2-5 Sept. 2014;(1):1023–30.

280. Gutberlet T, Hilbig H, Beddoe RE. Acid attack on hydrated cement - Effect of mineral acids on the degradation process. Cem Concr Res. 2015;74:35–43.

281. Monteny J, Vincke E, Beeldens A, De Belie N, Taerwe L, Van Gemert D, et al. Chemical, microbiological, and in situ test methods for biogenic sulfuric acid corrosion of concrete. Cem Concr Res. 2000 Apr 1;30(4):623–34.

282. Scrivener KL. Microstructure Development During the Hydration of Portland Cement. Imperial College of Science and Technology, University of London; 1984.

283. Agatzini-Leonardou S, Oustadakis P, Tsakiridis PE, Markopoulos C. Titanium leaching from red mud by diluted sulfuric acid at atmospheric pressure. J Hazard Mater. 2008;157(2–3):579–86.

284. Gräfe M, Power G, Klauber C. Bauxite residue issues: III. Alkalinity and associated chemistry. Hydrometallurgy. 2011;108(1–2):60–79.

285. Jen G, Stompinis N, Jones R. Chloride ingress in a belite-calcium sulfoaluminate cement matrix. Cem Concr Res. 2017;98:130–5.

286. Allevi S, Marchi M, Scotti F, Bertini S, Cosentino C. Hydration of calcium sulphoaluminate clinker with additions of different calcium sulphate sources. Mater Struct Constr. 2016;49(1–2):453–66.

287. Damidot D, Glasser FP. Thermodynamic investigation of the CaOAl2O3CaSO4H2O system at 25°C and the influence of Na2O. Cem Concr Res. 1993;23(1):221–38.

288. Bissonnette B, Pierre P, Pigeon M. Influence of key parameters on drying shrinkage of cementitious materials. Cem Concr Res. 1999 Oct 1;29(10):1655–62.

289. Thomas RJ, Lezama D, Peethamparan S. On drying shrinkage in alkali-activated concrete: Improving dimensional stability by aging or heat-curing. Cem Concr Res. 2017 Jan 1;91:13–23.

290. Drugă B, Ukrainczyk N, Weise K, Koenders E, Lackner S. Interaction between wastewater microorganisms and geopolymer or cementitious materials: Biofilm characterization and deterioration characteristics of mortars. Int Biodeterior Biodegrad. 2018;

291. Aboulela A, Peyre-Lavigne M, Bertron A. Investigation of test methods to qualify cementitious materials. In: Bertron A, Jonkers H, editors. Proceedings of RILEM TC 253-MCI Conference Microorganisms- Cementitious Materials Interactions PRO123, RILEM Edition. Toulouse; 2018. p. 45–56.

292. NF EN 196-2. Methods of testing cement - Part 2: Chemical analysis of cement.

293. Bureau of Analysed Samples Ltd. Certificat of analysis : BCS-CRM No. 353. Middlesbrough;

List of figures

List of figures

List of tables

List of tables